

**Harnessing the Reactivity of Late Transition Metals for the Making  
and Breaking of C-X (X = O, S, N) Bonds**

by

Addison N. Desnoyer

B.Sc. (Hons.), The University of British Columbia Okanagan, 2012

A THESIS SUBMITTED IN PARTIAL FULFILLMENT OF THE REQUIREMENTS FOR  
THE DEGREE OF

DOCTOR OF PHILOSOPHY

in

The Faculty of Graduate and Postdoctoral Studies

(Chemistry)

The University of British Columbia

(Vancouver)

July 2017

© Addison N. Desnoyer, 2017

## Abstract

This thesis explores the fundamental reactivity of  $\pi$ -complexes of rhodium and nickel, their reactivity to form well-defined 2-metallaoxetanes, as well as subsequent functionalization chemistry of these rare metallacycles. More generally, we also examine C-O and C-S bond cleavage processes.

In Chapter 1, we discuss the history of 2-metallaoxetanes, as well as outline some of the fundamental organometallic chemistry of group 10 transition metal complexes.

In Chapter 2, the chemistry of a well-defined 2-rhodaioxetane with unsaturated electrophiles is explored. In all cases, insertion into the Rh-O bond is observed. When electron-deficient alkynes are used as substrates, rhodadihydropyrans are formed. Reactivity studies have found these complexes to be robust. In contrast, when aldehydes are used, the product rhodaacetals are much less stable. Curiously, the aldehyde insertions were found to be reversible.

Chapter 3 outlines the reactivity of low-valent nickel complexes with three-membered oxacycles. When epoxides were used, isomerization to the corresponding aldehyde was observed as the primary reaction pathway. Experiments with tetrasubstituted epoxides indicate that these reactions occur *via* 2-nickela(II)oxetane intermediates. Further, catalytic functionalization was achieved using HBpin or B<sub>2</sub>pin<sub>2</sub>. When using oxaziridines as the three-membered heterocycle, N-O oxidative addition was found to rapidly generate oxazanickela(II)cyclobutanes. Fragmentation of these metallacycles resulted in the formation of a mixture of imine and aldehyde products.

Chapter 4 discusses the synthesis, mechanism of formation and reactivity of a family of well-defined 2-nickela(II)oxetanes. These nickelacycles are formed with retention of configuration, which had not been observed previously. Computational calculations were performed, which

support an unexpected bimetallic mechanism of oxidative addition that would allow for the observed stereochemistry. Reactivity studies indicate that the nickelaoxetanes are susceptible to protonolysis, insertion and oxidatively-induced reductive elimination reactions.

Chapter 5 describes the chemistry of nickel with esters and thioesters. For thioesters, C<sub>acyl</sub>-S bond cleavage followed by decarbonylation was observed to form methyl-thiolate complexes of nickel(II). In contrast, aryl esters were found to undergo C<sub>aryl</sub>-O oxidative addition, producing aryl-acetate nickel(II) complexes. Both of these classes of compounds were found to be competent in stoichiometric Suzuki-type cross-coupling reactions, but attempts to render the reactions catalytic have so far been unsuccessful.

## **Lay Summary**

Inorganic chemistry is the study of the structure and reactivity of metal (or metalloid) complexes. Oftentimes, the reactivity of these metals can be tuned by changing the structure of its ligands. The controlled reactivity of transition metal complexes is usually desired because it allows for the formation of new products that can be difficult to obtain through other means. In particular, chemists often strive to use transition metal complexes as a reaction catalyst; that is, something that allows a reaction to occur much faster than it would under ordinary conditions. Catalysts are also highly desirable because they can in principle be reused repeatedly. In this thesis, we perform fundamental reactivity studies of transition metal complexes in order to better understand the individual steps that occur during catalysis, thereby allowing for the development of reactions that are more efficient, cost-effective and produce less waste.

## Preface

Chapter 1 contains material that has been published as a Review Article in *Chemical Society Reviews* (*Chem. Soc. Rev.* **2017**, *46*, 197). All Schemes have been modified from the published version. I assembled the manuscript, with subsequent edits from Prof. Jennifer A. Love prior to submission.

Chapter 2 contains material that has been published as Communications in *Dalton Transactions* (*Dalton Trans.* **2014**, *43*, 30) and *Inorganic Chemistry* (*Inorg. Chem.* **2016**, *55*, 13). The rhodadihydropyran complexes **2.13** and **2.14** were initially prepared by Dr. Alex Dauth, my predecessor in the Love group, who collected preliminary characterization data on them. The X-ray Absorption Spectroscopy (XAS) analysis of complexes **1.31**, **1.32**, and **2.27** were performed by Dr. Shirin Behyan at the Canadian Light Source (CLS), and analysis of these data were performed by Dr. Shirin Behyan and Prof. Pierre Kennepohl. Dr. Brian O. Patrick performed the X-ray diffraction analyses and refined the structural data. All other experimental work was performed by me. I wrote the first draft for both manuscripts in this Chapter, with subsequent edits being made by all authors.

The chemistry in Chapter 3 was developed under my direct supervision. The work with epoxides in Sections 3.2 to 3.4 has been accepted for publication as a Communication in *Chemistry- A European Journal* (in press), while the oxaziridine chemistry in Section 3.5 is currently being pursued by Weiling Chiu, a PhD student in the Love group. We expect to submit a Communication based on our oxaziridine work shortly. I wrote the first drafts of these manuscript, with subsequent edits being made by all authors. Candy Cheung, an undergraduate researcher in the Love group, prepared imine complex **3.53**, as well as performed preliminary

reactivity studies of nickel complex **3.17** with oxaziridines. Jialing Geng, a MSc student in the Love group, first prepared ketone complex **3.26**, as well as performed initial hydrosilation and hydroboration experiments. Dr. Brian O. Patrick and Dr. Marcus W. Drover and performed the X-ray diffraction experiments and refinement of the structural data for all complexes except **3.34** and **3.62**. D. Dawson Beattie collected the data for these two complexes; refinement of the former was performed by Dr. Brian O. Patrick, while the latter was refined by me. All other experimental work was performed by me.

Parts of the results presented in Chapter 4 have been published as a Communication in the *Journal of the American Chemical Society (J. Am. Chem. Soc. 2015, 137, 12748)*. The computational work was performed by Eric G. Bowes, a PhD student in the Love group. Dr. Brian O. Patrick performed the data collection and refinement of the single crystal X-ray diffraction experiments. All other experimental work was performed by me. I wrote the first draft of the paper, with subsequent edits being made by all authors.

Parts of the work in Chapter 5 have been published as an Article in *Chemistry- A European Journal (Chem. Eur. J. 2016, 22, 4070)*. This chapter describes a research project that was initiated with Florian W. Friese, a visiting Scholar in the Love group from the Westfälische Wilhelms-Universität Münster, who prepared several of the  $\eta^2$ -carbonyl complexes and performed the initial cross-coupling work with boronic acids. Weiling Chiu, a PhD student in the Love group, optimized the cross-coupling experiments with both esters and thioester substrates, as well as prepared naphthyl complex **5.40**. X-ray diffraction analyses were performed by Dr. Brian O. Patrick and Dr. Marcus W. Drover. All other experimental work was performed by me. I wrote the first draft of the manuscript, with subsequent edits being performed based on input from all other authors. This Chapter also contains work that was performed by me at the Humboldt Universität zu Berlin

as a visiting scholar, where I worked with Prof. Dr. Thomas Braun and Theresia Ahrens, a PhD student in the Braun group.

# Table of Contents

Abstract.....	ii
Lay Summary.....	iv
Preface.....	v
Table of Contents.....	viii
List of Tables.....	x
List of Figures.....	xi
List of Schemes.....	xiii
List of Abbreviations.....	xvii
Acknowledgements.....	xxi
Dedication.....	xxiii
Chapter 1 : Transition Metal Complexes that Make and Break C-X (X = O, S, N) Bonds.....	1
1.1. 2-Metallaioxetanes as Reactive Intermediates and Well-Defined Complexes.....	2
1.2 Metallacycles of Nickel: Structure and Reactivity.....	23
1.3 Group Transfer Chemistry of Nickel Imidos.....	33
1.4 Oxidative Addition and Reductive Elimination Reactions of Late Transition Metals ..	38
1.5 Summary.....	47
Chapter 2 : Reactivity and Revisited Mechanism of Formation of a 2-Rhodaoxetane.....	49
2.1 Introduction.....	49
2.2 Insertion of Alkynes into a Rh-O Bond.....	54
2.3 Reactions of a 2-Rhodaoxetane with Other sp-Hybridized Electrophiles.....	60
2.4 Reversible Insertion of Aldehydes.....	64
2.5 Spectroscopic Analysis of Rhodium Oxidation States.....	70
2.6 Summary.....	75
2.7 Experimental.....	76
Chapter 3 : Exploring the Reactivity of Low-Valent Nickel with Three-Membered Oxacycles ..	95
3.1 Introduction.....	95
3.2 Isomerization of Epoxides.....	99
3.3 Oxidative Addition of Tetrasubstituted Epoxides.....	111
3.4 Functionalization of Epoxides.....	118
3.5 Reactivity with Oxaziridines.....	121

3.6	Summary .....	129
3.7	Experimental .....	130
Chapter 4 : Synthesis of 2-Nickela(II)oxetanes: Structure, Reactivity, and a New Mechanism of Formation.....		154
4.1	Introduction.....	154
4.2	Synthesis of Well-Defined 2-Nickela(II)oxetanes .....	157
4.3	Mechanistic Investigation by Density Functional Theory .....	167
4.4	Reactivity of Well-Defined 2-Nickela(II)oxetanes.....	172
4.5	Summary .....	181
4.6	Experimental.....	182
Chapter 5 : Adventures in C-O and C-S Bond Cleavage Using Nickel and Rhodium ....		197
5.1	Introduction .....	197
5.2	Reactivity of a Ketone and Thioesters with Nickel(0).....	201
5.3	Reactivity of Esters with Nickel(0).....	210
5.4	Reactivity of a Bridging Carbido Complex of Rhodium .....	219
5.5	Summary .....	229
5.6	Experimental .....	229
Chapter 6 : Overview and Future Work.....		254
6.1	Overview .....	254
6.2	Future Work .....	256
References.....		259
Appendix A: Crystallographic Data.....		286
Appendix B: NMR Spectra.....		301

## List of Tables

<b>Table 2.1</b> Scope of aldehyde insertion into <b>1.33</b> .....	67
<b>Table 3.1</b> Hydroboration of aryl epoxides with <b>3.20</b> and HBpin .....	119
<b>Table 5.1</b> Stoichiometric cross-coupling of thioesters with PhB(OH) <sub>2</sub> .....	209
<b>Table 5.2</b> Cross-coupling of esters with boronic acids .....	216

## List of Figures

<b>Figure 2.1</b> $^1\text{H}$ NMR spectrum (400 MHz, 25 °C, $\text{CD}_2\text{Cl}_2$ ) of <b>2.14</b> [ $\text{BAr}^{\text{F}_4}$ ]. Inset shows the resonance assigned to <b>H1</b> . * indicates residual DEAD.....	55
<b>Figure 2.2</b> Oak ridge thermal ellipsoid plot (ORTEP) diagram (50% probability ellipsoids) of <b>2.14</b> [ $\text{BAr}^{\text{F}_4}$ ]. H atoms, $\text{BAr}^{\text{F}_4}$ counterion and 0.5 $\text{H}_2\text{O}$ solvates omitted for clarity. ....	57
<b>Figure 2.3</b> Overlay of partial $^1\text{H}$ NMR spectra (400 MHz, 25 °C, acetone- $d_6$ ) of <b>2.14</b> [ $\text{BAr}^{\text{F}_4}$ ] after heating at 55 °C for 2 hr (purple trace), 6 hr (black trace), 22 hr (red trace) and 36 hr (green trace). ....	59
<b>Figure 2.4</b> $^1\text{H}$ NMR resonances for <b>H1</b> (right) and <b>H2</b> (left) of <b>2.22</b> when they are coupled (above) and decoupled (below) from the other. $[\text{Rh}] = (\text{TPA})\text{Rh}^+$ .....	62
<b>Figure 2.5</b> $^1\text{H}$ NMR spectrum (400 MHz, 25 °C, acetone- $d_6$ ) of <b>2.27</b> . Inset shows the resonance assigned to <b>H1</b> .....	65
<b>Figure 2.6</b> ORTEP (50% probability ellipsoids) of <b>2.27</b> [ $\text{BAr}^{\text{F}_4}$ ]. H atoms, $\text{BAr}^{\text{F}_4}$ counterion and 0.5 $\text{C}_6\text{H}_{14}$ solvates omitted for clarity. ....	66
<b>Figure 2.7</b> Region of the $^1\text{H}$ NMR spectra of <b>2.27</b> (above, $\text{R} = \text{H}$ ) and <b>2.32</b> (below, $\text{R} = \text{C}_6\text{F}_5$ ) showing the resonances of the $\text{RhCH}_2\text{CH}_2\text{O}$ group.....	68
<b>Figure 2.8</b> Rh K-edge XAS data for complexes <b>1.31</b> (---), <b>1.32</b> (.....), and <b>2.27</b> (—). The inset shows the first derivative of the XAS data near the edge. ....	73
<b>Figure 3.1</b> Overlay of the $^{31}\text{P}\{^1\text{H}\}$ NMR spectra of the reaction of styrene oxide <b>3.15</b> , $\text{Ni}(\text{COD})_2$ and dcype after heating at 75 °C for 0 hr (red trace), 1.5 hr (blue trace) and 8 hr (green trace)	101
<b>Figure 3.2</b> Synthesis and ORTEP diagram (50% probability ellipsoids) of complex <b>3.22</b> . All H atoms omitted for clarity. ....	103
<b>Figure 3.3</b> $^1\text{H}$ NMR spectrum (400 MHz, $\text{C}_6\text{D}_6$ , 25 °C) of <b>3.23</b> . Inset shows the <b>H1</b> and <b>H2</b> resonances. ....	105
<b>Figure 3.4</b> ORTEP diagram (50% probability ellipsoids) of complex <b>3.23</b> . All H atoms except <b>H1</b> omitted for clarity. ....	106
<b>Figure 3.5</b> Partial $^1\text{H}$ NMR spectrum (400 MHz, $\text{C}_6\text{D}_6$ , 25 °C) showing the methyl resonance of <b>3.24</b> . with (right) and without (left) $^{31}\text{P}$ decoupling.....	107
<b>Figure 3.6</b> ORTEP diagram (50% probability ellipsoids) of complex <b>3.24</b> . All H atoms omitted for clarity.....	108
<b>Figure 3.7</b> ORTEP diagram (50% probability ellipsoids) of complex <b>3.26</b> . All H atoms omitted for clarity.....	109
<b>Figure 3.8</b> ORTEP diagrams (50% probability ellipsoids) of complexes <b>3.30</b> (left) and <b>3.29</b> (right). All H atoms except <b>H1</b> omitted for clarity. ....	110
<b>Figure 3.9</b> Partial $^1\text{H}\{^{31}\text{P}\}$ NMR spectrum (400 MHz, $\text{C}_6\text{D}_6$ , 25 °C) showing the methyl and ABX resonances of <b>3.34</b> .....	112
<b>Figure 3.10</b> ORTEP diagram (50% probability ellipsoids) of complexes <b>3.34</b> . All H atoms except <b>H2</b> omitted for clarity .....	114
<b>Figure 3.11</b> ORTEP diagram (50% probability ellipsoids) of complexes <b>3.37</b> . All H atoms except <b>H2</b> omitted for clarity.....	115
<b>Figure 3.12</b> ORTEP diagram (50% probability ellipsoids) of complexes <b>3.38</b> . All H atoms omitted for clarity. This data is to demonstrate connectivity only. ....	116

<b>Figure 3.13</b> ORTEP diagram (50% probability ellipsoids) of complex <b>3.53</b> . All H atoms omitted for clarity.....	122
<b>Figure 3.14</b> ORTEP diagram (50% probability ellipsoids) of complex <b>3.54</b> . All H atoms omitted for clarity.....	123
<b>Figure 3.15</b> ORTEP diagram (50% probability ellipsoids) of complex <b>3.57</b> . All H atoms omitted for clarity.....	125
<b>Figure 3.16</b> Variable temperature $^{31}\text{P}\{^1\text{H}\}$ NMR spectra of the reaction of <b>3.20</b> with oxaziridine <b>3.60</b> at -50 °C (red trace), -30 °C (green trace) and 0 °C (black trace). .....	127
<b>Figure 3.17</b> ORTEP diagrams (50% probability ellipsoids) of complex <b>3.62</b> . All H atoms omitted for clarity. ....	128
<b>Figure 4.1</b> Partial HSQC spectrum of <b>4.21</b> showing the cyclohexyl resonances.....	159
<b>Figure 4.2</b> ORTEP (50% ellipsoids) diagrams of <b>4.21</b> . Hydrogen atoms omitted for clarity....	160
<b>Figure 4.3</b> Low-temperature $^{31}\text{P}\{^1\text{H}\}$ NMR spectrum (162 MHz, -50 °C, Tol- $d_8$ ) of the reaction of <b>3.20</b> with <b>4.20</b> .....	161
<b>Figure 4.4</b> ORTEP (50% ellipsoids) diagrams of <b>4.23</b> . Hydrogen atoms omitted for clarity....	163
<b>Figure 4.5</b> ORTEP (50% ellipsoids) diagrams of <b>4.28</b> . Hydrogen atoms omitted for clarity....	166
<b>Figure 4.6</b> DFT calculated reaction pathway (BP86/631-G(d,p)) for $\text{S}_{\text{N}}2$ -type ring-opening using a truncated dmpe ligand. Energies ( $\Delta\text{G}$ ) are reported in kcal/mol relative to <b>B_Me</b> .....	169
<b>Figure 4.7</b> DFT calculated reaction pathways (BP86/631-G(d,p)) for concerted (blue) and bimetallic (black) C-O oxidative addition. Energies ( $\Delta\text{G}$ ) are reported in kcal/mol relative to <b>B</b> (not shown). .....	171
<b>Figure 4.8</b> ORTEP (50% ellipsoids) diagrams of <b>4.35</b> . Hydrogen atoms omitted for clarity....	174
<b>Figure 4.9</b> ORTEP diagrams of <b>4.37</b> (30% ellipsoids). Hydrogen atoms omitted for clarity....	176
<b>Figure 4.10</b> ORTEP diagrams (30% ellipsoids) of <b>4.44</b> (left) and <b>4.45</b> (right). Hydrogen atoms omitted for clarity .....	179
<b>Figure 4.11</b> Synthesis and ORTEP diagram (30% ellipsoids) of <b>4.46</b> .....	181
<b>Figure 5.1</b> ORTEP diagram (30% ellipsoids) of bridging carbido complex <b>5.15</b> . Hydrogen atoms omitted for clarity. ....	200
<b>Figure 5.2</b> ORTEP (50% probability ellipsoids) diagram of <b>5.17</b> .....	202
<b>Figure 5.3</b> ORTEP (50% probability ellipsoids) diagram of complex <b>5.20</b> .....	203
<b>Figure 5.4</b> $^{31}\text{P}\{^1\text{H}\}$ NMR spectrum (162 MHz, $\text{C}_6\text{D}_6$ , 25 °C) of <b>5.20</b> .....	204
<b>Figure 5.5</b> ORTEP (50% probability ellipsoids) diagram of complex <b>5.21</b> .....	205
<b>Figure 5.6</b> ORTEP diagram of complex <b>5.24</b> . Thermal ellipsoids shown at 50% probability ..	206
<b>Figure 5.7</b> ORTEP diagram of complex <b>5.25</b> . Thermal ellipsoids shown at 50% probability. ..	207
<b>Figure 5.8</b> ORTEP diagram of complex <b>5.27</b> . Thermal ellipsoids shown at 50% probability ..	210
<b>Figure 5.9</b> ORTEP diagram of complex <b>5.30</b> . Thermal ellipsoids shown at 50% probability ..	211
<b>Figure 5.10</b> ORTEP diagram of complex <b>5.35</b> . Thermal ellipsoids shown at 50% probability ..	213
<b>Figure 5.11</b> ORTEP diagram of complex <b>5.37</b> . Thermal ellipsoids shown at 50% probability ..	217
<b>Figure 5.12</b> ORTEP diagram of complex <b>5.38</b> . Thermal ellipsoids shown at 50% probability ..	218
<b>Figure 5.13</b> Frontier molecular orbitals of complex <b>5.15</b> .....	221
<b>Figure 5.14</b> Overlay of $^{31}\text{P}\{^1\text{H}\}$ NMR spectra showing the conversion of <b>5.15</b> (•) to <b>5.44</b> (•) and subsequently to <b>5.45</b> (•) over 4 (green trace), 16 (blue trace), 24 (red trace) and 48 (purple trace) hours.....	223

## List of Schemes

<b>Scheme 1.1</b> The first reported 2-metallaioxetane .....	2
<b>Scheme 1.2</b> Sharpless ([2+2]) and CCN ([3+2]) mechanisms of olefin dihydroxylation .....	3
<b>Scheme 1.3</b> Milstein's catalytic epoxide isomerization .....	4
<b>Scheme 1.4</b> Synthesis of a 2-rhodaioxetane .....	5
<b>Scheme 1.5</b> Synthesis of a 2-titanaioxetane .....	6
<b>Scheme 1.6</b> Synthesis and reactivity of a 2-ruthenaioxetane .....	6
<b>Scheme 1.7</b> Schrock's synthesis of 2-metallaioxetanes of molybdenum and tungsten.....	7
<b>Scheme 1.8</b> Sundermeyer's syntheses of group 6 2-metallaioxetanes, including the first 2-chromaioxetane .....	7
<b>Scheme 1.9</b> Gal's synthesis of a 2-rhodaioxetane and rhodadioxolanes .....	9
<b>Scheme 1.10</b> Love's transmetalation of the Rh-O bond of a 2-rhodaioxetane.....	10
<b>Scheme 1.11</b> Love's proposed mechanism for olefin carbohydroxylation .....	11
<b>Scheme 1.12</b> Tejel's olefin oxidation via a 2-rhodaioxetane .....	12
<b>Scheme 1.13</b> Klemperer's synthesis and reactivity of a 2-iridaioxetane.....	12
<b>Scheme 1.14</b> Flood's synthesis and reactivity of a 2-iridaioxetane .....	13
<b>Scheme 1.15</b> Bera's synthesis and reactivity of a 2-iridaioxetane .....	14
<b>Scheme 1.16</b> Hillhouse's synthesis of 2-nickelaioxetanes .....	15
<b>Scheme 1.17</b> Doyle's catalytic cross-coupling of epoxides and boronic acids.....	16
<b>Scheme 1.18</b> Nickel complex isolated from Doyle's catalytic experiments .....	17
<b>Scheme 1.19</b> Jamison's catalytic reductive coupling of epoxides and alkynes .....	18
<b>Scheme 1.20</b> Puddephatt's transiently generated 2-platinaioxetane .....	19
<b>Scheme 1.21</b> Vedernikov's 2-platinaioxetane reductively eliminates to form epoxides .....	20
<b>Scheme 1.22</b> Sharp's reversible 2-platinaioxetane formation .....	21
<b>Scheme 1.23</b> Reactivity of Sharp's platinaioxetane .....	22
<b>Scheme 1.24</b> Synthesis of Cinelli's 2-auraioxetane .....	23
<b>Scheme 1.25</b> Reactivity of a nickel complex with CS <sub>2</sub> .....	23
<b>Scheme 1.26</b> Jones' synthesis and reactivity of a transient nickel sulfido.....	24
<b>Scheme 1.27</b> Synthesis and reactivity of nickel thiolate complexes .....	25
<b>Scheme 1.28</b> Oxidative addition of thiiranes with nickel(0).....	26
<b>Scheme 1.29</b> Synthesis and reactivity of nickel amido complexes .....	27
<b>Scheme 1.30</b> Oxidative addition of aziridines with nickel(0) .....	28
<b>Scheme 1.31</b> Synthesis and reactivity of nickel alkoxo complexes .....	29
<b>Scheme 1.32</b> Synthesis and reactivity of nickel alkoxo complexes .....	29
<b>Scheme 1.33</b> Synthesis and reductive elimination chemistry of nickel alkoxo complexes .....	31
<b>Scheme 1.34</b> Synthesis and reactivity of nickel alkoxo complexes .....	32
<b>Scheme 1.35</b> Nickel-mediated synthesis of a tetrahydrofuran ring.....	32
<b>Scheme 1.36</b> Nickel-mediated synthesis of a tetrahydrofuran ring.....	34
<b>Scheme 1.37</b> Reactivity of a nickel alkylidene with azides and N <sub>2</sub> O .....	35
<b>Scheme 1.38</b> Nickel-mediated amination of ethylene.....	36
<b>Scheme 1.39</b> Catalytic coupling of azides and CO to form isocyanate.....	37
<b>Scheme 1.40</b> Radical coupling and dehydrogenation of a nickel imido complex.....	38
<b>Scheme 1.41</b> Reversible C-S oxidative addition mediated by nickel.....	38

<b>Scheme 1.42</b> Oxidative addition of a CH <sub>3</sub> -O bond by palladium .....	39
<b>Scheme 1.43</b> C-O Reductive elimination proceeds via nucleophilic attack.....	40
<b>Scheme 1.44</b> C-O bond formation from a five-coordinate intermediate.....	41
<b>Scheme 1.45</b> C-O reductive elimination from a bimetallic palladium complex .....	41
<b>Scheme 1.46</b> C-S reductive elimination from palladium .....	42
<b>Scheme 1.47</b> Nickel-catalyzed cross-coupling of pivalates and azoles .....	43
<b>Scheme 1.48</b> Oxidative addition of esters with platinum.....	43
<b>Scheme 1.49</b> Oxidative addition of thioesters with platinum.....	44
<b>Scheme 1.50</b> Oxidative addition of aziridines with palladium.....	45
<b>Scheme 1.51</b> Oxidative addition of sulfoxides with nickel.....	45
<b>Scheme 1.52</b> C-O reductive elimination from nickel.....	46
<b>Scheme 1.53</b> C-X (X = O, S, N) reductive elimination with nickel.....	47
<b>Scheme 2.1</b> Could insertion of an electrophile (A=B) lead to productive reactivity? .....	49
<b>Scheme 2.2</b> Proposed mechanism of the Mirozoki-Heck reaction.....	50
<b>Scheme 2.3</b> Insertion of a pendant olefin into a rhodium-alkoxide bond .....	51
<b>Scheme 2.4</b> Insertion of DEAD into a rhodium-aryloxy bond.....	51
<b>Scheme 2.5</b> Reversible insertion of aldehydes and ketones into C-H bonds .....	52
<b>Scheme 2.6</b> Reversible insertion of methyl formate into a C-H bond.....	52
<b>Scheme 2.7</b> Insertion chemistry of complex <b>1.33</b> with acetone and acetonitrile .....	53
<b>Scheme 2.8</b> Insertion of electron-deficient acetylene dicarboxylates into the Rh-O bond of <b>1.33</b> . .....	54
<b>Scheme 2.9</b> Initial reactivity studies of <b>2.13</b> .....	58
<b>Scheme 2.10</b> Isomerization of <b>2.14</b> to <b>2.20</b> .....	59
<b>Scheme 2.11</b> Potential mechanism of isomerization of <b>2.14</b> to <b>2.20</b> . [Rh] = (TPA)Rh.....	60
<b>Scheme 2.12</b> Insertion of allene-type molecules into <b>1.33</b> .....	61
<b>Scheme 2.13</b> Insertion of allene-type molecules into <b>1.33</b> .....	63
<b>Scheme 2.14</b> Insertion of carbonyl compounds into <b>1.33</b> .....	64
<b>Scheme 2.15</b> Reversibility of aldehyde insertion into <b>1.33</b> and attempted transmetalation of <b>2.27</b> . [Rh] = (TPA)Rh <sup>+</sup> , R = C <sub>6</sub> F <sub>5</sub> . .....	69
<b>Scheme 2.16</b> Proposed mechanism for oxidative coupling of aldehydes and ethylene. [Rh] = (TPA)Rh <sup>+</sup> .....	70
<b>Scheme 2.17</b> Heyduk's oxidatively-induced C-C reductive elimination from zirconium(IV) ....	71
<b>Scheme 2.18</b> Synthesis of olefin complexes <b>2.36</b> and <b>2.37</b> .....	71
<b>Scheme 2.19</b> Proposed structural and electronic changes that occur during rotation of the ethylene ligand in <b>1.32''</b> . .....	74
<b>Scheme 2.20</b> Revised mechanism of formation of rhodaoxetane <b>1.33</b> . [Rh] = (TPA)Rh <sup>+</sup> .....	75
<b>Scheme 3.1</b> Contrasting reactivity of 2-metallaioxetanes of nickel and rhodium with alkynes ...	95
<b>Scheme 3.2</b> Coates' carbonylation of epoxides.....	97
<b>Scheme 3.3</b> 2-Nickela(II)oxetane <b>3.7</b> as a proposed intermediate in catalytic coupling of epoxide <b>3.5</b> and CO <sub>2</sub> . [Ni] = Ni(PCy <sub>3</sub> ) <sub>2</sub> or Ni(PPh <sub>3</sub> ) <sub>2</sub> .....	98
<b>Scheme 3.4</b> Synthesis of complexes <b>3.11</b> and <b>3.12</b> .....	98
<b>Scheme 3.5</b> Reactivity of <b>3.13</b> with epoxide <b>3.14</b> .....	99
<b>Scheme 3.6</b> Ligand screening for reactivity of nickel(0) with epoxides .....	100

<b>Scheme 3.7</b> Preparation of (dtbpe)nickel(0) synthons .....	102
<b>Scheme 3.8</b> Synthesis of complexes <b>3.23</b> and <b>3.24</b> .....	104
<b>Scheme 3.9</b> Synthesis of complexes <b>3.26</b> .....	109
<b>Scheme 3.10</b> Synthesis of complexes <b>3.29</b> and <b>3.30</b> .....	110
<b>Scheme 3.11</b> Synthesis of complexes <b>3.34</b> .....	113
<b>Scheme 3.12</b> Synthesis of complexes <b>3.36</b> and <b>3.37</b> .....	115
<b>Scheme 3.13</b> Potential mechanisms of oxidative addition of epoxides with nickel(0). [Ni] = (dtbpe)nickel(0) .....	117
<b>Scheme 3.14</b> Functionalization of styrene oxide with B <sub>2</sub> pin <sub>2</sub> or silanes .....	120
<b>Scheme 3.15</b> Proposed catalytic cycle for the hydroboration of epoxides. [Ni] = (dtbpe)Ni ....	120
<b>Scheme 3.16</b> Oxidation of platinum(II) with oxaziridine in protic solvent .....	121
<b>Scheme 3.17</b> Synthesis of complexes <b>3.52</b> and <b>3.53</b> . <sup>1</sup> H NMR yields in parentheses. ....	122
<b>Scheme 3.18</b> Synthesis and potential oxidation, deprotonation chemistry of complex <b>3.57</b> .....	124
<b>Scheme 3.19</b> Reactivity of <b>3.20</b> with oxaziridine <b>3.60</b> .....	126
<b>Scheme 3.20</b> Potential mechanism of formation of <b>3.54</b> and <b>3.66</b> from <b>3.63</b> .....	129
<b>Scheme 4.1</b> Oxidative cyclization of <b>4.1</b> with nickel(0) .....	154
<b>Scheme 4.2</b> Proposed mechanism of nickel-catalyzed Tischenko coupling .....	155
<b>Scheme 4.3</b> Proposed mechanism of nickel-catalyzed benzoxasilole synthesis .....	156
<b>Scheme 4.4</b> Ring-opening of cyclopropyl ketones mediated by nickel(0) .....	157
<b>Scheme 4.5</b> Initial synthesis of <b>4.21</b> . Isolated yield in parenthesis. Relative stereochemistry shown for clarity. ....	158
<b>Scheme 4.6</b> Low-temperature synthesis of <b>4.21</b> . Relative stereochemistry shown for clarity ...	162
<b>Scheme 4.7</b> Synthesis of <b>4.23</b> .....	162
<b>Scheme 4.8</b> Reactivity of <b>3.20</b> with cyclohexene oxide .....	164
<b>Scheme 4.9</b> Reactivity of <b>3.20</b> with oxyl radicals .....	164
<b>Scheme 4.10</b> Reactivity of <b>4.25</b> and <b>4.26</b> with epoxide <b>4.20</b> .....	165
<b>Scheme 4.11</b> Synthesis of 2-nickelaoxetanes <b>4.27</b> and <b>4.28</b> . Isolated yields in parentheses ....	166
<b>Scheme 4.12</b> Attempted reactions of acyclic epoxides with <b>3.20</b> .....	167
<b>Scheme 4.13</b> Protonolysis reactions of <b>4.21</b> .....	172
<b>Scheme 4.14</b> Deoxygenation of <b>4.21</b> with Ph <sub>3</sub> CBF <sub>4</sub> .....	173
<b>Scheme 4.15</b> Reactivity of <b>4.21</b> with carbon oxides .....	175
<b>Scheme 4.16</b> Proposed competing mechanisms of formation of <b>4.36</b> and <b>4.37</b> .....	177
<b>Scheme 4.17</b> Proposed mechanisms of formation of <b>4.40</b> and <b>4.20</b> <i>via</i> nickel(III) (upper pathway) or nickel(IV) (lower pathway). ....	178
<b>Scheme 4.18</b> Proposed mechanism of formation of <b>4.45</b> from <b>4.27</b> .....	180
<b>Scheme 5.1</b> Nickel complexes <b>5.2</b> and <b>5.3</b> can catalyze Tischenko-coupling of aldehydes .....	198
<b>Scheme 5.2</b> Nickel(0)-mediated decarbonylation of anhydrides .....	199
<b>Scheme 5.3</b> Rhodium(I)-mediated cleavage of trifluoroacetophenone .....	199
<b>Scheme 5.4</b> Synthesis of bridging carbido complex <b>5.15</b> .....	200
<b>Scheme 5.5</b> Synthesis of <b>5.17</b> . Isolated yields in parentheses .....	201
<b>Scheme 5.6</b> Synthesis of <b>5.20</b> and <b>5.21</b> . Isolated yields in parentheses .....	203
<b>Scheme 5.7</b> Syntheses of <b>5.24</b> and <b>5.25</b> . Isolated yields from the salt metathesis route in parentheses .....	206

<b>Scheme 5.8</b> Carbonylation of <b>5.25</b> with CO. [a] $^{31}\text{P}\{^1\text{H}\}$ NMR yield [b] $^1\text{H}$ NMR yield .....	208
<b>Scheme 5.9</b> Synthesis of complexes <b>5.27</b> and <b>5.28</b> . [a] Isolated yield. [b] $^1\text{H}$ NMR yield.....	209
<b>Scheme 5.10</b> Synthesis of <b>5.30</b> . Isolated yield in parentheses .....	211
<b>Scheme 5.11</b> Synthesis of complex <b>5.32</b> . Isolated yield in parentheses.....	212
<b>Scheme 5.12</b> Synthesis of complex <b>5.34</b> and <b>5.35</b> . $^1\text{H}$ NMR yields in parentheses.....	213
<b>Scheme 5.13</b> Regioselectivity of bond cleavage of esters vs. thioesters with complex <b>3.20</b> . [Ni] = (dtbpe)Ni. ....	214
<b>Scheme 5.14</b> Initial synthesis of biphenyl <b>5.36</b> . GC-FID yields in parentheses .....	215
<b>Scheme 5.15</b> Independent syntheses of complexes <b>5.37</b> and <b>5.38</b> . Isolated yields in parentheses .....	217
<b>Scheme 5.16</b> Synthesis of complex <b>5.40</b> . Nap = naphthyl. Isolated yield in parentheses.....	219
<b>Scheme 5.17</b> Synthesis of complex <b>5.15</b> .....	220
<b>Scheme 5.18</b> Hydrolysis of the SBpin groups of complex <b>5.15</b> by adventitious water yields <b>5.44</b> and <b>5.45</b> .....	222
<b>Scheme 5.19</b> No reaction was observed when <b>5.15</b> was treated with a variety of alkynes.....	224
<b>Scheme 5.20</b> Reactivity of <b>5.15</b> with thiophenol, isocyanates and a thioisocyanate .....	225
<b>Scheme 5.21</b> Reactivity of <b>5.15</b> with $\pi$ -acceptor ligands .....	226
<b>Scheme 5.22</b> Reactivity of <b>5.15</b> with OCS forms <b>5.48</b> , <b>5.14</b> and $\text{CS}_2$ .....	227
<b>Scheme 5.23</b> Reactivity of <b>5.8</b> with OCS forms <b>5.48</b> as the major product.....	227
<b>Scheme 5.24</b> Reactivity of <b>5.15</b> with $\text{PdCl}_2(\text{NPh})_2$ forms <b>5.51</b> .....	228
<b>Scheme 6.1</b> Hofmann's C-CN oxidative addition of benzonitrile with bis(NHC) complex <b>6.1</b>	257
<b>Scheme 6.2</b> A 2-nickela(II)oxetane supported by a P,N-type ancillary ligand .....	258
<b>Scheme 6.3</b> Resonance structures of a (dtbpe)nickel ketone complex.....	259

## List of Abbreviations

Ac	acetyl, COMe
AcOH	acetic acid
Ad	adamantyl, C <sub>10</sub> H <sub>15</sub>
Ar	aryl
BAr <sup>F</sup> <sub>4</sub>	tetrakis(3,5-bis(trifluoromethyl)phenyl)borate
Bn	benzyl, CH <sub>2</sub> C <sub>6</sub> H <sub>5</sub>
Boc	<i>tert</i> -butyloxycarbonyl
bpy	2,2'-bipyridyl
BrettPhos	2-(Dicyclohexylphosphino)-3,6-dimethoxy-2',4',6'-triisopropyl-1,1'-biphenyl
CHD	1,4-cyclohexadiene
Cn	1,4,7-triazacyclononane
Cn*	1,4,7-trimethyl-1,4,7-triazacyclononane
COD	1,5-cyclooctadiene
COE	cyclooctene
COSY	<sup>1</sup> H- <sup>1</sup> H correlation spectroscopy
COT	1,3,5,7-cyclooctatetraene
Cp	cyclopentadienyl, C <sub>5</sub> H <sub>5</sub>
Cp*	pentamethylcyclopentadienyl, C <sub>5</sub> Me <sub>5</sub>
Cy	cyclohexyl, C <sub>6</sub> H <sub>11</sub>
dba	dibenzylideneacetone
DCM	dichloromethane
dcype	bis(1,2-dicyclohexylphosphino)ethane
DEAD	diethylacetylene dicarboxylate
depe	bis(1,2-diethylphosphino)ethane
DFT	density functional theory
Dipp	2,6-di- <i>iso</i> -propylphenyl
dippe	bis(1,2-di- <i>iso</i> -propylphosphino)ethane
DMAD	dimethylacetylene dicarboxylate
DMAP	4-dimethylaminopyridine
dmpe	bis(1,2-dimethylphosphino)ethane

DMSO	dimethylsulfoxide
DPPBz	1,2-bis(diphenylphosphino)benzene
dppe	bis(1,2-diphenylphosphino)ethane
DPPF	1,1'-Bis(diphenylphosphino)ferrocene
dtbpe	bis(1,2-di- <i>tert</i> -butylphosphino)ethane
EI-MS	electron impact mass spectrometry
EPR	electron paramagnetic resonance
ESI	electrospray ionization
Et	ethyl, C <sub>2</sub> H <sub>5</sub>
Et <sub>2</sub> O	diethyl ether
Fc	ferrocenium, Cp <sub>2</sub> Fe <sup>+</sup>
GC	gas chromatography
HMBC	heteronuclear multiple bond coherence spectroscopy
HMDS	hexamethyldisilazide, N(SiMe <sub>3</sub> ) <sub>2</sub>
HOMO	highest occupied molecular orbital
HOTf	trifluoromethanesulfonic acid
HRMS	high-resolution mass spectrometry
HSQC	heteronuclear single quantum coherence spectroscopy
IAd	1,3-bis(adamantyl)imidazol-2-ylidene
IPr	1,3-bis(2,6-diisopropylphenyl)imidazol-2-ylidene
IR	infrared
IRC	intrinsic reaction coordinate
<sup>i</sup> Pr	<i>iso</i> -propyl, C <sub>3</sub> H <sub>7</sub>
KHMDS	potassium hexamethyldisilazide
LIFDI	liquid injection field desorption ionization
LUMO	lowest occupied molecular orbital
<i>m</i> CPBA	<i>meta</i> -chloroperoxybenzoic acid
Me	methyl, CH <sub>3</sub>
Mes	2,4,6-trimethylphenyl
NBE	norbornene
NFSI	N-Fluorobenzenesulfonimide

NHC	N-heterocyclic carbene
NMR	nuclear magnetic resonance
NOE	nuclear Overhauser effect
NOESY	nuclear Overhauser effect spectroscopy
NSERC	National Sciences and Engineering Research Council
ORTEP	Oakridge thermal ellipsoid plot
OTf	triflate, CF <sub>3</sub> SO <sub>3</sub>
PES	potential energy surface
Ph	phenyl, C <sub>6</sub> H <sub>5</sub>
PhINTs	N-( <i>p</i> -toluenesulfonyl)iminophenyliodinane
pin	pinacolato, OCM <sub>2</sub> CM <sub>2</sub> CO
PTFE	poly(tetrafluoroethylene)
<i>p</i> -Tol	<i>para</i> -tolyl
Py	pyridine, C <sub>5</sub> H <sub>4</sub> N
rt	room temperature
salph	6,6'-(((1E,1'E)-1,2-phenylenebis(methanylylidene)))bis(azanylylidene))bis(2,4-di- <i>tert</i> -butylphenolato)
<sup>t</sup> Bu	<i>tert</i> -butyl
TCNE	tetracyanoethylene
TEMPO	2,2,6,6-tetramethylpiperidin-1-yl)oxyl
terpy	terpyridine
Tf	triflyl, SO <sub>2</sub> CF <sub>3</sub>
TFA	trifluoroacetate
TFAH	trifluoroacetic acid
TFE	2,2,2-trifluoroethanol
THF	tetrahydrofuran
TMEDA	N,N,N',N'-tetramethylethylene-1,2-diamine
TMS	trimethylsilyl, SiMe <sub>3</sub>
Tol	toluene, C <sub>7</sub> H <sub>8</sub>
TPA	tris(2-pyridylmethyl)amine
Ts	tosyl, SO <sub>2</sub> - <i>p</i> -MeC <sub>6</sub> H <sub>4</sub>

UBC	The University of British Columbia
UV/vis	ultraviolet/visible
Xantphos	4,5-Bis(diphenylphosphino)-9,9-dimethylxanthene
XAS	X-ray absorption spectroscopy
Xyl	2,6-dimethylphenyl

## Acknowledgements

First, I'd like to thank my supervisor, Prof. Jennifer A. Love, for her support and encouragement over the last five years. Jen gave me the freedom to pursue even the craziest of my ideas (some of which actually worked!), in a research environment that fostered creativity and camaraderie. I would not be the scientist I am today without her influence, even if I haven't figured out how to deal with her terrible puns yet.

Thanks go to my supervisory committee for keeping me on the right track: Prof. Pierre Kennepohl, Prof. David Perrin, and Prof. Glenn Sammis. I would also like to acknowledge my first research supervisor, Prof. Kevin M. Smith, for teaching me the importance of enthusiasm and that radicals are not things to be feared.

Next, I would like to thank past and present members of the Love group: Tin Nguyen, Phil Provencher, Dr. Paul Bichler, Dr. Alex Sun, Dr. Alex Dauth, Nicole LaBerge, Hironobu Sakaguchi, Grete Hofmann, Annika Klose, as well as all the undergrads I've had the pleasure of working alongside.

In no particular order, special thanks go out to: Dr. Marcus W. Drover, whose excellence as a synthetic chemist is topped only by his excellence of character. Only Marcus could have taught me to appreciate the Oxford comma. To Eric G. Bowes, for gradually taking over my desk space, for having a messier fume hood than mine, and for providing me with endlessly entertaining stories because of his poor decisions. To Dr. Shrinwantu Pal, for being as thoughtful as anyone I know, and fully embracing the YOLO of the Love group. To Weiling Chiu, for introducing me to a unique blend of Indian-Chinese-Arab culture, for always being a beacon of cheer in the lab, and for being incredibly helpful with all things thesis-related, especially distributing them to my committee on

time despite the fact that I sent her to the wrong printing place. To Dawson Beattie, for always taking things way too far and loving every minute of it.

One of my greatest pleasures of my PhD has been seeing young scientists come into our group as budding organic chemists and leave as skilled organometallic chemists. Grace Ying, John Wheler, Candy Cheung and Florian W. Friese, it was an honour to watch you blossom in our group.

My work would not have been possible without the technical expertise of the support staff at UBC: Dr. Maria Ezhova, Derek Smith, Marshal Lapawa, Dr. Brian O. Patrick, Dr. Emily Seo, Brian Ditchburn, Ken Love and Milan Coschizza have all been invaluable to me in my time at UBC.

I would like to thank NSERC (CGSD-3 and MSFSS) for finally deciding I was worth funding. I'd also like to thank the Izaak Walton Killam Foundation for a doctoral fellowship and UBC (Laird, 4YF, Dr. F.J. Nicholson Scholarship) for additional funding.

My Mum and Dad both deserve some huge thanks for being so supportive and proud of me over the years, even when it is so hard to explain to people what it is I do. My dog Whiskey and my cat Alyst (get it? Cat Alyst?) also get a shout-out for providing me with an entirely different set of stresses and joys than those I get from the lab.

Finally, I would like to thank Caroline, for reading every single page of this thesis, for being incredibly supportive of me in my ventures, for being a constant source of new adventures, for making us urban gardeners and mountain climbers, for making our house a zoo, and for putting my pieces back together again whenever I fall apart. I'm so excited to start our next adventure together.

## Dedication

To Gladys Desnoyer  
And to Caroline M. Hedge

"I must not fear.  
Fear is the mind-killer.  
Fear is the little-death that brings total obliteration.  
I will face my fear.  
I will permit it to pass over me and through me.  
And when it has gone past I will turn the inner eye to see its path.  
Where the fear has gone there will be nothing. Only I will remain."  
- Litany against fear, *Dune* by Frank Herbert

"Oh my God, make it stahp!"  
- Caroline M. Hedge, on my repeated use of "thus" in this Thesis

## **Chapter 1 : Transition Metal Complexes that Make and Break C-X (X = O, S, N) Bonds**

The development of transition metal-catalyzed reactions that can selectively form carbon-carbon (C-C) bonds has dominated the fields of organic and inorganic chemistry for decades, and the literature is replete with examples of systems that are efficient, atom economical, and functional group tolerant.<sup>1</sup> In contrast, transition metal complexes that form carbon-heteroatom (C-X, X = N, O, S) bonds with the same degree of diversity and selectivity as C-C couplings have only recently been developed and studied in detail.<sup>2-8</sup> For example, pioneering mechanistic work by Sharpless and others has resulted in the growth of osmium-catalyzed olefin dihydroxylation into a powerful and easily utilized synthetic method, allowing for the it's widespread use in organic synthesis.<sup>9</sup>

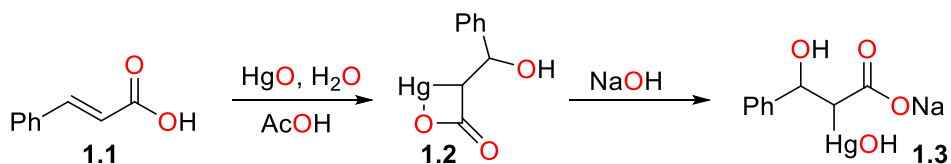
Inspired by such examples of rational catalyst design, one of the research themes in the Love group is the development of new catalytic processes that are based on the well-defined, organometallic reactivity of transition metal complexes, especially those that feature unusual structural motifs. For example, the Love group has focused on exploring the synthesis and fundamental reactivity of 2-metallaioxetanes with the goal of using this knowledge to develop new catalytic reactions.<sup>10, 11</sup>

Our group is also interested in examining the reactivity of organonickel complexes as potential catalysts. The chemistry of nickel has undergone a resurgence in recent years in both academia and industry relative to platinum and palladium. Despite significant advances in the field, perhaps most notably the shell higher olefin process and seminal work by Wilke,<sup>12</sup> nickel has only recently been considered a viable alternative to palladium. In addition to being more earth-abundant and less expensive than its heavier Group 10

congeners, nickel is much more likely than palladium or platinum to react *via* single electron (radical) processes. Thus, nickel offers the potential for reactivity that is *complementary* to that of the more established group 10 metals.

## 1.1. 2-Metallaioxetanes as Reactive Intermediates and Well-Defined Complexes

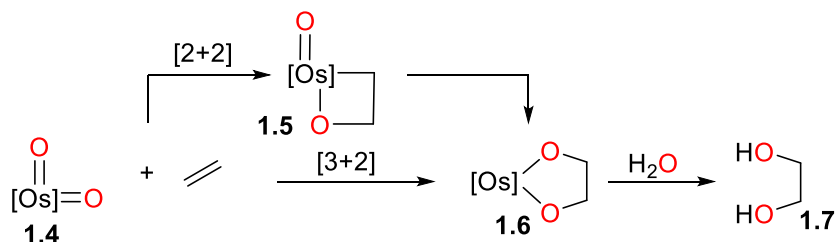
2-Metallaioxetanes are an unusual structural motif in which a metal atom and an oxygen atom are adjacent to each other in a four-membered ring. The first example of a 2-metallaioxetane in the literature was reported in 1900 (Scheme 1.1), when Biilmann described them as intermediates during the oxymercuration of olefins such as cinnamic acid.<sup>13</sup> Treating acid **1.1** with HgO in aqueous acetic acid yields mercuraoxetane **1.2**. Subsequent hydrolysis with base forms the ring-opened product **1.3**.



**Scheme 1.1** The first reported 2-metallaioxetane

Although several subsequent publications proposed 2-metallaioxetanes as reactive intermediates,<sup>14, 15</sup> perhaps the most controversial invocation of these oxametallacycles was made during the 1970's, when Sharpless and co-workers suggested their involvement in the mechanisms for olefin dihydroxylation and epoxidation.<sup>16</sup> They proposed that, when using osmium as the metal, the first step of the dihydroxylation involved the [2+2] cyclization of a metal-oxo complex **14**. with an alkene to yield a metallaioxetane **1.5**, which could undergo subsequent ring-expansion with the adjacent oxo moiety to yield

bis(alkoxide) complex **1.6** (Scheme 1.2). This intermediate could then undergo hydrolysis to yield the functionalized organic product **1.7**.

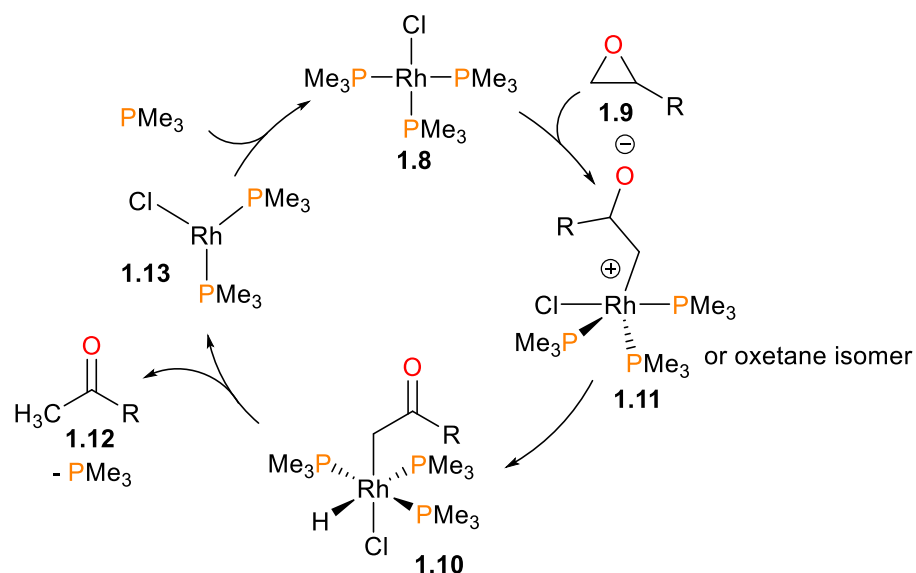


**Scheme 1.2** Sharpless ([2+2]) and CCN ([3+2]) mechanisms of olefin dihydroxylation

Initial experimental support for this stepwise mechanism included a non-linear Eyring plot of temperature and enantiomeric excess of the product.<sup>17</sup> Kinetic analyses of catalytic reactions with a wide array of both amine ligands and alkene substrates<sup>18</sup> was found to favour the Sharpless pathway. However, Corey strongly opposed this mechanism in favour of the traditional [3+2] mechanism (dubbed the Criegee-Corey-Noe mechanism, or CCN), ascribing the non-linear Eyring data reported by Sharpless to a rapid pre-equilibrium of olefin binding to the metal centre prior to [3+2] cyclization.<sup>19</sup> Eventually, in 1997 the groups of Sharpless, Singleton and Houk reported a joint experimental and theoretical work that supported the CCN pathway, based on comparison between computed and experimentally observed  $^{13}\text{C}$  and  $^2\text{H}$  kinetic isotope effects (KIEs).<sup>20</sup>

Milstein reported the first stable, isolable hydridoalkyl complex of rhodium in 1982,<sup>21</sup> when it was found that rhodium(I) complex **1.8** reacted with substituted epoxides **1.9** ( $\text{R} = \text{Me}$  or  $\text{Ph}$ ) to generate the complex **1.10** through either a 1,2-hydride shift or  $\beta$ -hydride elimination from zwitterionic intermediate **1.11** (or, alternatively, the ring-closed oxetane isomer). Complex **1.10** was characterized by nuclear magnetic resonance (NMR) spectroscopy and elemental analysis, and the presence of the ketone can be gleaned by the strong absorbance bands in the infrared (IR) spectra at  $1650\text{ cm}^{-1}$  and  $1625\text{ cm}^{-1}$  for  $\text{R}$

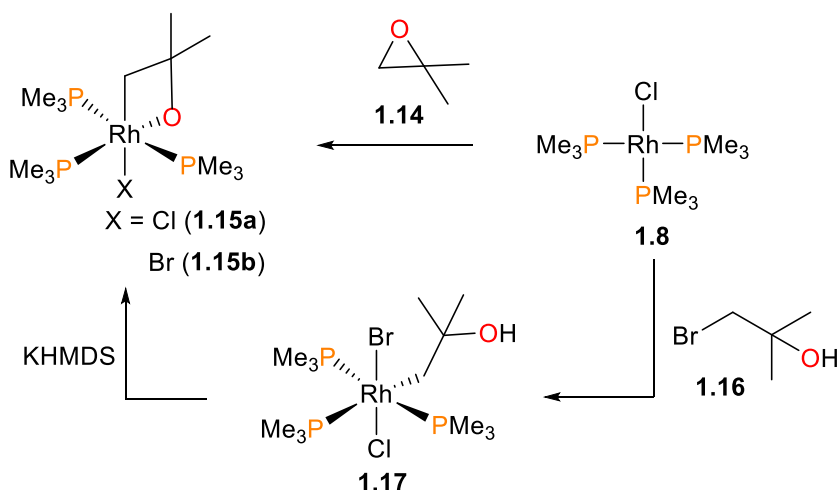
= Me and Ph, respectively. Gentle heating resulted in reductive elimination of the hydride and alkyl groups to generate ketones **1.12** and close the catalytic cycle. Crossover experiments indicated that reductive elimination is intramolecular, and kinetic analyses determined that the rate determining step was phosphine dissociation from **1.10** prior to rapid reductive elimination to generate rhodium(I) complex **1.13**, which would subsequently re-coordinate phosphine (see Scheme 1.3).



**Scheme 1.3** Milstein's catalytic epoxide isomerization

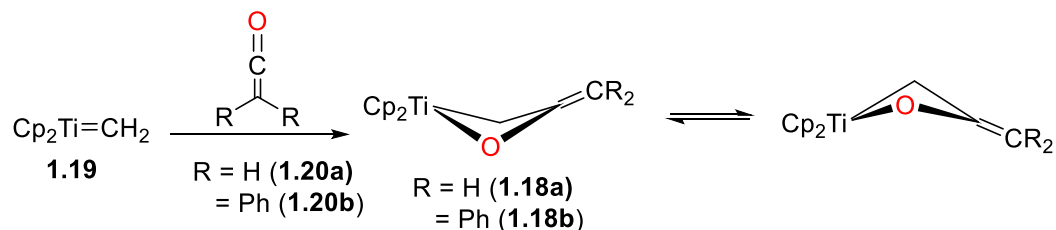
The authors proposed that complex **1.10** might also be formed *via* a rhodaoxetane isomer of intermediate **1.11**, which could undergo  $\beta$ -hydride elimination to yield the observed hydrido product. To shut down this  $\beta$ -elimination pathway, rhodium(I) complex **1.8** was reacted with isobutylene oxide **1.14**, as demonstrated in Scheme 1.4.<sup>22, 23</sup> The product of this reaction was found to be rhodaoxetane **1.15a**, which was formed in *ca.* 30% yield and characterized by NMR studies and X-ray diffraction experiments. Related complex **1.15b** could also be prepared independently *via* C-Br oxidative addition of

complex **1.8** with  $\alpha$ -bromoalcohol **1.16**, followed by deprotonation of the product **1.17** with the strong, hindered base potassium hexamethyldisilazide (KHMDS).



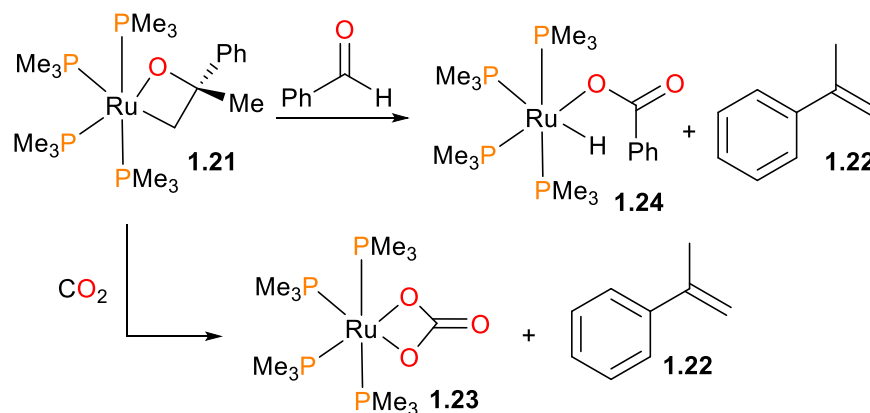
#### Scheme 1.4 Synthesis of a 2-rhodaioxetane

A classic example of an organometallic reaction whose mechanism typically invokes a metallaoxetane is the Tebbe olefination of carbonyl groups. Although to date no titanaoxetanes have been observed experimentally during this transformation, in 1988 the Grubbs group reported the synthesis of two titanaoxetanes **1.18** formed from the reaction of titanium methylidene **1.19** with ketenes **1.20** (see Scheme 1.5).<sup>24</sup> X-ray quality crystals could not be obtained, but the <sup>1</sup>H NMR spectral data indicated that the 2-titanaoxetane ring of **1.18** is puckered, and that interconversion between the two conformers occurs *via* a ring flip that is rapid at room temperature (rt). Interestingly, **1.18b** was found to be remarkably stable at up to 100 °C, demonstrating how appropriate substrate choice can be useful in the isolation of normally reactive intermediates.



**Scheme 1.5** Synthesis of a 2-titanaoxetane

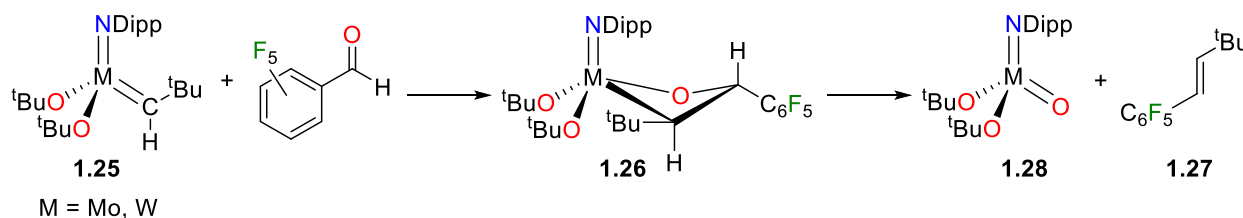
Hartwig, Bergman and Andersen synthesized the ruthenaoxetane **1.21**<sup>25, 26</sup> and reported its contrasting reactivity<sup>27</sup> compared to known, related iridium compounds.<sup>28</sup> For instance, it was found that **1.21** extruded  $\alpha$ -methylstyrene **1.22** when treated with either CO<sub>2</sub> or benzaldehyde (Scheme 1.6). In the case of the former, the bicarbonate complex **1.23** was obtained in 83% isolated yield. In the case of the latter, the hydrido benzoate complex **1.24** was formed in 53% yield by <sup>1</sup>H NMR spectroscopy.



**Scheme 1.6** Synthesis and reactivity of a 2-ruthenaoxetane

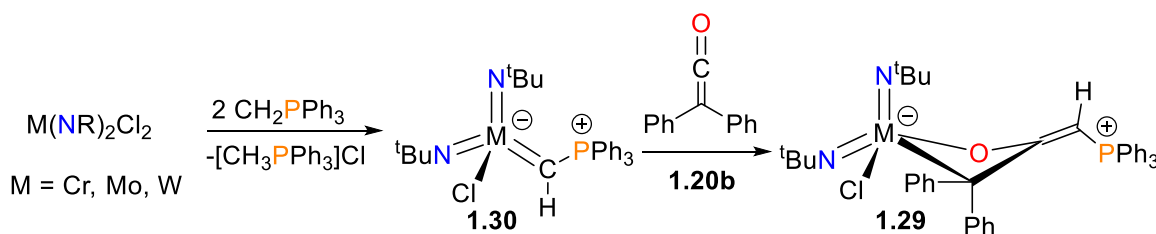
Bazan and Schrock have reported that 2-metallaioxetanes of molybdenum and tungsten can be formed when alkylidene precursors **1.25** are treated with pentafluorobenzaldehyde (Scheme 1.7).<sup>29</sup> The molybdenum complex **1.26** was crystallized from octane at -30 °C, and an X-ray diffraction study shows that the metallaioxetane ring is slightly puckered, with a dihedral angle of 21.3°. The Mo-O bond lengths of the two tert-butoxide ligands (1.860(3)

Å and 1.882(3) Å) are consistent with some degree of  $\pi$ -bonding between the  $d^0$  metal and the donor atoms. In contrast, the Mo-O bond length of the metallaoxetane moiety is much longer (1.995(3) Å). These oxacycles are inherently unstable, decomposing over several hours at room temperature, forming *trans*-alkene **1.27** and oxo complexes **1.28**, in reactivity reminiscent of the Wittig reaction.



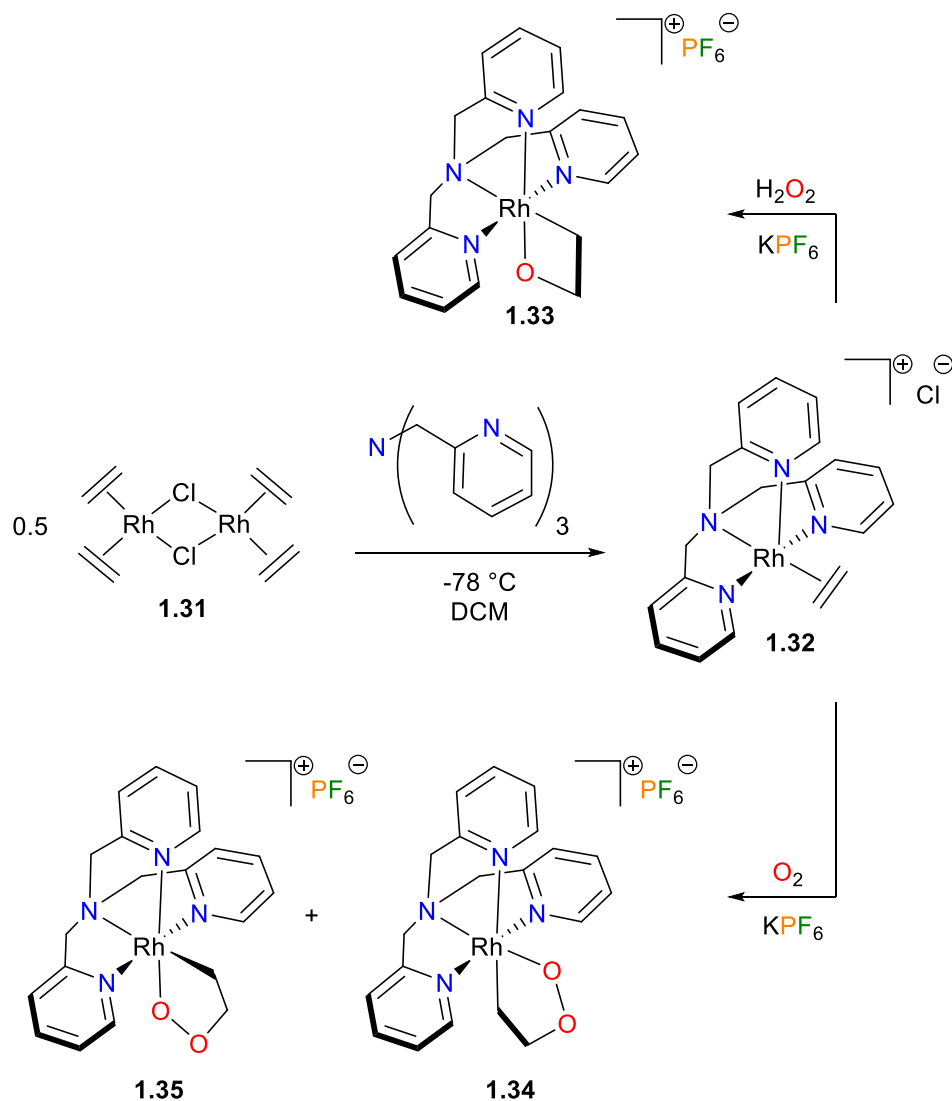
**Scheme 1.7** Schrock's synthesis of 2-metallaoxetanes of molybdenum and tungsten

Shortly thereafter, Sundermeyer and co-workers published the synthesis of related group 6 metallaoxetanes, **1.29** formed *via* the reaction of diphenylketene **1.20b** with M(VI) ylides **1.30** (see Scheme 1.8).<sup>30</sup> Included therein was the first example of a stable 2-chromaoxetane, a structural motif that was also proposed by Sharpless as an intermediate during chromyl chloride-catalyzed olefin epoxidation.<sup>16</sup> These metallaoxetanes are stable at room temperature, in contrast to the group 6 metallaoxetanes reported by Shrock.<sup>29</sup> The authors propose that this is due to resonance stabilization of the four-membered ring by the adjacent ylide moiety.



**Scheme 1.8** Sundermeyer's syntheses of group 6 2-metallaoxetanes, including the first 2-chromaoxetane

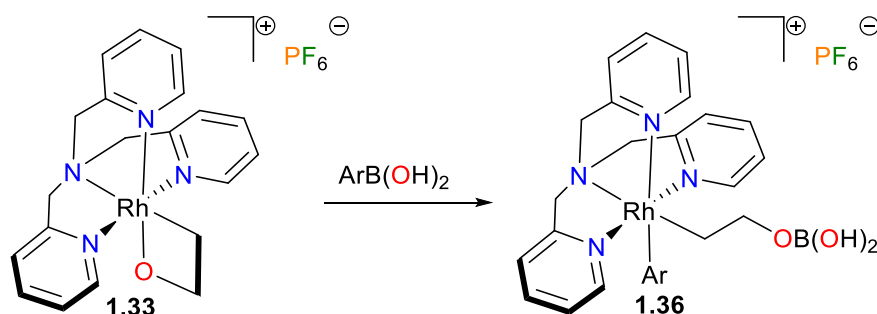
The first unsubstituted 2-metallaioxetane was reported by Gal and co-workers in 1997.<sup>31, 32</sup> The authors found that, when Cramer's dimer **1.31** was treated with tris(2-pyridylmethyl)amine (TPA) at low temperatures, the product was the cationic rhodium(I)-olefin complex **1.32**. Simple oxidation of **1.32** with aqueous H<sub>2</sub>O<sub>2</sub> resulted in the formation of 2-rhodaioxetane **1.33** in good yields. Curiously, only the isomer of **1.33** where the O-atom of the oxetane moiety is *cis* to the central TPA amine donor atom was observed (see Scheme 1.9). Conversely, when solid **1.32** is reacted with O<sub>2</sub>, a mixture of different rhodadioxolane isomers **1.34** and **1.35** are observed, corresponding to dioxygen insertion into both of the Rh-C bonds.<sup>33, 34</sup>



**Scheme 1.9** Gal's synthesis of a 2-rhodaioxetane and rhodadioxolanes

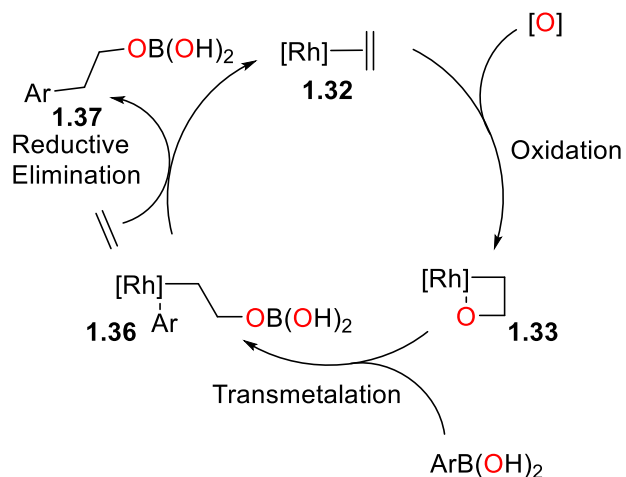
In 2010, the Love group reported that rhodaioxetane **1.33** can react with aryl- and alkenylboronic acids to yield ring-opened rhodium complexes **1.36**, as outlined in Scheme 1.10.<sup>35</sup> The products were characterized by a wide array of NMR spectroscopic techniques and mass spectrometry, as the products were resistant to crystallization. The transmetalation was observed to be general for arylboronic acids, but alkenylboronic acids were reluctant to undergo comparable reactivity. Initial mechanistic experiments indicate that coordination of the rhodaioxetane oxygen to the  $\text{sp}^2$ -hybridized boron of the boronic

acid yields an *ate*-complex, which undergoes subsequent aryl group transfer from boron to rhodium yielding the observed product.



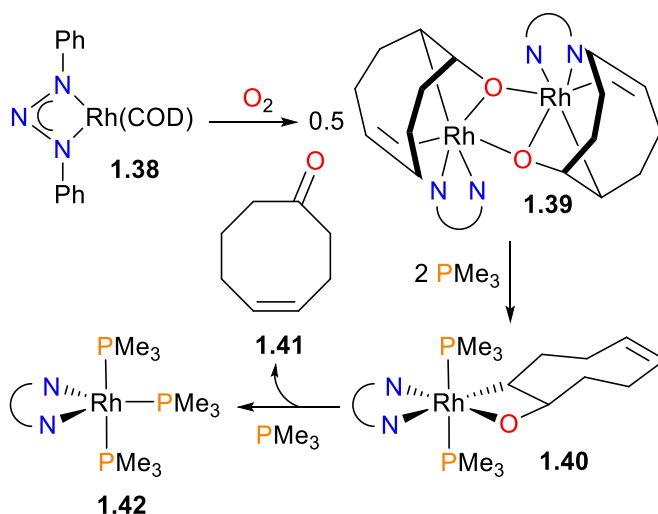
**Scheme 1.10** Love's transmetalation of the Rh-O bond of a 2-rhodaioxetane

The authors proposed that the above transmetalation chemistry could be incorporated into a new catalytic cycle that featured rhodaioxetane **1.33** as a well-defined intermediate. The proposed catalytic mechanism is shown in Scheme 1.11. Oxidation of a rhodium-bound olefin would generate rhodaioxetane **1.33**. Subsequent transmetalation with arylboronic acid would then form the ring-opened species **1.36**. Reductive elimination of the aryl and alkyl groups at rhodium would then release the product **1.37**, and coordination of another equivalent of olefin would close the catalytic cycle, regenerating **1.32**. This process, whose fundamental steps are similar to Suzuki-Miyaura coupling, would correspond to the carbohydroxylation of olefins. Importantly, both oxidation and transmetalation steps could be performed simultaneously in one pot without any decrease in yield. Unfortunately, the authors were unable to induce any clean reductive elimination from the rhodium(III) aryl complexes **1.36**. Indeed, these products were remarkably stable to thermolysis and the addition of a variety of additives.



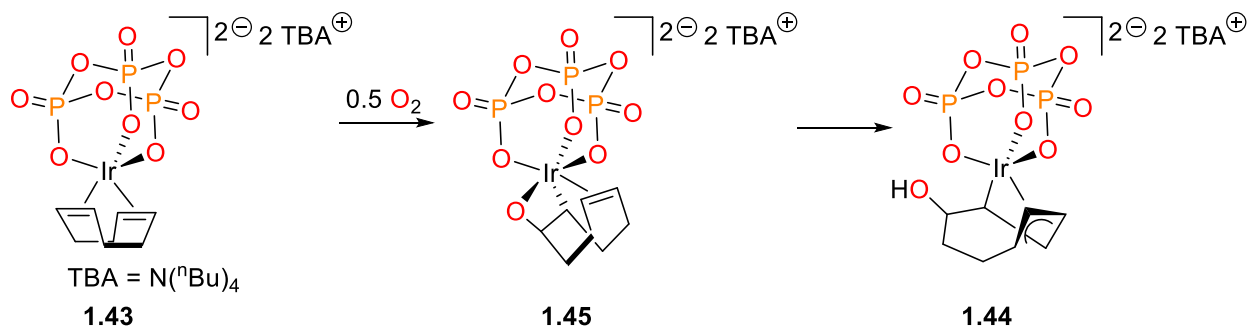
**Scheme 1.11** Love's proposed mechanism for olefin carbohydroxylation

Rhodium-mediated oxygenation of 1,4-cyclooctadiene (COD) with dioxygen has been reported by the Tejel group to proceed *via* a 2-rhodoxetane intermediate, which has been characterized by X-ray crystallography.<sup>36, 37</sup> Oxidation of starting material **1.38** with O<sub>2</sub> forms binuclear **1.39**, and addition of PMe<sub>3</sub> to this complex results in the formation of a mononuclear rhodoxetane **1.40**, which then releases the ketone product **1.41** (Scheme 1.12) upon coordination of another phosphine ligand. The authors propose that  $\beta$ -hydride elimination and reductive elimination occur prior to coordination of the final phosphine ligand to form the ultimate rhodium product **1.42**. Blum and Milstein have previously observed related  $\beta$ -hydride eliminations from iridium complexes.<sup>38</sup>



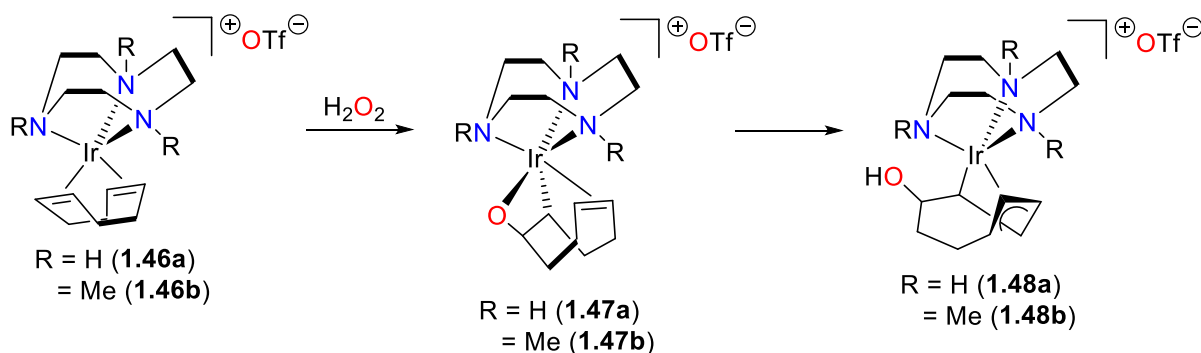
**Scheme 1.12** Tejel's olefin oxidation via a 2-rhodaioxetane

In an effort towards understanding the mechanism of ethylene oxidation on heterogeneous surfaces, Klemperer and Day prepared the iridium(I)-COD complex **1.43**,<sup>39</sup> bound by a polyoxoanionic ligand (Scheme 1.13). Volumetric gas buret measurements show that **1.43** reacts with one-half equivalent of dioxygen to ultimately form the  $\eta^3$ -allyl complex **1.44**. <sup>31</sup>P NMR spectroscopic experiments show that this transformation proceeds through several intermediates, including the iridaoxetane **1.45**, which could be isolated from acetonitrile and recrystallized from tetrahydrofuran (THF).



**Scheme 1.13** Klemperer's synthesis and reactivity of a 2-iridaoxetane

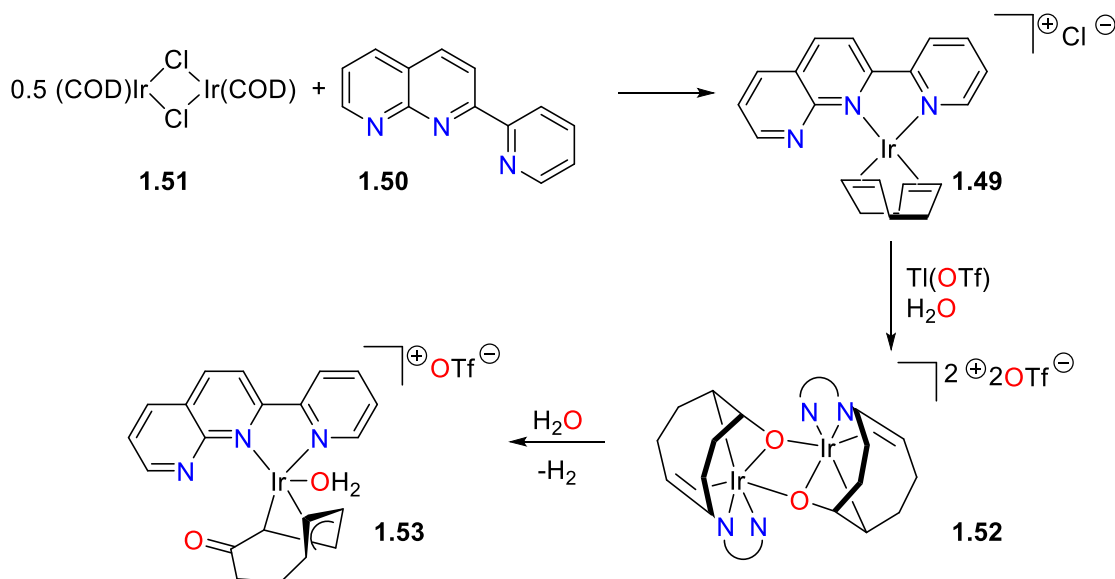
Oxidation of a related iridium(I)-COD complex was reported by the Flood group a decade later, this time featuring 1,4,7-triazacyclononane (Cn) ligands.<sup>40</sup> Oxidation of cationic complex **1.46a** with excess H<sub>2</sub>O<sub>2</sub> results in the formation of iridaoxetane **1.47a**. Heating samples of **1.47a** at 60 °C for 24 hours in CD<sub>3</sub>OD results in quantitative formation of a new complex **1.48a** (Scheme 1.14), which was characterized by a variety of NMR spectroscopic experiments and by X-ray crystallography as the η<sup>3</sup>-allyl complex. For the more electron-rich 1,4,7-trimethyl-1,4,7-triazacyclononane (Cn\*) ligand, the isomerization to **1.48b** from **1.47b** occurs rapidly at room temperature, although the iridaoxetane intermediate **1.47b** can be observed at low temperatures (-10 °C) by <sup>1</sup>H NMR spectroscopy.



**Scheme 1.14** Flood's synthesis and reactivity of a 2-iridaoxetane

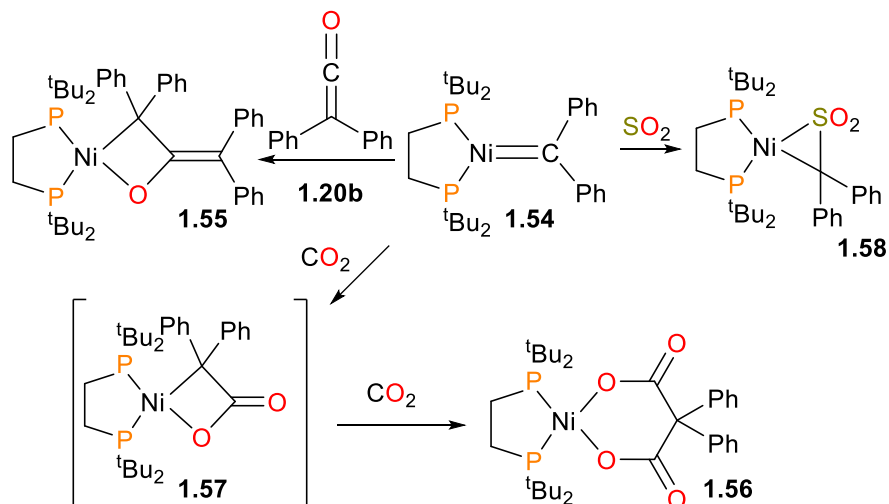
Recently, Bera and co-workers have disclosed the unusual oxidation of iridium-bound COD with water as the O-atom source.<sup>41</sup> Reasoning that a hydrogen bond-donor should lower the entropic barrier associated with hydration of metal-bound olefins, the authors prepared a series of cationic iridium-COD complexes such as **1.49** via simple ligand coordination of a series of ligands such as **1.50** with [(COD)IrCl]<sub>2</sub> **1.51**. Chloride abstraction using Tl(OTf) (OTf = trifluoromethanesulfonate) and addition of water resulted in the formation of iridaoxetane dimer **1.52**, isolated in 52% yield after 6 hours at room temperature. Further reaction of **1.52** with water (24 hours at room temperature) results in the 5-oxo-6-irida-1,2,3-allyl complex **1.53** (Scheme

1.15). Notably, dihydrogen evolution during this process was confirmed by gas chromatography (GC) analysis.



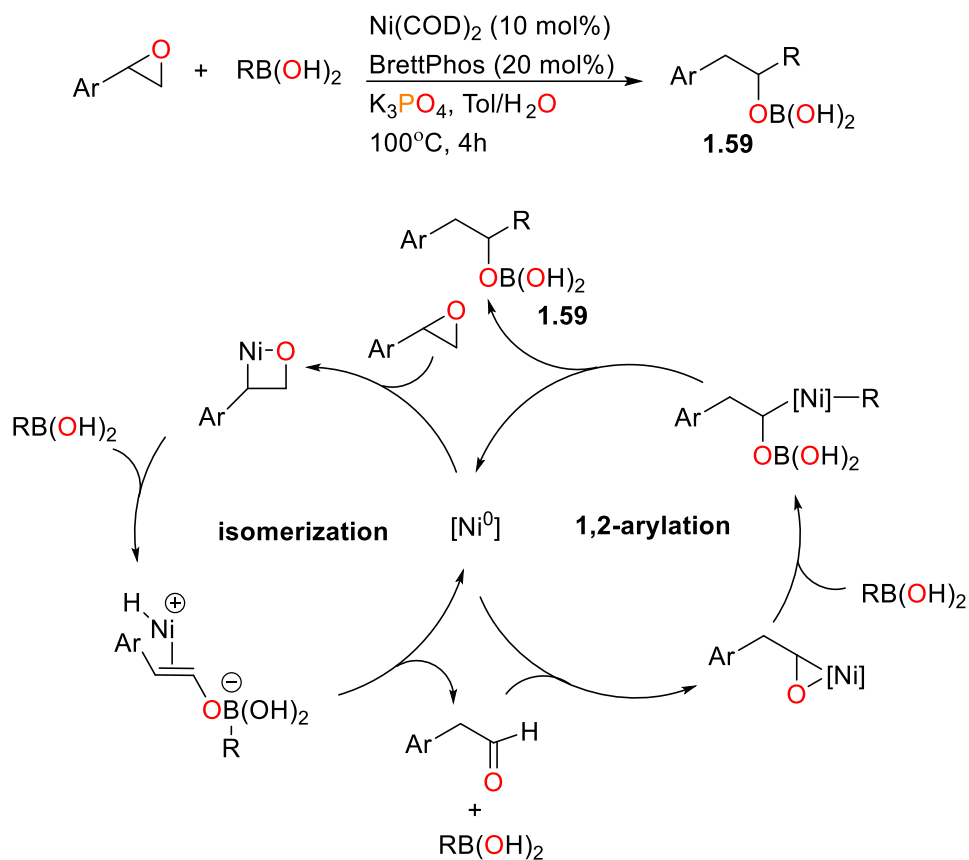
**Scheme 1.15** Bera's synthesis and reactivity of a 2-iridaoxetane

Mindiola and Hillhouse have reported that nickel alkylidene complex **1.54** could react with a variety of electrophiles to form cyclic products, as demonstrated in Scheme 1.16.<sup>42</sup> For example, alkylidene **1.54** reacts with diphenylketene *via* a formal [2+2] cyclization to generate the first example of a structurally well-defined nickela(II)oxetane, complex **1.55**. Two equivalents of smaller electrophiles (i.e. CO<sub>2</sub> in this case) were found to react at the metal centre to yield the six-membered nickelacycle **1.56**, presumably *via* insertion into the Ni-C bond of intermediate **1.57**. In addition, SO<sub>2</sub> was found to react at the Ni-C bond of **1.54** to generate a three-membered nickelacycle **1.58** *via* formation of a C-S bond.



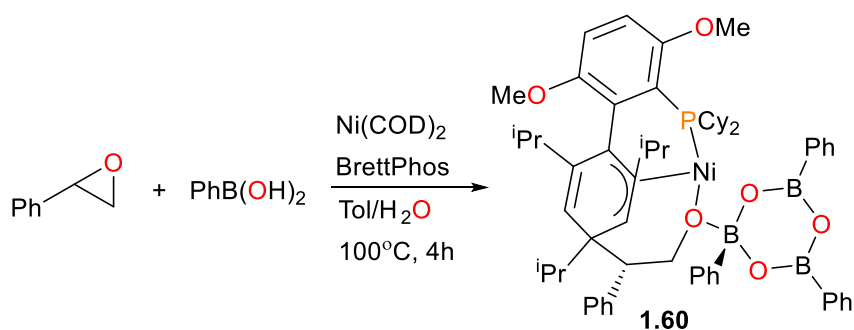
**Scheme 1.16** Hillhouse's synthesis of 2-nickelaoxetanes

Nielsen and Doyle have recently reported catalytic cross-coupling of epoxides and boronic acids catalyzed by nickel(0).<sup>43</sup> The authors propose that the mechanism of cross-coupling is bicyclic (see Scheme 1.17); first, the epoxide substrate is isomerized (possibly with assistance from the Lewis acidic boronic acid) to an arylacetaldehyde, which then undergoes a subsequent 1,2-arylation to form product **1.59**. Notably, both processes are nickel-catalyzed.



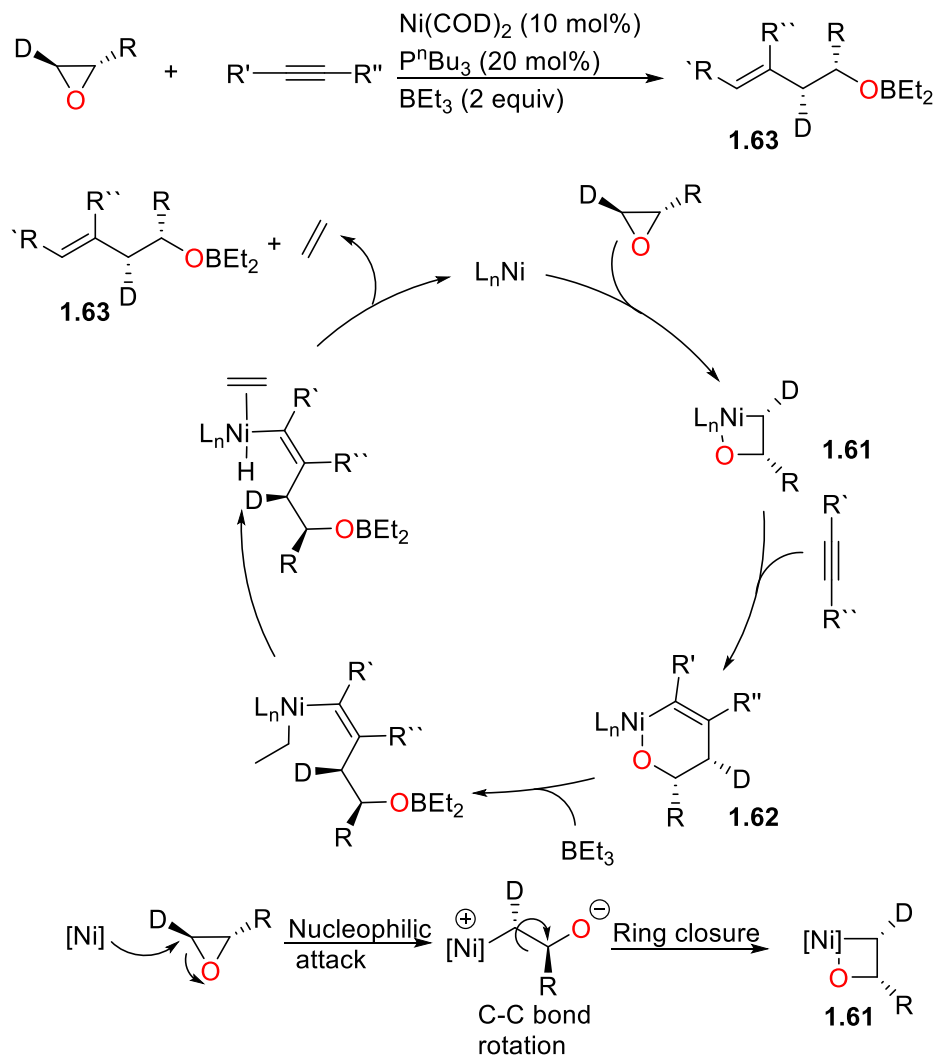
**Scheme 1.17** Doyle's catalytic cross-coupling of epoxides and boronic acids

From a catalytic reaction, red crystals were isolated and were determined to be complex **1.60** by X-ray diffraction analysis (Scheme 1.18). The mechanism of formation of **1.60** is not clear, but the complex is catalytically competent, although an induction period indicates it is an off-cycle species rather than an intermediate during catalysis.



**Scheme 1.18** Nickel complex isolated from Doyle's catalytic experiments

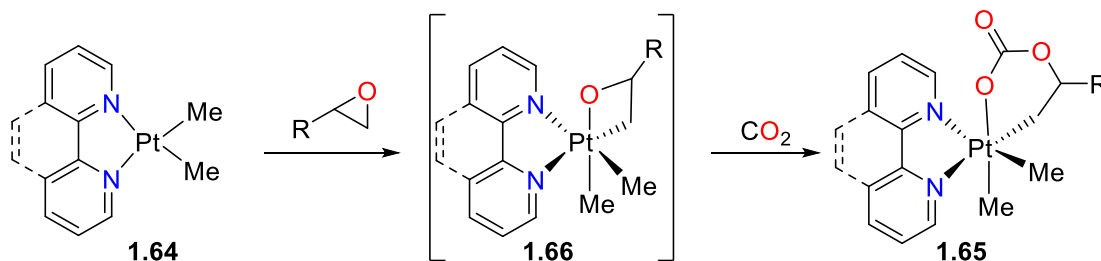
The Jamison group has also reported a nickel-catalyzed coupling reaction of epoxides that feature a nickelaoxetane as an intermediate. In 2003, Molinaro and Jamison published a report that detailed the reductive coupling of alkynes and epoxides, catalyzed by  $\text{Ni(COD)}_2$  and  $\text{P}^n\text{Bu}_3$ , along with the use of  $\text{BET}_3$  as a reductant.<sup>44</sup> Subsequent deuterium labelling studies found that oxidative addition of the least substituted C-O bond results in an inversion of stereochemical configuration of intermediate nickelaoxetane **1.61**,<sup>45</sup> consistent with an  $\text{S}_{\text{N}}2$ -type mechanism (see Scheme 1.19). Alkyne insertion into the Ni-C bond of the resulting nickelaoxetane (which was not observed experimentally) yields **1.62**. Subsequent transmetalation with  $\text{BET}_3$ ,  $\beta$ -hydride elimination and finally, reductive elimination to release the final product **1.63** and regenerate the nickel(0) catalyst.



**Scheme 1.19** Jamison's catalytic reductive coupling of epoxides and alkynes

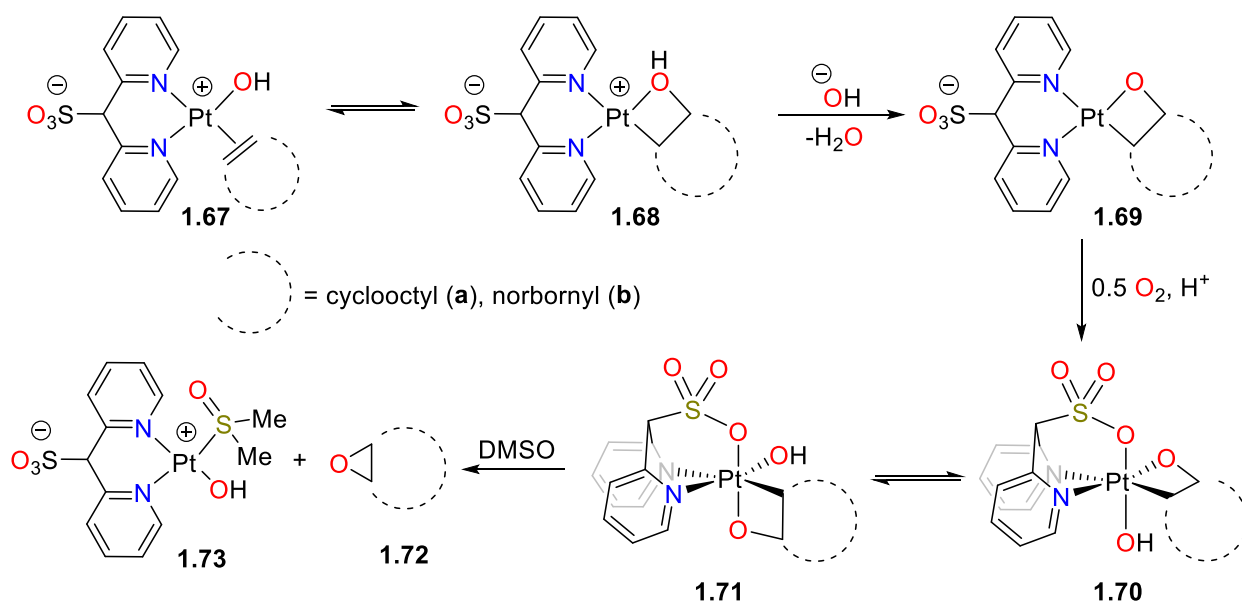
Puddephatt and co-workers have also probed the oxidative addition of epoxides with platinum(II) complexes.<sup>46, 47</sup> While reactions of complexes **1.64** with epoxides yielded complex mixtures under inert atmosphere, performing the reactions under  $\text{CO}_2$  gas resulted in the clean formation of the carbonate complexes **1.65**, presumably formed *via* insertion of  $\text{CO}_2$  into the Pt-O bond of intermediate **1.66** (Scheme 1.20). Oxidative addition of substituted epoxides occurred at the least-substituted C-O bond in all cases reported. ultraviolet/visible (UV/Vis) kinetics revealed an overall second order process, first order in both platinum(II) and epoxide but independent of  $\text{CO}_2$  concentration. Thus, the authors

concluded that the rate determining step is oxidative addition, and that both the thermodynamic activation parameters and the selectivity of oxidative addition (i.e. attack at the least substituted carbon) are consistent with an S<sub>N</sub>2-type mechanism.



**Scheme 1.20** Puddephatt's transiently generated 2-platinaoxetane

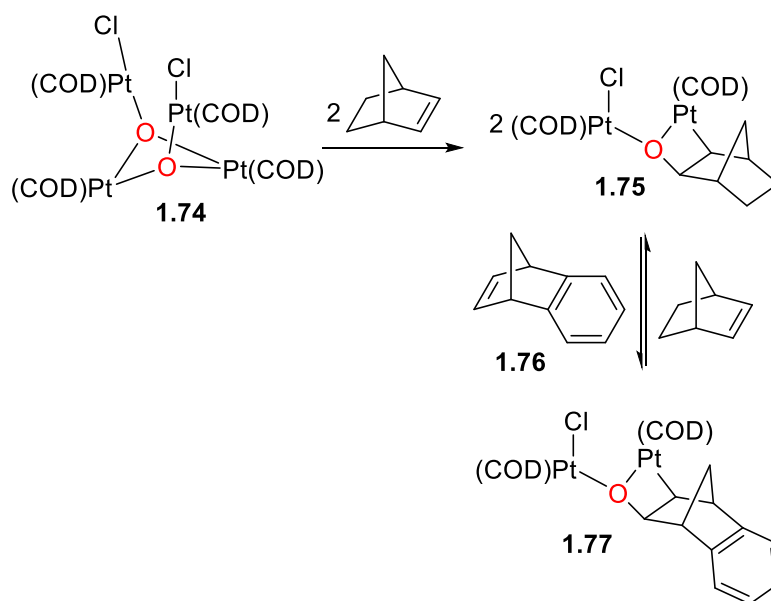
Examples of isolable platinaoxetanes have been reported by the Vedernikov group.<sup>48</sup> Reversible cyclization between the platinum-bound olefin and hydroxo groups of **1.67** forms the four-membered ring of complex **1.68**, which upon deprotonation gives anionic platinaoxetane **1.69** as a mixture of *cis* and *trans* isomers, depending on the orientation of the norbornyl or cyclooctyl ring relative to the sulfonate group. Oxidation with dioxygen in neutral or alkaline mixtures of 2,2,2-trifluoroethanol (TFE) and water yields the octahedral platinum(IV) complex **1.70**, with the pendant sulfonate moiety binding the apical site of the metal centre. Upon heating in dimethylsulfoxide (DMSO), isomerization to **1.71** occurs so that the O-atom of the oxetane moiety is *trans* to the sulfonate group (Scheme 1.21), and subsequent reductive elimination releases epoxide **1.72** and the cationic DMSO adduct **1.73**. This is the second example of direct C-O reductive elimination from a 2-metalla-oxetane, and the first that is clean and high-yielding.<sup>49</sup>



**Scheme 1.21** Vedernikov's 2-platinaoxetane reductively eliminates to form epoxides

The Sharp group has prepared platinum-oxo complex **1.74**, and explored its reactivity with ethylene.<sup>50</sup> Although the resulting reaction mixtures were complex, acetaldehyde was clearly identifiable as a major product.<sup>51</sup> In an effort to isolate any potential intermediates in this oxidative transformation, ethylene was replaced with norbornene. The resulting product characterized by NMR spectroscopy and X-ray diffraction as the binuclear platinaoxetane **1.75**, formed in nearly quantitative yield. Furthermore, alkene insertion was found to be reversible,<sup>52</sup> as treating **1.75** with norbornene derivative **1.76**, as shown in Scheme 1.22, gave the new platinaoxetane **1.77** in quantitative yield. Indeed, the reaction could also be pushed to completion in the opposite direction by adding a large excess of norbornene to **1.77** to reform **1.75**. The kinetics of this exchange were monitored by NMR spectroscopy, and surprisingly, it was found that the reaction is zero-order in platinaoxetane **1.75**. To test for the presence of a trace impurity that was catalyzing this exchange process, the rate of the reaction was examined as a function of *initial* concentration of **1.75**, and a directly proportional increase in the rate of reaction relative to the initial concentration of

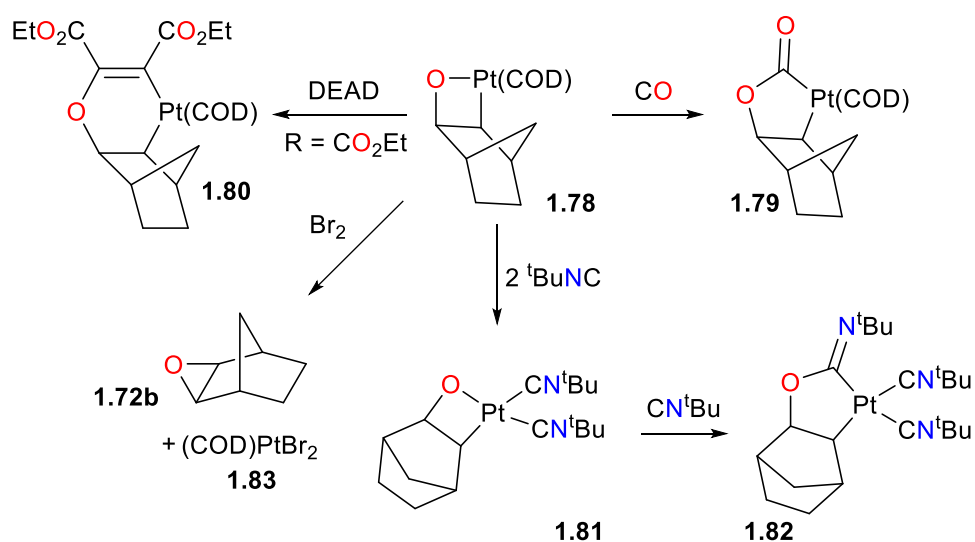
**1.75** was observed. This confirmed the presence of some catalyst in the alkene exchange process. A screening of possible impurities was performed, and it was found that Lewis acids had a dramatic effect on the rate of the exchange reaction, with  $\text{BF}_3\text{OEt}_2$  being the most efficient. The alkene exchange reaction occurred most rapidly when an excess of  $\text{BF}_3$  relative to platinum was used. Based on this, the authors propose that the actively exchanging species is a double Lewis acid adduct. The mono- $\text{BF}_3$  adduct of **1.75** was later prepared and fully characterized.<sup>53</sup> Further mechanistic studies also were consistent with protonations playing a key role in platinaoxetane formation.<sup>54</sup>



**Scheme 1.22** Sharp's reversible 2-platinaoxetane formation

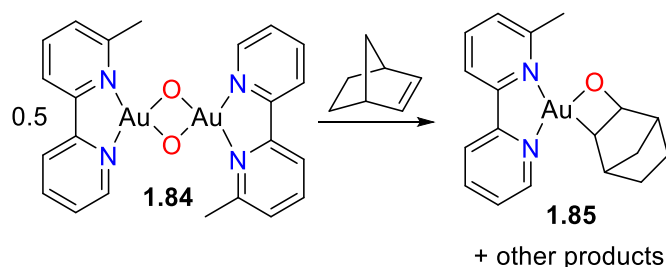
The reactivity of the related platinaoxetane **1.78** with small molecules was examined (Scheme 1.23), and it was found that complex **1.78** was amenable to insertion of a wide variety of electrophiles into the Pt-O bond to generate ring-expanded platinumacycles. For instance, CO can insert into the Pt-O bond to form acyl-platinum complex **1.79**. The electron-deficient alkyne diethylacetylene dicarboxylate (DEAD) also inserted cleanly to

generate the platinadihydropyran **1.80**, and similarly, tetracyanoethylene also inserted into the same bond. Reacting **1.78** with 2 equivalents of <sup>t</sup>BuNC first results in displacement of the COD ligand, yielding **1.81**, while a third equivalent of isocyanide then inserts into the Pt-O bond to give the five-membered platinacycle **1.82**. Lastly, reacting **1.78** with Br<sub>2</sub> results in formation of the norbornene oxide **1.72b** *via* C-O bond formation, with **1.83** as the organometallic product, formed in quantitative yield.



### Scheme 1.23 Reactivity of Sharp's platinaoxetane

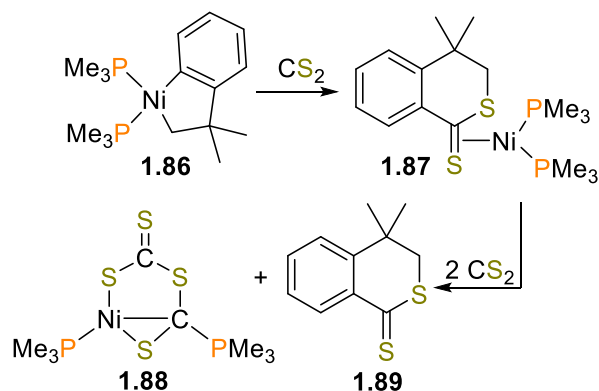
Binuclear gold-oxo complexes of the type **1.84** have been found to react with strained alkenes to generate oxygenated products.<sup>49</sup> In the case of norbornene, auroxetane **1.85** was isolated from the reaction mixture (Scheme 1.24). The organic products observed were a complex mixture of diols, aldehydes and epoxide **1.72b**, all derived from norbornene.



**Scheme 1.24** Synthesis of Cinellu's 2-auraoxetane

## 1.2 Metallacycles of Nickel: Structure and Reactivity

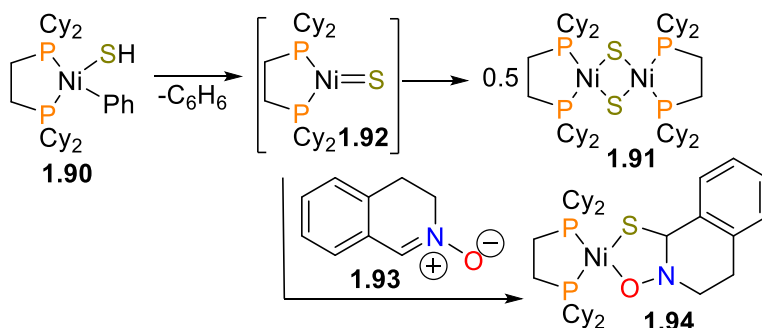
Carmona and co-workers have reported that complex **1.86** reacts with one equivalent of  $\text{CS}_2$  to generate the dithialactone complex **1.87**.<sup>55</sup> Low-temperature NMR experiments revealed that the  $\text{CS}_2$  group inserts first into the Ni-C<sub>aryl</sub> bond prior to C-S reductive elimination. In addition, treating **1.87** with an additional two equivalents of  $\text{CS}_2$  yields Iber's complex **1.88** and releases the dithiolactone product **1.89** (see Scheme 1.25).



**Scheme 1.25** Reactivity of a nickel complex with  $\text{CS}_2$

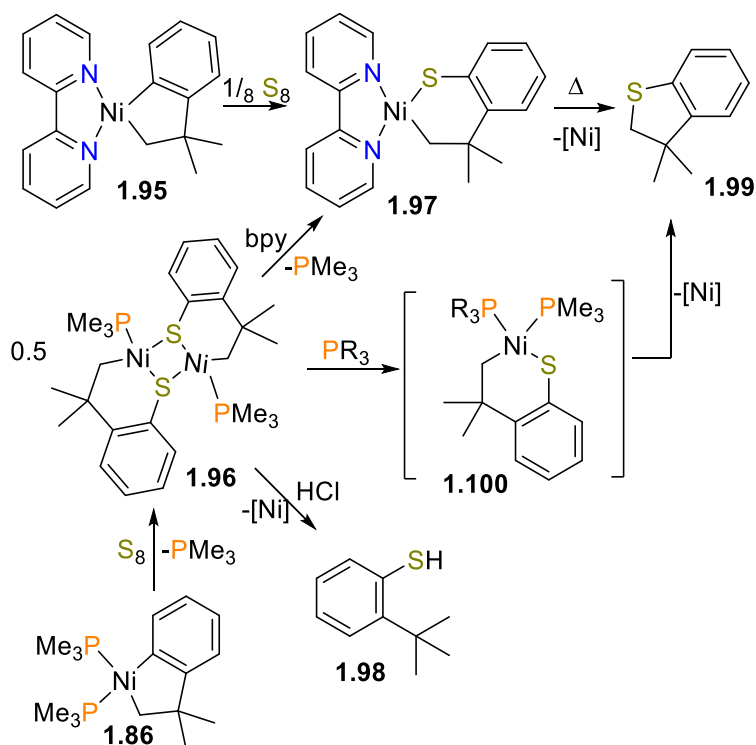
Vicic and Jones also reported one of the first examples of a transiently generated terminal sulfide of nickel.<sup>56</sup> Mild heating of complex **1.90** resulted in the release of benzene and the quantitative formation of bridging sulfide dimer **1.91**, likely formed *via* sulfide **1.92**

(Scheme 1.26). If the same reaction took place in the presence of nitron **1.93**, new product **1.94** was observed, characterized by NMR spectroscopy and X-ray diffraction studies.



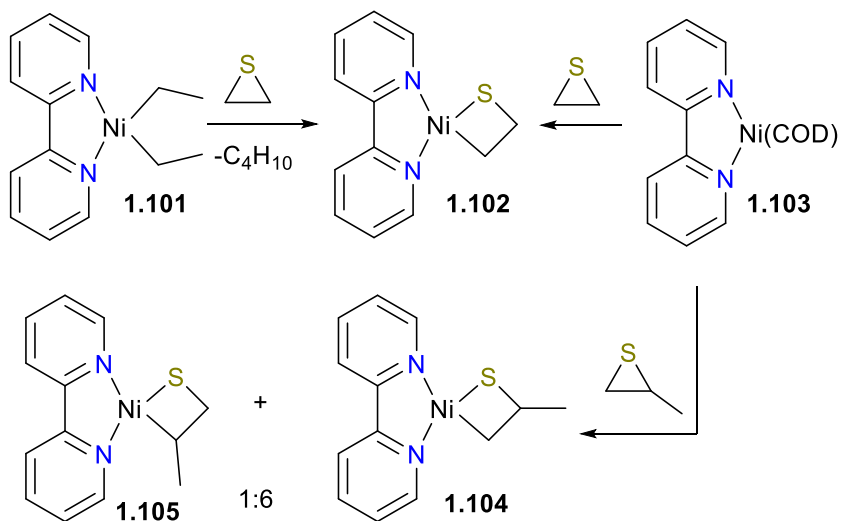
**Scheme 1.26** Jones' synthesis and reactivity of a transient nickel sulfido

Han and Hillhouse have reported that elemental sulfur,  $S_8$ , can oxidize nickel alkyl complexes bearing either bipyridine (**1.95**) or phosphines (**1.86**) as ancillary ligands (Scheme 1.27). The phosphine complex **1.96** can be converted to the bipyridine complex **1.97** by a simple ligand exchange reaction. Protonolysis of the Ni-C and Ni-S bonds with HCl yields aromatic thiol **1.98** in 88% yield. Heating samples of **1.96** for 24 hours at 100 °C results in the formation of thioether **1.99** via C-S reductive elimination. Initial mechanistic studies show that the rate of formation of thioether is faster in the presence of added phosphines. The authors propose that formation of an intermediate species, complex **1.100**, which is detectable by NMR spectroscopy, thus directly precedes the C-S reductive elimination.<sup>57</sup> Oxidation of platinum alkyls with  $S_8$  has also been reported.<sup>58, 59</sup>



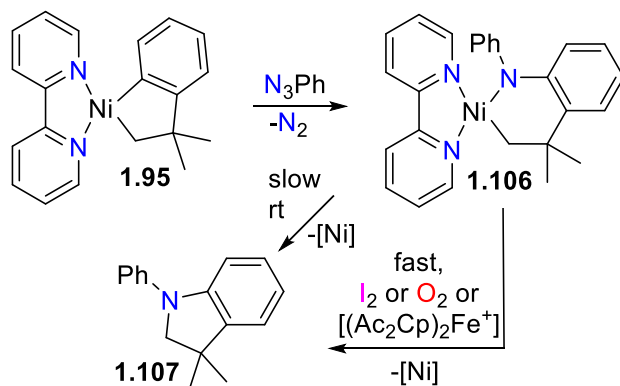
**Scheme 1.27** Synthesis and reactivity of nickel thiolate complexes

In 1994, Matsunaga and Hillhouse found that reacting the nickel(II) complex **1.101** with ethylene sulfide yielded the thianickelacyclobutane complex **1.102** after 7 hours at room temperature in THF (Scheme 1.28). The authors proposed that complex **1.101** first reductively eliminates butane to yield a reactive (bpy)nickel(0) (bpy = 2,2'-bipyridyl) complex, which can subsequently oxidatively add to the C-S bond of the thirane to give the observed product. Consistent with this hypothesis, they found that using **1.103** as an alternate starting material allowed for the reaction to proceed under much milder conditions (30 minutes at 0 °C) with comparable yields. Expanding the substrate scope, the authors found that reaction of propylene sulfide with complex **1.103** resulted in a 6:1 mixture of isomers **1.104** and **1.105**, indicating that steric interactions contribute appreciably to the site of oxidative addition.



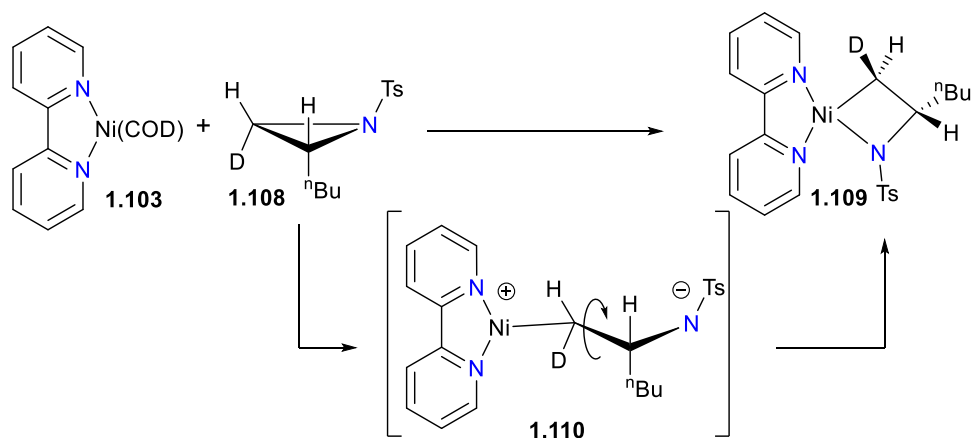
**Scheme 1.28** Oxidative addition of thiranes with nickel(0)

Oxidatively-induced reductive elimination has been observed for nickel alkyl-amido complexes, as shown in Scheme 1.29.<sup>60</sup> For example, treatment of complex **1.95** with phenylazide gave complex **1.106**. Complex **1.106** was found to be thermally unstable, reductively eliminating to compound **1.107** when stored at room temperature over the course of 2 days. This process could be greatly accelerated by adding an oxidant, either in the form of  $\text{I}_2$ ,  $\text{O}_2$ , or the single-electron oxidant acetyl ferrocenium  $[(\text{AcCp})_2\text{Fe}^+]$ . Koo and Hillhouse demonstrated that this process could be used for the nickel-mediated synthesis of a variety of indolines *via* the coupling of phenethyl Grignard reagents and arylazides.<sup>61</sup> These reactions were not limited to cyclic species, as untethered alkyl-amido complexes of nickel were found to undergo similar reactivity when exposed to the same group of oxidants.<sup>60</sup> The Hillhouse group also communicated the analogous reactivity of other bipyridyl-ligated complexes of nickel with arylazides.<sup>62</sup>



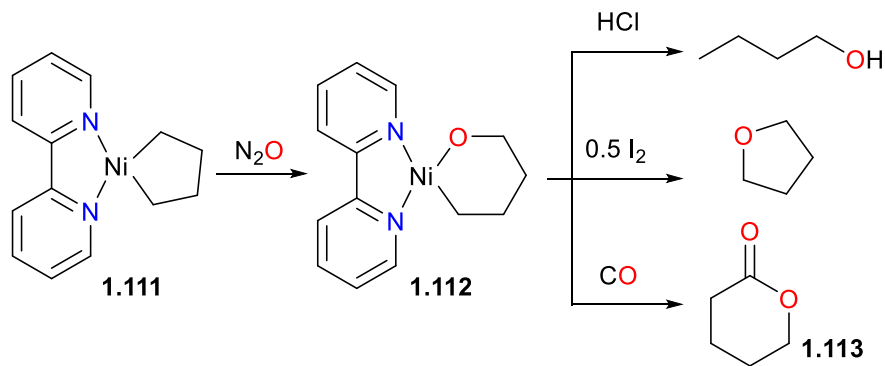
**Scheme 1.29** Synthesis and reactivity of nickel amido complexes

In 2002, Lin, Clough and Hillhouse reported a study of **1.103** with aziridines to yield azanickelacyclobutanes.<sup>63</sup> Elegant use of deuterium labelling on the aziridine substrate **1.108** demonstrated that this oxidative addition occurred with inversion of the stereochemical configuration at the methylene carbon, consistent with an  $S_N2$ -type oxidative addition mechanism. The authors proposed that the azanickelacyclobutane product **1.109** is formed *via*  $S_N2$ -type ring-opening to give zwitterionic intermediate **1.110**, which upon C-C rotation can close *via* attack on the tosyl-stabilized amide on the cationic metal centre (see Scheme 1.30). Curiously, upon oxidatively-induced reductive elimination from complex **1.109**, the *syn*-aziridine **1.108** is regenerated in high yield, indicating that the reductive elimination also proceeds with inversion of stereochemistry. The nickel species after reductive elimination was not characterized. Notably, the groups of Doyle<sup>64</sup> and Jamison<sup>65</sup> have since built on this fundamental stoichiometric study to develop new catalytic cross-coupling reactions. More recently, Xi and co-workers have prepared a related azanickelacyclobutane by reaction of 1,3-bis(2,6-diisopropylphenyl)imidazol-2-ylidene (IPr) and Ni(COD)<sub>2</sub> with 2,6-diazasemibulvalene.<sup>66</sup>



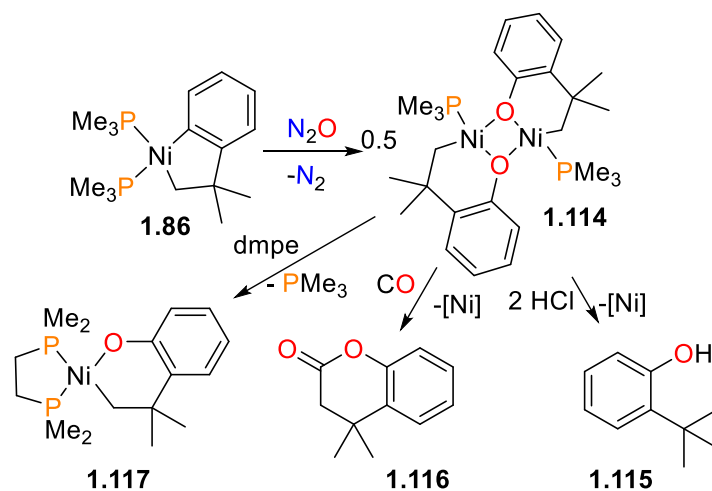
**Scheme 1.30** Oxidative addition of aziridines with nickel(0)

Early work in the Hillhouse group was spent developing the use of nitrous oxide ( $\text{N}_2\text{O}$ ) as an O-atom transfer reagent on late transition metals. For instance, in 1993 Hillhouse and co-workers reported that the metallacycle **1.111** reacts with 1 atm of  $\text{N}_2\text{O}$  in benzene at 50 °C to produce the ring-expanded mixed alkyl-alkoxide complex **1.112**, as shown in Scheme 1.31.<sup>67</sup> Later reactivity studies of **1.112** found that it was susceptible to protonolysis with HCl to release n-butanol, oxidatively-induced reductive elimination when treated with one half of an equivalent of iodine to generate THF, as well as insertion and reductive elimination when treated with an excess of CO to generate lactone **1.113**.<sup>68</sup> Related formation of acyclic esters from the treatment of (bpy)nickel(II) complexes with CO have also been reported by the group of Yamamoto.<sup>69, 70</sup>



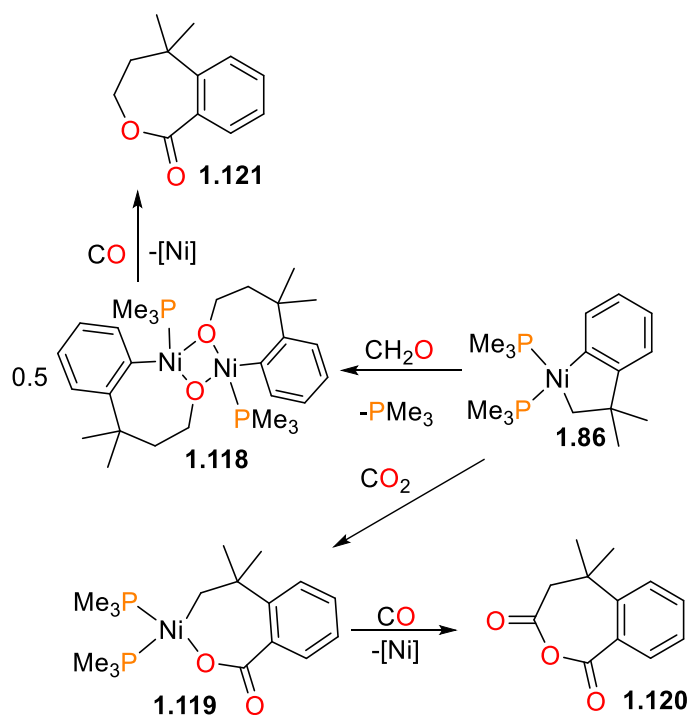
**Scheme 1.31** Synthesis and reactivity of nickel alkoxo complexes

Perhaps not surprisingly, the use of smaller, more labile phosphines as ancillary ligands led to the formation of binuclear species, bridged by the alkoxide groups (Scheme 1.32).<sup>71</sup> Oxidation of **1.86** with  $\text{N}_2\text{O}$  yields **1.114**. Once again, these dimeric species were found to be susceptible to protonolyses with strong acids, forming alcohol **1.115**, and insertion and reductive elimination when treated with  $\text{CO}$ , resulting in the formation of lactone **1.116**. The addition of chelating ligands, such as 1,2-bis(dimethylphosphino)ethane (dmpe), 1,10-phenanthroline (phen) or bpy, after oxidation with  $\text{N}_2\text{O}$  resulted in the formation of mononuclear complexes such as **1.117**.



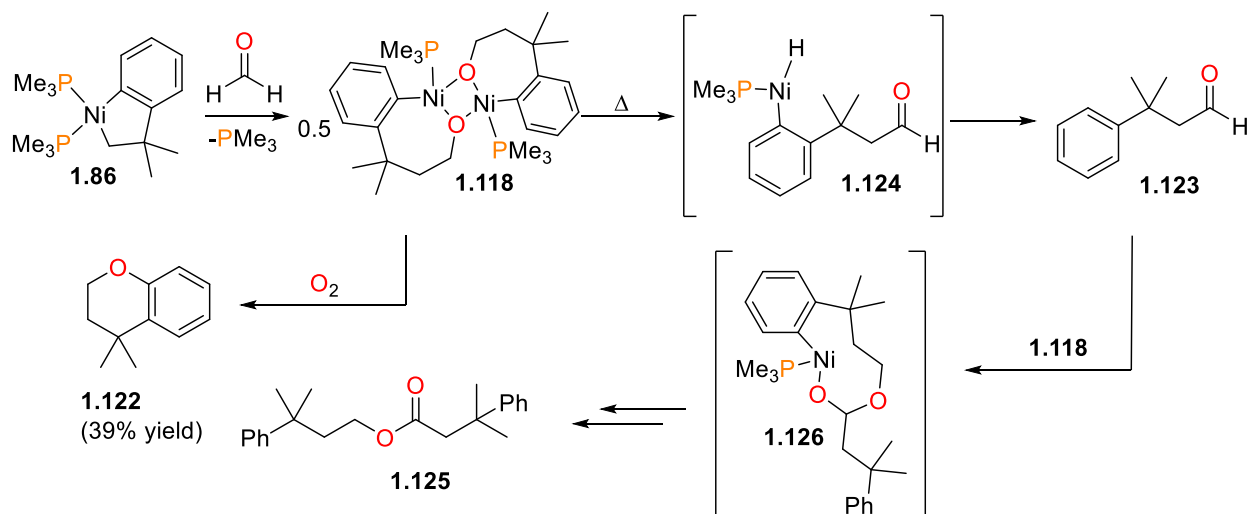
**Scheme 1.32** Synthesis and reactivity of nickel alkoxo complexes

Carmona and co-workers reported the small molecule reactivity of cyclometalated **1.86**, as shown in Scheme 1.33.<sup>72</sup> Stirring complex **1.86** with polymeric paraformaldehyde yields **1.118**, which is the product of insertion into the C<sub>alkyl</sub>-Ni bond. While complex **1.86** was characterized definitively by an X-ray diffraction study, the structure of **1.118** was assigned based on NMR spectral data, particularly the strong coupling to a <sup>31</sup>P nucleus ( $J = 88$  Hz) for the *ipso* aromatic carbon resonance in the <sup>13</sup>C NMR spectrum. The structure was found to be binuclear on the basis of elemental analysis (which showed loss of one equivalent of PMe<sub>3</sub>) as well as by molecular weight determinations. Reacting **1.86** with CO<sub>2</sub> results in insertion into the C<sub>aryl</sub>-Ni bond, generating nickelalactone **1.120**. Exposing **1.119** to an atmosphere of CO results in insertion and reductive elimination to generate the cyclic anhydride **1.120**, which could be isolated after workup as colourless crystals. Similarly, treating **1.118** with CO results in insertion and reductive elimination to form lactone **1.121**.



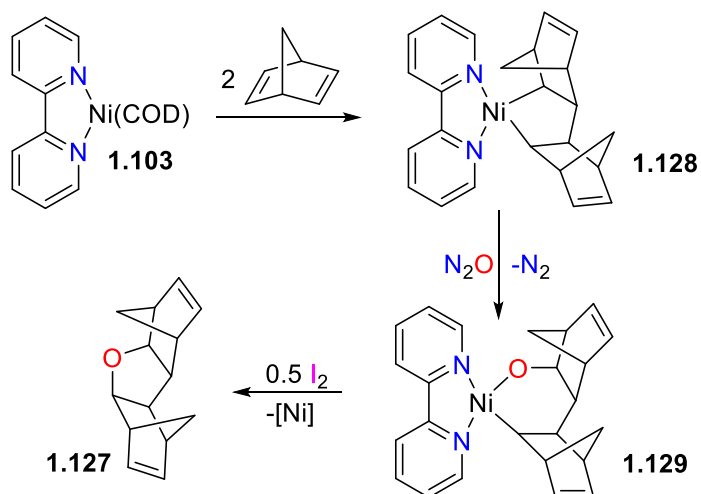
**Scheme 1.33** Synthesis and reductive elimination chemistry of nickel alkoxo complexes

Subsequently, Hillhouse demonstrated that **1.118** could react with dry  $\text{O}_2$  to yield chroman **1.122** in modest 39 % yield (see Scheme 1.34).<sup>73</sup> In contrast, when complex **1.118** was heated in the absence of an oxidant, the main organic product isolated was found to be aldehyde **1.123**, which the authors assigned as being formed *via*  $\beta$ -H elimination from **1.118**, followed by reductive elimination of the aryl and hydrido groups of intermediate **1.124**. In addition, the aldehyde product was also found to be a suitable candidate for insertion chemistry, as it could react with another equivalent of **1.118** to undergo Tischenko-like coupling to generate ester **1.125** *via* intermediate **1.127**.



**Scheme 1.34** Synthesis and reactivity of nickel alkoxo complexes

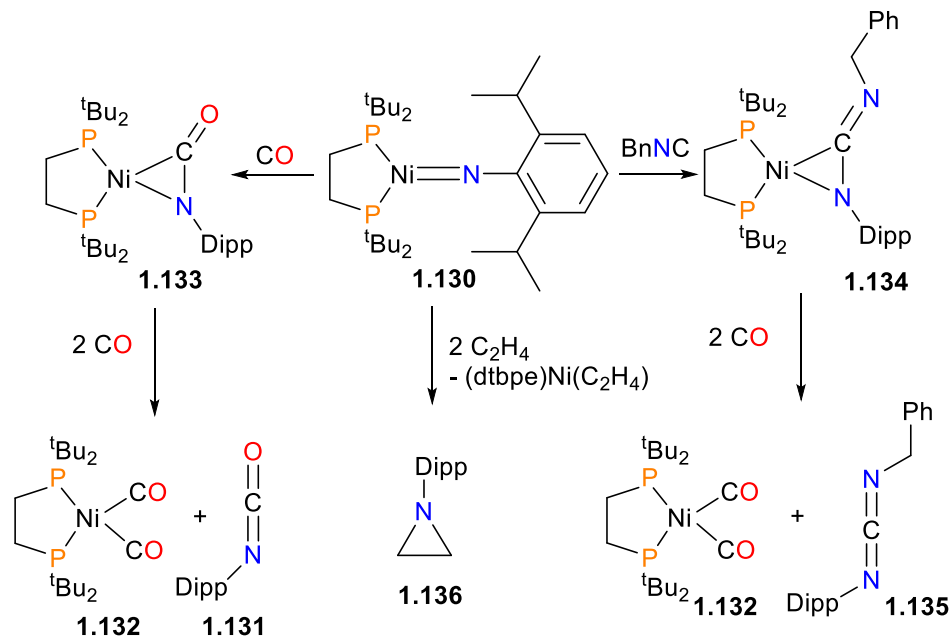
In related work, it was demonstrated that **1.103** could be used to effect the synthesis of more complex tetrahydrofuran derivatives such as **1.127** (see Scheme 1.35).<sup>74</sup> The mechanism involves olefin cyclodimerization to give **1.128**, followed by O-atom insertion with  $\text{N}_2\text{O}$  to generate nickelacycle **1.129**, followed by oxidatively-induced reductive elimination with  $\text{I}_2$  to generate the cyclic ether.



**Scheme 1.35** Nickel-mediated synthesis of a tetrahydrofuran ring

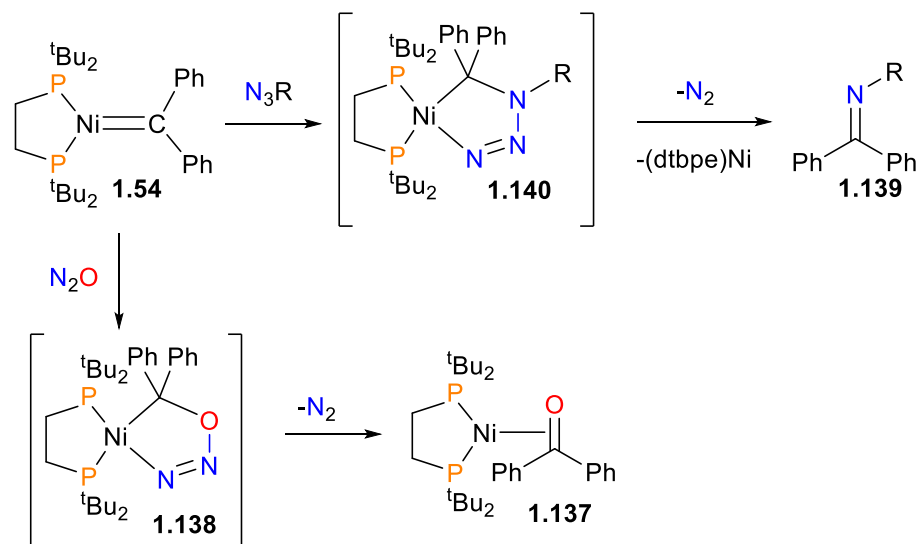
### 1.3 Group Transfer Chemistry of Nickel Imidos

Mindiola and Hillhouse were the first to report the synthesis and structure of a nickel imido complex, **1.130**.<sup>75</sup> Subsequent reactivity studies found that the imido group could be coupled to CO to generate isocyanate **1.131** and carbonyl complex **1.132** *via* complex **1.133**.<sup>76</sup> In addition, the imido could also be coupled to benzyl isocyanide to generate the  $\eta^2$ -bound carbodiimide complex **1.134**, which was characterized by X-ray diffraction studies. Exposure of **1.134** to an atmosphere of CO gas caused the release of the organic carbodiimide fragment **1.135**, concomitant with the formation of complex **1.132**. Shortly thereafter, Waterman and Hillhouse reported that complex **1.130** could also be used to aziridinate ethylene to aziridine **1.136** (Scheme 1.36).<sup>77</sup> Interestingly, deuterium labeling studies demonstrated that this aziridination reaction occurred with retention of stereochemistry. A more detailed study on the reactivity of **1.130** was published by the Hillhouse group in 2014.<sup>78</sup>



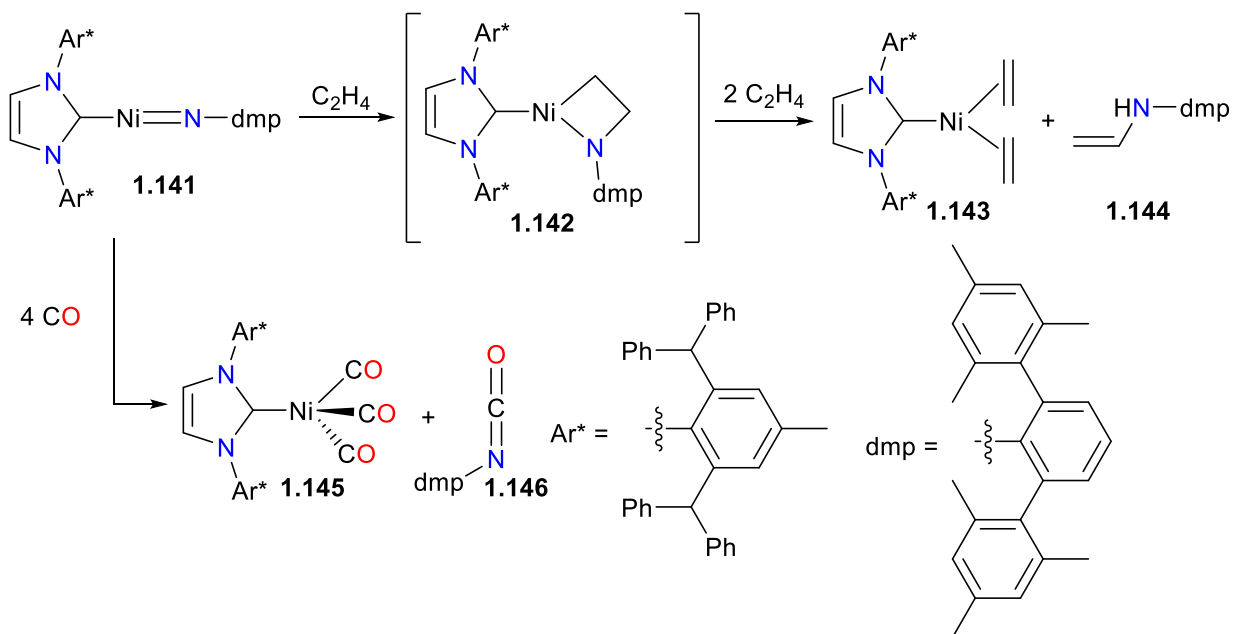
**Scheme 1.36** Nickel-mediated synthesis of a tetrahydrofuran ring

Alkylidene complex **1.54** demonstrates rich cyclization chemistry, as it reacts with N<sub>2</sub>O to yield benzophenone adduct **1.137** via O-atom transfer to the alkylidene group.<sup>79</sup> This transformation likely occurs via the formation of five-membered intermediate **1.138**, which eliminates N<sub>2</sub> to generate the observed product, as shown in Scheme 1.37. Analogously, organic azides can also react with alkylidene **1.54** to give N<sub>2</sub> and imines **1.139** via C-N coupling. This transformation also likely occurs via a five-membered intermediate **1.140**, as indicated by density functional theory (DFT) studies.



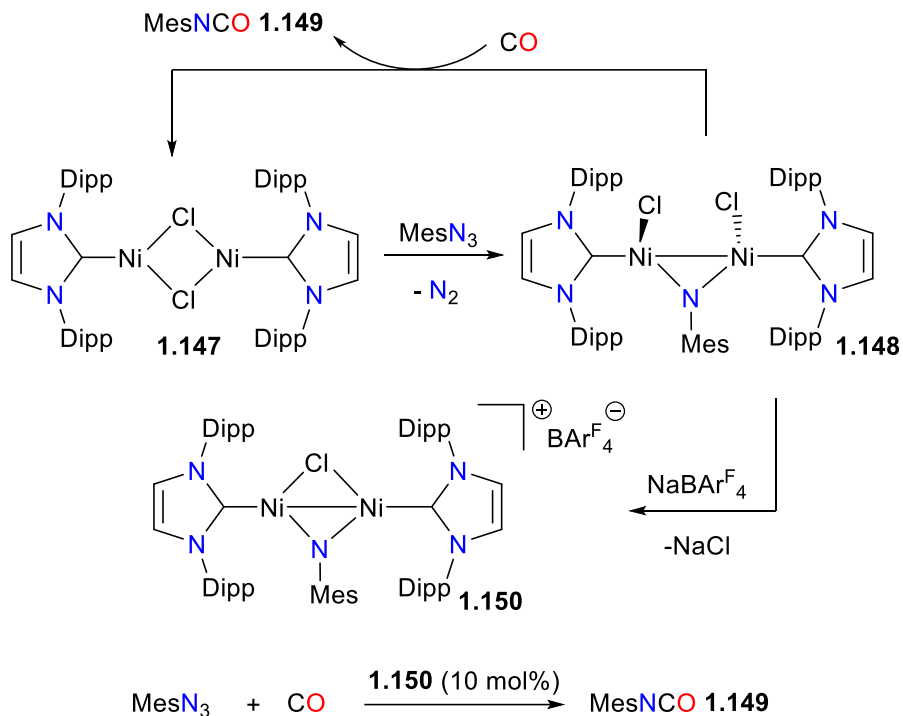
**Scheme 1.37** Reactivity of a nickel alkylidene with azides and  $N_2O$

Extremely bulky N-heterocyclic carbenes (NHCs) have recently received much attention due to their ability to kinetically stabilize otherwise reactive moieties. An elegant example of this is the preparation of nickel nitrene complex **1.141**, which features both very bulky  $Ar^*$  groups on the N atoms of the NHC as well as large mesityl substituents at the ortho positions of the imido aryl group (Scheme 1.38).<sup>80</sup> Treatment of **1.141** with ethylene at room temperature yielded the azametallacyclobutane **1.142**, which was characterized by NMR spectroscopic experiments but could not be isolated. Over the course of 12 hours under an atmosphere of ethylene, **1.142** yielded complex **1.143** and vinylamine **1.144**. The authors propose that the amine is formed *via* either a 1,2-hydride shift or  $\beta$ -H elimination from **1.142** and subsequent N-H reductive elimination. The imido could also be coupled to CO to generate nickel(0) complex **1.145** and isocyanate **1.146**.



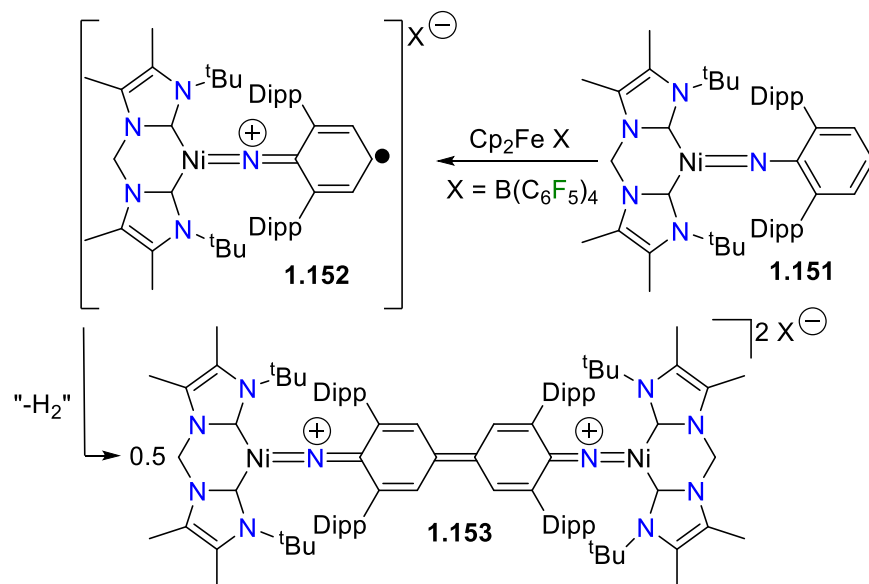
### Scheme 1.38 Nickel-mediated amination of ethylene

Other NHC ligands can also be useful for the preparation of isocyanates *via* the coupling of a imido group and CO.<sup>81</sup> For instance, treating nickel complex **1.147** with MesN<sub>3</sub> yields the bridging imido complex **1.148**, which releases MesNCO **1.149** when reacted with CO. Attempts to render this transformation catalytic were hampered by the rapid disproportionation of **1.147** under an atmosphere of CO. This decomposition pathway can be circumvented somewhat *via* chloride abstraction from **1.148** with NaBARF<sub>4</sub> to yield the bridging chloride dimer **1.150**, which is a competent catalyst for the formation of MesNCO **1.149** from MesN<sub>3</sub> and CO. Using 10 mol% **1.150** as a catalyst gave MesNCO in 52% yield after 6 hours at room temperature (Scheme 1.39).



**Scheme 1.39** Catalytic coupling of azides and CO to form isocyanate

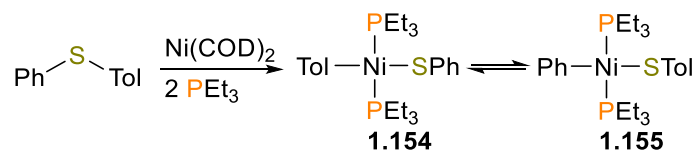
Bidentate NHCs have also been reported to stabilize nickel imidos.<sup>82</sup> In fact, treatment of the chelating NHC complex **1.151** with  $\text{Cp}_2\text{FeB}(\text{C}_6\text{F}_5)_4$  results in ligand-based oxidation to generate a carbon-centred radical species **1.152**, which can undergo C-C coupling and formal dehydrogenation with another equivalent of itself to form binuclear quinoneimine complex **1.153**, as outlined in Scheme 1.40. These Gomberg-type couplings of nitrogen-based radicals that are delocalized across an aromatic ring have also been reported for copper<sup>83,84, 85</sup> and rhodium.<sup>86</sup> Bai and Stephan have published related chemistry using a nickel(I) synthon with aryl azides.<sup>87</sup> Other groups have also observed C-N bond formation upon treating group 10 complexes with nitrene precursors.<sup>88</sup>



**Scheme 1.40** Radical coupling and dehydrogenation of a nickel imido complex

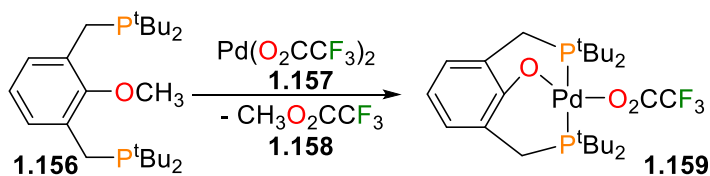
## 1.4 Oxidative Addition and Reductive Elimination Reactions of Late Transition Metals

Yamamoto and co-workers described one of the earliest examples of reversible C-S oxidative addition and reductive elimination when they reported that nickel(II) complexes **1.154** and **1.155** could interconvert *via* reversible oxidative addition and reductive elimination steps (Scheme 1.41).<sup>89</sup> Variable temperature NMR spectral studies revealed that **1.154** and **1.155** were in equilibrium. More recently, analogous reactivity using (dippe)palladium(0) has been reported by the Jones group.<sup>90</sup>



**Scheme 1.41** Reversible C-S oxidative addition mediated by nickel

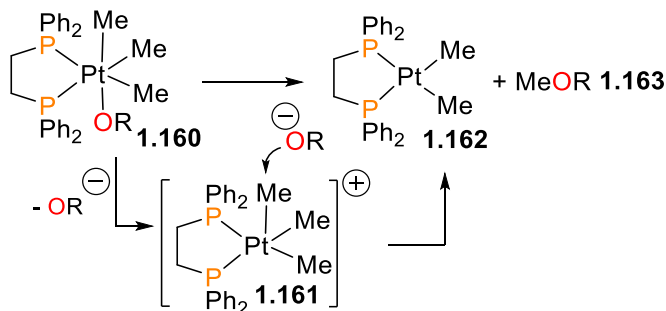
One of the earliest examples of C-O activation of aromatic methyl esters was reported by the Milstein group.<sup>91, 92</sup> Treating a pincer ligand precursor **1.156** with palladium(II) complex **1.157** resulted in the release of methyl trifluoroacetate **1.158** (Scheme 1.42), as detected by <sup>1</sup>H NMR spectroscopy, and the formation of phenoxy complex **1.159** via cleavage of the alkyl C-O bond. Complex **1.159** is produced in quantitative yield after heating for 3 hours at 80 °C in benzene. It is noteworthy that activation of the aromatic C-O bond is observed when the same aryl ether is treated with rhodium(I) as the metal. Related complexes of palladium<sup>93</sup> and nickel<sup>92, 94</sup> have since been reported to undergo similar C-O activations.



**Scheme 1.42** Oxidative addition of a CH<sub>3</sub>-O bond by palladium

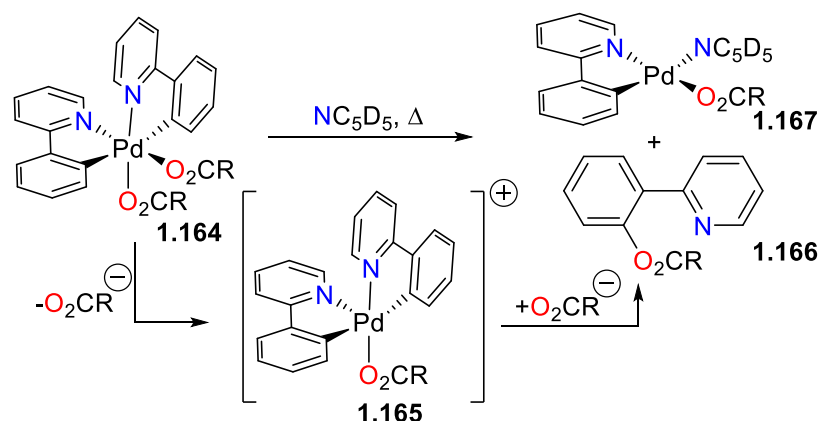
Williams and Goldberg have reported seminal work on the mechanism of C-O reductive elimination from platinum(IV) complexes **1.160**.<sup>95-97</sup> Dissociation of the alkoxide group from **1.160** generates a cationic five-coordinate intermediate **1.161**. The C-O bond forming step is likely the nucleophilic attack of alkoxide onto the electrophilic methyl group bound to platinum, resulting in reduction of platinum(IV) to platinum(II) and the formation of both **1.162** and ether **1.163**, as shown in Scheme 1.43. This type of nucleophilic attack was first demonstrated by Luinstra and Bercaw, who performed mechanistic studies on Shilov's methane oxidation system. It was found that platinum(IV) alkyls react with either water or chloride to form alcohols and alkyl chlorides, respectively. Deuterium labelling

experiments found an inversion of stereochemical configuration at carbon, consistent with an S<sub>N</sub>2-type attack at the platinum-bound alkyl.<sup>98</sup>



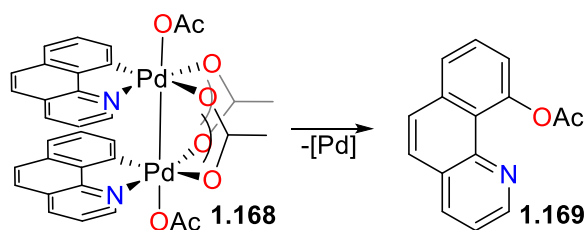
**Scheme 1.43** C-O Reductive elimination proceeds via nucleophilic attack

Sanford and co-workers have examined related chemistry with palladium,<sup>99, 100</sup> and found that for complex **1.164**, while C-O reductive elimination again proceeds through a five-coordinate intermediate (i.e. **1.165**), it is the palladium-bound carboxylate that couples with the phenylpyridyl ligand. This results in direct reductive elimination at the metal centre, rather than nucleophilic attack of the alkoxide, to generate the C-O bond of **1.166** and palladium product **1.167** (Scheme 1.44). Direct C-O reductive elimination was demonstrated through several crossover experiments.<sup>101</sup> It is worth noting that an earlier DFT study by a different group indicated that C-O reductive elimination occurred directly through the octahedral complex **1.164**.<sup>102</sup> Canty and co-workers have also explored C-O bond forming reactions with similar palladium complexes, but were unable to detect the palladium(IV) species responsible for C-O bond formation.<sup>103, 104</sup> The Sanford group has since expanded the scope this transformation to C<sub>sp</sub><sup>3</sup>-O reductive elimination, and in this case detailed mechanistic studies point towards nucleophilic attack of alkoxide as the key C-O bond forming step.<sup>105</sup>



**Scheme 1.44** C-O bond formation from a five-coordinate intermediate

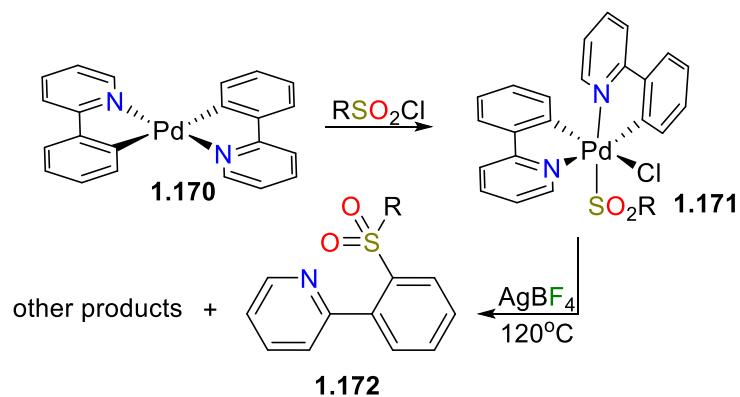
The first well-defined example of bimetallic carbon-heteroatom reductive elimination was reported by Powers and Ritter in their landmark 2009 study.<sup>106</sup> The authors demonstrated that bimetallic palladium(III) complex **1.168**, which is only stable at low temperatures (but was nevertheless fully characterized, including by X-ray diffraction), produces aromatic acetate **1.169** (see Scheme 1.45) in 64% yield *via* C-O reductive elimination.<sup>107-109</sup> Labelling experiments demonstrate that both bridging and terminal acetates exchange at a rate much faster than C-O bond formation. Related bimetallic complexes of platinum(III) have been shown to be active in the oxidation of alkynes.<sup>110</sup>



**Scheme 1.45** C-O reductive elimination from a bimetallic palladium complex

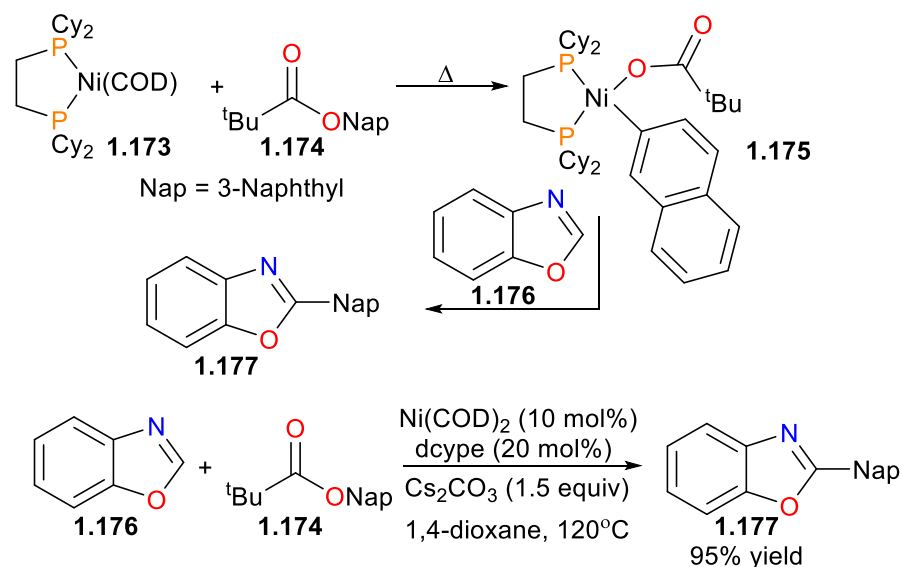
Inspired by Sanford (*vide supra*), Zhao and Dong have oxidized palladium(II) complex **1.170** with sulfonyl chlorides.<sup>111</sup> Thermolyzing palladium(IV) complexes **1.171** in the

presence of silver salts results in predominantly C-S reductive elimination to form aromatic sulfonyl **1.172** (Scheme 1.46), as well as the products of C-C and C-Cl reductive eliminations in minor amounts. Crossover experiments indicate that these reductive eliminations occur directly from palladium(IV).



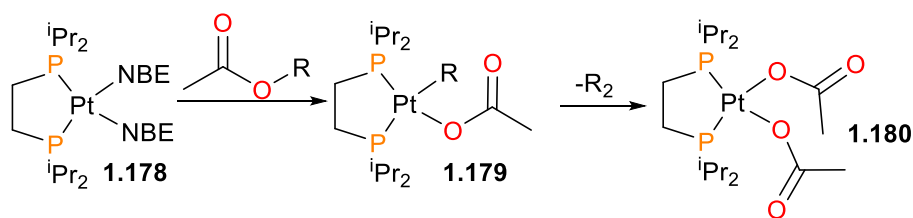
#### Scheme 1.46 C-S reductive elimination from palladium

Itami and co-workers have found that arylpivalates can be coupled with azoles to generate biaryls using nickel catalysis.<sup>112</sup> Mechanistic studies indicate that the combination of **1.173** and naphthylpivalate **1.174** react when heated *via* the oxidative addition of the C<sub>aryl</sub>-O bond, generating the fully characterized aryl-pivalate nickel(II) complex **1.175**. Subsequent heating of **1.175** with the azole **1.176** furnishes the cross-coupled product **1.177** (Scheme 1.47). Nickel(0) complexes with bidentate phosphine ligands have also been demonstrated to be good catalysts for the oxidative coupling of ethylene and CO<sub>2</sub> to form acrylate.<sup>113</sup>



**Scheme 1.47** Nickel-catalyzed cross-coupling of pivalates and azoles

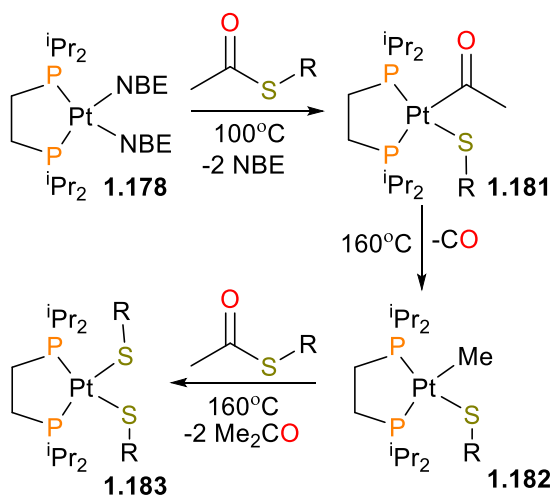
The group of Jones has performed reactivity studies of a low-valent platinum complex **1.178** with esters,<sup>114</sup> and found that C-O cleavage occurred to form acetate complexes of type **1.179**. Subsequent disproportionation resulted in the formation of a bis(acetate) complex **1.180**, as shown in Scheme 1.48.



**Scheme 1.48** Oxidative addition of esters with platinum

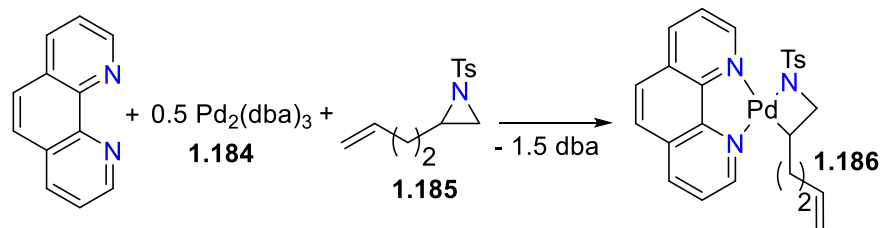
Jones and co-workers have demonstrated that thioesters can also be activated with platinum(0) complexes, although high temperatures are required.<sup>115</sup> Heating **1.178** with a 5-fold excess of thioester results in C<sub>acyl</sub>-S bond cleavage. Subsequent heating of the platinum(II) complex **1.181** results in decarbonylation of the acyl ligand to generate a methyl thiolate **1.182**, which can undergo further reaction with thioester to generate a

bis(thiolate) **1.183** with concomitant release of acetone, as shown in Scheme 1.49. The same group has also examined similar reactivity of **1.178** with thioethers.<sup>116</sup> Others have demonstrated related C-S oxidative addition reactions of sulfones with palladium<sup>117</sup> and nickel.<sup>118</sup>



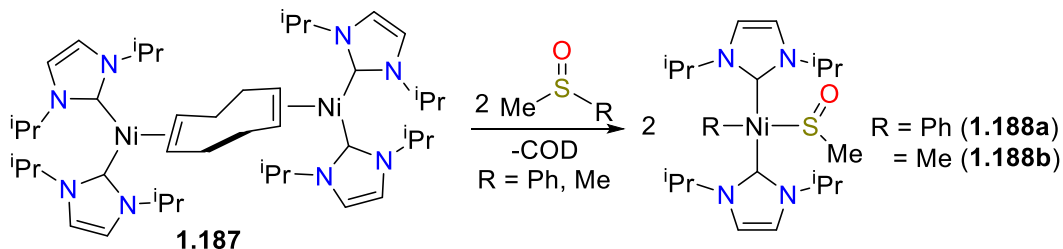
**Scheme 1.49** Oxidative addition of thioesters with platinum

Ney and Wolfe have reported the synthesis of a group 10 azametallacyclobutane. Mixing Pd<sub>2</sub>(dba)<sub>3</sub> (**1.184**, dba = dibenzylideneacetone), phenanthroline and aziridine **1.185** formed palladacycle **1.186** in 45% isolated yield (Scheme 1.50).<sup>119</sup> The presence of the pendant olefin was found to be important, with the authors proposing it serves as a directing group for the palladium(0) prior to oxidative addition. However, it should be noted that using a more reactive nosyl-substituted aziridine obviated the need for the olefin tail. Similar to Hillhouse's system,<sup>63</sup> deuterium labelling studies found that the oxidative addition proceeds with inversion of stereochemical configuration.



**Scheme 1.50** Oxidative addition of aziridines with palladium

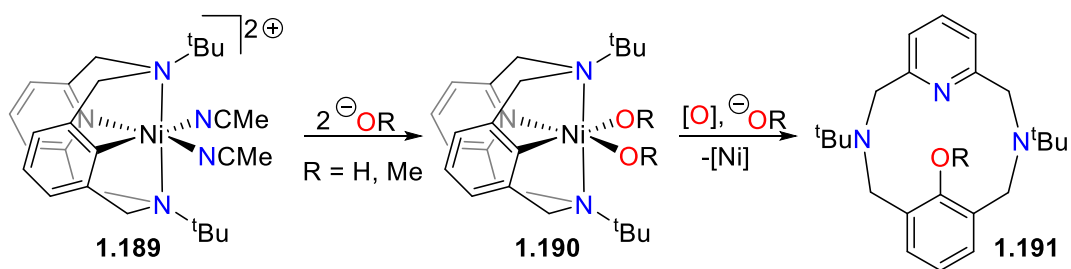
Radius and co-workers have examined the reactivity of nickel(0) complex **1.187** with methyl sulfoxides.<sup>120</sup> Analysis of the products by electron impact mass spectrometry (EI-MS) and elemental analysis showed the incorporation of the sulfoxide moiety into the bis(carbene) fragment, along with concomitant loss of COD (Scheme 1.51). The <sup>1</sup>H NMR data revealed that the carbene ligands adopt a *trans* orientation, ruling out the formation of an η<sup>2</sup>-type binding mode of the S=O group to nickel. Tellingly, complex **1.188b** displays two inequivalent resonances for the methyl groups; one at 2.35 ppm, while the other resonates much more upfield at -0.52 ppm. This latter shift is typical of nickel-bound methyl groups, indicative of C-S oxidative addition. Indeed, this structural assignment was ultimately corroborated by single crystal X-ray diffraction experiments for both complexes **1.188a** and **1.188b**. This family of complexes demonstrated the first general example of metal-mediated C-S bond cleavage in sulfoxides.



**Scheme 1.51** Oxidative addition of sulfoxides with nickel

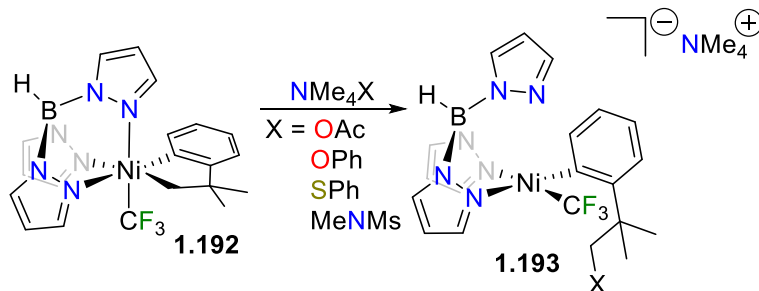
Mirica and co-workers have studied C-O reductive elimination from high-valent nickel bearing a pyridophane ligand (see Scheme 1.52).<sup>121</sup> Reacting cationic complex **1.189** with

excess of either hydroxide or methoxide forms complex **1.190**, which decomposes overnight at room temperature. Complexes **1.190** were characterized by electron paramagnetic resonance (EPR) spectroscopy and a low-resolution crystal structure. When treated with the oxidant  $\text{PhI}(\text{PyOMe})_2(\text{OTf})_2$  and additional alkoxide, **1.190** undergoes C-O reductive elimination to form the functionalized ligand **1.191**. The authors propose that this process occurs by sequential steps of alkoxide coordination to the nickel centre to form an *ate* complex, which then is oxidized to nickel(IV), followed by rapid C-O reductive elimination.



**Scheme 1.52** C-O reductive elimination from nickel

Recently, Camasso and Sanford<sup>122</sup> have reported the synthesis and reactivity of a very rare example of a well-defined nickel(IV) complex **1.192** that can undergo carbon-heteroatom coupling reactions when treated with nucleophiles, as outlined in Scheme 1.53. Crucial to the reactivity observed is the ability of the tris(pyrazolyl)borate ligand to change binding modes from  $\kappa^3$  to  $\kappa^2$  upon reduction of the metal centre during the formation of product **1.193**. Initial kinetic analyses found that the rate of the coupling reactions is first-order in both nickel species and  $\text{NMe}_4\text{X}$ , which indicates an  $\text{S}_{\text{N}}2$ -type mechanism of C-X bond formation. This proposal was also supported by a strong correlation between the initial rate of the coupling reaction and the Swain-Scott nucleophilicity parameters of the  $\text{NMe}_4\text{X}$  reagent.



**Scheme 1.53** C-X (X = O, S, N) reductive elimination with nickel

## 1.5 Summary

Over the last several decades, 2-metallaioxetanes have gone from being putative intermediates to well-defined complexes for a range of transition metals, in large part due to stabilization from the ancillary ligand(s) on the metal centre. Once formed, these oxacycles can undergo a myriad of reaction pathways, including both intramolecular (i.e. alkene elimination, as shown for complex **1.26** or isomerization to ketones, as is seen for compound **1.40**), and intermolecular pathways (i.e. transmetalation of rhodaoxetane **1.33** with boronic acids to form **1.36**, or the insertion chemistry of platinaoxetane **1.78**).

Equally as rich is the organometallic chemistry of group 10 complexes, especially nickel. Recent work from Hillhouse, Jones, and several others have highlighted the ability of low-valent group 10 compounds to break C-X (X = O, S, N) bonds *via* oxidative addition pathways (i.e. the formation of azametallacyclobutanes **1.109** and **1.186**, the synthesis of platinum complexes **1.78** and **1.80**, as well as nickel complex **1.175**). Importantly, the converse of these reactions (i.e. C-X reductive elimination from high-valent group 10 compounds) has also been shown to be not only feasible, but rapid and high-yielding under

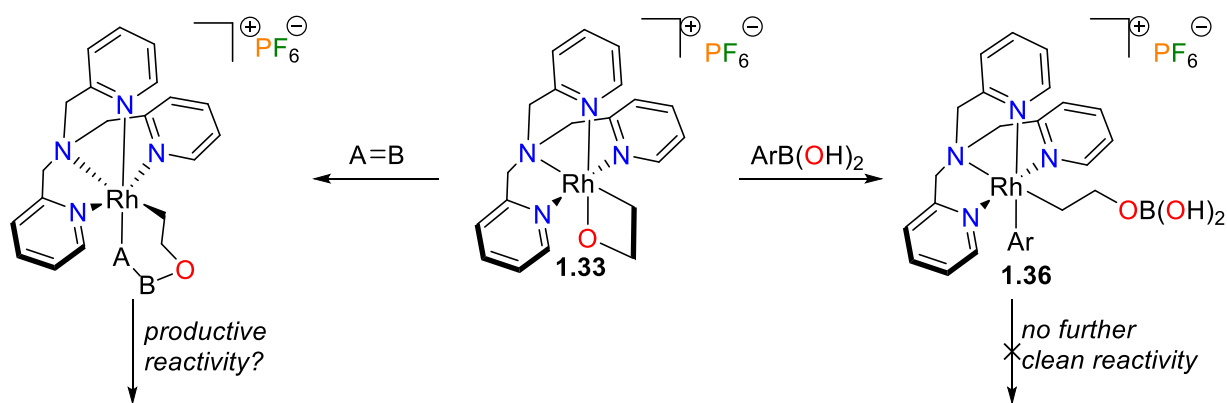
the appropriate conditions, as highlighted in the work of Sanford, Ritter, and Mirica, amongst others.

The work in this thesis was undertaken to expand on the fundamental organometallic chemistry of 2-metallaioxetanes of rhodium and nickel. In the case of the former, we sought to describe the reactivity of complex **1.33** with an array of molecules that had previously been unexplored, in the hopes of developing a potentially catalytic transformation. In the case of the latter, almost no experimental work had been done to prepare and characterize 2-nickelaoxetanes, let alone explore their reactivity or mechanisms of formation. In addition, we also undertook studies to examine the electronic structure of  $\pi$ -complexes of rhodium, as well as investigated small molecule activation with low-valent complexes of both rhodium and nickel.

## Chapter 2 : Reactivity and Revisited Mechanism of Formation of a 2-Rhodaioxetane

### 2.1 Introduction

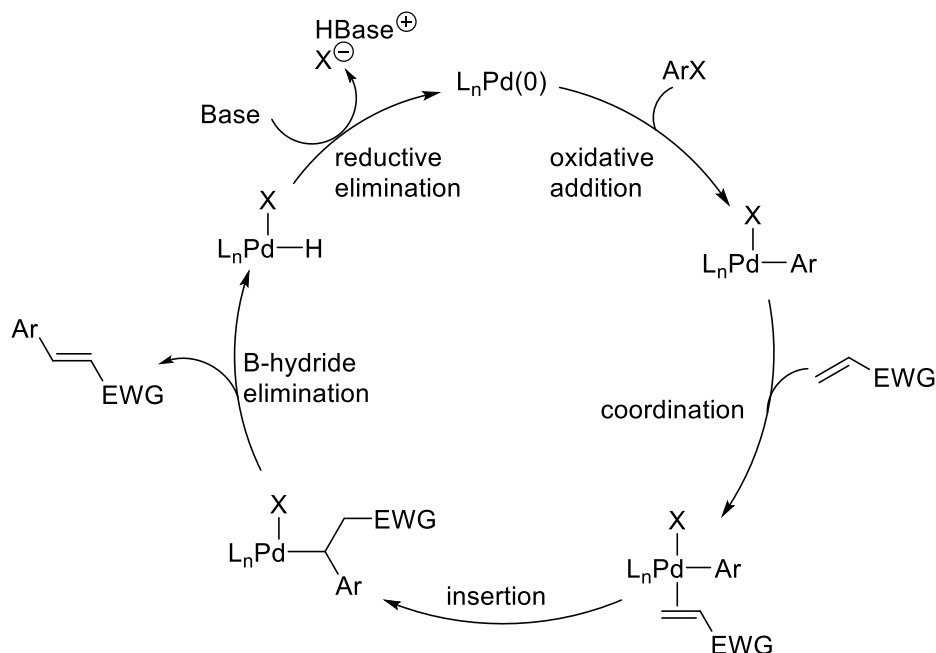
As outlined in Chapter 1, 2-metallaioxetanes of a wide array of transition metals can be prepared given suitable conditions to stabilize these otherwise reactive moieties. Previous research in the Love group has focused on exploring the feasibility of utilizing 2-rhodaioxetane **1.33** as a well-defined intermediate in some new catalytic protocol for the functionalization of olefins. Given the ease of transmetalation of **1.33** with aryl- and alkenylboronic acids, a potential carbohydroxylation of olefins was envisioned.<sup>35</sup> Unfortunately, the final reductive elimination step required to close the catalytic cycle was not achieved with a wide variety of experimental conditions. This chapter explores the fundamental reactivity of **1.33** in hope of identifying an alternate reaction pathway that would be more amenable to catalytic turnover (Scheme 2.1).



**Scheme 2.1** Could insertion of an electrophile ( $\text{A}=\text{B}$ ) lead to productive reactivity?

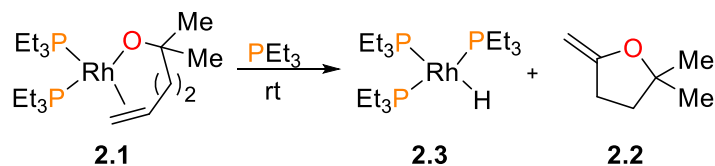
One of the most common fundamental organometallic reactions is the insertion of an unsaturated unit into a metal-carbon (M-C) bond. A classic example of this reactivity is the

Heck reaction (Scheme 2.2), which allows for the coupling of aryl halides or triflates with alkenes to form substituted alkenes *via* palladium catalysis.<sup>1</sup>



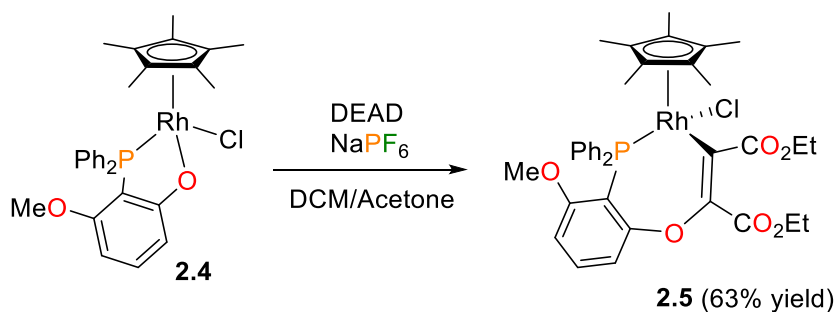
**Scheme 2.2** Proposed mechanism of the Mirozoki-Heck reaction

In contrast, the corresponding insertion into a M-X bond ( $X = O, S,$  or  $N$ ) is much rarer, with many examples being reported only recently.<sup>5</sup> For example, Zhao, Incarvito and Hartwig have prepared rhodium(I) complex **2.1** that features tethered alkoxy and olefin co-ligands.<sup>123</sup> Treating complex **2.1** with additional  $PEt_3$  ligand at room temperature results in the clean formation of substituted tetrahydrofuran **2.2** (Scheme 2.3) and hydride **2.3**. Kinetic analysis of the formation of product **2.2** indicates that the reaction is unimolecular, and a similar rate of formation of **2.2** in cyclohexane, benzene and THF indicate that the reaction likely does not proceed through ionic intermediates. Deuterium labelling studies found the product formed as a single isomer, consistent with *syn* addition of the metal and alkoxy across the  $C=C$  double bond.



**Scheme 2.3** Insertion of a pendant olefin into a rhodium-alkoxide bond

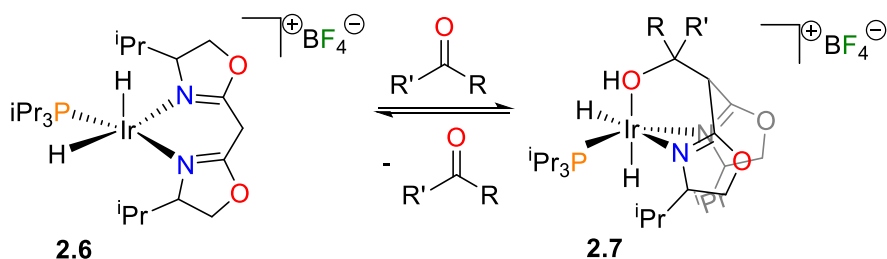
Yamamoto and co-workers have also demonstrated alkyne insertion into rhodium-aryloxide bonds, as outlined in Scheme 2.4.<sup>124</sup> Stirring rhodium complex **2.4** and DEAD in dichloromethane (DCM)/acetone for 5 hours results in the formation of complex **2.5** in modest (63%) isolated yield. Key to this process is the presence of NaPF<sub>6</sub>, which presumably abstracts chloride from the rhodium centre, forming a cationic metal complex and opening up a coordination site for the alkyne to bind prior to insertion. When the reaction was performed without added NaPF<sub>6</sub>, the starting material was recovered in quantitative yield.



**Scheme 2.4** Insertion of DEAD into a rhodium-aryloxide bond

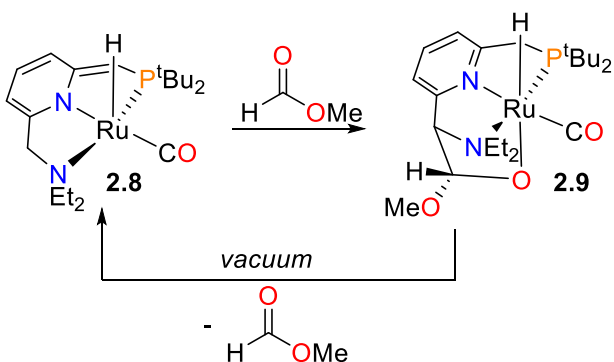
Importantly, insertion reactions can occasionally be reversible. For example, Sola and co-workers have found that iridium(III) hydride complex **2.6** can react with aldehydes or ketones by insertion of the electrophile into a C-H bond of the bis(oxazoline) ligand backbone (Scheme 2.5). The equilibria of these transformations were found to be quite dependent on the bulk and electronic

nature of the carbonyl substrate; for acetaldehyde (i.e. R = Me, R' = H) the equilibrium lies far to the right. In contrast, when 1-phenylpropanone (i.e. R = Me, R' = CH<sub>2</sub>Ph) was used as substrate, the insertion products **2.7** (as a mixture of isomers) and starting material **2.6** equilibrated to a 61:39 ratio at room temperature.



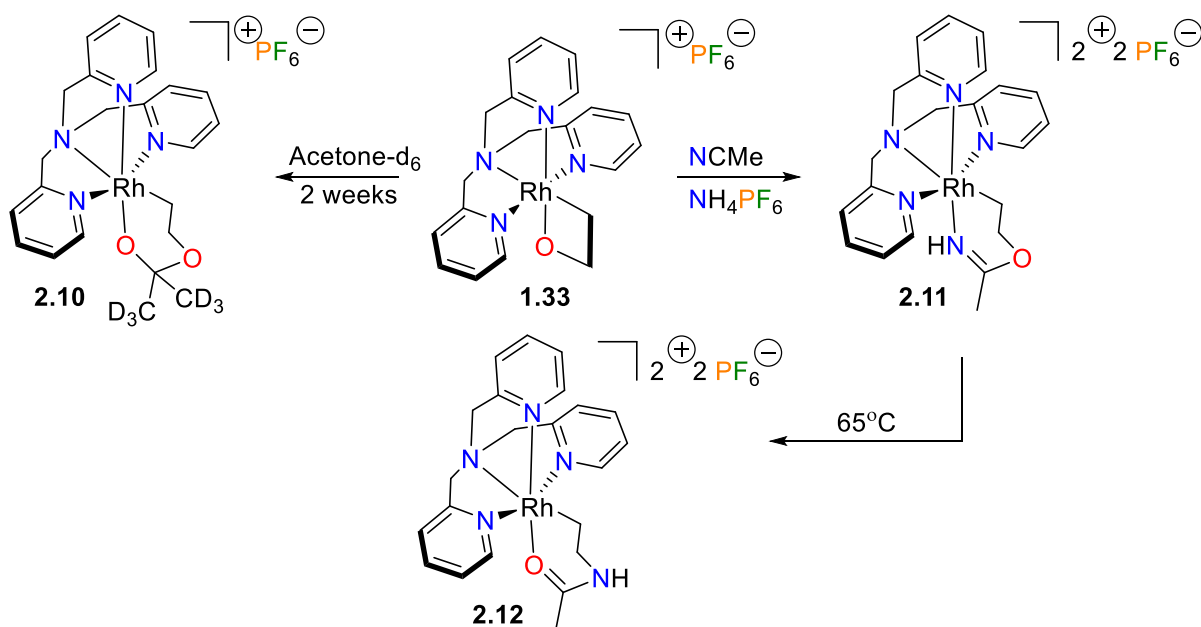
**Scheme 2.5** Reversible insertion of aldehydes and ketones into C-H bonds

Ruthenium complex **2.8**, which is a highly active hydrogenation catalyst, has been shown to react reversibly with carbonyl-containing compounds such as methyl formate to produce **2.9**. Two-dimensional NMR spectroscopy experiments reveal that a C-C bond forming reaction has occurred between the N-arm of the pincer ligand and the formate, resulting in the stereoisomer depicted in Scheme 2.6, a structural assignment that was also supported by X-ray crystallography. This C-C bond forming process was shown to be completely reversible, as exposure of **2.9** to high vacuum was sufficient to remove the formate moiety, resulting in quantitative recovery of **2.8**.



**Scheme 2.6** Reversible insertion of methyl formate into a C-H bond

In fact, Gal and co-workers had noted some examples of insertion chemistry of **1.33** with certain unsaturated solvents (Scheme 2.7). For instance, samples of rhodaoxetane **1.33** that had been dissolved in acetone- $d_6$  for 2 weeks displayed new signals corresponding to the rhodaketal **2.10**. Notably, the decrease in the coupling constant of the RhCH<sub>2</sub>CH<sub>2</sub>O group ( $^3J_{H,H} = 5.6$  Hz for **2.10**, as opposed to 7.4 Hz for **1.33**) was indicative of ring expansion from a four-membered ring to a six-membered ring.<sup>32</sup> Acetonitrile could also insert cleanly into the Rh-O bond of **1.33** in the presence of acid, resulting in the quantitative formation of imino ester **2.11**.<sup>125</sup> Interestingly, heating **2.11** at 65 °C for 4 hours isomerizes the imino ester to amide **2.12**. The reaction can be performed in CD<sub>3</sub>CN with no incorporation of deuterium into the final product, demonstrating that the reaction is unimolecular. In addition, the isomerization process is also tolerant of up to 10 equivalents of added H<sub>2</sub>O, indicating that both imino ester **2.11** and amide **2.12** are relatively stable towards hydrolysis.

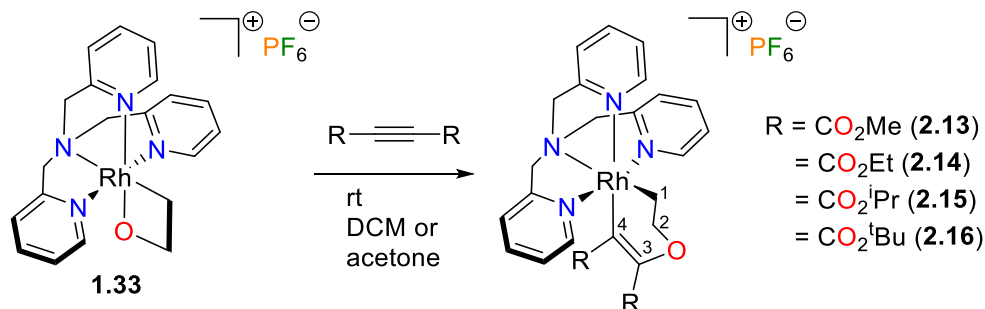


**Scheme 2.7** Insertion chemistry of complex **1.33** with acetone and acetonitrile

Herein, we report our efforts towards expanding the insertion chemistry of **1.33** with unsaturated electrophiles such as electron-deficient alkynes, heterocumulenes and aldehydes. We also describe X-ray absorption spectroscopic experiments on ethylene complex **1.32**, shedding new light on the electronic nature of the olefin ligand and the role it plays in the mechanism of formation of **1.33**.

## 2.2 Insertion of Alkynes into a Rh-O Bond

In line with de Bruin's original report, we found that **1.33** was unreactive towards simple internal alkynes, such as diphenylacetylene, ethyl 2-butynoate and ethyl 3-phenylpropiolate; and room temperature reactions with the terminal alkyne ethyl propiolate led to decomposition to a mixture of unidentified products. However, **1.33** reacted readily with electron-deficient alkynes of the form  $\text{RO}_2\text{CC}\equiv\text{CCO}_2\text{R}$  to give complexes **2.13** to **2.16** after stirring at room temperature in DCM or acetone (see Scheme 2.8).



**Scheme 2.8** Insertion of electron-deficient acetylene dicarboxylates into the Rh-O bond of **1.33**.

The characterization data for **2.14** will be discussed as a representative example.  $^1\text{H}$  NMR spectroscopy reveals that in solution, **2.14** maintains the same plane of symmetry found in **1.33**, as the two equatorial arms of the TPA ligand are equivalent (Figure 2.1). Insertion of the alkyne into the Rh-O bond rather than the Rh-C bond is clearly shown by the  $^{103}\text{Rh}$  coupling found in the

resonance for **H1** ( $\delta = 3.13$  ppm, dt,  $^3J_{\text{H,H}} = 7.3$  Hz,  $^2J_{\text{Rh,H}} = 2.9$  Hz; see Scheme 2.8 for numbering). Interestingly, the peaks of the axial methylene protons of the equivalent TPA arms have shifted dramatically downfield from **1.33** ( $\delta = 5.18$  ppm, d[AB],  $^2J_{\text{H,H}} = 15.3$  Hz) to **2.14** ( $\delta = 5.96$  ppm, d[AB],  $^2J_{\text{H,H}} = 16.3$  Hz), which could be because of close contact with the nearby carbonyl moiety (*vide infra*).

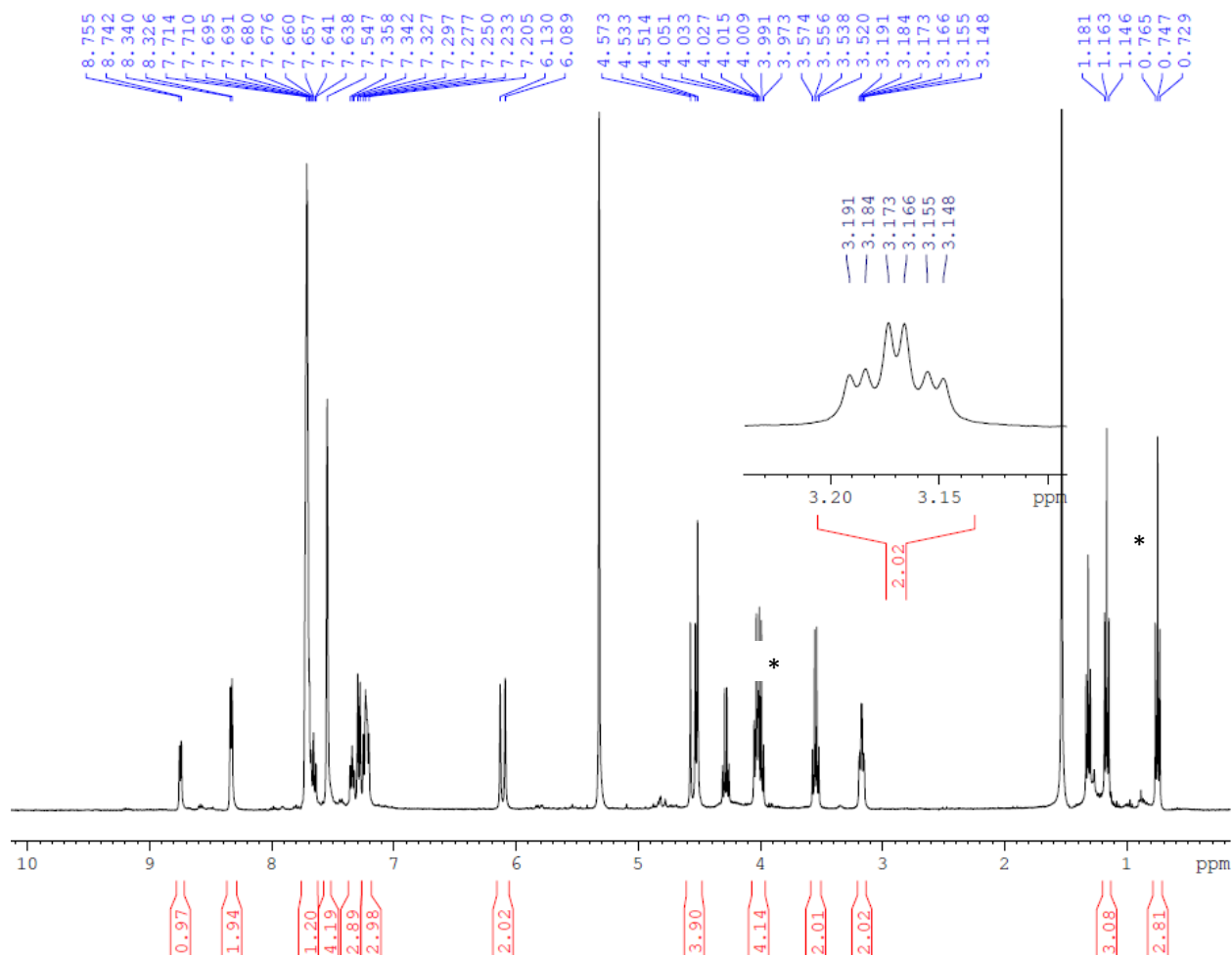


**Figure 2.1**  $^1\text{H}$  NMR spectrum (400 MHz, 25 °C,  $\text{CD}_2\text{Cl}_2$ ) of **2.14**[ $\text{BAR}^{\text{F}}_4$ ]. Inset shows the resonance assigned to **H1**. \* indicates residual DEAD.

$^{13}\text{C}$  NMR spectroscopy also supported the proposed structure of **2.14**, notably showing a doublet for **C1** ( $\delta = 29.5$  ppm,  $^1J_{\text{Rh,C}} = 26.9$  Hz) and for **C4** ( $\delta = 141.52$  ppm,  $^1J_{\text{Rh,C}} = 34.5$  Hz),

although the latter is, not surprisingly, of low intensity. Full characterization of **2.14** was completed with the use of 2D NMR spectroscopic techniques such as  $^1\text{H}$ - $^1\text{H}$  correlation spectroscopy (COSY), nuclear Overhauser effect spectroscopy (NOESY), heteronuclear single quantum coherence spectroscopy (HSQC) and heteronuclear multiple bond coherence spectroscopy (HMBC), as well as high-resolution mass spectrometry (HRMS) to confirm the empirical formula.

The use of tetrakis[(3,5-trifluoromethyl)phenyl]borate ( $\text{BAr}^{\text{F}_4}$ ) as a counterion allowed for X-ray quality crystals to be grown, and the molecular structure of **2.14**[ $\text{BAr}^{\text{F}_4}$ ] was confirmed by X-ray diffraction (Figure 2.2). In the solid phase, the metallacycle adopts a puckered conformation, with O1 pointed towards one of the equatorial arms of the TPA ligand. This is in contrast to the NMR data, which indicates that, in solution, **2.14** maintains a plane of symmetry through the axial TPA arm. Lowering of the temperature to  $-70\text{ }^\circ\text{C}$  did not lead to a breaking of the symmetry in solution but showed only a broadening of the metallacycle resonances as judged by  $^1\text{H}$  NMR spectroscopy. Together, these data suggest that the metallacycle bears a low energy barrier to inversion.<sup>126</sup> The C3-C4 bond length is  $1.339(4)\text{ \AA}$ , typical for a C-C double bond. The geometry at rhodium is a distorted octahedron, with Rh-N bond lengths similar to those in related complexes.<sup>32, 125, 127-129</sup> As expected from the  $^1\text{H}$  NMR spectrum, the axial methylene protons of the equivalent TPA arm are close to the carbonyl oxygen at around  $2.29\text{ \AA}$ .

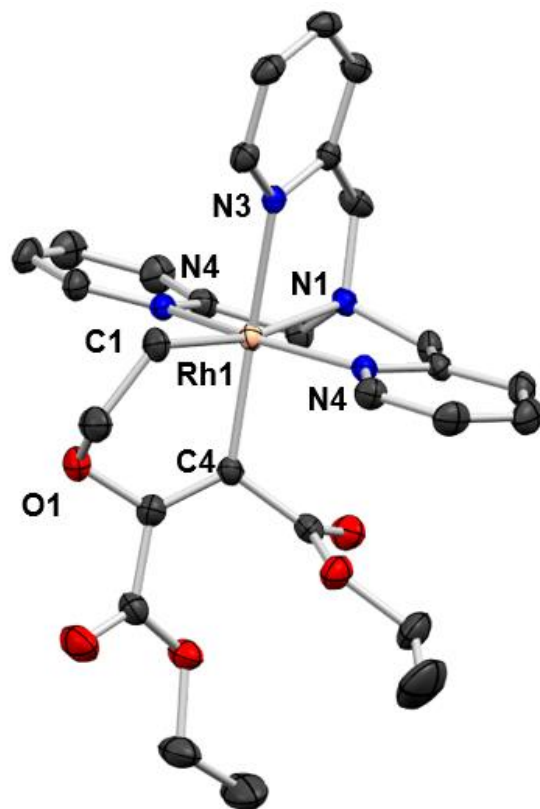
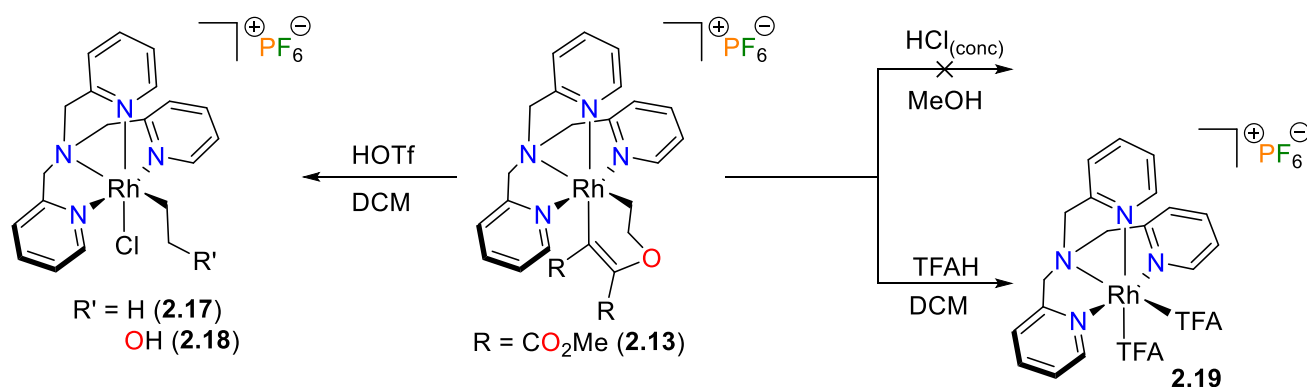


**Figure 2.2** Oak ridge thermal ellipsoid plot (ORTEP) diagram (50% probability ellipsoids) of **2.14**[BAr<sup>F</sup><sub>4</sub>]. H atoms, BAr<sup>F</sup><sub>4</sub> counterion and 0.5 H<sub>2</sub>O solvates omitted for clarity.

Despite the fact that similar reactions of **1.33** have been proposed to be acid catalyzed,<sup>127</sup> the rate of alkyne insertion was found to be unaffected by the presence of Na<sub>2</sub>CO<sub>3</sub>. The insertions of these acetylene dicarboxylates into rhodium-alkoxide bonds<sup>124, 130</sup> as well as the Pt-O bond of a platinaoxetane<sup>131</sup> are known, although the insertion of diethylacetylene dicarboxylate into **1.33**, which is complete after 1 hour, is notably faster than the corresponding platinaoxetane reaction, which requires 20 hours. This transformation is also in contrast to that of a similar ruthenaoxetane where insertion occurs across the Ru-C bond<sup>132-134</sup> and electron-rich alkynes react faster than electron-deficient alkynes.

In an attempt to cleave the coupled organic fragment, **2.13** was reacted with various acids and monitored by mass spectrometry (Scheme 2.9). While **2.13** reacts with trifluoromethanesulfonic acid (HOTf) in DCM over 3 hours to give a mixture of **2.17** and **2.18**,<sup>32</sup> using the less acidic trifluoroacetic acid (TFAH) yields the bis(trifluoroacetate) complex **2.19**<sup>135</sup> after 1.5 hours. Unfortunately, the organic fragment appears to undergo hydrolysis and its ultimate fate remains to be determined. Other acids, such as acetic acid (AcOH) and HCl, were found to be ineffective at cleaving the Rh-C bonds.



**Scheme 2.9** Initial reactivity studies of **2.13**

Heating **2.14** at 55 °C in acetone- $d_6$  for 36 hours resulted in the clean conversion to a new product (**2.20**, see Figure 2.3) with the same  $m/z$  ratio in the mass spectrum, which in addition to the similarities between the  $^1\text{H}$  and  $^{13}\text{C}$  NMR data of **2.14** and **2.20**, could indicate an isomerization process.

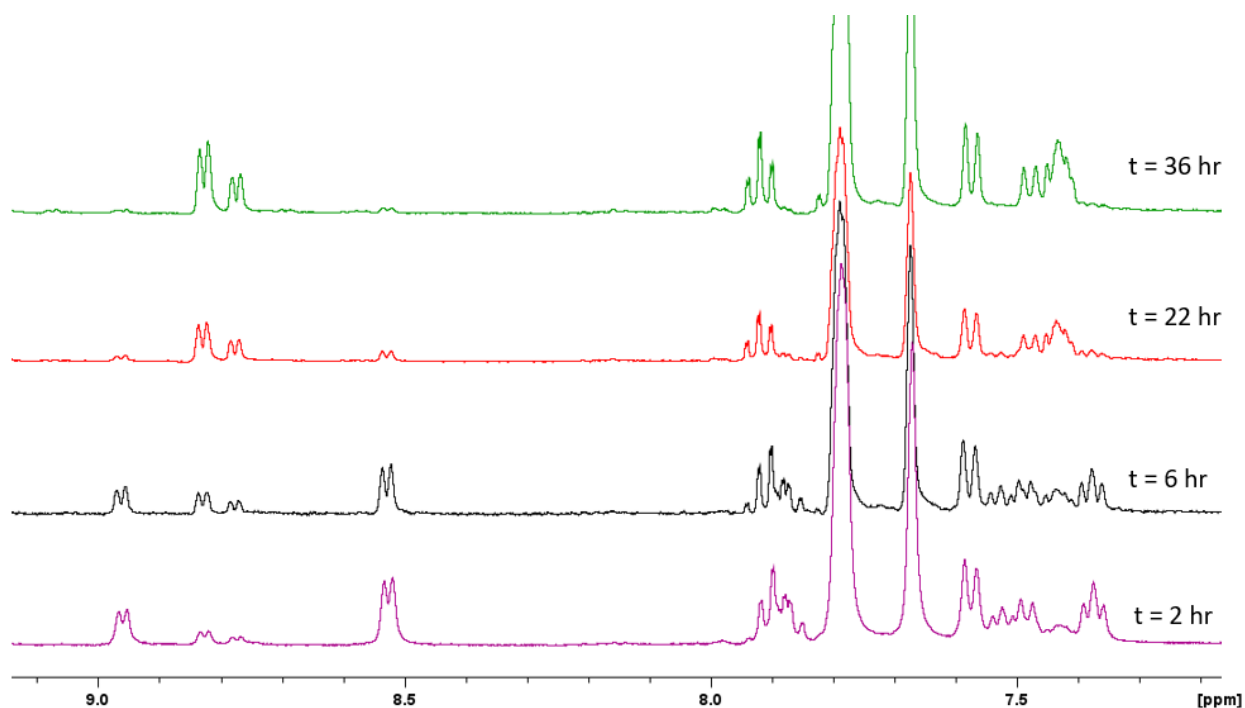
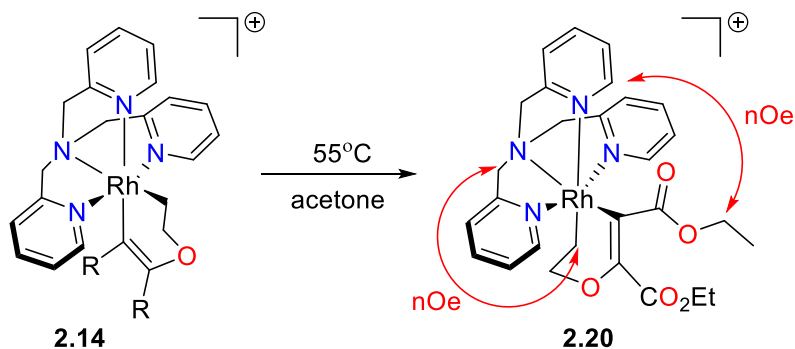


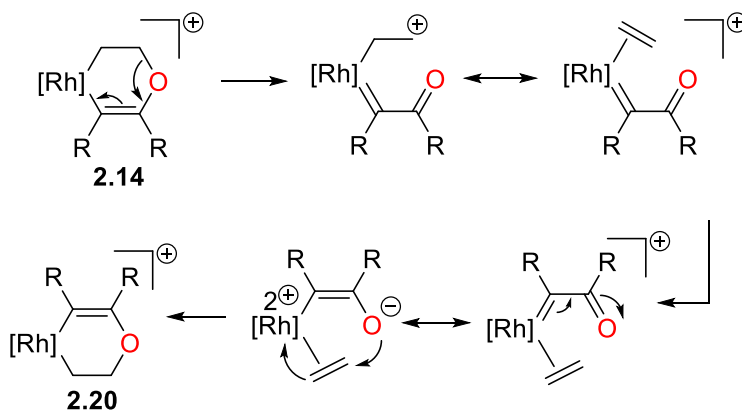
**Figure 2.3** Overlay of partial  $^1\text{H}$  NMR spectra (400 MHz, 25 °C, acetone- $d_6$ ) of **2.14**[ $\text{Bar}^{\text{F}}_4$ ] after heating at 55 °C for 2 hr (purple trace), 6 hr (black trace), 22 hr (red trace) and 36 hr (green trace).

Tellingly, a 2D NOESY spectrum revealed strong contact peaks between the signals for **H1** and the axial methylene resonance of the TPA scaffold, indicating that the  $\text{CH}_2\text{CH}_2$  moiety derived from ethylene is now *trans* to the axial pyridine nitrogen instead of the central amine nitrogen (Scheme 2.10).



**Scheme 2.10** Isomerization of **2.14** to **2.20**

This rearrangement has not been observed in these TPA systems before, and is counterintuitive from a simple steric perspective. In related work, the Gal group propose that the mechanism of isomerization of **2.11** to **2.12** proceeds *via* a Ritter-like mechanism.<sup>125</sup> If the isomerization to **2.20** follows a similar mechanism, it would involve the formation of a Schrock carbene, as outlined in Scheme 2.11.



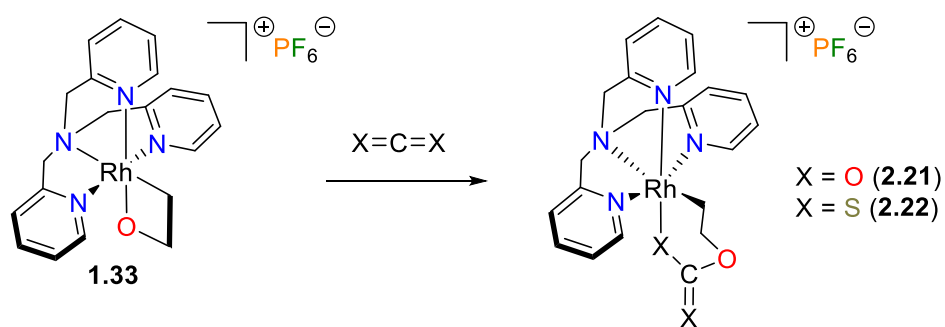
**Scheme 2.11** Potential mechanism of isomerization of **2.14** to **2.20**. [Rh] = (TPA)Rh

A simpler mechanism would be the dissociation of one pyridyl arm, followed by sequential Berry-type pseudorotation from the resulting five-coordinate intermediate, then pyridyl recoordination. Unfortunately, attempts to grow X-ray quality crystals of **2.20** were ultimately unsuccessful. At this time, we do not have sufficient data to support one potential isomerization mechanism over another.

### 2.3 Reactions of a 2-Rhodaoxetane with Other *sp*-Hybridized Electrophiles

As our attempts to release the organic moiety from the rhodadihydropyrans were unsuccessful, we turned our attention to other unsaturated electrophilic reagents. We targeted substrates that would form Rh-X rather than Rh-C bonds upon insertion, as we posited that these would be more

reactive. While **1.33** showed no reactivity with *tert*-butyl isocyanide or trimethylsilyldiazomethane, stirring a solution of **1.33** under an atmosphere of CO<sub>2</sub> led to the formation of a mixture of **2.18** and the bicarbonate insertion product **2.21** as indicated by <sup>1</sup>H NMR spectroscopy and HRMS (Scheme 2.12). These mixtures persisted despite initial attempts to optimize the reaction, which has so far precluded the full characterization of **2.21**. While crystals could be grown from the reaction mixture, they were not of sufficient quality for an X-ray diffraction study.



### Scheme 2.12 Insertion of allene-type molecules into **1.33**

In a similar fashion, the addition of excess CS<sub>2</sub> at -78 °C to a solution of **1.33** was found to consume the starting material and give a new major product, **2.22** (76% NMR yield), which was characterized by <sup>1</sup>H, <sup>13</sup>C, and 2D NMR spectroscopic techniques, as well as HRMS. Like **2.13-2.16**, metallacycle **2.22** maintains C<sub>s</sub> symmetry in solution, and insertion into the Rh-O bond rather than the Rh-C bond is demonstrated by <sup>103</sup>Rh coupling in both the <sup>1</sup>H and <sup>13</sup>C NMR spectra. The RhCH<sub>2</sub>CH<sub>2</sub>O moiety of **2.22** displays unusual multiplicities for this family of compounds (Figure 2.4). The splitting remains the same in both CD<sub>2</sub>Cl<sub>2</sub> and acetone-d<sub>6</sub>, and variable temperature NMR studies down to -70 °C show only a slight broadening of the peaks. COSY and <sup>1</sup>H{<sup>1</sup>H} NMR experiments show that **H2** is solely coupled to **H1**, and **H1** is coupled to both **H2** and Rh with a <sup>2</sup>J<sub>Rh,H</sub> of 2.6 Hz. This could be the result of second-order coupling between protons that are

chemically equivalent but not magnetically equivalent, although why **2.22** is the only complex in this family of insertion products to display this type of coupling is unclear.

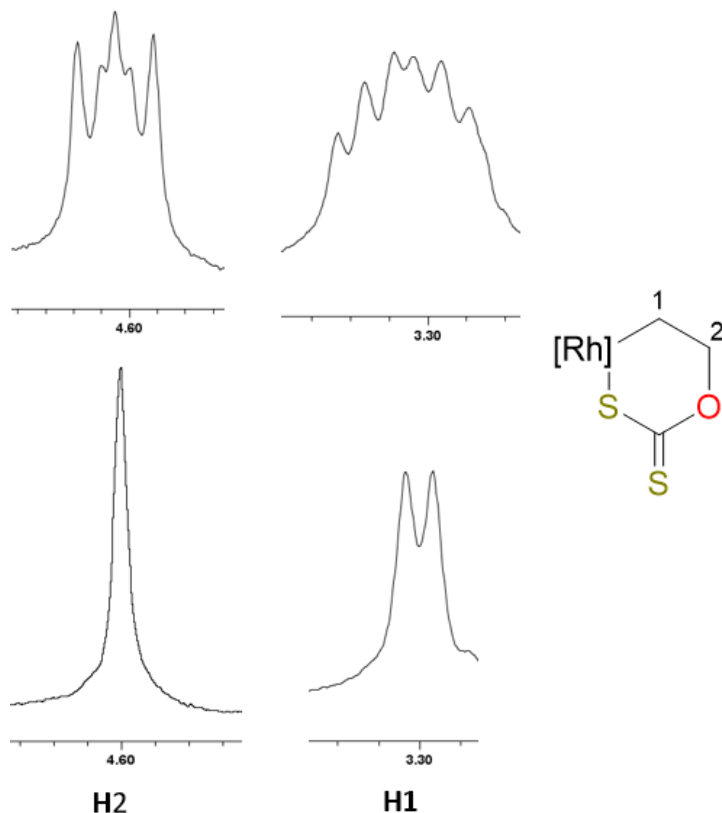


**Figure 2.4**  $^1\text{H}$  NMR resonances for **H1** (right) and **H2** (left) of **2.22** when they are coupled (above) and decoupled (below) from the other.  $[\text{Rh}] = (\text{TPA})\text{Rh}^+$

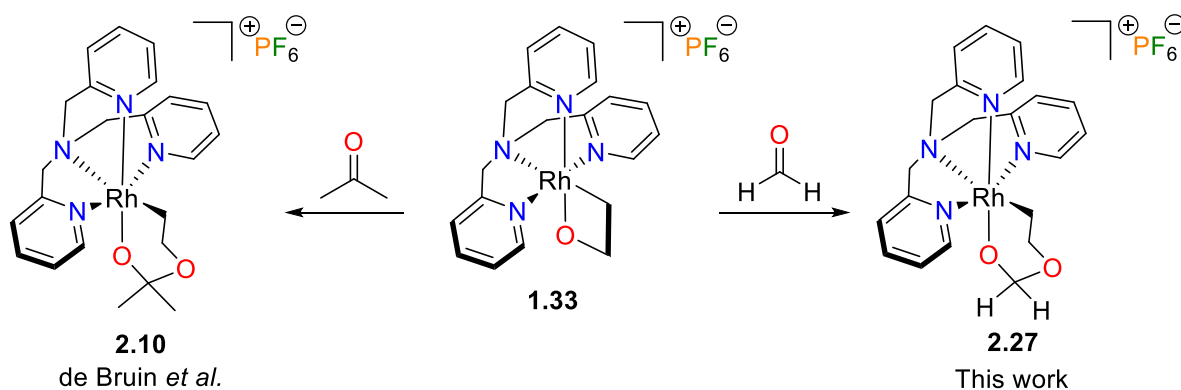
Complex **2.22** was found to be thermally unstable, decomposing in solution after 5 days at room temperature, but keeping for 3 weeks when stored at  $-20\text{ }^\circ\text{C}$ . No trace of the direct reductive elimination product xanthate could be observed from decomposed samples of **2.22** by either  $^1\text{H}$  NMR spectroscopy or electrospray ionization (ESI) mass spectrometry.

In an attempt to explore the regioselectivity of heterocumulene insertion, **1.33** was reacted with diphenylketene, a series of isothiocyanates ( $\text{RNCS}$ ,  $\text{R} = \text{Me}$ ,  $\text{Et}$ ,  $^i\text{Pr}$  and  $^t\text{Bu}$ ) as well as



## 2.4 Reversible Insertion of Aldehydes

It was previously reported by de Bruin that **1.33** reacted slowly with acetone to generate rhodaketal **2.10** (*vide supra*).<sup>32</sup> We reasoned that aldehydes should react more rapidly, anticipating less steric interaction of aldehyde insertion relative to that of ketones, as well as increased electrophilicity. Accordingly, complex **1.33** was found to react rapidly with paraformaldehyde to cleanly and quantitatively generate the rhodaacetal **2.27** (98% NMR yield, 59% isolated, Scheme 2.14).



### Scheme 2.14 Insertion of carbonyl compounds into **1.33**

The  $^1\text{H}$  NMR spectrum of **2.27** is similar to the previously discussed insertion products, as the equatorial TPA arms are again equivalent (Figure 2.5). Notably, the resonance for **H1** ( $\delta = 3.10$  ppm, dt,  $^3J_{\text{H,H}} = 5.9$  Hz,  $^2J_{\text{Rh,H}} = 2.7$  Hz) shows a smaller  $^3J_{\text{H,H}}$  coupling constant compared to that of **1.33** ( $\delta = 2.31$  ppm, dt,  $^3J_{\text{H,H}} = 7.5$  Hz,  $^2J_{\text{Rh,H}} = 2.3$  Hz), which is attributed to the release of ring strain from the expanded metallacycle. The presence of the six-membered ring, as opposed to a ring-opened species, is firmly demonstrated by the  $^{103}\text{Rh}$  coupling shown by **H3** ( $\delta = 4.13$  ppm, d,  $^3J_{\text{Rh,H}} = 1.1$  Hz), which would not be present if the O atom of the aldehyde moiety were not coordinated to rhodium.

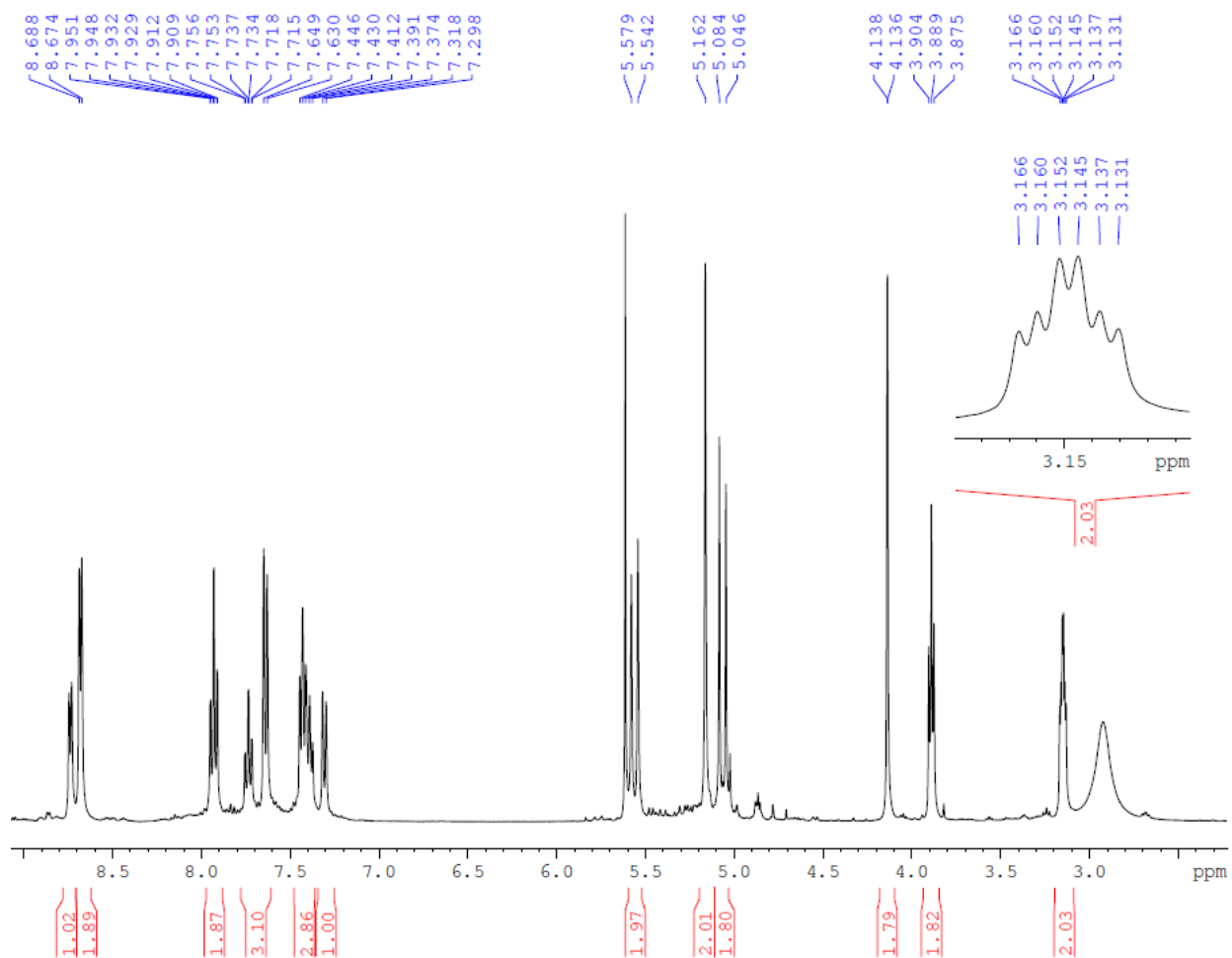


**Figure 2.5**  $^1\text{H}$  NMR spectrum (400 MHz, 25 °C, acetone- $\text{d}_6$ ) of **2.27**. Inset shows the resonance assigned to **H1**.

X-ray quality crystals of **2.27**[**BAr** $^{\text{F}}_4$ ] could be grown from DCM/hexanes (Figure 2.6). The solid-state structure confirmed that suggested from the NMR data. The acetal ring adopts a chair conformation, and the Rh-O bond is longer than that reported for **1.33** by 0.1 Å, but still in the range of reported bond lengths for rhodium-alkoxide bonds (2.00 to 2.11 Å).<sup>32</sup> Of note, the C3-O2 bond, at 1.349(11) Å, is much shorter than the C3-O1 bond at 1.450(11) Å. Like **2.14**[**BAr** $^{\text{F}}_4$ ], the TPA scaffold of **2.27**[**BAr** $^{\text{F}}_4$ ] is unremarkable amongst the family of TPA rhodium complexes.<sup>127</sup>

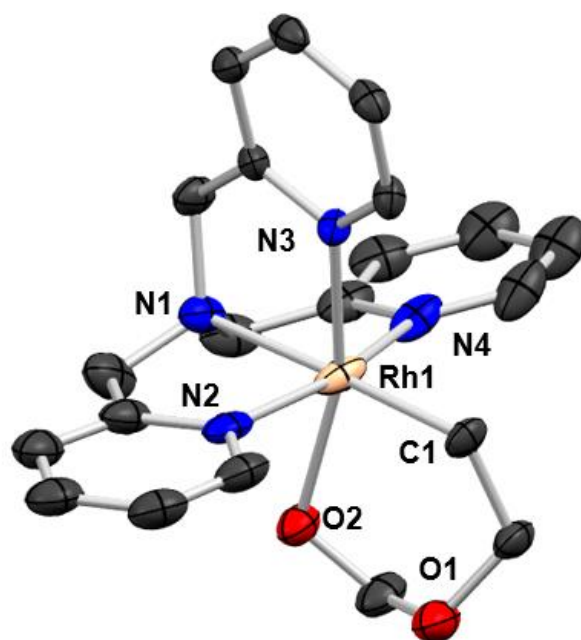


**Figure 2.6** ORTEP (50% probability ellipsoids) of **2.27**[BAr<sup>F</sup><sub>4</sub>]. H atoms, BAr<sup>F</sup><sub>4</sub> counterion and 0.5 C<sub>6</sub>H<sub>14</sub> solvates omitted for clarity.

Complex **1.33** was also found to react with substituted aldehydes, although lower temperatures and longer reaction times were required for clean formation of [**2.28-2.32**]<sup>+</sup> (Table 2.1). Both aliphatic aldehydes and electron-poor aromatic aldehydes underwent insertion, while more electron-rich aromatic aldehydes only gave trace products. The insertion of aldehydes into rhodium-alkoxide bonds has been reported by Hartwig<sup>136, 137</sup> and invoked by Tejel;<sup>138</sup> likewise, the insertion of benzaldehyde into a stannaoxetane is also known.<sup>139</sup>

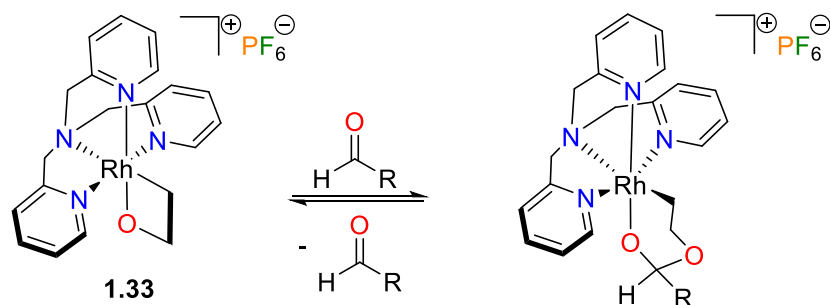


**Table 2.1** Scope of aldehyde insertion into **1.33**

Compound	R	Temp.	Time	% Yield <sup>c</sup>
2.27	H	rt	30 min <sup>a</sup>	98
2.28	Me	-20 °C	17 h <sup>b</sup>	81
2.29	Et	-20 °C	19 h <sup>b</sup>	82
2.30	<sup>i</sup> Pr	-20 °C	45 h <sup>b</sup>	80
2.31	<i>p</i> -NO <sub>2</sub> C <sub>6</sub> H <sub>4</sub>	rt	18 h <sup>b</sup>	85
2.32	C <sub>6</sub> F <sub>5</sub>	-20 °C	17 h <sup>b</sup>	63

<sup>a</sup> Time required for **1.33** to be consumed in the presence of 5 equiv of aldehyde <sup>b</sup> Time required for **1.33** to be consumed in the presence of 3 equiv of aldehyde <sup>c</sup> NMR yields based on comparison to 1,3,5-trimethoxybenzene as internal standard.

The incorporation of the acetal functionality into **2.27-2.32** is supported by the <sup>13</sup>C NMR shifts of **C3**, which lie between 95 and 110 ppm, typical for that functional group. The incorporation of a substituent at **C3** disrupts the symmetry of the complex, as all three of the TPA arms are rendered inequivalent. In addition, each of the protons of the RhCH<sub>2</sub>CH<sub>2</sub>O fragment become diastereotopic; with their own unique set of signals which are characteristic of **2.28-2.32** (Figure 2.7). **H2a** appears as an apparent doublet of triplets that is deshielded relative to **H2b**, which appears as a doublet of doublets of doublets.

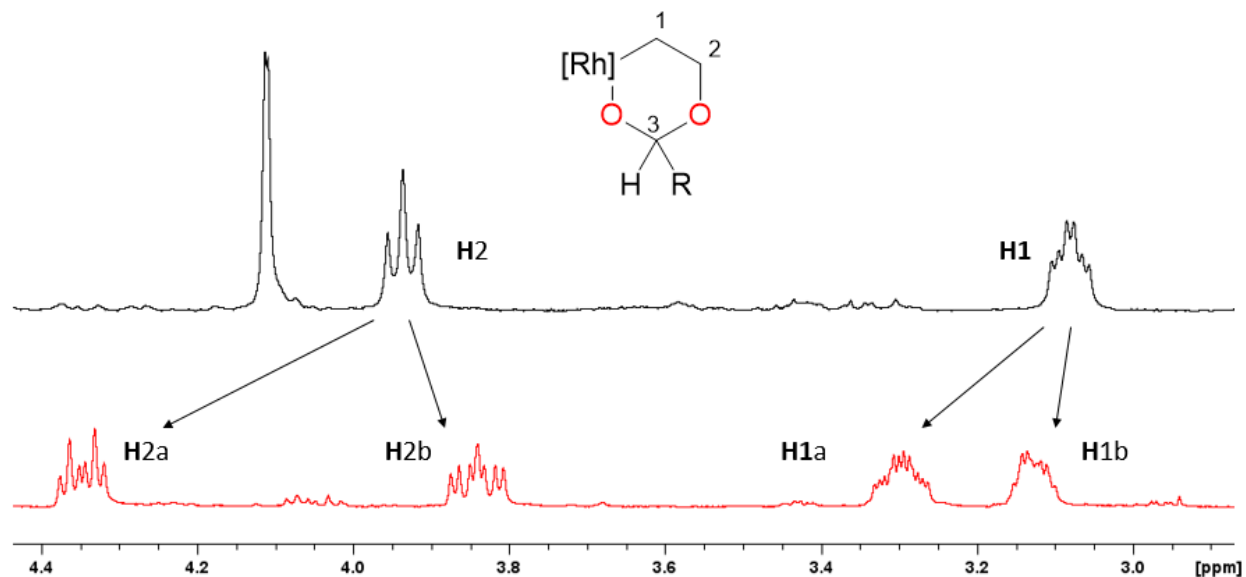
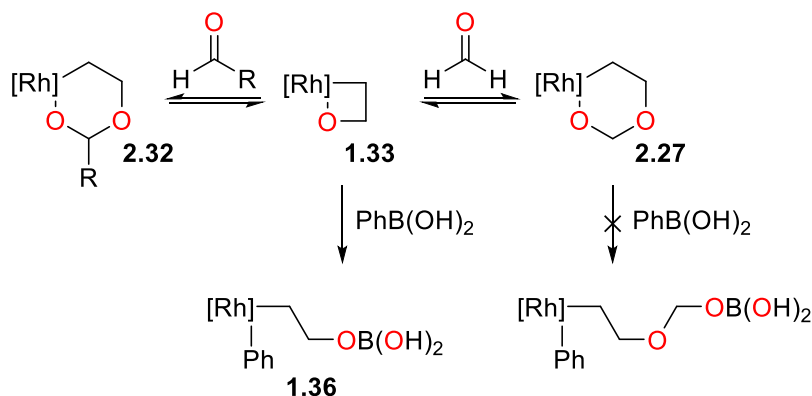


**Figure 2.7** Region of the  $^1\text{H}$  NMR spectra of **2.27** (above,  $\text{R} = \text{H}$ ) and **2.32** (below,  $\text{R} = \text{C}_6\text{F}_5$ ) showing the resonances of the  $\text{RhCH}_2\text{CH}_2\text{O}$  group

The chemical shift of the **H3** resonances are quite sensitive to the electronic nature of the  $\text{R}$  group, as it ranges from 3.47 ppm for complex **2.30** ( $\text{R} = \text{iPr}$ ) to 5.02 ppm for complex **2.31** ( $\text{R} = p\text{-NO}_2\text{C}_6\text{H}_4$ ). The relative configuration of the protons in the metallacycle could be assigned using a 2D NOESY experiment and were found to adopt a gauche orientation. The two Me groups of **2.30** are diastereotopic with unique signals in the  $^1\text{H}$  and  $^{13}\text{C}$  NMR spectra.

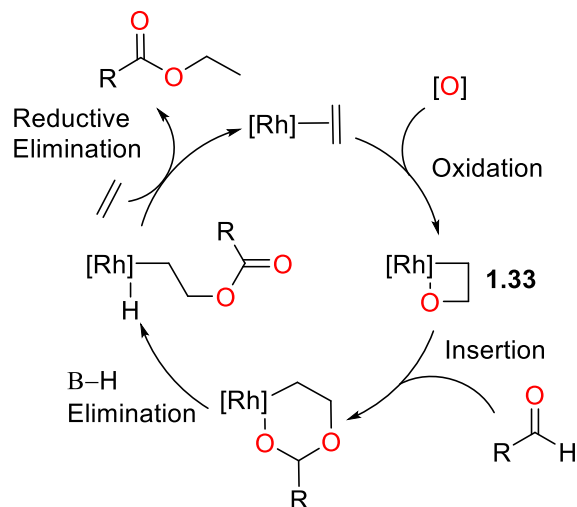
It is noteworthy that the insertion of aldehydes into the  $\text{Rh-O}$  bond of **1.33** was found to be reversible and dependent on the solvent. For example, **2.27** in  $\text{CD}_2\text{Cl}_2$  or acetone- $\text{d}_6$  was found to be stable for weeks at room temperature, but removal of the solvent *in vacuo* followed by extraction of the residue with MeOD showed only **2.27** after 10 minutes, but an approximately equimolar amount of **2.27** and **1.33** after 22 hours. NMR spectroscopy samples of substituted complexes **2.28-2.32** were also found to release their respective aldehydes on standing in  $\text{CD}_2\text{Cl}_2$ , and addition of an eight-fold excess of  $\text{C}_6\text{F}_5\text{CHO}$  to **2.27** in acetone- $\text{d}_6$  caused complete conversion

of **2.27** to **2.32** after 21 hours. This is consistent with extrusion of formaldehyde from **2.27** to regenerate **1.33**, which subsequently undergoes insertion of  $C_6F_5CHO$  to form **2.32** (see Scheme 2.15). In addition, attempts to transmetalate **2.27** with  $PhB(OH)_2$  resulted in the clean formation of **1.36** consistent with our previous report on the conversion of rhodaoxetane **1.33** to complex **1.36**. This is also consistent with regeneration of **1.33** from **2.27**, followed by transmetalation to yield **1.36**. We believe that aldehyde elimination proceeds by heterolysis of the Rh-O bond, and thus, the hydrogen bonding ability of the solvent plays an important role in these reactions, likely stabilizing zwitterionic intermediates.



**Scheme 2.15** Reversibility of aldehyde insertion into **1.33** and attempted transmetalation of **2.27**.  $[Rh] = (TPA)Rh^+$ ,  $R = C_6F_5$ .

The expanded metallacycles of **2.27-2.32** possess a  $\beta$ -H derived from the aldehyde moiety. Thus, analogous to the Heck reaction, we envisioned a process whereby elimination of this hydride, followed by reductive elimination, would result in the oxidative coupling of an aldehyde and ethylene. Coordination of another equivalent of ethylene would then be expected to close the catalytic cycle (Scheme 2.16). Related metallacycles of nickel have been shown to undergo C-O reductive elimination or  $\beta$ -hydride elimination when exposed to either oxidants or higher temperatures, respectively.<sup>73</sup>



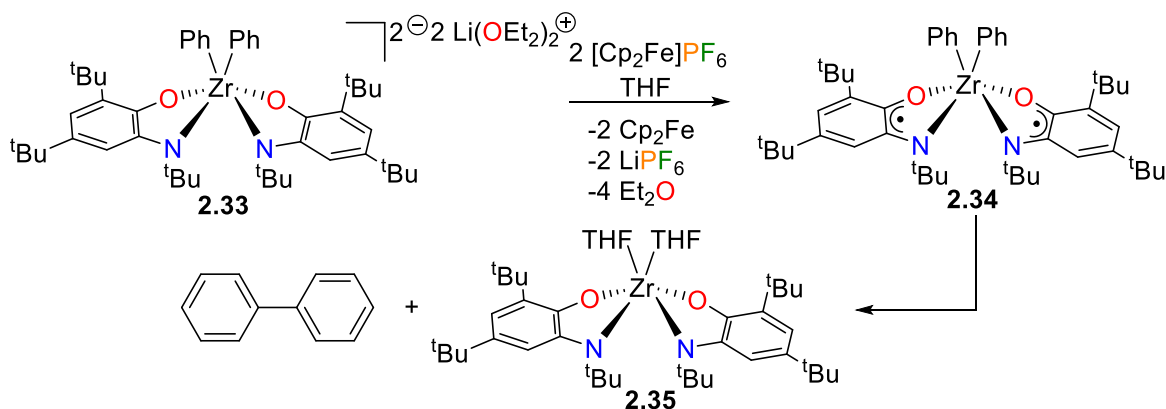
**Scheme 2.16** Proposed mechanism for oxidative coupling of aldehydes and ethylene. [Rh] = (TPA)Rh<sup>+</sup>

Initial reactivity studies of **2.27** have found that it decomposes slowly in the presence of oxidants such as Br<sub>2</sub>, H<sub>2</sub>O<sub>2</sub> and AgOTf, typically yielding mixtures that contain acetaldehyde and formaldehyde. Similar results are obtained upon heating **2.27** at 55 °C in acetone-d<sub>6</sub> over several days. Attempted photolysis of **2.27** under short-wave UV light for several days was also ineffective at inducing clean reactivity from the complex.

## 2.5 Spectroscopic Analysis of Rhodium Oxidation States

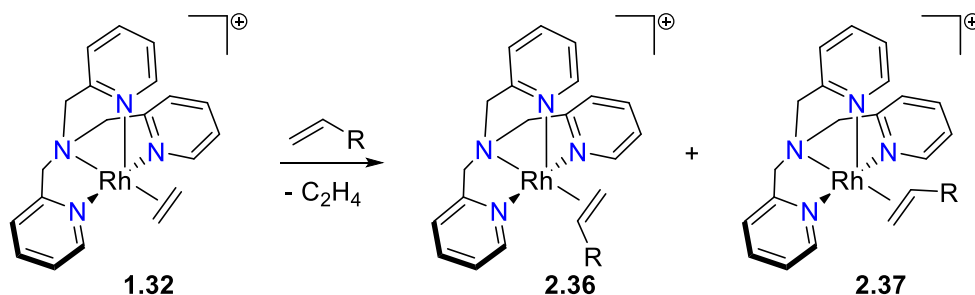
Recently, the chemistry of organometallic complexes with redox-active ligands has undergone tremendous growth,<sup>140-143</sup> in no small part because these ligands can enable “non-classical” reactivity from both base<sup>144</sup>-and noble-metal<sup>145</sup> complexes. This approach of using the ligand manifold as an “electron reservoir” is utilized in nature to great effect.<sup>146</sup> For instance, the metalloenzyme galactose oxidase uses a single copper ion in conjunction with a modified tyrosinyl ligand to perform the 2-electron oxidation of alcohols to aldehydes.<sup>147</sup> In a recent synthetic example, Heyduk has reported that zirconium(IV) complexes outfitted with aminophenolate ligands such as **2.33** can be oxidized with chlorine to form ligand-based biradical complexes<sup>148</sup> or

ferrocenium to induce C-C reductive elimination from intermediate **2.34**, resulting in the formation of biphenyl and **2.35** (Scheme 2.17).<sup>149</sup>



**Scheme 2.17** Heyduk's oxidatively-induced C-C reductive elimination from zirconium(IV)

Prior work in the Love group found that the ethylene ligand of complex **1.32** can be exchanged for substituted olefins (Scheme 2.18),<sup>150</sup> resulting in the formation of two isomers: **2.36**, in which the R group is proximal to the apical pyridyl arm of the TPA ligand, and **2.37**, in which the R group is distal to the pyridyl arm.



**Scheme 2.18** Synthesis of olefin complexes **2.36** and **2.37**.

Curiously, we noted that although isomers **2.36** and **2.37** show exchange peaks in their 2D NOESY spectra with free olefin, they do not show exchange peaks with each other. We proposed that this was due to a dissociative mechanism of olefin binding to rhodium. Thus, **2.36** and **2.37** can interconvert *via* olefin dissociation and re-coordination, but cannot interconvert through

simple rotation of the bound olefin. These results prompted us, in collaboration with the Kennepohl group at the University of British Columbia (UBC), to probe the nature of the metal-olefin bond in greater detail through a combination of computational and spectroscopic studies on the parent ethylene complex **1.32**.

NMR spectroscopy, in particular coupling constants, have frequently been used to determine the oxidation states of transition metal complexes.<sup>151</sup> The coupling constants of the ethylene carbons resonances of **1.32** ( $\delta = 25.0$  ppm, d,  $^1J_{\text{Rh,C}} = 19.7$  Hz and  $\delta = 27.2$  ppm, d,  $^1J_{\text{Rh,C}} = 18.0$  Hz)<sup>32</sup> are remarkably large for well-defined ethylene complexes of rhodium,<sup>152-154</sup> and are actually very similar to that for rhodaoxetane **1.33** ( $\delta = 1.3$  ppm, d,  $^1J_{\text{Rh,C}} = 18.4$  Hz).<sup>32</sup> This points towards a metallacyclopropane description of the metal-olefin bonding in **1.32**. To unambiguously assign the oxidation state of rhodium in **1.32**, we turned to X-ray absorption spectroscopy (XAS), which is effective in elucidating the spectroscopic oxidation state of transition metals.<sup>155-159</sup> Solid-state rhodium K-edge XAS data reveal only small differences in the near-edge spectra between **1.32** and **2.27** (Figure 2.8). Both the shape and energy of the near-edge spectra are almost identical, suggesting that there is little to no difference in electronics at the metal centre. As such, the spectroscopic oxidation states of these two complexes are the same. For comparison, we note that the rhodium K-edge XAS spectrum for Cramer's dimer (**1.31**) shows a significantly lower energy onset to ionization. From the first derivative of the edge spectra, the ionization energy is approximately 3eV lower for **1.31** as compared to both **1.32** and **2.27**. These differences are similar to those observed in analogous rhodium-dioxygen complexes, where rhodium K-edge XAS data can distinguish between rhodium(I)-(dioxygen) and rhodium(III)-(peroxo) species.<sup>160, 161</sup>

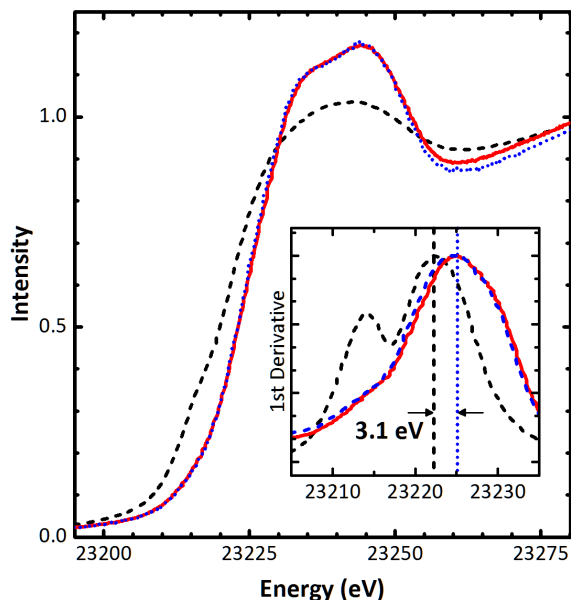
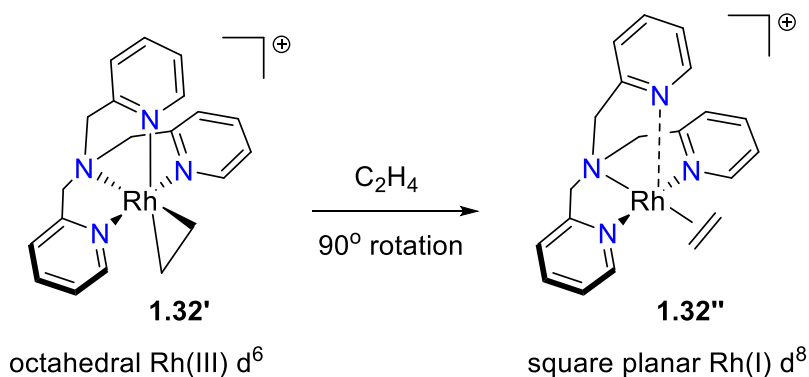


**Figure 2.8** Rh K-edge XAS data for complexes **1.31** (---), **1.32** (·····), and **2.27** (—). The inset shows the first derivative of the XAS data near the edge.

To further probe the electronic structure of **1.32**, we undertook a density functional theory (DFT) investigation of olefin binding in this system.<sup>162</sup> A relaxed coordinate scan indicated that rotation of the ethylene ligand at the metal centre is *highly* unfavourable, with a calculated energy barrier of nearly 100 kJ/mol. Rotation of the ligand is accompanied by a marked decrease in the ethylene C-C bond distance ( $\approx 0.6$  Å) and concomitant increase in the bond distance to one of the pyridyl arms. Intriguingly, ethylene rotation leads to significant electronic and geometric reorganization (**1.32''**) which suggests that formation of a square planar rhodium(I)  $d^8$  adduct occurs during ligand rotation (Scheme 2.19).

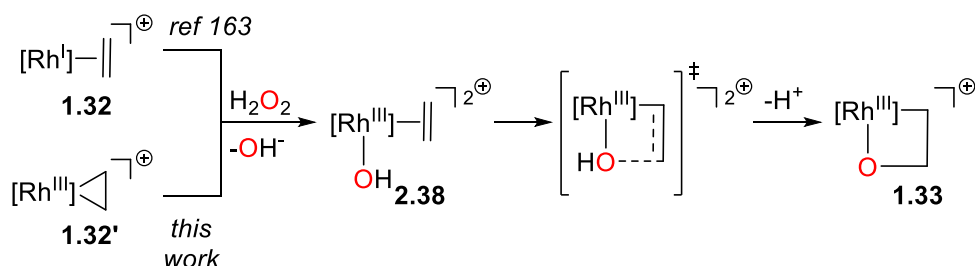


**Scheme 2.19** Proposed structural and electronic changes that occur during rotation of the ethylene ligand in **1.32''**.

Based on these results, it became apparent that complex **1.32** is best described as a rhoda(III)cyclopropane (**1.32'**, Scheme 2.19) that is electronically more similar to the rhoda(III)oxetane **1.33** and rhoda(III)acetal **2.27** than weakly bound ethylene adducts such as **1.31**. This characterization is consistent with the inability of **2.36** and **2.37** to interconvert by bond rotation of the alkene ligand.

The predominantly metallacyclopropane-like electronic structure of **1.32'** should have significant implications with regards to the reactivity of such species, including the mechanism of formation of **1.33** from **1.32**. This mechanism was investigated computationally by Budzelaar and Blok in 2004.<sup>163</sup> As originally formulated,  $\text{H}_2\text{O}_2$  oxidizes the rhodium centre from rhodium(I) to rhodium(III), which allows for internal nucleophilic attack from a bound hydroxo ligand to the olefin adduct (Scheme 2.20). Complex **1.33** arises from cyclization of the rhodium-hydroxyl intermediate **2.38** with the bound olefin, generating the final metallaoxetane product following deprotonation. However, given that the metal centre is already oxidized to rhodium(III) (**1.32'**, *vide supra*), the peroxide-initiated redox chemistry must be *ligand-centered*<sup>164</sup> rather than metal-centered. As expected, the calculated ethylene C-C bond distance in the rhodium(III) hydroxo intermediate (**2.38**) first identified by Budzelaar is extremely short ( $\approx 1.35 \text{ \AA}$ ) and the ethylene

fragment adopts a nearly planar geometry. The changes observed upon oxidation of **1.32'** are predominantly associated with *formal oxidation of the X<sub>2</sub>-type C<sub>2</sub>H<sub>4</sub> group* to form a rhodium(III)-ethylene adduct where the ethylene is now an L-type ligand; the peroxide oxidation does little to change the electron density at the metal centre. The primary role of the peroxide is thus to activate the ethylene ligand for nucleophilic attack *via* ligand oxidation. Consistent with this formulation, the DFT-calculated barrier to rotation of the ethylene ligand in intermediate **2.38** is less than 10 kJ/mol, which is an order of magnitude lower than that calculated for complex **1.32'**. Scheme 2.20 outlines the reaction of **1.32'** with H<sub>2</sub>O<sub>2</sub> to form intermediate **2.38** and rhodaoxetane **1.33**.



**Scheme 2.20** Revised mechanism of formation of rhodaoxetane **1.33**. [Rh] = (TPA)Rh<sup>+</sup>

## 2.6 Summary

In conclusion, we have demonstrated that rhodaoxetane **1.33** is capable of reacting cleanly with a variety of unsaturated molecules *via* insertion into the Rh-O bond. The resulting six-membered metallacycles display a wide range of stabilities. In the case of aldehydes, insertion was found to be reversible. Although we envisioned a new catalytic cycle that would oxidatively couple olefins and aldehydes, we were unable to induce the necessary  $\beta$ -hydride elimination step from the rhodaacetal complexes arising from aldehyde insertion. Characterization of these complexes was performed using primarily NMR spectroscopy and mass spectrometry. In addition, through collaboration with the Kennepohl group at UBC, we have re-examined the electronic structure of rhodium-

ethylene complex **1.32**, and found *via* rhodium K-edge XAS data that the complex is more accurately described as a rhoda(III)cyclopropane. Thus, the oxidation of complex **1.32** with H<sub>2</sub>O<sub>2</sub> that leads to the formation of rhodaoxetane **1.33** is more accurately described as a *ligand-centred* oxidation rather than a *metal-centred* oxidation, as had been previously described in the literature.

## 2.7 Experimental

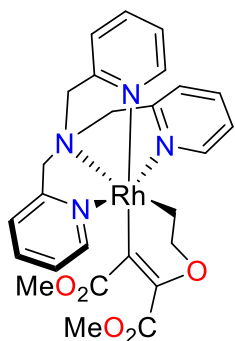
**General Considerations:** All reactions were carried out under nitrogen using standard Schlenk techniques. All reagents were used as received from commercial suppliers with no further purification. Tris(2-pyridylmethyl)amine was prepared by a slight modification of the literature procedure<sup>165</sup> and recrystallized from boiling petroleum ether (bp 35-60 °C) to give bright yellow flakes. Rhodaoxetane **1.33**,<sup>32</sup> NaBAR<sub>4</sub><sup>F</sup><sup>166</sup> and ethyl 3-phenylpropiolate<sup>167</sup> were prepared according to the literature procedures. The counteranion for all cationic rhodium complexes reported here was PF<sub>6</sub> unless otherwise stated. NMR yields are averaged over at least two separate reactions and were determined by referencing well-resolved product signals versus the aryl protons of 1,3,5-trimethoxybenzene or the methyl protons of acetophenone as an internal standard. The relaxation delay for quantitative <sup>1</sup>H NMR spectroscopic experiments was set to at least 5 times the longest T<sub>1</sub> present. Room temperature corresponds to ~25 °C. See Appendix A for detailed crystallographic data.

NMR spectra were recorded on Bruker Avance 300 and 400 MHz spectrometers and are referenced to residual protio solvent (5.32 ppm for CD<sub>2</sub>Cl<sub>2</sub>, 2.05 ppm for acetone-d<sub>6</sub>, and 3.31 ppm for MeOD) for <sup>1</sup>H NMR, solvent peaks (53.84 ppm for CD<sub>2</sub>Cl<sub>2</sub>, 29.84 ppm for acetone-d<sub>6</sub> and 49.00 ppm for MeOD) for <sup>13</sup>C NMR and 1-fluoro-3-nitrobenzene (-112.0 ppm) for <sup>19</sup>F NMR. Mass

spectrometry data were recorded on a Waters LC/MS for low resolution and a Waters/Micromass LCT for high resolution.

## II. Organometallic Syntheses

### Synthesis of 2.13



To a suspension of **1.33** (19.7 mg, 0.034 mmol, 1.0 equiv) in dichloromethane (5 mL) was added dimethylacetylene dicarboxylate (4.2  $\mu$ L, 1.0 equiv). The resulting pale yellow slurry was stirred at room temperature for 1 hour, during which time the solution became homogeneous and darker yellow. To this solution was added Et<sub>2</sub>O (15 mL), which caused the precipitation of a fine, white solid. The supernatant was decanted, the residue was washed with hexanes and dried *in vacuo* to give 14.6 mg (60 % yield) of **2.13**.

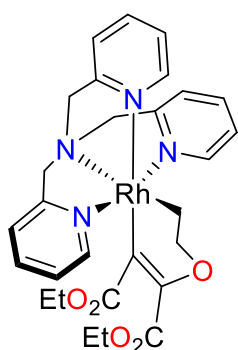
<sup>1</sup>H NMR (400 MHz, CD<sub>2</sub>Cl<sub>2</sub>)  $\delta$ . 8.73 (d,  $J_{\text{H,H}} = 5.5$  Hz, 1H), 8.30 (d,  $J_{\text{H,H}} = 5.6$  Hz, 2H), 7.76-7.69 (m, 3H), 7.40-7.32 (m, 4H), 7.21 (t,  $J_{\text{H,H}} = 6.5$  Hz, 2H), 5.90 (d[AB],  $^2J_{\text{H,H}} = 16.3$  Hz, 2H), 4.76 (d[AB],  $^2J_{\text{H,H}} = 16.3$  Hz, 2H) 4.69 (s, 2H), 4.02 (t,  $J_{\text{H,H}} = 7.4$  Hz, 2H), 3.55 (s, 3H), 3.14 (dt,  $^3J_{\text{H,H}} = 7.4$  Hz,  $^2J_{\text{Rh,H}} = 2.8$  Hz, 2H), 3.12 (s, 3H).

<sup>13</sup>C{<sup>1</sup>H} NMR (100 MHz, CD<sub>2</sub>Cl<sub>2</sub>)  $\delta$  177.5 (s), 165.1 (s), 161.7 (s), 160.5 (s), 151.5 (s), 149.1 (s), 147.8 (s), 141.9 (d,  $^1J_{\text{Rh,C}} = 34.4$  Hz), 139.5 (s), 139.0 (s), 125.4 (s), 124.8 (s), 123.8 (s), 122.8 (s),

72.7 (s), 68.9 (s), 66.0 (s), 51.9 (s), 29.4 (d,  $^1J_{\text{Rh,C}} = 27.1$  Hz). An HSQC experiment showed that the resonance for one of the Me groups was overlapping with the solvent signal.

HRMS (ESI) Calcd: 579.1115 ( $\text{C}_{26}\text{H}_{28}\text{N}_4\text{O}_5\text{Rh}^+$ ). Found 579.1110.

### Synthesis of 2.14



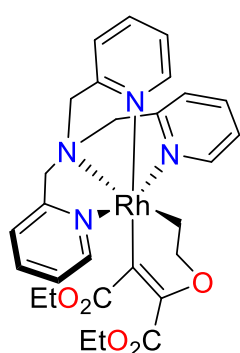
To a suspension of **1.33** (19.8 mg, 0.034 mmol) in dichloromethane (5 mL) was added diethylacetylene dicarboxylate (5.5  $\mu\text{L}$ , 1.0 equiv). The resulting slurry was stirred at room temperature for 1 hour, during which time the solution became homogeneous and darker yellow. To this solution was added  $\text{Et}_2\text{O}$  (15 mL), which caused the precipitation of a fine, white solid. The supernatant was decanted, the residue was washed with hexanes and dried *in vacuo* to give 11.8 mg (46 % yield) of **2.14**.

$^1\text{H}$  NMR (400 MHz,  $\text{CD}_2\text{Cl}_2$ )  $\delta$  8.73 (d,  $J_{\text{H,H}} = 5.7$  Hz, 1H), 8.32 (d,  $J_{\text{H,H}} = 5.8$  Hz, 2H), 7.75-7.68 (m, 3H), 7.40-7.31 (m, 4H), 7.21 (t,  $J_{\text{H,H}} = 6.7$  Hz, 2H), 5.96 (d[AB],  $^2J_{\text{H,H}} = 16.3$  Hz, 2H), 4.74 (d[AB],  $^2J_{\text{H,H}} = 16.3$  Hz, 2H), 4.68 (s, 2H), 4.03 (t,  $J_{\text{H,H}} = 7.4$  Hz, 2H), 3.99 (q,  $J_{\text{H,H}} = 7.3$  Hz, 2H), 3.59 (q,  $J_{\text{H,H}} = 7.3$  Hz, 2H), 3.13 (dt,  $^3J_{\text{H,H}} = 7.3$  Hz,  $^2J_{\text{Rh,H}} = 2.9$  Hz, 2H), 1.16 (t,  $^3J_{\text{H,H}} = 7.1$  Hz, 3H), 0.76 (t,  $^3J_{\text{H,H}} = 7.2$  Hz, 3H).

$^{13}\text{C}\{^1\text{H}\}$  NMR (100 MHz,  $\text{CD}_2\text{Cl}_2$ )  $\delta$ . 177.4 (s), 165.1 (s), 161.2 (s), 160.5 (s), 151.6 (s), 149.3 (s), 147.8 (s), 141.5 ppm (d,  $^1J_{\text{Rh,C}} = 34.5$  Hz), 139.4 (s), 138.9 (s), 125.3 (s), 124.8 (s), 123.9 (s), 122.7 (s), 72.5 (s), 68.8 (s), 65.9 (s), 61.0 (s), 60.9 (s), 29.4 (d,  $^1J_{\text{Rh,C}} = 26.7$  Hz), 14.4 (s), 13.8 (s).

HRMS (ESI) Calcd: 607.1428 ( $\text{C}_{28}\text{H}_{32}\text{N}_4\text{O}_5\text{Rh}^+$ ). Found 607.1436.

### Synthesis of **2.14**[ $\text{BAr}^{\text{F}}_4$ ]



Cramer's dimer,  $[\text{Rh}(\text{Cl})(\text{C}_2\text{H}_4)_2]_2$  (34.8 mg, 0.090 mmol, 0.5

equiv) and TPA (52.8 mg, 0.18 mmol, 1.0 equiv) were placed in

a round bottom flask and the mixture was then cooled in a  $-78$

$^{\circ}\text{C}$  bath. The flask was evacuated and backfilled with nitrogen

gas three times. Sparged dichloromethane (2 mL) was added, and

the suspension was stirred at  $-78$   $^{\circ}\text{C}$  for 1 hour. The acetone/dry ice bath was then replaced with

an ice/brine bath, and subsequently 30 % aqueous  $\text{H}_2\text{O}_2$  (40  $\mu\text{L}$ , 0.35 mmol, 2.0 equiv) was added

to the reaction mixture, which quickly developed a red-brown residue. After stirring for 1 hour,

the pale yellow supernatant was decanted and the residue was dried *in vacuo* before  $\text{NaBAr}^{\text{F}}_4$

(164.9 mg, 0.19 mmol, 1.0 equiv) and dichloromethane (2 mL) was added. After stirring this

orange-yellow solution for 20 minutes, diethylacetylene dicarboxylate (40  $\mu\text{L}$ , 0.25 mmol, 1.4

equiv) was added, causing a colour change to dark brown after a few minutes. The reaction was

stirred for an additional hour, then was filtered through celite, which stranded a dark residue on

the pad and gave an amber filtrate which was evaporated to dryness. Recrystallization of the solid

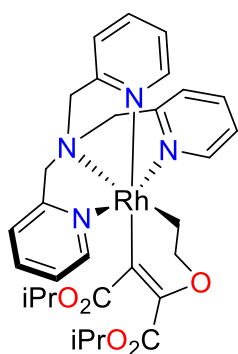
residue from slow evaporation of a 2:1 DCM/hexanes solution gave 41.3 mg of **2.14**[ $\text{BAr}^{\text{F}}_4$ ] (15

% yield) as X-ray quality crystals. Despite washing the crystals with hexanes,  $^1\text{H}$  and  $^{13}\text{C}$  NMR spectroscopy show residual diethylacetylene dicarboxylate.

$^1\text{H}$  NMR (400 MHz,  $\text{CD}_2\text{Cl}_2$ )  $\delta$  8.75 (d,  $J_{\text{H,H}} = 5.4$  Hz, 1H), 8.33 (d,  $J_{\text{H,H}} = 5.6$  Hz, 2H), 7.78 (broad s, 8H), 7.72 (dt,  $^3J_{\text{H,H}} = 7.8$  Hz,  $^4J_{\text{H,H}} = 1.4$  Hz, 2H), 7.66 (dt,  $^3J_{\text{H,H}} = 7.9$  Hz,  $^4J_{\text{H,H}} = 1.5$  Hz, 1H), 7.55 (broad s, 4H), 7.34 (t,  $J_{\text{H,H}} = 6.4$  Hz, 1H), 7.29 (d,  $J_{\text{H,H}} = 7.8$  Hz, 2H), 7.26-7.18 (m, 3H), 6.11 (d[AB],  $^2J_{\text{H,H}} = 16.2$  Hz, 2H), 4.55 (d[AB],  $^2J_{\text{H,H}} = 16.2$  Hz, 2H), 4.51 (s, 2H), 4.03 (t,  $J_{\text{H,H}} = 7.2$  Hz, 2H), 4.00 (q,  $J_{\text{H,H}} = 7.2$  Hz, 2H), 3.55 (q,  $J_{\text{H,H}} = 7.2$  Hz, 2H), 3.17 (dt,  $^3J_{\text{H,H}} = 7.2$ ,  $^2J_{\text{Rh,H}} = 2.9$  Hz, 2H), 1.16 (t,  $J_{\text{H,H}} = 7.1$  Hz, 3H), 0.75 (t,  $J_{\text{H,H}} = 7.2$  Hz, 3H).

$^{13}\text{C}\{^1\text{H}\}$  NMR (100 MHz,  $\text{CD}_2\text{Cl}_2$ )  $\delta$  177.6 (s), 164.4 (s), 162.1 (q,  $^1J_{\text{B,C}} = 49.9$  Hz), 161.2 (s), 159.4 (s), 152.0 (s), 149.8 (s), 148.3 (s), 139.5 (s), 139.1 (s), 135.2 (broad s), 129.2 (q,  $^2J_{\text{C,F}} = 32.3$  Hz), 125.8 (s), 125.1 (s), 125.0 (q,  $^1J_{\text{C,F}} = 270.0$  Hz), 123.5 (s), 122.2 (s), 117.9 (m), 72.5 (s), 69.2 (s), 66.1 (s), 61.1 (s), 61.0 (s), 29.8 (d,  $^1J_{\text{Rh,C}} = 27.6$  Hz), 14.4 (s), 13.7 (s). The resonance due to C4 could not be observed, probably due to coupling to  $^{103}\text{Rh}$  and the low intensity of quaternary carbon signals. The resonance may also be overlapping with signals from the  $\text{BARF}_4$  anion.

### Synthesis of 2.15



To a solution of **[3]PF<sub>6</sub>** (0.028 mmol) in 0.5 mL of  $\text{CD}_2\text{Cl}_2$  in an NMR tube was added a solution of diisopropylacetylene dicarboxylate (6.0 mg, 0.030 mmol) in 0.25 mL  $\text{CD}_2\text{Cl}_2$ . The tube was inverted three times to thoroughly mix the contents, then left to stand at room temperature overnight.  $^1\text{H}$  NMR and MS analysis

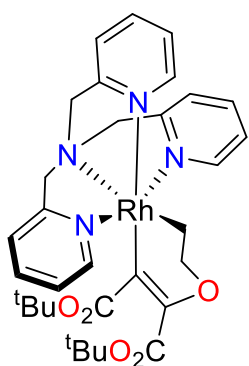
showed the formation of **[7]PF<sub>6</sub>** as well as other unidentified byproducts. The presence of these

impurities allowed for only partial assignment of the  $^1\text{H}$  NMR data, as the aromatic region contained many overlapping peaks.

$^1\text{H}$  NMR (400 MHz,  $\text{CD}_2\text{Cl}_2$ ):  $\delta$  8.71 (d,  $J_{\text{H,H}} = 5.5$  Hz, 1H), 8.32 (d,  $J_{\text{H,H}} = 6.0$  Hz, 2H), 6.10 (d[AB],  $^2J_{\text{H,H}} = 16.1$  Hz, 2H), 4.82 (sept,  $J_{\text{H,H}} = 6.3$  Hz, 1H), 4.71 (d[AB],  $^2J_{\text{H,H}} = 16.1$  Hz, 2H), 4.65 (s, 2H), 4.59 (sept,  $J_{\text{H,H}} = 6.2$  Hz, 1H), 4.03 (t,  $J_{\text{H,H}} = 7.1$  Hz, 2H), 3.13 (dt,  $^3J_{\text{H,H}} = 7.1$  Hz,  $^2J_{\text{Rh,H}} = 2.8$  Hz, 2H), 1.15 (d,  $J_{\text{H,H}} = 6.3$  Hz, 6H), 0.74 (d,  $J_{\text{H,H}} = 6.3$  Hz, 6H).

HRMS (ESI) Calcd: 635.1741 ( $\text{C}_{28}\text{H}_{32}\text{N}_4\text{O}_5\text{Rh}^+$ ). Found 635.1747.

### Synthesis of 2.16



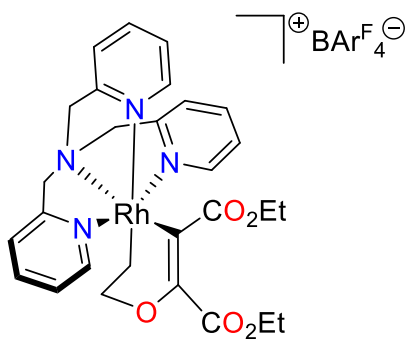
To a solution of **[3]PF<sub>6</sub>** (0.039 mmol) in 0.5 mL of  $\text{CD}_2\text{Cl}_2$  in an NMR tube was added a solution of di-tert-butylacetylene dicarboxylate (8.6 mg, 0.038 mmol) in 0.25 mL  $\text{CD}_2\text{Cl}_2$ . The tube was inverted three times to thoroughly mix the contents, then left to stand at room temperature overnight.  $^1\text{H}$  NMR and MS analysis

showed the formation of **[8]PF<sub>6</sub>** as well as other unidentified byproducts. The presence of these impurities allowed for only partial assignment of the  $^1\text{H}$  NMR data, as the aromatic region contained many overlapping peaks.

$^1\text{H}$  NMR (400 MHz,  $\text{CD}_2\text{Cl}_2$ )  $\delta$  8.56 (d,  $J_{\text{H,H}} = 5.6$  Hz, 1H), 8.32 (d,  $J_{\text{H,H}} = 5.9$  Hz, 2H), 6.20 (d[AB],  $^2J_{\text{H,H}} = 16.0$  Hz, 2H), 4.67 (d[AB],  $^2J_{\text{H,H}} = 16.0$  Hz, 2H), 4.59 (s, 2H), 3.99 (t,  $J_{\text{H,H}} = 7.6$  Hz, 2H), 3.08 (dt,  $^3J_{\text{H,H}} = 7.4$  Hz,  $^3J_{\text{Rh,H}} = 3.0$  Hz, 2H), 1.22 (s, 9H), 0.97 (s, 9H).

LRMS (ESI) 663.3 ( $\text{C}_{32}\text{H}_{40}\text{N}_4\text{O}_5\text{Rh}^+$ ).

### Synthesis of **2.20**[ $\text{BAr}^{\text{F}}_4$ ]



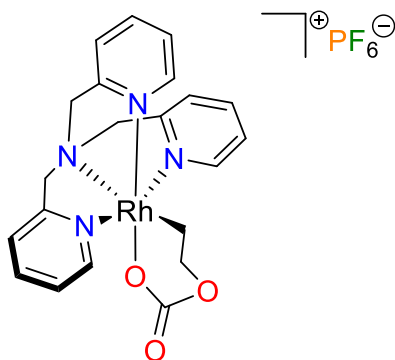
A screw-cap NMR tube was charged with **2.14**[ $\text{BAr}^{\text{F}}_4$ ] in 0.6 mL of acetone- $d_6$ . The tube was placed in an oil bath set to 55 °C and was monitored periodically by  $^1\text{H}$  NMR spectroscopy. After 22 hours, the spectrum showed the major component to be **2.20**[ $\text{BAr}^{\text{F}}_4$ ], while the minor component was unreacted **2.14**[ $\text{BAr}^{\text{F}}_4$ ]. After 36 hours, **2.14**[ $\text{BAr}^{\text{F}}_4$ ] had been completely consumed.

$^1\text{H}$  NMR (400 MHz, acetone- $d_6$ )  $\delta$  8.83 (d,  $J_{\text{H,H}} = 5.5$  Hz, 2H), 8.77 (d,  $J_{\text{H,H}} = 5.6$  Hz, 1H), 7.92 (dt,  $^3J_{\text{H,H}} = 6.2$  Hz,  $^4J_{\text{H,H}} = 1.7$  Hz, 2H), 7.82-7.76 (m, 9H), 7.69-7.65 (m, 4H), 7.57 (d,  $J_{\text{H,H}} = 5.7$  Hz, 2H), 7.50-7.39 (m, 4H), 5.44 (d[AB],  $^2J_{\text{H,H}} = 16.3$  Hz, 2H), 5.03 (d[AB],  $^2J_{\text{H,H}} = 16.7$  Hz, 2H), 4.86 (s, 2H), 4.43 (q,  $J_{\text{H,H}} = 7.2$  Hz, 2H), 4.22 (q,  $J_{\text{H,H}} = 7.1$  Hz, 2H), 3.35-3.27 (m, 2H), 2.56-2.50 (m, 2H), 1.33 (t,  $J_{\text{H,H}} = 7.2$  Hz, 3H), 1.31 (t,  $J_{\text{H,H}} = 7.2$  Hz, 3H).

$^{13}\text{C}\{^1\text{H}\}$  NMR (100 MHz, acetone- $d_6$ )  $\delta$  177.4 (s), 164.6 (s), 162.6 (q,  $^1J_{\text{B,C}} = 49.9$  Hz) 158.9 (s), 154.8 (s), 150.4 (s), 147.9 (s), 139.4 (s), 135.5 (br s), 130.0 (m), 126.1 (s), 125.3 (q,  $^1J_{\text{C,F}} = 270$  Hz), 125.3 (s), 124.6 (s), 123.4 (s), 118.5 (m), 69.4 (s), 69.3 (s), 66.9 (s), 61.0 (s), 60.7 (s), 23.3 (s), 14.7 (s), 14.5 (s). Three of the four quaternary carbon signals of the metallacycle could not be located, probably due to the typical low intensity of quaternary carbon signals or overlap with resonances from the  $\text{BAr}^{\text{F}}_4$  anion.

LRMS (ESI) 607.1 ( $\text{C}_{28}\text{H}_{32}\text{N}_4\text{O}_5\text{Rh}^+$ ).

### Synthesis of 2.21



To a sample of **1.33** in 0.6 mL of  $\text{CD}_2\text{Cl}_2$  in a J-Young NMR tube was added a small chip of dry ice. After an initial burst of gas, the tube was sealed and left to stand overnight at room temperature. After releasing the pressure the following morning, the solution was analyzed by  $^1\text{H}$  NMR and MS and found to be a mixture of **2.21** and **2.18**. Subsequent attempts to prepare **2.21**

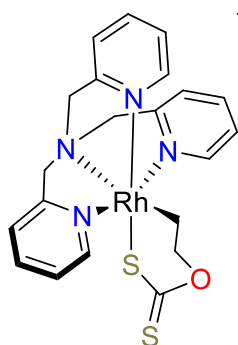
by stirring **1.33** under 1 or 4 atmospheres of  $\text{CO}_2$ , as well as using MeOD as the solvent resulted in a lower yield of **2.21** by  $^1\text{H}$  NMR analysis. As a result of the presence of **2.18**, not all of the peaks in the aromatic region could be assigned with confidence.

$^1\text{H}$  NMR (400 MHz,  $\text{CD}_2\text{Cl}_2$ )  $\delta$  8.54 (d,  $J_{\text{H,H}} = 5.4$  Hz, 1H), 8.49 (d,  $J_{\text{H,H}} = 5.4$  Hz, 2H), 7.87 (dt,  $^3J_{\text{H,H}} = 7.8$  Hz,  $^4J_{\text{H,H}} = 1.4$  Hz, 2H), 7.67 (dt,  $^3J_{\text{H,H}} = 7.9$ ,  $^4J_{\text{H,H}} = 1.6$  Hz, 1H), 7.57 (d,  $J_{\text{H,H}} = 7.8$  Hz, 2H), 7.51 (d,  $J_{\text{H,H}} = 7.8$  Hz, 1H), 7.38 (t,  $J_{\text{H,H}} = 7.1$  Hz, 1H), 7.28 (t,  $J_{\text{H,H}} = 7.3$  Hz, 2H), 5.64

(d[AB],  $^2J_{\text{H,H}} = 15.4$  Hz, 2H), 5.09 (d[AB],  $^2J_{\text{H,H}} = 15.5$  Hz, 2H), 5.05 (s, 2H), 4.08 (t,  $J_{\text{H,H}} = 5.5$  Hz, 2H), 3.42-3.37 (m, 2H).

HRMS (ESI) Calcd: 481.0747 ( $\text{C}_{21}\text{H}_{22}\text{N}_4\text{O}_3\text{Rh}^+$ ). Found 481.0742.

### Synthesis of 2.22



In a Wilmad screw-cap NMR tube, a solution of **1.33** (5.0 mg, 0.0086 mmol) in  $\text{CD}_2\text{Cl}_2$  (0.6 mL) was chilled to  $-78$  °C. An excess of  $\text{CS}_2$  (1.0  $\mu\text{L}$ , 1.8 equiv) was added *via* microsyringe, the tube was inverted three times to thoroughly mix and the solution was left to slowly warm to room temperature over the course of 12 hours,

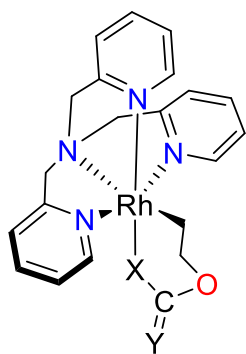
giving compound **2.22** in 76% yield by  $^1\text{H}$  NMR spectroscopy, as well as other minor TPA-containing impurities. Compound **2.22** was found to decompose in solution at room temperature over ~5 days but was stable for 3 weeks when stored at  $-20$  °C.

$^1\text{H}$  NMR (400 MHz,  $\text{CD}_2\text{Cl}_2$ )  $\delta$  8.67 (d,  $J_{\text{H,H}} = 5.7$  Hz, 1H), 8.33 (d,  $J_{\text{H,H}} = 5.6$  Hz, 2H), 7.82 (dt,  $^3J_{\text{H,H}} = 5.6\text{Hz}$ ,  $^4J_{\text{H,H}} = 1.4$  Hz, 2H), 7.72 (dt,  $^3J_{\text{H,H}} = 7.8$  Hz,  $^4J_{\text{H,H}} = 1.4$  Hz, 1H), 7.52 (d,  $J_{\text{H,H}} = 7.8$  Hz, 2H), 7.38-7.28 (m, 4H), 5.36 (d[AB],  $^2J_{\text{H,H}} = 15.8$  Hz, 2H), 5.05 (d[AB],  $^2J_{\text{H,H}} = 15.8$  Hz, 2H), 4.95 (s, 2H), 4.60 (m, 2H), 3.30 (m, 2H).

$^{13}\text{C}\{^1\text{H}\}$  NMR (100 MHz,  $\text{CD}_2\text{Cl}_2$ )  $\delta$  223.7 (s), 164.0 (s), 162.2 (s), 150.0 (s), 147.8 (s), 140.0 (s), 139.8 (s), 126.4 (s), 125.9 (s), 125.0 (s), 123.0 (s), 78.8 (s), 67.7 (s), 66.8 (s), 33.3 (d,  $^1J_{\text{Rh,C}} = 26.3$  Hz).

HRMS (ESI) Calcd: 513.0290 ( $\text{C}_{21}\text{H}_{22}\text{N}_4\text{OS}_2\text{Rh}^+$ ). Found 513.0302.

### Reaction of **1.33** with MeNCS



X = S, Y = NMe **2.23**  
X = NMe, Y = S **2.24**

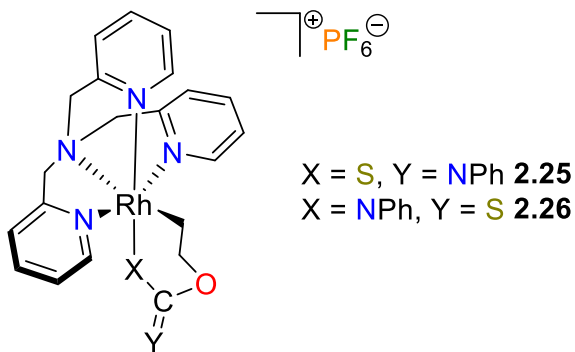
To a solution of **1.33** (0.014 mmol) in  $\text{CD}_2\text{Cl}_2$  (0.6 mL) was added an excess of MeNCS (1.9  $\mu\text{L}$ , 0.029 mmol), and the tube was inverted three times to mix the contents. The tube was then stored in a freezer at  $-20\text{ }^\circ\text{C}$  overnight.  $^1\text{H}$  NMR analysis showed a mixture of what are tentatively assigned

as **2.23** and **2.24** in a ratio of 2.3 : 1. The  $^1\text{H}$  NMR spectra of each could only be partially assigned due to many overlapping peaks.

**2.23**:  $^1\text{H}$  NMR (400 MHz,  $\text{CD}_2\text{Cl}_2$ )  $\delta$  8.69 (d,  $J = 5.8$  Hz, 1H), 5.52 (d[AB],  $^2J = 16.1$  Hz, 2H), 5.19 (d[AB],  $^2J = 16.3$  Hz, 2H), 4.80 (s, 2H), 4.08 (t,  $J = 6.8$  Hz, 2H), 3.55 (dt,  $^3J_{\text{H,H}} = 6.8$  Hz,  $^2J_{\text{Rh,H}} = 2.7$  Hz, 2H), 2.88 (s, 3H).

**2.24:**  $^1\text{H}$  NMR (400 MHz,  $\text{CD}_2\text{Cl}_2$ )  $\delta$  8.65 (d,  $J = 5.6$  Hz, 1H), 5.50 (d[AB],  $^2J = 15.4$  Hz, 2H), 5.04 (d[AB],  $^2J = 15.5$  Hz, 2H), 4.96 (s, 2H), 4.44 (t,  $J = 5.4$  Hz, 2H), 3.10-3.04 (m, 2H), 2.54 (s, 3H).

### Reaction of **1.33** with PhNCS

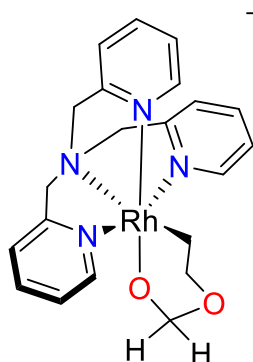


To a solution of **1.33** (0.017 mmol) in  $\text{CD}_2\text{Cl}_2$  (0.6 mL) was added PhNCS (2.0  $\mu\text{L}$ , 0.017 mmol), and the tube was inverted three times to mix the contents. After 30 minutes at room temperature, the solution had developed a pale yellow precipitate, and  $^1\text{H}$  NMR analysis showed a mixture of what are tentatively assigned as **2.25** and **2.26** in a ratio of 1.1 : 1. The  $^1\text{H}$  NMR spectra of each could only be partially assigned due to many overlapping resonances.

**2.25:**  $^1\text{H}$  NMR (400 MHz,  $\text{CD}_2\text{Cl}_2$ )  $\delta$  8.78 (d,  $J_{\text{H,H}} = 5.9$  Hz, 1H), 8.54 (d,  $J_{\text{H,H}} = 5.6$  Hz, 2H), 6.53 (d,  $J_{\text{H,H}} = 7.6$  Hz, 2H), 4.34 (t,  $J_{\text{H,H}} = 6.5$  Hz, 2H), 3.73 (dt,  $^3J_{\text{H,H}} = 6.4$  Hz,  $^2J_{\text{Rh,H}} = 2.7$  Hz, 2H).

**2.26:**  $^1\text{H}$  NMR (400 MHz,  $\text{CD}_2\text{Cl}_2$ )  $\delta$  8.64 (d,  $J_{\text{H,H}} = 5.9$  Hz, 1H), 8.45 (d,  $J_{\text{H,H}} = 5.6$  Hz, 2H), 5.90 (d,  $J_{\text{H,H}} = 7.6$  Hz, 2H), 4.57 (t,  $J_{\text{H,H}} = 5.6$  Hz, 2H), 3.15-3.10 (m, 2H).

## Synthesis of 2.27



To a solution of **1.33** (25.5 mg, 0.044 mmol) in dichloromethane (5 mL) was added an excess of paraformaldehyde (8.0 mg, 6.1 equiv). The resulting slurry was stirred at room temperature for 1 hour before being filtered through celite. To this yellow filtrate was added Et<sub>2</sub>O (15 mL), which caused the precipitation of a fine, white solid. The very pale yellow supernatant was

decanted, and the residue was dried *in vacuo* to give 15.9 mg (59 % yield) of **2.27**.

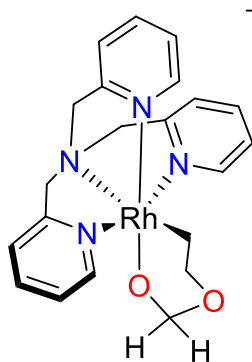
<sup>1</sup>H NMR (400 MHz, CD<sub>2</sub>Cl<sub>2</sub>) δ 8.54 (d, *J*<sub>H,H</sub> = 5.8 Hz, 1H), 8.47 (d, *J*<sub>H,H</sub> = 5.4 Hz, 2H), 7.79 (dt, <sup>3</sup>*J*<sub>H,H</sub> = 7.8, <sup>4</sup>*J*<sub>H,H</sub> = 1.5 Hz, 2H), 7.61 (dt, <sup>3</sup>*J*<sub>H,H</sub> = 7.9, <sup>4</sup>*J* = 1.3 Hz, 1H), 7.48 (d, *J*<sub>H,H</sub> = 8.0 Hz, 2H), 7.30 (t, *J*<sub>H,H</sub> = 6.4 Hz, 2H), 7.25-7.22 (m, 2H), 5.52 (d[AB], <sup>2</sup>*J*<sub>H,H</sub> = 14.9 Hz, 2H), 4.91 (s, 2H), 4.87 (d[AB], <sup>2</sup>*J*<sub>H,H</sub> = 14.9 Hz, 2H), 4.10 (d, <sup>3</sup>*J*<sub>Rh,H</sub> = 1.1 Hz, 2H), 3.93 (t, *J*<sub>H,H</sub> = 5.9 Hz, 2H), 3.07 (dt, <sup>3</sup>*J*<sub>H,H</sub> = 5.9, <sup>2</sup>*J*<sub>Rh,H</sub> = 2.7 Hz, 2H).

<sup>1</sup>H NMR (400 MHz, acetone-d<sub>6</sub>) δ 8.74 (d, *J*<sub>H,H</sub> = 5.4 Hz, 1H), 8.68 (d, *J*<sub>H,H</sub> = 5.5 Hz, 2H), 7.93 (dt, <sup>3</sup>*J*<sub>H,H</sub> = 7.9, <sup>4</sup>*J* = 1.3 Hz, 2H), 7.74 (dt, <sup>3</sup>*J*<sub>H,H</sub> = 7.9, <sup>4</sup>*J*<sub>H,H</sub> = 1.3 Hz, 1H), 7.64 (d, *J*<sub>H,H</sub> = 7.8 Hz, 2H), 7.43 (t, *J*<sub>H,H</sub> = 6.5 Hz, 2H), 7.40 (t, *J*<sub>H,H</sub> = 6.6 Hz, 1H), 7.31 (d, *J*<sub>H,H</sub> = 7.8 Hz, 1H), 5.56 (d[AB], <sup>2</sup>*J*<sub>H,H</sub> = 14.9 Hz, 2H), 5.16 (s, 2H), 5.06 (d[AB], <sup>2</sup>*J*<sub>H,H</sub> = 14.9 Hz, 2H), 4.13 (d, <sup>3</sup>*J*<sub>Rh,H</sub> = 1.1 Hz, 2H), 3.89 (t, *J*<sub>H,H</sub> = 5.9 Hz, 2H), 3.15 (dt, <sup>3</sup>*J*<sub>H,H</sub> = 5.9, <sup>2</sup>*J*<sub>Rh,H</sub> = 2.7 Hz, 2H).

$^{13}\text{C}\{^1\text{H}\}$  NMR (100 MHz,  $\text{CD}_2\text{Cl}_2$ )  $\delta$  164.8 (s), 163.6 (s), 151.1 (s), 148.9 (s), 139.5 (s), 138.7 (s), 125.5 (s), 125.2 (s), 124.5 (s), 122.5 (s), 95.9 (s), 69.7 (s), 66.1 (s), 65.1 (s), 28.4 (d,  $^1J_{\text{Rh,C}} = 27.7$  Hz).

HRMS (ESI) Calcd: 467.0954 ( $\text{C}_{21}\text{H}_{24}\text{N}_4\text{O}_2\text{Rh}^+$ ). Found 467.0956.

### Synthesis of **2.27**[ $\text{BAr}^{\text{F}}_4$ ]



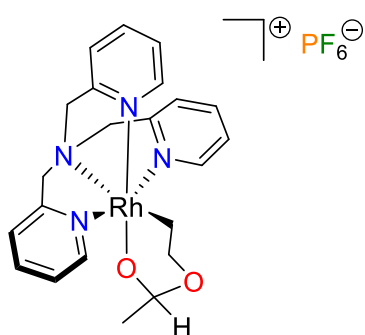
Cramer's dimer  $[\text{Rh}(\text{Cl})(\text{C}_2\text{H}_4)_2]_2$  (20.8 mg, 0.053 mmol) and TPA (31.2 mg, 0.11 mmol) were combined in a 2 mL screw-cap reaction vial, which was flushed with  $\text{N}_2$  and then chilled to  $-78^\circ\text{C}$ . Sparged dichloromethane (2 mL) was added, and the slurry was stirred for 1 hour. The acetone/dry ice bath was then replaced with a brine/ice bath, and 30% aqueous  $\text{H}_2\text{O}_2$  (24  $\mu\text{L}$ , 0.21 mmol) was added. The reaction mixture immediately faded in colour from orange-yellow to pale yellow and developed a brown precipitate. The mixture stirred for 1 hour, after which the pale yellow supernatant was decanted and the residue was dried *in vacuo*.  $\text{NaBAr}^{\text{F}}_4$  (93.3 mg, 0.11 mmol) was then added in dichloromethane (2 mL). After stirring for 20 minutes, an excess of paraformaldehyde (14.0 mg, 0.47 mmol) was added, and the slurry was stirred for 1 hour. The reaction mixture was then filtered through celite and taken to dryness *in vacuo* to yield a yellow oil. Recrystallization of this oil from a ~3:1 mixture of hexanes/dichloromethane at  $-20^\circ\text{C}$  afforded X-ray quality crystals of **2.27**[ $\text{BAr}^{\text{F}}_4$ ].

### General preparation of substituted rhodaacetals

To a solution of **1.33** in 0.6 mL of  $\text{CD}_2\text{Cl}_2$  in a Wilmad screw-cap NMR tube was added 3 equiv of the appropriate aldehyde. The tube was inverted three times to thoroughly mix the contents

before being stored at the appropriate temperature (reactions at -20 °C were stored in a freezer at that temperature). The reaction was monitored periodically by <sup>1</sup>H NMR spectroscopy until complete consumption of **1.33** was observed. Excess aldehyde from complexes **2.28-2.30** could be removed by pumping the solution to dryness *in vacuo* and redissolving the residue in dichloromethane or acetone.

### Synthesis of 2.28



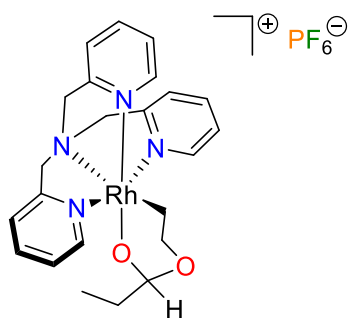
The title compound was prepared using the general method above with 1.0 μL of acetaldehyde and a reaction time of 17 hours at -20 °C. NMR yield: 81%.

<sup>1</sup>H NMR (400 MHz, CD<sub>2</sub>Cl<sub>2</sub>) δ. 8.55-8.50 (m, 2H), 8.45 (d, *J*<sub>H,H</sub> = 5.5 Hz, 1H), 7.80 (dt, <sup>3</sup>*J*<sub>H,H</sub> = 7.9 Hz, <sup>4</sup>*J*<sub>H,H</sub> = 1.6 Hz, 1H), 7.76 (dt, <sup>3</sup>*J*<sub>H,H</sub> = 7.7 Hz, <sup>4</sup>*J*<sub>H,H</sub> = 1.5 Hz, 1H), 7.59 (dt, <sup>3</sup>*J*<sub>H,H</sub> = 7.8 Hz, <sup>4</sup>*J*<sub>H,H</sub> = 1.4 Hz, 1H), 7.49 (d, *J*<sub>H,H</sub> = 7.8 Hz, 1H), 7.44 (d, *J*<sub>H,H</sub> = 7.8 Hz, 1H), 7.31-7.25 (m, 2H), 7.25-7.16 (m, 2H), 5.54 (d[AB], <sup>2</sup>*J*<sub>H,H</sub> = 14.9 Hz, 1H), 5.49 (d[AB], <sup>2</sup>*J*<sub>H,H</sub> = 14.7 Hz, 1H), 4.89 (s, 2H), 4.86 (d[AB], <sup>2</sup>*J*<sub>H,H</sub> = 14.9 Hz, 1H), 4.82 (d[AB], <sup>2</sup>*J*<sub>H,H</sub> = 14.8 Hz, 1H), 4.11 (q, *J*<sub>H,H</sub> = 4.9 Hz, 1H), 4.07 (apparent dt, <sup>2</sup>*J*<sub>H,H</sub> ≈ <sup>3</sup>*J*<sub>H,H</sub> = 12.8 Hz, <sup>3</sup>*J*<sub>H,H</sub> = 4.5 Hz, 1H), 3.65 (ddd, <sup>2</sup>*J*<sub>H,H</sub> = 12.9 Hz, <sup>3</sup>*J*<sub>H,H</sub> = 10.4 Hz, <sup>3</sup>*J*<sub>H,H</sub> = 3.8 Hz, 1H), 3.15-3.08 (m, 1H), 3.03-2.98 (m, 1H), 0.84 (d, *J*<sub>H,H</sub> = 4.9 Hz, 3H).

<sup>13</sup>C{<sup>1</sup>H} NMR (100 MHz, CD<sub>2</sub>Cl<sub>2</sub>) δ 164.8 (s), 164.7 (s), 163.5 (s), 151.5 (s), 150.5 (s), 149.2 (s), 139.3 (s), 139.2 (s), 138.5 (s), 125.6 (s), 125.3 (s), 125.2 (s), 124.4 (s), 124.2 (s), 122.4 (s), 100.0 (s), 68.4 (s), 66.2 (s), 65.9 (s), 64.9 (s), 31.0 (s), 30.2 (d, <sup>1</sup>*J*<sub>Rh,C</sub> = 27.7 Hz).

HRMS (ESI) Calcd. 488.1111 (C<sub>22</sub>H<sub>26</sub>N<sub>4</sub>O<sub>2</sub>Rh<sup>+</sup>). Found 488.1107.

### Synthesis of 2.29



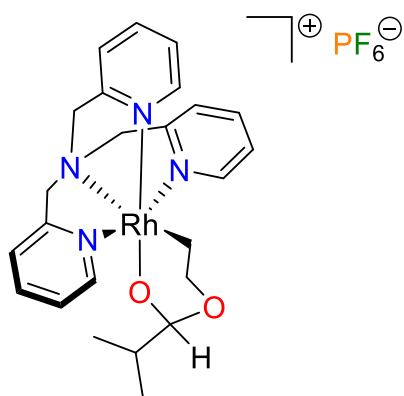
The title compound was prepared using the general method above with 1.2  $\mu$ L of propionaldehyde and a reaction time of 19 hours at -20 °C. NMR yield: 82%.

<sup>1</sup>H NMR (400 MHz, CD<sub>2</sub>Cl<sub>2</sub>)  $\delta$ . 8.55 (d,  $J_{\text{H,H}} = 5.6$  Hz, 1H), 8.50 (d,  $J_{\text{H,H}} = 5.6$  Hz, 1H), 8.45 (d,  $J_{\text{H,H}} = 5.7$  Hz, 1H), 7.80 (dt,  $^3J_{\text{H,H}} = 7.8$  Hz,  $^4J = 1.3$  Hz, 1H), 7.76 (dt,  $^3J_{\text{H,H}} = 7.7$  Hz,  $^4J_{\text{H,H}} = 1.4$  Hz, 1H), 7.59 (dt,  $^3J_{\text{H,H}} = 7.8$  Hz,  $^4J_{\text{H,H}} = 1.4$  Hz, 1H), 7.49 (d,  $J_{\text{H,H}} = 8.0$  Hz, 1H), 7.45 (d,  $J_{\text{H,H}} = 7.9$  Hz, 1H), 7.32 -7.25 (m, 2H), 7.24-7.17 (m, 2H), 5.54 (d[AB],  $^2J_{\text{H,H}} = 15.0$  Hz, 1H), 5.48 (d[AB],  $^2J_{\text{H,H}} = 14.8$  Hz, 1H), 4.91 (s, 2H), 4.88 (d[AB],  $^2J_{\text{H,H}} = 15.0$  Hz, 1H), 4.83 (d[AB],  $^2J_{\text{H,H}} = 14.7$  Hz, 1H), 4.08 (apparent dt,  $J_{\text{H,H}} = 12.7$  Hz,  $J_{\text{H,H}} = 4.6$  Hz, 1H), 3.77 (dd,  $J_{\text{H,H}} = 5.7$  Hz,  $J_{\text{H,H}} = 4.6$  Hz, 1H), 3.67 (ddd,  $^2J_{\text{H,H}} = 13.2$ ,  $^3J_{\text{H,H}} = 10.3$ ,  $^3J_{\text{H,H}} = 3.9$  Hz, 1H), 3.11 (m, 1H), 3.00 (m, 1H), 2.44 (dq,  $J_{\text{H,H}} = 7.4$  Hz,  $J_{\text{H,H}} = 1.4$  Hz, 2H), 1.07 (t,  $J_{\text{H,H}} = 7.4$  Hz, 3H).

<sup>13</sup>C{<sup>1</sup>H} NMR (100 MHz, CD<sub>2</sub>Cl<sub>2</sub>)  $\delta$  164.7 (2 overlapping signals), 163.5 (s), 151.5 (s), 154.4 (s), 149.20 (s), 139.4 (s), 139.2 (s), 138.6 (s), 126.6 (s), 125.3 (s), 125.1 (s), 124.4 (s), 124.2 (s), 122.4 (s), 104.6 (s), 68.6 (s), 66.2 (s), 65.9 (s), 64.9 (s), 31.6 (s), 30.1 (d,  $^1J_{\text{Rh,C}} = 27.7$  Hz), 10.2 (s).

HRMS (ESI) Calcd: 495.1267 (C<sub>23</sub>H<sub>28</sub>N<sub>4</sub>O<sub>2</sub>Rh<sup>+</sup>). Found 495.1250.

## Synthesis of 2.30



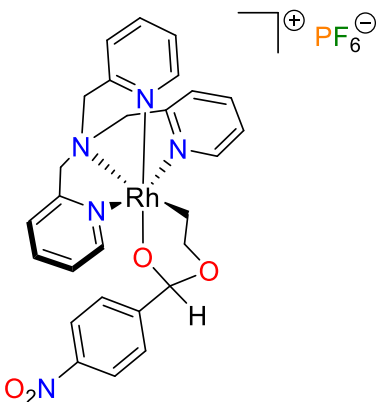
The title compound was prepared using the general method above with 1.5  $\mu\text{L}$  of isobutyraldehyde and a reaction time of 45 hours at  $-20\text{ }^\circ\text{C}$ . NMR yield: 80%.

$^1\text{H}$  NMR (400 MHz,  $\text{CD}_2\text{Cl}_2$ )  $\delta$  8.88 (d,  $J_{\text{H,H}} = 5.7$  Hz, 1H), 8.49 (d,  $J_{\text{H,H}} = 5.5$  Hz, 1H), 8.46 (d,  $J_{\text{H,H}} = 5.5$  Hz, 1H), 7.80 (dt,  $^3J_{\text{H,H}} = 7.9$ ,  $^4J_{\text{H,H}} = 1.4$  Hz, 1H), 7.76 (dt,  $^3J_{\text{H,H}} = 7.7$ ,  $^4J_{\text{H,H}} = 1.3$  Hz, 1H), 7.59 (dt,  $^3J_{\text{H,H}} = 7.8$  Hz,  $^4J_{\text{H,H}} = 1.4$  Hz, 1H), 7.49 (d,  $J_{\text{H,H}} = 7.8$  Hz, 1H), 7.44 (d,  $J_{\text{H,H}} = 8.0$  Hz, 1H), 7.32-7.27 (m, 2H), 7.24-7.18 (m, 2H), 5.51 (d[AB],  $^2J_{\text{H,H}} = 14.7$  Hz, 1H), 5.47 (d[AB],  $^2J_{\text{H,H}} = 14.9$  Hz, 1H), 4.90 (s, 2H), 4.88 (d[AB],  $^2J_{\text{H,H}} = 15.9$  Hz, 1H), 4.84 (d[AB],  $^2J_{\text{H,H}} = 15.2$  Hz, 1H), 4.10 (apparent dt,  $J_{\text{H,H}} = 12.8$  Hz,  $J_{\text{H,H}} = 4.6$  Hz, 1H), 3.67 (ddd,  $J_{\text{H,H}} = 13.3$  Hz,  $J_{\text{H,H}} = 10.1$  Hz,  $J_{\text{H,H}} = 3.8$  Hz, 1H), 3.47 (d,  $J_{\text{H,H}} = 5.6$  Hz, 1H), 3.15-3.08 (m, 1H), 3.02-2.96 (m, 1H), 1.25 (m, 1H), 0.62 (d,  $J_{\text{H,H}} = 6.8$  Hz, 3H), 0.59 (d,  $J_{\text{H,H}} = 6.8$  Hz, 3H).

$^{13}\text{C}\{^1\text{H}\}$  NMR (100 MHz,  $\text{CD}_2\text{Cl}_2$ )  $\delta$  164.8 (s), 164.7 (s), 163.5 (s), 151.5 (s), 150.2 (s), 149.2 (s), 139.3 (s), 139.1 (s), 138.5 (s), 125.6 (s), 125.2 (s), 125.1 (s), 124.3 (s), 124.1 (s), 122.4 (s), 108.1 (s), 69.0 (s), 66.3 (s), 65.9 (s), 65.0 (s), 35.5 (s), 30.3 (d,  $^1J_{\text{Rh,C}} = 27.9$  Hz), 18.9 (s), 18.3 (s).

HRMS (ESI) Calcd: 509.1424 ( $\text{C}_{24}\text{H}_{30}\text{N}_4\text{O}_2\text{Rh}^+$ ). Found 509.1429.

## Synthesis of 2.31



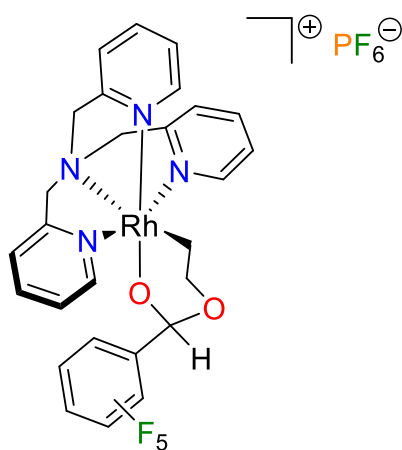
The title compound was prepared using the general method above with 2.4 mg of *p*-nitrobenzaldehyde and a reaction time of 18 hours at room temperature. NMR yield: 85 %.

$^1\text{H}$  NMR (400 MHz,  $\text{CD}_2\text{Cl}_2$ )  $\delta$  8.58-8.53 (m, 3H), 7.95 (d,  $J_{\text{H,H}} = 8.8$  Hz, 2H), 7.83 (dt,  $^3J_{\text{H,H}} = 7.9$  Hz,  $^4J_{\text{H,H}} = 1.5$  Hz, 1H), 7.75 (dt,  $^3J_{\text{H,H}} = 7.9$  Hz,  $^4J_{\text{H,H}} = 1.5$  Hz, 1H), 7.62 (dt,  $^3J_{\text{H,H}} = 7.9$  Hz,  $^4J_{\text{H,H}} = 1.5$  Hz, 1H), 7.53 (d,  $J_{\text{H,H}} = 7.6$  Hz, 1H), 7.38 (d,  $J_{\text{H,H}} = 7.8$  Hz, 1H), 7.34 (t,  $J_{\text{H,H}} = 6.8$  Hz, 1H), 7.32-7.26 (m, 3H), 7.26-7.20 (m, 2H), 5.54 (d[AB],  $^2J_{\text{H,H}} = 15.0$  Hz, 1H), 5.43 (d[AB],  $^2J_{\text{H,H}} = 15.0$  Hz, 1H), 5.02 (s, 1H), 4.97 (d[AB],  $^2J_{\text{H,H}} = 15.0$  Hz, 1H), 4.96 (s, 2H), 4.87 (d[AB],  $^2J_{\text{H,H}} = 14.9$  Hz, 1H), 4.24 (apparent dt,  $J_{\text{H,H}} = 12.8$  Hz,  $J_{\text{H,H}} = 4.3$  Hz, 1H), 3.94 (ddd,  $J_{\text{H,H}} = 12.8$  Hz,  $J_{\text{H,H}} = 10.3$  Hz,  $J_{\text{H,H}} = 4.2$  Hz, 1H), 3.29-3.20 (m, 1H), 3.18-3.11 (m, 1H).

$^{13}\text{C}\{^1\text{H}\}$  NMR (100 MHz,  $\text{CD}_2\text{Cl}_2$ )  $\delta$  164.8 (s), 164.6 (s), 163.6 (s), 152.9 (s), 151.6 (s), 151.2 (s), 150.4 (s), 149.3 (s), 147.1 (s), 139.6 (s), 139.4 (s), 138.8 (s), 127.1 (s), 125.8 (s), 125.4 (s), 125.3 (s), 124.2 (s), 123.1 (s), 122.5 (s), 101.2 (s), 69.1 (s), 66.4 (s), 66.1 (s), 65.0 (s), 30.4 (d,  $^1J_{\text{Rh,C}} = 27.3$  Hz).

HRMS (ESI) Calcd. 588.1118 ( $\text{C}_{27}\text{H}_{27}\text{N}_5\text{O}_4\text{Rh}^+$ ). Found 588.1116.

## Synthesis of 2.32



The title compound was prepared using the general method above with 2.0  $\mu\text{L}$  of pentafluorobenzaldehyde and a reaction time of 17 hours at  $-20\text{ }^\circ\text{C}$ . NMR yield: 63 %.

$^1\text{H}$  NMR (400 MHz,  $\text{CD}_2\text{Cl}_2$ )  $\delta$  8.60-8.51 (m, 3H), 7.85 (dt,  $^3J_{\text{H,H}} = 7.8\text{ Hz}$ ,  $^4J_{\text{H,H}} = 1.5\text{ Hz}$ , 1H), 7.80 (dt,  $^3J_{\text{H,H}} = 7.7\text{ Hz}$ ,  $^4J_{\text{H,H}} = 1.5\text{ Hz}$ , 1H), 7.63 (dt,  $^3J_{\text{H,H}} = 7.8\text{ Hz}$ ,  $^4J_{\text{H,H}} = 1.4\text{ Hz}$ , 1H), 7.53 (d,  $J_{\text{H,H}} = 7.8\text{ Hz}$ , 1H), 7.44 (d,  $J_{\text{H,H}} = 7.9\text{ Hz}$ , 1H), 7.38-7.29 (m 2H), 7.27-7.21 (m, 2H), 5.48 (d[AB],  $^2J_{\text{H,H}} = 14.9\text{ Hz}$ , 1H), 5.36 (d[AB],  $^2J_{\text{H,H}} = 15.1\text{ Hz}$ , 1H), 4.96 (s, 1H), 4.94 (s, 2H), 4.91 (d[AB],  $^2J_{\text{H,H}} = 15.0\text{ Hz}$ , 1H), 4.84 (d[AB],  $^2J_{\text{H,H}} = 14.9\text{ Hz}$ , 1H), 4.32 (apparent dt,  $J_{\text{H,H}} = 12.8\text{ Hz}$ ,  $J_{\text{H,H}} = 4.9\text{ Hz}$ , 1H), 3.81 (ddd,  $J_{\text{H,H}} = 13.4\text{ Hz}$ ,  $J_{\text{H,H}} = 9.8\text{ Hz}$ ,  $J_{\text{H,H}} = 4.2\text{ Hz}$ , 1H), 3.30-3.22 (m, 1H), 3.13-3.06 (m, 1H).

$^{13}\text{C}\{^1\text{H}\}$  NMR (100 MHz,  $\text{CD}_2\text{Cl}_2$ )  $\delta$  165.1 (s), 164.8 (s), 163.7 (s), 151.4 (s), 150.1 (s), 149.2 (s), 139.7 (s), 139.4 (s), 138.8 (s), 125.8 (s), 125.3 (s), 125.2 (s), 124.5 (s), 124.1 (s), 122.6 (s), 97.3 (s), 69.7 (s), 66.4 (s), 66.0 (s), 65.2 (s), 30.1 (d,  $^1J_{\text{Rh,C}} = 27.6\text{ Hz}$ ). The aryl resonances of the  $\text{C}_6\text{F}_5$  ring could not be located, probably due broadening due to  $^{13}\text{C}$ - $^{19}\text{F}$  coupling and the low intensity of quaternary carbon signals.

$^{19}\text{F}\{^1\text{H}\}$  NMR (280 MHz,  $\text{CD}_2\text{Cl}_2$ )  $\delta$  -73.8 (d,  $^1J_{\text{P,F}} = 712\text{ Hz}$ ), -140.7 (m), -151.9 (m), -163.6 (m).

HRMS (ESI) Calcd: 633.0796 (C<sub>27</sub>H<sub>23</sub>N<sub>4</sub>O<sub>2</sub>F<sub>5</sub>Rh<sup>+</sup>). Found 633.0792.

### **X-ray Absorption Spectroscopy**

Data Collection: Rh K-edge XANES spectra were acquired at the hard X-ray microanalysis (HXMA) superconducting wiggler beamline (06ID-1), using a double crystal monochromator including two crystal pairs of Si(111) and Si(220), at the Canadian Light Source (CLS). Powder samples of Rh complexes were sandwiched between Kapton tape and placed inside a Teflon sample holder and positioned in front of X-ray beam. Spectral data were recorded in fluorescence mode using a 32-element Ge detector with simultaneous measurements of Ru reference spectra for energy calibration at 22117 eV. To increase signal to noise ratio, three spectra were acquired for each sample.

Data Processing and Analysis: Rh K-edge XAS data were analysed using SIXpack.<sup>168</sup> All acceptable scans acquired by 32-element Ge detector were averaged and fit to a linear background and subtracted from the entire spectrum and normalized to an edge jump of 1.0.

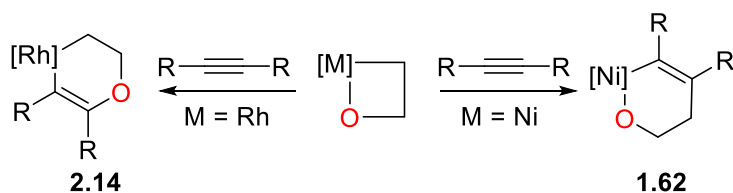
### **Density Functional Theory Calculations**

Initial geometries for all molecules were obtained from crystallographic coordinates (where available) or constructed from standard models. Geometry optimizations and numerical frequency calculations were performed using version 3.0.3 of the ORCA computational chemistry package. Scalar relativistic effects were included using ZORA corrections as implemented in ORCA 3.0.3 using the auxiliary (/J) basis set.<sup>169, 170</sup> Molecular geometries were optimized using the B3LYP functional and all electron basis sets (def2-TZVP) for all atoms. Computational efficiency was improved by applying the RI approximation (RIJCOSX) for the hybrid functional.<sup>171</sup> All calculations were performed with a dense integration grid (ORCA Grid6).

# Chapter 3 : Exploring the Reactivity of Low-Valent Nickel with Three-Membered Oxacycles

## 3.1 Introduction

Our inspiration for the work outlined in this Chapter is twofold; first, we were intrigued by the difference in reactivity between the 2-nickelaoxetane invoked by Jamison<sup>44</sup> and that of the 2-rhodaoxetane observed by us as detailed in Chapter 2. In particular, whereas the 2-rhodaoxetane **1.33** was found to insert alkynes and other electrophiles into the *Rh-O* bond of the metallaioxetane moiety, nickelaoxetane **1.61** (Scheme 3.1, see Chapter 1) was proposed to undergo insertion of alkynes into the *Ni-C* bond.



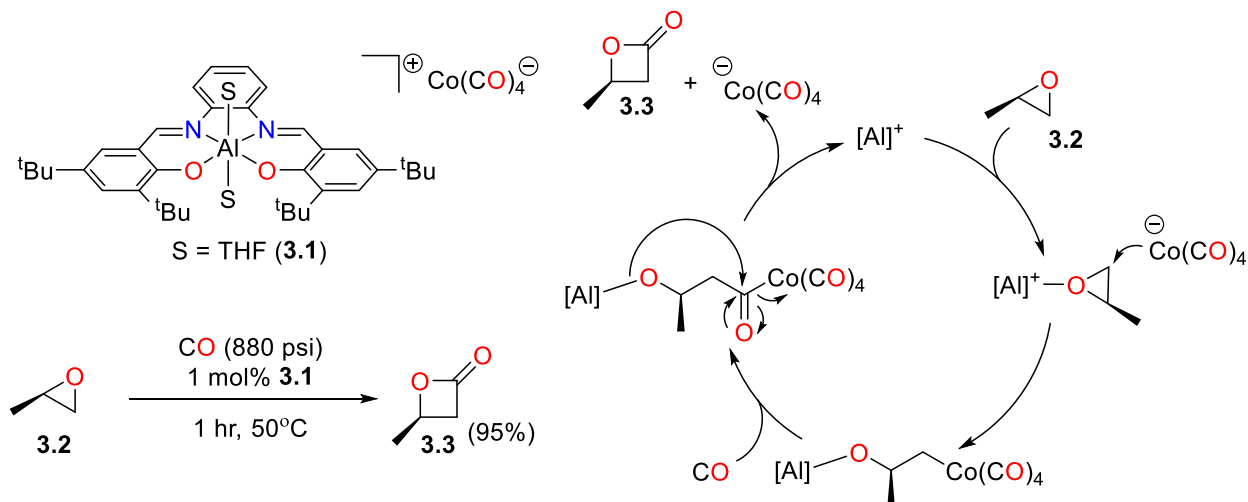
**Scheme 3.1** Contrasting reactivity of 2-metallaioxetanes of nickel and rhodium with alkynes

Our second inspiration was the paucity of well-defined examples of 2-nickelaoxetanes in the literature, despite several groups proposing them as intermediates in a variety of nickel-mediated transformations of epoxides.<sup>14, 43-45, 172</sup> Indeed, before our work in this field, the only reported example of a 2-nickelaoxetane was a complex published by the Hillhouse group where the oxetane moiety was formed *via* reaction of a nickel(II) alkylidene with diphenylketene.<sup>42</sup> During the course of our work here, the same group published another paper that demonstrated that these formal [2+2] cyclizations could also be applied to the reaction of diphenylketene with nickel(II) imido complexes.<sup>78</sup>

Epoxides are valuable chemical feedstocks, owing to the ease of their synthesis from either alkene- or carbonyl-containing precursors and their subsequent tendency to ring-open.<sup>173</sup> Asymmetric protocols like the Sharpless<sup>174</sup> and Jacobsen<sup>175, 176</sup> epoxidations, as well as Jacobsen's hydrolytic kinetic resolution system<sup>177, 178</sup> allow for the ready synthesis and enantioenrichment of a wide array of epoxides, which are powerful intermediates for natural product synthesis.

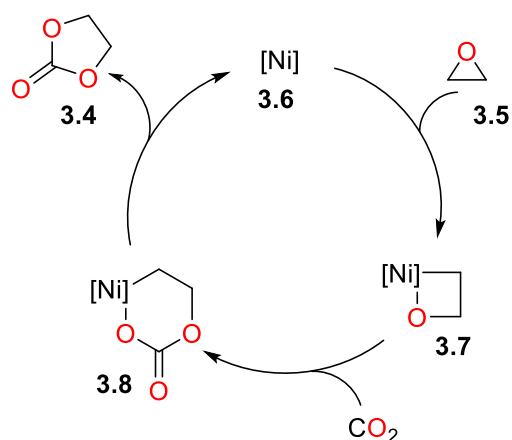
Early work on coupling reactions of epoxides focused on the use of the use of hard, carbon-based nucleophiles such as cyanide, Grignard, and alkyllithium reagents as coupling partners.<sup>179</sup> More recently, the groups of Doyle<sup>43</sup> and Jamison<sup>44</sup> have reported much milder nickel-catalyzed couplings of epoxides with boronic acids and alkynes, respectively (see Chapter 1). Radical coupling reactions of epoxides using both early<sup>180-185</sup> and late<sup>186, 187</sup> transition metals have also been recognized for their synthetic utility.

Epoxide carbonylation is another vibrant field of research, as the lactone products are themselves useful starting materials for the preparation of biodegradable polymers.<sup>188, 189</sup> In a pioneering study, Coates and co-workers demonstrated that an Al/Co system **3.1** can cleanly carbonylate propylene oxide **3.2**, amongst other epoxides, to the corresponding  $\beta$ -lactones such as **3.3**.<sup>190</sup> The proposed mechanism of this carbonylation is outlined in Scheme 3.2. First, coordination of the O atom of the epoxide to the Lewis acidic aluminium activates the three-membered ring towards nucleophilic attack from the cobaltate anion. The ring-opened species can then insert CO, and subsequent ring-closure *via* attack of the alkoxy group at the acyl moiety releases the product ester and regenerates the Lewis acid/Lewis base catalyst pair.



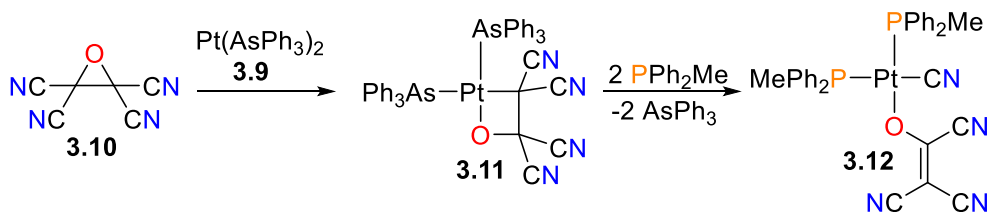
**Scheme 3.2** Coates' carbonylation of epoxides

Similarly, epoxides can also be coupled to  $\text{CO}_2$  to form cyclic carbonates using transition metal catalysis.<sup>191</sup> In 1973, De Pasquale reported that certain nickel(0) complexes with monodentate phosphine ligands could catalyze the formation of ethylene carbonate **3.4** in moderate yield (60%) by heating ethylene oxide **3.5** to 100 °C in benzene in a steel autoclave pressurized with 500 psi of  $\text{CO}_2$ .<sup>14</sup> The proposed mechanism, outlined in Scheme 3.3, features oxidative addition of nickel(0) complex **3.6** into the C-O bond of **3.5**, followed by insertion of  $\text{CO}_2$  into nickelaoxetane **3.7** to form metallacarboxylate **3.8**, which subsequently reductively eliminates **3.4** to regenerate the nickel(0) catalyst. Related oxidative addition steps have also been proposed in other nickel-mediated reactions,<sup>192</sup> including the halogenation of fluorinated epoxides.<sup>172, 193</sup>



**Scheme 3.3** 2-Nickela(II)oxetane **3.7** as a proposed intermediate in catalytic coupling of epoxide **3.5** and CO<sub>2</sub>. [Ni] = Ni(PCy<sub>3</sub>)<sub>2</sub> or Ni(PPh<sub>3</sub>)<sub>2</sub>

Shortly thereafter, data in support of this proposed oxidative addition step was put forth by the Ibers group, who found that a related low-valent Group 10 complex, Pt(AsPh<sub>3</sub>)<sub>2</sub> (**3.9**), could add cleanly to the C-O bond of tetracyanooxirane **3.10** to form a well-defined platinaoxetane **3.11** (Scheme 3.4) that was characterized by X-ray crystallography.<sup>194</sup> It was also found that addition of neutral ligands such as PPh<sub>2</sub>Me resulted in β-migration of a cyano group, forming enolate complex **3.12**.<sup>195</sup>



**Scheme 3.4** Synthesis of complexes **3.11** and **3.12**

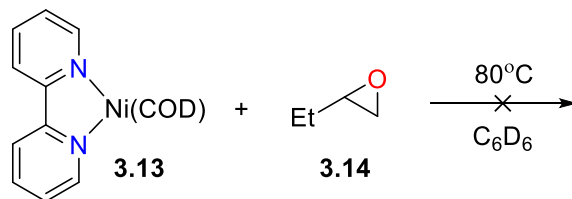
Herein, we describe our efforts to prepare well-defined 2-metalla-oxetanes of nickel formed *via* the oxidative addition of nickel(0) with epoxides, the reactivity of these rare metallacycles, as well as the development of a new protocol for the catalytic hydroboration of epoxides that likely feature

2-nickelaoxetanes as reactive intermediates. Finally, we also discuss the reactivity of nickel(0) with oxaziridines.

## 3.2 Isomerization of Epoxides

Our starting point for this work was to investigate whether well-known nickel(0) complexes would react with simple, commercially available epoxides. For our initial studies, we chose (bpy)Ni(COD) **3.13** as a source of low-valent nickel, given the success the Hillhouse group and others have had utilizing this particular complex for other stoichiometric<sup>63, 196</sup> and catalytic<sup>197</sup> transformations.

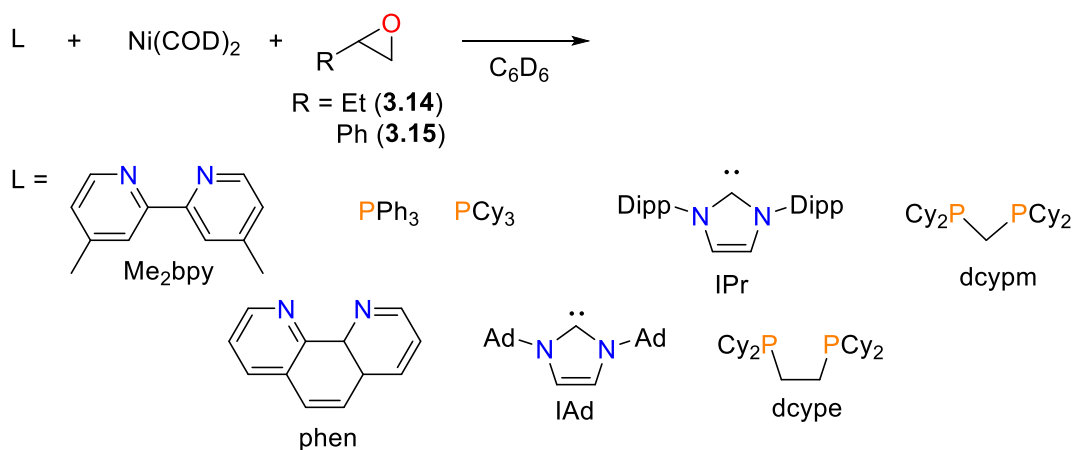
Complex **3.13** did not react with alkyl epoxide **3.14** under a variety of conditions employed, including prolonged refluxing in C<sub>6</sub>D<sub>6</sub> (Scheme 3.5). Attempts to perform “COD-free” reactions<sup>65</sup> (i.e. the *in situ* reduction of (bpy)nickel(II) complexes with manganese or zinc dust) were similarly unsuccessful.



### Scheme 3.5 Reactivity of **3.13** with epoxide **3.14**

Given the lack of reactivity with bpy as an ancillary ligand, we next decided to examine a series of different L or L<sub>2</sub>-type ligands for the nickel centre. We reasoned that a strongly electron-donating ligand would increase the electron density at the metal centre, facilitating oxidative addition into the C-O bond. We also desired a ligand that would contain enough steric bulk to kinetically stabilize a potential four-membered ring against intermolecular decomposition.

Our initial screening of ancillary ligands, shown in Scheme 3.2.2, featured bpy-derivatives such as Me<sub>2</sub>bpy and phen,<sup>65</sup> bulky NHC ligands such as IPr<sup>198</sup> and 1,3-bis(adamantyl)imidazol-2-ylidene (IAd),<sup>199-201</sup> as well as both monodentate phosphines (PPh<sub>3</sub> and PCy<sub>3</sub><sup>202</sup>) and bidentate phosphines with differing bite angles (bis(1,2-dicyclohexylphosphino)ethane (dcype)<sup>203</sup> and dcypm<sup>204, 205</sup>). As a general procedure, we combined either 1 or 2 equivalents of the ancillary ligand with 1 equivalent of Ni(COD)<sub>2</sub>, followed by addition of either alkyl epoxide **3.14** or styrene oxide **3.15** in C<sub>6</sub>D<sub>6</sub> (Scheme 3.6). The reactions were then monitored by NMR spectroscopy.



**Scheme 3.6** Ligand screening for reactivity of nickel(0) with epoxides

Although both the Me<sub>2</sub>bpy and phen reactions with styrene oxide **3.15** changed colour from purple to dark green upon addition of the epoxide, the <sup>1</sup>H NMR spectra of these reactions only contained broad resonances, possibly indicating the presence of paramagnetic species. Both of these reactions rapidly changed colour from dark green to dark brown upon exposure to air, and no tractable products could be subsequently isolated.

More promising were the reactions of 1,2-bis(dicyclohexyl)phosphinoethane (dcype) complexes of nickel with styrene oxide **3.15**, which could be conveniently monitored by <sup>31</sup>P{<sup>1</sup>H}NMR spectroscopy. Room temperature mixing of all three reagents in C<sub>6</sub>D<sub>6</sub>

resulted only in the formation of (dcype)Ni(COD) **3.16**,<sup>112</sup> which resonates as a singlet at 60.4 ppm (Figure 3.1, red trace). Heating the solution at 75 °C in an oil bath for 1.5 hours (blue trace) results in the formation of a new complex which displays an asymmetric coordination environment at the metal centre. While further heating at 75 °C (8 hours, green trace) does consume all of the **3.16**, additional unidentified byproducts are formed. The resonances for the new product are also significantly decreased in intensity, perhaps indicating that the complex is thermally sensitive.

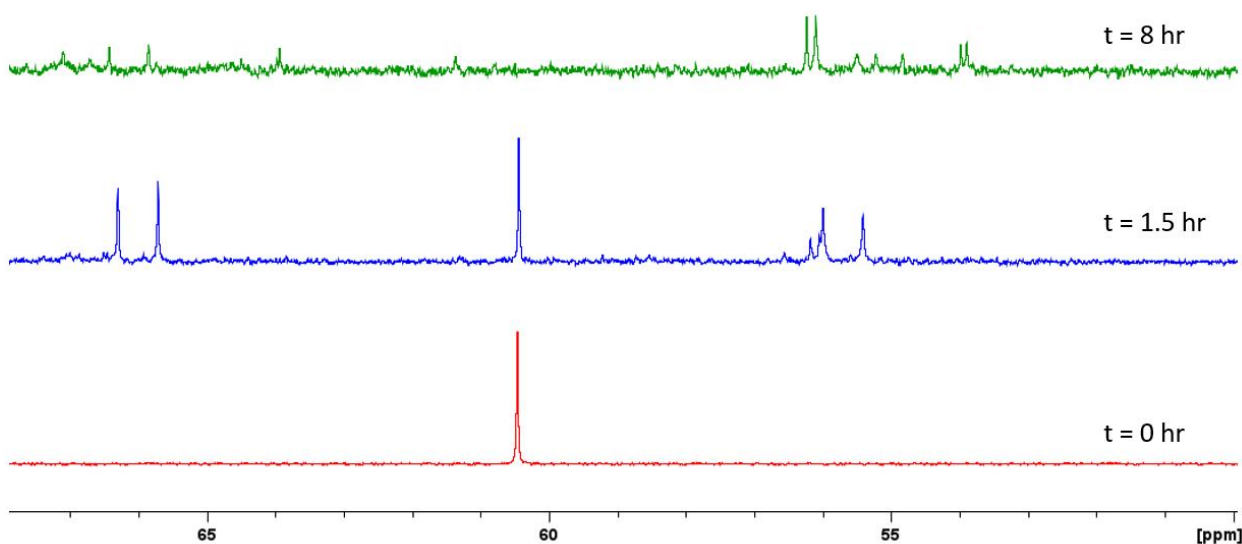
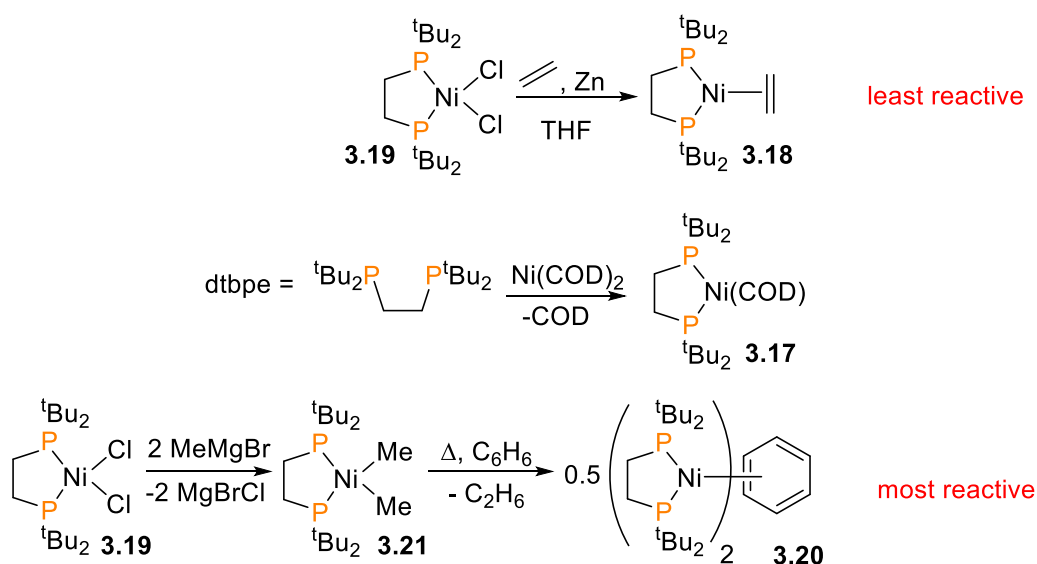


**Figure 3.1** Overlay of the  $^{31}\text{P}\{^1\text{H}\}$  NMR spectra of the reaction of styrene oxide **3.15**,  $\text{Ni}(\text{COD})_2$  and dcype after heating at 75 °C for 0 hr (red trace), 1.5 hr (blue trace) and 8 hr (green trace)

Importantly, the magnitude of the  $^2J_{\text{P,P}}$  coupling constants in asymmetric nickel complexes that contain at least two P donor atoms can be used as an indicator of the nickel oxidation state. As through-bond coupling is electron-mediated, more electron-rich metal centres (i.e. those in low oxidation states) will display higher coupling constant values than those with less electron-rich metal centers (i.e. those in higher oxidation states). An overview of the literature shows that the typical coupling constant value for nickel(II) complexes falls in the range of 5-30 Hz, while those

for formally nickel(0) complexes tend to be in the range of 45-80 Hz<sup>76, 113, 151, 206-213</sup> (although there are notable exceptions to this trend).<sup>214</sup> Based on this, the transiently-generated product ( $^2J_{P,P} = 70$  Hz) appears to be a nickel(0) complex.

Encouraged by the relatively clean reactivity of **3.16** with epoxide **3.15**, we prepared 1,2-bis(*tert*-butyl)phosphinoethane (dtbpe) as our idealized ancillary ligand, believing that the increase in steric bulk would be sufficient to impart increased thermal stability to any resulting organometallic complexes formed from the reaction of low-valent nickel with epoxides. The ligand dtbpe has a rich history with nickel, having been developed by Pörschke<sup>215-217</sup> and popularized by the Hillhouse group<sup>218</sup> and others.<sup>219, 220</sup> Numerous synthetic routes are available for the preparation of (dtbpe)nickel(0) synthons of varying reactivities, as outlined in Scheme 3.7. The COD complex **3.17** can be prepared by addition of dtbpe to Ni(COD)<sub>2</sub> in THF.<sup>215</sup> The ethylene complex **3.18** can be prepared cleanly *via* reduction of (dtbpe)NiCl<sub>2</sub> **3.19** with Zn under an atmosphere of ethylene. <sup>215, 219</sup> Lastly, the arene dimer **3.20** can be prepared by alkylation of **3.19** with 2 equivalents of MeMgBr, followed by thermolysis of (dtbpe)NiMe<sub>2</sub> **3.21** in benzene.<sup>216</sup>



**Scheme 3.7** Preparation of (dtbpe)nickel(0) synthons

Our earliest experiments utilized (dtbpe)nickel complexes **3.17** and **3.18**, as they were the simplest to prepare. Mixing equimolar amounts of ethylene complex **3.18** with freshly-prepared styrene oxide **3.15** in Tol- $d_8$  resulted in the formation of a new nickel(II) complex **3.22**, as observed by  $^{31}\text{P}\{^1\text{H}\}$  NMR spectroscopy. Upon standing overnight at room temperature, small crystals formed in the NMR tube. X-ray diffraction analysis revealed that the new product was not due to any reaction of **3.18** with styrene oxide, but rather, from C-Cl oxidative addition of residual dichloromethane remaining from the synthesis of styrene oxide (Figure 3.2). Related reactions of DCM with complexes of rhodium,<sup>221, 222</sup> iridium<sup>223</sup> and other Group 10 metals<sup>224-227</sup> have been observed over the last 3 decades.

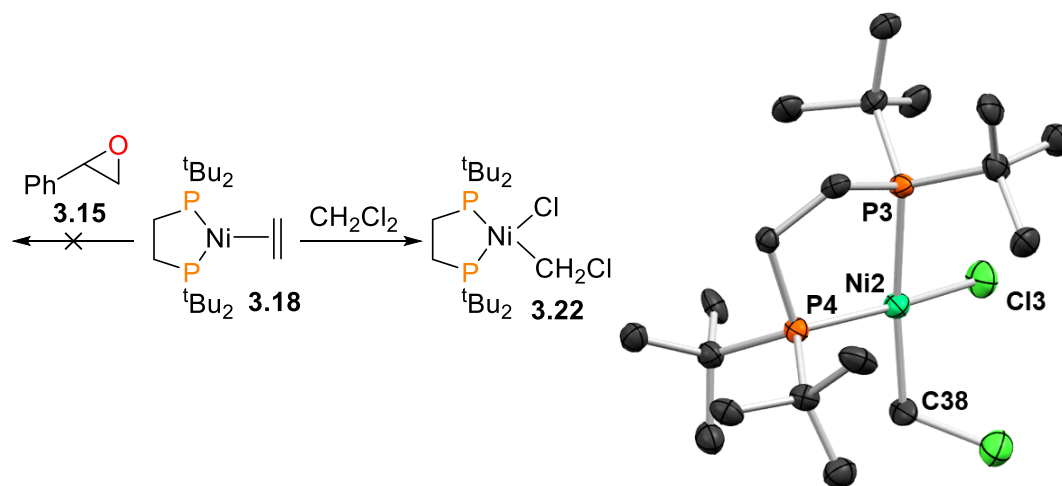
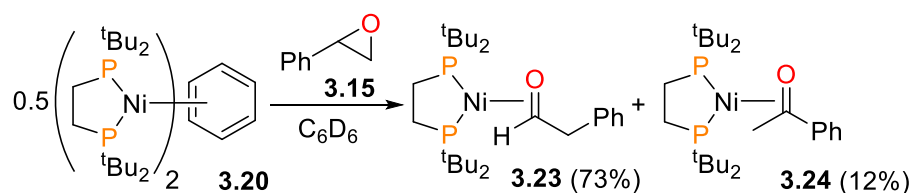


**Figure 3.2** Synthesis and ORTEP diagram (50% probability ellipsoids) of complex **3.22**. All H atoms omitted for clarity.

For the rest of our studies, we turned to arene dimer **3.20** as our preferred starting material, as it is the most reactive nickel(0) source and can be prepared on large scale as a pure, crystalline solid. Addition of purified styrene oxide **3.15** to an orange-red solution of **3.20** in  $\text{C}_6\text{D}_6$  results in the formation of a mixture of products as determined by  $^{31}\text{P}\{^1\text{H}\}$  NMR spectroscopy. The major

product **3.23**, formed in 73% yield, displays two doublets at 94.6 and 83.9 ppm that show large  $^2J_{P,P}$  values of 74 Hz, indicative of an asymmetric coordination geometry at a nickel(0) centre.<sup>151</sup> The minor product **3.24**, formed in 12% yield by  $^1\text{H}$  NMR spectroscopy, displays similar spectroscopic features, i.e. two [AB] doublets at 87.1 and 85.9 ppm with  $^2J_{P,P}$  values of 75 Hz. The major and minor products were identified as the  $\eta^2$ -bound aldehyde complex **3.23** and ketone complex **3.24**, respectively, formed by isomerization of epoxide **3.15** (Scheme 3.8). Ogoshi has reported that a related nickel(0) complex is capable of isomerizing **3.15** to phenylacetaldehyde.<sup>228</sup> The isomerization products **3.23** and **3.24** were also prepared independently *via* the addition of the appropriate organic carbonyl to complex **3.20**, and were characterized by  $^1\text{H}$ ,  $^{13}\text{C}$  and  $^{31}\text{P}$  NMR spectroscopic methods, as well as 2-dimensional methods such as HMBC, HSQC, NOESY and COSY spectroscopic experiments.



### Scheme 3.8 Synthesis of complexes **3.23** and **3.24**

The  $^{31}\text{P}\{^1\text{H}\}$  and  $^1\text{H}$  NMR spectra of **3.23** show an asymmetric phosphine ligand, as each of the *tert*-butyl groups are inequivalent. The aldehydic proton resonance (ddd,  $\delta = 4.98$ ,  $^3J_{H,H} = 6.9$  Hz,  $^3J_{H,P} = 3.1$ ,  $^3J_{H,P} = 0.9$  Hz) is remarkably shielded, demonstrating a significant extent of backbonding from the metal centre to the  $\pi^*$  orbital of the C=O group (Figure 3.3). In addition, the methylene resonances of the aldehyde moiety are diastereotopic and display coupling to a single  $^{31}\text{P}$  nucleus as well as the  $^1\text{H}$  coupling. Curiously, the aldehydic proton couples to only one

of the two adjacent methylene protons. An HSQC experiment ruled out that the bound aldehyde adopted the enol tautomer, which would be consistent with the observed coupling.

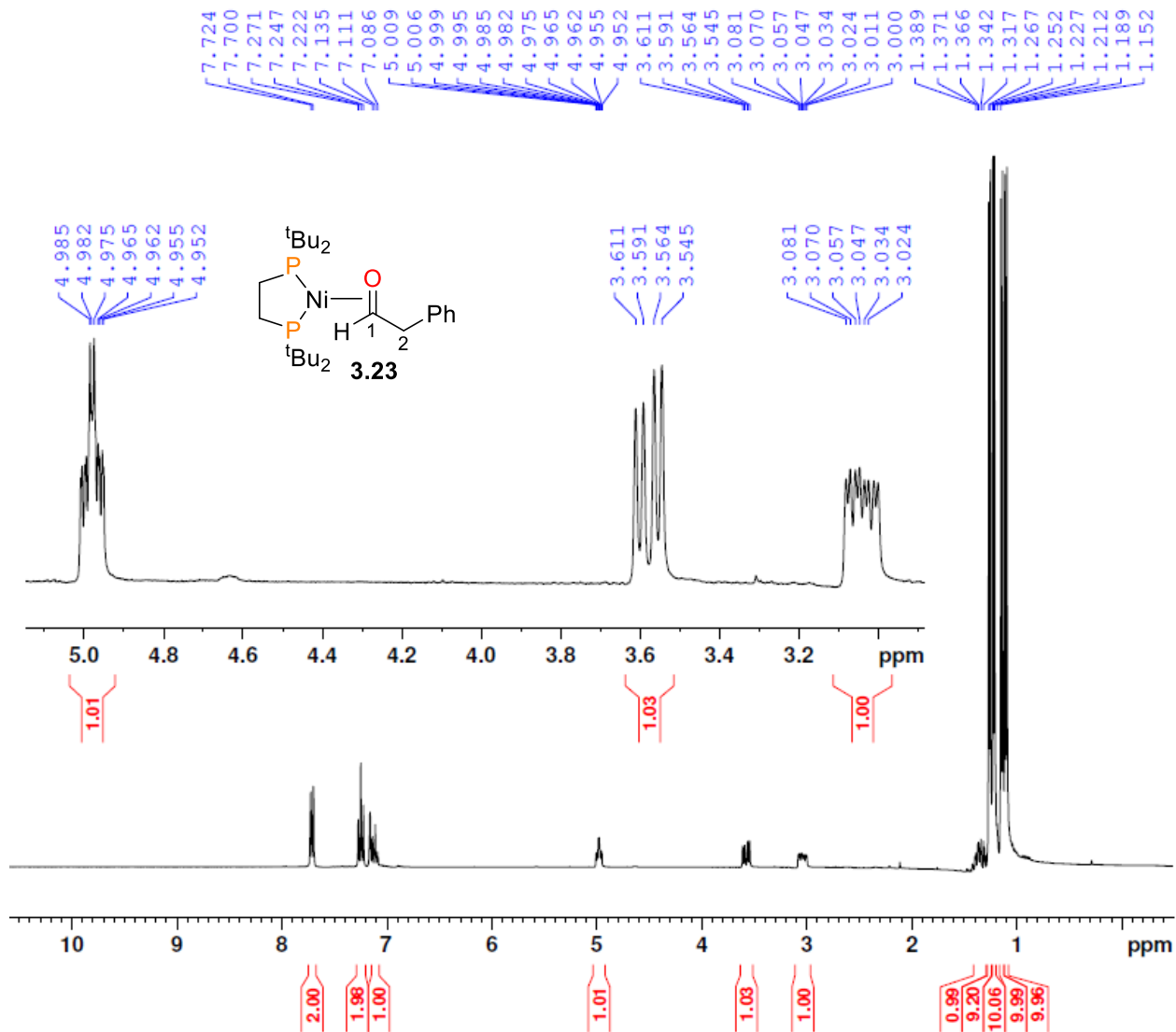


**Figure 3.3**  $^1\text{H}$  NMR spectrum (400 MHz,  $\text{C}_6\text{D}_6$ , 25  $^\circ\text{C}$ ) of **3.23**. Inset shows the **H1** and **H2** resonances.

Additionally, examination of the  $^{13}\text{C}$  NMR spectrum of **3.23** shows that the *ipso*-carbon of the aromatic ring resonates as a doublet of doublets ( $\delta = 142.7$ ,  $J_{\text{C,P}} = 9, 2$  Hz) due to coupling to  $^{31}\text{P}$ , while all other aromatic carbon resonances appear as singlets. This most likely indicates an  $\eta^1$ -

interaction of the aromatic ring with the nickel centre. Variable temperature NMR experiments in toluene- $d_8$  up to 100 °C displayed minimal changes in the appearance of the *ipso*-carbon resonance, showing that the interaction is quite strong. These types of  $\eta^1$  interactions have been previously observed crystallographically in (dtbpe)Ni complexes,<sup>229</sup> as well as systems with palladium.<sup>230, 231</sup> Complex **3.23** was recrystallized from Et<sub>2</sub>O at -35 °C to yield orange crystals suitable for diffraction analysis, and the solid-state structure is shown in Figure 3.4. In contrast to the NMR spectral data, the aromatic ring is held away from the metal centre in the solid state. The C-O bond length of the phenylacetaldehyde ligand has lengthened to 1.332(3) Å, again demonstrating a high degree of backbonding.

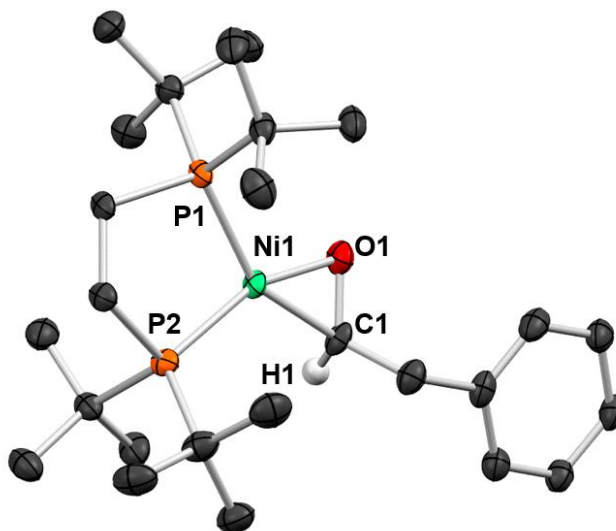


**Figure 3.4** ORTEP diagram (50% probability ellipsoids) of complex **3.23**. All H atoms except **H1** omitted for clarity.

Like **3.23**, the <sup>1</sup>H NMR spectrum of **3.24** also displays four upfield doublets that each integrate to 9 protons, indicating that the *tert*-butyl groups on the phosphine ligand are inequivalent. Coupling of the dtbpe donor atoms to the acetophenone moiety can be observed in the methyl

resonance, which appears as a doublet of doublets ( $\delta = 2.04$  ppm,  ${}^3J_{\text{H,P}} = 8.0$ ,  ${}^3J_{\text{H,P}} = 1.5$  Hz) that collapses to a singlet upon  ${}^{31}\text{P}$  decoupling (Figure 3.5).

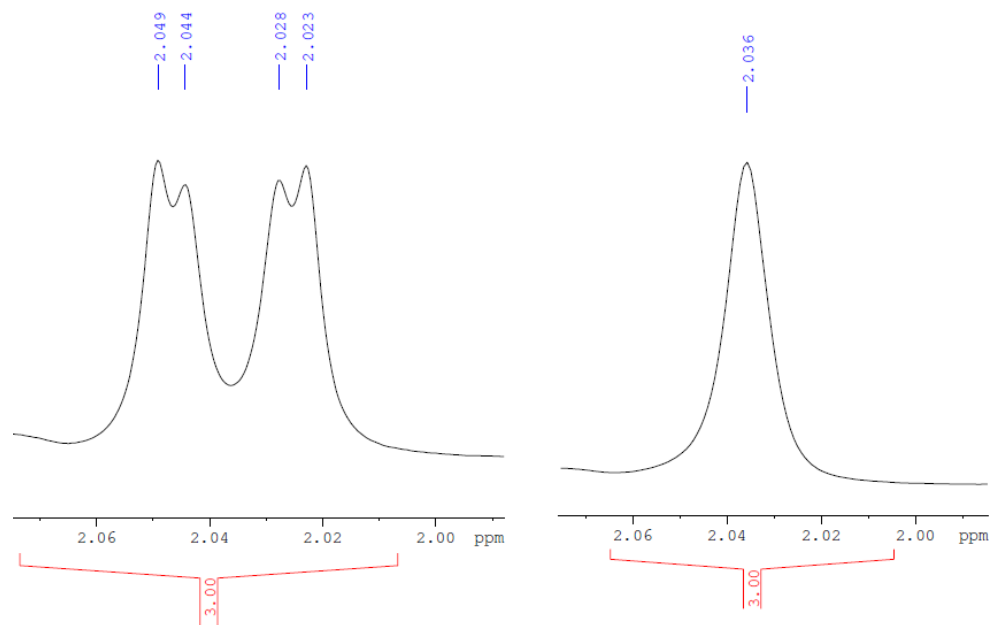


**Figure 3.5** Partial  ${}^1\text{H}$  NMR spectrum (400 MHz,  $\text{C}_6\text{D}_6$ , 25  $^\circ\text{C}$ ) showing the methyl resonance of **3.24**, with (right) and without (left)  ${}^{31}\text{P}$  decoupling.

The  ${}^{13}\text{C}$  NMR spectrum of **3.24** also supports the proposed structure. Perhaps the most striking feature of the  ${}^{13}\text{C}$  NMR spectrum is that the carbonyl resonance of the acetophenone moiety appears at 80.6 ppm. Unlike the  ${}^{13}\text{C}$  NMR data for **3.23**, the aromatic resonances of complex **3.24** all display small but equivalent coupling (3 Hz) to a single  ${}^{31}\text{P}$  nucleus, indicating a weak  $\eta^6$ -type interaction of the metal centre with the aromatic ring in solution. This type of “ring-walking” of nickel with conjugated aromatic systems has been observed previously in cross-coupling reactions.<sup>232</sup> Cooling a concentrated toluene solution of **3.24** to  $-30$   $^\circ\text{C}$  allowed for the growth of dark red crystals which were suitable for X-ray diffraction. The crystals feature two independent molecules in the unit cell (see Figure 3.6). The geometry about the metal centre is distorted square

planar, similar to other  $\eta^2$ -ketone complexes of nickel,<sup>212, 233-235</sup> with the C-O bond length of the acetophenone ligand lengthened to 1.345(2) Å.

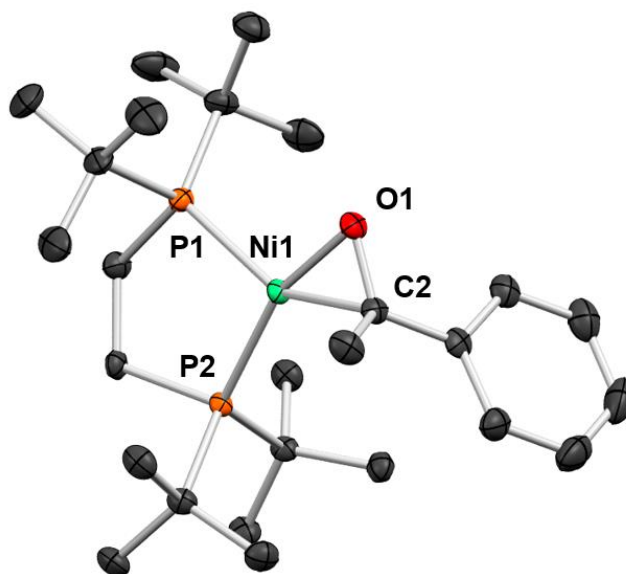
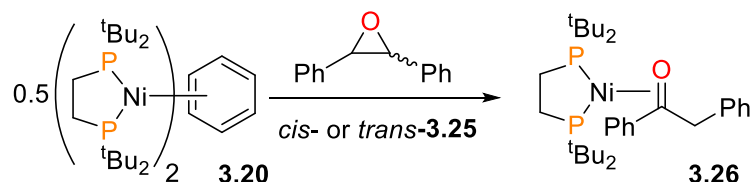


**Figure 3.6** ORTEP diagram (50% probability ellipsoids) of complex **3.24**. All H atoms omitted for clarity.

To probe the lability of these  $\pi$ -bound ligands, we reacted **3.23** with an excess of acetophenone and **3.24** with an excess of phenylacetaldehyde. In both cases, no reaction was observed over several days at room temperature, and heating to 80 °C was required for ligand exchange to occur. These exchange experiments were complicated by the decomposition of **3.23** to a currently-unidentified nickel(0) complex at the elevated temperatures required for ligand exchange. Thus, ligand exchange is quite slow in these complexes.

In an attempt to gain insight into the scope and mechanism of this epoxide isomerization process, we then reacted a variety of substituted epoxides with complex **3.20**. *cis*- and *trans*-Stilbene oxides (**3.25**) isomerize at room temperature within seconds to give the same organometallic species (in 97% <sup>1</sup>H NMR yield from *cis*-**3.25** and 88% <sup>1</sup>H NMR yield from *trans*-

**3.25**), which was again unambiguously identified by independent synthesis as the ketone complex **3.26** (Scheme 3.9).



### Scheme 3.9 Synthesis of complexes **3.26**

Complex **3.26** could be isolated as an orange powder by cooling a saturated pentanes solution to  $-30\text{ }^{\circ}\text{C}$ . Blocky, red crystals could be grown by cooling an  $\text{Et}_2\text{O}$  solution of **3.26**, and the solid-state structure is shown in Figure 3.7. Isomerization of *trans*-stilbene oxide has previously been reported using nucleophilic reagents like  $\text{LiNEt}_2$ <sup>236</sup> and  $\text{Co}(\text{CO})_4^-$ <sup>237</sup>.

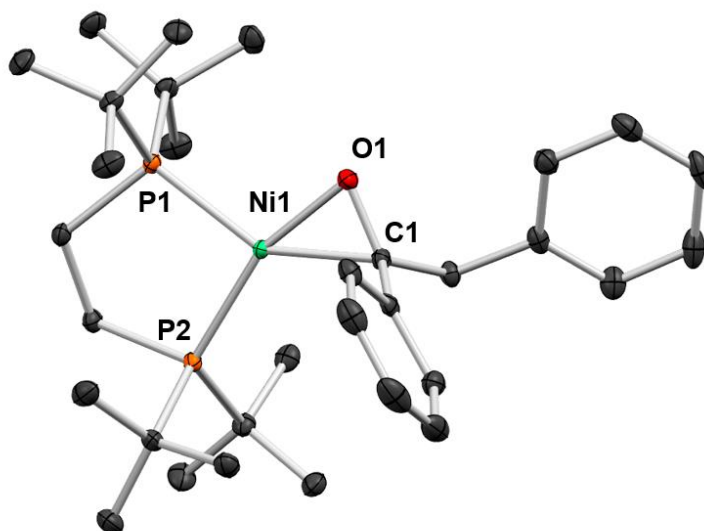
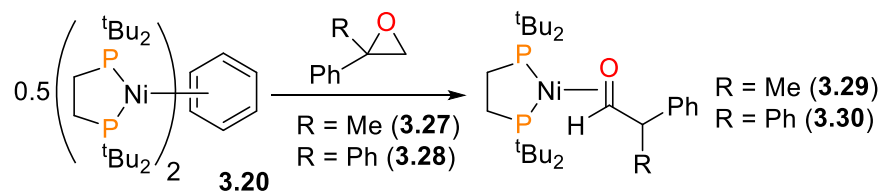


**Figure 3.7** ORTEP diagram (50% probability ellipsoids) of complex **3.26**. All H atoms omitted for clarity.

1,1-Disubstituted epoxides **3.27** and **3.28** also reacted cleanly with **3.20** to generate aldehyde complexes **3.29** (93%  $^1\text{H}$  NMR yield) and **3.30** (78%  $^1\text{H}$  NMR yield, Scheme 3.10). Of note, these

reactions are much slower than the above-mentioned isomerization reactions of 1- and 1,2-substituted epoxides, requiring several hours at room temperature before reaching completion.



### Scheme 3.10 Synthesis of complexes 3.29 and 3.30

Due to the contiguous stereogenic centres, complex **3.29** forms as an equimolar mixture of diastereomers when prepared by reacting **3.20** with either epoxide **3.27** or 2-phenylpropionaldehyde. Crystallization of **3.29** from cold Et<sub>2</sub>O gives a crystalline solid that <sup>1</sup>H NMR spectroscopic analysis shows to be a 15:2 mixture of diastereomers. X-ray diffraction analysis of a single crystal selected from the mixture yields the structure of a sole diastereomer (see Figure 3.8)

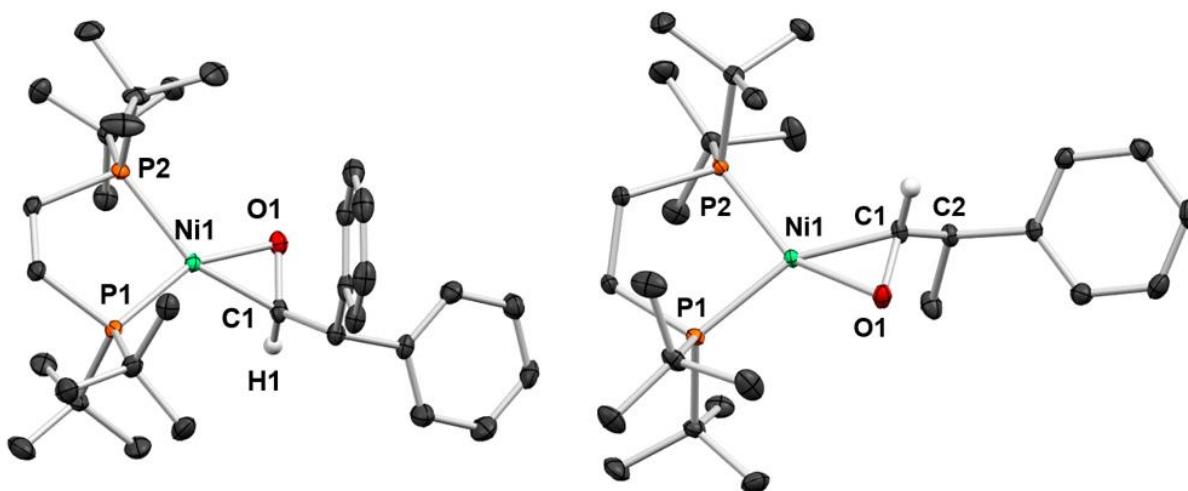


**Figure 3.8** ORTEP diagrams (50% probability ellipsoids) of complexes **3.30** (left) and **3.29** (right). All H atoms except **H1** omitted for clarity.

Importantly, reacting enantiopure epoxide (R)-**3.27**<sup>238</sup> with **3.20** also results in an equimolar mixture of the diastereomers of **3.29**, which indicates that some step along the conversion of **3.20** to **3.29** proceeds with scrambling of configuration.

In an attempt to observe any intermediates during the isomerization process, we reacted **3.20** with *trans*-**3.25** at -50 °C in toluene-*d*<sub>8</sub>. In these experiments, however, we observed only the formation of **3.26** with concomitant decrease of the signals of **3.20**, as observed by <sup>31</sup>P NMR spectroscopy. Similarly, the reactions of **3.27** and **3.28** with **3.20**, which require hours at room temperature, also do not show any detectable intermediates. Based on these data, we propose that these isomerization reactions proceed by rate limiting C-O oxidative addition, followed by fast β-hydride elimination and C-H reductive elimination to form the observed nickel(0) products.

### 3.3 Oxidative Addition of Tetrasubstituted Epoxides

The formation of aldehydes from epoxides is well known to proceed *via* Lewis acid catalysis.<sup>239,</sup><sup>240</sup> However, Ni(0) is a notably poor Lewis acid, especially when chelated by an electron-donating phosphine ligand.<sup>43</sup> In contrast, recent work with both Al/Co<sup>241</sup> and Rh<sup>242</sup> has demonstrated epoxide isomerizations proceeding *via* nucleophilic attack typically form ketones, although an exception is the Pd system reported by Kulasegaram and Kulawiec.<sup>243-245</sup> To explore the ring-opening step, we prepared a series of tetrasubstituted epoxides which we anticipated would not undergo rapid β-hydride elimination upon reaction with **3.20**. While tetraphenyl epoxide **3.31** did react with **3.20**, the new product unexpectedly resonated as a singlet in the <sup>31</sup>P{<sup>1</sup>H} NMR spectrum, and we were unable to purify it by recrystallization, or even to identify it by its NMR spectral data. We then turned to methyl-substituted *cis*-**3.32** and reacted it with **3.20**. Monitoring the reaction at 60 °C *via* <sup>31</sup>P NMR spectroscopy reveals the formation of an asymmetric intermediate **3.33** (<sup>2</sup>*J*<sub>P,P</sub> = 29 Hz)<sup>78</sup> as well as a final nickel(II) product, **3.34** (<sup>2</sup>*J*<sub>P,P</sub> = 13 Hz).

Complete conversion to **3.34** was observed after heating for 10 hours. Surprisingly, the  $^1\text{H}$  NMR spectrum of **3.34** showed an ABX spin system inconsistent with the expected nickelaoxetane product of simple C-O oxidative addition (Figure 3.9).

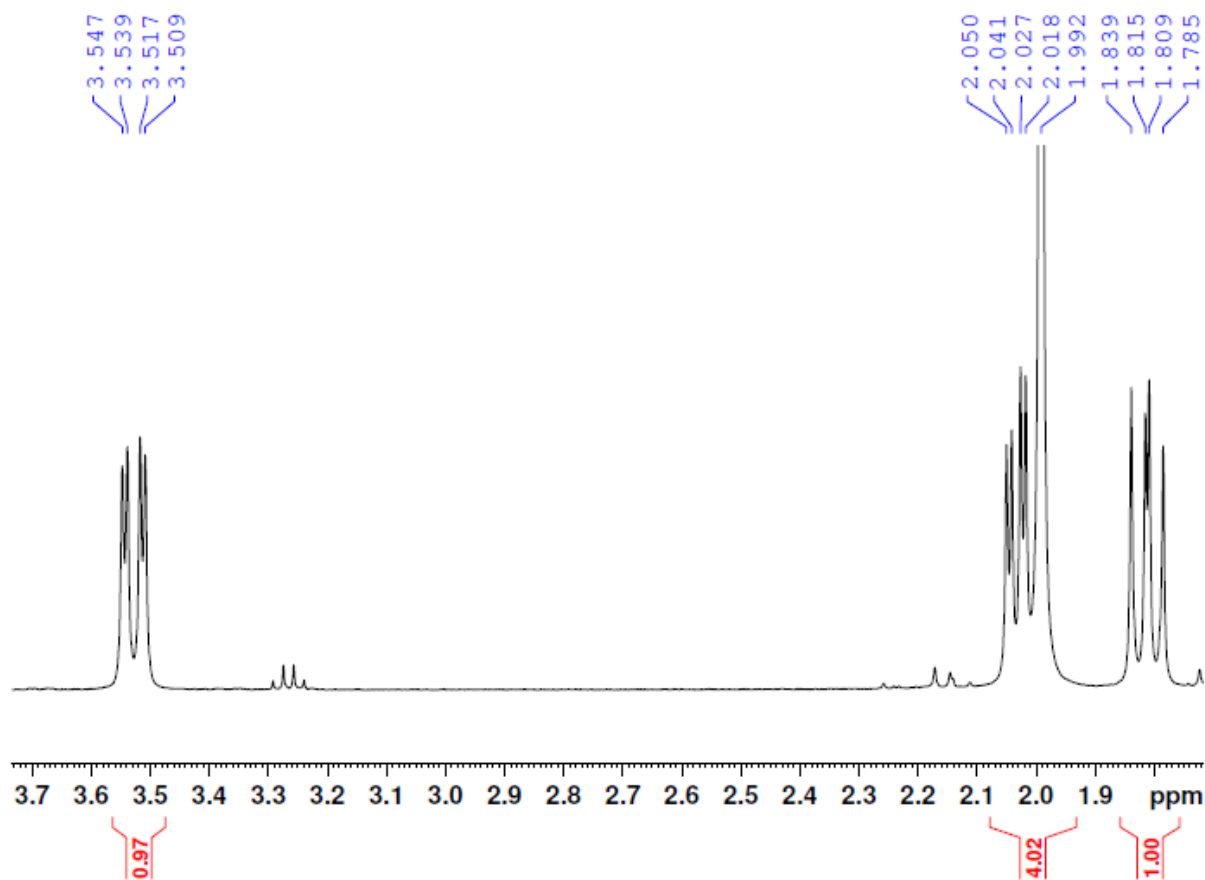
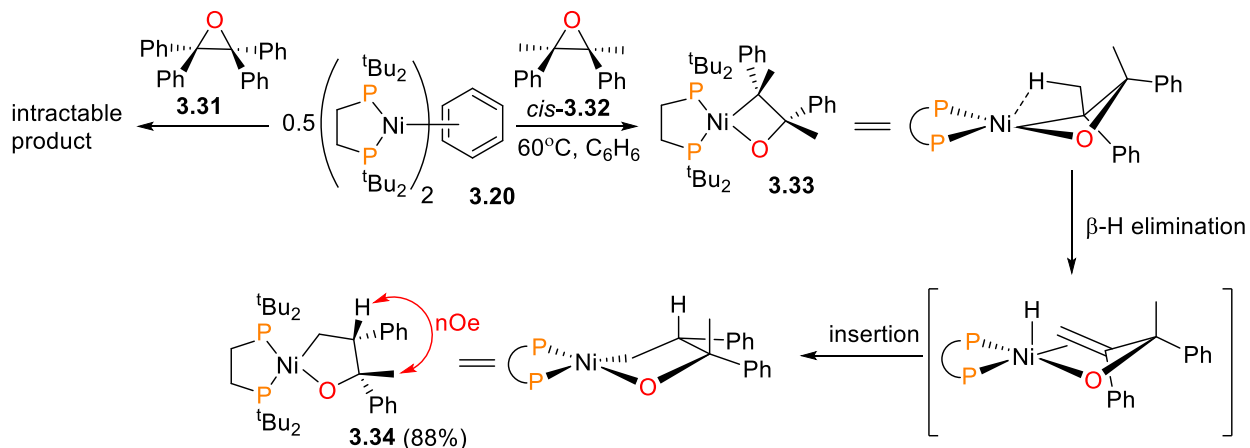


**Figure 3.9** Partial  $^1\text{H}\{^{31}\text{P}\}$  NMR spectrum (400 MHz,  $\text{C}_6\text{D}_6$ , 25  $^\circ\text{C}$ ) showing the methyl and ABX resonances of **3.34**

Further analysis by 2-D NMR spectroscopic experiments (HMBC and HSQC) reveal that **3.34** is the five-membered metallacycle shown in Scheme 3.11. We propose that **3.34** is formed by

oxidative addition of nickel(0) into the C-O bond of *cis*-**3.32**, followed by  $\beta$ -hydride elimination of a methyl C-H bond and rapid insertion of the hydride into the newly-formed styrenyl olefin.



### Scheme 3.11 Synthesis of complexes **3.34**

A 2D-NOESY experiment demonstrates that **3.34** is formed as a single diastereomer, indicating that the oxidative addition step proceeds with *retention* of configuration. Earlier work by Jamison<sup>44, 45</sup> invoked the formation of nickelaoxetane intermediates *via* an  $S_N2$  type mechanism (i.e. with *inversion* of configuration). Related mechanistic work from Hillhouse<sup>63</sup> and Jamison<sup>65, 246</sup> on the synthesis of azanickelacyclobutanes from nickel(0) and aziridines found an  $S_N2$  type mechanism of oxidative addition to be operative. Recrystallization of **3.34** from cold pentanes formed yellow crystals suitable for X-ray diffraction analysis, and the solid-state structure of **3.34** is shown in Figure 3.10.

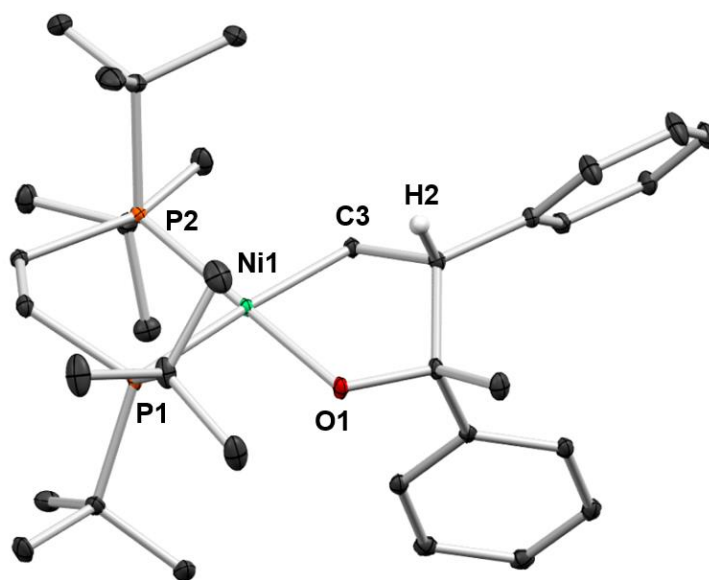
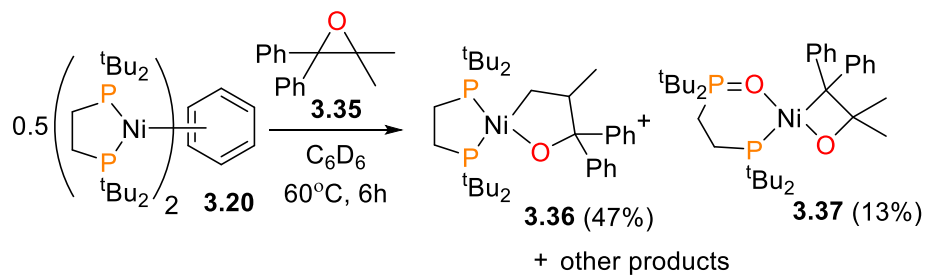


**Figure 3.10** ORTEP diagram (50% probability ellipsoids) of complexes **3.34**. All H atoms except **H2** omitted for clarity

In order to probe the regioselectivity of oxidative addition, we also prepared tetrasubstituted epoxide **3.35** and reacted it with **3.20**. While no reaction was observed at room temperature, heating the solution at 60 °C for 6 hours results in the colour darkening from red-orange to very dark red-brown. Analysis of the solution by  $^{31}\text{P}$  NMR spectroscopy shows the formation of a complex mixture of products, including singly oxidized dtbpe ligand (dtbpeO),<sup>113, 247</sup> as well as two major new organometallic species. The main organometallic product, complex **3.36**, displays two doublets at 77.9 ppm and 71.8 ppm with small  $^2J_{\text{P,P}}$  values of 14 Hz. Subsequent NMR spectroscopic experiments found that **3.36** is the five-membered nickelacycle in Scheme 3.12, analogous to **3.34**. The second product, complex **3.37**, resonates as one doublet at 70.8 ppm and another at 29.4 ppm, which is dramatically shifted upfield for nickel complexes of dtbpe. The  $^{31}\text{P}\{^1\text{H}\}$  NMR spectrum of complex **3.37** shows even smaller  $^2J_{\text{P,P}}$  coupling of 6 Hz.



**Scheme 3.12** Synthesis of complexes **3.36** and **3.37**

Complexes **3.36** and **3.37** could be separated by repeated extractions of the crude reaction mixture with cold pentanes. Gratifyingly, cooling a concentrated Et<sub>2</sub>O solution of complex **3.37** resulted in small crystals that were of sufficient quality to be analyzed by X-ray diffraction (see Figure 3.11). The structure was determined to be the nickelaoxetane shown in Scheme 3.12.

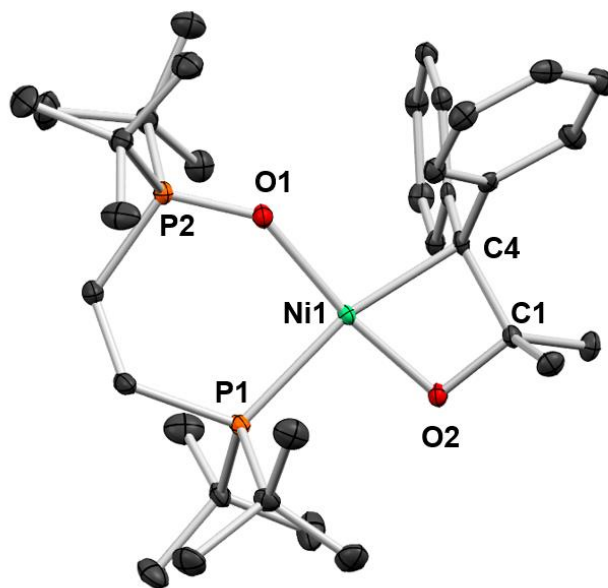


**Figure 3.11** ORTEP diagram (50% probability ellipsoids) of complexes **3.37**. All H atoms except **H2** omitted for clarity.

Curiously, the dtbpe ligand of **3.37** has been oxidized by a single O atom, giving a rare example of a dtbpeO complex of nickel. The Ni-O bond of the oxetane ring is 1.840(2) Å, and the Ni-C bond length is 1.986(2) Å, which are slightly longer and shorter, respectively, to the corresponding

bond lengths in other nickelaoxetanes. We have only observed the isomer of **3.37** where the O atoms are *trans*. We initially hypothesized that **3.37** was formed *via* oxidative addition of nickel(0) into the phenyl-substituted C-O bond of **3.35**, with subsequent oxidation of one phosphine arm by trace *meta*-chloroperoxybenzoic acid (*m*CPBA) remaining from the synthesis of **3.35**. However, independent experiments reveal that equimolar mixtures of **3.20**, **3.35** and *m*CPBA do not increase the amount of **3.37** formed. Based on this, we do not believe that *m*CPBA is the source of the O atom in the dtbpeO ligand.

In our attempts to recrystallize complex **3.36**, we were able to isolate small crystals of the nickelaoxetane **3.38**, which does not contain an oxidized dtbpe ligand. Unfortunately, the crystals examined by X-ray diffraction methods were twinned to such an extent that satisfactory data for publication was not obtained. In addition, we were unable to obtain NMR spectroscopic data of requisite quality for structural assignment. We have included a ORTEP depiction of the crude structural data in Figure 3.12 merely to demonstrate connectivity.

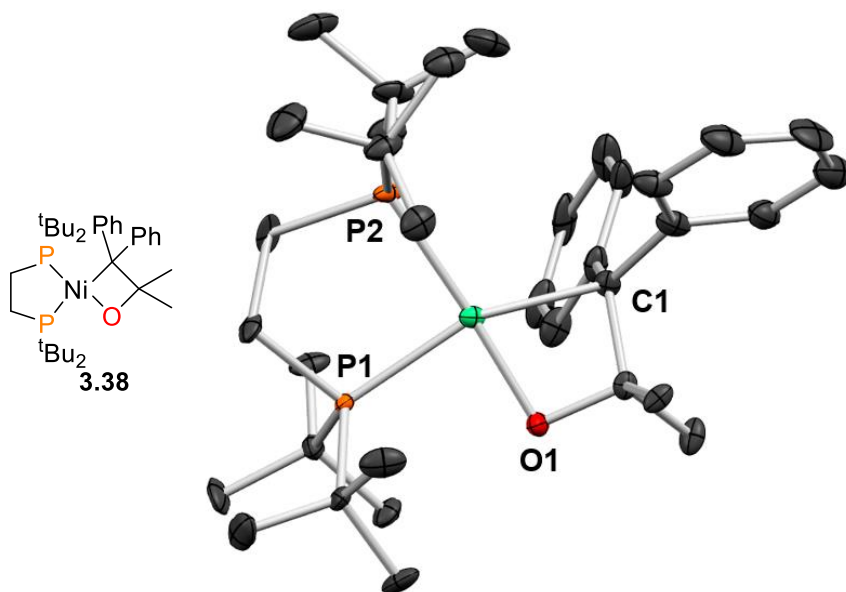
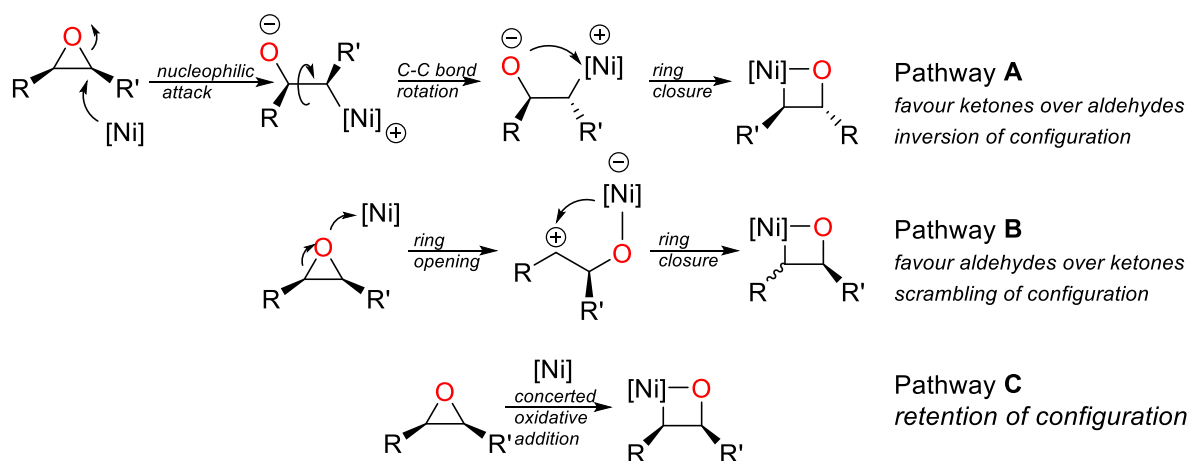


**Figure 3.12** ORTEP diagram (50% probability ellipsoids) of complexes **3.38**. All H atoms omitted for clarity. This data is to demonstrate connectivity only.

Possible mechanisms of oxidative addition of nickel(0) with epoxides are outlined in Scheme 3.13. Pathway **A**, which features an  $S_N2$  type attack of the metal at the least substituted carbon, has been reported by Jamison,<sup>44, 45</sup> and has also been proposed by Hillhouse,<sup>63</sup> Wolfe<sup>119</sup> and others.<sup>47</sup> Pathway **B** is analogous to the Meinwald rearrangement, where nickel(0) would act as a Lewis acid.<sup>241</sup> Binding of the O atom of the epoxide to the metal would precede ring-opening to form the most stable carbocation, which would subsequently be attacked by nickel(0) to form a nickelaoxetane. Formation of the carbocation would result in a scrambling of configuration at the nickelaoxetane carbon. Pathway **C** features a concerted oxidative addition of a C-O bond of the epoxide across the metal centre, and would result in a *retention* of configuration. Based on the fact that we see retention of configuration in the synthesis of **3.34** and moderate selectivity for the aldehyde isomerization products over the ketone isomerization products, we favour Pathway **C** as the most likely for oxidative addition of epoxides with (dtbpe)nickel(0).



**Scheme 3.13** Potential mechanisms of oxidative addition of epoxides with nickel(0). [Ni] = (dtbpe)nickel(0).

### 3.4 Functionalization of Epoxides

Given the rapid rate of epoxide isomerization discussed in the previous section, we sought to find a way to close a potential catalytic cycle featuring this isomerization step. Our group has recently become interested in selective hydroboration of carbonyl compounds using late transition metals.<sup>248</sup> As such, we were curious to determine if these  $\eta^2$ -carbonyl complexes derived from epoxide isomerization could undergo hydroboration chemistry.<sup>249-254</sup>

While heating a catalytic amount of **3.20** (i.e. 5 mol% **3.20**, 10 mol% Ni) with styrene oxide **3.15** in C<sub>6</sub>D<sub>6</sub> only resulted in the formation of **3.23** and **3.24** (i.e. with no appreciable amount of free phenylacetaldehyde in solution), addition of HBpin<sup>197</sup> (pin = pinacolato) to the yellow solution resulted in an instant colour change to dark red, and <sup>1</sup>H NMR spectroscopic analysis reveals the formation of boronate ester PhCH<sub>2</sub>CH<sub>2</sub>OBpin (**3.39**) in 31% yield, which could be increased to 72% upon heating for 22 hours at 80 °C. Interestingly, of the two isomerization products formed, only **3.23** reacts with HBpin under these conditions. As observed by <sup>31</sup>P NMR spectroscopy, the resting state of these catalytic reactions is complex **3.24**.

We next examined the scope of styrene oxide derivatives that could undergo this hydroboration process with HBpin (Table 3.1). Although electron-rich epoxides (entries 2 and 3) produced better yields than electron-poor epoxides (entries 4 and 5) at room temperature, moderate yields of boronate esters were observed for all the *para*-substituted styrene derivatives tested after heating at 80 °C for 22 hours. Bulkier epoxides such as xylyloxirane (entry 6) gave only trace hydroboration product under the typical reaction conditions, demonstrating a sensitivity to the sterics of the substrate.

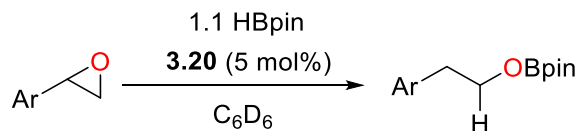
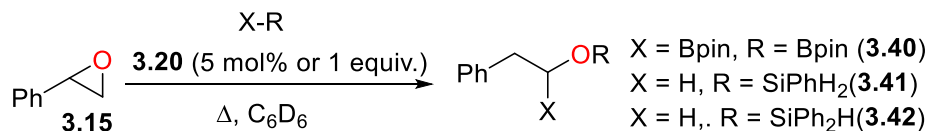


**Table 3.1** Hydroboration of aryl epoxides with **3.20** and HBpin

Entry	Ar	% Yield <sup>[a]</sup>
1	Ph	72 (31)
2	<i>p</i> -MeC <sub>6</sub> H <sub>4</sub>	43 (15)
3	<i>p</i> -MeOC <sub>6</sub> H <sub>4</sub>	46 (6)
4	C <sub>6</sub> F <sub>5</sub>	41 (trace)
5	<i>p</i> -ClC <sub>6</sub> H <sub>4</sub>	39 (trace)
6	Xyl	2 (trace)

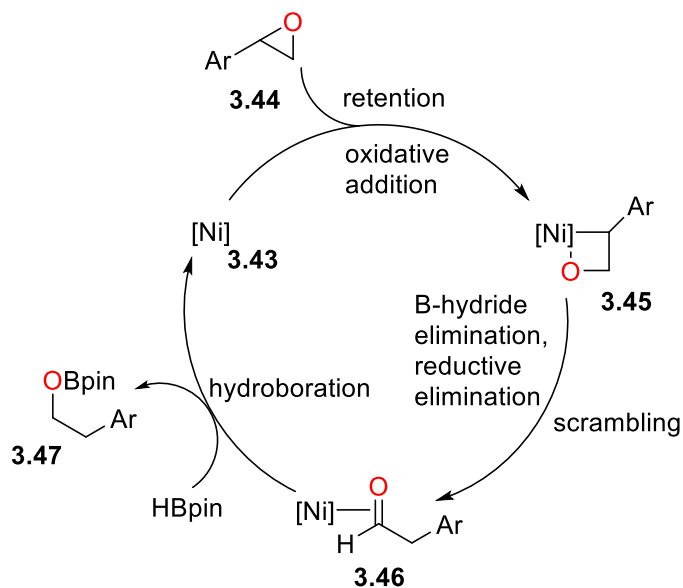
[a] Yields determined by <sup>1</sup>H NMR spectroscopy after 22 hours at 80 °C. Values in brackets are yields after 10 minutes at room temperature. 1,3,5-trimethoxybenzene was used as internal standard.

Upon prolonged heating, catalytic diboration<sup>255</sup> with B<sub>2</sub>pin<sub>2</sub> was also found to give functionalized product PhCH<sub>2</sub>CH(Bpin)OBpin **3.40** in 45% yield, along with a significant amount of protodeboration product **3.39** (14% yield). Catalytic reactions with 1,1-disubstituted epoxides **3.27** or **3.28** resulted in complex mixtures that contained only trace yields of the desired hydroboration products. We attribute this to a greatly reduced rate of reaction of substituted aldehyde complexes **3.29** and **3.30** with HBpin. Indeed, equimolar amounts of HBpin and pure **3.30** require 16 hours before reaching completion at room temperature. We also found that complex **3.20** could facilitate stoichiometric hydrosilation<sup>253, 256</sup> of **3.15** (i.e. forming **3.41** in 44% yield and **3.42** in 57% yield), at elevated temperatures (Scheme 3.14). Ongoing work in our laboratory is aimed at expanding the catalytic functionalization of **3.15** and other epoxides described herein.



**Scheme 3.14** Functionalization of styrene oxide with B<sub>2</sub>pin<sub>2</sub> or silanes

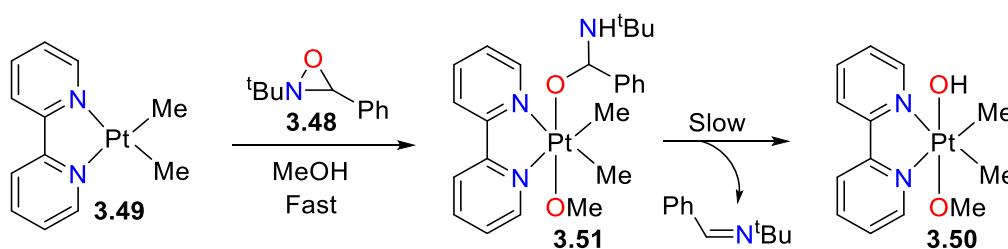
Based on the available data, we propose the following mechanism for the isomerization and hydroboration of epoxides (Scheme 3.15): first, oxidative addition of the (dtbpe)nickel(0) fragment **3.43** into the more substituted C-O bond of aryl epoxide **3.44** yields a 2-nickelaoxetane intermediate (**3.45**) with retention of configuration. Subsequent β-hydride elimination and reductive elimination (or, Ni-O bond heterolysis followed by 1,2-hydride migration) reduces the metal centre and forms the η<sup>2</sup>-aldehyde complex **3.46** along with scrambling of configuration. Direct reaction of this species with HBpin regenerates the nickel(0) catalyst and releases the product boronate ester **3.47**.



**Scheme 3.15** Proposed catalytic cycle for the hydroboration of epoxides. [Ni] = (dtbpe)Ni

### 3.5 Reactivity with Oxaziridines

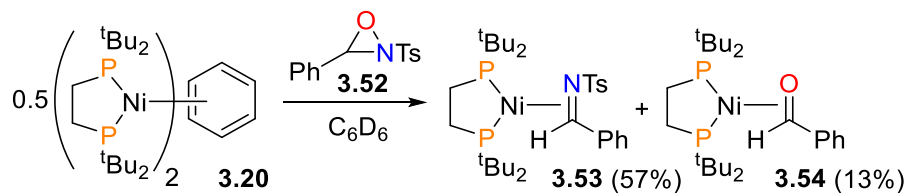
Oxaziridines are commonly used reagents in organic synthesis,<sup>257, 258</sup> but have been relatively unexplored in the field of organometallic chemistry. In a recent example, Puddephatt and co-workers reported that, in protic solvents, oxaziridine **3.48** can oxidize dimethylplatinum(II) complex **3.49** to platinum(IV) hydroxo species **3.50** via hemiaminal intermediate **3.51** (Scheme 3.16).<sup>259</sup>



**Scheme 3.16** Oxidation of platinum(II) with oxaziridine in protic solvent

The most common mode of reactivity of oxaziridines with redox-active transition metal complexes is their isomerization to the corresponding amides.<sup>260</sup> Oxaziridines can also be used as electrophilic O-atom transfer (OAT) reagents, as well as amination<sup>261</sup> and oxyamination reagents.<sup>262-264</sup> Given the myriad potential reactivity pathways possible, we were interested in exploring the chemistry of **3.20** with oxaziridines. In particular, we believed that the relatively weak N-O bond of oxaziridines would be primed for the oxidative addition chemistry we had observed for epoxides, perhaps enabling further productive reactivity.

Addition of Davis' oxaziridine (**3.52**)<sup>265</sup> to a C<sub>6</sub>D<sub>6</sub> solution of **3.20** resulted in the formation of two organometallic products, complexes **3.53** and **3.54**, as determined by <sup>31</sup>P{<sup>1</sup>H} NMR spectroscopy (Scheme 3.17). The first product, complex **3.53**, displaying two [AB] doublets at 85.1 and 84.1 ppm with a <sup>2</sup>J<sub>P,P</sub> of 43 Hz, was determined to be the η<sup>2</sup>-imine complex shown in Scheme 3.5.1. The <sup>1</sup>H NMR spectroscopic yield for **3.53** was 57%.



**Scheme 3.17** Synthesis of complexes **3.52** and **3.53**.  $^1H$  NMR yields in parentheses.

Complex **3.53** was also prepared independently by addition of the imine TsN=CHPh (**3.55**) to **3.20**. Complex **3.53** was fully characterized by  $^1H$  and  $^{13}C$  NMR spectroscopy, as well as EI mass spectrometry. Dark red, X-ray diffraction quality crystals could be grown *via* slow evaporation of a saturated Et<sub>2</sub>O solution at room temperature (see Figure 3.13 for solid-state structure). The C-N bond length was found to be appreciably lengthened at 1.409(4) Å, which is longer than that of several related structures.<sup>212</sup> Curiously, although imine **3.55** is the byproduct of OAT from **3.52** and dtbpe is prone to oxidation, we did not detect any dtbpeO or dtbpeO<sub>2</sub> in the reaction mixtures.

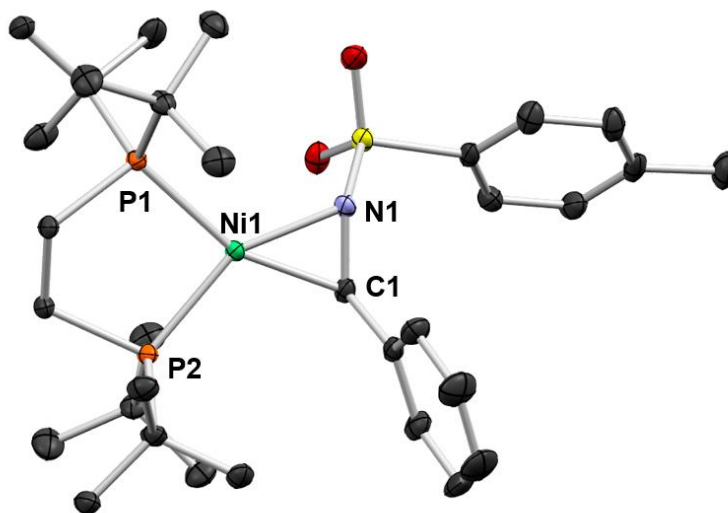


**Figure 3.13** ORTEP diagram (50% probability ellipsoids) of complex **3.53**. All H atoms omitted for clarity.

The other product of the reaction (**3.54**, formed in 13% yield by  $^1\text{H}$  NMR spectroscopy) displays two [AB] doublets at 90.1 and 88.1 ppm with large  $^2J_{\text{P,P}}$  values of 70 Hz. The similarities to related complexes prepared by our group hinted that the other product could be an  $\eta^2$ -carbonyl complex of Ni(0). A  $^{31}\text{P}$ - $^1\text{H}$  HMBC experiment showed cross peaks between the two [AB] doublets and a resonance in the  $^1\text{H}$  NMR spectrum at 5.92 ppm. This resonance appears as a doublet of doublets ( $J_{\text{H,P}} = 6.2$ ,  $J_{\text{H,P}} = 4.2$  Hz) which collapses to a broad singlet on  $^{31}\text{P}$  decoupling. An HSQC experiment showed a strong cross peak for this  $^1\text{H}$  resonance with a  $^{13}\text{C}$  resonance at 78.8 ppm. The chemical shift and multiplicity (d,  $J_{\text{C,P}} = 22$  Hz) of this  $^{13}\text{C}$  resonance are also consistent with a  $\pi$ -bound aldehyde complex. The product was ultimately identified as the  $\eta^2$ -benzaldehyde complex **3.53**, which was again confirmed *via* independent synthesis and comparison of the spectral data with that of the reaction mixture. Like **3.53**, complex **3.54** was fully characterized *via* NMR spectroscopy, elemental analysis, EI mass spectrometry and X-ray diffraction (see Figure 3.14 for solid-state structure).

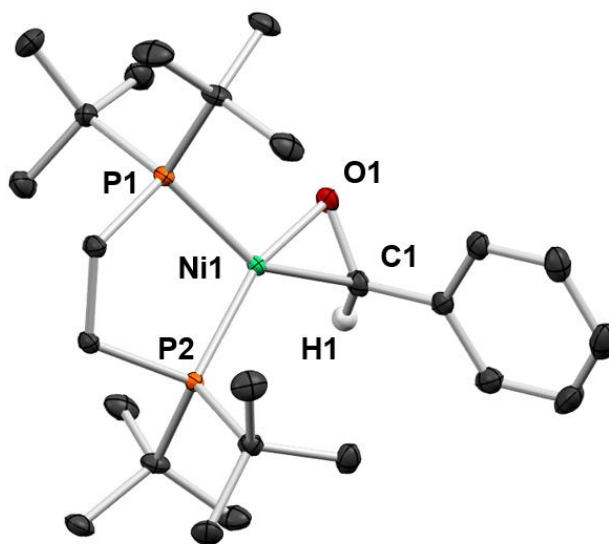
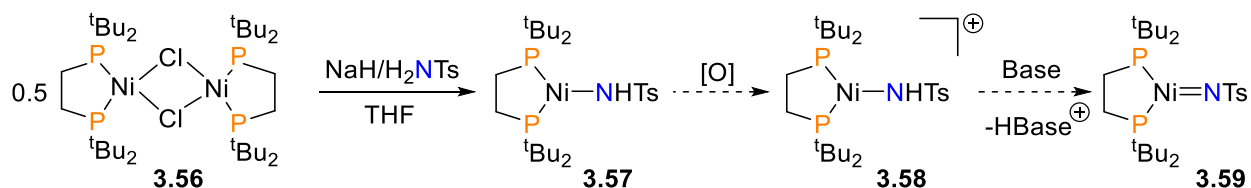


**Figure 3.14** ORTEP diagram (50% probability ellipsoids) of complex **3.54**. All H atoms omitted for clarity.

Mass spectrometric analysis (ESI) of the crude reaction mixture after exposure to air showed a strong peak at  $m/z$  546, which corresponds to the [(dtbpe)NiNHTs] cation. Curious about the origin of this complex, we sought to prepare it independently using a classic route for the synthesis of nickel(II) imido complexes (Scheme 3.18).<sup>75</sup>



**Scheme 3.18** Synthesis and potential oxidation, deprotonation chemistry of complex **3.57**

Addition of NaH and H<sub>2</sub>NTs to a solution of [(dtbpe)NiCl]<sub>2</sub> **3.56** resulted in a colour change from red to dark brown, and washing of the crude product with pentanes yielded a pale yellow solid. Recrystallization of the crude from Et<sub>2</sub>O resulted in a mixture of orange crystals of the starting material, as well as pale yellow plates, which were found by X-ray diffraction analysis to be the desired nickel(I) amido complex **3.57** (see Figure 3.15 for solid-state structure). Further work is required to both optimize the synthesis and complete the characterization of **3.57**. The oxidation and deprotonation chemistry of **3.57** is an ongoing project in the Love group, potentially providing access to nickel(II) complexes such as **3.58** and **3.59** that are not available *via* the more modern method of reacting a nickel(0) source with aryl- or alkylazides.<sup>266</sup>

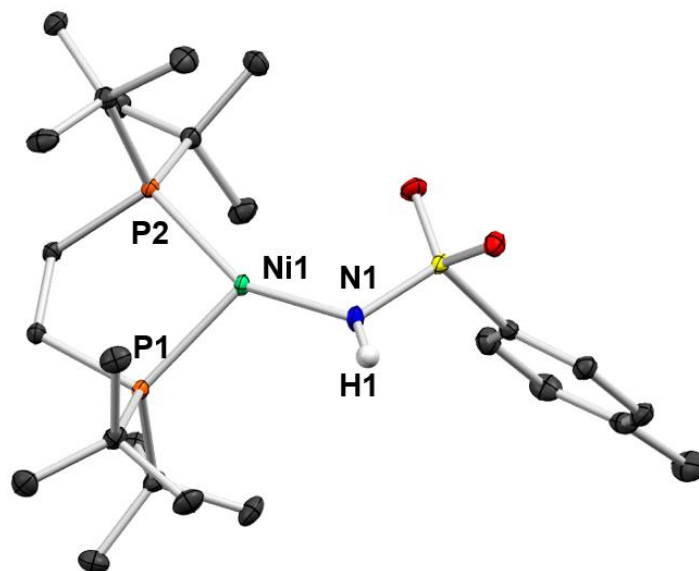
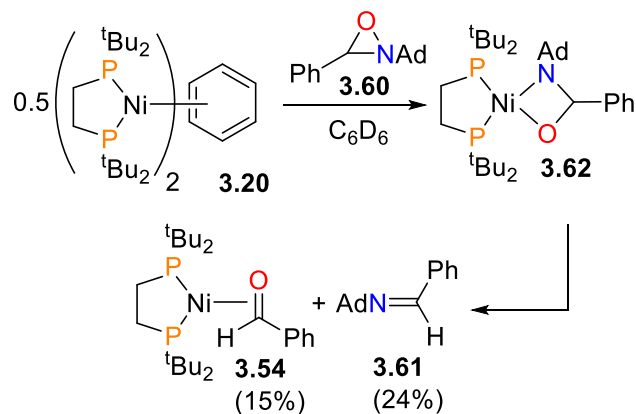


**Figure 3.15** ORTEP diagram (50% probability ellipsoids) of complex **3.57**. All H atoms omitted for clarity.

Although we initially hypothesized that **3.54** was formed *via* hydrolysis of either the free imine **3.55** or the bound imine of **3.53**, there was no trace of free H<sub>2</sub>NTs in the <sup>1</sup>H NMR spectrum of the reaction mixtures. In addition, both **3.53** and **3.55** have been found to be stable in the presence of a large excess of water in C<sub>6</sub>D<sub>6</sub> over 24 hours. Based on these data, we deemed hydrolysis by adventitious water to be unlikely, and consequently were interested in determining the mechanism of formation of both **3.53** and **3.54**.

Low-temperature (-50 °C) addition of **3.52** to **3.20** in Tol-d<sub>8</sub> did not reveal the presence of any intermediates detectable by <sup>31</sup>P{<sup>1</sup>H} NMR spectroscopy. As a result, we sought to slow the reaction down by increasing the steric bulk at the N-substituent. N-Adamantyl oxaziridine (**3.60**) was prepared according to literature procedure<sup>267</sup> and reacted with **3.20** in C<sub>6</sub>D<sub>6</sub> (Scheme 3.19).



**Scheme 3.19** Reactivity of **3.20** with oxaziridine **3.60**.

The reaction mixture immediately changed colour from red-orange to dark purple upon mixing, although subsequent  $^{31}\text{P}\{^1\text{H}\}$  NMR analysis revealed no new resonances. The  $^1\text{H}$  NMR spectrum of this solution only contained broad resonances. After standing at room temperature for 1 hour, the solution changed from purple to brown-red, and  $^1\text{H}$  NMR spectroscopy shows the conversion of the purple complex to a mixture of **3.54** (15%  $^1\text{H}$  NMR yield) and the free imine AdN=CHPh (**3.61**, 24%  $^1\text{H}$  NMR yield). In this case, low-temperature ( $-50\text{ }^\circ\text{C}$ ) addition of **3.60** to **3.20** in  $\text{C}_6\text{D}_8$  revealed two resonances ( $\delta = 66.1\text{ ppm}$  and  $51.6\text{ ppm}$ ) in the  $^{31}\text{P}\{^1\text{H}\}$  NMR spectrum. These resonances broaden significantly upon warming to  $-30\text{ }^\circ\text{C}$ , and are undetectable when the solution is further warmed to  $0\text{ }^\circ\text{C}$  (Figure 3.16).

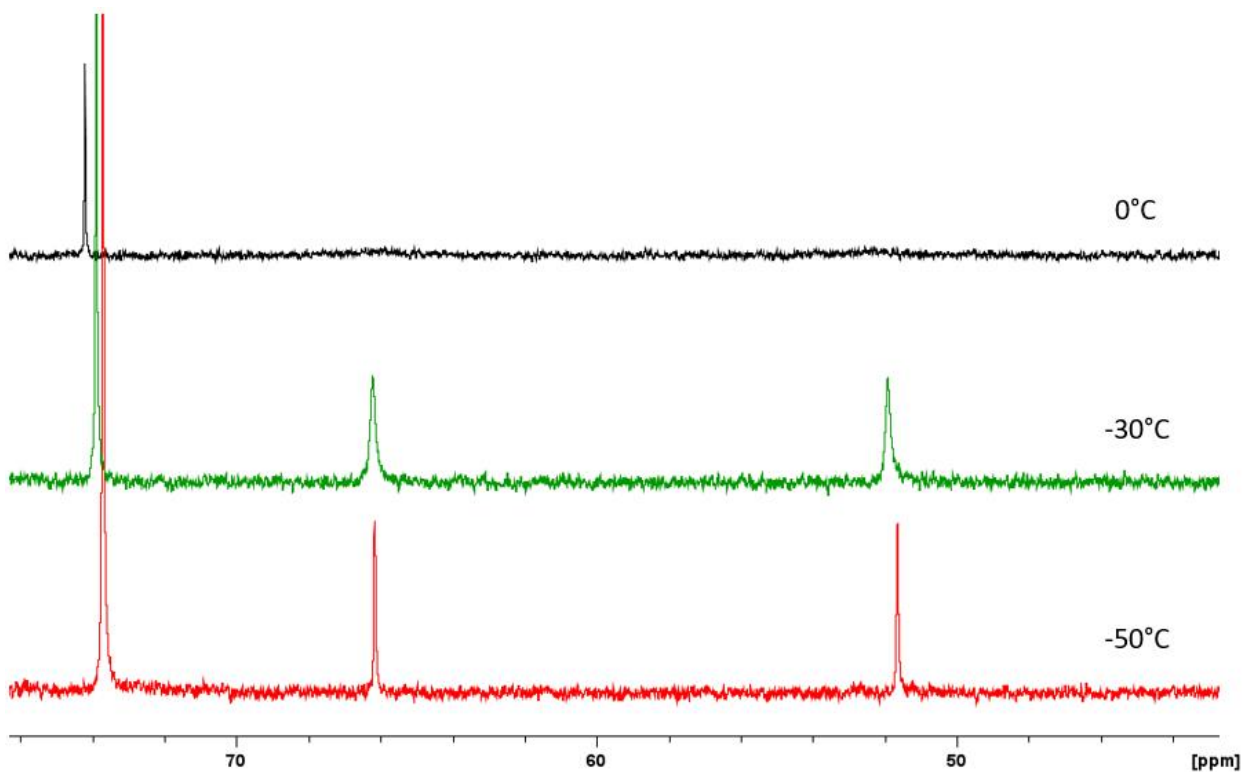


**Figure 3.16** Variable temperature  $^{31}\text{P}\{^1\text{H}\}$  NMR spectra of the reaction of **3.20** with oxaziridine **3.60** at  $-50^\circ\text{C}$  (red trace),  $-30^\circ\text{C}$  (green trace) and  $0^\circ\text{C}$  (black trace).

If care is taken to keep the reaction of **3.20** with **3.60** cold, intermediate **3.62** can be isolated in 88% yield as a dark powder, and large purple blocks can be grown from a concentrated  $\text{Et}_2\text{O}$  solution upon standing at  $-30^\circ\text{C}$ . Single crystal X-ray diffraction experiments determined that the structure of **3.62** is the nickel(II) oxazanickelacyclobutane depicted in Figure 3.17, formed *via* oxidative addition of the N-O bond.

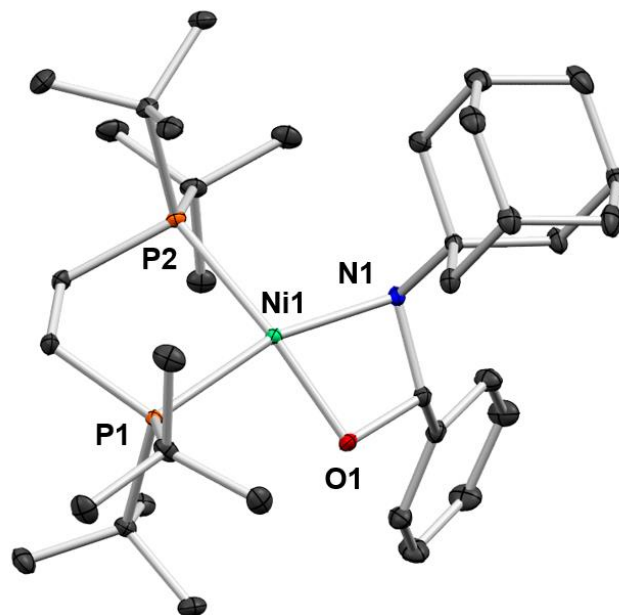
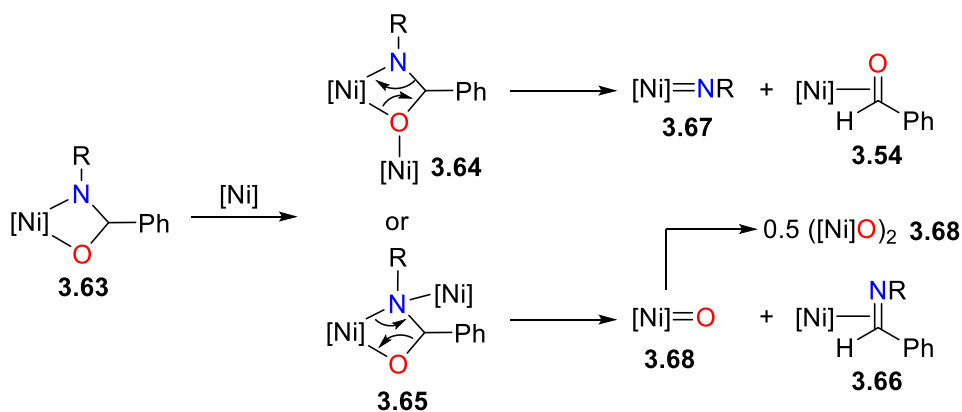


**Figure 3.17** ORTEP diagrams (50% probability ellipsoids) of complex **3.62**. All H atoms omitted for clarity.

Related metallacycles have been reported by the Hillhouse group, formed *via* reactions of imido complexes (dtbpe)Ni=NR with C=O-containing molecules like CO<sub>2</sub> and benzaldehyde.<sup>78</sup> Oxazametallacycles of early transition metals have also been reported by related synthetic routes.<sup>268, 269</sup> While the oxidative addition of the N-O bond of an oxaziridine has been invoked in palladium-catalyzed ethoxycarbonylation,<sup>270</sup> to the best of our knowledge, this is the first well-defined example of such a process.

A mechanism that could explain the unusual product distribution of the reactions of **3.20** with oxaziridines is outlined in Scheme 3.20. Oxidative addition of the N-O bond of the oxaziridine results in formation of an oxazanickelacyclobutane **3.63**. Coordination of another equivalent of nickel to either of the heteroatoms would form of bimetallics **3.64** or **3.65**, and formal [2+2] cycloreversion would then form either benzaldehyde complex **3.54** or imine complex **3.66**, along with an additional equivalent of either nickel(II) imido **3.67** or nickel(II) oxo **3.68**. Related complexes of nickel are known to rapidly dimerize,<sup>271-278</sup> and would likely be insoluble. For the

case of oxaziridine **3.60**, the lack of any detectable **3.67**, which has previously been prepared by Waterman and Hillhouse,<sup>266</sup> argues against this particular mechanism.



**Scheme 3.20** Potential mechanism of formation of **3.54** and **3.66** from **3.63**

## 3.6 Summary

In conclusion, this chapter describes the reactivity of low-valent nickel with three-membered oxacycles. Arene complex **3.20** was found to preferentially isomerize a variety of epoxides into their corresponding aldehydes. These aldehyde complexes of nickel(0) were characterized by an array of experimental methods, including X-ray diffraction, multinuclear NMR spectroscopy and mass spectrometry. Experiments with tetrasubstituted epoxides indicate that these isomerization reactions likely proceed *via* 2-nickela(II)oxetane intermediates, and that the oxidative addition of the C-O bond proceeds with *retention* of configuration. Catalytic functionalization of styrenyl epoxides was also achieved using HBpin and **3.20** as a catalyst. In addition, the chemistry of **3.20** with common oxaziridines was explored. It was found that oxidative addition of the metal into the weak N-O bond resulted in the formation of unstable oxazanickelacyclobutanes, which could fragment to form either imines or aldehydes. Overall, this work demonstrates that oxidative addition of

(dtbpe)nickel(0) into three-membered heterocycles is a viable reaction pathway for both catalytic and stoichiometric transformations.

## 3.7 Experimental

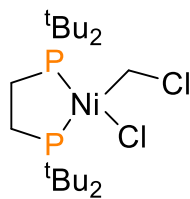
**General Considerations:** Unless stated otherwise, all reactions were performed in a glovebox or on a Schlenk line under an atmosphere of pure N<sub>2</sub> using standard Schlenk techniques. Anhydrous pentanes, toluene, diethyl ether, benzene, hexanes and tetrahydrofuran were purchased from Aldrich, sparged with N<sub>2</sub>, and dried further by passage through towers containing activated alumina and molecular sieves. Tol-d<sub>8</sub>, C<sub>6</sub>D<sub>6</sub> and THF-d<sub>8</sub> were purchased from Aldrich and dried over sodium/benzophenone before being distilled and degassed by three freeze-pump-thaw cycles. Epoxides **3.14** and **3.15** were purchased from commercial suppliers. Epoxides *cis*- and *trans*-**3.25** and **3.31** were prepared from *m*CPBA oxidation<sup>279</sup> of commercially available alkenes. Epoxides **3.27**, **3.28** and all epoxides in Table 3.4.1 were prepared through Corey-Chaykovsky conditions<sup>43, 280</sup> of commercially available benzaldehydes. Enantiopure epoxide (R)-**3.27** was prepared according to literature procedure.<sup>238</sup> Epoxides *cis*-**3.32** and *trans*-**3.32** were prepared *via m*CPBA oxidation of a 2:1 mixture of *cis*- and *trans*-2,3-diphenylbutene, which was synthesized according to literature procedure.<sup>281</sup> The resulting epoxides, whose spectral data match the literature,<sup>282</sup> could be separated by flash chromatography on silica gel (30:1 hexanes:EtOAc). Epoxide **3.35** was prepared as described below. All other epoxides were purified by either distillation or column chromatography, degassed by three freeze-pump-thaw cycles and stored under nitrogen at -30 °C over activated 4 Å molecular sieves. Oxaziridines **3.52** and **3.60** were prepared from *m*CPBA oxidation of imines **3.55**<sup>283</sup> and **3.61**,<sup>267</sup> respectively, according to literature procedures. Oxaziridine **3.52** was purified by column chromatography on silica gel (10:1 hexanes:EtOAc), while oxaziridine **3.60** was purified by recrystallization from boiling petroleum ether. Arene dimer

**3.20**,<sup>216</sup> ethylene complex **3.18**,<sup>219</sup> COD complex **3.17**,<sup>215</sup> dichloride **3.19**<sup>217</sup> and nickel(I) dimer **3.56**<sup>78</sup> were prepared according to the literature procedures. All other chemicals were purchased from commercial suppliers and used as received.

NMR spectra were recorded on 300, 400 and 600 MHz spectrometers and are referenced to residual protio solvent (7.16 ppm for C<sub>6</sub>D<sub>5</sub>H, 2.08 ppm for C<sub>6</sub>D<sub>5</sub>CD<sub>2</sub>H, 3.58 ppm for THF-d<sub>7</sub> and 7.26 for CHCl<sub>3</sub>) for <sup>1</sup>H NMR spectroscopy, solvent peaks (128.06 ppm for C<sub>6</sub>D<sub>6</sub>, 20.43 ppm for C<sub>6</sub>D<sub>5</sub>CD<sub>2</sub>H, 67.21 ppm for THF-d<sub>7</sub> and 77.16 for CHCl<sub>3</sub>) for <sup>13</sup>C NMR spectroscopy. <sup>31</sup>P{<sup>1</sup>H} NMR spectra were referenced to 85 % H<sub>3</sub>PO<sub>4</sub> at 0 ppm. NMR spectra were taken at 25 °C unless otherwise noted. NMR yields are averaged over at least two separate experiments and are performed using 1,3,5-trimethoxybenzene as internal standard. Mass spectra and elemental analyses were performed by the microanalytic services at the Department of Chemistry of the University of British Columbia. See Appendix A for detailed crystallographic data.

## Organometallic Syntheses

### Synthesis of **3.22**

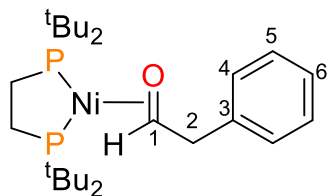


To a solution of ethylene complex **3.18** (12.0 mg, 0.0296 mmol, 1.0 equiv.) in 0.4 mL Tol-d<sub>8</sub> was added a solution of freshly prepared **3.15** (6.0 mg, 0.0500 mmol, 1.7 equiv.) in 0.2 mL Tol-d<sub>8</sub> in a J-Young NMR tube. The yellow solution was

monitored by <sup>31</sup>P{<sup>1</sup>H} NMR spectroscopy for several hours at room temperature, revealing the growth of a new nickel(II) species. After standing overnight at room temperature, the supernatant changed from yellow to orange, and small orange crystals had formed in the NMR tube. X-ray diffraction analysis revealed that the crystals were complex **3.22**.

$^{31}\text{P}$  NMR (162 MHz,  $\text{C}_6\text{D}_6$ )  $\delta$  78.3 (d[AB],  $J_{\text{P,P}} = 19$  Hz), 75.4 (d[AB],  $J_{\text{P,P}} = 19$  Hz).

### Synthesis of **3.23**



To a red-orange solution of **3.20** (35.7 mg, 0.043 mmol, 1.0 equiv) in 4 mL of  $\text{Et}_2\text{O}$  was added phenylacetaldehyde (17.5 mg, 0.146 mmol, 3.4 equiv) in 4 mL of  $\text{Et}_2\text{O}$ , resulting in a colour change to yellow. The solution was then stirred at room temperature for 2 hours. The volatiles were removed *in vacuo* to give a yellow residue, which was extracted with a minimum amount of  $\text{Et}_2\text{O}$  and filtered through glass fiber to give a yellow solution. On standing at  $-30$  °C overnight, yellow crystals formed. The supernatant was decanted, and the solids were dried *in vacuo* to yield 39.2 mg (92% yield) of **3.23** as X-ray quality crystals.

$^1\text{H}$  NMR (400 MHz,  $\text{C}_6\text{D}_6$ )  $\delta$  7.72 (d,  $J_{\text{H,H}} = 7.2$  Hz, 2H, **H4**), 7.25 (app. t,  $J_{\text{H,H}} = 7.2$  Hz, 2H, **H5**), 7.11 (app. t,  $J_{\text{H,H}} = 7.3$  Hz, 1H, **H6**), 4.98 (ddd,  $J_{\text{H,H}} = 6.9$  Hz,  $J_{\text{H,P}} = 3.1, 0.9$  Hz, 1H, **H1**), 3.58 (dd,  $J_{\text{H,H}} = 14.0$  Hz,  $J_{\text{H,P}} = 5.9$  Hz, 1H, **H2**), 3.04 (ddd,  $J_{\text{H,H}} = 13.9$  Hz,  $J_{\text{H,P}} = 3.1$  Hz, 1H, **H2**), 1.43-1.28 (m, 4H,  $\text{PCH}_2\text{CH}_2\text{P}$ ), 1.26 (d,  $J_{\text{H,P}} = 4.6$  Hz, 9H,  $\text{C}(\text{CH}_3)_3$ ), 1.22 (d,  $J_{\text{H,P}} = 4.5$  Hz, 9H,  $\text{C}(\text{CH}_3)_3$ ), 1.14 (d,  $J_{\text{H,P}} = 5.3$  Hz, 9H,  $\text{C}(\text{CH}_3)_3$ ), 1.10 (d,  $J_{\text{H,P}} = 5.3$  Hz, 9H,  $\text{C}(\text{CH}_3)_3$ ).

$^{31}\text{P}$  NMR (162 MHz,  $\text{C}_6\text{D}_6$ )  $\delta$  94.6 (d[AB],  $J_{\text{P,P}} = 74$  Hz), 83.9 (d[AB],  $J_{\text{P,P}} = 74$  Hz).

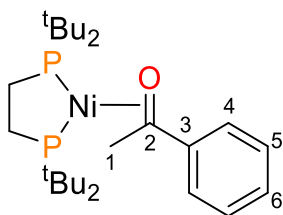
$^{13}\text{C}\{^1\text{H}\}$  NMR (100 MHz,  $\text{C}_6\text{D}_6$ )  $\delta$  142.68 (dd,  $J_{\text{C,P}} = 9, 2$  Hz, **C3**), 129.58 (s, **C4**), 128.41 (s, **C5**), 125.50 (s, **C6**), 80.83 (d,  $J_{\text{C,P}} = 25$  Hz, **C1**), 48.90 (br s, **C2**), 34.76 (dd,  $J_{\text{C,P}} = 14, 5$  Hz,  $\text{C}(\text{CH}_3)_3$ ),

34.30 (dd,  $J_{C,P} = 11, 4$  Hz,  $C(CH_3)_3$ ), 34.04 (dd,  $J_{C,P} = 7, 3$  Hz,  $C(CH_3)_3$ ), 33.79 (dd,  $J_{C,P} = 6, 2$  Hz,  $C(CH_3)_3$ ), 30.79 (d,  $J_{C,P} = 7$  Hz,  $C(CH_3)_3$ ), 30.65 (d,  $J_{C,P} = 7$  Hz,  $C(CH_3)_3$ ), 30.57 (d,  $J_{C,P} = 6$  Hz,  $C(CH_3)_3$ ), 30.40 (d,  $J_{C,P} = 7$  Hz,  $C(CH_3)_3$ ), 24.75 (dd,  $J_{C,P} = 21, J_{C,P} = 18$  Hz,  $PCH_2CH_2P$ ), 20.79 (app. t,  $J_{C,P} = 13$  Hz,  $PCH_2CH_2P$ ).

Anal. Calcd: C, 62.80; H, 9.73. Found: C, 61.81; H, 9.51. Although satisfactory elemental analysis could not be obtained after repeated attempts, the data here is included to demonstrate our best results.

LRMS (EI) 496 [ $M^+$ ]

### Synthesis of **3.24**



To a red-orange solution of **3.20** (36.5 mg, 0.044 mmol, 1.0 equiv) in 4 mL of  $Et_2O$  was added acetophenone (15.8 mg, 0.132 mmol, 3.0 equiv) in 4 mL of  $Et_2O$ , resulting in a colour change to orange. The solution was then stirred at room temperature for 2 hours. The volatiles were removed *in vacuo* to give an orange residue, which was extracted with a minimum amount of  $Et_2O$  and filtered through glass fiber to give an orange solution. On standing at  $-30$  °C overnight, an orange powder formed. The supernatant was decanted, and the solids were dried *in vacuo* to yield 31.5 mg (72% yield) of **3.24** as an orange powder. X-ray quality crystals were grown by cooling a concentrated toluene solution of **3.24** to  $-30$  °C.

$^1\text{H}$  NMR (400 MHz,  $\text{C}_6\text{D}_6$ )  $\delta$  7.91 (d,  $J_{\text{H,H}} = 7.8$  Hz, 2H, **H4**), 7.25 (t,  $J_{\text{H,H}} = 7.6$  Hz, 2H, **H5**), 7.12-7.08 (m, 1H, **H6**), 2.04 (dd,  $J_{\text{H,P}} = 8.6$ ,  $J_{\text{H,P}} = 1.5$  Hz, 3H, **H1**), 1.33 (d,  $J_{\text{H,P}} = 4.9$  Hz, 9H,  $\text{C}(\text{CH}_3)_3$ ), 1.30 (d,  $J_{\text{H,P}} = 5.0$  Hz, 9H,  $\text{C}(\text{CH}_3)_3$ ), 1.28-1.19 (m, 4H,  $\text{PCH}_2\text{CH}_2\text{P}$ ), 1.12 (d,  $J_{\text{H,P}} = 11.5$  Hz, 9H,  $\text{C}(\text{CH}_3)_3$ ), 0.73 (d,  $J_{\text{H,P}} = 11.8$  Hz, 9H,  $\text{C}(\text{CH}_3)_3$ ).

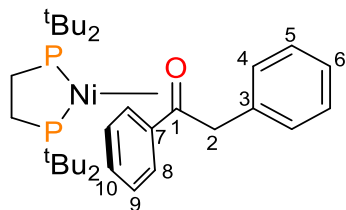
$^{31}\text{P}$  NMR (162 MHz,  $\text{C}_6\text{D}_6$ )  $\delta$  87.1 (d[AB],  $J_{\text{P,P}} = 75$  Hz), 85.9 (d[AB],  $J_{\text{P,P}} = 75$  Hz).

$^{13}\text{C}\{^1\text{H}\}$  NMR (100 MHz,  $\text{C}_6\text{D}_6$ )  $\delta$  153.5 (d,  $J_{\text{C,P}} = 3$  Hz, **C3**), 128.0 (**C4**, overlapping with solvent signal as shown by HSQC), 124.7 (d,  $J_{\text{C,P}} = 3$  Hz, **C5**), 122.9 (d,  $J_{\text{C,P}} = 3$  Hz, **C6**), 80.6 (d,  $J_{\text{C,P}} = 24$  Hz, **C2**), 34.7 (m,  $\text{C}(\text{CH}_3)_3$ ), 34.6 (m,  $\text{C}(\text{CH}_3)_3$ ), 34.2 (dd,  $J_{\text{C,P}} = 7$  Hz,  $J_{\text{C,P}} = 3$  Hz,  $\text{C}(\text{CH}_3)_3$ ), 33.8 (dd,  $J_{\text{C,P}} = 5$  Hz,  $J_{\text{C,P}} = 3$  Hz,  $\text{C}(\text{CH}_3)_3$ ), 30.7 (d,  $J_{\text{C,P}} = 3$  Hz,  $\text{C}(\text{CH}_3)_3$ ), 30.64 (d,  $J_{\text{C,P}} = 3$  Hz,  $\text{C}(\text{CH}_3)_3$ ), 30.6 (d,  $J_{\text{C,P}} = 7$  Hz,  $\text{C}(\text{CH}_3)_3$ ), 30.1 (d,  $J_{\text{C,P}} = 6$  Hz,  $\text{C}(\text{CH}_3)_3$ ), 27.3 (app. t,  $J_{\text{C,P}} = 2$  Hz, **C1**), 25.0 (dd,  $J_{\text{C,P}} = 22$  Hz,  $J_{\text{C,P}} = 20$  Hz,  $\text{PCH}_2\text{CH}_2\text{P}$ ), 20.1 (dd,  $J_{\text{C,P}} = 13$  Hz,  $J_{\text{C,P}} = 11$  Hz,  $\text{PCH}_2\text{CH}_2\text{P}$ ).

Anal. Calcd: C, 62.80; H, 9.73. Found: C, 63.08; H, 9.67.

LRMS (EI) 496 [ $\text{M}^+$ ]

## Synthesis of 3.26



To a red-orange solution of **3.20** (41.6 mg, 0.050 mmol, 1.0 equiv) in 4 mL of Et<sub>2</sub>O was added deoxybenzoin (23.3 mg, 0.119 mmol, 2.4 equiv) in 4 mL of Et<sub>2</sub>O, resulting in a colour change to orange. The solution was then stirred at room temperature for 2 hours. The volatiles were then removed *in vacuo* to give an orange residue, which was extracted with a minimum amount pentanes and filtered through glass fiber to give an orange solution. On standing at -30 °C overnight, an orange solid precipitated. The supernatant was decanted, and the solids dried *in vacuo* to yield 53.2 mg (93% yield) of **3.26** over several fractions. X-ray quality crystals were grown by cooling a saturated Et<sub>2</sub>O solution of **3.26** to -30 °C.

<sup>1</sup>H NMR (400 MHz, C<sub>6</sub>D<sub>6</sub>) 7.90 (d,  $J_{H,H} = 8.0$  Hz, 2H, **H4** or **H8**), 7.75 (d,  $J_{H,H} = 7.4$  Hz, 2H, **H4** or **H8**), 7.13 (t,  $J_{H,H} = 7.7$  Hz, 2H, **H5** or **H9**), 7.10 (t,  $J_{H,H} = 7.5$  Hz, 2H, **H5** or **H9**), 6.95 (m, 2H, **H6** and **H10**), 4.46 (dd,  $J_{H,H} = 14.5$  Hz,  $J_{H,P} = 5.2$  Hz, 1H, **H2**), 3.44 (dd,  $J_{H,H} = 14.4$  Hz,  $J_{H,P} = 3.2$  Hz, 1H, **H2**), 1.31 (d,  $J_{H,P} = 11.8$  Hz, 9H, C(CH<sub>3</sub>)<sub>3</sub>), 1.30 (d,  $J_{H,P} = 11.8$  Hz, 9H, C(CH<sub>3</sub>)<sub>3</sub>), 1.16 (d,  $J_{H,P} = 11.8$  Hz, 9H, C(CH<sub>3</sub>)<sub>3</sub>), 0.87-1.11 (m, 4H, PCH<sub>2</sub>CH<sub>2</sub>P), 0.73 (d,  $J_{H,P} = 12.2$  Hz, 9H, C(CH<sub>3</sub>)<sub>3</sub>).

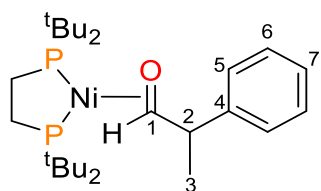
<sup>31</sup>P NMR (162 MHz, C<sub>6</sub>D<sub>6</sub>) δ 87.2 (d[AB],  $J_{P,P} = 73$  Hz), 85.0 (d[AB],  $J_{P,P} = 73$  Hz).

$^{13}\text{C}\{^1\text{H}\}$  NMR (100 MHz,  $\text{C}_6\text{D}_6$ )  $\delta$  151.3 (d,  $J_{\text{C,P}} = 5$  Hz, **C3** or **C7**), 140.3 (dd,  $J_{\text{C,P}} = 9$  Hz,  $J_{\text{C,P}} = 2$  Hz, **C3** or **C7**), 129.8 (s, **C4** or **C8**), 128.2 (s, **C5** or **C9**), 127.9 (s, **C5** or **C9**), 125.6 (s, **C4** or **C8**), 125.0 (d,  $J_{\text{C,P}} = 3$  Hz, **C6** or **C10**), 122.8 (d,  $J_{\text{C,P}} = 3$  Hz, **C6** or **C10**), 84.0 (d,  $J_{\text{C,P}} = 26$  Hz, **C1**), 47.2 (br. s, **C2**), 34.8 (dd,  $J_{\text{C,P}} = 9$  Hz,  $J_{\text{C,P}} = 5$  Hz,  $\text{C}(\text{CH}_3)_3$ ), 34.7 (dd,  $J_{\text{C,P}} = 9$  Hz,  $J_{\text{C,P}} = 4$  Hz,  $\text{C}(\text{CH}_3)_3$ ), 34.1 (dd,  $J_{\text{C,P}} = 8$  Hz,  $J_{\text{C,P}} = 2$  Hz,  $\text{C}(\text{CH}_3)_3$ ), 33.8 (dd,  $J_{\text{C,P}} = 6$ ,  $J_{\text{C,P}} = 3$  Hz,  $\text{C}(\text{CH}_3)_3$ ), 30.8-30.5 (m, 3  $\text{C}(\text{CH}_3)_3$ ), 30.1 (d,  $J_{\text{C,P}} = 6$  Hz,  $\text{C}(\text{CH}_3)_3$ ), 25.1 (dd,  $J_{\text{C,P}} = 21$  Hz,  $J_{\text{C,P}} = 19$  Hz,  $\text{PCH}_2\text{CH}_2\text{P}$ ), 20.1 (dd,  $J_{\text{C,P}} = 14$  Hz,  $J_{\text{C,P}} = 11$  Hz,  $\text{PCH}_2\text{CH}_2\text{P}$ ).

Anal. Calcd: C, 67.03; H, 9.14. Found: C, 66.36; H, 9.58. Although satisfactory analysis could not be obtained after repeated attempts, the data here is included to demonstrate our best results.

LRMS (EI) 572 [ $\text{M}^+$ ]

### Synthesis of **3.29**



To a red-orange solution of **3.20** (45.1 mg, 0.054 mmol, 1.0 equiv) in 5 mL of  $\text{Et}_2\text{O}$  was added 2-phenylpropionaldehyde (20.4 mg, 0.152 mmol, 2.8 equiv) in 4 mL of  $\text{Et}_2\text{O}$ . The solution was then stirred at

room temperature for 2 hours, during which time the colour changed from red-orange to yellow.

The volatiles were removed *in vacuo* to give a yellow residue, which was extracted with a minimum amount pentanes and filtered through glass fiber to give a yellow solution. On standing at  $-30$  °C, yellow crystals of **3.29** formed. The supernatant was decanted, and the crystals dried *in vacuo* to yield 42.3 mg (76% yield) of **3.29** over several fractions. X-ray quality crystals were

grown by cooling a saturated Et<sub>2</sub>O solution of **3.29** to -30 °C. Analysis by NMR of the crystals obtained from both Et<sub>2</sub>O and pentanes show a 15:2 mixture of diastereomers.

### Major diastereomer of **3.29**

<sup>1</sup>H NMR (400 MHz, C<sub>6</sub>D<sub>6</sub>) δ 7.79 (d,  $J_{H,H} = 7.5$  Hz, 2H, **H5**), 7.26 (t,  $J_{H,H} = 7.2$  Hz, 2H, **H6**), 7.11 (t,  $J_{H,H} = 7.2$  Hz, 1H, **H7**), 5.06 (dd,  $J_{H,P} = 6.2$  Hz,  $J_{H,P} = 2.4$  Hz, 1H, **H1**), 3.56 (app. pent.,  $J_{H,P} = J_{H,H} = 6.8$  Hz, 1H, **H2**), 1.71 (d,  $J_{H,H} = 7.0$  Hz, 3H, **H3**), 1.27 (d,  $J_{H,P} = 12.0$  Hz, 9H, C(CH<sub>3</sub>)<sub>3</sub>), 1.25 (d,  $J_{H,P} = 12.1$  Hz, 9H, C(CH<sub>3</sub>)<sub>3</sub>), 1.11 (br. d,  $J_{H,P} = 11.8$  Hz, 18H, 2 C(CH<sub>3</sub>)<sub>3</sub>). Although the resonances for the ethylene backbone of the dtbpe ligand could not be directly observed, they were detected indirectly *via* an HSQC experiment at around 1.44 ppm and 1.13 ppm.

<sup>31</sup>P NMR (162 MHz, C<sub>6</sub>D<sub>6</sub>) δ 93.7 (d[AB],  $J_{P,P} = 76$  Hz), 82.7 (d[AB],  $J_{P,P} = 75$  Hz).

<sup>13</sup>C{<sup>1</sup>H} NMR (100 MHz, C<sub>6</sub>D<sub>6</sub>) δ 148.8 (dd,  $J_{C,P} = 9$  Hz,  $J_{C,P} = 2$  Hz, **C4**), 128.6 (s, **C5**), 128.3 (s, **C6**), 125.7 (s, **C7**), 86.0 (d,  $J_{C,P} = 25$  Hz, **C1**), 49.5 (s, **C2**), 34.8 (dd,  $J_{C,P} = 14$  Hz,  $J_{C,P} = 5$  Hz, C(CH<sub>3</sub>)<sub>3</sub>), 34.2 (dd,  $J_{C,P} = 8$  Hz,  $J_{C,P} = 4$  Hz, C(CH<sub>3</sub>)<sub>3</sub>), 34.1 (dd,  $J_{C,P} = 7$  Hz,  $J_{C,P} = 3$  Hz, C(CH<sub>3</sub>)<sub>3</sub>), 34.0 (dd,  $J_{C,P} = 7$  Hz,  $J_{C,P} = 2$  Hz, C(CH<sub>3</sub>)<sub>3</sub>), 30.7 (d,  $J_{C,P} = 7$  Hz, C(CH<sub>3</sub>)<sub>3</sub>), 30.6 (d,  $J_{C,P} = 6$  Hz, C(CH<sub>3</sub>)<sub>3</sub>), 30.5 (d,  $J_{C,P} = 5$  Hz, C(CH<sub>3</sub>)<sub>3</sub>), 30.4 (d,  $J_{C,P} = 5$  Hz, C(CH<sub>3</sub>)<sub>3</sub>), 24.7 (dd,  $J_{C,P} = 22$  Hz,  $J_{C,P} = 18$  Hz, PCH<sub>2</sub>CH<sub>2</sub>P), 21.2 (s, **C3**), 20.8 (app. t,  $J_{C,P} = 13$  Hz, PCH<sub>2</sub>CH<sub>2</sub>P).

### Minor diastereomer of **3.29**

Due to the weak signal intensity and overlap with the resonances from the major diastereomer, the NMR data for the minor diastereomer could only be partially assigned.

$^1\text{H}$  NMR (600 MHz,  $\text{C}_6\text{D}_6$ )  $\delta$  7.72 (d,  $J_{\text{H,H}} = 8.0$  Hz, 2H, **H5**), 5.00 (br. d.,  $J_{\text{H,H}} = 6.3$  Hz, 1H, **H1**), 3.28 (app. pent.,  $J_{\text{H,H}} = 6.8$  Hz, 1H, **H2**), 1.78 (d,  $J_{\text{H,H}} = 7.1$  Hz, 3H, **H3**), 0.96 (d,  $J_{\text{H,P}} = 12.1$  Hz, 9H,  $\text{C}(\text{CH}_3)_3$ ).

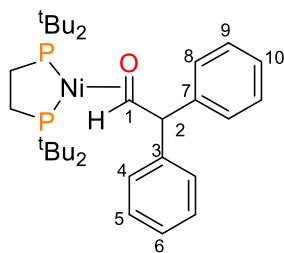
$^{31}\text{P}$  NMR (162 MHz,  $\text{C}_6\text{D}_6$ )  $\delta$  93.8 (d[AB],  $J_{\text{P,P}} = 73$  Hz), 82.7 (d[AB],  $J_{\text{P,P}} = 73$  Hz).

$^{13}\text{C}\{^1\text{H}\}$  NMR (125 MHz,  $\text{C}_6\text{D}_6$ )  $\delta$  147.7 (d,  $J_{\text{C,P}} = 3$  Hz, **C4**), 130.0 (s, **C5**), 125.4 (s, **C7**), 86.0 (d,  $J_{\text{C,P}} = 27$  Hz, **C1**), 48.4 (s, **C3**), 24.8 (app. t,  $J_{\text{C,P}} = 21$  Hz,  $\text{PCH}_2\text{CH}_2\text{P}$ ), 22.7 (s, **C3**), 20.4 (app. t,  $J_{\text{C,P}} = 13$  Hz,  $\text{PCH}_2\text{CH}_2\text{P}$ ).

Anal. Calcd: C, 63.42; H, 9.86. Found: C, 63.46; H, 10.15.

LRMS (EI) 510 [ $\text{M}^+$ ]

### Synthesis of **3.30**



To a red-orange solution of **3.20** (48.5 mg, 0.058 mmol, 1.0 equiv) in 4 mL of  $\text{Et}_2\text{O}$  was added diphenylacetaldehyde (25.1 mg, 0.128 mmol, 2.2 equiv) in 4 mL  $\text{Et}_2\text{O}$ , resulting in an instant colour change to yellow. The solution was stirred at room temperature for 2 hours, then the volatiles were removed *in vacuo* to yield a yellow residue. The residue was extracted with a minimum

volume of pentanes, then filtered through glass fiber into a 5-dram vial. The yellow solution was stored at -30 °C overnight, resulting in the formation of yellow crystals of **3.30**. The supernatant was decanted, and after drying *in vacuo*, 61.7 mg (92% yield) of **3.30** was collected over several fractions. X-ray quality crystals of **10** were grown by cooling a pentanes solution of **3.30** at -30 °C.

<sup>1</sup>H NMR (400 MHz, C<sub>6</sub>D<sub>6</sub>) δ 7.89 (d,  $J_{\text{H,H}} = 8.1$  Hz, 2H, **H4** or **H8**), 7.85 (d,  $J_{\text{H,H}} = 7.1$  Hz, 2H, **H4** or **H8**), 7.18-7.11 (m, 4H, **H5** and **H9**), 7.04-6.98 (m, 2H, **H6** and **H10**), 5.25 (ddd,  $J_{\text{H,P}} = 6.3$  Hz,  $J_{\text{H,P}} = 2.4$  Hz,  $J_{\text{H,H}} = 1.4$  Hz, 1H, **H1**), 4.59 (dd,  $J_{\text{H,P}} = 5.0$  Hz,  $J_{\text{H,H}} = 1.3$  Hz, 1H, **H2**). 1.29 - 1.23 (m, 2H, PCH<sub>2</sub>CH<sub>2</sub>P), 1.22 (d,  $J_{\text{H,P}} = 11.8$  Hz, 9H, C(CH<sub>3</sub>)<sub>3</sub>), 1.18-1.10 (m, 2H, PCH<sub>2</sub>CH<sub>2</sub>P), 1.08 (d,  $J_{\text{H,P}} = 12.0$  Hz, 9H, C(CH<sub>3</sub>)<sub>3</sub>), 1.05 (d,  $J_{\text{H,P}} = 12.0$  Hz, 9H, C(CH<sub>3</sub>)<sub>3</sub>), 0.91 (d,  $J_{\text{H,P}} = 12.2$  Hz, 9H, C(CH<sub>3</sub>)<sub>3</sub>).

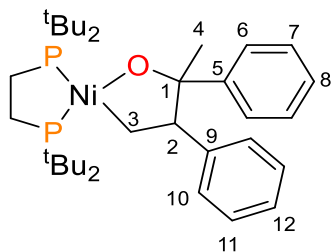
<sup>31</sup>P NMR (162 MHz, C<sub>6</sub>D<sub>6</sub>) δ 93.1 (d[AB],  $J_{\text{P,P}} = 71$  Hz), 82.1 (d[AB],  $J_{\text{P,P}} = 71$  Hz).

<sup>13</sup>C{<sup>1</sup>H} NMR (100 MHz, C<sub>6</sub>D<sub>6</sub>) δ 147.0 (dd,  $J_{\text{C,P}} = 9$  Hz,  $J_{\text{C,P}} = 2$  Hz, **C3** or **C7**), 145.3 (d,  $J_{\text{C,P}} = 2$  Hz, **C3** or **C7**), 131.2 (s, **C5** or **C9**), 129.5 (s, **C5** or **C9**), 129.0 (s, **C4** or **C8**), 128.6 (s, **C4** or **C8**), 125.7 (s, **C6** or **C10**), 125.5 (s, **C6** or **C10**), 83.1 (dd,  $J_{\text{C,P}} = 26$  Hz,  $J_{\text{C,P}} = 2$  Hz, **C1**), 60.5 (br. s, **C2**), 35.0 (dd,  $J_{\text{C,P}} = 14$  Hz,  $J_{\text{C,P}} = 4$  Hz, C(CH<sub>3</sub>)<sub>3</sub>), 34.2 (dd,  $J_{\text{C,P}} = 7$  Hz,  $J_{\text{C,P}} = 4$  Hz, C(CH<sub>3</sub>)<sub>3</sub>), 34.0 (dd,  $J_{\text{C,P}} = 6$  Hz,  $J_{\text{C,P}} = 2$  Hz, C(CH<sub>3</sub>)<sub>3</sub>), 33.8 (dd,  $J_{\text{C,P}} = 12$  Hz,  $J_{\text{C,P}} = 4$  Hz, C(CH<sub>3</sub>)<sub>3</sub>), 30.7-30.5 (m, 3 C(CH<sub>3</sub>)<sub>3</sub>), 30.4 (d,  $J_{\text{C,P}} = 7$  Hz, C(CH<sub>3</sub>)<sub>3</sub>), 24.7 (dd,  $J_{\text{C,P}} = 21$  Hz,  $J_{\text{C,P}} = 18$  Hz, PCH<sub>2</sub>CH<sub>2</sub>P), 20.5 (app. t,  $J_{\text{C,P}} = 13$  Hz, PCH<sub>2</sub>CH<sub>2</sub>P).

Anal. Calcd: C, 67.03; H, 9.14. Found: C, 68.51; H, 9.25. Analysis of isolated **10** via NMR spectroscopy and X-ray diffraction reveals that a small amount of diphenylacetaldehyde co-crystallizes with complex **10**. Although satisfactory elemental analysis could not be obtained after repeated attempts, the data here is included to demonstrate our best results.

LRMS (EI) 572 [M<sup>+</sup>]

### Synthesis of **3.34**



To a red-orange solution of **3.20** (74.0 mg, 0.089 mmol, 1.0 equiv) in 5 mL of benzene was added epoxide *cis*-**3.32** (43.3 mg, 0.193 mmol, 2.2 equiv) in 5 mL of benzene. The red-orange solution was then transferred to a Teflon-sealed Schlenk flask, and heated in an oil bath at 60 °C for 16 hours, during which time the colour changed from red-orange to dark red, then finally to amber. The volatiles were then removed *in vacuo* to give a yellow-brown residue, which was extracted with a minimum amount pentanes and filtered through glass fiber to give a yellow solution. On standing at -30 °C overnight, yellow crystals formed. The supernatant was decanted, and the crystals dried *in vacuo* to yield 93.7 mg (88% yield) of **3.34** over two fractions. X-ray quality crystals were grown by cooling a concentrated pentanes solution of **3.34** to -30 °C.

<sup>1</sup>H{<sup>31</sup>P} NMR (400 MHz, C<sub>6</sub>D<sub>6</sub>) δ 7.74 (d, *J*<sub>H,H</sub> = 7.3 Hz, 2H, **H6**), 7.29 (t, *J*<sub>H,H</sub> = 7.5 Hz, 2H, **H7**), 7.23 (d, *J*<sub>H,H</sub> = 7.3 Hz, 2H, **H10**), 7.14-7.09 (m, 3H, **H8** + **H11**), 7.05 (t, *J*<sub>H,H</sub> = 7.2 Hz, 1H, **H12**),

3.53 (dd,  $J_{H,H} = 12.0$  Hz,  $J_{H,H} = 3.4$  Hz, 1H, **H2**), 2.03 (dd,  $^2J_{H,H} = 9.5$  Hz,  $J_{H,H} = 3.5$  Hz, 1H, **H3**), 2.00 (s, 3H, **H4**), 1.81 (dd,  $J_{H,H} = 12.1$  Hz,  $^2J_{H,H} = 9.5$  Hz, 1H, **H3**), 1.51 (s, 9H, C(CH<sub>3</sub>)<sub>3</sub>), 1.43 (s, 9H, C(CH<sub>3</sub>)<sub>3</sub>), 1.13 (s, 9H, C(CH<sub>3</sub>)<sub>3</sub>), 1.06 (s, 9H, C(CH<sub>3</sub>)<sub>3</sub>). Although the resonances for the methylene groups of the dtbpe ligand could not be clearly distinguished, an HSQC experiment showed that they are located at 1.33, 1.13, 1.12 and 0.93 ppm.

<sup>31</sup>P{<sup>1</sup>H} NMR (162 MHz, C<sub>6</sub>D<sub>6</sub>) δ 79.7(d[AB],  $J_{P,P} = 13$  Hz), 71.8 (d[AB].  $J_{P,P} = 13$  Hz).

<sup>13</sup>C{<sup>1</sup>H} NMR (100 MHz, C<sub>6</sub>D<sub>6</sub>) δ 150.9 (s, **C5**), 147.8 (t,  $J_{P,C} = 4$  Hz, **C9**), 129.7 (s, **C10**), 128.9 (s, **C6**), 127.3 (s, **C11**), 126.2 (s, **C7**), 125.4 (s, **C12**), 124.9 (s, **C8**), 84.3 (dd,  $J_{P,C} = 11$  Hz,  $J_{P,C} = 2$  Hz, **C1**), 66.9 (t,  $J_{P,C} = 5$  Hz, **C2**), 36.1 (dd,  $J_{P,C} = 15$  Hz,  $J_{P,C} = 2$  Hz, C(CH<sub>3</sub>)<sub>3</sub>), 35.6 (dd,  $J_{P,C} = 17$  Hz,  $J_{P,C} = 3$  Hz, C(CH<sub>3</sub>)<sub>3</sub>), 34.9 (d,  $J_{P,C} = 8$  Hz, C(CH<sub>3</sub>)<sub>3</sub>), 34.6 (d,  $J_{P,C} = 5$  Hz, C(CH<sub>3</sub>)<sub>3</sub>), 33.2 (s, **C4**), 30.8-30.6 (m, 2 C(CH<sub>3</sub>)<sub>3</sub>), 30.6 (d,  $J_{P,C} = 4$  Hz, C(CH<sub>3</sub>)<sub>3</sub>), 30.3 (d,  $J_{P,C} = 4$  Hz, C(CH<sub>3</sub>)<sub>3</sub>), 27.9 (dd,  $J_{P,C} = 67$  Hz,  $J_{P,C} = 24$  Hz, **C3**), 26.0 (dd,  $J_{P,C} = 24$  Hz,  $J_{P,C} = 17$  Hz, PCH<sub>2</sub>CH<sub>2</sub>P), 18.9 (app. t,  $J_{P,C} = 11$  Hz, PCH<sub>2</sub>CH<sub>2</sub>P).

Anal. Calcd: C, 67.90; H, 9.39. Found: C, 67.96; H, 9.08.

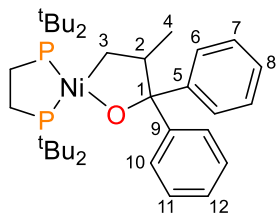
LRMS (EI) 600 [M<sup>+</sup>], 585 [M<sup>+</sup>-Me]

### Synthesis of **3.36**, **3.37** and **3.38**

To a red-orange solution of **3.20** (85.6 mg, 0.103 mmol, 1.0 equiv) in 5 mL of benzene was added epoxide **3.35** (46.1 mg, 0.206 mmol, 2.0 equiv) in 5 mL of benzene. The red-orange solution was then transferred to a Teflon-sealed Schlenk flask, and heated in an oil bath at 60 °C for 16 hours, during which time the colour changed from red-orange to very dark red. The volatiles were then removed *in vacuo* to give a dark red-brown residue, which was extracted with a minimum amount of cold pentanes and filtered through glass fiber to give a dark red solution. On standing at -30 °C overnight, a dark red solid formed. The supernatant was decanted, and the solids dried *in vacuo* to yield 58.5 mg (47% yield) of **3.36** as an impure powder. Despite repeated efforts, we have been unable to obtain analytically pure **3.36** or grow sufficient quality crystals for an X-ray diffraction study. In our attempts to recrystallize complex **3.36** from pentanes, we did manage to isolate small crystals of complex **3.38**, the analogue of complex **3.37** where the dtbpe ligand has not been oxidized. However, the crystals were twinned to an extent that rendered the data insufficient for publication. In addition, we were unable to obtain NMR data of sufficient quality for structural assignment. We have included a ORTEP depiction of **3.38** (*vide supra*) merely to demonstrate connectivity.

The residue remaining on the filter pad from above was extracted with Et<sub>2</sub>O, and filtered into a 5-dram vial to give a yellow solution, which was concentrated *in vacuo* and stored at -30 °C overnight to form brown-yellow crystals of **3.37** (8.1 mg, 13% yield) which were suitable for X-ray diffraction analysis.

### Characterization data for 3.36



$^1\text{H}$  NMR (400 MHz,  $\text{C}_6\text{D}_6$ )  $\delta$  7.97 (d,  $J_{\text{H,H}} = 7.7$  Hz, 2H, **H6** or **H10**), 7.94 (d,  $J_{\text{H,H}} = 7.7$  Hz, 2H, **H6** or **H10**), 7.31 (t,  $J_{\text{H,H}} = 7.4$  Hz, 4H, **H7** and **H11**), 7.13-7.06 (m, 2H, **H8** and **H12**), 3.07-2.98 (m, 1H, **H2**), 1.90-1.82 (m, 1H, **H3**), 1.76-1.68 (m, 1H, **H3**), 1.44 (d,  $J_{\text{H,P}} = 11.7$  Hz, 9H,  $\text{C}(\text{CH}_3)_3$ ), 1.44 (d,  $J_{\text{H,H}} = 6.5$  Hz, 3H, **H4**), 1.33 (d,  $J_{\text{H,P}} = 11.9$  Hz, 9H,  $\text{C}(\text{CH}_3)_3$ ), 1.16-1.08 (m, 13H,  $\text{C}(\text{CH}_3)_3$  and  $\text{PCH}_2\text{CH}_2\text{P}$ ), 0.99 (d,  $J_{\text{H,P}} = 12.2$  Hz, 9H,  $\text{C}(\text{CH}_3)_3$ ).

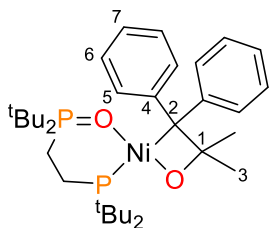
$^{31}\text{P}$  NMR (162 MHz,  $\text{C}_6\text{D}_6$ )  $\delta$  77.3 (d,  $J_{\text{P,P}} = 14$  Hz), 71.2 (d,  $J_{\text{P,P}} = 14$  Hz).

$^{13}\text{C}\{^1\text{H}\}$  NMR (100 MHz,  $\text{C}_6\text{D}_6$ )  $\delta$  155.4 (s, **C5** or **C9**), 152.5 (s, **C5** or **C9**), 128.9 (s, **C6** or **C10**), 127.9 (s, **C6** or **C10**), 127.2 (s, **C7** or **C11**), 126.9 (s, **C7** or **C11**), 124.8 (s, **C8** or **C12**), 124.6 (s, **C8** or **C12**), 90.4 (d,  $J_{\text{C,P}} = 12$  Hz, **C1**), 49.5 (t,  $J_{\text{C,P}} = 5$  Hz, **C2**), 36.0 (dd,  $J_{\text{C,P}} = 16$  Hz,  $J_{\text{C,P}} = 2$  Hz,  $\text{C}(\text{CH}_3)_3$ ), 35.6 (dd,  $J_{\text{C,P}} = 16$  Hz,  $J_{\text{C,P}} = 3$  Hz,  $\text{C}(\text{CH}_3)_3$ ), 34.7 (d,  $J_{\text{C,P}} = 6$  Hz,  $\text{C}(\text{CH}_3)_3$ ), 34.6 (d,  $J_{\text{C,P}} = 6$  Hz,  $\text{C}(\text{CH}_3)_3$ ), 30.7 (d,  $J_{\text{C,P}} = 5$  Hz,  $\text{C}(\text{CH}_3)_3$ ), 30.6-30.4 (m, 3  $\text{C}(\text{CH}_3)_3$ ), 30.0 (d,  $J_{\text{C,P}} = 24$  Hz, **C3**), 25.8 (dd,  $J_{\text{C,P}} = 23$  Hz,  $J_{\text{C,P}} = 17$  Hz,  $\text{PCH}_2\text{CH}_2\text{P}$ ), 21.4 (s, **C4**), 18.9 (dd,  $J_{\text{C,P}} = 12$  Hz,  $J_{\text{C,P}} = 10$  Hz,  $\text{PCH}_2\text{CH}_2\text{P}$ ).

Anal. Calcd: C, 67.90; H, 9.39. Found: C, 65.62; H, 9.47. Although satisfactory elemental analysis could not be obtained after repeated attempts, the data here is included to demonstrate our best results.

LRMS (EI) 600 [M<sup>+</sup>]

### Characterization data for 3.37



<sup>1</sup>H NMR (600 MHz, C<sub>6</sub>D<sub>6</sub>) δ 8.43 (d, *J*<sub>H,H</sub> = 7.6 Hz, 4H, **H5**), 7.36 (t, *J*<sub>H,H</sub> = 7.5 Hz, 4H, **H6**), 7.23 (t, *J*<sub>H,H</sub> = 7.3 Hz, 2H, **H7**), 1.69 (s, 6H, **H3**), 1.58 (d, *J*<sub>H,P</sub> = 11.8 Hz, 18H, 2 C(CH<sub>3</sub>)<sub>3</sub>), 1.22-1.18 (m, 2H, PCH<sub>2</sub>CH<sub>2</sub>P), 1.09-1.04 (m, 2H, PCH<sub>2</sub>CH<sub>2</sub>P), 0.65 (d, *J*<sub>H,P</sub> = 13.8 Hz, 18H, 2 C(CH<sub>3</sub>)<sub>3</sub>).

<sup>31</sup>P NMR (162 MHz, C<sub>6</sub>D<sub>6</sub>) δ 70.8 (d, *J*<sub>P,P</sub> = 6 Hz), 29.4 (d, *J*<sub>P,P</sub> = 6 Hz).

<sup>13</sup>C{<sup>1</sup>H} NMR (125 MHz, C<sub>6</sub>D<sub>6</sub>) δ 151.2 (d, *J*<sub>C,P</sub> = 5 Hz, **C4**), 130.5 (d, *J*<sub>C,P</sub> = 5 Hz, **C5**), 127.5 (s, **C6**), 121.7 (s, **C7**), 85.4 (s, **C1**), 35.8 (d, *J*<sub>C,P</sub> = 60 Hz, C(CH<sub>3</sub>)<sub>3</sub>), 34.2 (d, *J*<sub>C,P</sub> = 5 Hz, C(CH<sub>3</sub>)<sub>3</sub>), 33.9 (s, **C3**), 30.1 (d, *J*<sub>C,P</sub> = 6 Hz, C(CH<sub>3</sub>)<sub>3</sub>), 26.6 (s, C(CH<sub>3</sub>)<sub>3</sub>), 24.1 (d, *J*<sub>C,P</sub> = 63 Hz, **C2**), 15.6 (d, *J*<sub>C,P</sub> = 51 Hz, PCH<sub>2</sub>CH<sub>2</sub>P), 12.1 (d, *J*<sub>C,P</sub> = 5 Hz, PCH<sub>2</sub>CH<sub>2</sub>P).

Anal. Calcd: C, 66.14; H, 9.14. Found: C, 62.32; H, 8.67. Although satisfactory elemental analysis could not be obtained after repeated attempts, the data here is included to demonstrate our best results.

LRMS (EI) 616 [M<sup>+</sup>]

#### IV. Isomerization and Exchange Experiments

##### Isomerization of **3.15** with complex **3.20**

A solution of complex **3.20** (8.3 mg, 0.010 mmol, 1.0 equiv) and trimethoxybenzene as internal standard in 0.5 mL C<sub>6</sub>D<sub>6</sub> was added to a vial containing **3.15** (4.1 mg, 0.034 mmol, 3.4 equiv.), resulting in a colour change from red-orange to yellow instantly. Analysis of the solution by <sup>31</sup>P{<sup>1</sup>H} and <sup>1</sup>H NMR spectroscopy reveals the presence of **3.23** in 73% yield and **3.24** in 12% yield.

##### Isomerization of *cis*-**3.25** with complex **3.20**

A solution of complex **3.20** (7.7 mg, 0.093 mmol, 1.0 equiv) and trimethoxybenzene as internal standard in 0.5 mL C<sub>6</sub>D<sub>6</sub> was added to a vial containing *cis*-**3.25** (5.8 mg, 0.030 mmol, 3.1 equiv.), resulting in a colour change from red-orange to orange instantly. Analysis of the solution by <sup>31</sup>P{<sup>1</sup>H} and <sup>1</sup>H NMR spectroscopy reveals the presence of **3.26** in 97% yield.

##### Isomerization of *trans*-**3.25** with complex **3.20**

A solution of complex **3.20** (8.0 mg, 0.096 mmol, 1.0 equiv) and trimethoxybenzene as internal standard in 0.5 mL C<sub>6</sub>D<sub>6</sub> was added to a vial containing *trans*-**3.25** (5.2 mg, 0.026

mmol, 2.6 equiv.), resulting in a colour change from red-orange to orange instantly. Analysis of the solution by  $^{31}\text{P}\{^1\text{H}\}$  and  $^1\text{H}$  NMR spectroscopy reveals the presence of **3.26** in 88% yield.

#### **Isomerization of 3.27 with complex 3.20**

A solution of complex **3.20** (7.7 mg, 0.0093 mmol, 1.0 equiv) and trimethoxybenzene as internal standard in 0.5 mL  $\text{C}_6\text{D}_6$  was added to a vial containing **3.27** (5.9 mg, 0.044 mmol, 4.7 equiv.), resulting in a colour change from red-orange to yellow over 6 hours. Analysis of the solution by  $^{31}\text{P}\{^1\text{H}\}$  and  $^1\text{H}$  NMR spectroscopy reveals the presence of **3.29** in 93% yield.

#### **Isomerization of 3.28 with complex 3.20**

A solution of complex **3.20** (7.7 mg, 0.0093 mmol, 1.0 equiv) and trimethoxybenzene as internal standard in 0.5 mL  $\text{C}_6\text{D}_6$  was added to a vial containing **3.28** (5.1 mg, 0.026 mmol, 2.8 equiv.), resulting in a colour change from red-orange to yellow over 4 hours. Analysis of the solution by  $^{31}\text{P}\{^1\text{H}\}$  and  $^1\text{H}$  NMR spectroscopy reveals the presence of **3.30** in 78% yield.

#### **Reaction of 3.23 with acetophenone**

Complexes **3.23** (6.4 mg, 0.013 mmol, 1.0 equiv) was dissolved in 0.5 mL of  $\text{C}_6\text{D}_6$  and added to a vial containing acetophenone (14.0 mg, 0.117 mmol, 9.0 equiv.). The solution was transferred to a J-young NMR tube, and monitored by  $^{31}\text{P}\{^1\text{H}\}$  NMR spectroscopy. No change was observed in the reaction after 2 days at room temperature. The tube was then placed in an oil bath at 80 °C for 24 hours. Subsequent analysis by  $^{31}\text{P}\{^1\text{H}\}$  NMR spectroscopy reveals that the reaction contains trace ( $\approx 10\%$ ) ligand exchange product **3.24**,

as well as the formation of a small amount of a new nickel(0) complex ( $\delta = 94.5$  ppm,  $J_{P,P} = 71$  Hz,  $\delta = 83.6$  ppm,  $J_{P,P} = 71$  Hz) that we have thus far been unable to identify. Additional heating of the tube at 80 °C for 4 days resulted in further ligand exchange ( $\approx 40\%$  yield of **3.24**), as well as further formation of the new nickel(0) product and a concomitant decrease in **3.23**.

### **Reaction of 3.24 with phenylacetaldehyde**

Complexes **3.24** (8.9 mg, 0.018 mmol, 1.0 equiv) was dissolved in 0.5 mL of C<sub>6</sub>D<sub>6</sub> and added to a vial containing phenylacetaldehyde (16.4 mg, 0.136 mmol, 7.6 equiv.). The solution was transferred to a J-young NMR tube, and monitored by <sup>31</sup>P{<sup>1</sup>H} NMR spectroscopy. No change was observed in the reaction after 2 days at room temperature. The tube was then placed in an oil bath at 80 °C for 2 hours. Subsequent analysis <sup>31</sup>P{<sup>1</sup>H} NMR spectroscopy reveals that the reaction contains trace ( $\approx 15\%$ ) ligand exchange product **3.23**, as well as the formation of a small amount of a new nickel(0) complex ( $\delta = 94.5$  ppm,  $J_{P,P} = 71$  Hz,  $\delta = 83.6$  ppm,  $J_{P,P} = 71$  Hz ) that we have thus far been unable to identify. Additional heating of the tube at 80 °C for 2 days resulted in further ligand exchange ( $\approx 45\%$  yield of **3.23**), as well as further formation of the new nickel(0) product and a concomitant decrease in **3.24**.

### **Attempted isolation of unknown nickel(0) product**

In an attempt to identify the nickel(0) product formed above, separate solutions of **3.23** and **3.24** in C<sub>6</sub>D<sub>6</sub> were heated at 80 °C in J-young NMR tubes. While no change was observed in the solution containing **3.24**, the solution containing **3.23** developed a brown precipitate, and the formation of the nickel(0) contaminant was observed by <sup>31</sup>P{<sup>1</sup>H} NMR

spectroscopy. Unfortunately, we were unable to isolate any tractable amounts of the unknown product for further structural analysis.

## V. Hydroboration Experiments

A solution of complex **3.20** (4.0 mg, 0.005 mmol) and trimethoxybenzene as internal standard in 0.4 mL of C<sub>6</sub>D<sub>6</sub> was added to a solution of styrenyl epoxide (0.1 mmol, 20 equiv) dissolved in 0.3 mL of C<sub>6</sub>D<sub>6</sub>. To this was added a solution of HBpin (14.1 mg, 22 equiv.) dissolved in 0.3 mL C<sub>6</sub>D<sub>6</sub>. The solutions were mixed *via* pipette, then transferred to J-young NMR tubes and analyzed by <sup>1</sup>H NMR spectroscopy. The tubes were then placed in an oil bath at 80 °C for 22 hours before being analyzed again by <sup>1</sup>H NMR spectroscopy and GC/MS.

## VI. Hydrosilation or Diboration Experiments

### Catalytic Diboration of **3.15** with B<sub>2</sub>pin<sub>2</sub>

A solution of complex **3.20** (4.9 mg, 0.0059 mmol, 1.0 equiv.) and trimethoxybenzene as internal standard in 0.4 mL of C<sub>6</sub>D<sub>6</sub> was added to a solution of styrene oxide **3.15** (14.2 mg, 0.118 mmol, 20.0 equiv) dissolved in 0.3 mL of C<sub>6</sub>D<sub>6</sub>. To this was added B<sub>2</sub>pin<sub>2</sub> (34.1 mg, 0.134 mmol, 22.8 equiv.). The solution was mixed *via* pipette, then transferred to a J-young NMR tube. The tube was then placed in an oil bath at 90 °C for 3 days before being analyzed by <sup>1</sup>H NMR spectroscopy and GC/MS, revealing the presence of diborylated product PhCH<sub>2</sub>CH(Bpin)OBpin (**3.40**) in 45% yield and boronate ester PhCH<sub>2</sub>CH<sub>2</sub>OBpin (**3.39**) in 14% yield.

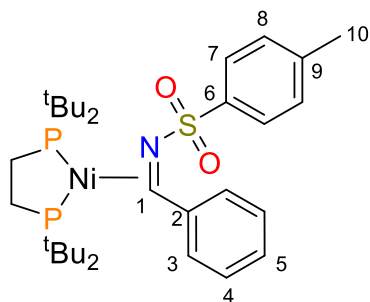
### Stoichiometric Hydrosilation of **3.15** with $\text{PhSiH}_3$

A solution of complex **3.20** (15.3 mg, 0.018 mmol, 1.0 equiv.) and trimethoxybenzene as internal standard in 0.4 mL of  $\text{C}_6\text{D}_6$  was added to a solution of styrene oxide **3.15** (4.9 mg, 0.041 mmol, 2.3 equiv) dissolved in 0.3 mL of  $\text{C}_6\text{D}_6$ . To this was added  $\text{PhSiH}_3$  (4.8 mg, 0.044 mmol, 2.4 equiv.). The solution was mixed *via* pipette, then transferred to a J-young NMR tube. The tube was then placed in an oil bath at 60 °C for 20 hours before being analyzed by  $^1\text{H}$  NMR spectroscopy and GC/MS, revealing the presence of hydrosilation product  $\text{PhCH}_2\text{CH}_2\text{OSiH}_2\text{Ph}$  (**3.41**) in 44% yield.

### Stoichiometric Hydrosilation of **3.15** with $\text{Ph}_2\text{SiH}_2$

A solution of complex **3.20** (8.8 mg, 0.011 mmol, 1.0 equiv.) and trimethoxybenzene as internal standard in 0.4 mL of  $\text{C}_6\text{D}_6$  was added to a solution of styrene oxide **3.15** (4.6 mg, 0.038 mmol, 3.5 equiv.) dissolved in 0.3 mL of  $\text{C}_6\text{D}_6$ . To this was added  $\text{Ph}_2\text{SiH}_2$  (5.8 mg, 0.032 mmol, 2.9 equiv.). The solution was mixed *via* pipette, then transferred to a J-young NMR tube. The tube was then placed in an oil bath at 90 °C for 22 hours before being analyzed by  $^1\text{H}$  NMR spectroscopy and GC/MS, revealing the presence of hydrosilation product  $\text{PhCH}_2\text{CH}_2\text{OSiHPh}_2$  (**3.42**) in 44% yield.

### Synthesis of **3.53**



To a red-orange solution of **3.20** (36.7 mg, 0.0441 mmol, 1.0 equiv) in 4 mL of  $\text{Et}_2\text{O}$  was added imine **3.55** (23.7 mg, 0.0914 mmol, 2.1 equiv) in 4 mL of  $\text{Et}_2\text{O}$ , resulting in a colour change to red. The solution was then stirred at room temperature for 2 hours.

The volatiles were removed *in vacuo* to give a red residue, which was extracted with a minimum

amount of Et<sub>2</sub>O and filtered through glass fiber to give a red-orange solution. On standing at -30 °C overnight, red crystals formed. The supernatant was decanted, and the solids were dried *in vacuo* to yield 40.2 mg (72% yield) of **3.53** as X-ray quality crystals.

<sup>1</sup>H NMR (400 MHz, C<sub>6</sub>D<sub>6</sub>) δ 8.16 (d,  $J_{\text{H,H}} = 8.2$  Hz, 2H, **H7**), 7.56 (d,  $J_{\text{H,H}} = 6.9$  Hz, 2H, **H8**), 7.02 (t,  $J_{\text{H,H}} = 7.6$  Hz, 2H, **H4**), 6.92 (m, 1H, **H5**), 6.65 (d,  $J_{\text{H,H}} = 8.1$  Hz, 2H, **H3**), 4.90 (dd,  $J_{\text{H,P}} = 7.0$  Hz,  $J_{\text{H,P}} = 2.0$  Hz, 1H, **H1**), 1.70 (s, 3H, **H10**), 1.51 (d,  $J_{\text{H,P}} = 12.2$  Hz, 9H, C(CH<sub>3</sub>)<sub>3</sub>), 1.47 (d,  $J_{\text{H,P}} = 12.0$  Hz, 9H, C(CH<sub>3</sub>)<sub>3</sub>), 1.28 (d,  $J_{\text{H,P}} = 12.4$  Hz, 9H, C(CH<sub>3</sub>)<sub>3</sub>), 0.61 (d,  $J_{\text{H,P}} = 12.1$  Hz, 9H, C(CH<sub>3</sub>)<sub>3</sub>). Although the resonances for the methylene groups of the phosphine backbone were obscured, they could be detected indirectly through an HSQC experiment around 1.38 ppm and 1.20 ppm.

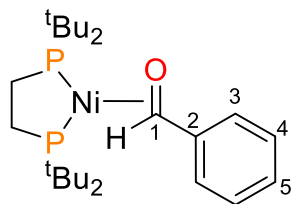
<sup>31</sup>P NMR (162 MHz, C<sub>6</sub>D<sub>6</sub>) δ 85.12 (d[AB],  $J_{\text{P,P}} = 44$  Hz), 84.17 (d[AB],  $J_{\text{P,P}} = 43$  Hz).

<sup>13</sup>C{<sup>1</sup>H} NMR (100 MHz, C<sub>6</sub>D<sub>6</sub>) δ 148.3 (s, **C2** or **C6**), 143.45 (s, **C2** or **C6**), 140.29 (s), 128.93 (s), 128.35 (overlapping with the solvent signal, was detected indirectly using an HSQC experiment), 127.11 (s), 126.16 (s), 124.30 (s), 55.90 (d,  $J_{\text{C,P}} = 27$  Hz, **C1**), 35.85 (dd,  $J_{\text{C,P}} = 15$  Hz,  $J_{\text{C,P}} = 2$  Hz, C(CH<sub>3</sub>)<sub>3</sub>), 35.14 (dd,  $J_{\text{C,P}} = 14$  Hz,  $J_{\text{C,P}} = 4$  Hz, C(CH<sub>3</sub>)<sub>3</sub>), 34.89 (dd,  $J_{\text{C,P}} = 9$  Hz,  $J_{\text{C,P}} = 3$  Hz, C(CH<sub>3</sub>)<sub>3</sub>), 34.51 (d,  $J_{\text{C,P}} = 11$  Hz, C(CH<sub>3</sub>)<sub>3</sub>), 31.20 (d,  $J_{\text{C,P}} = 5$  Hz, C(CH<sub>3</sub>)<sub>3</sub>), 30.91 (d,  $J_{\text{C,P}} = 7$  Hz, C(CH<sub>3</sub>)<sub>3</sub>), 30.82 (d,  $J_{\text{C,P}} = 6$  Hz, C(CH<sub>3</sub>)<sub>3</sub>), 29.85 (d,  $J_{\text{C,P}} = 5$  Hz, C(CH<sub>3</sub>)<sub>3</sub>), 23.62 (app. t,  $J_{\text{C,P}} = 17$  Hz, PCH<sub>2</sub>CH<sub>2</sub>P), 21.82 (dd,  $J_{\text{C,P}} = 16$  Hz,  $J_{\text{C,P}} = 13$  Hz, PCH<sub>2</sub>CH<sub>2</sub>P), 20.96 (s, **C10**).

Anal. Calcd: C, 60.39; H, 8.39; N, 2.20; Found: C, 60.01; H, 8.45; N, 2.12.

LRMS (EI) 635 [M<sup>+</sup>]

### Synthesis of 3.54



To a red-orange solution of **3.20** (48.6 mg, 0.0584 mmol, 1.0 equiv) in 4 mL of Et<sub>2</sub>O was added benzaldehyde (18.9 mg, 0.178 mmol, 3.0 equiv) in 4 mL of Et<sub>2</sub>O, resulting in a colour change to orange-yellow. The

solution was then stirred at room temperature for 2 hours. The volatiles were removed *in vacuo* to give an orange residue, which was extracted with a minimum amount of Et<sub>2</sub>O and filtered through glass fiber to give a orange-yellow solution. On standing at -30 °C overnight, red crystals formed. The supernatant was decanted, and the solids were dried *in vacuo* to yield 51.3 mg (91% yield) of **3.54** as X-ray quality crystals.

<sup>1</sup>H NMR (400 MHz, C<sub>6</sub>D<sub>6</sub>) δ 7.78 (d, *J*<sub>H,H</sub> = 7.3 Hz, 2H, **H3**), 7.21 (t, *J*<sub>H,H</sub> = 7.6 Hz, 2H, **H4**), 7.09 (t, *J*<sub>H,H</sub> = 7.3 Hz, 1H, **H5**), 5.87 (dd, *J*<sub>H,P</sub> = 6.3, 4.2 Hz, 1H, **H1**), 1.30 (d, *J*<sub>H,P</sub> = 9.8 Hz, 9H, C(CH<sub>3</sub>)<sub>3</sub>), 1.28 (d, *J*<sub>H,P</sub> = 9.8 Hz, 9H, C(CH<sub>3</sub>)<sub>3</sub>), 1.17 (d, *J*<sub>H,P</sub> = 12.1 Hz, 9H, C(CH<sub>3</sub>)<sub>3</sub>), 0.73 (d, *J*<sub>H,P</sub> = 12.3 Hz, 9H, C(CH<sub>3</sub>)<sub>3</sub>). Although the methylene resonances of the phosphine backbone could not be resolved, they were detected indirectly *via* an HSQC experiment at around 1.37 and 1.31 ppm.

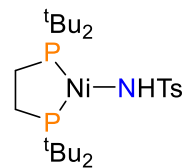
<sup>31</sup>P NMR (162 MHz, C<sub>6</sub>D<sub>6</sub>) δ 90.0 (d[AB], *J*<sub>P,P</sub> = 71 Hz), 88.2 (d[AB], *J*<sub>P,P</sub> = 71 Hz).

$^{13}\text{C}\{^1\text{H}\}$  NMR (100 MHz,  $\text{C}_6\text{D}_6$ )  $\delta$  152.3 (d,  $J_{\text{C,P}} = 6$  Hz, C2), 128.4 (d,  $J_{\text{C,P}} = 3$  Hz, C3), 124.0 (d,  $J_{\text{C,P}} = 3$  Hz, C4), 123.6 (d,  $J_{\text{C,P}} = 3$  Hz, C5), 79.0 (d,  $J_{\text{C,P}} = 21$  Hz, C1), 34.9 (dd,  $J_{\text{C,P}} = 13$  Hz,  $J_{\text{C,P}} = 5$  Hz, C(CH $_3$ ) $_3$ ), 34.6 (dd,  $J_{\text{C,P}} = 12$  Hz,  $J_{\text{C,P}} = 4$  Hz, C(CH $_3$ ) $_3$ ), 34.2 (dd,  $J_{\text{C,P}} = 8$ ,  $J_{\text{C,P}} = 4$  Hz, C(CH $_3$ ) $_3$ ), 33.7 (dd,  $J_{\text{C,P}} = 7$ ,  $J_{\text{C,P}} = 2$  Hz, C(CH $_3$ ) $_3$ ), 30.9 (d,  $J_{\text{C,P}} = 8$  Hz, C(CH $_3$ ) $_3$ ), 30.6 (d,  $J_{\text{C,P}} = 6$  Hz, C(CH $_3$ ) $_3$ ), 30.4 (d,  $J_{\text{C,P}} = 7$  Hz, C(CH $_3$ ) $_3$ ), 30.0 (d,  $J_{\text{C,P}} = 6$  Hz, C(CH $_3$ ) $_3$ ), 24.6 (dd,  $J_{\text{C,P}} = 21$  Hz,  $J_{\text{C,P}} = 19$  Hz, PCH $_2$ CH $_2$ P), 20.7 (dd,  $J_{\text{C,P}} = 14$ ,  $J_{\text{C,P}} = 12$  Hz, PCH $_2$ CH $_2$ P).

Anal. Calcd: C, 62.13; H, 9.59. Found: C, 62.52; H, 9.66.

LRMS (EI) 482 [ $\text{M}^+$ ]

### Synthesis of **3.57**

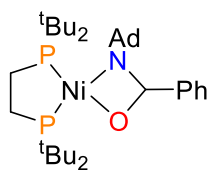


A suspension of NaH (45.9 mg, 1.913 mmol, 2.32 equiv) in 3 mL of THF and a solution H $_2$ NTS (315.7 mg, 1.844 mmol, 2.23 equiv.) in 3 mL of THF were both chilled in a -30 °C freezer for 30 minutes. The amine solution was then added dropwise to the NaH slurry, which was allowed to warm to room temperature and stirred for 1 hour. The cloudy, colourless mixture was then returned to the freezer for 30 minutes. In a separate vial, dimer **3.55** (681.4 mg, 0.826 mmol, 1.00 equiv.) was dissolved in 5 mL of THF and also chilled in the freezer for 30 minutes. Both vials were then removed from the freezer, and the amide solution was added dropwise to the solution of **3.56**, resulting in colour change from red to dark brown. After stirring at room temperature for 2 hours, the volatiles were removed *in vacuo*, and the dark brown residue was extracted with pentanes and filtered through glass fiber, yielding a dark brown filtrate and a yellow residue on the filter pad. Extraction of this residue with Et $_2$ O gave an orange filtrate, which

was concentrated *in vacuo* and stored at -30 °C overnight to yield ≈50 mg of crystalline solid. Examining the crystals through a microscope revealed a mixture of orange crystals of **3.56** and pale yellow plates that were shown by X-ray diffraction studies to be **3.57**.

Analysis of the crystalline mixture by  $^{31}\text{P}\{^1\text{H}\}$  and  $^1\text{H}$  NMR spectroscopy revealed only broad, paramagnetic peaks.

### Synthesis of **3.62**



A red-orange solution of **3.20** (34.2 mg, 0.0411 mmol, 1.0 equiv) in 6 mL of  $\text{Et}_2\text{O}$  and a solution of oxaziridine **3.60** (20.5 mg, 0.0803 mmol, 2.0 equiv) in 3 mL  $\text{Et}_2\text{O}$  were both chilled in the glovebox freezer at -30 °C. After 20 minutes,

the solutions were removed from the freezer, and the solution of **3.60** was poured into the solution of **3.20**, causing an instant colour change to dark purple. The solution was returned to the freezer for 1 hour, then quickly filtered through glass fiber while cold to give a dark purple solution. Removal of the volatiles *in vacuo* yielded 45.0 mg (88% yield) of **3.62** as a dark purple powder. X-ray quality crystals were grown by cooling a concentrated  $\text{Et}_2\text{O}$  solution of **3.62** at -30 °C overnight. Complex **3.62** was found to be unstable even in the solid state at -30 °C, decomposing to a mixture of compounds, including **3.54**, after several days.

Due to the thermal instability of **3.62**, we were unable to achieve satisfactory analytic data.

Analysis of **3.62** by  $^{31}\text{P}\{^1\text{H}\}$  and  $^1\text{H}$  NMR spectroscopy revealed only very broad peaks.

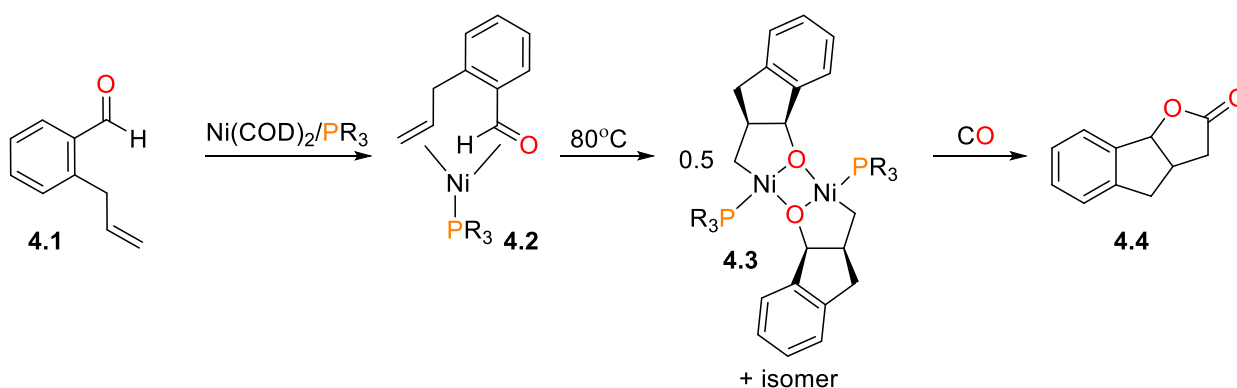
LRMS (EI) 630  $[\text{M}-\text{H}]^+$

# Chapter 4 : Synthesis of 2-Nickela(II)oxetanes: Structure, Reactivity, and a New Mechanism of Formation

## 4.1 Introduction

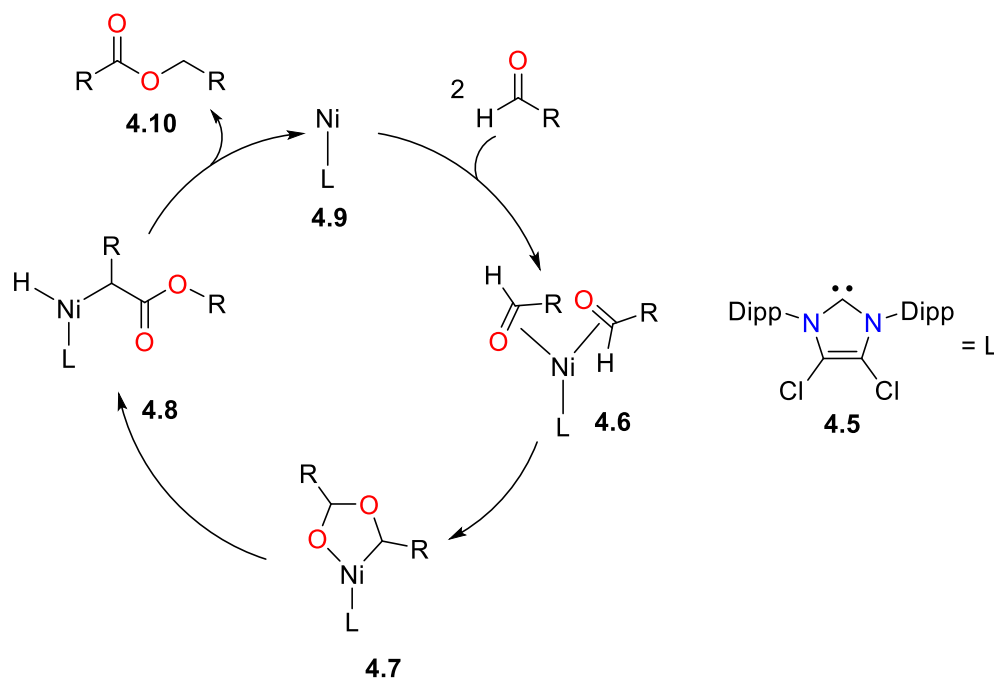
The work described in Chapter 3 demonstrates that 2-nickela(II)oxetanes can be formed by the reaction of nickel(0) with epoxides, and can be quite reactive, often decomposing by  $\beta$ -hydride elimination. In an effort to identify a possible epoxide that would obviate this undesired reaction pathway, we turned to the literature to ascertain some fundamental reactivity of nickel(0) that could be exploited towards our synthetic target.

In 2004, Ogoshi and co-workers reported the first example of a well-defined oxidative cyclization reaction between an aldehyde and an alkene at a nickel centre (Scheme 4.1).<sup>284</sup> They found that when aldehyde **4.1** was treated with an equimolar amounts of  $\text{Ni}(\text{COD})_2$  and  $\text{PR}_3$  ( $\text{R} = \text{Cy}$  or  $\text{Ph}$ ), nickel adduct **4.2** was formed in high yield.  $^1\text{H}$  NMR spectroscopy clearly shows that both alkene and aldehyde moieties are bound to the metal centre. Upon heating at  $80^\circ\text{C}$ , oxidative cyclization results in the formation of a new C-C bond, forming the nickel(II) complex **4.3** as a mixture of isomers. Stirring **4.3** under CO (3 atm), lactone **4.4** is produced in high yield as the sole organic product along with  $\text{Ni}(\text{PR}_3)_n(\text{CO})_{4-n}$ .



**Scheme 4.1** Oxidative cyclization of **4.1** with nickel(0)

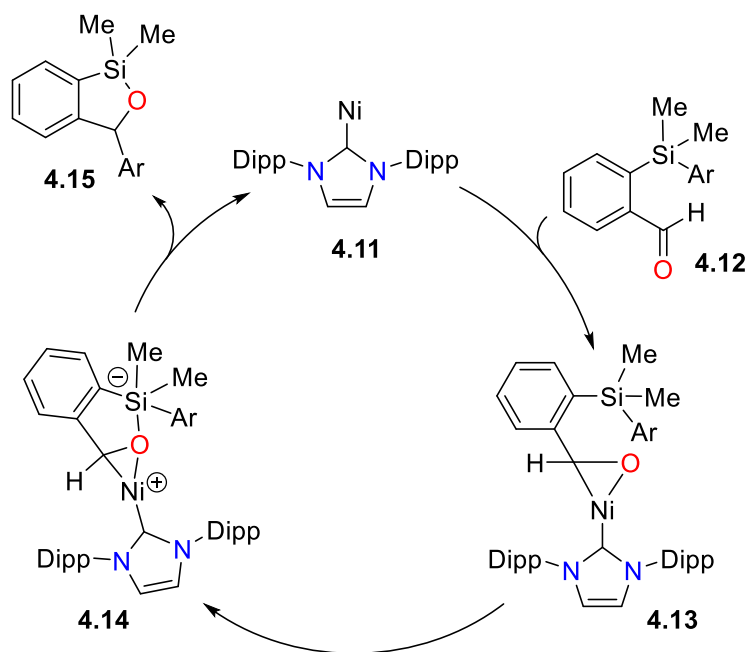
Several years later, the same group reported that N-heterocyclic carbenes can also be used as ligands for the functionalization of aldehydes.<sup>285</sup> For example, Ni(COD)<sub>2</sub> and the ligand **4.5** can catalyze the Tischenko coupling of aldehydes with low (i.e. 1 to 3 mol%) catalyst loadings. Conversely, NMR experiments at -60 °C with higher catalyst loading (20 mol%) reveal that the nickel centre coordinates two equivalents of aldehyde (**4.6**) prior to oxidative cyclization to form **4.7**. Rapid β-hydride elimination forms intermediate **4.8** and reductive elimination regenerates the nickel(0) catalyst **4.9** and releases the ester product **4.10** (Scheme 4.2).



**Scheme 4.2** Proposed mechanism of nickel-catalyzed Tischenko coupling

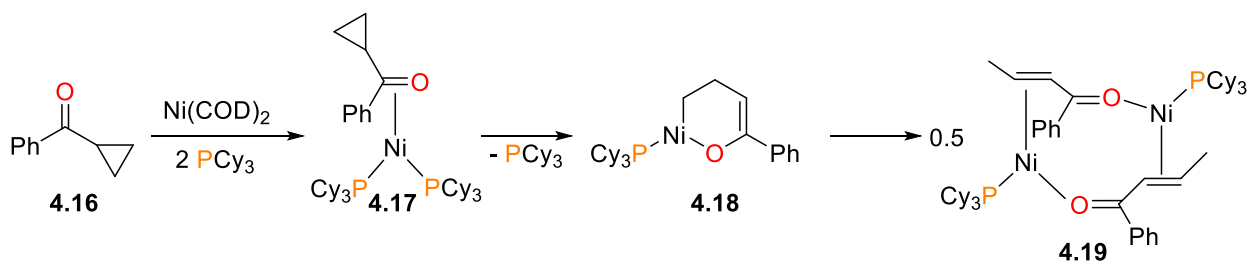
More recently, coordination of nickel(0) **4.11** to aromatic aldehydes **4.12** has been utilized for the catalytic synthesis of benzoxasiloles (Scheme 4.3).<sup>286</sup> Again, stoichiometric NMR spectroscopic experiments at low temperatures reveal that  $\eta^2$ -aldehyde complex **4.13** (Ar = Ph) is an intermediate in this process. The authors propose that coordination of the

metal to the aldehyde activates the oxygen towards nucleophilic attack at the silicon, forming silicate intermediate **4.14**. Curiously, subsequent aryl group transfer to release product **4.15** occurs *via* an intermolecular process, as demonstrated by scrambling during crossover experiments.



**Scheme 4.3** Proposed mechanism of nickel-catalyzed benzoxasilole synthesis

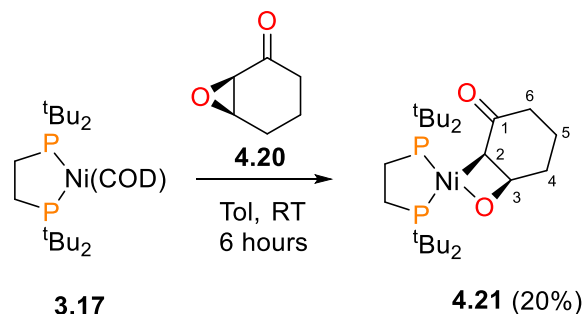
Finally, the Ogoshi group has also reported a study on the reactivity of cyclopropyl ketones with nickel(0).<sup>198, 202</sup> Reacting ketone **4.16** with Ni(COD)<sub>2</sub> and 2 equiv. of PCy<sub>3</sub> results in the formation of  $\eta^2$ -carbonyl complex **4.17** (Scheme 4.4). After 5 hours at room temperature, oxidative addition of the cyclopropyl group to the nickel(0) centre results in ring-opening, and **4.17** completely converts to the nickelaenolate **4.18**. After a subsequent 36 hours at room temperature, **4.18** decomposes to the binuclear enone complex **4.19** in 68% yield.



**Scheme 4.4** Ring-opening of cyclopropyl ketones mediated by nickel(0)

## 4.2 Synthesis of Well-Defined 2-Nickela(II)oxetanes

Inspired by the above reports, we prepared epoxide **4.20**<sup>287</sup> and reacted it with (dtbpe)Ni(COD) **3.17**<sup>215</sup> in C<sub>6</sub>D<sub>6</sub> at room temperature (Scheme 4.5). Monitoring the reaction by <sup>31</sup>P{<sup>1</sup>H} NMR spectroscopy reveals the formation of a mixture of products over the course of six hours. The major product appears as two doublets ( $\delta = 72.7$  and  $71.5$  ppm) with small <sup>2</sup>J<sub>P,P</sub> values of 6 Hz, indicative of coupling through a nickel(II) centre.<sup>151, 288</sup> Removing the volatiles *in vacuo* and extracting the resulting residue with pentanes allowed for the isolation of the major product **4.21** in 20% yield as an analytically pure orange powder. A variety of NMR spectroscopy and X-ray crystallography techniques were employed to determine the structure of **4.21**, which was found to be the first example of an isolable nickela(II)oxetane derived from nickel and epoxides. Exclusive oxidative addition into the stronger C2-O bond of **4.20** was observed, with no evidence of C3-O oxidative addition by either <sup>1</sup>H or <sup>31</sup>P{<sup>1</sup>H} NMR spectroscopy.



**Scheme 4.5** Initial synthesis of **4.21**. Isolated yield in parenthesis. Relative stereochemistry shown for clarity.

The  $^1\text{H}$  NMR spectrum of **4.21** displays a downfield multiplet for **H3** ( $\delta = 5.78$  ppm; see Scheme 4.2.1 for numbering). A COSY experiment shows that this resonance is coupled to another at 2.87 ppm, which is assigned as the resonance for **H2**. Importantly, a NOESY experiment shows strong correlations between the **H2** and **H3** protons, indicative of *cis* stereochemistry. Each of the methylene resonances of the cyclohexyl ring are diastereotopic, which complicates the aliphatic region of the  $^1\text{H}$  NMR spectrum, however, they can each be assigned on the basis of COSY, HSQC and HMBC experiments (see Figure 4.1 for HSQC spectrum). The presence of the unbound ketone is shown by the downfield shift of the **C1** resonance in the  $^{13}\text{C}\{^1\text{H}\}$  NMR spectrum ( $\delta = 211.7$ , apparent t,  $^3J_{\text{C,P}} = 2$  Hz).

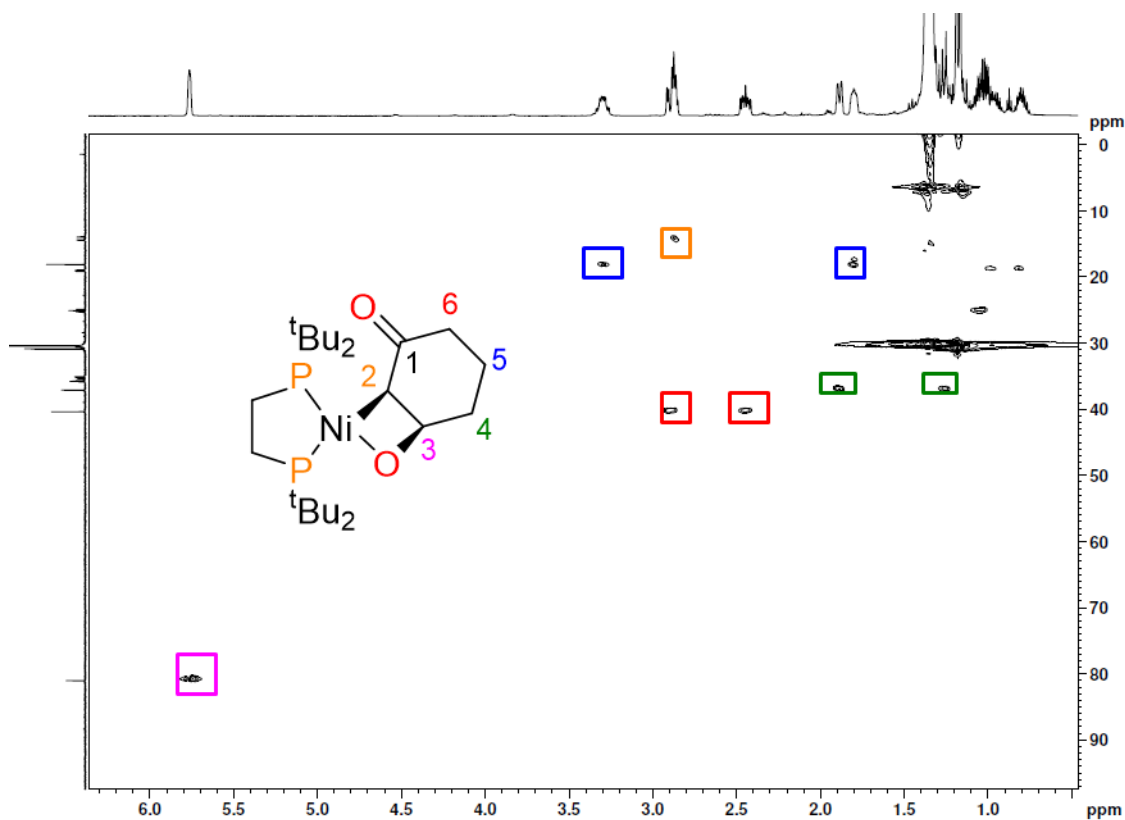


**Figure 4.1** Partial HSQC spectrum of **4.21** showing the cyclohexyl resonances

The slow evaporation of a cold Et<sub>2</sub>O solution of **4.21** allowed for the growth of dark red, X-ray quality crystals, and the structure of **4.21** was confirmed by an X-ray diffraction study (Figure 4.2). The geometry at the nickel is square planar, with a Ni-O distance of 1.832(1) Å and a Ni-C distance of 2.014(2) Å. The metallacycle bond lengths are relatively similar to the metallaioxetanes reported by the Hillhouse group,<sup>42, 78</sup> which at the time were the only well-defined 2-nickela(II)oxetanes described in the literature.

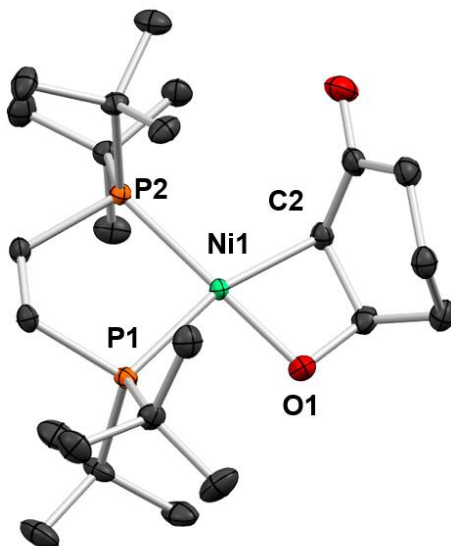


**Figure 4.2** ORTEP (50% ellipsoids) diagrams of **4.21**. Hydrogen atoms omitted for clarity.

With **4.21** in hand, we sought to explore the mechanism of formation and reactivity of this species. We speculated that COD could be competing with **4.20** at the nickel(0) centre, resulting in low yields of **4.21**.<sup>63, 65</sup> Consequently, we explored other sources of (dtbpe)nickel(0) as starting materials. While (dtbpe)Ni(C<sub>2</sub>H<sub>4</sub>) **3.18**<sup>219</sup> was found to be unreactive with **4.20**, the arene adduct [(dtbpe)Ni]<sub>2</sub>(μ-η<sup>2</sup>:η<sup>2</sup>-C<sub>6</sub>H<sub>6</sub>) **3.20**<sup>216</sup> was found to rapidly generate **4.21** at room temperature in 60% isolated yield. In an attempt to observe any intermediates during this transformation, we performed low-temperature NMR studies on the reaction of **3.20** with **4.20** (Scheme 4.6).

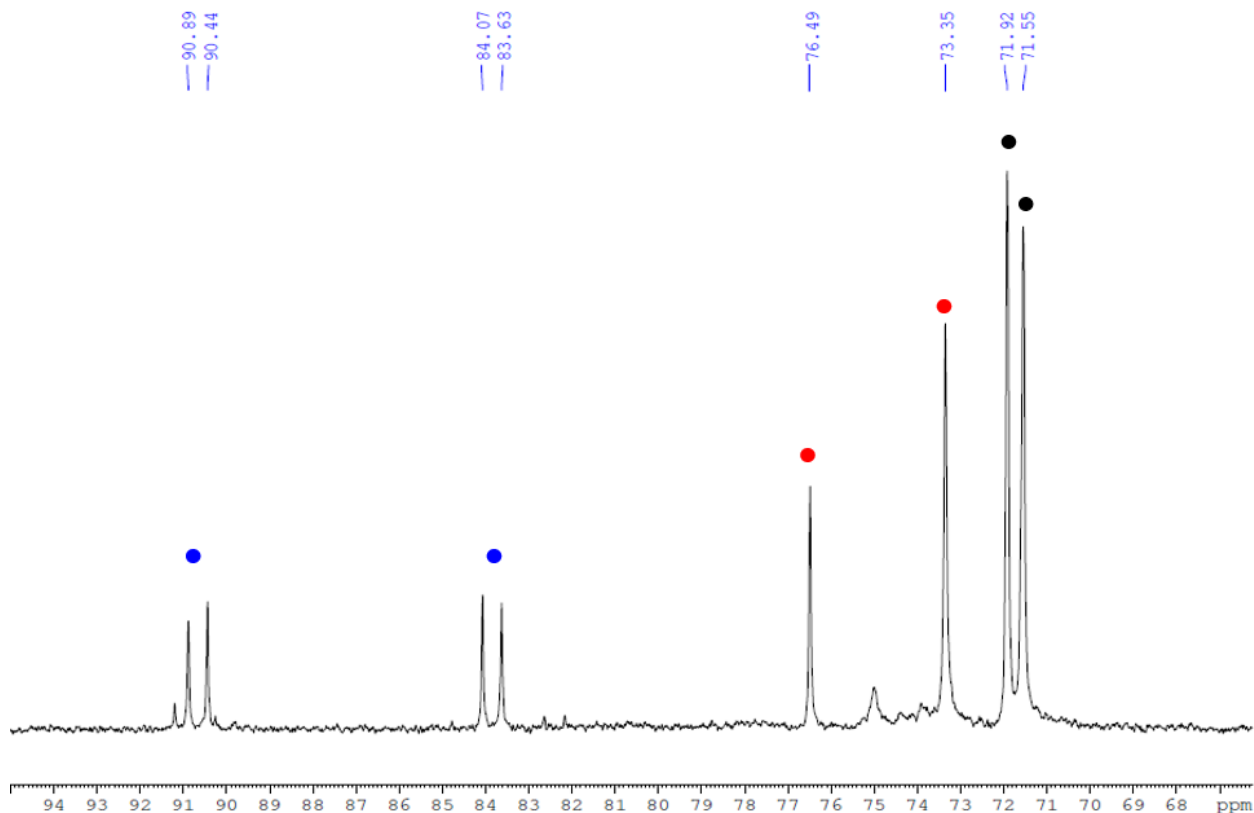
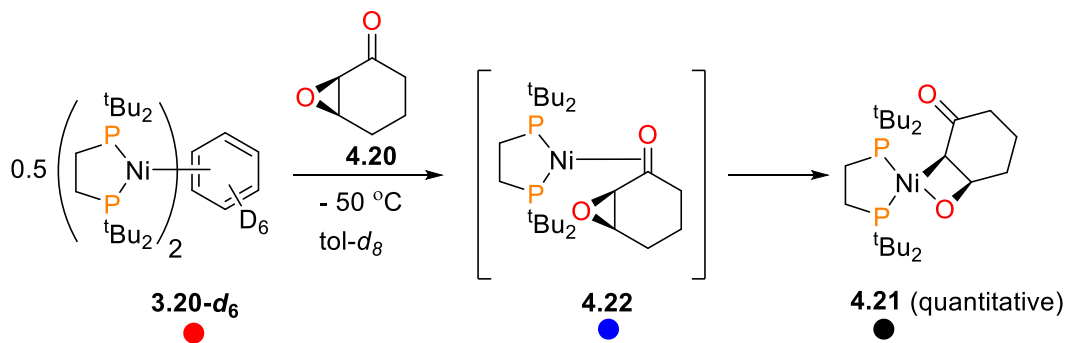


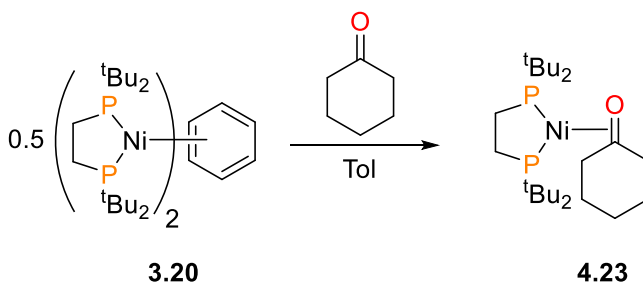
**Figure 4.3** Low-temperature  $^{31}\text{P}\{^1\text{H}\}$  NMR spectrum (162 MHz,  $-50\text{ }^\circ\text{C}$ , Tol- $d_8$ ) of the reaction of **3.20** with **4.20**

Even at  $-50\text{ }^\circ\text{C}$ , NMR spectroscopy showed that the main species in solution is **4.21** (black dots, Figure 4.3), highlighting the facile oxidative addition process. In addition, both  $^{31}\text{P}\{^1\text{H}\}$  and  $^{13}\text{C}\{^1\text{H}\}$  NMR spectroscopies reveal the transient existence of a nickel(0) complex (blue dots), which we assign as the asymmetric  $\eta^2$ -ketone complex **4.22** (Scheme 4.2.2). Warming the solution to  $-15\text{ }^\circ\text{C}$  resulted in the disappearance of the resonances of **4.22** in the  $^{31}\text{P}\{^1\text{H}\}$  NMR spectrum and the complete conversion to **4.21**. This shows that **4.22** is either an intermediate along the pathway to **4.21**, or possibly in an off-path equilibrium with some intermediate between **3.20** and **4.21**. In contrast, the reaction of **3.17** with **4.20** was found to not proceed below room temperature.



**Scheme 4.6** Low-temperature synthesis of **4.21**. Relative stereochemistry shown for clarity

As **4.22** proved too reactive to isolate, we sought to prepare an analogue that did not contain the epoxide moiety. Addition of cyclohexanone to a solution of **3.20** resulted in an immediate colour change from red to yellow. Crystallization of the crude product from pentanes afforded the  $\eta^2$ -ketone adduct **4.23**, which was fully characterized by EI-MS, EA and multinuclear NMR experiments (Scheme 4.7).



**Scheme 4.7** Synthesis of **4.23**

The  $^{31}\text{P}\{^1\text{H}\}$  NMR spectrum of **4.23** features two doublets ( $\delta = 91.4$  and  $82.6$  ppm) with large  $^2J_{\text{P,P}}$  values of 79 Hz. The *tert*-butyl groups of the dtbpe ligand resonate as two doublets in the  $^1\text{H}$  NMR spectrum that each integrate to 18 protons, indicating the complex exhibits  $C_s$  symmetry in solution. Similar to the other  $\pi$ -bound carbonyl complexes of nickel(0) described in Chapter 3, the carbonyl resonance of **4.23** appears as a doublet ( $^2J_{\text{C,P}} = 29$  Hz) at 89.4 ppm. X-ray quality crystals of **4.23** could be grown by cooling a

concentrated pentanes solution down to  $-35\text{ }^{\circ}\text{C}$  overnight, and the solid-state structure is shown in Figure 4.4. As expected, **4.22** and **4.23** are spectroscopically similar, in particular regarding the coupling constants in the  $^{13}\text{C}\{^1\text{H}\}$  and  $^{31}\text{P}\{^1\text{H}\}$  NMR spectra. Complex **4.23** was found to be thermally robust, as no decomposition was observed after heating at  $80\text{ }^{\circ}\text{C}$  in  $\text{C}_6\text{D}_6$  over the course of 3 days.

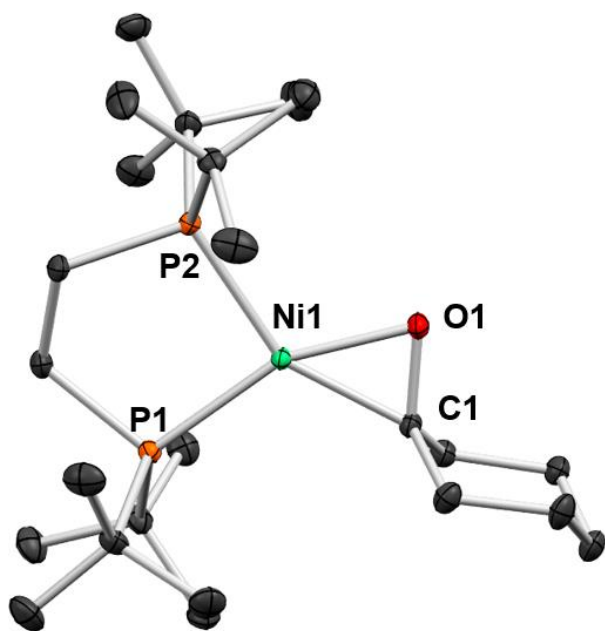
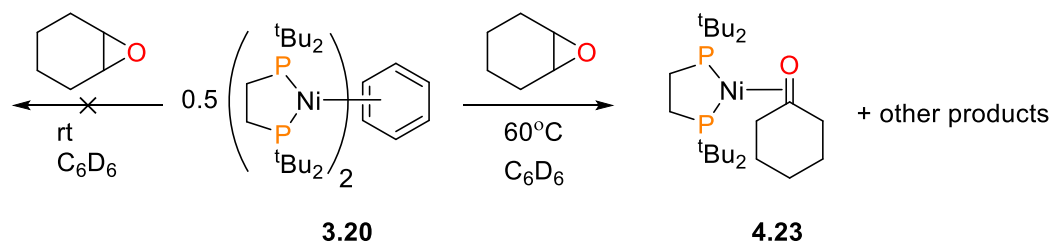


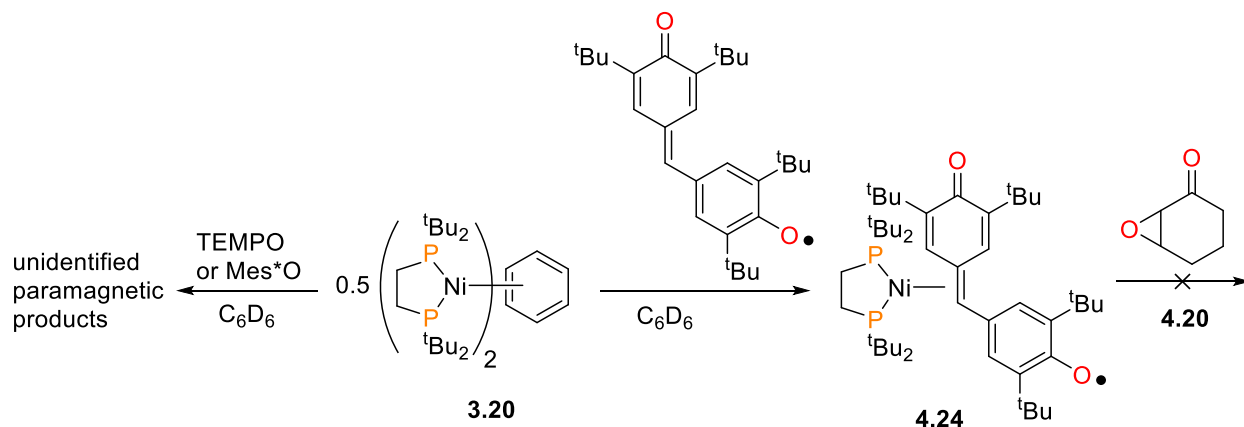
**Figure 4.4** ORTEP (50% ellipsoids) diagrams of **4.23**. Hydrogen atoms omitted for clarity.

In addition, we found that equimolar amounts of either **3.17** or **3.20** and cyclohexene oxide in  $\text{C}_6\text{D}_6$  resulted in no reaction over several days at room temperature, which highlights the importance of the ketone moiety in this C-O oxidative addition reaction (*vide infra*). Heating solutions of **3.20** and cyclohexene oxide at  $60\text{ }^{\circ}\text{C}$  for 16 hours results in a mixture of products, the major component of which was **4.23** (Scheme 4.8). Thus, the epoxide isomerization reported in Chapter 3 is also operative for cyclohexene oxide, although more forcing conditions are required.



**Scheme 4.8** Reactivity of **3.20** with cyclohexene oxide

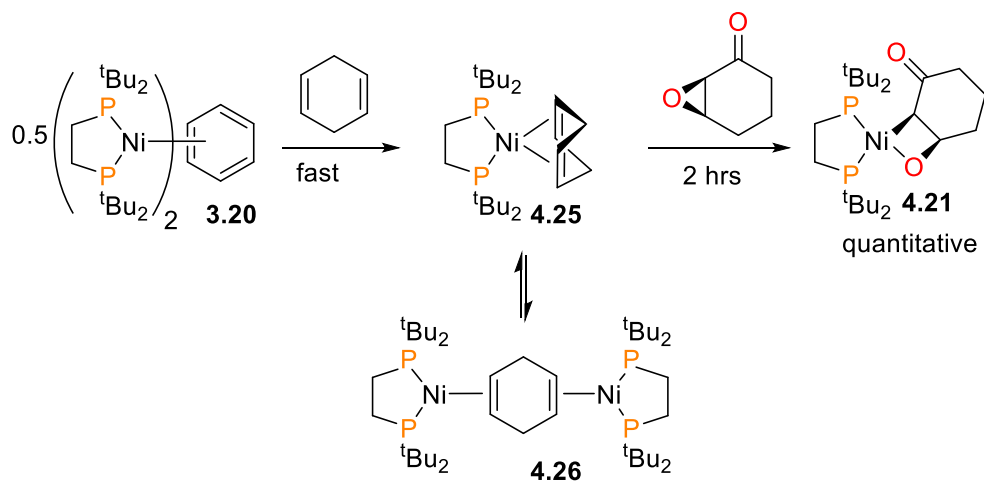
Given the propensity of nickel to perform single electron chemistry,<sup>235</sup> we desired to probe a potential radical mechanism for the formation of **4.21** by performing the reaction of **3.20** with **4.20** in the presence of a suitable radical trap. While stabilized oxyl radicals like 2,2,6,6-tetramethylpiperidin-1-yl)oxyl (TEMPO) are frequently used as radical traps,<sup>289</sup> we found **3.20** and equimolar TEMPO rapidly reacted together to form a very dark purple paramagnetic species that is currently unidentified. Similar results were obtained with the tri-*tert*-butylphenoxy radical (Mes\*O).<sup>290</sup> We also attempted to react **3.20** with galvinoxyl, and while initial NMR spectroscopy experiments indicate the formation of a  $\pi$ -bound alkene complex **4.24**, this complex was unreactive upon addition of epoxide **4.20** (Scheme 4.9).



**Scheme 4.9** Reactivity of **3.20** with oxyl radicals

We eventually identified 1,4-cyclohexadiene (CHD) as a suitable reagent, as it has very weak C-H bonds that are prone to react with free radicals.<sup>291</sup> Addition of an excess of CHD to a solution

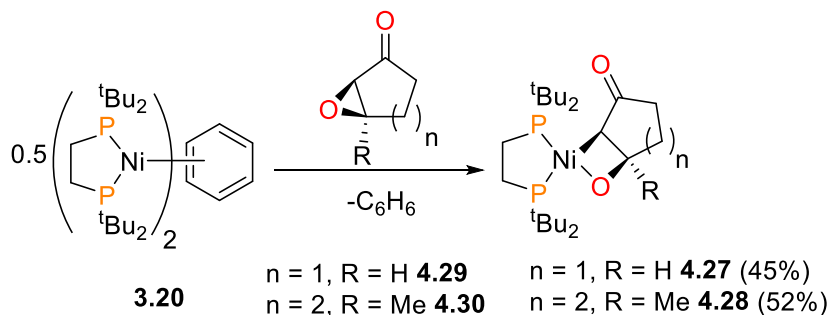
of **3.20** results in 2 new singlets ( $\delta = 85.3$  and  $81.0$  ppm) in the  $^{31}\text{P}\{^1\text{H}\}$  NMR spectrum. Subsequent  $^1\text{H}$  and  $^{13}\text{C}\{^1\text{H}\}$  NMR spectroscopic experiments indicate that the products are the  $\eta^2$ -alkene complexes **4.25** and **4.26** (Scheme 4.10). These results are not surprising, given that both **3.17**<sup>215</sup> and **3.20**<sup>216</sup> interchange between monometallic and bimetallic structures in solution. Addition of epoxide **4.20** to a mixture of **4.25** and **4.26** in  $\text{C}_6\text{D}_6$  at room temperature resulted in the clean and quantitative formation of **4.21** over the course of 2 hours, as observed by  $^{31}\text{P}\{^1\text{H}\}$  and  $^1\text{H}$  NMR spectroscopy. Although not conclusive, we assume that any radical species formed by ring-opening of the epoxide would also react with CHD (resulting in a concomitant decrease in the yield of **4.21**). Thus, we believe these results support that a radical mechanism is not operative for the formation of **4.21**.



**Scheme 4.10** Reactivity of **4.25** and **4.26** with epoxide **4.20**

We also prepared complexes **4.27** and **4.28** from epoxides **4.29** and **4.30** using the same synthetic route (Scheme 4.11). The NMR spectroscopic data of **4.27** and **4.28** were all analogous to those of **4.21**. To explore the potential reversibility of nickelaoxetane formation, an excess of epoxide **4.29** was added to a solution of **4.21** in  $\text{C}_6\text{D}_6$ . No formation

of **4.27** was detected after three days at room temperature, indicating the reaction is irreversible under these conditions.



**Scheme 4.11** Synthesis of 2-nickelaoxetanes **4.27** and **4.28**. Isolated yields in parentheses

Both complexes **4.27** and **4.28** could be isolated in moderate yields. Although X-ray quality crystals of **4.27** eluded us, we were able to obtain the crystal structure of nickelaoxetane **4.28** (Figure 4.5), which was very similar to **4.21**.

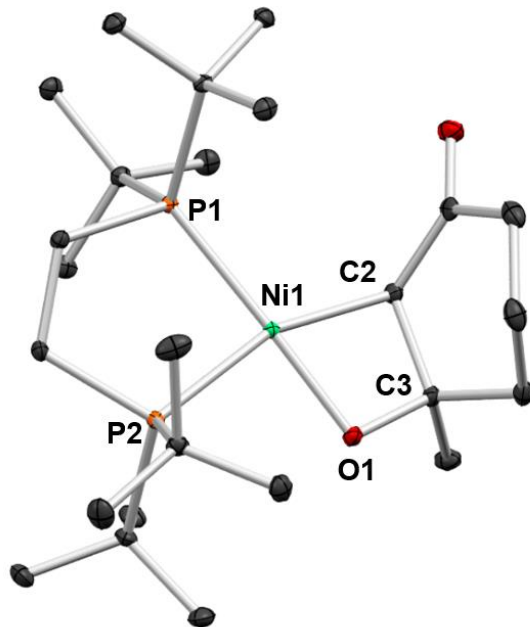
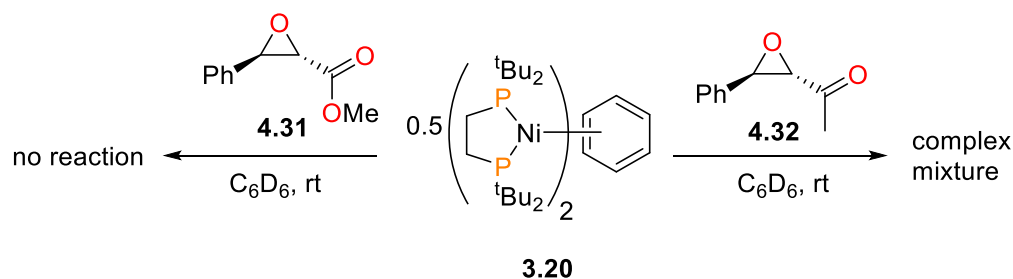


**Figure 4.5** ORTEP (50% ellipsoids) diagrams of **4.28**. Hydrogen atoms omitted for clarity

In contrast to the nickelaoxetanes in reported Chapter 3, complexes **4.21** and **4.27** do not undergo  $\beta$ -hydride elimination. We propose that this is due to **C2** and **C3** being tethered together, preventing the orbital overlap required for  $\beta$ -hydride elimination. To probe this hypothesis, we attempted to expand the epoxide scope to acyclic compounds that featured adjacent carbonyl groups (Scheme 4.12). However, when we reacted **3.20** with either **4.31** or **4.32** we observed either no reaction over several days in the case of **4.31** or rapid decomposition to multiple unidentified products in the case of **4.32**. Although preliminary, we believe these data support our hypothesis that tethering of the **C2** and **C3** is required to stabilize the nickelaoxetane moiety.



**Scheme 4.12** Attempted reactions of acyclic epoxides with **3.20**

### 4.3 Mechanistic Investigation by Density Functional Theory

The Jamison group has previously proposed that low-valent nickel can react with epoxides *via* an  $S_N2$ -type attack, resulting in an inversion of stereochemical configuration at the carbon.<sup>44, 45, 47</sup> Hillhouse has also reported a similar mechanism for the oxidative addition of (bpy)Ni(COD) (bpy = 2,2'-bipyridyl) to a variety of N-tosylaziridines to generate azanickelacyclobutanes.<sup>63</sup> We believe that in our system **4.21** is formed by a different mechanism, as the oxetane retains the *cis* configuration of the epoxide. In order to gain insight into the mechanism of our transformation, DFT calculations<sup>292, 293</sup> were

performed by Eric G. Bowes, a PhD candidate in the Love group. Intermediates and transition states were first located using a truncated bis(1,2-dimethylphosphino)ethane (dmpe) ligand, followed by modelling using the full dtbpe ligand scaffold.

Figure 4.6 shows the first possible process we examined. Dissociation of COD or C<sub>6</sub>H<sub>6</sub> from **A** or **B** leads to the formation of an unsaturated nickel(0) complex **C**, which reacts with the epoxide **4.20** to form an  $\eta^2$ -ketone complex **D**. Two conformers are possible for the  $\eta^2$ -ketone complex: **D**, in which the epoxide oxygen is located on the same face of the six-membered ring as the nickel centre, and **D'** in which the oxygen atom is found on the opposite face. Curiously, when using the dmpe ligand set, an intermediate was located on the potential energy surface (PES) that corresponded to initial C-C oxidative addition of the (dmpe)nickel(0) fragment. This intermediate, **H\_Me**, was connected to the zwitterionic product of S<sub>N</sub>2 ring-opening (**G\_Me**) *via* transition state **HG<sup>TS</sup>\_Me**, as shown by intrinsic reaction coordinate (IRC) calculations. Although we were unable to surmise an intuitive reaction pathway to lead to from **G\_Me** to the final nickelaoxetane product **F\_Me**, a simple geometry optimization shows that **F\_Me** is quite stable ( $\Delta G = -28.8$  kcal/mol relative to **B\_Me**). The energy profile calculated with the full dtbpe ligand is qualitatively similar, although we were unable to locate **H**, the initial C-C oxidative addition intermediate.

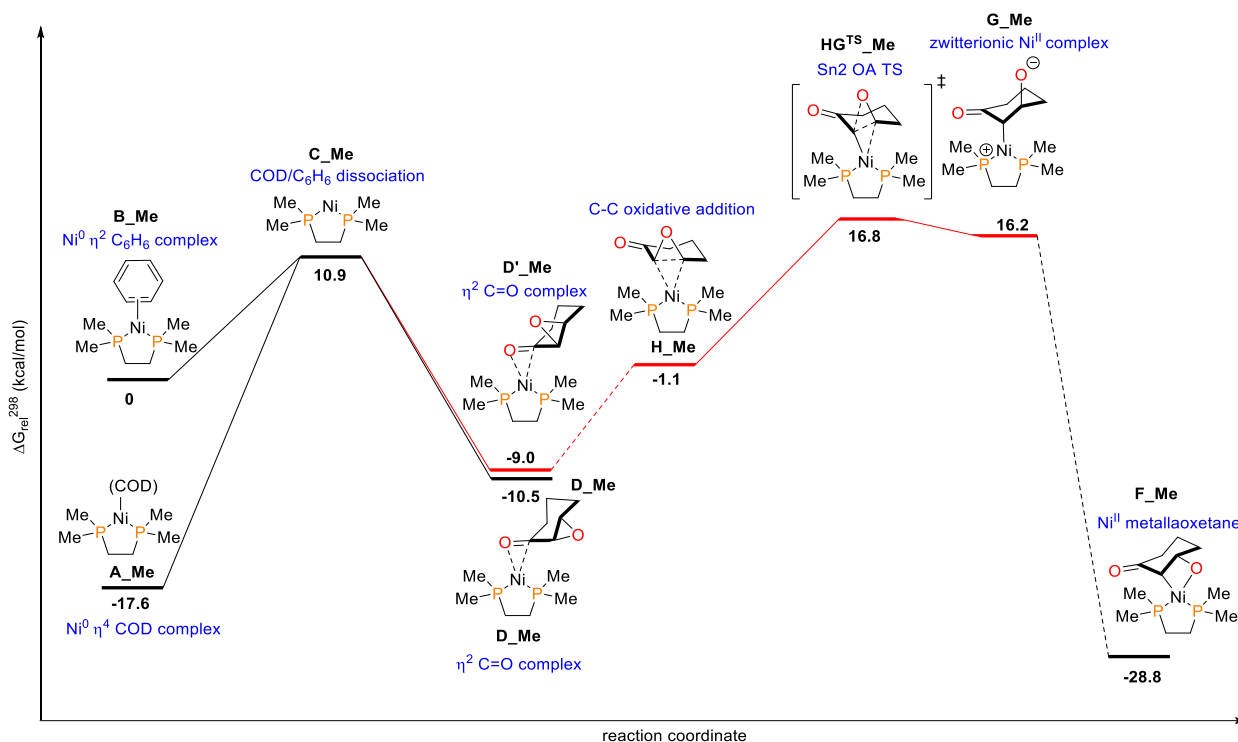


**Figure 4.6** DFT calculated reaction pathway (BP86/631-G(d,p)) for  $S_N2$ -type ring-opening using a truncated dmpe ligand. Energies ( $\Delta G$ ) are reported in kcal/mol relative to **B\_Me**

Next, we attempted to locate a concerted C-O oxidative addition pathway directly from intermediate **D** (Figure 4.7, black pathway). Though we were unable to locate a direct path linking **D** to the metallaoxetane product, a high energy intermediate **E** ( $\Delta G = 10.2$  kcal/mol) was located on the PES best described as an  $\eta^5$ -O,C,C,C,H complex in which the nickel(0) centre is found in an approximately tetrahedral geometry. Oxidative addition proceeds through transition state **EF<sup>TS</sup>** with a barrier of 24.5 kcal/mol (**D**→**EF<sup>TS</sup>**) to generate the final metallaoxetane product **F**. We were unable to definitively establish the connectivity of **D** with **E**, and therefore it is possible that the  $\eta^2$ -ketone complex is formed in an off-pathway equilibrium and intermediate **E** is formed directly from free **C** and epoxide **4.20**.

We were surprised to find that (dtbpe)nickel(0) could act to effectively stabilize the alkoxide group, as our calculations show that the energy of the nickel(0)-stabilized

zwitterionic product is lowered by 24.7 kcal/mol.<sup>233</sup> In light of this, we explored the possibility of a stepwise ring-opening/ring-closing mechanism that would allow for retention of stereochemistry (Figure 4.7, blue pathway). In calculations involving the dmpe ligand, a bimetallic complex was identified in which the epoxide oxygen binds a second (dmpe)nickel(0) fragment. For the energetics in this discussion we assume the second nickel(0) fragment is generated by dissociation from **B**. Formation of the bimetallic species is endergonic (+8.0 kcal/mol compared to the  $\eta^2$ -ketone complex) and the intermediate exists in a shallow well on the PES, with epoxide opening proceeding through a transition state that was calculated to have a slightly negative  $\Delta G$  value. In calculations involving the full dtbpe ligand, no epoxide complex was located, and ring opening was found to be barrierless upon approach of the nickel(0) fragment toward the epoxide oxygen of **D'**. The resultant ring-opened structure **bmI** is an  $\eta^3$ -oxallylnickel complex, analogous to those previously described,<sup>198, 294, 295</sup> with  $\Delta G = -17.2$  kcal/mol. This species is 9.6 kcal/mol lower in energy than the bimetallic zwitterion that would result from  $S_N2$  attack on the  $\alpha$ -carbon. No transition state was located for subsequent ring closure leading to metallaoxetane **bmII** ( $\Delta G = -26.7$  kcal/mol) but we expect this intramolecular process to be facile. In the formation of **bmII** the oxallylic nickel re-adopts a  $\eta^2$ -ketone binding mode. Formation of the observed product **F** and regeneration of **B** by loss of nickel(0) from the carbonyl is calculated to have a negligible free energy change. It is also expected that **bmII** can act as a source of free nickel(0) for further metallacycle formation.

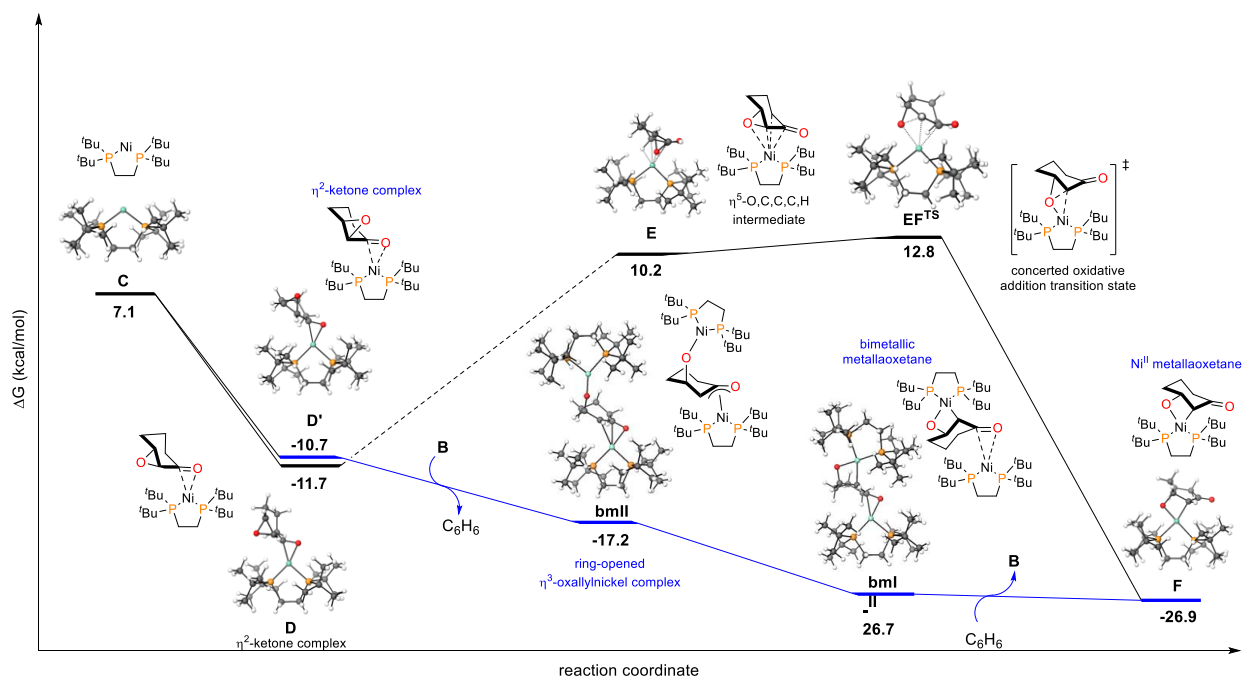


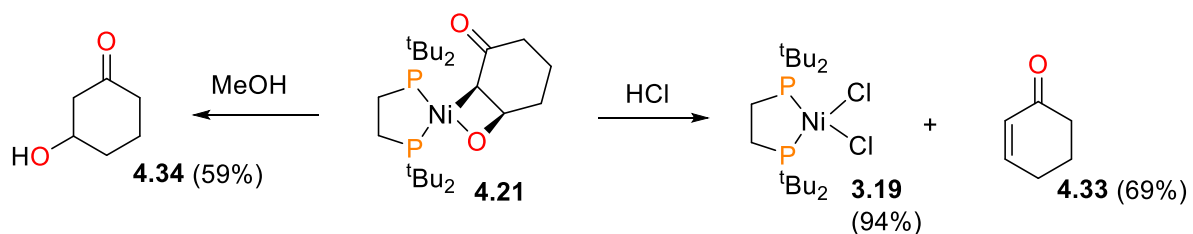
**Figure 4.7** DFT calculated reaction pathways (BP86/631-G(d,p)) for concerted (blue) and bimetallic (black) C-O oxidative addition. Energies ( $\Delta G$ ) are reported in kcal/mol relative to **B** (not shown).

Notably, no conversion to **bmII** was observed experimentally upon addition of arene complex **3.20** to nickelaoxetane **4.21**. The lower energetics of the bimetallic pathway are more consistent with the rapid rate of formation of **4.21** that we observe. Unfortunately, our attempts to obtain kinetic data by low-temperature ( $-50\text{ }^{\circ}\text{C}$ )  $^{31}\text{P}\{^1\text{H}\}$  NMR spectroscopy were unsuccessful, as under pseudo first-order conditions (i.e. 7 equiv. of epoxide **4.20**) the reaction is nearly complete within the time required to acquire the first spectrum. We believe that stopflow spectrophotometry would be an ideal manifold for studying this transformation, as both **3.20** and **4.21** are quite different colours. These experiments will need to be done in collaboration with a group outside UBC, as the chemistry department currently lacks the necessary equipment required for these air-sensitive manipulations. Although our DFT calculations favour a stepwise mechanism, we cannot conclusively rule

out a concerted mechanism at this time, and further mechanistic studies are ongoing within our group.

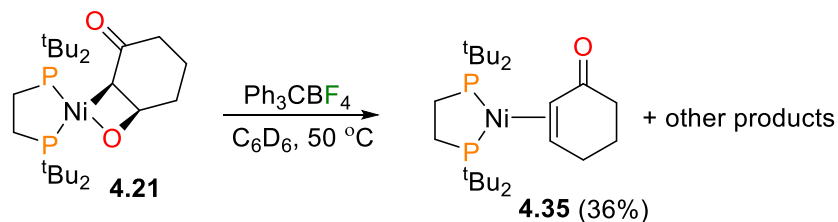
#### 4.4 Reactivity of Well-Defined 2-Nickela(II)oxetanes

We then explored the reactivity of **4.21**. Protonolysis of **4.21** with an excess of HCl in C<sub>6</sub>D<sub>6</sub> resulted in the rapid precipitation of a red solid, identified as (dtbpe)NiCl<sub>2</sub> **3.19**<sup>217</sup> and isolated in 94% yield. The organic product was identified by GC-MS and <sup>1</sup>H NMR spectroscopy as 2-cyclohexenone **4.33** (69% yield), presumably formed *via* acid-induced elimination from liberated 3-hydroxycyclohexanone **4.34**. Indeed, using less acidic sources of protons such as MeOH results in the formation of alcohol **4.34** in 59% yield by <sup>1</sup>H NMR spectroscopy (Scheme 4.13).



**Scheme 4.13** Protonolysis reactions of **4.21**

Treatment of **4.21** with Ph<sub>3</sub>CBF<sub>4</sub> or BF<sub>3</sub>OEt gave complex **4.35** as the major organometallic product *via* deoxygenation of the nickelaoxetane ring (Scheme 4.14). In the case of Ph<sub>3</sub>CBF<sub>4</sub>, complex **4.35** was formed in 36% <sup>1</sup>H NMR spectroscopic yield, and singly oxidized phosphine ligand (dtbpeO)<sup>113, 247</sup> was also observed by <sup>31</sup>P{<sup>1</sup>H} NMR spectroscopy. The crude reaction mixture also contained **4.33** (26% yield), free dtbpe and a dark precipitate presumed to be nickel black.



**Scheme 4.14** Deoxygenation of **4.21** with  $\text{Ph}_3\text{CBF}_4$

Interestingly, the conversion of **4.21** to **4.35** results in the formal reduction of the nickel centre. Alkene extrusions have been reported for a few examples of 2-metallaioxetanes of other transition metals.<sup>52, 296</sup> Complex **4.35** was prepared independently by the addition of cyclohexenone **4.33** to arene **3.20**, and fully characterized by our standard methods of NMR spectroscopy, EI-mass spectrometry and elemental analysis. The binding of the nickel centre to the alkene rather than the ketone can be seen clearly in the  $^1\text{H}$  NMR spectrum of **4.35**, as the resonances for **H2** ( $\delta = 4.12$  ppm, ddd,  $^3J_{\text{H,H}} = 8.7$  Hz,  $^3J_{\text{H,P}} = 6.3$  Hz,  $^3J_{\text{H,P}} = 3.4$  Hz) and **H3** ( $\delta = 3.25$  ppm, m) are shifted upfield relative to typical alkene signals. The  $^{13}\text{C}\{^1\text{H}\}$  NMR spectrum also supports this binding mode, as seen by the resonance at 202.7 ppm for **C1**. The solid-state structure of **4.35** is shown in Figure 4.8.

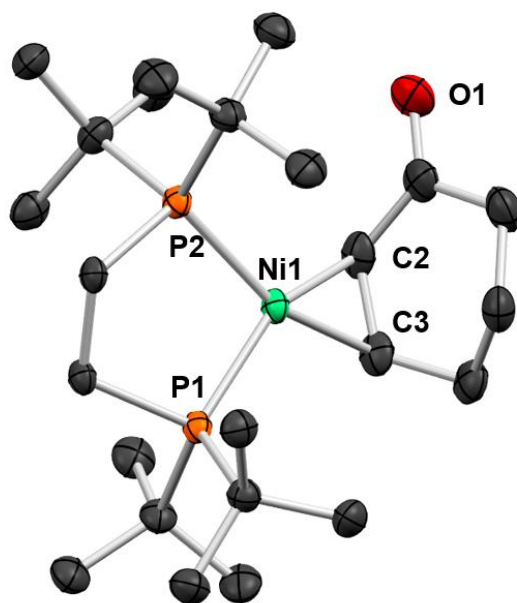
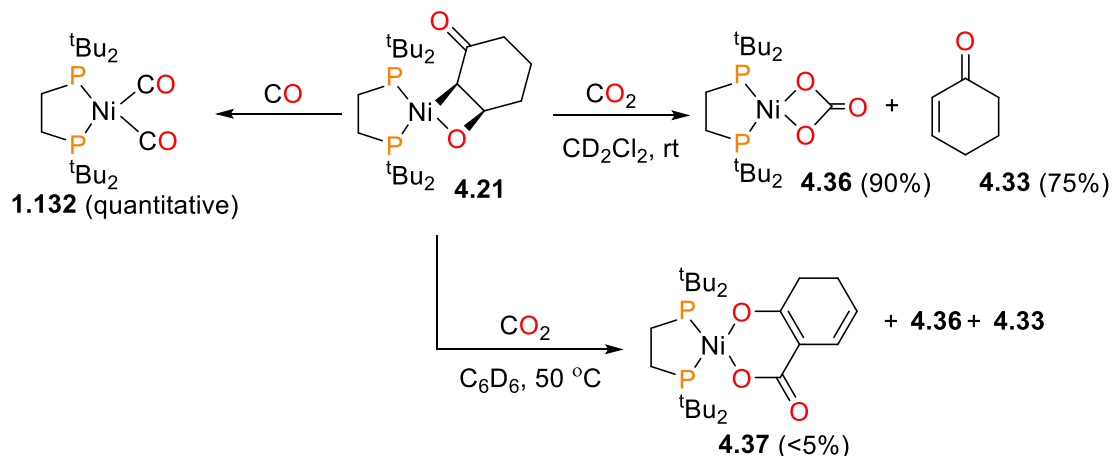


**Figure 4.8** ORTEP (50% ellipsoids) diagrams of **4.35**. Hydrogen atoms omitted for clarity.

While **4.21** was found to be unreactive with both ethylene and diphenylacetylene, stirring a solution of **4.21** in  $C_6D_6$  under 1 atm of CO for 16 hours resulted in a colour change from orange-red to pale yellow.<sup>131</sup> Analysis of the reaction mixture by  $^{31}P\{^1H\}$  NMR spectroscopy revealed the complete formation of  $(dtbpe)Ni(CO)_2$  **1.136**.<sup>215</sup> In contrast, reacting **4.21** with  $CO_2$  in  $CD_2Cl_2$  yields  $(dtbpe)Ni(CO_3)$  **4.36**<sup>213</sup> as the major product (>90% yield by  $^{31}P\{^1H\}$  NMR spectroscopy) along with **4.33** (75% yield by  $^1H$  NMR spectroscopy, see Scheme 4.15).



**Scheme 4.15** Reactivity of **4.21** with carbon oxides

In addition, if the reaction of **4.21** with  $\text{CO}_2$  is performed in benzene or toluene at  $50\text{ }^\circ\text{C}$ , orange crystals of **4.37** suitable for X-ray diffraction analysis (Figure 4.9) can also be obtained from the reaction mixture. While the insertion of a  $\text{CO}_2$  unit does indeed result in ring expansion, the bicyclic moiety of **4.37** appears to have undergone an elimination reaction to form an alkene. This group is clearly seen in the  $^1\text{H}$  NMR spectrum of **4.37**. We have been unable to characterize complex **4.37** fully, as it is formed in low yields (<5% by  $^1\text{H}$  NMR spectroscopy) and readily decomposes.

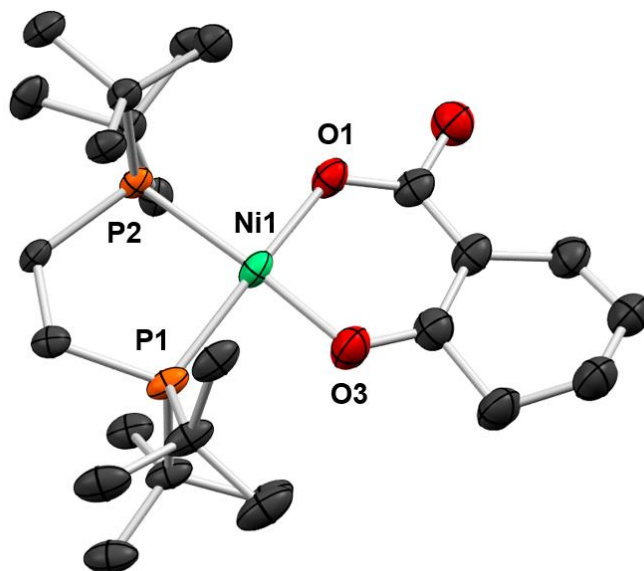
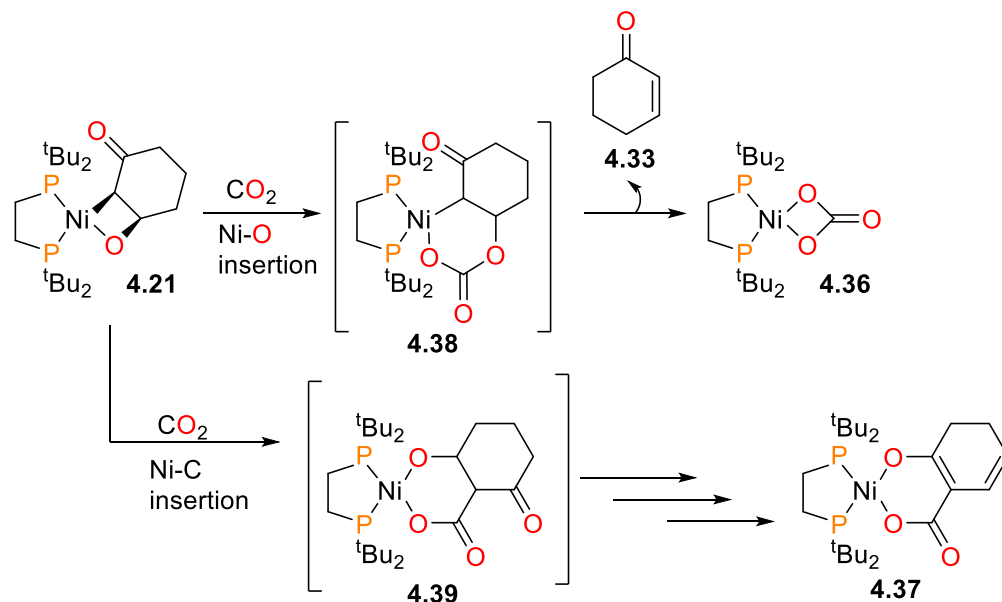


**Figure 4.9** ORTEP diagrams of **4.37** (30% ellipsoids). Hydrogen atoms omitted for clarity.

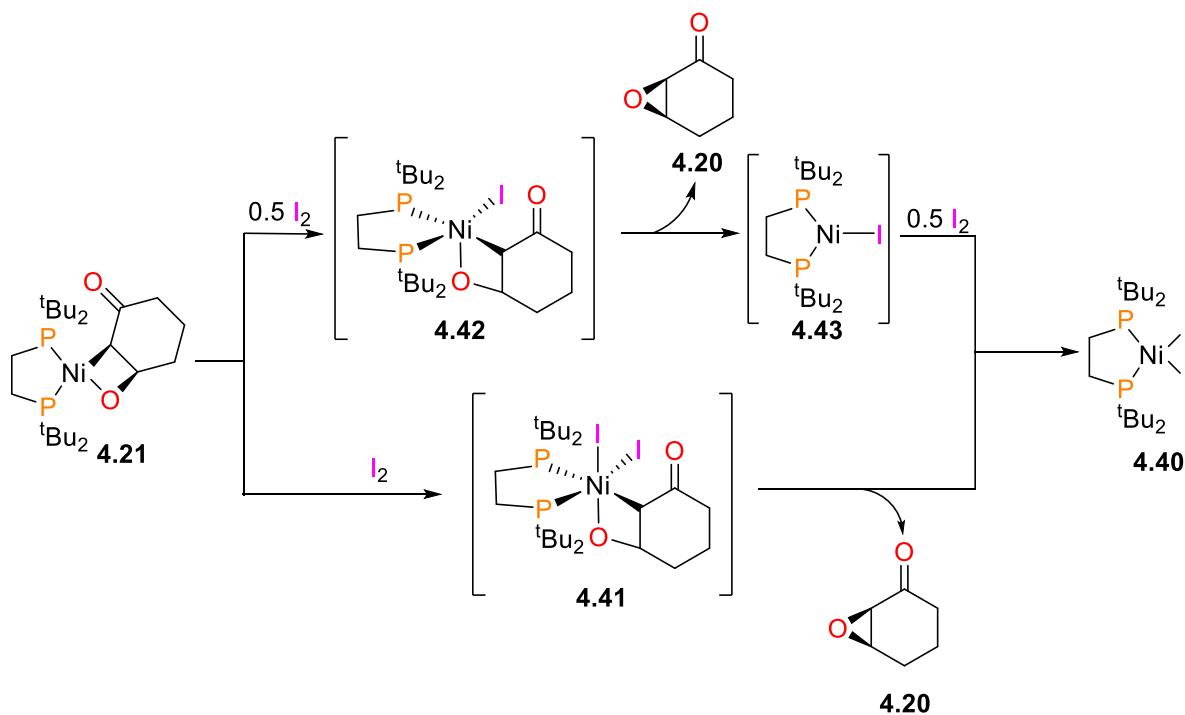
We propose that **4.36** and **4.37** are formed *via* competing mechanisms of CO<sub>2</sub> insertion into either the Ni-O bond (to generate **4.38** followed by rapid elimination of enone **4.33**, see Scheme 4.16) or *via* a competing, higher energy pathway that first involves CO<sub>2</sub> insertion into the Ni-C bond of **4.21** to form intermediate **4.39**, eventually generating **4.37**.



**Scheme 4.16** Proposed competing mechanisms of formation of **4.36** and **4.37**

Oxidatively-induced reductive elimination has been well-documented for first-row transition metals, including nickel.<sup>63, 73, 297, 298</sup> While **4.21** was found to be unreactive with O<sub>2</sub>, addition of I<sub>2</sub> to **4.21** results in an immediate colour change from red-orange to dark green. Analysis of the resulting solution by EI-MS and UV/Vis spectroscopy reveals the formation of paramagnetic (dtbpe)NiI<sub>2</sub> (**4.40**),<sup>299</sup> isolated in 93% yield. In addition, GC analysis of the crude mixture shows the presence of **4.20** in 81% yield. Two potential pathways for this reaction are outlined in Scheme 4.17. In one case, an equivalent of I<sub>2</sub> oxidizes the metal centre of **4.21**, forming an unstable nickel(IV) complex **4.41** that undergoes C-O reductive elimination to form epoxide **4.20** and **4.40**. In the other pathway, **4.21** could react with one half equivalent of iodine (i.e. a radical iodine atom) to form a nickel(III) intermediate **4.42**, which would release epoxide **4.20** *via* C-O reductive elimination. The resulting nickel(I) complex **4.43** would then be oxidized by an additional half equivalent of iodine to the final nickel(II) product **4.40**. Although Camasso and Sanford have recently reported C-O reductive elimination from a well-defined nickel(IV)

complex,<sup>122</sup> we currently favour the nickel(III) pathway, given that hard ligands like  $\text{CF}_3$ <sup>300</sup> and multidentate N-donor ligands<sup>121, 301</sup> are typically required to stabilize nickel(IV).



**Scheme 4.17** Proposed mechanisms of formation of **4.40** and **4.20** *via* nickel(III) (upper pathway) or nickel(IV) (lower pathway).

Interestingly, the addition of a methyl group at the C3 position dramatically reduces the reactivity of the nickelaoxetane ring. For example, we found that complex **4.28** was inert under an atmosphere of  $\text{CO}_2$  for several days at room temperature. Similarly, heating **4.28** at  $60^\circ\text{C}$  in the presence of  $\text{Ph}_3\text{CBF}_4$  resulted in no change to the  $^{31}\text{P}\{^1\text{H}\}$  NMR spectrum.

In our attempts to grow X-ray quality crystals of the five-membered analogue **4.27**, we reacted arene **3.20** with 5 equivalents of epoxide **4.29** in  $\text{Et}_2\text{O}$  and allowed the solvent to slowly evaporate at room temperature over the course of several days. We were able to isolate small amounts of orange-red crystals from this experiment that were subjected to X-ray diffraction analysis (Figure 4.10). To our surprise, the unit cell was comprised of two molecules of complex **4.44**, the

cyclopentenone analogue of complex **4.35**, as well as a ring-expanded complex **4.45**, formed by insertion of another equivalent of epoxide **4.29** into the Ni-C bond of nickelaoxetane **4.27** (Scheme 4.18).

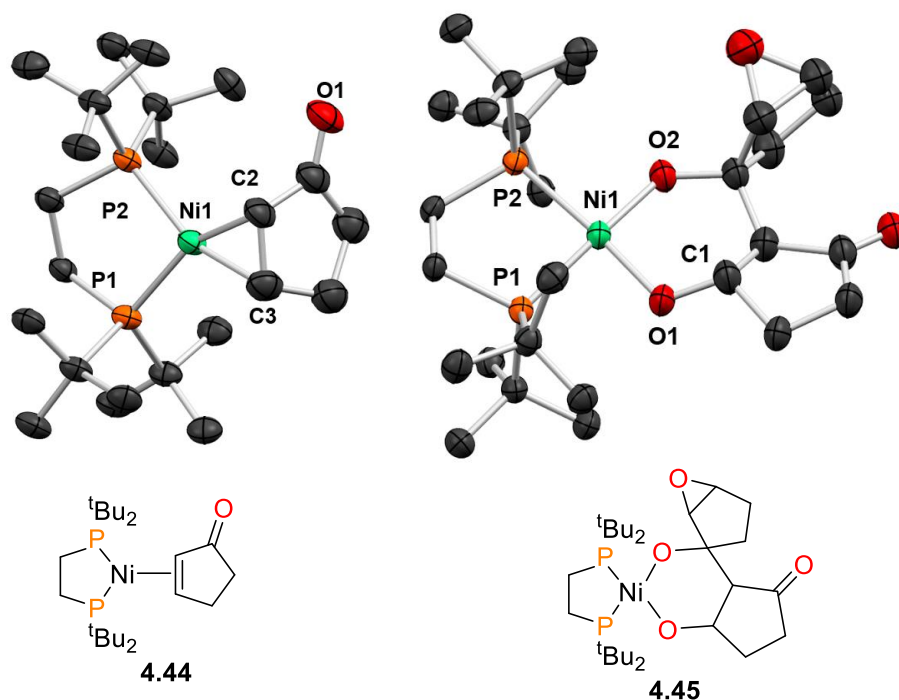
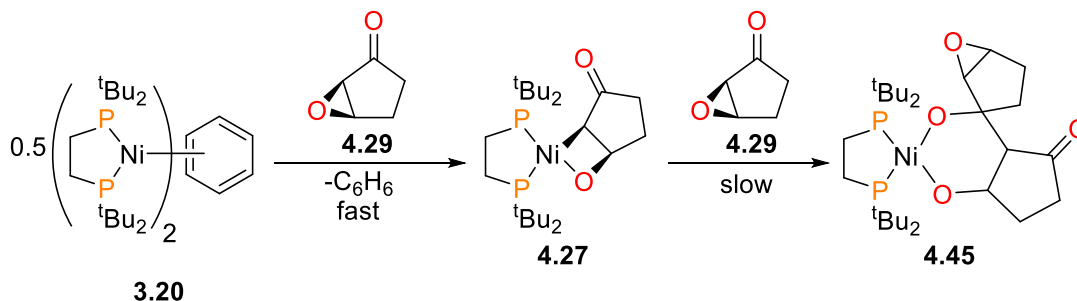


**Figure 4.10** ORTEP diagrams (30% ellipsoids) of **4.44** (left) and **4.45** (right). Hydrogen atoms omitted for clarity

Unfortunately, analysis of the remaining solid by <sup>1</sup>H and <sup>31</sup>P{<sup>1</sup>H} NMR spectroscopy showed a complex mixture of products. Subsequent attempts to form **4.45** cleanly in solution *via* the addition of a large excess (>10 equiv.) of **4.29** to arene **3.20** in C<sub>6</sub>D<sub>6</sub> showed only initial formation of nickelaoxetane **4.27** followed by gradual decomposition to the same intractable mixture of products over several days. We propose that insertion of the ketone moiety of **4.29** into the Ni-C bond of **4.27** is quite slow. Given the small amount of crystals formed during our crystallization experiment, we are uncertain at this point whether the alkene complex **4.44** is formed by deoxygenation of nickelaoxetane **4.27** or *via* simple

coordination of (dtbpe)nickel(0) to trace cyclopentenone remaining from the synthesis of epoxide **4.29**.



**Scheme 4.18** Proposed mechanism of formation of **4.45** from **4.27**

To explore whether the insertion of **4.29** into nickelaoxetane **4.27** could be encouraged at higher temperatures, we treated a  $\text{C}_6\text{D}_6$  solution of **4.27** with 1 equiv. of epoxide **4.29** and heated the red-orange solution at  $50\text{ }^\circ\text{C}$  for 5 hours. These conditions resulted in the deposition of blocky, dark-red crystals in the NMR tube. Analysis of the pale pink supernatant by  $^{31}\text{P}\{^1\text{H}\}$  NMR spectroscopy revealed no detectable resonances, indicating that the majority of the phosphorous-containing material had precipitated from solution. X-ray diffraction experiments on the crystals showed that the product of this reaction was not the expected insertion product **4.45**, but rather the bis(enolate) complex **4.46** (Figure 4.11). Unfortunately, in our hands the synthesis of **4.46** was not reproducible, and complete characterization of it remains outstanding. Formal dehydrogenation of organic moieties bound to nickel have been reported recently by Hillhouse<sup>82</sup> and Ogoshi.<sup>302</sup> Further studies on the mechanism of dehydrogenation and synthetic utility of both **4.37** and **4.46** are currently underway in our laboratory.

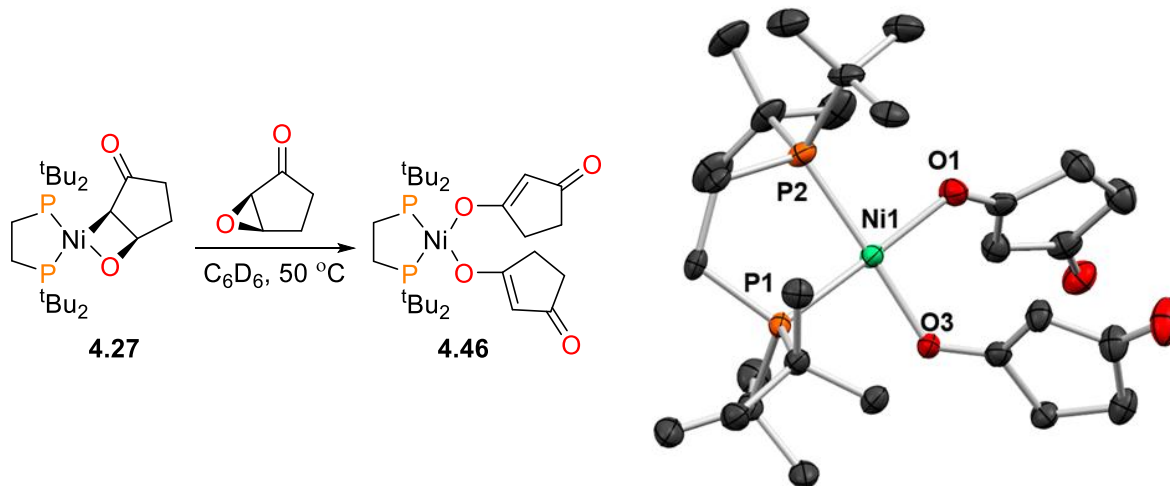


**Figure 4.11** Synthesis and ORTEP diagram (30% ellipsoids) of **4.46**

## 4.5 Summary

Overall, this Chapter demonstrates that elusive 2-nickela(II)oxetanes can be synthesized from epoxides and nickel(0) given judicious choice of organic substrate and organometallic precursor. A family of these rare nickelacycles was prepared and their structures determined through a combination of NMR spectroscopy, X-ray crystallography, mass spectrometry and elemental analysis.

Interestingly, the C-O oxidative addition step was found to proceed with *retention* of configuration, which stands in contrast to several other related systems in the literature that proceed with *inversion* of configuration.<sup>44, 45, 47, 63</sup> Possible mechanisms that would account for the observed stereochemistry of the product were explored using computational methods, and an unusual bimetallic mechanism was found to be more energetically accessible than the unimolecular pathway examined.

Finally, the fundamental reactivity of these nickelaoxetanes is also reported. Protonolysis with both strong and weak acids resulted in cleavage of the Ni-C and Ni-O

bonds of the four-membered ring, and treating **4.21** with strong Lewis acids instead results in deoxygenation of the oxetane moiety. Interestingly, reacting **4.21** with CO<sub>2</sub> resulted in a mixture of products indicative of competing Ni-C and Ni-O insertion reactions. Lastly, **4.21** was also found to be susceptible to oxidatively-induced reductive elimination when reacted with iodine, regenerating epoxide **4.20**.

## 4.6 Experimental

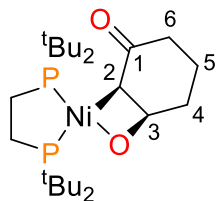
**I. General Considerations:** Unless stated otherwise, all reactions were performed in a glovebox under an atmosphere of pure nitrogen using standard Schlenk techniques. Anhydrous pentanes, toluene, diethyl ether, and tetrahydrofuran were purchased from Aldrich, sparged with dinitrogen, and dried further by passage through towers containing activated alumina and molecular sieves. C<sub>6</sub>D<sub>6</sub> and toluene-*d*<sub>8</sub> were purchased from Aldrich and dried over sodium/benzophenone before being distilled and degassed by three freeze-pump-thaw cycles. CD<sub>2</sub>Cl<sub>2</sub> was purchased from Aldrich and dried over CaH<sub>2</sub> before being distilled and degassed by three freeze-pump-thaw cycles. Cyclohexanone, **4.33** and cyclohexene oxide were dried over activated 4 Å molecular sieves and degassed by three freeze-pump-thaw cycles. Iodine was sublimed before use. Cyclic epoxides **4.20**, **4.29** and **4.30** were prepared according to the literature procedure,<sup>287</sup> degassed via three freeze-pump-thaw cycles and stored at -35 °C over activated 4 Å molecular sieves. Complexes **3.17**,<sup>215</sup> **3.20**,<sup>216</sup> **3.19**,<sup>217</sup> and **4.36**<sup>303</sup> were prepared according to literature procedures. Complex **3.20-d**<sub>6</sub> was prepared analogously to **3.20** using C<sub>6</sub>D<sub>6</sub> instead of C<sub>6</sub>H<sub>6</sub>.

NMR spectra were recorded on 300, 400 and 600 MHz spectrometers and are referenced to residual protio solvent (7.16 ppm for C<sub>6</sub>D<sub>5</sub>H, 2.08 ppm for the methyl resonance of toluene-*d*<sub>8</sub>, 5.32 ppm for CDHCl<sub>2</sub>) for <sup>1</sup>H NMR spectroscopy, solvent peaks (128.06 ppm for C<sub>6</sub>D<sub>6</sub>, 53.84 ppm for CD<sub>2</sub>Cl<sub>2</sub>, 20.43 ppm for the methyl resonance of toluene-*d*<sub>8</sub>) for <sup>13</sup>C NMR spectroscopy. <sup>31</sup>P{<sup>1</sup>H}

NMR spectra were referenced to 85 % H<sub>3</sub>PO<sub>4</sub> at 0 ppm. NMR yields are averaged over at least two separate experiments and are performed using 1,3,5-trimethoxybenzene as internal standard. NMR spectra were acquired at 25 °C unless specified otherwise. Mass spectra and elemental analyses were performed by the microanalytic services at the Department of Chemistry of the University of British Columbia. See Appendix A for detailed crystallographic data.

## II. Organometallic Syntheses

### Synthesis of **4.21**



In a 50 mL Schlenk flask containing a Teflon stir bar, complex **3.20-d<sub>6</sub>** (41.2 mg, 0.0491 mmol) was dissolved in 3 mL Et<sub>2</sub>O to give an orange-red solution.

To this was added a solution of epoxide **2** (20.6 mg, 0.184 mmol, 3.9 equiv) in Et<sub>2</sub>O (3 mL), resulting in a colour change to orange-brown. The flask was

sealed with a glass stopper (silicone grease), and the solution was stirred at rt for 1 hour before being taken to dryness *in vacuo*. The orange residue was extracted with pentanes, filtered through glass fiber to give an orange filtrate and stored at -35 °C, yielding 28.8 mg (60% yield) of **3** as an orange powder in two crops. Red, X-ray quality crystals of **4.21** were grown by the slow evaporation of a saturated Et<sub>2</sub>O solution at -35 °C over several days.

<sup>1</sup>H NMR (600 MHz, C<sub>6</sub>D<sub>6</sub>) δ 5.79-5.76 (m, 1H, **H3**), 3.35-3.25 (m, 1H, **H5**), 2.94-2.83 (m, 2H, **H2** + **H6**), 2.50-2.40 (m, 1H, **H6**), 1.92-1.85 (m, 1H, **H4**), 1.84-1.76 (m, 1H, **H5**), 1.39-1.32 (m, 28 H, 3 C(CH<sub>3</sub>)<sub>3</sub> + **H4**), 1.28-1.24 (m 1H, PCH<sub>2</sub>CH<sub>2</sub>P), 1.17 (d, *J*<sub>H,P</sub> = 12.9 Hz, 9H, C(CH<sub>3</sub>)<sub>3</sub>), 1.09-0.92 (m, 3H, PCH<sub>2</sub>CH<sub>2</sub>P), 0.84-0.75 (m, 1H, PCH<sub>2</sub>CH<sub>2</sub>P).

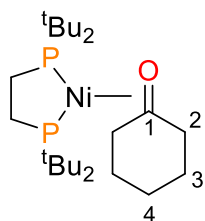
<sup>31</sup>P NMR (162 MHz, C<sub>6</sub>D<sub>6</sub>) 72.7 (d, <sup>2</sup>*J*<sub>P,P</sub> = 6 Hz), 71.5 (d, <sup>2</sup>*J*<sub>P,P</sub> = 6 Hz).

$^{13}\text{C}\{^1\text{H}\}$  NMR (150 MHz,  $\text{C}_6\text{D}_6$ )  $\delta$  211.7 (app. t,  $J_{\text{C,P}} = 3$  Hz, **C1**), 81.0 (d,  $J_{\text{C,P}} = 2$  Hz, **C3**), 40.4 (s, **C6**), 37.1 (s, **C4**), 35.8 (d,  $J_{\text{C,P}} = 12$  Hz, **C(CH<sub>3</sub>)<sub>3</sub>**), 35.7 (d,  $J_{\text{C,P}} = 10$  Hz, **C(CH<sub>3</sub>)<sub>3</sub>**), 35.3 (d,  $J_{\text{C,P}} = 14$  Hz, **C(CH<sub>3</sub>)<sub>3</sub>**), 35.1 (d,  $J_{\text{C,P}} = 10$  Hz, **C(CH<sub>3</sub>)<sub>3</sub>**), 30.8 (d,  $J_{\text{C,P}} = 5$  Hz, **C(CH<sub>3</sub>)<sub>3</sub>**), 30.4-30.3 (m, 3 **C(CH<sub>3</sub>)<sub>3</sub>**), 25.1 (app. t,  $J_{\text{C,P}} = 20$  Hz, **PCH<sub>2</sub>CH<sub>2</sub>P**), 19.0 (dd,  $J_{\text{C,P}} = 14, 10$  Hz, **PCH<sub>2</sub>CH<sub>2</sub>P**), 18.1 (s, **C5**), 14.2 (dd,  $J_{\text{C,P}} = 46, 7$  Hz, **C2**).

Anal. Calcd: C, 58.91; H, 9.89. Found: C, 59.20; H, 10.01.

LRMS (EI) 488 [ $\text{M}^+$ ]

### Synthesis of **4.23**



In a 20 mL scintillation vial, a toluene solution (2 mL) of complex **3.20** (60.3 mg, 0.0724 mmol) was combined with a toluene solution (2 mL) of cyclohexanone (30.8 mg, 0.314 mmol, 4.5 equiv), resulting in a colour change from orange-red to yellow. The vial was capped, and the solution was stirred at rt for 45 minutes before being taken to dryness *in vacuo*. The yellow residue was extracted with pentanes and filtered through glass fiber. Upon cooling at  $-35$  °C, 53.2 mg (77% yield) of **4.23** were isolated as yellow, X-ray quality crystals over two crops.

$^1\text{H}$  NMR (400 MHz,  $\text{C}_6\text{D}_6$ )  $\delta$  2.54 (tt,  $J_{\text{H,P}} = 12.2$  Hz,  $J_{\text{H,P}} = 4.1$  Hz, 2H, **H2**), 2.27 (qt,  $J_{\text{H,H}} = 13.2$  Hz,  $J_{\text{H,H}} = 3.6$  Hz, 2H, **H3**), 1.91-1.80 (m 5H, **H2** + **H3** + **H4**), 1.67 (qt,  $J_{\text{H,H}} = 13.1$  Hz,  $J_{\text{H,H}} =$

3.3 Hz, 1H, **H4**), 1.41-1.30 (m, 2H, PCH<sub>2</sub>CH<sub>2</sub>P), 1.27 (m,  $J_{H,P}$  = 11.9 Hz, 18H, 2 C(CH<sub>3</sub>)<sub>3</sub>), 1.23-1.17 (m, 2H, PCH<sub>2</sub>CH<sub>2</sub>P), 1.15 (d,  $J_{H,P}$  = 11.9 Hz, 18H, 2 C(CH<sub>3</sub>)<sub>3</sub>).

<sup>31</sup>P NMR (162 MHz, C<sub>6</sub>D<sub>6</sub>) δ 91.4 (d[AB],  $^2J_{P,P}$  = 79 Hz), 82.6 (d[AB],  $^2J_{P,P}$  = 79 Hz).

<sup>13</sup>C{<sup>1</sup>H} NMR (100 MHz, C<sub>6</sub>D<sub>6</sub>) δ 89.4 (d,  $J_{C,P}$  = 29 Hz, **C1**), 44.9 (s, **C2**), 34.6 (d,  $J_{C,P}$  = 6 Hz, C(CH<sub>3</sub>)<sub>3</sub>), 34.5 (d,  $J_{C,P}$  = 6 Hz, C(CH<sub>3</sub>)<sub>3</sub>), 33.9 (d,  $J_{C,P}$  = 3 Hz, C(CH<sub>3</sub>)<sub>3</sub>), 33.8 (d,  $J_{C,P}$  = 3 Hz, C(CH<sub>3</sub>)<sub>3</sub>), 30.6 (m, 3 C(CH<sub>3</sub>)<sub>3</sub>), 29.3 (d,  $J_{C,P}$  = 8 Hz, C(CH<sub>3</sub>)<sub>3</sub>), 29.1 (s, **C3**), 26.5 (s, **C4**), 25.3 (dd,  $J_{C,P}$  = 23,  $J_{C,P}$  = 18 Hz, PCH<sub>2</sub>CH<sub>2</sub>P), 20.2 (app. t,  $J_{C,P}$  = 12 Hz, PCH<sub>2</sub>CH<sub>2</sub>P).

Anal. Calcd: C, 60.65; H, 10.60. Found: C, 60.81; H, 10.84.

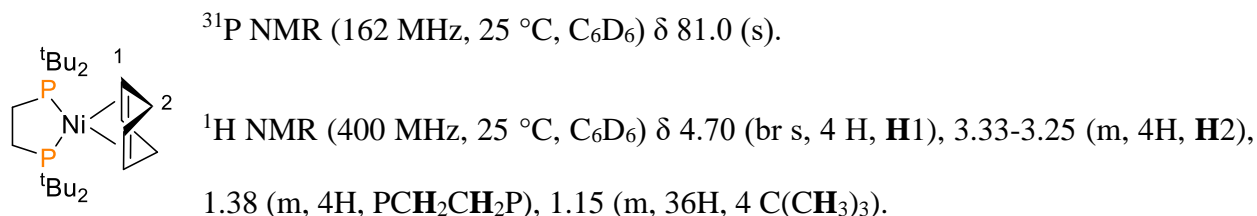
LRMS (EI) 474 [M<sup>+</sup>]

### Synthesis of 4.25 and 4.26

Complex **3.20** (61.0 mg, 0.0733 mmol) was dissolved in 5 mL of Et<sub>2</sub>O in a 20 mL scintillation vial. To this red-orange solution was added a solution of 1,4-cyclohexadiene (16.8 mg, 0.210 mmol, 2.9 equiv) in 3 mL of Et<sub>2</sub>O. Upon addition, the colour of the solution changed within seconds from red-orange to orange-yellow. The solution was stirred at rt for 1 hour, then the volatiles were removed *in vacuo* to yield an orange residue. The residue was extracted with 10 mL of pentanes and filtered to yield an orange-yellow filtrate. After standing overnight at -30 °C, a yellow powder was isolated by decanting the supernatant and drying the solid *in vacuo*. The yield was 39.5 mg. Analysis of the solid by <sup>1</sup>H, <sup>31</sup>P{<sup>1</sup>H} and <sup>13</sup>C{<sup>1</sup>H} NMR spectroscopy revealed that

the powder was a 1.8:1 mixture of **4.25** and **4.26**. The combined yield of **4.25** and **4.26** was 59% based on nickel.

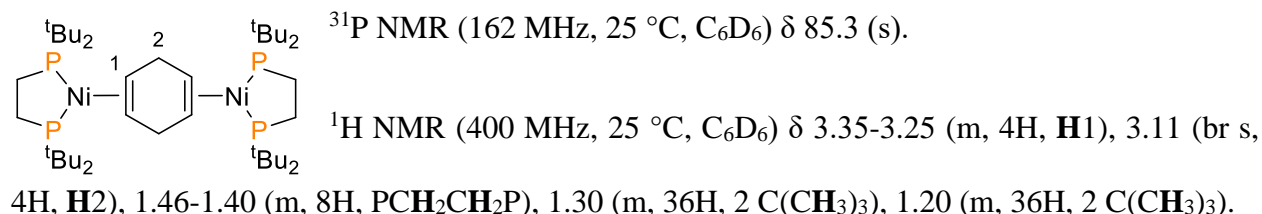
### Spectroscopic data for **4.25**



$^{13}\text{C}$  NMR (100 MHz, 25 °C,  $\text{C}_6\text{D}_6$ )  $\delta$  89.6 (br s, **C1**), 34.6 (m,  $\text{C}(\text{CH}_3)_3$ ), 30.7 (m,  $\text{C}(\text{CH}_3)_3$ ), 29.7 (s, **C2**), 23.6 (m,  $\text{PCH}_2\text{CH}_2\text{P}$ ).

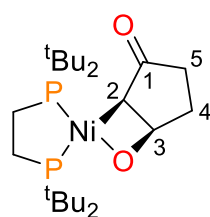
LRMS (EI) 456 [ $\text{M}^+$ ]

### Spectroscopic data for **4.26**



$^{13}\text{C}$  NMR (100 MHz, 25 °C,  $\text{C}_6\text{D}_6$ )  $\delta$  54.1 (app. t,  $J_{\text{C,P}} = 9$  Hz, **C1**), 34.6 (m,  $\text{C}(\text{CH}_3)_3$ ), 34.4 (m,  $\text{C}(\text{CH}_3)_3$ ), 32.1 (s, **C2**), 31.2 (m,  $\text{C}(\text{CH}_3)_3$ ), 30.6 ( $\text{C}(\text{CH}_3)_3$ ), 23.9 (m,  $\text{PCH}_2\text{CH}_2\text{P}$ ).

### Synthesis of **4.27**



In a 50 mL Schlenk flask, complex **3.20** (54.3 mg, 0.0652 mmol) was dissolved in 3 mL  $\text{Et}_2\text{O}$  to give an orange-red solution. To this was added a solution of epoxide **4.29** (18.2 mg, 0.216 mmol, 3.3 equiv) in  $\text{Et}_2\text{O}$  (2 mL), resulting in a colour change to orange-brown. The flask was sealed with a glass stopper (silicone grease), and the solution was stirred at rt for 30 minutes before being taken to dryness *in*

*vacuo*. The brown residue was extracted with pentanes, filtered through glass fiber to give an orange filtrate and dried *in vacuo* to give 27.9 mg (45% yield) of **4.27** as an orange powder.

$^1\text{H}$  NMR (600 MHz,  $\text{C}_6\text{D}_6$ )  $\delta$  6.02-5.97 (m, 1H, **H3**), 3.72-3.63 (m, 1H, **H5**), 2.38-2.30 (m, 2H, **H2** + **H5**), 2.08 (dd,  $J_{\text{H,H}} = 12.7$  8.5 Hz, 1H, **H4**), 1.93-1.83 (m, 1H, **H4**), 1.33 (d,  $J_{\text{H,P}} = 12.0$  Hz, 9H,  $\text{C}(\text{CH}_3)_3$ ), 1.30 (d,  $J_{\text{H,P}} = 12.3$  Hz, 9H,  $\text{C}(\text{CH}_3)_3$ ), 1.28 (d,  $J_{\text{H,P}} = 7.0$  Hz, 9H,  $\text{C}(\text{CH}_3)_3$ ), 1.26 (d,  $J_{\text{H,P}} = 7.3$  Hz, 9H  $\text{C}(\text{CH}_3)_3$ ), 1.08-0.98 (m, 1H  $\text{PCH}_2\text{CH}_2\text{P}$ ), 0.94-0.79 (m, 3H,  $\text{PCH}_2\text{CH}_2\text{P}$ ).

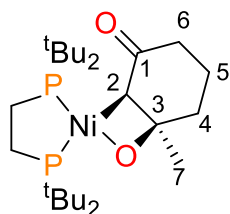
$^{31}\text{P}$  NMR (162 MHz,  $\text{C}_6\text{D}_6$ ) 76.6 (d,  $^2J_{\text{P,P}} = 7$  Hz), 74.8 (d,  $^2J_{\text{P,P}} = 7$  Hz).

$^{13}\text{C}\{^1\text{H}\}$  NMR (150 MHz,  $\text{C}_6\text{D}_6$ )  $\delta$  217.8 (br s, **C1**), 86.3 (d,  $J_{\text{C,P}} = 2$  Hz, **C3**), 39.3 (s, **C4**), 37.4 (s, **C5**), 35.6 (d,  $J_{\text{C,P}} = 13$  Hz,  $\text{C}(\text{CH}_3)_3$ ), 35.5 (d,  $J_{\text{C,P}} = 14$  Hz,  $\text{C}(\text{CH}_3)_3$ ), 35.3 (d,  $J_{\text{C,P}} = 14$  Hz,  $\text{C}(\text{CH}_3)_3$ ), 34.5 (d,  $J_{\text{C,P}} = 9$  Hz,  $\text{C}(\text{CH}_3)_3$ ), 30.7 (d,  $J_{\text{C,P}} = 4$  Hz,  $\text{C}(\text{CH}_3)_3$ ), 30.6 (d,  $J_{\text{C,P}} = 4$  Hz,  $\text{C}(\text{CH}_3)_3$ ), 30.5 (d,  $J_{\text{C,P}} = 4$  Hz,  $\text{C}(\text{CH}_3)_3$ ), 30.1 (d,  $J_{\text{C,P}} = 3$  Hz,  $\text{C}(\text{CH}_3)_3$ ), 24.5 (app. t,  $J_{\text{C,P}} = 19$  Hz,  $\text{PCH}_2\text{CH}_2\text{P}$ ), 19.1 (dd,  $J_{\text{C,P}} = 14, 11$  Hz,  $\text{PCH}_2\text{CH}_2\text{P}$ ), 9.0 (dd,  $J_{\text{C,P}} = 48, 8$  Hz, **C2**).

Anal. Calcd: C, 58.13; H, 9.76. Found: C, 58.53; H, 9.64.

LRMS (EI) 474 [M<sup>+</sup>]

### Synthesis of **4.28**



In a 50 mL Schlenk flask, complex **3.20** (57.0 mg, 0.0685 mmol) was dissolved in 2 mL toluene to give an orange-red solution. To this was added a solution of epoxide **4.30** (27.2 mg, 0.216 mmol, 3.3 equiv) in toluene (2 mL),

resulting in a colour change to orange-brown. The flask was sealed with a glass stopper (silicone grease), and the solution was stirred at rt for 30 minutes before being taken to dryness *in vacuo*. The brown residue was extracted with pentanes, filtered through glass fiber to give an orange filtrate and stored at -35 °C, yielding 35.6 mg (52% yield) of orange, X-ray quality crystals of **4.28** in two crops.

$^1\text{H}$  NMR (400 MHz,  $\text{C}_6\text{D}_6$ )  $\delta$  3.29-3.15 (m, 1H, **H5**), 2.85 (dd,  $J_{\text{H,H}} = 18.2$  Hz, 6.2 Hz, 1H, **H6**), 2.52 (d,  $J_{\text{H,H}} = 6.4$  Hz, 1H, **H6**), 2.44-2.32 (m, 1H, **H2**), 1.86-1.77 (m, 1H, **H4**), 1.73-1.65 (m, 1H, **H5**), 1.48 (s, 3H, **H7**), 1.38 (d,  $J_{\text{H,P}} = 12.2$  Hz, 9H,  $\text{C}(\text{CH}_3)_3$ ), 1.36-1.34 (m, 10H, **H4** +  $\text{C}(\text{CH}_3)_3$ ), 1.33 (d,  $J_{\text{H,P}} = 6.5$  Hz, 9H,  $\text{C}(\text{CH}_3)_3$ ), 1.29-1.22 (m, 4H,  $\text{PCH}_2\text{CH}_2\text{P}$ ), 1.17 (d,  $J_{\text{H,P}} = 12.6$  Hz, 9H,  $\text{C}(\text{CH}_3)_3$ ).

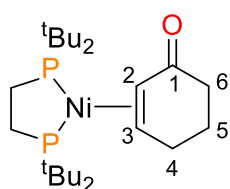
$^{31}\text{P}\{^1\text{H}\}$  NMR (162 MHz,  $\text{C}_6\text{D}_6$ )  $\delta$  72.7 (d[AB],  $^2J_{\text{P,P}} = 7$  Hz), 71.3 (d[AB],  $^2J_{\text{P,P}} = 7$  Hz).

$^{13}\text{C}\{^1\text{H}\}$  NMR (100 MHz,  $\text{C}_6\text{D}_6$ )  $\delta$  211.4 (app. t,  $J_{\text{C,P}} = 3$  Hz, **C1**), 82.8 (s, **C3**), 41.9 (s, **C6**), 39.8 (s, **C7**), 36.3 (s, **C4**), 35.8 (d,  $J_{\text{C,P}} = 12$  Hz,  $\text{C}(\text{CH}_3)_3$ ), 35.5 (d,  $J_{\text{C,P}} = 10$  Hz,  $\text{C}(\text{CH}_3)_3$ ), 35.3 (d,  $J_{\text{C,P}} = 14$  Hz,  $\text{C}(\text{CH}_3)_3$ ), 35.0 (d,  $J_{\text{C,P}} = 8$  Hz,  $\text{C}(\text{CH}_3)_3$ ), 30.9 (d,  $J_{\text{C,P}} = 5$  Hz,  $\text{C}(\text{CH}_3)_3$ ), 30.5-30.3 (m, 3  $\text{C}(\text{CH}_3)_3$ ), 25.2 (app. t,  $J_{\text{C,P}} = 20$  Hz,  $\text{PCH}_2\text{CH}_2\text{P}$ ), 23.5 (dd,  $J_{\text{C,P}} = 46$  Hz, 6 Hz, **C2**), 19.4 (s, **C5**), 19.0 (dd,  $J_{\text{C,P}} = 14$  Hz, 10 Hz,  $\text{PCH}_2\text{CH}_2\text{P}$ ).

Anal. Calcd: C, 59.66; H, 10.01. Found: C, 58.39; H, 10.11. Although satisfactory elemental analysis could not be obtained after repeated attempts, the data here is included to demonstrate our best results.

LRMS (EI) 502 [M+]

### Synthesis of 4.35



In a 25 mL Schlenk flask, complex **3.20-d<sub>6</sub>** (41.6 mg, 0.0499 mmol) was dissolved in 4 mL of Et<sub>2</sub>O to give an orange-red solution. To this solution was added **4.33** (15.6 mg, 0.163 mmol, 3.4 equiv) in Et<sub>2</sub>O (2 mL), resulting in an immediate colour change to yellow. The flask was sealed with a glass stopper (silicone grease), and the solution was stirred at rt for 15 minutes before being taken to dryness *in vacuo*. The yellow residue was extracted with pentanes, and upon cooling to -35 °C yielded 35.4 mg (75% yield) of **4.35** as orange, X-ray quality crystals in two crops.

<sup>1</sup>H NMR (400 MHz, C<sub>6</sub>D<sub>6</sub>) δ 4.18 (ddd, <sup>3</sup>J<sub>H,H</sub> = 8.7 Hz, J<sub>H,P</sub> = 6.3 Hz, 3.4 Hz, 1H, **H2**), 3.29-3.21 (m, 1H, **H3**), 2.49 (br d, <sup>2</sup>J<sub>H,H</sub> = 16.0 Hz, 1H, **H6**), 2.29-2.15 (m, 2H, **H4** + **H6**), 1.91-1.83 (m, 2H, **H4** + **H5**), 1.78-1.71 (m, 1H, **H5**), 1.40-1.22 (m, 4H, PCH<sub>2</sub>CH<sub>2</sub>P), 1.20 (d, J<sub>H,P</sub> = 11.8 Hz, 9H, C(CH<sub>3</sub>)<sub>3</sub>), 1.14 (d, J<sub>H,P</sub> = 12.0 Hz, 9H, C(CH<sub>3</sub>)<sub>3</sub>), 1.06 (d, J<sub>H,P</sub> = 11.8 Hz, 9H, C(CH<sub>3</sub>)<sub>3</sub>), 1.02 (d, J<sub>H,P</sub> = 11.9 Hz, 9H, C(CH<sub>3</sub>)<sub>3</sub>).

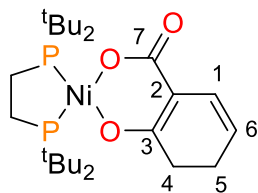
<sup>31</sup>P NMR (162 MHz, C<sub>6</sub>D<sub>6</sub>) δ 85.7 (d, <sup>2</sup>J<sub>P,P</sub> = 61 Hz), 79.5 (d, <sup>2</sup>J<sub>P,P</sub> = 61 Hz).

<sup>13</sup>C{<sup>1</sup>H} NMR (100 MHz, C<sub>6</sub>D<sub>6</sub>) δ 202.7 (t, J<sub>C,P</sub> = 3 Hz, **C1**), 63.3 (dd, J<sub>C,P</sub> = 13 Hz, 2 Hz, **C2**), 48.5 (d, J<sub>C,P</sub> = 25 Hz, **C3**), 39.0 (s, **C6**), 35.5 (dd, J<sub>C,P</sub> = 9 Hz, 3 Hz, C(CH<sub>3</sub>)<sub>3</sub>), 35.1-34.8 (m, 3 C(CH<sub>3</sub>)<sub>3</sub>), 30.7-30.4 (m, 4 C(CH<sub>3</sub>)<sub>3</sub>), 29.0 (dd, J<sub>C,P</sub> = 3 Hz, 1 Hz, **C4**), 25.4 (s, **C5**), 24.0 (dd, J<sub>C,P</sub> = 19 Hz, 15 Hz, PCH<sub>2</sub>CH<sub>2</sub>P), 22.8 (dd, J<sub>C,P</sub> = 16 Hz, 14 Hz, PCH<sub>2</sub>CH<sub>2</sub>P).

Anal. Calcd: C, 60.91; H, 10.22. Found: C, 61.03; H, 10.42.

LRMS (EI) 472 [M+]

### Synthesis of 4.37



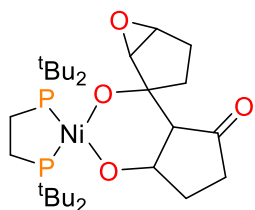
Complex **4.21** was dissolved in toluene (2 mL) in a Teflon-sealed Schlenk bomb. The flask was removed from the glovebox and attached to a Schlenk line. The orange-red solution was then frozen in a liquid nitrogen bath, and the headspace was evacuated. The flask was then backfilled with CO<sub>2</sub> gas and warmed to room temperature with a constant flow of CO<sub>2</sub>. Once the solution had completely warmed, the flask was sealed and placed in a 50 °C oil bath overnight, allowing for the deposition of orange crystals in the reaction vessel. The yellow supernatant was decanted, and the crystals were washed with pentanes and dried *in vacuo*. Analysis of the crystals by <sup>31</sup>P, <sup>1</sup>H and <sup>13</sup>C NMR spectroscopy revealed them to mostly consist of **4.36** with a small amount of **4.37**. Attempts to purify **4.37** by recrystallization were unsuccessful, as it displays similar solubility to **4.36** and decomposed readily in our hands.

<sup>1</sup>H NMR (600 MHz, CD<sub>2</sub>Cl<sub>2</sub>) δ 6.42 (d, *J*<sub>H,H</sub> = 9.7 Hz, 1H, **H1**), 5.14-5.10 (m, 1H, **H6**), 2.15-2.10 (m, 2H, **H5**), 2.09-2.04 (m, 2H, **H4**), 1.57 (d, *J*<sub>H,P</sub> = 13.0 Hz, 18H, C(CH<sub>3</sub>)<sub>3</sub>), 1.53 (d, *J*<sub>H,P</sub> = 13.0 Hz, 18H, C(CH<sub>3</sub>)<sub>3</sub>). The methylene resonances of the dtbpe ligand could not be located due to overlapping impurities.

<sup>31</sup>P NMR (162 MHz, CD<sub>2</sub>Cl<sub>2</sub>) δ 79.8 (d[AB], <sup>2</sup>*J*<sub>P,P</sub> = 51 Hz), 79.0 (d[AB], <sup>2</sup>*J*<sub>P,P</sub> = 51 Hz).

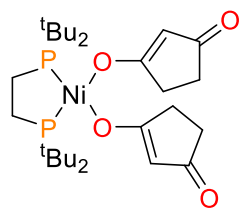
$^{13}\text{C}$  NMR (150 MHz,  $\text{CD}_2\text{Cl}_2$ )  $\delta$  174.0 (s, C3), 167.2 (s, C7), 138.4 (s, C2), 127.9 (s, C1), 111.4 (s, C6), 36.5 (d,  $J_{\text{C,P}} = 15$  Hz,  $\text{C}(\text{CH}_3)_3$ ), 36.4 (d,  $J_{\text{C,P}} = 15$  Hz,  $\text{C}(\text{CH}_3)_3$ ), 33.4 (s, C4), 30.3 (d,  $J_{\text{C,P}} = 2$  Hz,  $\text{C}(\text{CH}_3)_3$ ), 30.2 (d,  $J_{\text{C,P}} = 2$  Hz,  $\text{C}(\text{CH}_3)_3$ ), 23.5 (s, C5).

### Synthesis of 4.45



In the glovebox, a 5-dram vial was charged with a red solution of **3.20** (30.7 mg, 0.036 mmol, 1.0 equiv.) in 4 mL  $\text{Et}_2\text{O}$ . To this was added a solution of epoxide **4.29** (19.2 mg, 0.196 mmol, 5.4 equiv.) in 4 mL of  $\text{Et}_2\text{O}$ , resulting in a colour change to orange-red. A stir bar was added, and the reaction was stirred for 1 hour at room temperature. The stir bar was then removed, and the cap of the vial was loosened to allow for slow evaporation of the  $\text{Et}_2\text{O}$  solvent. After sitting at room temperature for several days, small orange-red crystals formed on the walls of the vial, which were analyzed by X-ray diffraction experiments and found to contain both **4.44** and **4.45** in the unit cell.

### Synthesis of 4.46

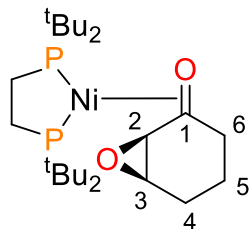


To a solution of **4.27** (9.7 mg, 0.020 mmol, 1.0 equiv.) in  $\text{C}_6\text{D}_6$  was added epoxide **4.29** (2.2 mg, 0.022 mmol, 1.1 equiv.). The orange-red solution was then transferred to a J-Young tube, sealed, and removed from the glovebox. The tube was placed in a 50 °C oil bath for 5 hours, during which time blocky red crystals deposited on the walls of the tube. After removing the tube from the bath, the supernatant was examined by  $^{31}\text{P}\{^1\text{H}\}$  NMR spectroscopy, revealing no detectable resonances. The tube was then returned to the glovebox, and the supernatant was decanted from the crystals.

Analysis of the crystals by X-ray diffraction experiments reveal that they are the bis(enolate) complex **4.46**.

### III. Mechanistic Studies of the Formation of **4.21**

#### Low-temperature synthesis of **4.21**



Complex **3.20-d<sub>6</sub>** (24.2 mg, 0.0289 mmol) was dissolved in 0.3 mL of tol-*d*<sub>8</sub>.

This red-orange solution was transferred to a screw-cap NMR tube and frozen in liquid nitrogen. To the top of this frozen solution was added a solution of **4.20** (6.3 mg, 0.0566 mmol, 2.0 equiv) in tol-*d*<sub>8</sub> (0.2 mL). The

tube was then placed in a -78 °C bath to thaw before being quickly placed in an NMR spectrometer pre-cooled to -70 °C. The spectrometer was then warmed to -50 °C, and the sample was analyzed by <sup>31</sup>P{<sup>1</sup>H} and <sup>13</sup>C NMR spectroscopy.

#### Spectroscopic data for **4.22**

<sup>31</sup>P NMR (162 MHz, -50 °C, tol-*d*<sub>8</sub>) δ 90.7 (d[AB], <sup>2</sup>J<sub>P,P</sub> = 72 Hz), 83.9 (d[AB], <sup>2</sup>J<sub>P,P</sub> = 72 Hz).

<sup>13</sup>C NMR (100 MHz, -50 °C, tol-*d*<sub>8</sub>) δ 81.3 (d, J<sub>C,P</sub> = 31 Hz, C1), 66.1 (s, C3), 61.6 (s, C2), 56.0 (s, C6), 55.9 (s, C4), 15.8 (s, C5). The signals for the dtbpe ligand of **4.22** could not be assigned due to overlap with the corresponding ligand signals for **3.20**, **3.20'** and **4.21**.

### IV. Reactivity of Studies of **4.21**

#### Reaction of **4.21** with HCl

In a glovebox, complex **4.21** (5.1 mg, 0.0104 mmol) and trimethoxybenzene (2.1 mg, 0.0124 mmol) were dissolved in 0.6 mL of C<sub>6</sub>D<sub>6</sub> in a 1-dram vial. The vial was taken out of the glovebox,

and 1 drop of 1.2 M HCl<sub>(aq)</sub> was added, resulting in an immediate colour change from orange-red to red-pink, as well as the precipitation of a red solid. After 20 minutes, the pale pink supernatant was decanted and analyzed by <sup>1</sup>H NMR spectroscopy, and was found to contain enone **4.33** in 69% yield. The red precipitate was dried *in vacuo* and identified as (dtbpe)NiCl<sub>2</sub> **3.19** by EI-MS and UV/Vis spectroscopy. The isolated yield was 4.4 mg (94%).

#### **Reaction of 4.21 with MeOH**

In a glovebox, complex **4.21** (9.2 mg, 0.0188 mmol) and trimethoxybenzene (1.4 mg, 0.0083 mmol) were dissolved in 0.6 mL CDCl<sub>3</sub> to give an orange solution, which was transferred to a screw-cap NMR tube. Using a microsyringe, 2.5 μL of MeOH were then added through the septum of the cap and mixed, resulting in a gradual colour change from orange to red-pink over the course of 2 hours. The solution was then analyzed *via* <sup>1</sup>H NMR spectroscopy and GC-MS, revealing the formation of alcohol **4.34** in 59% yield.

#### **Reaction of 4.21 with Ph<sub>3</sub>CBF<sub>4</sub>**

In a glovebox, complex **4.21** (8.2 mg, 0.0168 mmol) and trimethoxybenzene (1.8 mg, 0.0107 mmol) was dissolved in 0.6 mL C<sub>6</sub>D<sub>6</sub> and transferred to a J-Young NMR tube. To the orange-red solution was added Ph<sub>3</sub>CBF<sub>4</sub> (4.0 mg, 0.0121 mmol). The tube was then sealed and removed from the glovebox. Monitoring the reaction for 24 hours at room temperature revealed minimal consumption of **4.21**. The tube was then placed in a 50 °C oil bath for 16 hours, resulting in a colour change from orange-red to yellow and the precipitation of a black solid. Analysis of the solution by <sup>31</sup>P and <sup>1</sup>H NMR spectroscopy, as well as EI-MS revealed the formation of **4.35** in 36% yield, as well as enone **4.33** in 26% yield. Free dtbpe was observed by <sup>31</sup>P NMR spectroscopy but could not be accurately quantified by <sup>1</sup>H NMR spectroscopy due to overlapping peaks.

### Reaction of 4.21 with CO

Complex **4.21** was dissolved in 0.6 mL C<sub>6</sub>D<sub>6</sub> and transferred to a J-Young NMR tube. The NMR tube was sealed and removed from the glovebox. After placing the tube on a Schlenk line, the solution was frozen in a -78 °C bath. The headspace was then evacuated and backfilled with CO gas. The bath was then removed, and the solution was allowed to come to room temperature under a constant flow of CO. The tube was then sealed and monitored by <sup>31</sup>P{<sup>1</sup>H} NMR spectroscopy, which revealed the consumption of **4.21** and the quantitative generation of (dtbpe)Ni(CO)<sub>2</sub> **1.132**. No intermediates were observed in the <sup>31</sup>P{<sup>1</sup>H} NMR spectra. After the reaction was complete, the supernatant was analyzed *via* GC-MS. The only identifiable organic components were enone **4.33** and alcohol **4.34** in trace amounts.

### High-temperature reaction of 4.21 with CO<sub>2</sub>

Complex **4.21** (25.3 mg, 0.0517 mmol) was dissolved in toluene (2 mL) in a Teflon-sealed Schlenk bomb. The flask was removed from the glovebox and attached to the Schlenk line. The orange-red solution was then frozen in a liquid nitrogen bath, and the headspace was evacuated. The flask was then backfilled with CO<sub>2</sub> gas and warmed to room temperature with a constant flow of CO<sub>2</sub>. Once the solution had completely warmed, the flask was sealed and placed in a 50 °C oil bath overnight, allowing for the deposition of a small amount of orange crystals of **4.37** in the reaction vessel. The yellow-brown supernatant was decanted and allowed to slowly evaporate, yielding yellow crystals of **4.36**. The remaining supernatant was decanted, and the crystals of **4.36** were dried *in vacuo* (yield = 8.3 mg, 37%). Complex **4.36** was identified by <sup>31</sup>P, <sup>1</sup>H and <sup>13</sup>C NMR spectroscopy.

### Room temperature reaction of 4.21 with CO<sub>2</sub>

Complex **4.21** (8.3 mg, 0.0170 mmol) and trimethoxybenzene (2.7 mg, 0.0161 mmol) were dissolved in 0.5 mL CD<sub>2</sub>Cl<sub>2</sub>. The red solution was transferred to a screw-cap NMR tube, sealed,

and removed from the glove box. CO<sub>2</sub> (0.8 mL, 0.033 mmol) was injected into the tube through the septum using a 1 mL syringe, and the solution was inverted 3 times to mix. The reaction was monitored by <sup>1</sup>H and <sup>31</sup>P NMR spectroscopy, and revealed the conversion of complex **4.21** into complex **4.36** and enone **4.33** over the course of 2.5 hours at room temperature. No intermediates were observed during the course of the reaction. The final yield of enone **4.33** was 75%, and while the <sup>1</sup>H NMR yield of complex **4.36** could not be reliably determined due to overlapping signals, <sup>31</sup>P{<sup>1</sup>H} NMR spectroscopy indicates >90% conversion of **4.21** to **4.36**.

### Reaction of **4.21** with I<sub>2</sub>

In a glovebox, complex **4.21** (13.5 mg, 0.0276 mmol) was dissolved in 1.00 mL of THF to give an orange-red solution. This was then added rapidly to a 1-dram vial charged with I<sub>2</sub> (7.3 mg, 0.0288 mmol, 1.05 equiv) and a stir bar. The colour of the solution changed within seconds from orange-red to dark green, and was stirred at rt for 45 minutes. An aliquot of the solution was then analyzed by GC-FID, which showed the formation of epoxide **4.20** in 81% yield. The remaining solution was taken to dryness *in vacuo*. The residue was then washed with pentanes and dried *in vacuo* overnight to yield a blue-green powder (16.2 mg, 93% yield), identified as paramagnetic (dtbpe)NiI<sub>2</sub> **4.40** by UV/Vis spectroscopy and EI-MS.

## VII. Computational Details

Density functional theory was employed using Gaussian 09, revision D.01.<sup>304</sup> The gradient-corrected functional BP86 (incorporating Becke's exchange functional<sup>305</sup> and the correlation functional of Perdew<sup>306</sup>) was used in all calculations, and geometry optimisations were performed with no symmetry restrictions. The double- $\zeta$  basis set 6-31G(d,p) was used for non-metal atoms in all calculations, and the LANL2DZ basis set and associated effective core-potential was used for Ni. Analytical computation of the Hessian matrix was performed on each output geometry to

ensure the presence of local minima and maxima. Statistical mechanics calculations of entropic and thermal effects were performed using the rigid rotor and harmonic oscillator approximations at 298.15 K and 1 atm. Connectivity between transition states and intermediates was established by means of intrinsic reaction coordinate (IRC) calculations. NBO analysis was performed using the NBO 3.1 program as implemented in Gaussian 09. Intermediates and transition states along the reaction pathway were initially located using the truncated dmpe (bis(dimethylphosphino)ethane) ligand, followed by full modelling of the dtbpe ligand. Upon comparison of the X-ray structure for the metallacycle to optimized structures, it was found that the truncated dmpe ligand provided more accurate bond lengths, especially for the P-Ni bonds. The use of the dispersion-corrected BP86-D3 functional did not improve the calculated bond metrics.

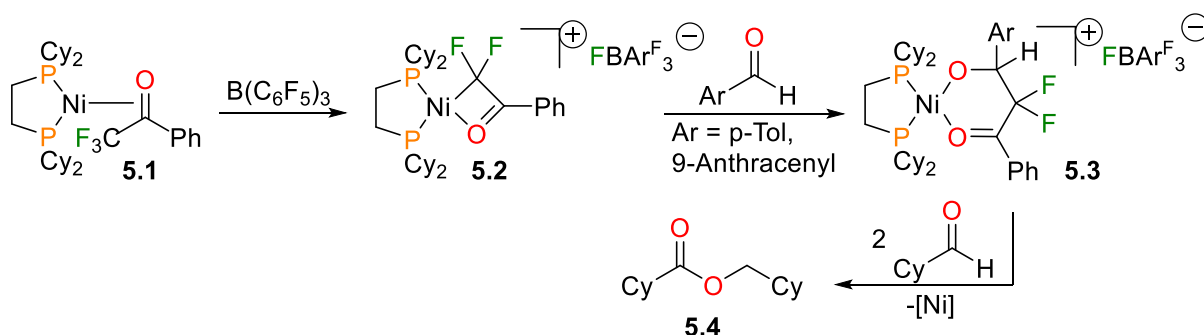
# Chapter 5 : Adventures in C-O and C-S Bond Cleavage Using Nickel and Rhodium

## 5.1 Introduction

After the successful utilization of ketones as directing groups for nickel(0) described in Chapter 4, we were inspired to determine what other C-O or C-S oxidative addition reactions could be induced by the motif of pre-coordination described in Chapter 4. Among carbonyl compounds, esters are known to show relatively low reactivity towards nickel complexes, although there are several early reports of C-O bond cleavage using nickel(0).<sup>307-309</sup> Since esters are a cheap and naturally abundant feedstock, the direct activation of C-O bonds of esters is of great interest.<sup>310-312</sup> The utility of esters as the electrophilic source in Suzuki-type cross coupling reactions has recently been realized by Garg<sup>313</sup> and Shi<sup>314, 315</sup> using aryl pivalates with aryl boronic acids and aryl boroxines, respectively. Subsequently, Itami succeeded in the isolation and structural elucidation of an arynickel(II) pivalate as an intermediate in catalytic C-H/C-O biaryl coupling.<sup>112</sup> Our group has also recently demonstrated decarbonylative cross-coupling of esters with arylboronic acids by nickel catalysis as an alternative to aryl halide-based Suzuki coupling.<sup>316</sup>

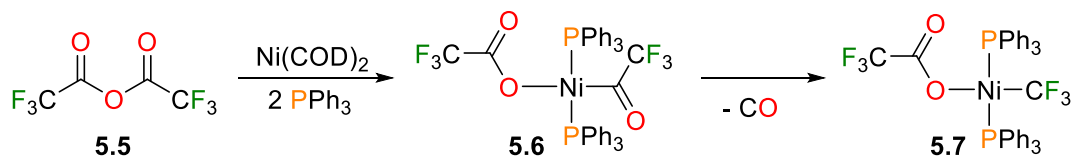
Interestingly, thioesters often show complementary activation pathways relative to esters. For instance, Jones' report of platinum(0)-mediated C-S bond activation of aliphatic thioesters displayed an initial C<sub>acyl</sub>-S bond cleavage yielding a platinum acyl-thiolate complex.<sup>115</sup> Upon heating, CO is released and activation of a second equivalent of thioester led to a platinum dithiolate complex. In addition, Riordan has reported that the use of a comparable nickel(0) complex led to the cleavage of the C<sub>acyl</sub>-S bond of thioesters having an electron-deficient C<sub>6</sub>F<sub>5</sub> substituent.<sup>317</sup>

Recently, Ogoshi and co-workers have shown that trifluoroacetophenone complex **5.1**, which is qualitatively similar to complexes described here in Chapters 3 and 4, reacts with Lewis acidic  $B(C_6F_5)_3$  via fluoride abstraction to form cationic nickel enolate complex **5.2**. This nickel(II) product can then insert aldehydes into the Ni-C bond to generate the six-membered nickelacycles of type **5.3**.<sup>209</sup> Curiously, both **5.2** and **5.3** are competent catalysts for Tischenko-type coupling of aldehydes to form esters. Stoichiometric studies indicated that the first equivalent of aldehyde is not incorporated into the ester, as treating **5.3** with two equivalents of cyclohexylcarbaldehyde resulted in the quantitative formation of ester **5.4** shown in Scheme 5.1.



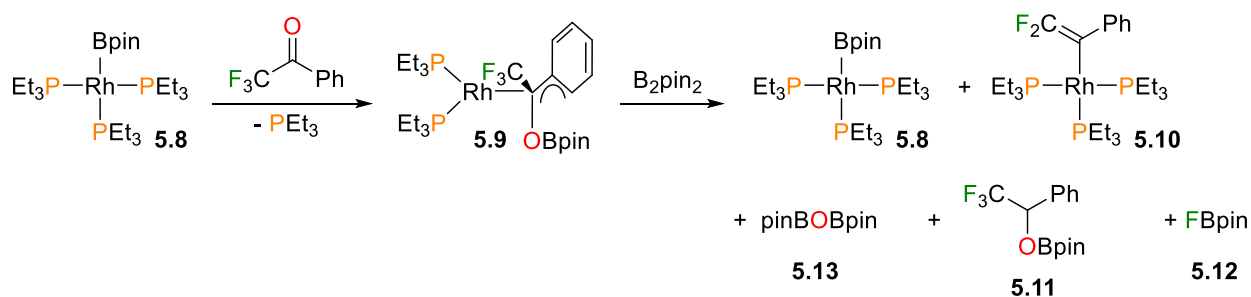
**Scheme 5.1** Nickel complexes **5.2** and **5.3** can catalyze Tischenko-coupling of aldehydes

Maleckis and Sanford have reported that nickel phosphine complexes can also be used to cleave the C-O bond of anhydrides,<sup>214</sup> as shown in Scheme 5.2. After oxidative addition of fluorinated anhydride **5.5**, the nickel-acyl moiety of intermediate **5.6** rapidly undergoes decarbonylation to form trifluoromethyl complex **5.7**. Although the phosphine ligands of **5.7** are sufficiently labile to be replaced by bis(1,2-diphenylphosphino)ethane (dppe), further attempts to use **5.7** as a cross-coupling catalyst by reacting it with transmetalating reagents like  $Ph_2Zn$  resulted only in complex mixtures and homocoupling.



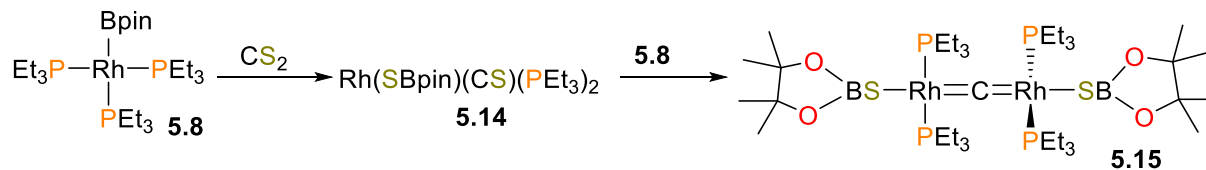
**Scheme 5.2** Nickel(0)-mediated decarbonylation of anhydrides

In related work, Braun and co-workers have demonstrated that trifluoroacetophenone can react with rhodium(I) boryl complex **5.8** to form an  $\eta^3$ -benzyl complex **5.9** by insertion of the ketone into the rhodium-boryl bond.<sup>318</sup> Functionalization of **5.9** could be achieved by reacting it with an equivalent of  $B_2pin_2$ , which forms a multitude of products, including equimolar amounts of **5.8** and the alkenyl complex **5.10** as the organometallic species, as well as boronate ester **5.11**, FBpin **5.12** and pinBOBpin **5.13** (Scheme 5.3).



**Scheme 5.3** Rhodium(I)-mediated cleavage of trifluoroacetophenone

The Braun group has also reported that rhodium boryl complex **5.8** reacts rapidly with an equivalent of  $CS_2$  to form the thiocarbonyl complex **5.14**,<sup>319</sup> which is only stable in the presence of free  $PEt_3$ . While a peak in the mass spectrum was observed for  $n = 2$ , a single, broad resonance was observed in the  $^{31}P\{^1H\}$  NMR spectrum, along with no peak for free  $PEt_3$ . Thus, the authors speculate that these data may be a sign of rapid exchange with free phosphine. Treating **5.14** with another equivalent of rhodium boryl **5.8** resulted in rapid precipitation of an orange product, which could be recrystallized and characterized as dinuclear complex **5.15**, a remarkable bridging carbido complex of rhodium (Scheme 5.4).



**Scheme 5.4** Synthesis of bridging carbido complex **5.15**

The most noteworthy spectroscopic feature of complex **5.15** is the  $^{13}\text{C}$  NMR resonance of the bridging carbon atom. When the  $^{13}\text{C}$  isotopologue is prepared using  $^{13}\text{CS}_2$ , the carbide resonates as a triplet of pentets at 439.4 ppm due to coupling to 2 equivalent rhodium atoms and 4 equivalent phosphorous nuclei. X-ray quality crystals of **5.15** could be grown from cooling a methylcyclohexane solution, and the solid-state structure is shown in Figure 5.1.

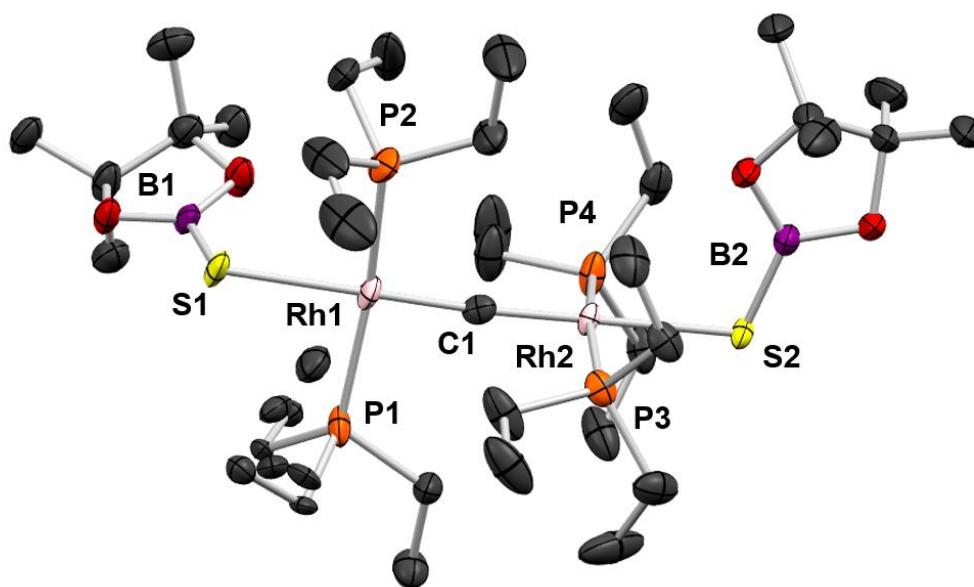


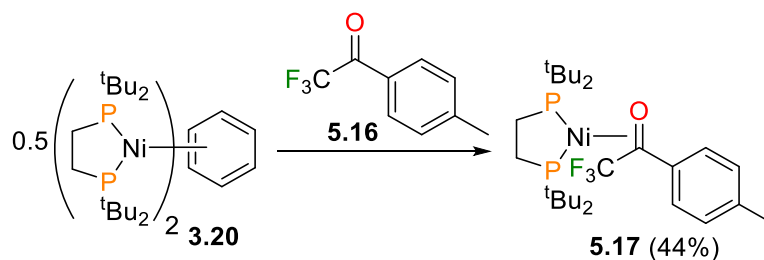
**Figure 5.1** ORTEP diagram (30% ellipsoids) of bridging carbido complex **5.15**. Hydrogen atoms omitted for clarity.

The nickel chemistry described in this Chapter took root when Florian W. Friese, an undergraduate student from the Westfälische Wilhelms-Universität Münster, joined the Love group for a brief research internship. He performed some of the initial organometallic work, as well as cross-coupling reactions with boronic acids. Weiling Chiu, a PhD student in the Love group, also

contributed to the cross-coupling studies, as well as synthesized and characterized complex **5.40**. The rhodium work was performed at the Humboldt Universität zu Berlin during the course of a 4-month National Sciences and Engineering Research Council (NSERC) Michael Smith Foreign Study Supplement, in collaboration with Prof. Dr. Thomas Braun and Theresia Ahrens, a PhD student in the Braun group.

## 5.2 Reactivity of a Ketone and Thioesters with Nickel(0)

At the outset of our work on this project, we were concerned that C-F activation of the pendant  $\text{CF}_3$  group would be a prominent decomposition pathway, as nickel-mediated C-F activation is well-known.<sup>320, 321</sup> Indeed, Pörschke has demonstrated that **3.20** can activate  $\text{C}_6\text{F}_6$  under thermolytic conditions.<sup>216</sup> Thus, we sought to first prepare a trifluoromethyl ketone complex derived from **3.20** and examine its reactivity. Addition of ketone **5.16** to a solution of **3.20** in benzene results in an immediate colour change from red-orange to yellow. Recrystallization of the crude product from  $\text{Et}_2\text{O}$  yields X-ray quality crystals of the  $\eta^2$ -ketone complex **5.17** (see Scheme 5.5) in 44% isolated yield, which was characterized by multinuclear NMR spectroscopic experiments, electron-impact mass spectrometry (EI-MS), elemental analysis (EA) and X-ray diffraction studies.



**Scheme 5.5** Synthesis of **5.17**. Isolated yields in parentheses

The NMR spectroscopic features of **5.17** are comparable to related complexes.<sup>233, 235, 322-326</sup> The coordination of the ketone to nickel generates a  $C_1$  symmetric complex, with each of the four <sup>t</sup>Bu groups rendered inequivalent. The most notable feature is the downfield shifted resonance ( $\delta = 74.5$  ppm) of the carbonyl carbon, which is broadened significantly, presumably due to coupling to both <sup>31</sup>P and <sup>19</sup>F nuclei. The solid-state structure is shown in Figure 5.2, and demonstrates a C-O bond length of 1.345(2) Å, which is elongated relative to most ketones due to the significant back-donation from the nickel centre to the C=O  $\pi^*$  orbital.

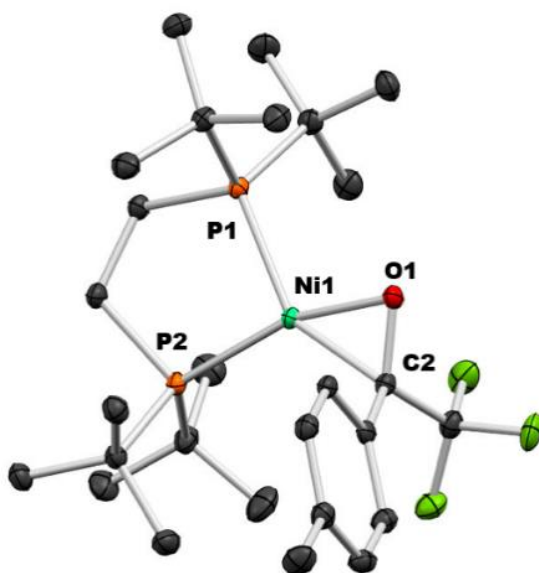
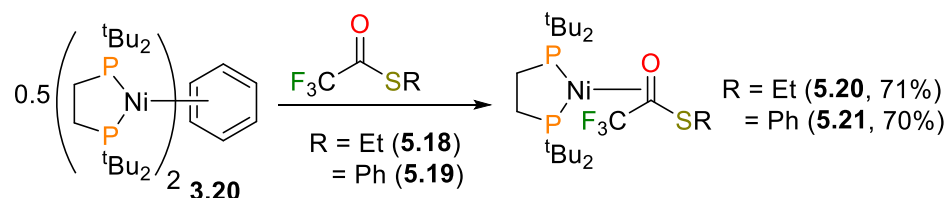


**Figure 5.2** ORTEP (50% probability ellipsoids) diagram of **5.17**

We found that heating **5.17** at 70 °C in C<sub>6</sub>D<sub>6</sub> in a sealed tube for 3 days results in no observable reaction *via* <sup>31</sup>P{<sup>1</sup>H}, <sup>19</sup>F{<sup>1</sup>H} and <sup>1</sup>H NMR spectroscopic experiments. Even subsequent heating at 110 °C for a further 24 hours results in no change to the NMR spectra of **5.17**. As a result, we conclude that the pendant CF<sub>3</sub> group is inactive towards thermally induced C-F activation. Concomitant with our studies on this system, Ogoshi and co-workers published their elegant report on the C-F activation of related complexes using Lewis acids (*vide supra*).<sup>209</sup>

We then turned our attention to other carbonyl-bearing substrates (see Scheme 5.6). Addition of CF<sub>3</sub>-containing thioesters **5.18** and **5.19** to complex **3.20** results in the formation of η<sup>2</sup>-bound thioester complexes **5.20** and **5.21**. After workup, complexes **5.20** and **5.21** can be isolated in 71% and 70% yield, respectively. These complexes were fully characterized by standard analytical methods such as mass spectrometry, elemental analysis and multinuclear NMR spectroscopy.



**Scheme 5.6** Synthesis of **5.20** and **5.21**. Isolated yields in parentheses

Yellow, needle-like crystals of **5.20** could be grown by cooling a concentrated Et<sub>2</sub>O sample at -35 °C overnight, and the solid-state structure is shown in Figure 5.3. Analogously to complex **5.17**, complex **5.20** shows a significantly long C-O bond length of 1.347(1) Å.

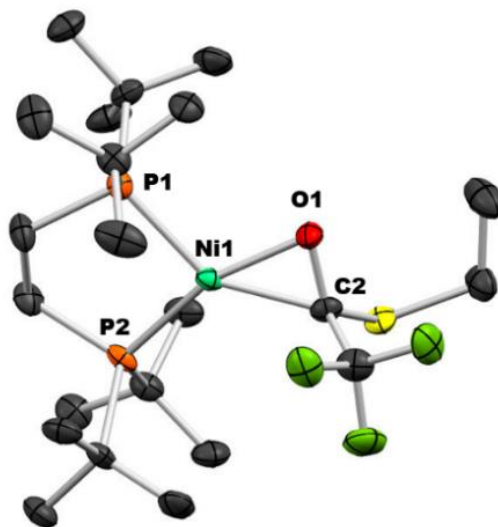


**Figure 5.3** ORTEP (50% probability ellipsoids) diagram of complex **5.20**

The  $^{31}\text{P}\{^1\text{H}\}$  NMR spectrum of complex **5.20** (see Figure 5.4) displays two resonances for the dtbpe ligand; an [AB] doublet ( $\delta = 93.1\text{ ppm}$ ,  $^2J_{\text{P,P}} = 48\text{ Hz}$ ) that we assigned as the resonance for **P2** (i.e. the phosphorous atom *trans* to the oxygen of the thioester moiety) and a doublet of quartets ( $\delta = 90.1\text{ ppm}$ ,  $^2J_{\text{P,P}} = 48\text{ Hz}$ ,  $^4J_{\text{P,F}} = 11\text{ Hz}$ ) that was assigned as the resonance for **P1**.

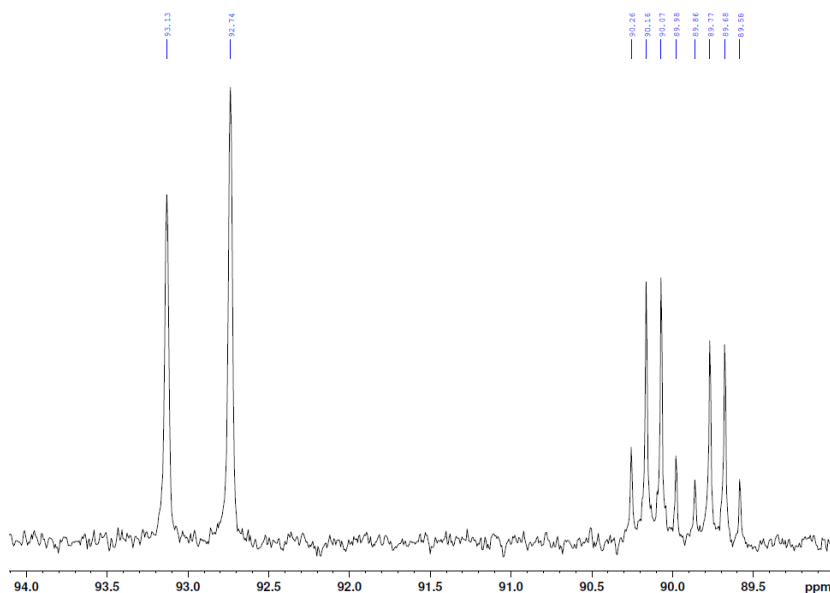


**Figure 5.4**  $^{31}\text{P}\{^1\text{H}\}$  NMR spectrum (162 MHz,  $\text{C}_6\text{D}_6$ , 25 °C) of **5.20**

Dark red, X-ray quality crystals of complex **5.21** can be grown *via* the slow evaporation of a concentrated toluene solution over several days, and the solid-state structure is shown in Figure 5.5.

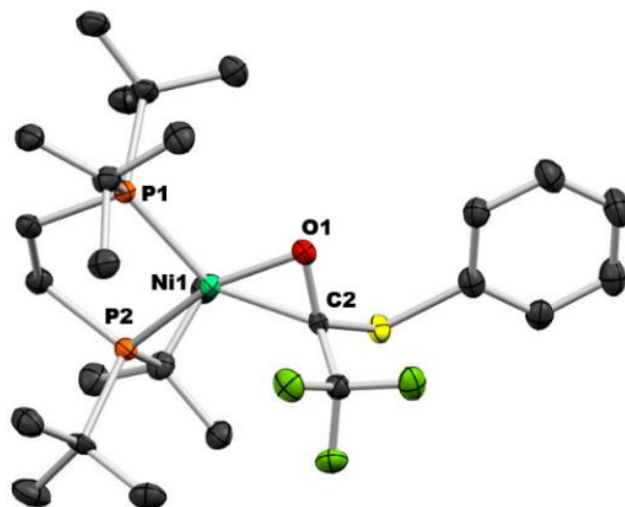
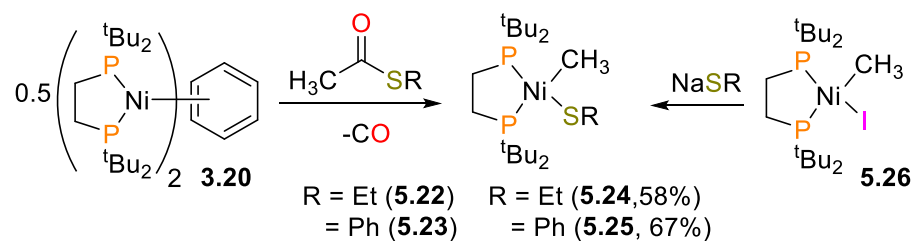


**Figure 5.5** ORTEP (50% probability ellipsoids) diagram of complex **5.21**

In sharp contrast to the formation of  $\eta^2$ -carbonyl complexes, reacting acetylthioesters **5.22** or **5.23** with **3.20** yields a mixture of products as determined by  $^{31}\text{P}\{^1\text{H}\}$  NMR spectroscopy. One product, present in both reactions, is readily identified as  $(\text{dtbpe})\text{Ni}(\text{CO})_2$  (**1.132**) *via* its characteristic  $^{31}\text{P}$  NMR chemical shift ( $\delta = 94.8$  ppm).<sup>215</sup> The other main products in each case display two doublets with small coupling constants consistent with oxidation to nickel(II).<sup>151, 288</sup> Following purification by recrystallization, complexes **5.24** (formed in 29% yield by  $^1\text{H}$  NMR spectroscopy) and **5.25** (formed in 49% yield by  $^1\text{H}$  NMR spectroscopy) were identified as methylnickel complexes derived from decarbonylation of the thioester moiety, comparable to Jones' system using platinum.<sup>115</sup> Complexes **5.24** and **5.25** could be prepared independently *via* a metathesis reaction of a sodium thiolate with  $(\text{dtbpe})\text{Ni}(\text{Me})\text{I}$  (**5.26**) in 58% and 67% isolated yield, respectively (see Scheme 5.7).



**Scheme 5.7** Syntheses of **5.24** and **5.25**. Isolated yields from the salt metathesis route in parentheses

The solid-state structure of complex **5.24** was determined *via* single-crystal X-ray diffraction studies (Figure 5.6). Although analytically pure, dark red crystals of complex **5.24** could be grown *via* recrystallization from pentanes at  $-30\text{ }^\circ\text{C}$ , complex **5.24** was found to be thermally sensitive, as it decomposes in the solid-state at room temperature over the course of two weeks and in solution over a few days (*vide infra*).

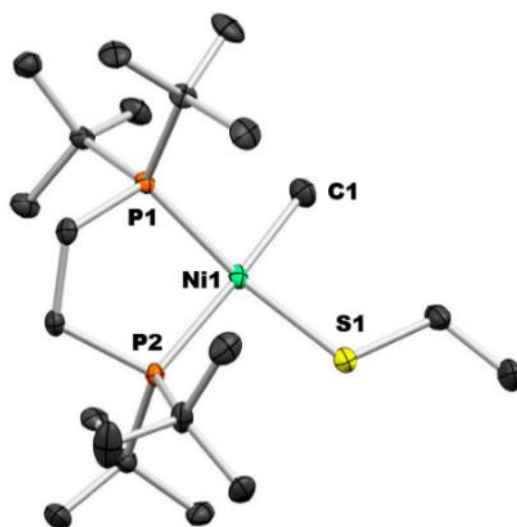


**Figure 5.6** ORTEP diagram of complex **5.24**. Thermal ellipsoids shown at 50% probability

In contrast to complex **5.24**, complex **5.25** was found to be thermally robust; heating solutions of complex **5.25** in  $\text{C}_6\text{D}_6$  at  $50\text{ }^\circ\text{C}$  for 1 week result in no change to the  $^1\text{H}$  and  $^{31}\text{P}\{^1\text{H}\}$  NMR

spectra. Red-orange crystals of complex **5.25** could be grown by cooling a saturated Et<sub>2</sub>O solution to -30 °C, and the solid-state structure is shown in Figure 5.7.

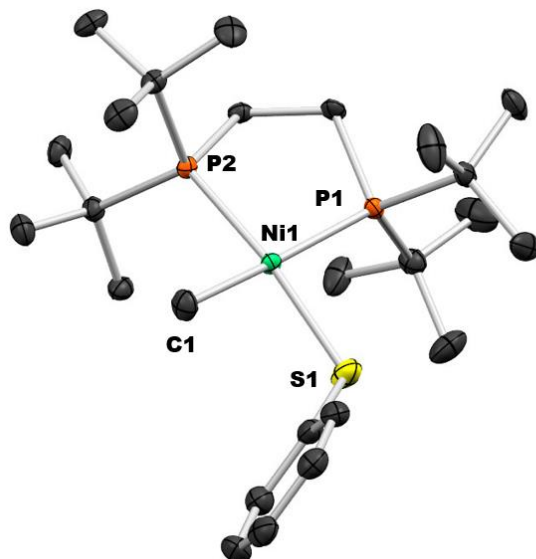
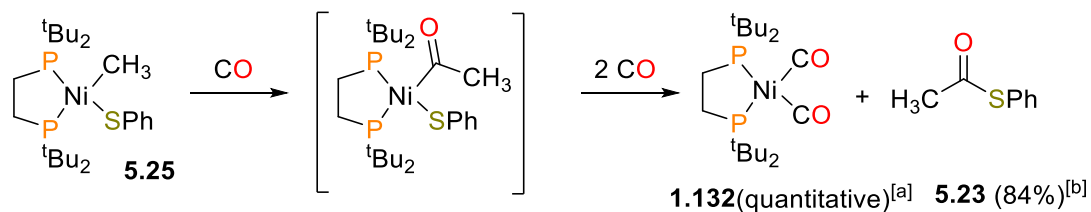


**Figure 5.7** ORTEP diagram of complex **5.25**. Thermal ellipsoids shown at 50% probability.

Intrigued by the rapid decarbonylation of acetylthioesters, we sought to explore whether the reaction could be pushed in the reverse direction. Indeed, exposure of a solution of **5.25** to 1 atm of CO gas results in the formation of **1.132** as the major organometallic species. In addition, thioester **5.23** is also formed, as determined by GC-MS and <sup>1</sup>H NMR spectroscopy (84% yield, see Scheme 5.8). Although at this point, CO insertion into the nickel-thiolate bond cannot be excluded, we propose that **5.23** is formed by insertion of CO into the nickel-methyl bond of **5.25**,<sup>70</sup> followed by reductive elimination.



**Scheme 5.8** Carbonylation of **5.25** with CO. [a]  $^{31}\text{P}\{^1\text{H}\}$  NMR yield [b]  $^1\text{H}$  NMR yield

While heating samples of **5.20** and **5.21** results in decarbonylation leading to the formation of **1.132**, we were unable to detect any formation of  $\text{RSCF}_3$  ( $\text{R} = \text{Et}, \text{Ph}$ ) by  $^1\text{H}$  and  $^{19}\text{F}\{^1\text{H}\}$  NMR spectroscopy or GC-MS analysis. Given the success our group and others have had using boronic acids as transmetalation reagents,<sup>35, 43, 316, 327, 328</sup> we sought to explore the feasibility of C-S bond formation by combining complex **3.20**, thioesters **5.18**, **5.19**, **5.22** or **5.23** and  $\text{PhB}(\text{OH})_2$  in one pot (see Table 5.1). Although we are able to form substituted sulfides in appreciable yields, we found that attempts to render the cross-coupling reactions catalytic are hampered by the formation of complex **1.132**, which is unreactive to further productive chemistry under the conditions employed. We currently hypothesize that these cross-coupling reactions occur *via*  $\text{C}_{\text{acyl}}\text{-S}$  oxidative addition, decarbonylation, transmetalation and C-C reductive elimination steps.

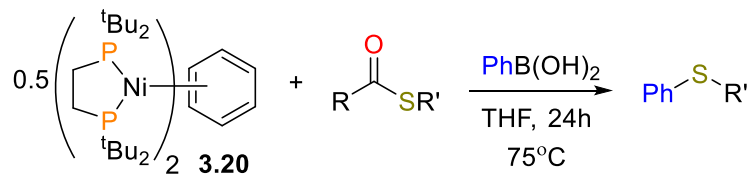
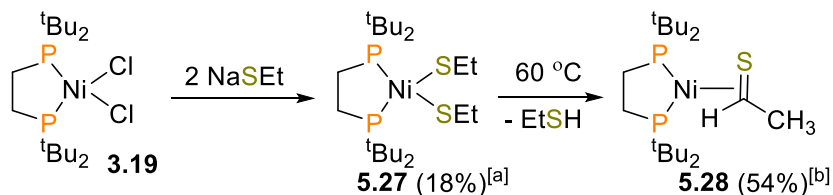


**Table 5.1** Stoichiometric cross-coupling of thioesters with PhB(OH)<sub>2</sub>

R	R'	% Yield <sup>[a]</sup>
CF <sub>3</sub>	Et	35
CF <sub>3</sub>	Ph	73
CH <sub>3</sub>	Et	0
CH <sub>3</sub>	Ph	12

[a] Yields determined by GC-FID analysis

Performing GC-MS analyses confirmed the presence of disulfides (RSSR, R = Et or Ph) in low yields during the cross-coupling reactions. Given the possibility of ligand scrambling,<sup>329, 330</sup> we wondered if the disulfide could be formed *via* reductive elimination from (dtbpe)Ni(SR)<sub>2</sub>.<sup>331-333</sup> To probe this possibility, we prepared dithiolate **5.27** by reaction of 2 equiv. of NaSEt with (dtbpe)NiCl<sub>2</sub> **3.19**, (Scheme 5.9). Complex **5.27** was fully characterized, and the solid-state structure is shown in Figure 5.8.



**Scheme 5.9** Synthesis of complexes **5.27** and **5.28**. [a] Isolated yield. [b] <sup>1</sup>H NMR yield

Heating complex **5.27** in C<sub>6</sub>D<sub>6</sub> at 60 °C results not in the formation of EtSSEt, but rather the thioacetaldehyde complex **5.28** in 54% yield by <sup>1</sup>H NMR spectroscopy. Concomitant formation of EtSH is also observed in 46% yield by <sup>1</sup>H NMR spectroscopy. Indeed, complex **5.28** is one of the decomposition products observed when **5.24** is stored for extended periods of time, presumably

forming along with concomitant expulsion of methane. Eliminations of this type from zirconium dithiolates has been reported previously by Buchwald.<sup>334</sup> Based on this, it seems unlikely that the disulfides observed during the cross-coupling are derived from **5.27**. We currently hypothesize that the presence of the disulfides is indicative of a radical process, and further mechanistic studies are currently underway in our laboratory.

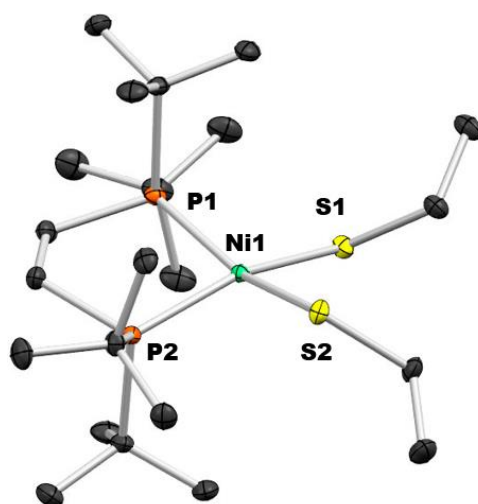
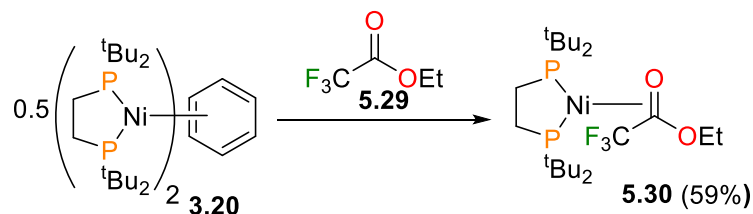


**Figure 5.8** ORTEP diagram of complex **5.27**. Thermal ellipsoids shown at 50% probability

### 5.3 Reactivity of Esters with Nickel(0)

Given the successful oxidative addition chemistry observed with thioesters, we next targeted esters as reaction partners for complex **3.20**. While **3.20** was found to be unreactive with 10 equiv. of EtOAc, addition of trifluoromethyl derivative **5.29** to an orange-red solution of **3.20** results in a gradual colour change to yellow, and the  $\eta^2$ -carbonyl complex **5.30** could be isolated in 59% yield after recrystallization of the crude product from pentanes (see Scheme 5.10).



**Scheme 5.10** Synthesis of **5.30**. Isolated yield in parentheses

Yellow, blocky crystals of **5.30** suitable for X-ray diffraction analysis could be grown from slow evaporation of a saturated toluene solution. The solid-state structure of **5.30** (Figure 5.9) is analogous to that of **5.20**, including the notably elongated C-O bond length of 1.317(3) Å.

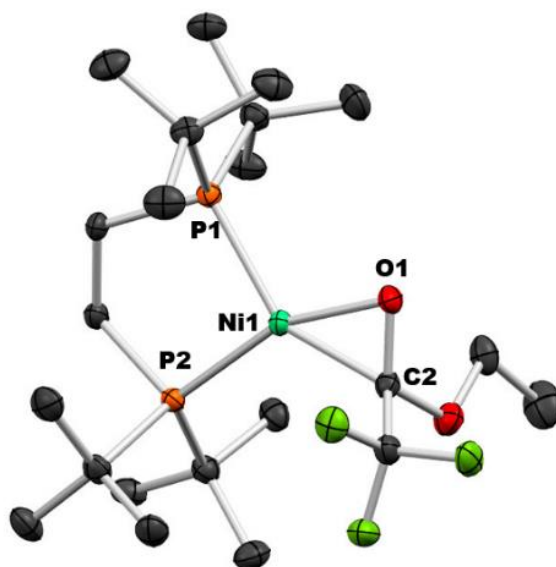
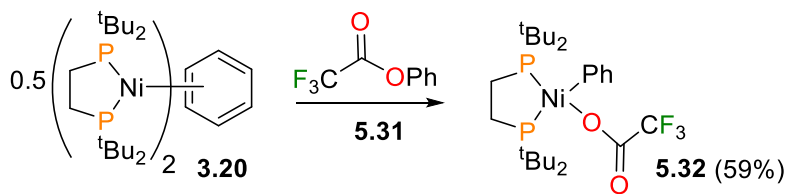


**Figure 5.9** ORTEP diagram of complex **5.30**. Thermal ellipsoids shown at 50% probability

In contrast, **3.20** was found to react rapidly with phenyl ester **5.31** to give **5.32** in 59% isolated yield, which is the product of C<sub>aryl</sub>-O bond cleavage (see Scheme 5.11).<sup>335-338</sup> Although we were able to grow red crystals of complex **5.32**, they were too disordered to extract meaningful crystallographic data. Nevertheless, the structure of **5.32** can be assigned using NMR spectroscopy. In particular, the large coupling constants for the *ipso*-carbon resonance ( $\delta = 150.8$  ppm, dd,  $^2J_{C,P}$

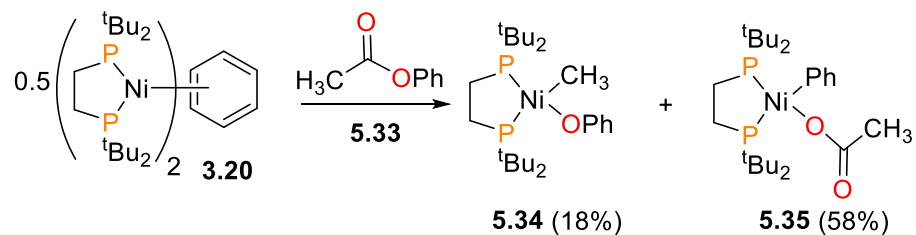
= 80 Hz,  $^2J_{C,P} = 41$  Hz) are indicative of a phenyl group bound to a diphosphine nickel species.<sup>339</sup>

340



**Scheme 5.11** Synthesis of complex **5.32**. Isolated yield in parentheses

To our surprise, reacting phenyl acetate **5.33** with complex **3.20** results in a complex mixture of products, as determined by  $^{31}\text{P}\{^1\text{H}\}$  and  $^1\text{H}$  NMR spectroscopy (see Scheme 5.12). One minor product, formed in 18% yield by  $^1\text{H}$  NMR spectroscopy, was characterized as complex **5.34**, which is the product of  $\text{C}_{\text{acyl-O}}$  bond cleavage followed by decarbonylation. This is analogous to the thioester reactivity already discussed (*vide supra*). Complex **5.34** could also be prepared independently from a salt metathesis reaction of NaOPh with **5.26**. The major product, complex **5.35** (58% yield by  $^1\text{H}$  NMR spectroscopy) was characterized as the product of  $\text{C}_{\text{aryl-O}}$  oxidative addition. Notably, the Houk group has recently published a comprehensive computational work<sup>338</sup> examining the origins of selectivity in Itami's cross-coupling of benzoxazole with aryl pivalates using (dcype)Ni(COD) as a catalyst.<sup>112</sup> Based on their DFT calculations, Houk and co-workers propose that although  $\text{C}_{\text{acyl-O}}$  bond cleavage is energetically more accessible than  $\text{C}_{\text{aryl-O}}$  bond cleavage, subsequent decarbonylation would generate a sterically very encumbered *tert*-butylnickel intermediate, which prohibits further reactivity. It is interesting to point out here that although the product of decarbonylation is much less sterically hindered, the main product observed is still the result of  $\text{C}_{\text{aryl-O}}$  oxidative addition.



**Scheme 5.12** Synthesis of complex **5.34** and **5.35**.  $^1\text{H}$  NMR yields in parentheses

Although similar solubilities of **5.34** and **5.35** rendered purification by recrystallization difficult, X-ray quality crystals of **5.35** could be grown by cooling a concentrated pentanes solution, and the structure of **5.35** was confirmed by an X-ray diffraction study (see Figure 5.10). To date, we have been unable to prepare **5.35** in pure form, either by purification of the reaction of **3.20** with **5.33** or by independent synthesis.

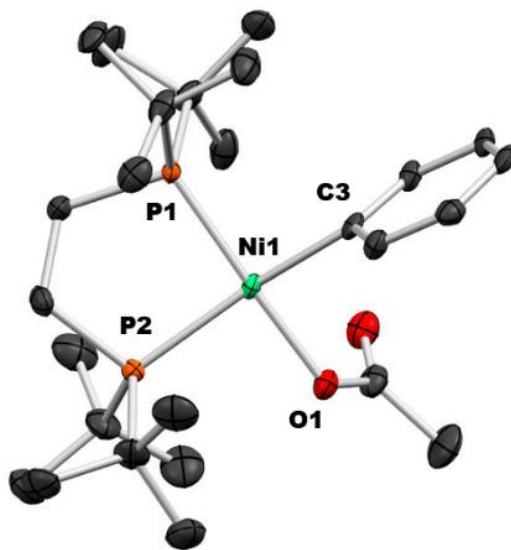
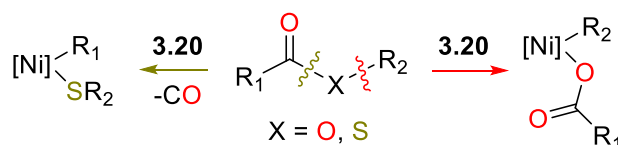


**Figure 5.10** ORTEP diagram of complex **5.35**. Thermal ellipsoids shown at 50% probability

The dependence of which C-X bond ( $X = \text{O}, \text{S}$ ) is cleaved during oxidative addition is outlined in Scheme 5.13. This type of selectivity change is normally observed when altering the phosphine ligand, and is unusual for a given nickel(0) system. For instance, our group has recently reported

that cross-coupling reactions of esters and boronic acids catalyzed by Ni(COD)<sub>2</sub> and PCy<sub>3</sub> can form appreciable amounts of ketones as byproducts, in addition to the desired biaryls.<sup>316</sup> The formation of ketones indicates that C<sub>acyl</sub>-O oxidative addition has occurred, and that transmetalation of the nascent nickel alkoxide is competitive with decarbonylation. A broader protocol was recently reported by Itami using PBu<sub>3</sub> as ancillary ligand, and detailed computational modelling indicates that C<sub>acyl</sub>-O oxidative addition is favoured due to a π-bonding interaction between the nickel and the aromatic ring substituent of the ester.<sup>310</sup> In contrast, Itami has also demonstrated that use of dcype instead of PCy<sub>3</sub> results in C<sub>aryl</sub>-O oxidative addition.<sup>112, 341, 342</sup> Thus, it appears that the regioselectivity of oxidative addition is due not only to the denticity of the ancillary ligand, but also depends on the structure of the organic substrate.



**Scheme 5.13** Regioselectivity of bond cleavage of esters vs. thioesters with complex **3.20**. [Ni] = (dtbpe)Ni.

Esters have recently received much attention as cross-coupling partners in organic synthesis.<sup>343, 344</sup> We envisioned that **5.32** and **5.35** could serve as intermediates in the cross-coupling of aryl esters with boronic acids (see Scheme 5.14). While heating **5.32** at 70 °C for 24 hours and reacting **5.32** with phenylboronic acid at room temperature yielded only trace amounts of biphenyl, refluxing a toluene solution of **3.20**, esters **5.31** or **5.33** and PhB(OH)<sub>2</sub> in stoichiometric amounts for 24 hours results in the formation of biphenyl **5.36** in 10% and 78% yield, respectively, as shown by GC-FID analysis of the crude reaction mixture. Of note, replacing PhB(OH)<sub>2</sub> with Ph<sub>2</sub>Zn under identical reaction conditions results in generally poorer yields of **5.36** (16% and 26%, respectively).



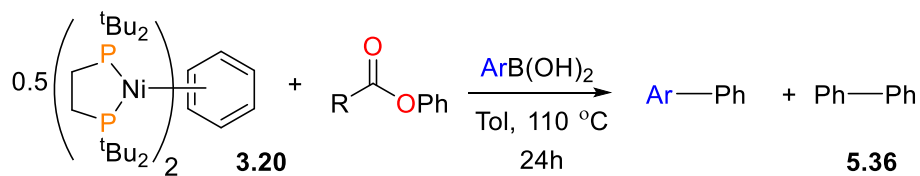


**Table 5.2** Cross-coupling of esters with boronic acids

R	Ar	% Yield Ar-Ph <sup>[a]</sup>	% Yield <b>5.36</b> <sup>[a]</sup>
CH <sub>3</sub>	Ph	77	-
CH <sub>3</sub>	<i>p</i> -OMeC <sub>6</sub> H <sub>4</sub>	16	6
CH <sub>3</sub>	<i>p</i> -OCF <sub>3</sub> C <sub>6</sub> H <sub>4</sub>	6	6
CF <sub>3</sub>	Ph	10	-
CF <sub>3</sub>	<i>p</i> -OMeC <sub>6</sub> H <sub>4</sub>	31	6

[a] Yields determined by GC-FID analysis

Attempts to induce catalytic turnover were not met with success, as lowering the loading of complex **3.20** results in a dramatic decrease in the yield of biaryl product. During the course of our cross-coupling studies, we noted the formation of a red precipitate as the reactions progressed. From cross-coupling reactions of ester **5.31**, red crystals of the bis(trifluoroacetate) complex **5.37** could be isolated from the reaction mixture that were suitable for an X-ray diffraction study (see Figure 5.11).

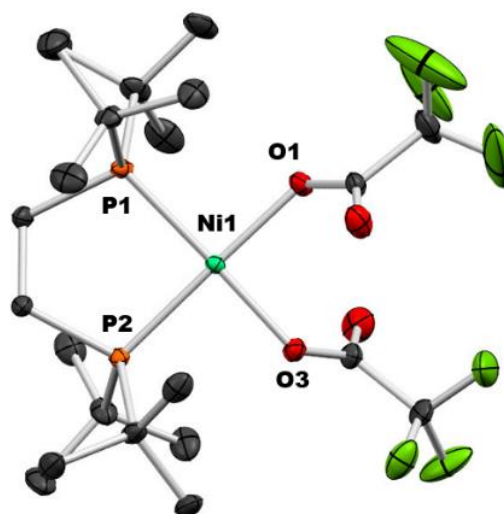
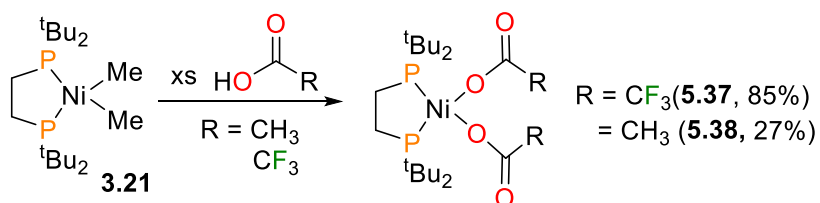


**Figure 5.11** ORTEP diagram of complex **5.37**. Thermal ellipsoids shown at 50% probability

These acetate complexes could also be prepared independently *via* the protonolysis of dimethyl complex **3.21** with trifluoroacetic acid or acetic acid, as shown in Scheme 5.15. Both complexes are insoluble in nonpolar solvents, and therefore can be easily isolated after they precipitate from solution. Large, blocky crystals of **5.37** could be grown by cooling a concentrated THF solution to  $-30\text{ }^{\circ}\text{C}$ , while smaller red-orange crystals of **5.38** could be prepared by cooling a concentrated toluene solution to  $-30\text{ }^{\circ}\text{C}$ .



**Scheme 5.15** Independent syntheses of complexes **5.37** and **5.38**. Isolated yields in parentheses

The solid-state structure of **5.38** is shown in Figure 5.12. Of note, two equivalents of acetic acid were found hydrogen-bonding to the carbonyl oxygen atoms of the acetate ligands (not shown).

The persistence of excess acetic acid in the product is likely the reason that the resonances in the  $^1\text{H}$  and  $^{31}\text{P}\{^1\text{H}\}$  NMR spectra of **5.38** prepared by protonolysis are broad.

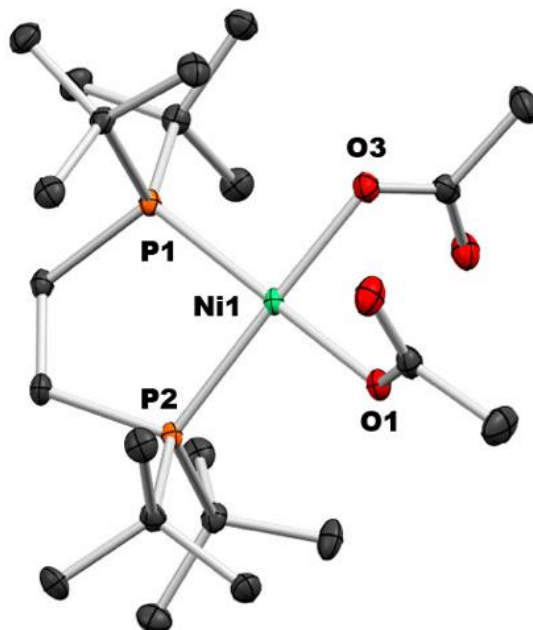
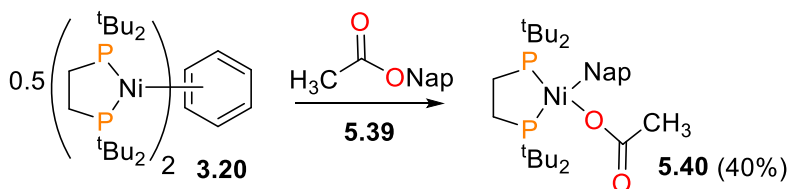


**Figure 5.12** ORTEP diagram of complex **5.38**. Thermal ellipsoids shown at 50% probability

Naphthyl esters and ethers have been demonstrated to be more reactive than their phenyl counterparts for cross-coupling reactions with nickel.<sup>345-347</sup> In an attempt to improve our own cross-coupling, Weiling Chiu, a PhD candidate in the Love group, prepared naphthyl ester **5.39** and reacted it with **3.20** (see Scheme 5.16). Gratifyingly, the reaction produced a single product, complex **5.40**, which was recrystallized from pentanes in 40% isolated yield and characterized as the naphthyl analogue of **5.35**. Unfortunately, while combining **3.20**, **5.39** and  $\text{PhB}(\text{OH})_2$  in THF at 50 °C for 24 hours results in the formation of 2-phenylnaphthalene in 89% yield, as shown by GC-FID analysis, we were unable to achieve catalytic turnover, as once again decreasing the loading of nickel drastically decreased the yield of biaryl. We are currently attempting to render

the cross-coupling reactions reported herein catalytic, as well as exploring further mechanistic studies on these transformations.

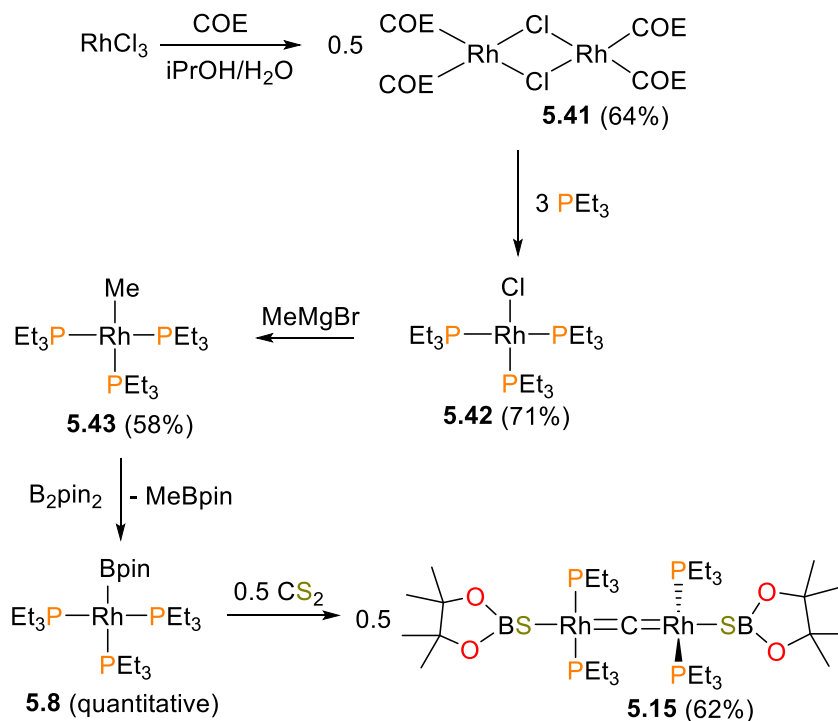


**Scheme 5.16** Synthesis of complex **5.40**. Nap = naphthyl. Isolated yield in parentheses

## 5.4 Reactivity of a Bridging Carbido Complex of Rhodium

Carbido complexes of transition metals have recently come under new scrutiny, given the discovery of the interstitial carbon atom in nitrogenase enzymes.<sup>348-351</sup> In addition, these unusual ligands have also been shown to be formed by catalyst deactivation during olefin metathesis.<sup>352</sup> Following the Braun group's report of the synthesis of complex **5.15** *via* a rare example of double C=S scission,<sup>353</sup> we set out to explore its reaction chemistry. Complex **5.15** was prepared according to the literature procedure, and was isolated as an orange powder in moderate yield (Scheme 5.17).<sup>319</sup> Refluxing  $\text{RhCl}_3 \cdot 3\text{H}_2\text{O}$  with excess cyclooctene (COE) in a mixture of water and isopropanol yields the orange dimer **5.41** after washing with hexanes and drying *in vacuo*. Addition of  $\text{PEt}_3$  gave the chloride complex **5.42** as a tacky red solid, which upon alkylation with  $\text{MeMgBr}$  produced the thermally-sensitive methyl complex **5.43** as a dark orange-red oil. Finally, in a two-step, one-pot procedure, complex **5.43** was dissolved in  $\text{C}_6\text{H}_{12}$  in a poly(tetrafluoroethylene) (PTFE) tube and treated with  $\text{B}_2\text{pin}_2$  for 3 hours. Although no change is observed to the yellow colour of the solution,  $^{31}\text{P}\{^1\text{H}\}$  NMR spectroscopy reveals complete conversion of **5.43** to the very reactive boryl **5.8**. Then, addition of 0.5 equiv. of  $\text{CS}_2$  results in rapid colour change to dark brown

and the precipitation of **5.15** as an orange powder. Carbido **5.15** could be subsequently purified by recrystallization from hexanes.



### Scheme 5.17 Synthesis of complex **5.15**

Initial density functional theory (DFT) calculations on **5.15**, performed by Dr. Mike Ahrens of the Braun group, yielded the Frontier Orbitals depicted in Figure 5.13. The highest occupied molecular orbital (HOMO) is primarily metal-based, with small contributions from the C atom. The lowest unoccupied molecular orbital (LUMO) is composed primarily of a carbon-based p-orbital, orthogonal to the Rh-C-Rh axis, with small contributions from metal-based d-orbitals with  $\pi^*$  symmetry relative to the carbon orbital. Thus, the LUMO appears to be a Rh=C antibonding

orbital. Not surprisingly, the LUMO+1 also appears to have the same symmetry.

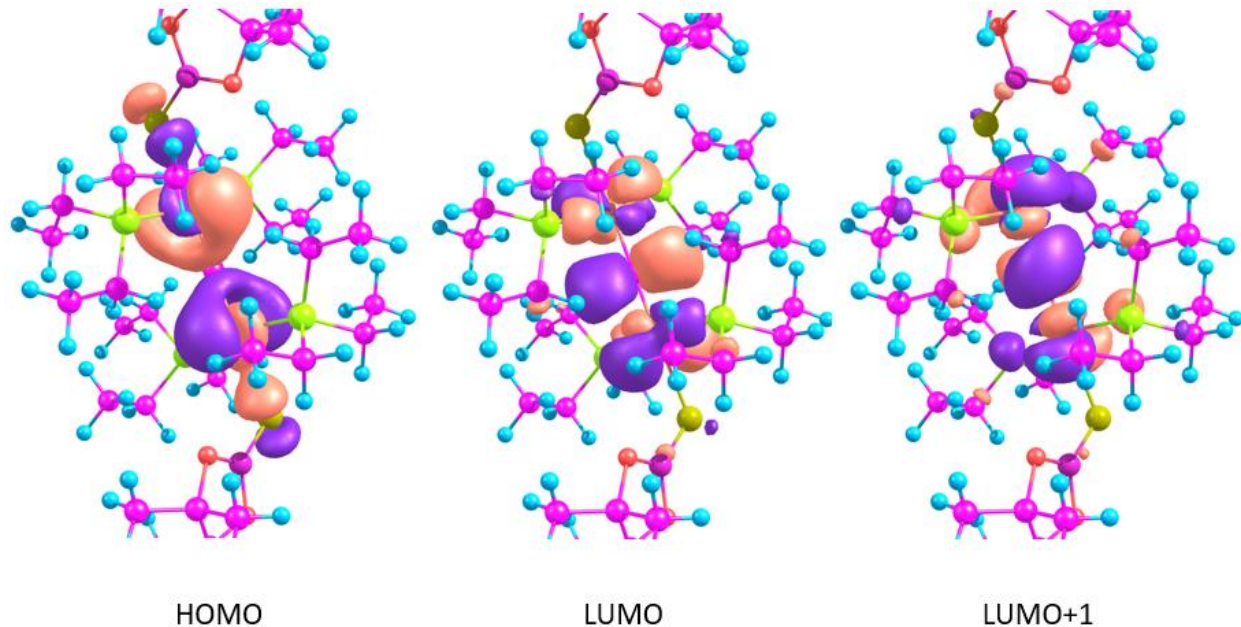
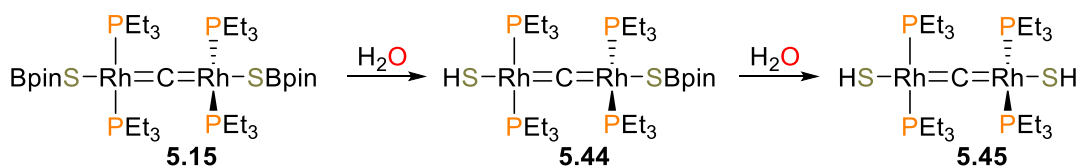


**Figure 5.13** Frontier molecular orbitals of complex **5.15**

We observed early on that complex **5.15** was thermally sensitive, as even gentle heating at 50 °C for three hours resulted in the darkening of the solution from orange to brown and the formation of a dark, insoluble precipitate. Free  $\text{PEt}_3$  was observed in the supernatant of these mixtures by  $^{31}\text{P}\{^1\text{H}\}$  NMR spectroscopy. Thus, we performed the majority of reactions of **5.15** at room temperature. Preliminary reactivity studies of complex **5.15** were also complicated by slow hydrolyses of the SBpin groups (Scheme 5.18). This reactivity had been observed previously on treatment of **5.15** with MeOH.



**Scheme 5.18** Hydrolysis of the SBpin groups of complex **5.15** by adventitious water yields **5.44** and **5.45**

Treating a  $\text{C}_6\text{D}_6$  solution of **5.15** with 10 equivalents of 4-dimethylaminopyridine (DMAP) results in the slow hydrolysis of **5.15** with adventitious water rather than reaction with DMAP. A representative series of  $^3\text{P}\{^1\text{H}\}$  NMR spectra are shown in Figure 5.14. The growth and decay of the asymmetric complex **5.44** can clearly be observed during the course of 2 days at room temperature, and the final product of this reaction is the bis(hydrothiolate) complex **5.45**. The upfield chemical shifts of the resonances of the hydrothiolate protons of **5.44** ( $\delta = -2.11$  ppm, dt,  $^3J_{\text{P,H}} = 16$  Hz,  $^2J_{\text{Rh,H}} = 2$  Hz) and **5.45** ( $\delta = -2.09$  ppm, dt,  $^3J_{\text{P,H}} = 15$  Hz,  $^2J_{\text{Rh,H}} = 1$  Hz) make hydrolysis easily detectable by  $^1\text{H}$  NMR spectroscopy.

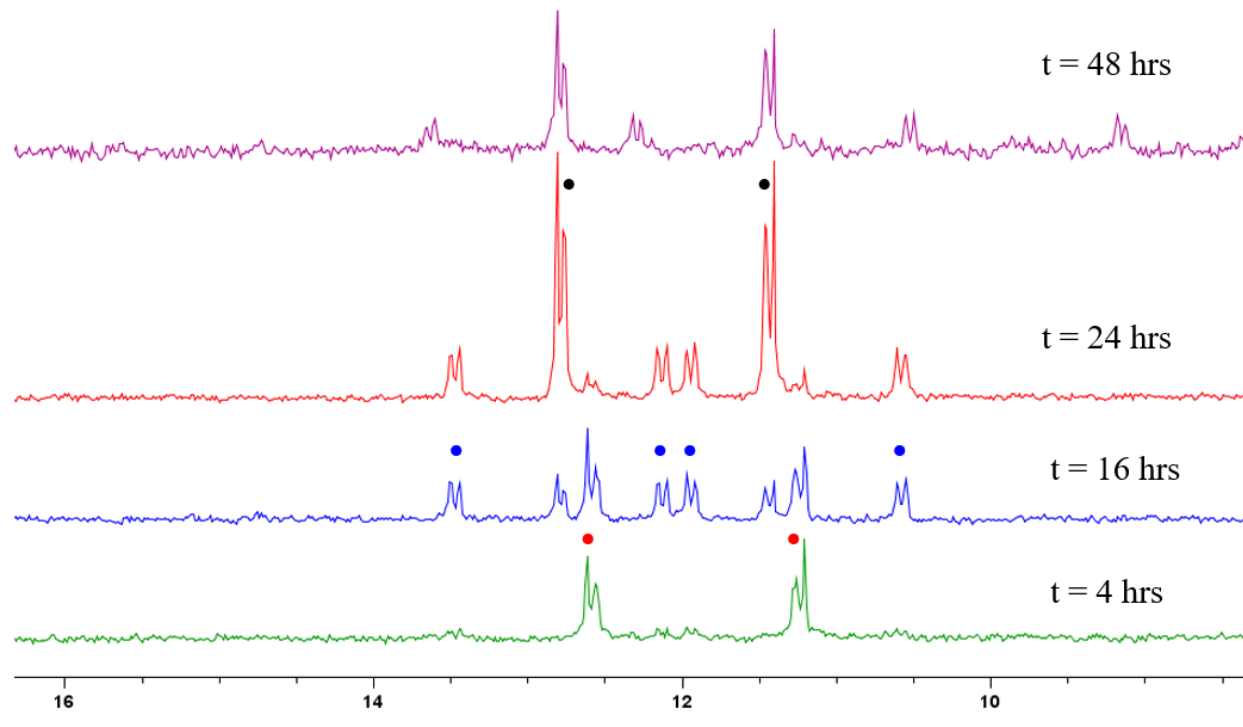
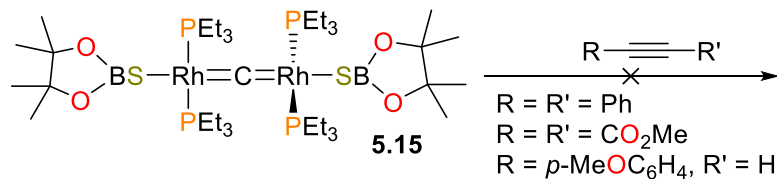


**Figure 5.14** Overlay of  $^{31}\text{P}\{^1\text{H}\}$  NMR spectra showing the conversion of **5.15** (•) to **5.44**(•) and subsequently to **5.45**(•) over 4 (green trace), 16 (blue trace), 24 (red trace) and 48 (purple trace) hours

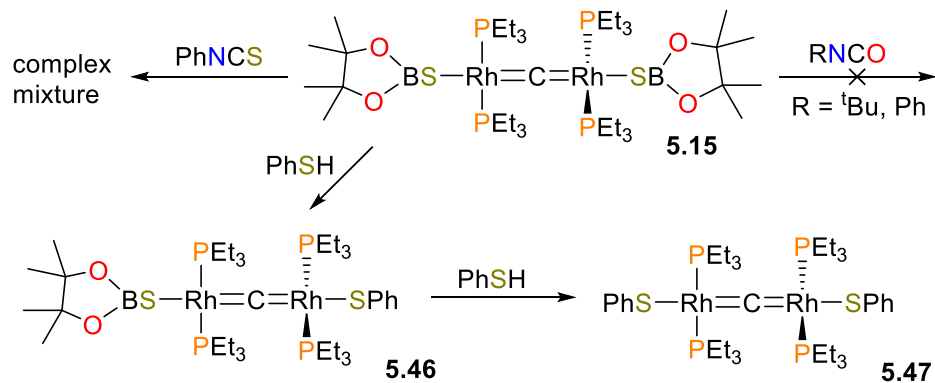
Given that the LUMO of complex **5.15** appears to be of  $\pi^*$  symmetry, we hypothesized that **5.15** could be amenable to cyclization chemistry with an appropriate organic reagent. Hillhouse has reported related formal [2+2] cyclizations of nickel alkylidene complexes with heterocumulenes such as diphenylketene and  $\text{CO}_2$ .<sup>42</sup> Unfortunately, it was discovered that **5.15** was unreactive to most of the alkenes and alkynes we attempted to use as substrates (Scheme 5.19). No reaction other than hydrolysis was observed by  $^{31}\text{P}\{^1\text{H}\}$  and  $^1\text{H}$  NMR spectroscopy when solutions of **5.15** were treated with equimolar amounts of diphenylacetylene ( $\text{Ph}_2\text{C}_2$ ), dimethylacetylene dicarboxylate (DMAD), or *p*-methoxyphenylacetylene. In contrast, addition of an equimolar amount of tetracyanoethylene (TCNE) to an orange solution of **5.15** results in an immediate bleaching of the colour to pale yellow and the formation of a black precipitate that we

were unable to characterize further. The only resonances detectable in the  $^{31}\text{P}\{^1\text{H}\}$  NMR spectrum of this reaction were residual **5.15** and oxidized phosphine ligand, ( $\text{O}=\text{PEt}_3$ ).



**Scheme 5.19** No reaction was observed when **5.15** was treated with a variety of alkynes

We then turned our attention to other unsaturated organic molecules. Unfortunately, isocyanates ( $^t\text{BuNCO}$  and  $\text{PhNCO}$ ) proved to be just as unreactive as alkynes, with no new products being formed after several days at room temperature. On a more encouraging note, reacting **5.15** with phenylisothiocyanate ( $\text{PhNCS}$ ) did result in the formation of at least 3 new products over 1 day at room temperature. However, these new products were ultimately unidentified, as the reaction was still slow and the products decomposed, with approximately 50% of complex **5.15** still remaining in solution. Given the meagre success of this reaction, we then attempted to react **5.15** with thiophenol ( $\text{PhSH}$ ) as a sulfur-based nucleophile. However,  $^1\text{H}$  and  $^{31}\text{P}\{^1\text{H}\}$  NMR spectra of the reaction indicate that the reaction proceeds analogously to the hydrolysis of **5.15**, and that the binuclear core of the carbido moiety is retained (Scheme 5.20). Complete characterization of **5.46** and **5.47** remains outstanding.



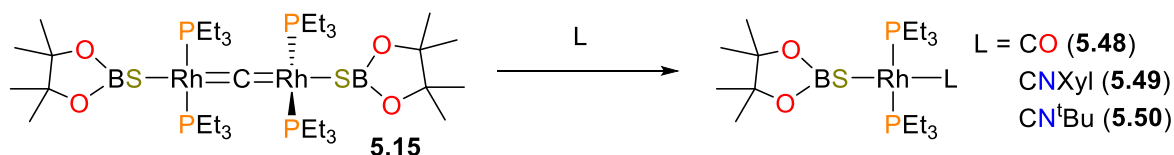
**Scheme 5.20** Reactivity of **5.15** with thiophenol, isocyanates and a thioisocyanate

We hypothesized that  $\text{CO}_2$  could serve as a potential substrate. A solution of **5.15** in  $\text{C}_6\text{D}_6$  was placed into a J-Young NMR tube and charged with 1 atm of  $\text{CO}_2$  before being sealed and monitored by  $^{31}\text{P}\{^1\text{H}\}$  NMR spectroscopy. Gradually, a new, asymmetric species began to appear that was neither **5.44** or **5.45** (the products of hydrolysis). After six days at room temperature, the NMR spectrum displayed an approximate 2:3 ratio of the new product to complex **5.15**. The  $^{31}\text{P}\{^1\text{H}\}$  NMR data for this new species ( $\delta = 11.7$  ppm, dd,  $^1J_{\text{Rh,P}} = 158$  Hz,  $^2J_{\text{P,P}} = 7$  Hz and  $\delta = 15.0$  ppm, dd,  $^1J_{\text{Rh,P}} = 173$  Hz,  $^2J_{\text{P,P}} = 7$  Hz), in particular the large Rh-P coupling constants, indicates that the binuclear structural motif is maintained. However, characterization of the new product was thwarted by decomposition on standing for longer periods of time, as well as incomplete consumption of **5.15**.

Given the paucity of clean and quantitative reactivity we had observed thus far with **5.15** and unsaturated organic compounds, we then sought to examine other types of reagents. For example, the Lau group have recently demonstrated N-N coupling upon reaction of an electrophilic nitride with anilines.<sup>354</sup> Intrigued by the possibility of analogous C-N bond formation,<sup>355</sup> we reacted **5.15** with *p*-fluoroaniline, but unfortunately, no reaction occurred. We also examined the possibility of C-F bond formation *via* reaction of **5.15** with a variety of fluorinating agents, both nucleophilic

(CsF) and electrophilic, such as N-fluoropyridinium tetrafluoroborate or N-fluorobenzenesulfonimide (NFSI). No clean reactivity was observed in any of the above cases.

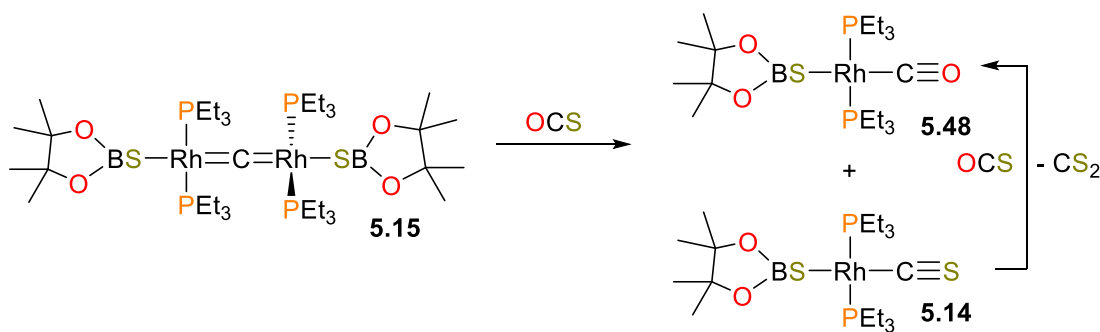
We then turned our attention to  $\pi$ -acceptor ligands, such as CO, xyllysiocyanide (CNXyl) and *tert*-butylisocyanide (<sup>t</sup>BuNC). Curiously, the NMR spectral data for each reaction indicates the formation of a major phosphorous-containing product, tentatively assigned as complexes **5.48-5.50** based on their similar spectral features to previously reported compounds (Scheme 5.21).<sup>356</sup> In particular, **5.48** shows a strong absorbance band at 1941 cm<sup>-1</sup> in its IR spectrum, which is similar to other rhodium(I) carbonyl compounds.<sup>318, 319</sup> The independent syntheses of **5.48-5.50** will require more experimental effort, as initial attempts to prepare them as pure compounds *via* alternate methods were unsuccessful. Importantly, experiments with isotopically labelled **5.15**-<sup>13</sup>C demonstrated that the carbido carbon atom is not retained in the structures of **5.48-5.50**. The fate of this carbon atom is currently unknown, and future work will be aimed towards determining its ultimate destination.



**Scheme 5.21** Reactivity of **5.15** with  $\pi$ -acceptor ligands

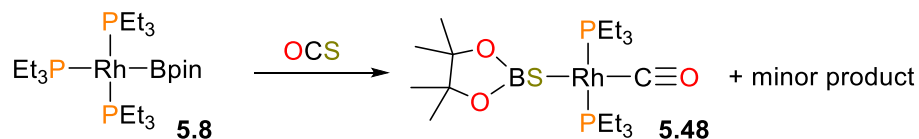
The group of Johnson has demonstrated that terminal carbide complexes of ruthenium can undergo oxidation reactions to form either carbonyl or thiocarbonyl complexes when treated with O- or S-based oxidants, respectively.<sup>357</sup> In order to explore potential redox chemistry of **5.15**, we reacted it with a variety of reductants (such as HSiEt<sub>3</sub>) and oxidants (AgOTf, trimethylamine-N-oxide and pyridine-N-oxide), but once again observed no clean reaction over the course of days. When stronger oxidants such as *m*CPBA or benzoylperoxide were used, complex mixtures of multiple products were obtained. Notably, in the case of *m*CPBA, complex **5.48** was observed as

a minor product in approximately 10% yield. The main product of this reaction is oxidized phosphine ligand, O=P<sub>Et</sub><sub>3</sub>. We also found that **5.15** reacts over several hours with OCS to yield a mixture of two products, the major of which is **5.48** (Scheme 5.22). The minor product was identified as thiocarbonyl **5.14**, which has also been previously reported.<sup>319</sup> Continued stirring of this mixture under OCS resulted in the conversion of **5.14** to **5.48**.



**Scheme 5.22** Reactivity of **5.15** with OCS forms **5.48**, **5.14** and CS<sub>2</sub>

Using **5.15**-<sup>13</sup>C in this reaction reveals the formation of <sup>13</sup>CS<sub>2</sub> and O<sup>13</sup>CS, as demonstrated by <sup>13</sup>C NMR spectroscopy. Thus, we believe that the products of this reaction are formed *via* metathesis-like equilibria that would allow for the scrambling of <sup>13</sup>C into the heterocumulenes. We also found that the rhodium boryl complex **5.8** reacted analogously to **5.15** when exposed to OCS, albeit much faster (Scheme 5.23). Preparative scale reactions to isolate **5.48** by this methodology were unsuccessful.

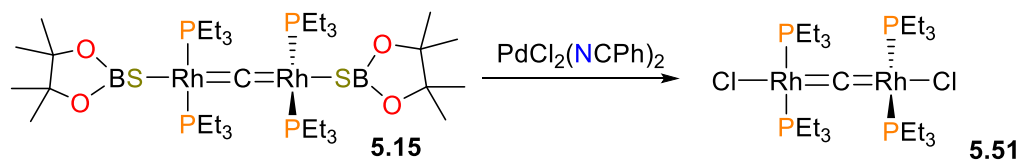


**Scheme 5.23** Reactivity of **5.8** with OCS forms **5.48** as the major product

In an attempt to broaden the scope of oxidants that could react cleanly with **5.15**, we attempted reaction of **5.15** with ethylene sulfide as an S-atom transfer reagent. However, no formation of

**5.14** was observed by  $^{31}\text{P}\{^1\text{H}\}$  NMR spectroscopy; the only reaction observed over the course of 1 day was the formation of  $\text{S}=\text{PEt}_3$  along with a concomitant decrease in the signals of **5.15** in the NMR spectrum. We also attempted C-N bond formation *via* reaction of **5.15** with the N-based oxidant 1-azidoadamantane ( $\text{N}_3\text{Ad}$ ), however, no reaction was observed over several days.

Finally, we were intrigued by an earlier report from the Grubbs group that described ruthenium carbido complexes acting as  $\sigma$ -donor ligands towards other transition metals, such as molybdenum and palladium.<sup>358</sup> While **5.15** was unreactive towards  $\text{Cr}(\text{CO})_6$ , addition of 1 equivalent of  $\text{PdCl}_2(\text{NCPh})_2$  to a solution of **5.15** in benzene resulted in the immediate formation of a black precipitate. After stirring for 4 hours, the volatiles were removed *in vacuo* and the residue was extracted with hexanes and filtered to yield a brown solution. The solution was slowly concentrated to incipient precipitation, then stored at  $-30\text{ }^\circ\text{C}$  overnight to yield complex **5.51** as a brown-yellow powder, which was isolated by decanting the supernatant and drying *in vacuo*. The unoptimized yield of **5.51** was approximately 30%. The structure of **5.51** was assigned by NMR spectroscopy and LIFDI-MS analysis to be the result of sulfido metathesis, shown in Scheme 5.24. Attempts to react **5.15** with other palladium complexes such as  $\text{PdCl}_2(\text{CNXyl})_2$  and  $\text{PdCl}_2(\text{PPh}_3)(\text{CNXyl})$  resulted in mixtures of **5.49**, **5.51** and other unidentified products. Future work on this project will require the completion of the characterization of complexes **5.48-5.50** and **5.51**, as well as the fate of the carbido atom on reaction of **5.15** with  $\pi$ -acceptor ligands to form **5.48-5.50**.



**Scheme 5.24** Reactivity of **5.15** with  $\text{PdCl}_2(\text{NCPh})_2$  forms **5.51**

## 5.5 Summary

In this Chapter, we have examined the reactivity of **3.20** with a family of thioesters and esters. For trifluoroacetyl thioesters, simple binding of the (dtbpe)nickel moiety to the carbonyl group occurs to yield  $\eta^2$ -thioester complexes. In the case of acetyl thioesters, subsequent C<sub>acyl</sub>-S oxidative addition and decarbonylation forms methyl-thiolate nickel(II) complexes as the main products. Interestingly, regeneration of the thioester can be induced by treating the nickel(II) products with an atmosphere of CO gas. When trifluoroacetyl esters are used as substrates, binding of the nickel to the carbonyl moiety is similarly observed. However, for aryl-substituted esters, a C<sub>aryl</sub>-O oxidative addition step yields aryl-acetate nickel(II) complexes as the products. Suzuki-type cross-coupling with boronic acids was found to be viable in a stoichiometric fashion, yielding either sulfides or biaryls from the thioesters or esters, respectively. Attempts to render these processes catalytic were hindered by poisoning of the nickel(0) with the CO byproduct (forming (dtbpe)Ni(CO)<sub>2</sub> **1.132**) in the case of the former, and by ligand scrambling to form insoluble bis(acetate) complexes in the case of the latter. In addition, we also report the reactivity of rhodium carbide complex **5.15** with an array of reagents, most of which led to decomposition. Surprisingly, when **5.15** is treated with strong  $\pi$ -acceptor ligands like CO and isocyanides, leads to the loss of the carbide ligand. Also of note, when **5.15** is treated with OCS, a mixture of **5.14** and **5.48** are formed, likely *via* a metathesis-like process (Scheme 5.22).

## 5.6 Experimental

**I. General Considerations:** Unless stated otherwise, all reactions were performed in a glovebox or on a Schlenk line under an atmosphere of pure N<sub>2</sub> using standard Schlenk techniques. Anhydrous pentanes, toluene, diethyl ether, and tetrahydrofuran were purchased from Aldrich,

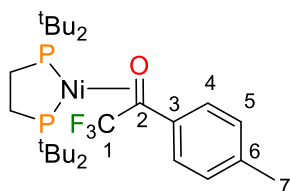
sparged with N<sub>2</sub>, and dried further by passage through towers containing activated alumina and molecular sieves. C<sub>6</sub>D<sub>6</sub> was purchased from Aldrich and dried over sodium/benzophenone before being distilled and degassed by three freeze-pump-thaw cycles. CD<sub>2</sub>Cl<sub>2</sub> was purchased from Aldrich and dried over CaH<sub>2</sub> before being distilled and degassed by three freeze-pump-thaw cycles. Ketone **5.16** was prepared following a slight modification to a literature procedure.<sup>359</sup> Thioesters **5.18**, **5.22** and **5.23** were purchased from Aldrich, while thioester **5.19** was prepared according to a literature procedure.<sup>360</sup> All thioesters were dried by stirring over CaH<sub>2</sub> before being distilled and degassed by three freeze-pump-thaw cycles. All thioesters were stored under N<sub>2</sub> at -30 °C over activated 4 Å molecular sieves. Ethyl acetate, esters **5.29** and **5.31** were purchased from Aldrich, while **5.33**<sup>361</sup> and **5.39**<sup>4 362</sup> were prepared according to literature procedures. Ethyl acetate, **5.29**, **5.31** and **5.33** were dried by stirring over CaH<sub>2</sub> before being distilled and degassed by three freeze-pump-thaw cycles. All esters were stored under N<sub>2</sub> at -30 °C, and EtOAc, **5.29**, **5.31** and **5.33** were stored over activated 4Å molecular sieves. Complexes **3.20**,<sup>216</sup> **5.26**,<sup>217</sup> **3.19**,<sup>217</sup> **3.21**,<sup>217</sup> and **5.15**<sup>319</sup> were prepared according to literature procedures. NaSet,<sup>363</sup> NaSPh<sup>364</sup> and NaOPh<sup>364</sup> were prepared according to literature procedures. All other chemicals were purchased from commercial suppliers and used as received.

NMR spectra were recorded on 300, 400 and 600 MHz spectrometers and are referenced to residual protio solvent (7.16 ppm for C<sub>6</sub>D<sub>5</sub>H, 5.32 ppm for CDHCl<sub>2</sub>) for <sup>1</sup>H NMR spectroscopy, solvent peaks (128.06 ppm for C<sub>6</sub>D<sub>6</sub>, 53.84 ppm for CD<sub>2</sub>Cl<sub>2</sub>) for <sup>13</sup>C NMR spectroscopy. <sup>31</sup>P{<sup>1</sup>H} NMR spectra were referenced to 85 % H<sub>3</sub>PO<sub>4</sub> at 0 ppm. NMR yields are averaged over at least two separate experiments and are performed using 1,3,5-trimethoxybenzene as internal standard. EI-MS and elemental analyses were performed by the microanalytic services at the Department of Chemistry of the University of British Columbia. LIFDI-MS data were measured with a

Micromass Q-Tof-2 instrument equipped with a Linden LIFDI source (Linden CMS GmbH). Infrared spectra were recorded with a Bruker Vertex 70 spectrometer equipped with an ATR unit (diamond). See Appendix A for detailed crystallographic data.

## II. Organometallic Syntheses

### Synthesis of 5.17



In a 5-dram vial, complex **3.20** (37.0 mg, 0.0444 mmol, 1.00 equiv.) was dissolved in 3 mL of C<sub>6</sub>H<sub>6</sub> to give an orange-red solution. To this solution was added ketone **5.16** (16.0 mg, 0.0850 mmol, 1.9 equiv.), resulting in a gradual colour change to yellow-orange over several minutes. The solution was stirred at room temperature for 30 minutes, then the volatiles were removed *in vacuo* to give a yellow-orange residue. This residue was dissolved in a minimum of Et<sub>2</sub>O and filtered through glass fiber into a 1-dram vial. After standing at -30 °C overnight, red, X-ray quality crystals formed, which were collected by decanting the supernatant and dried *in vacuo* to give 21.0 mg (44% yield) of complex **5.17**.

<sup>1</sup>H NMR (600 MHz, C<sub>6</sub>D<sub>6</sub>) δ 8.12 (d, <sup>3</sup>J<sub>H,H</sub> = 7.9 Hz, 2H, **H4**), 7.15 (d, <sup>3</sup>J<sub>H,H</sub> = 8.1 Hz, 2H, **H5**), 2.18 (s, 3H, **H7**), 1.26 (d, <sup>3</sup>J<sub>H,P</sub> = 10.9 Hz, 18H, 2 C(CH<sub>3</sub>)<sub>3</sub>), 1.18 (d, <sup>3</sup>J<sub>H,P</sub> = 12.1 Hz, 9H, C(CH<sub>3</sub>)<sub>3</sub>), 1.15-1.06 (m, 4H, PCH<sub>2</sub>CH<sub>2</sub>P), 0.75 (d, <sup>3</sup>J<sub>H,P</sub> = 12.1 Hz, 9H, C(CH<sub>3</sub>)<sub>3</sub>).

<sup>13</sup>C{<sup>1</sup>H} NMR (150 MHz, C<sub>6</sub>D<sub>6</sub>) δ 142.3 (br. s, **C6**), 133.7 (br. s, **C3**), 129.3 (br. s, **C4**), 125.6 (s, **C5**), 74.8 (dd, <sup>2</sup>J<sub>C,P</sub> = 33 Hz, <sup>2</sup>J<sub>C,P</sub> = 27 Hz, **C2**), 34.8 (dd, <sup>1</sup>J<sub>C,P</sub> = 14 Hz, <sup>3</sup>J<sub>C,P</sub> = 4 Hz, C(CH<sub>3</sub>)<sub>3</sub>), 34.6 (dd, <sup>1</sup>J<sub>C,P</sub> = 9 Hz, <sup>3</sup>J<sub>C,P</sub> = 3 Hz, C(CH<sub>3</sub>)<sub>3</sub>), 34.4 (dd, <sup>1</sup>J<sub>C,P</sub> = 13 Hz, <sup>3</sup>J<sub>C,P</sub> = 5 Hz, C(CH<sub>3</sub>)<sub>3</sub>), 34.1 (dd, <sup>1</sup>J<sub>C,P</sub> = 9 Hz, <sup>3</sup>J<sub>C,P</sub> = 3 Hz, C(CH<sub>3</sub>)<sub>3</sub>), 30.5 (d, <sup>2</sup>J<sub>C,P</sub> = 6 Hz, C(CH<sub>3</sub>)<sub>3</sub>), 30.3 (t, <sup>2</sup>J<sub>C,P</sub> = 5 Hz,

$\text{C}(\text{CH}_3)_3$ , 30.0 (d,  $^2J_{\text{C,P}} = 5$  Hz, 2  $\text{C}(\text{CH}_3)_3$ ), 25.0 (app. t,  $^1J_{\text{C,P}} = ^2J_{\text{C,P}} = 20$  Hz,  $\text{PCH}_2\text{CH}_2\text{P}$ ), 21.3 (s, **C7**), 20.0 (dd,  $^1J_{\text{C,P}} = 14$  Hz,  $^2J_{\text{C,P}} = 11$  Hz,  $\text{PCH}_2\text{CH}_2\text{P}$ ). The resonance for **C1** could not be observed, presumably due to coupling to  $^{19}\text{F}$  and the low signal intensity typical of quaternary carbons.

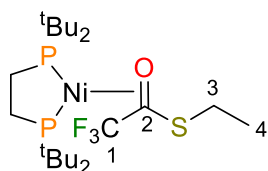
$^{31}\text{P}\{^1\text{H}\}$  NMR (121 MHz,  $\text{C}_6\text{D}_6$ )  $\delta$  89.8-89.4 (m).

$^{19}\text{F}\{^1\text{H}\}$  NMR (282 MHz,  $\text{C}_6\text{D}_6$ )  $\delta$  -61.7 (m).

LRMS (EI) 564 [ $\text{M}^+$ ]

Anal. Calcd: C, 57.37; H, 8.38. Found: C, 57.27; H, 8.63.

### Synthesis of **5.20**



In a 5-dram vial, complex **3.20** (100.7 mg, 0.121 mmol, 1.00 equiv.) was dissolved in 3 mL of  $\text{C}_6\text{H}_6$  to give an orange-red solution. To this solution was added thioester **5.18** (40.2 mg, 0.254 mmol, 2.54 equiv.), resulting in a gradual colour change to yellow over several minutes. The solution was stirred at room temperature for 30 minutes, then the volatiles were removed *in vacuo* to give a yellow residue. This residue was dissolved in a minimum of  $\text{Et}_2\text{O}$  and filtered through glass fiber into a 1-dram vial. After standing at  $-35$  °C overnight, yellow, X-ray quality crystals formed, which were collected by decanting the supernatant and dried *in vacuo* to give 92.4 mg (71% yield) of complex **5.20**.

$^1\text{H}$  NMR (600 MHz,  $\text{C}_6\text{D}_6$ )  $\delta$  3.29 (dq,  $^2J_{\text{H,H}} = 12.4$  Hz,  $^3J_{\text{H,H}} = 7.5$  Hz, 1H, **H3**), 3.15 (dq,  $^2J_{\text{H,H}} = 12.4$  Hz,  $^3J_{\text{H,H}} = 7.5$  Hz, 1H, **H3**), 1.46 (t,  $^3J_{\text{H,H}} = 7.4$  Hz, 3H, **H4**), 1.36 (d,  $^3J_{\text{H,P}} = 12.2$  Hz, 9H,  $\text{C}(\text{CH}_3)_3$ ), 1.42-1.36 (m, 2H,  $\text{PCH}_2\text{CH}_2\text{P}$ ), 1.33 (d,  $^3J_{\text{H,P}} = 12.2$  Hz, 9H,  $\text{C}(\text{CH}_3)_3$ ), 1.26 (d,  $^3J_{\text{H,P}} = 12.5$  Hz, 9H,  $\text{C}(\text{CH}_3)_3$ ), 1.24 (d,  $^3J_{\text{H,P}} = 12.5$  Hz, 9H,  $\text{C}(\text{CH}_3)_3$ ) 1.09-1.04 (m, 2H,  $\text{PCH}_2\text{CH}_2\text{P}$ ).

$^{13}\text{C}\{^1\text{H}\}$  NMR (150 MHz,  $\text{C}_6\text{D}_6$ )  $\delta$  125.0 (dq,  $^1J_{\text{C,F}} = 280$  Hz,  $^3J_{\text{C,P}} = 3$  Hz, **C1**), 76.5 – 75.0 (m, **C2**), 34.7 (dd,  $^1J_{\text{C,P}} = 15$  Hz,  $^3J_{\text{C,P}} = 3$  Hz,  $\text{C}(\text{CH}_3)_3$ ), 34.6 (dd,  $^1J_{\text{C,P}} = 15$  Hz,  $^3J_{\text{C,P}} = 3$  Hz,  $\text{C}(\text{CH}_3)_3$ ), 34.3 (dd,  $^1J_{\text{C,P}} = 11$  Hz,  $^3J_{\text{C,P}} = 2$  Hz,  $\text{C}(\text{CH}_3)_3$ ), 34.1 (dd,  $^1J_{\text{C,P}} = 11$  Hz,  $^3J_{\text{C,P}} = 1.5$  Hz,  $\text{C}(\text{CH}_3)_3$ ), 30.6 (d,  $^2J_{\text{C,P}} = 6$  Hz,  $\text{C}(\text{CH}_3)_3$ ), 30.5 (d,  $^2J_{\text{C,P}} = 6$  Hz,  $\text{C}(\text{CH}_3)_3$ ), 30.3 (d,  $^2J_{\text{C,P}} = 6$  Hz,  $\text{C}(\text{CH}_3)_3$ ), 30.2 (d,  $^2J_{\text{C,P}} = 6$  Hz,  $\text{C}(\text{CH}_3)_3$ ), 26.8 (d,  $^4J_{\text{C,P}} = 6$  Hz, **C3**), 25.1 (app. t,  $^1J_{\text{C,P}} = ^2J_{\text{C,P}} = 19$  Hz,  $\text{PCH}_2\text{CH}_2\text{P}$ ), 20.2 (dd,  $^1J_{\text{C,P}} = 16$  Hz,  $^2J_{\text{C,P}} = 10$  Hz,  $\text{PCH}_2\text{CH}_2\text{P}$ ), 16.3 (s, **C4**).

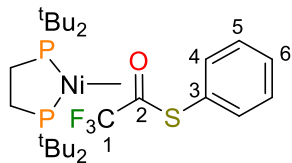
$^{31}\text{P}\{^1\text{H}\}$  NMR (162 MHz,  $\text{C}_6\text{D}_6$ )  $\delta$  93.11 (d,  $^2J_{\text{P,P}} = 48$  Hz), 90.11 (dq,  $^2J_{\text{P,P}} = 48$  Hz,  $^4J_{\text{P,F}} = 11$  Hz).

$^{19}\text{F}\{^1\text{H}\}$  NMR (282 MHz,  $\text{C}_6\text{D}_6$ )  $\delta$  -64.7 (d,  $^4J_{\text{P,F}} = 11$  Hz).

LRMS (EI) 534 [M+]

Anal. Calcd: C, 49.36; H, 8.47. Found: C, 49.65; H, 8.49.

## Synthesis of 5.21



In a 50 mL Schlenk flask, complex **3.20** (53.0 mg, 0.0637 mmol, 1.00 equiv.) was dissolved in 5 mL of Et<sub>2</sub>O to give an orange-red solution. To this solution was added thioester **5.19** (33.4 mg, 0.162 mmol, 2.54 equiv.), resulting in a gradual colour change to dark brown over several minutes. The solution was stirred at room temperature for 5 hours, then the volatiles were removed *in vacuo* to give a brown residue. This residue was dissolved in a minimum (0.5 mL) of THF, filtered through glass fiber into a 1-dram vial, then carefully layered with pentanes (3.5 mL). After standing at -30 °C overnight, a red-orange powder formed, which was collected by decanting the supernatant and dried *in vacuo* to give 52.2 mg (70% yield) of complex **5.21**. X-ray quality crystals of **5.21** could be grown by slow evaporation of a concentrated toluene solution.

<sup>1</sup>H NMR (400 MHz, C<sub>6</sub>D<sub>6</sub>) δ 8.02 (d, <sup>3</sup>J<sub>H,H</sub> = 7.7 Hz, 2H, **H4**), 7.07 (app. t, <sup>3</sup>J<sub>H,H</sub> = 7.3 Hz, 2H, **H5**), 6.94 (app. t, <sup>3</sup>J<sub>H,H</sub> = 7.6 Hz, 1H, **H6**), 1.45-1.33 (m, 2H, PCH<sub>2</sub>CH<sub>2</sub>P), 1.27 (d, <sup>3</sup>J<sub>P,H</sub> = 12.7 Hz, 10H, C(CH<sub>3</sub>)<sub>3</sub> + PCH<sub>2</sub>CH<sub>2</sub>P), 1.21 (d, <sup>3</sup>J<sub>P,H</sub> = 12.6 Hz, 9H, C(CH<sub>3</sub>)<sub>3</sub>), 1.15 (m, 18H, 2 C(CH<sub>3</sub>)<sub>3</sub>), 1.07-1.00 (m, 1H, PCH<sub>2</sub>CH<sub>2</sub>P).

<sup>13</sup>C{<sup>1</sup>H} NMR (100 MHz, C<sub>6</sub>D<sub>6</sub>) δ 138.1 (d, <sup>4</sup>J<sub>C,P</sub> = 8 Hz, **C3**), 131.5 (s, **C4**), 128.4 (s, **C6**), 126.0 (s, **C5**), 34.9 (dd, <sup>1</sup>J<sub>C,P</sub> = 15 Hz, <sup>3</sup>J<sub>C,P</sub> = 2 Hz, C(CH<sub>3</sub>)<sub>3</sub>), 34.8 (dd, <sup>1</sup>J<sub>C,P</sub> = 15 Hz, <sup>3</sup>J<sub>C,P</sub> = 3 Hz, C(CH<sub>3</sub>)<sub>3</sub>), 34.5 (dd, <sup>1</sup>J<sub>C,P</sub> = 11, <sup>3</sup>J<sub>C,P</sub> = 2 Hz, C(CH<sub>3</sub>)<sub>3</sub>), 34.3 (dd, <sup>1</sup>J<sub>C,P</sub> = 12 Hz, <sup>3</sup>J<sub>C,P</sub> = 1 Hz, C(CH<sub>3</sub>)<sub>3</sub>), 30.7 (d, <sup>2</sup>J<sub>C,P</sub> = 15 Hz, C(CH<sub>3</sub>)<sub>3</sub>), 30.6 (d, <sup>2</sup>J<sub>C,P</sub> = 15 Hz, C(CH<sub>3</sub>)<sub>3</sub>), 30.3 (d, <sup>2</sup>J<sub>C,P</sub> = 20 Hz, C(CH<sub>3</sub>)<sub>3</sub>), 30.2 (d, <sup>2</sup>J<sub>C,P</sub> = 20 Hz, C(CH<sub>3</sub>)<sub>3</sub>), 25.0 (dd, <sup>1</sup>J<sub>C,P</sub> = 20 Hz, <sup>2</sup>J<sub>C,P</sub> = 19 Hz, PCH<sub>2</sub>CH<sub>2</sub>P), 20.2 (dd, <sup>1</sup>J<sub>C,P</sub> = 16 Hz, <sup>2</sup>J<sub>C,P</sub> = 10 Hz, PCH<sub>2</sub>CH<sub>2</sub>P). The resonances of **C1** and **C2** could not be

detected, probably due to coupling to both  $^{31}\text{P}$  and  $^{19}\text{F}$  nuclei as well as the low signal intensity typical of quaternary carbons.

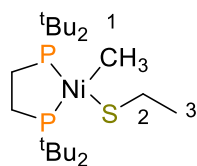
$^{31}\text{P}\{^1\text{H}\}$  NMR (162 MHz,  $\text{C}_6\text{D}_6$ )  $\delta$  92.4 (m), 89.0 (m).

$^{19}\text{F}\{^1\text{H}\}$  NMR (282 MHz,  $\text{C}_6\text{D}_6$ )  $\delta$  -64.3 (br. s).

LRMS (EI) 582 [M+]

Anal. Calcd: C, 53.53; H, 7.78. Found: C, 53.16; H, 7.68.

### Synthesis of 5.24



In a 5-dram vial, complex **5.26** (51.3 mg, 0.0988 mmol, 1.00 equiv.) was dissolved in 5 mL of THF to give a brown solution. To this solution was added NaSEt (10.4 mg, 0.124 mmol, 1.25 equiv.), and the solution was stirred for 1

hour at room temperature, during which time the colour changed from brown to dark brown-red.

The volatiles were then removed *in vacuo* to give a dark brown residue, which was extracted with pentanes and filtered through glass fiber. The resulting dark brown-red filtrate was taken to dryness *in vacuo* to give a brown residue. This residue was extracted with a minimum amount of pentanes, then filtered through glass fiber into a 5-dram vial. After standing at  $-30\text{ }^\circ\text{C}$  overnight, dark red, X-ray quality crystals formed, which were collected by decanting the supernatant and dried *in vacuo* to give 26.0 mg (58% yield) of complex **5.24**. Complex **5.24** was found to be thermally

unstable, decomposing in the solid state and in solution to give complex **5.28**, amongst other products.

$^1\text{H}$  NMR (400 MHz,  $\text{C}_6\text{D}_6$ )  $\delta$  2.80 (dq,  $^3J_{\text{H,H}} = 7.4$  Hz,  $^4J_{\text{H,P}} = 3.5$  Hz, 2H, **H2**), 1.69 (t,  $^3J_{\text{H,H}} = 7.3$  Hz, 3H, **H3**), 1.44 (d,  $J_{\text{H,P}} = 11.7$  Hz, 18H, 2 C(**CH**<sub>3</sub>)<sub>3</sub>), 1.30-1.24 (m, 2H, P**CH**<sub>2</sub>CH<sub>2</sub>P), 1.19 (d,  $J_{\text{H,P}} = 11.7$  Hz, 18H, 2 C(**CH**<sub>3</sub>)<sub>3</sub>), 1.30-1.24 (m, 2H, P**CH**<sub>2</sub>CH<sub>2</sub>P), 0.51 (dd,  $^3J_{\text{H,P}} = 7.5$  Hz,  $^3J_{\text{H,P}} = 4.1$  Hz, 3H, **H1**).

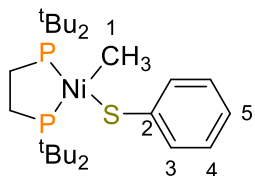
$^{13}\text{C}\{^1\text{H}\}$  NMR (100 MHz,  $\text{C}_6\text{D}_6$ )  $\delta$  36.1 (d,  $^1J_{\text{C,P}} = 13$  Hz, 2 C(**CH**<sub>3</sub>)<sub>3</sub>), 35.8 (d,  $^1J_{\text{C,P}} = 8$  Hz, 2 C(**CH**<sub>3</sub>)<sub>3</sub>), 31.0 (d,  $^1J_{\text{C,P}} = 4$  Hz, 2 C(**CH**<sub>3</sub>)<sub>3</sub>), 30.9 (d,  $^1J_{\text{C,P}} = 4$  Hz, 2 C(**CH**<sub>3</sub>)<sub>3</sub>), 24.7 (dd,  $^1J_{\text{C,P}} = 21$  Hz,  $^2J_{\text{C,P}} = 13$  Hz, P**CH**<sub>2</sub>CH<sub>2</sub>P), 21.4 (dd,  $^1J_{\text{C,P}} = 15$  Hz,  $^2J_{\text{C,P}} = 13$  Hz, P**CH**<sub>2</sub>CH<sub>2</sub>P), 20.3 (d,  $^4J_{\text{C,P}} = 3$  Hz, **C3**), 18.5 (dd,  $^3J_{\text{C,P}} = 13$  Hz,  $^3J_{\text{C,P}} = 3$  Hz, **C2**), -10.6 (dd,  $^2J_{\text{C,P}} = 58$  Hz,  $^2J_{\text{C,P}} = 27$  Hz, **C1**).

$^{31}\text{P}\{^1\text{H}\}$  NMR (162 MHz,  $\text{C}_6\text{D}_6$ ) 76.0 (s), 69.4 (s).

The EI-MS of **5.24** shows a peak at  $m/z = 436$ , which is the  $[\text{M}^+]$  peak for complex **5.28**, indicating that **5.24** is decomposing to **5.28** under ionization conditions.

Anal. Calcd: C, 55.64; H, 10.67. Found: C, 55.48; H, 10.71.

## Synthesis of 5.25



In a 5-dram vial, complex **5.26** (50.0 mg, 0.0963 mmol, 1.00 equiv.) was dissolved in 8 mL of THF to give a brown solution. To this solution was added NaSPh (144.0 mg, 1.090 mmol, 11.3 equiv.), and the resulting slurry was stirred at room temperature for 24 hours. The mixture was then filtered through glass fiber, and the resulting dark orange filtrate was taken to dryness *in vacuo* to give an orange residue. This residue was extracted with a minimum amount of Et<sub>2</sub>O, then filtered through glass fiber into a 5-dram vial. After standing at -30 °C overnight, dark red, X-ray quality crystals formed, which were collected by decanting the supernatant and dried *in vacuo* to give 32.2 mg (67% yield) of complex **5.25**.

<sup>1</sup>H NMR (400 MHz, C<sub>6</sub>D<sub>6</sub>) δ 7.92 (d, <sup>3</sup>J<sub>H,H</sub> = 7.6 Hz, 2H, **H3**), 7.18 (t, <sup>3</sup>J<sub>H,H</sub> = 7.5 Hz, 2H, **H4**), 7.06 (t, <sup>3</sup>J<sub>H,H</sub> = 7.3 Hz, 1H, **H5**), 1.43 (d, <sup>3</sup>J<sub>H,P</sub> = 11.9 Hz, 18H, 2 C(CH<sub>3</sub>)<sub>3</sub>), 1.35-1.24 (m, 4H, PCH<sub>2</sub>CH<sub>2</sub>P), 1.13 (d, <sup>3</sup>J<sub>H,P</sub> = 12.0 Hz, 18H, 2 C(CH<sub>3</sub>)<sub>3</sub>), 0.30 (dd, <sup>3</sup>J<sub>H,P</sub> = 6.4 Hz, <sup>3</sup>J<sub>H,P</sub> = 6.2 Hz, 3H, **H1**).

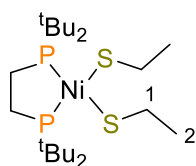
<sup>13</sup>C{<sup>1</sup>H} NMR (100 MHz, C<sub>6</sub>D<sub>6</sub>) δ 146.5 (dd, <sup>3</sup>J<sub>C,P</sub> = 14 Hz, <sup>3</sup>J<sub>C,P</sub> = 3 Hz, **C2**), 137.5 (s, **C3**), 127.7 (s, **C4**), 123.3 (s, **C5**), 36.3 (d, <sup>1</sup>J<sub>C,P</sub> = 14 Hz, 2 C(CH<sub>3</sub>)<sub>3</sub>), 35.8 (d, <sup>1</sup>J<sub>C,P</sub> = 8 Hz, 2 C(CH<sub>3</sub>)<sub>3</sub>), 31.0-30.9 (m, overlapping 4 C(CH<sub>3</sub>)<sub>3</sub>), 25.4 (dd, <sup>1</sup>J<sub>C,P</sub> = 21 Hz, <sup>2</sup>J<sub>C,P</sub> = 13 Hz, PCH<sub>2</sub>CH<sub>2</sub>P), 21.5 (app. t, <sup>1</sup>J<sub>C,P</sub> = <sup>2</sup>J<sub>C,P</sub> = 14 Hz, PCH<sub>2</sub>CH<sub>2</sub>P), -4.6 (dd, <sup>2</sup>J<sub>C,P</sub> = 57 Hz, <sup>2</sup>J<sub>C,P</sub> = 28 Hz, **C1**).

<sup>31</sup>P{<sup>1</sup>H} NMR (162 MHz, C<sub>6</sub>D<sub>6</sub>) δ 78.3 (d, <sup>2</sup>J<sub>P,P</sub> = 4 Hz), 70.8 (d, <sup>2</sup>J<sub>P,P</sub> = 4 Hz).

LRMS (EI) 500 [M<sup>+</sup>]

Anal. Calcd: C, 59.89; H, 9.65. Found: C, 59.53; H, 9.66.

### Synthesis of **5.27**



In a 50 mL Schlenk flask, complex **3.19** (265.5 mg, 0.593 mmol, 1.00 equiv.)

was combined with NaSEt (106.7 mg, 1.27 mmol, 2.14 equiv.) and 15 mL of

THF was added. The colour of the solution quickly changed from red to dark

brown, and the resulting solution was stirred for 1 hour at room temperature. The volatiles were

then removed *in vacuo* to yield a dark brown residue. This residue was extracted with a minimum

of Et<sub>2</sub>O and filtered through glass fiber to yield a very dark brown filtrate. After standing at -30 °C

overnight, dark brown, X-ray quality crystals formed, which were collected by decanting the

supernatant and dried *in vacuo* to give 54.1 mg (18% yield) of complex **5.27**.

<sup>1</sup>H NMR (400 MHz, C<sub>6</sub>D<sub>6</sub>) δ 3.18 (q, <sup>3</sup>J<sub>H,H</sub> = 7.4 Hz, 4H, **H1**), 1.69 (t, <sup>3</sup>J<sub>H,H</sub> = 7.4 Hz, 6H, **H2**), 1.41 (d, <sup>3</sup>J<sub>H,P</sub> = 11.1 Hz, 36H, 4 C(CH<sub>3</sub>)<sub>3</sub>), 1.16 (d, <sup>2</sup>J<sub>H,P</sub> = 9.8 Hz, 4H, PCH<sub>2</sub>CH<sub>2</sub>P).

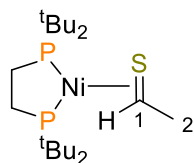
<sup>13</sup>C{<sup>1</sup>H} NMR (150 MHz, C<sub>6</sub>D<sub>6</sub>) δ 37.2-36.9 (m, 4 C(CH<sub>3</sub>)<sub>3</sub>), 31.1 (s, 4 C(CH<sub>3</sub>)<sub>3</sub>), 27.3 (s, **C1**), 23.1-22.7 (m, PCH<sub>2</sub>CH<sub>2</sub>P), 20.8 (s, **C2**).

<sup>31</sup>P{<sup>1</sup>H} NMR (162 MHz, C<sub>6</sub>D<sub>6</sub>) δ 72.3 (s).

The EI-MS of **5.27** shows a peak at  $m/z = 436$ , which is the  $[M^+]$  peak for complex **5.28**, indicating that **5.27** decomposes to **5.28** under ionization conditions

Anal. Calcd: C, 52.91; H, 10.09. Found: C, 52.75; H, 9.96.

### Synthesis of **5.28**



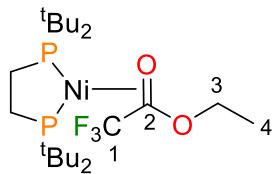
Complex **5.27** was dissolved in  $C_6D_6$  (0.5 mL) and the dark brown solution was transferred to a J-Young tube. The tube was heated in a  $60\text{ }^\circ\text{C}$  oil bath for 16 hours, and the resulting dark brown solution was analyzed by EI-MS and NMR spectroscopy.

$^1\text{H}$  NMR (300 MHz,  $C_6D_6$ )  $\delta$  4.03 (app. sext.,  $^3J_{\text{H,P}} = 5.8\text{ Hz}$ ,  $^3J_{\text{H,H}} = 5.8\text{ Hz}$ , 1H, **H1**), 1.94 (ddd,  $^4J_{\text{H,P}} = 7.3\text{ Hz}$ ,  $^4J_{\text{H,P}} = 1.3\text{ Hz}$ ,  $^3J_{\text{H,H}} = 5.8\text{ Hz}$ , 3H, **H2**), 1.25-1.16 (m, 18H, 2  $C(\text{CH}_3)_3$ ), 1.09 (d,  $^3J_{\text{H,P}} = 4.7\text{ Hz}$ , 9H,  $C(\text{CH}_3)_3$ ), 1.05 (d,  $^3J_{\text{H,P}} = 4.6\text{ Hz}$ , 9H,  $C(\text{CH}_3)_3$ ). The resonances for the methylene protons of the dtbpe ligand could not be reliably assigned due to overlap with multiple other peaks.

$^{31}\text{P}\{^1\text{H}\}$  NMR (120 MHz,  $C_6D_6$ )  $\delta$  99.0 (d,  $^2J_{\text{P,P}} = 35\text{ Hz}$ ), 90.9 (d,  $^2J_{\text{P,P}} = 35\text{ Hz}$ ).

LRMS (EI) 436  $[M^+]$

## Synthesis of 5.30



In a 50 mL Schlenk flask, complex **3.20** (42.8 mg, 0.0514 mmol, 1.00 equiv.) was dissolved in 5 mL of  $C_6H_6$  to give an orange-red solution. To this solution was added ester **5.29** (20.1 mg, 0.141 mmol, 2.75 equiv.), resulting in a gradual colour change to yellow over several minutes. The solution was stirred at room temperature for 45 minutes, then the volatiles were removed *in vacuo* to give a yellow residue. This residue was dissolved in a minimum of pentanes and filtered through glass fiber into a 1-dram vial. After standing at  $-30\text{ }^\circ\text{C}$  overnight, a yellow powder formed, which was collected by decanting the supernatant and dried *in vacuo* to give 53.4 mg (59% yield) of complex **5.30**. Yellow, X-ray quality crystals of **5.30** could be grown *via* the slow evaporation of a concentrated toluene solution.

$^1\text{H}$  NMR (400 MHz,  $C_6D_6$ )  $\delta$  4.03 (dq,  $^2J_{\text{H,H}} = 9.8\text{ Hz}$ ,  $^3J_{\text{H,H}} = 7.0\text{ Hz}$ , 1H, **H3**), 3.91 (dq,  $^2J_{\text{H,H}} = 9.8\text{ Hz}$ ,  $^3J_{\text{H,H}} = 7.3\text{ Hz}$ , 1H, **H3**), 1.50-1.33 (m, 2H,  $\text{PCH}_2\text{CH}_2\text{P}$ ), 1.26 (t,  $^3J_{\text{H,H}} = 7.1\text{ Hz}$ , 3H, **H4**), 1.22 (d,  $^3J_{\text{H,P}} = 10.4\text{ Hz}$ , 9H,  $\text{C}(\text{CH}_3)_3$ ), 1.19 (d,  $^3J_{\text{H,P}} = 7.1\text{ Hz}$ , 9H,  $\text{C}(\text{CH}_3)_3$ ), 1.17-1.13 (m, 18H, 2  $\text{C}(\text{CH}_3)_3$ ), 1.09-0.99 (m, 2H,  $\text{PCH}_2\text{CH}_2\text{P}$ ).

$^{13}\text{C}\{^1\text{H}\}$  NMR (100 MHz,  $C_6D_6$ )  $\delta$  122.2 (qt,  $^1J_{\text{C,F}} = 252\text{ Hz}$ ,  $^4J_{\text{C,P}} = 7\text{ Hz}$ , **C1**), 94.1 (m, **C2**), 59.6 (s, **C3**), 34.6 (app. t,  $J_{\text{C,P}} = 3\text{ Hz}$ ,  $\text{C}(\text{CH}_3)_3$ ), 34.4 (app. t,  $J_{\text{C,P}} = 4\text{ Hz}$ ,  $\text{C}(\text{CH}_3)_3$ ), 34.2 (dd,  $^1J_{\text{C,P}} = 8\text{ Hz}$ ,  $^2J_{\text{C,P}} = 2\text{ Hz}$ ,  $\text{C}(\text{CH}_3)_3$ ), 34.1 (dd,  $^1J_{\text{C,P}} = 9\text{ Hz}$ ,  $^2J_{\text{C,P}} = 2\text{ Hz}$ ,  $\text{C}(\text{CH}_3)_3$ ), 30.6 (d,  $^1J_{\text{C,P}} = 6\text{ Hz}$ ,  $\text{C}(\text{CH}_3)_3$ ), 30.3 (m, 2  $\text{C}(\text{CH}_3)_3$ ), 30.1 (d,  $^2J_{\text{C,P}} = 6\text{ Hz}$ ,  $\text{C}(\text{CH}_3)_3$ ), 24.8 (app. t,  $J_{\text{C,P}} = 24\text{ Hz}$ ,  $\text{PCH}_2\text{CH}_2\text{P}$ ), 20.0 (dd,  $^1J_{\text{C,P}} = 14\text{ Hz}$ ,  $^2J_{\text{C,P}} = 10\text{ Hz}$ ,  $\text{PCH}_2\text{CH}_2\text{P}$ ), 15.9 (s, **C4**).

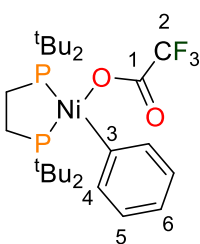
$^{31}\text{P}\{^1\text{H}\}$  NMR (162 MHz,  $\text{C}_6\text{D}_6$ )  $\delta$  92.4(d[AB],  $^2J_{\text{P,P}} = 63$  Hz), 82.4 (d[AB]q,  $^2J_{\text{P,P}} = 63$  Hz,  $^4J_{\text{P,F}} = 10$  Hz).

$^{19}\text{F}\{^1\text{H}\}$  NMR (376 MHz,  $\text{C}_6\text{D}_6$ )  $\delta$  -71.2 (d,  $^4J_{\text{P,F}} = 10$  Hz).

LRMS (EI) 518 [ $\text{M}^+$ ]

Anal. Calcd: C, 50.89; H, 8.74. Found: C, 50.94; H, 8.80.

### Synthesis of **5.32**



In a 50 mL Schlenk flask, complex **3.20** (54.2 mg, 0.0651 mmol, 1.00 equiv.) was dissolved in 10 mL of  $\text{Et}_2\text{O}$  to give an orange-red solution. To this solution was added ester **5.31** (29.2 mg, 0.154 mmol, 2.37 equiv.), resulting in a gradual colour change to light orange over several minutes. After stirring for 45 minutes, the solution had developed an orange precipitate. The mixture was stirred for a subsequent 4 hours before the volatiles were removed *in vacuo* to yield an orange residue. This residue was dissolved in a minimum (0.5 mL) of THF, filtered through glass fiber into a 1-dram vial, then carefully layered with pentanes (3.5 mL). After standing at  $-30$  °C overnight, a red-orange powder formed, which was collected by decanting the supernatant and dried *in vacuo* to give 43.5 mg (59% yield) of complex **5.32**. Although crystals of **5.32** could be grown *via* the slow evaporation of a THF solution, they were not of sufficient quality for an X-ray diffraction study.

$^1\text{H}$  NMR (600 MHz,  $\text{C}_6\text{D}_6$ )  $\delta$  8.00 (br. t,  $^3J_{\text{H,H}} = 6.6$  Hz, 2H, **H4**), 7.09 (br. t,  $^3J_{\text{H,H}} = 7.5$  Hz, 2H, **H5**), 6.95 (t,  $^3J_{\text{H,H}} = 7.2$  Hz, 1H, **H6**), 1.26 (d,  $^3J_{\text{H,P}} = 12.2$  Hz, 18H, 2  $\text{C}(\text{CH}_3)_3$ ), 1.10 (d,  $^3J_{\text{H,P}} = 13.0$  Hz, 18H, 2  $\text{C}(\text{CH}_3)_3$ ), 0.86 (m, 4H,  $\text{PCH}_2\text{CH}_2\text{P}$ ).

$^{13}\text{C}\{^1\text{H}\}$  NMR (150 MHz,  $\text{C}_6\text{D}_6$ )  $\delta$  160.8 (q,  $^2J_{\text{C,F}} = 38$  Hz, **C1**), 150.5 (dd,  $^2J_{\text{C,P}} = 80$  Hz,  $^2J_{\text{C,P}} = 41$  Hz, **C3**), 138.1 (s, **C5**) 126.0 (dd,  $^3J_{\text{C,P}} = 6$  Hz,  $^3J_{\text{C,P}} = 2$  Hz, **C4**), 123.5 (s, **C6**), 116.2 (q,  $^1J_{\text{C,F}} = 291$  Hz, **C2**), 37.2 (d,  $^1J_{\text{C,P}} = 19$  Hz, 2  $\text{C}(\text{CH}_3)_3$ ), 34.6 (d,  $^1J_{\text{C,P}} = 8$  Hz, 2  $\text{C}(\text{CH}_3)_3$ ), 30.7 (d,  $^2J_{\text{C,P}} = 3$  Hz,  $\text{C}(\text{CH}_3)_3$ ), 30.1 (d,  $^2J_{\text{C,P}} = 5$  Hz,  $\text{C}(\text{CH}_3)_3$ ), 25.8 (dd,  $^1J_{\text{C,P}} = 22$  Hz,  $^2J_{\text{C,P}} = 19$  Hz,  $\text{PCH}_2\text{CH}_2\text{P}$ ), 18.3 (dd,  $^1J_{\text{C,P}} = 15$  Hz,  $^2J_{\text{C,P}} = 8$  Hz,  $\text{PCH}_2\text{CH}_2\text{P}$ ).

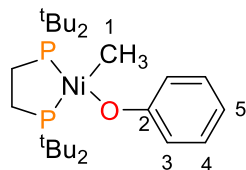
$^{31}\text{P}\{^1\text{H}\}$  NMR (162 MHz,  $\text{C}_6\text{D}_6$ )  $\delta$  73.4 (s), 71.6 (s).

$^{19}\text{F}\{^1\text{H}\}$  NMR (282 MHz,  $\text{C}_6\text{D}_6$ )  $\delta$  -75.4 (s).

LRMS (EI) 566 [ $\text{M}^+$ ]

Anal. Calcd: C, 55.05; H, 8.00. Found: C, 54.02; H, 7.73. Although satisfactory elemental analyses could not be obtained, the data here are included to demonstrate our best results to date.

### Synthesis of **5.34**



In a 5-dram vial, complex **5.26** (50.5 mg, 0.0973 mmol, 1.00 equiv.) was dissolved in 2 mL of THF to give a brown solution. To this solution was added NaOPh (13.3 mg, 0.115 mmol, 1.18 equiv.), and the solution was

stirred for 1 hour at room temperature, during which time the colour changed from brown to yellow. The volatiles were then removed *in vacuo* to give a dark yellow-brown residue, which was extracted with pentanes and filtered through glass fiber. The resulting yellow filtrate was taken to dryness *in vacuo* to give a yellow residue. This residue was extracted with a minimum amount of pentanes, then filtered through glass fiber into a 5-dram vial. After standing at -30 °C overnight, a yellow powder formed, which was collected by decanting the supernatant and dried *in vacuo* to give 23.0 mg (49% yield) of complex **5.34**.

$^1\text{H}$  NMR (400 MHz,  $\text{C}_6\text{D}_6$ )  $\delta$  7.43 (t,  $^3J_{\text{H,H}} = 7.6$  Hz, 2H, **H4**), 7.25 (d,  $^3J_{\text{H,H}} = 7.9$  Hz, 2H, **H3**), 6.80 (t,  $^3J_{\text{H,H}} = 7.2$  Hz, 1H, **H5**), 1.32 (d,  $^3J_{\text{H,P}} = 11.8$  Hz, 18H,  $\text{C}(\text{CH}_3)_3$ ), 1.26-1.18 (m, 4H,  $\text{PCH}_2\text{CH}_2\text{P}$ ), 1.12 (d,  $^3J_{\text{H,P}} = 12.2$  Hz, 18H,  $\text{C}(\text{CH}_3)_3$ ), 0.47 (app. t,  $^3J_{\text{H,P}} = 4.8$  Hz, 3H, **H1**).

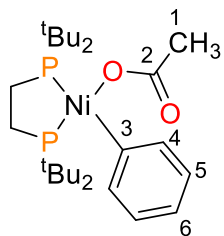
$^{13}\text{C}\{^1\text{H}\}$  NMR (100 MHz,  $\text{C}_6\text{D}_6$ )  $\delta$  168.4 (br. s, **C2**), 129.1 (s, **C4**), 123.0 (s, **C3**), 112.8 (s, **C5**), 36.2 (d,  $^1J_{\text{C,P}} = 18$  Hz,  $\text{C}(\text{CH}_3)_3$ ), 34.5 (d,  $^1J_{\text{C,P}} = 6$  Hz,  $\text{C}(\text{CH}_3)_3$ ), 31.0 (d,  $^2J_{\text{C,P}} = 3$  Hz,  $\text{C}(\text{CH}_3)_3$ ), 30.6 (d,  $^2J_{\text{C,P}} = 4$  Hz,  $\text{C}(\text{CH}_3)_3$ ), 27.0 (dd,  $^1J_{\text{C,P}} = 24$  Hz,  $^2J_{\text{C,P}} = 18$  Hz,  $\text{PCH}_2\text{CH}_2\text{P}$ ), 18.9 (app. t,  $J_{\text{C,P}} = 10$  Hz,  $\text{PCH}_2\text{CH}_2\text{P}$ ), -2.6 (dd,  $^2J_{\text{C,P}} = 69$  Hz,  $^2J_{\text{C,P}} = 35$  Hz, **C1**).

$^{31}\text{P}\{^1\text{H}\}$  NMR (162 MHz,  $\text{C}_6\text{D}_6$ )  $\delta$  79.3 (d,  $^2J_{\text{P,P}} = 9$  Hz), 68.4 (d,  $^2J_{\text{P,P}} = 9$  Hz).

LRMS (EI) 484 [ $\text{M}^+$ ]

Despite repeated attempts, satisfactory elemental analyses for complex **5.34** could not be obtained.

## Synthesis of 5.35



In a 5-dram vial, complex **5.35** (40.0 mg, 0.0481 mmol, 1.00 equiv.) was dissolved in 4 mL of benzene to give an orange-red solution. To this solution was added ester **5.33** (23.0 mg, 0.169 mmol, 3.51 equiv.), resulting in a gradual colour change to light orange over several minutes. After stirring for 1.5 hours, the volatiles were removed *in vacuo* to yield an orange residue. This residue was extracted with a minimum of pentanes and filtered through glass fiber into a 1-dram vial. After standing at -30 °C overnight, an orange powder formed, which was collected by decanting the supernatant and dried *in vacuo* to give 31.1 mg of product. Analysis of the solid by  $^1\text{H}$ ,  $^{31}\text{P}$  and  $^{13}\text{C}$  NMR spectroscopy indicated it was a mixture that contained complex **3.53**, as well as complexes **3.54** and **1.132** and several other unidentified products. X-ray quality crystals of **3.53** could be obtained from this mixture. Attempts to purify **3.53** by recrystallization from  $\text{Et}_2\text{O}$  and toluene were unsuccessful. Partial assignments of the resonances of **5.35** were made with the aid of COSY, HSQC and HMBC experiments.

$^1\text{H}$  NMR (600 MHz,  $\text{C}_6\text{D}_6$ )  $\delta$  8.20 (app. t,  $^3J_{\text{H,H}} = ^4J_{\text{H,P}} = 6.5$  Hz, 2H, **H4**), 6.98-6.92 (m, 3H, **H5+H6**), 1.86 (s, 3H, **H1**), 1.32 (d,  $^3J_{\text{H,P}} = 11.9$  Hz, 18H, 2  $\text{C}(\text{CH}_3)_3$ ), 1.17 (d,  $^3J_{\text{H,P}} = 12.8$  Hz, 18H, 2  $\text{C}(\text{CH}_3)_3$ ). The resonances for the methylene protons of the dtbpe ligand could not be discerned due to multiple overlapping peaks.

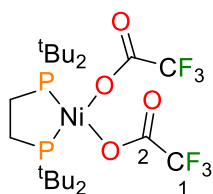
$^{13}\text{C}\{^1\text{H}\}$  NMR (100 MHz,  $\text{C}_6\text{D}_6$ )  $\delta$  168.5 (m, **C2**), 154.6 (dd,  $^2J_{\text{C,P}} = 85$  Hz,  $^2J_{\text{C,P}} = 39$  Hz, **C3**), 138.5 (s, **C4**), 125.5 (dd,  $J_{\text{C,P}} = 7$  Hz,  $J_{\text{C,P}} = 3$  Hz, **C5**), 113.1 (s, **C6**), 37.0 (dd,  $^1J_{\text{C,P}} = 18$  Hz,  $^2J_{\text{C,P}} = 2$  Hz, 2  $\text{C}(\text{CH}_3)_3$ ), 36.2 (dd,  $^1J_{\text{C,P}} = 18$  Hz,  $^2J_{\text{C,P}} = 2$  Hz, 2  $\text{C}(\text{CH}_3)_3$ ) 30.7-30.6 (m, 4  $\text{C}(\text{CH}_3)_3$ ),

25.4 (m, C1). The resonances for the methylene carbons of the dtbpe ligand could not be reliable assigned due to multiple overlapping peaks.

$^{31}\text{P}\{^1\text{H}\}$  NMR (162 MHz,  $\text{C}_6\text{D}_6$ )  $\delta$  79.0 (d,  $^2J_{\text{P,P}} = 10$  Hz), 68.0 (d,  $^2J_{\text{P,P}} = 10$  Hz).

LRMS (EI) 512 [ $\text{M}^+$ ]

### Synthesis of 5.37



In a 50 mL Schlenk flask, complex **3.19** (172.2 mg, 0.384 mmol, 1.00 equiv.) was suspended in 15 mL of  $\text{Et}_2\text{O}$ . The flask was sealed, then removed from the glovebox and placed on a Schlenk line. The flask was cooled to  $-40$  °C in an acetonitrile/dry ice bath, and  $\text{MeMgBr}$  (0.26 mL of a 3.0M solution in  $\text{Et}_2\text{O}$ , 78 mmol, 2.04 equiv.) was added dropwise. The resulting slurry was stirred for 4 hours at  $-40$  °C, resulting in a colour change from red to brown. The flask was then warmed to room temperature, and the volatiles were removed *in vacuo* to yield a brown residue. The flask was then taken back into the glovebox, and the residue was extracted with pentanes and filtered through glass fiber until the rinsings were colourless, giving a dark brown filtrate. This solution was concentrated *in vacuo* to a volume of 15 mL, then transferred to a 50 mL Schlenk flask and removed from the glovebox. After placing the flask on the Schlenk line, an excess of trifluoroacetic acid (0.11 mL, 1.437 mmol, 3.74 equiv.) was added, resulting in the immediate precipitation of an orange solid. The orange mixture was stirred for 1 hour, then taken to dryness *in vacuo* and returned to the glovebox. The orange residue was extracted with a minimum of THF and filtered to yield an orange filtrate, which upon standing at  $-30$  °C yielded orange, X-ray quality crystals of complex **5.37** (197.8 mg, 85% yield).

$^1\text{H}$  NMR (400 MHz,  $\text{CD}_2\text{Cl}_2$ )  $\delta$  1.74 (d,  $^2J_{\text{H,P}} = 10.1$  Hz, 4H,  $\text{PCH}_2\text{CH}_2\text{P}$ ), 1.56 (d,  $^3J_{\text{H,P}} = 12.9$  Hz, 36H, 4  $\text{C}(\text{CH}_3)_3$ ).

$^{13}\text{C}\{^1\text{H}\}$  NMR (100 MHz,  $\text{CD}_2\text{Cl}_2$ )  $\delta$  162.2 (q,  $^2J_{\text{C,F}} = 36$  Hz, C2), 115.3 (q,  $^1J_{\text{C,F}} = 291$  Hz, C1), 37.8 (t,  $^1J_{\text{C,P}} = 8$  Hz, 4  $\text{C}(\text{CH}_3)_3$ ), 29.9 (s, 4  $\text{C}(\text{CH}_3)_3$ ), 23.1 (t,  $^1J_{\text{C,P}} = ^2J_{\text{C,P}} = 18$  Hz,  $\text{PCH}_2\text{CH}_2\text{P}$ ).

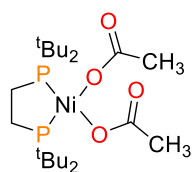
$^{31}\text{P}\{^1\text{H}\}$  NMR (162 MHz,  $\text{CD}_2\text{Cl}_2$ )  $\delta$  85.3 (s).

$^{19}\text{F}\{^1\text{H}\}$  NMR (382 MHz,  $\text{CD}_2\text{Cl}_2$ )  $\delta$  -75.7 (s).

LRMS (EI) 602 [ $\text{M}^+$ ]

Anal. Calcd: C, 43.81; H, 6.68. Found: C, 43.66; H, 6.65.

### Synthesis of **5.38**



In a 50 mL Schlenk flask, complex **3.19** (198.9 mg, 0.444 mmol, 1.00 equiv.) was suspended in 15 mL of  $\text{Et}_2\text{O}$ . The flask was sealed, then removed from the glovebox and placed on a Schlenk line. The flask was cooled to  $-40$  °C in an acetonitrile/dry ice bath, and  $\text{MeMgBr}$  (0.32 mL of a 3.0M solution in  $\text{Et}_2\text{O}$ , 0.96 mmol, 2.16 equiv.) was added dropwise. The resulting slurry was stirred for 4 hours at  $-40$  °C, resulting in a colour change from red to brown. The flask was then warmed to room temperature, and the volatiles were removed *in vacuo* to yield a brown residue. The flask was then taken back into the

glovebox, and the residue was extracted with pentanes and filtered through glass fiber until the rinsings were colourless, giving a dark brown filtrate. This solution was concentrated *in vacuo* to a volume of 15 mL, then transferred to a 50 mL Schlenk flask and removed from the glovebox. After placing the flask on the Schlenk line, an excess of glacial acetic acid (0.11 mL, 1.92 mmol, 4.33 equiv.) was added, resulting in the immediate precipitation of an orange-red solid. The orange-red mixture was stirred for 1 hour, then taken to dryness *in vacuo* and returned to the glovebox. The red residue was extracted with a minimum of toluene and filtered to yield a red filtrate, which upon standing at -30 °C yielded dark red, X-ray quality crystals of complex **5.38** (73.2 mg, 27% yield). The crystal structure shows two molecules of acetic acid per molecule **5.38**.

$^1\text{H}$  NMR (400 MHz,  $\text{CD}_2\text{Cl}_2$ )  $\delta$  1.68 (br. s, 36H, 4  $\text{C}(\text{CH}_3)_3$ ), 1.23 (br. d,  $^2J_{\text{H,P}} = 13.1$  Hz, 4H,  $\text{PCH}_2\text{CH}_2\text{P}$ ). The  $^1\text{H}$  NMR spectrum of **5.38** displayed very broad resonances, and the other peaks could not be discerned (see Figure S42).

$^{13}\text{C}\{^1\text{H}\}$  NMR (100 MHz,  $\text{CD}_2\text{Cl}_2$ )  $\delta$  33.9 (br. s, 4  $\text{C}(\text{CH}_3)_3$ ), 26.4 (s, 4  $\text{C}(\text{CH}_3)_3$ ). The other peaks could not be discerned (see Figure S43).

$^{31}\text{P}\{^1\text{H}\}$  NMR (162 MHz,  $\text{CD}_2\text{Cl}_2$ )  $\delta$  64.2 (s).

Anal. Calcd for **5.38**•2HOAc: C, 50.75; H, 8.85. Found: C, 52.30; H, 9.54. Although satisfactory elemental analyses could not be obtained, the data here are included to demonstrate our best results to date.

### Reaction of 5.25 with CO

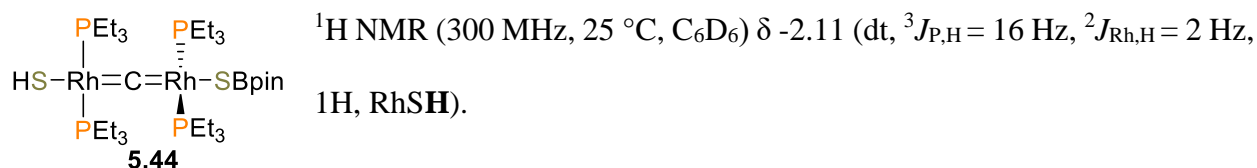
Complex **5.25** (5.0 mg, 0.010 mmol) and trimethoxybenzene (1.5 mg, 0.009 mmol) were dissolved in 0.5 mL C<sub>6</sub>D<sub>6</sub>, and the resulting brown-orange solution was transferred to a screw-cap Wilmad NMR tube fitted with a Teflon septum. To this tube was added CO gas (0.5 mL, 0.245 mmol, 24.5 equiv.) *via* syringe, resulting in an immediate colour change to dark brown-purple. NMR analysis revealed the quantitative formation of complex **1.132** by <sup>31</sup>P{<sup>1</sup>H} NMR spectroscopy, as well as thioester **5.23** in 84% yield by <sup>1</sup>H NMR spectroscopy.

### General procedure for Cross-Coupling Experiments

Complex **3.20** (14.9 mg, 1.00 equiv.) was dissolved in 1.5 ml of solvent in a 1-dram vial in a glove-box. The appropriate ester or thioester (2.5 equiv.) was added and the mixture was stirred for 5 minutes. Arylboronic acid (2.2 equiv.) was added and the reaction mixture was transferred into a teflon-sealed Schlenk tube and heated to the specified temperature for 24 hours. Upon completion, the mixture was cooled to room temperature and analyzed by GC-MS and GC-FID.

### Attempted Reaction of 5.15 with DMAP

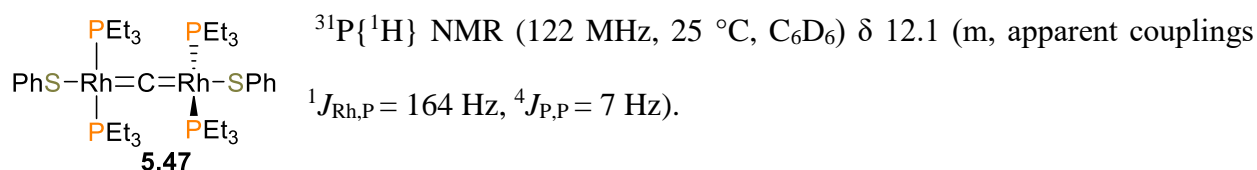
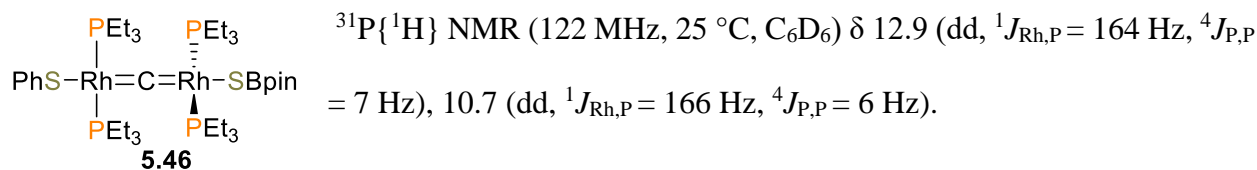
Complex **5.15** (7.3 mg, 0.0073 mmol, 1.0 equiv.) was dissolved in 0.5 mL C<sub>6</sub>D<sub>6</sub> to give an orange solution. To this was added DMAP (8.4 mg, 0.0640 mmol, 8.8 equiv.). The solution was mixed, then transferred to an NMR tube. The tube was sealed and removed from the glovebox. The reaction was monitored by <sup>31</sup>P{<sup>1</sup>H} and <sup>1</sup>H NMR spectroscopy over the course of several days, showing only the slow hydrolysis of **5.15** to **5.44** and subsequently **5.45**.<sup>319</sup> Due to multiple overlapping peaks, the NMR data for **5.44** could only be partially assigned.



$^{31}\text{P}\{^1\text{H}\}$  NMR (122 MHz, 25 °C,  $\text{C}_6\text{D}_6$ )  $\delta$  12.8 (dd,  $^1J_{\text{Rh,P}} = 162$  Hz,  $^4J_{\text{P,P}} = 7$  Hz), 11.2 (dd,  $^1J_{\text{Rh,P}} = 166$  Hz,  $^4J_{\text{P,P}} = 7$  Hz).

### Reaction of 5.15 with Thiophenol

Complex **5.15** (9.2 mg, 0.0091 mmol, 1.0 equiv.) was dissolved in 0.5 mL  $\text{C}_6\text{D}_6$  to give an orange solution. The solution was mixed, then transferred to an NMR tube. The tube was sealed and removed from the glovebox and placed on a Schlenk line. To this was added PhSH (8.4 mg, 0.0640 mmol, 8.8 equiv.). The reaction was monitored by  $^{31}\text{P}\{^1\text{H}\}$  and  $^1\text{H}$  NMR spectroscopy over the course of several days, showing the conversion of **5.15** to **5.46** and subsequently **5.47**. Due to multiple overlapping peaks, the NMR data for **5.46** and **5.47** could only be partially assigned.



### Reaction of 5.15 with $\text{CO}_2$

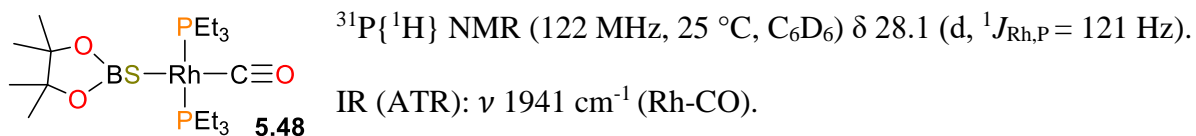
Complex **5.15** (9.7 mg, 0.0096 mmol, 1.0 equiv.) was dissolved in 0.5 mL  $\text{C}_6\text{D}_6$  to give an orange solution. The solution was mixed, then transferred to a J-Young NMR tube. The tube was sealed and removed from the glovebox and placed on a Schlenk line. The solution in the tube was frozen in a liquid nitrogen bath, then the headspace was evacuated. The bath was removed, and the tube was backfilled with  $\text{CO}_2$ . After warming to room temperature, the tube was sealed again and the

reaction was monitored by  $^{31}\text{P}\{^1\text{H}\}$  and  $^1\text{H}$  NMR spectroscopy over the course of two weeks, showing both the growth and decay of an unidentified product, as well as unconsumed **5.15**.

$^{31}\text{P}\{^1\text{H}\}$  NMR (122 MHz, 25 °C,  $\text{C}_6\text{D}_6$ ) data of unidentified product:  $\delta$  15.0 (app. dd,  $J_{\text{Rh,P}} = 173$  Hz,  $J_{\text{P,P}} = 8$  Hz), 11.6 (app. dd,  $J_{\text{Rh,P}} = 159$  Hz,  $J_{\text{P,P}} = 7$  Hz).

### Reaction of **5.15** with CO

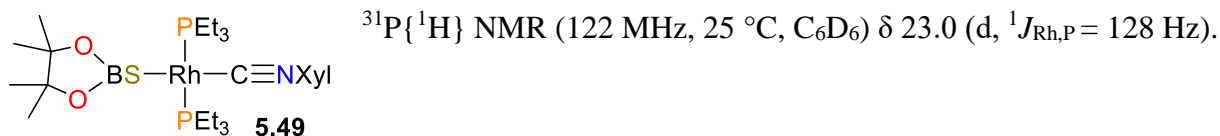
Complex **5.15** (9.7 mg, 0.0096 mmol, 1.0 equiv.) was dissolved in 0.5 mL  $\text{C}_6\text{D}_6$  to give an orange solution. The solution was mixed, then transferred to a J-Young NMR tube. The tube was sealed and removed from the glovebox and placed on a Schlenk line. The solution in the tube was frozen in a liquid nitrogen bath, then the headspace was evacuated. The bath was removed, and the tube was backfilled with CO. After warming to room temperature, the tube was sealed again and the reaction was monitored by  $^{31}\text{P}\{^1\text{H}\}$  and  $^1\text{H}$  NMR spectroscopy showing rapid conversion of **5.15** to **5.48**.



### Reaction of **5.15** with CNXyl

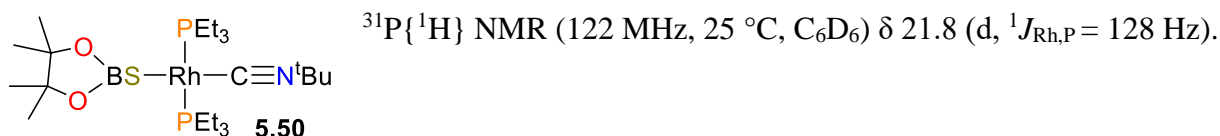
Complex **5.15** (7.9 mg, 0.0078 mmol, 1.0 equiv.) was dissolved in 0.5 mL  $\text{C}_6\text{D}_6$  to give an orange solution. The solution was mixed, then transferred to an NMR tube. The tube was sealed and removed from the glovebox and placed on a Schlenk line. To this was added XylNC (3.1 mg, 0.0236 mmol, 3.0 equiv.). The reaction was monitored by  $^{31}\text{P}\{^1\text{H}\}$  and  $^1\text{H}$  NMR spectroscopy over

the course of several days, showing the conversion of **5.15** to **5.49** Due to multiple overlapping peaks, the NMR data for **5.49** could only be partially assigned.



### Reaction of **5.15** with $\text{CN}^t\text{Bu}$

Complex **5.15** (7.6 mg, 0.0075 mmol, 1.0 equiv.) was dissolved in 0.5 mL  $\text{C}_6\text{D}_6$  to give an orange solution. The solution was mixed, then transferred to an NMR tube. The tube was sealed and removed from the glovebox and placed on a Schlenk line. To this was added  $^t\text{BuNC}$  (2.0  $\mu\text{L}$ , 0.0177 mmol, 2.4 equiv.). The reaction was monitored by  $^{31}\text{P}\{^1\text{H}\}$  and  $^1\text{H}$  NMR spectroscopy over the course of several days, showing the conversion of **5.15** to **5.50** Due to multiple overlapping peaks, the NMR data for **5.50** could only be partially assigned.



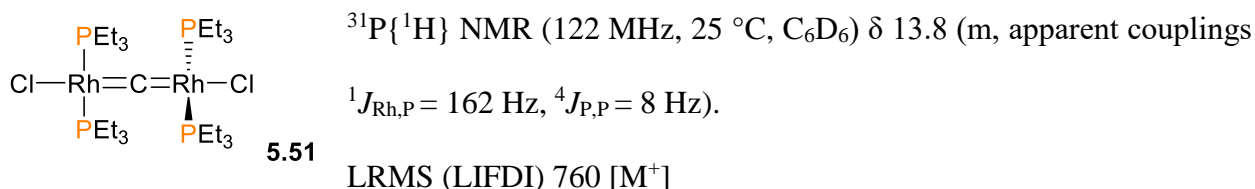
### Reaction of **5.15** with OCS

Complex **5.15** (8.2 mg, 0.0081 mmol, 1.0 equiv.) was dissolved in 0.5 mL  $\text{C}_6\text{D}_6$  to give an orange solution. The solution was mixed, then transferred to a J-Young NMR tube. The tube was sealed and removed from the glovebox and placed on a Schlenk line. The solution in the tube was frozen in a liquid nitrogen bath, then the headspace was evacuated. The bath was removed, and the tube was backfilled with OCS. After warming to room temperature, the tube was sealed again and the

reaction was monitored by  $^{31}\text{P}\{^1\text{H}\}$  and  $^1\text{H}$  NMR spectroscopy, showing initially the formation of approximately equimolar amounts of **5.14** and **5.48**, which upon standing converted to solely **5.48**.

### Reaction of **5.15** with $\text{Pd}(\text{NPh})_2\text{Cl}_2$

A Schlenk flask was charged with  $\text{Pd}(\text{NPh})_2\text{Cl}_2$  (40.0 mg, 0.104 mmol, 1.0 equiv.) and a small stir bar. To this flask was added a dark red benzene solution (5 mL) of complex **5.15** (100.8 mg, 0.100 mmol, 1.0 equiv.), resulting in a colour change to dark brown. The reaction mixture was stirred for 2 hours, then the volatiles were removed *in vacuo* to yield a dark brown residue. This residue was extracted with hexanes (2 x 5 mL) and filtered through celite, giving a brown filtrate and stranding an insoluble, black precipitate on the filter pad. This filtrate was taken to dryness *in vacuo*, then extracted with a minimum volume of hexanes (5 mL), then filtered through glass fiber into a Schlenk flask. Storing the brown solution at  $-35\text{ }^\circ\text{C}$  resulted in the precipitation of **5.51** (23.2 mg, 30% yield) as a brown powder after decanting the supernatant and drying *in vacuo*.



### Computational Details

Density functional calculations were performed by Dr. Mike Ahrens of the Braun group, using Gaussian 09, revision D.01.<sup>304</sup> The functional B3LYP was used in all calculations, and geometry optimisations were performed with no symmetry restrictions. The double- $\zeta$  basis set 6-31G(d,p)

was used for non-metal atoms in all calculations, and the RECP/cc-pvdz basis set was used for Rh. NBO analysis was performed using the NBO 3.1 program as implemented in Gaussian 09.

## Chapter 6 : Overview and Future Work

### 6.1 Overview

2-Metallaoxetanes have been frequently invoked as reactive intermediates in organometallic processes over the last several decades, but only in a few cases have well-defined examples been reported. The work presented in this Thesis was motivated by a desire to expand on the synthesis and fundamental reactivity of 2-metallaoxetanes of rhodium and nickel. More broadly, the work described over the course of the preceding Chapters was performed with an eye towards the development of new catalytic processes based on the individual steps we had studied.

In Chapter 2, the insertion chemistry of rhodaoxetane **1.33** with a wide range of unsaturated electrophiles was examined. Electron-deficient acetylene dicarboxylates were found to readily insert into the Rh-O bond of **1.33**, yielding six-membered rhodadihydropyrans that were remarkably stable (Scheme 2.8). In contrast, while heterocumulenes such as CO<sub>2</sub>, CS<sub>2</sub> and isothiocyanates also inserted into the Rh-O bond of **1.33**, the ring-expanded products displayed a much greater thermal instability, decomposing even when stored at low temperatures (Scheme 2.12). Finally, a family of aldehydes was also found to be competent substrates for insertion into the Rh-O bond of **1.33** to form rhodaacetals (Table 2.1). Notably, these insertions were reversible and solvent-dependent. Although we envisioned a Heck-like mechanism for the coupling of olefins and aldehydes *via* these rhodaacetals, we were unable to induce the  $\beta$ -hydride elimination step required for catalytic turnover. We also performed XAS studies on the olefin complex **1.32** to rigorously determine its electronic structure. Our results indicate that **1.32** is best described as a metallacyclopropane (Scheme 2.19). This result implies that the role of H<sub>2</sub>O<sub>2</sub> in the formation of **1.33** from **1.32** is not to oxidize the metal, as had been previously described in the literature, but rather, to oxidize the ethylene ligand.

In Chapter 3, the chemistry of low-valent nickel complexes, outfitted with a bulky, electron-rich dtbpe ligand, with simple styrenyl epoxides was explored. The arene dimer **3.20** was found to rapidly isomerize styrene oxide **3.15** to a mixture of  $\eta^2$ -aldehyde and -ketone complexes, with the aldehyde complex being the major product (Scheme 3.8). Similar results were obtained with 1,1- and 1,2-disubstituted epoxides. Experiments with tetrasubstituted epoxides indicate that these reactions are occurring *via* 2-nickela(II)oxetane intermediates, and that the oxidative addition step occurs with retention of configuration (Scheme 3.11). Catalytic functionalization of styrene oxide was achieved by heating in the presence of HBpin or B<sub>2</sub>pin<sub>2</sub> and substoichiometric **3.20** (5 mol%, i.e. 10 mol% in Ni, Table 3.1). Furthermore, the chemistry of **3.20** with oxaziridines was investigated. Reacting **3.20** with Davis' oxaziridine **3.51** was found to rapidly generate a mixture of  $\eta^2$ -imine and -aldehyde complexes (Scheme 3.17). Use of a bulkier oxaziridine **3.60** allowed for the isolation of a dark purple intermediate in this unusual fragmentation process, identified by X-ray crystallography as an oxazanickela(II)cyclobutane (Scheme 3.19).

In Chapter 4, the synthesis, mechanism of formation, and reactivity of a family of well-defined 2-nickela(II)oxetanes is presented (Schemes 4.5 and 4.11). The use of a ketone moiety as a directing group allowed for the rapid and quantitative formation of the four-membered oxacycles even at low temperatures, and tethering of the C2 and C3 carbons prevented the rampant  $\beta$ -hydride elimination that was observed in Chapter 3. Notably, the nickelaoxetanes in this Chapter are also formed with retention of configuration. Low-temperature NMR experiments indicate that the reactions proceed *via* an  $\eta^2$ -ketone intermediate. Theoretical calculations were performed to probe a mechanism that would account for the observed stereochemistry of the product, and an unexpected bimetallic pathway was identified as being the most energetically accessible of those

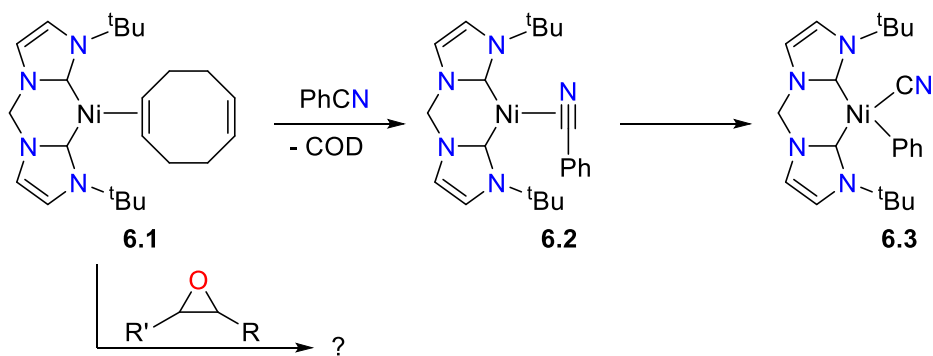
examined (Figure 4.7). Reactivity studies on **4.21** show that it is susceptible to protonolysis, insertion, deoxygenation and oxidatively-induced reductive elimination.

Finally, in Chapter 5, the chemistry of **3.20** with a family esters and thioesters was developed. For trifluoroacetyl thioesters, the products were found to be simple  $\eta^2$ -thioester complexes (Scheme 5.6). However, in the case of acetyl thioesters, subsequent  $C_{\text{acyl}}-S$  oxidative addition and decarbonylation was found to occur, yielding methyl-thiolate complexes of nickel(II) as the products (Scheme 5.7). In contrast, when aryl-substituted esters were used as substrates,  $C_{\text{aryl}}-O$  oxidative addition was found to occur, yielding aryl-acetate nickel(II) complexes as the products (Schemes 5.11 and 5.12). Suzuki-type cross-couplings of these nickel(II) products were attempted with boronic acids, and while moderate stoichiometric yields of sulfides and biaryls were obtained, we were unable to successfully achieve catalytic turnover. This was due in part to poisoning of the nickel(0) species by the CO generated from decarbonylation of the thioesters. In addition, ligand scrambling was observed during the ester cross-coupling experiments, resulting in the precipitation of insoluble bis(acetate) complexes from solution (Scheme 5.15). We also report that when the bridging carbide complex **5.15** is reacted with strong  $\pi$ -acceptor ligands, loss of the carbido atom occurs, as demonstrated by isotopic labelling experiments. In addition, **5.15** reacts with OCS to form mixtures of carbonyl **5.48** and thiocarbonyl **5.14**, likely by a metathesis-like mechanism (Scheme 5.22).

## 6.2 Future Work

The substitution of phosphine ligands with N-heterocyclic carbenes is ubiquitous across the fields of inorganic chemistry. Arguably, the most prominent examples of this trend are the development of Grubbs' second generation olefin metathesis catalyst,<sup>365, 366</sup> as well as the emergence of NHC-ligated palladium catalysts for cross-coupling reactions.<sup>367-370</sup> Some of the

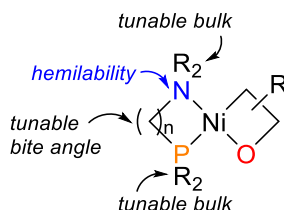
many reasons for the popularity of NHC ligands are their strong  $\sigma$ -donating character, their easily tuned steric parameters and their thermal robustness relative to phosphine ligands. Indeed, many of these were features that we desired when we originally identified dtbpe as the optimal ligand for the chemistry described in Chapters 3-5. In addition, NHCs are generally not susceptible to decomposition by oxidation to the same extent that electron-rich phosphines such as dtbpe are. Thus, it seems logical that an extension of the work described herein would focus on the design and reactivity of NHC analogues of the low-valent nickel complexes used here. Progress towards this end has already been reported by Hofmann and co-workers,<sup>371</sup> who have recently described the synthesis of bis(NHC) complexes of platinum(0) and nickel(0) such as **6.1** (Scheme 6.1). Importantly, they found that C-CN oxidative addition of the bound benzonitrile of **6.2** to form nickel(II) complex **6.3** is faster and irreversible in comparison to the same reaction with bis(1,2-di-*iso*-propylphosphino)ethane (dippe) as the ancillary ligand. The groups of Hillhouse<sup>80, 372-375</sup> and Ogoshi<sup>198, 376, 377</sup> have also reported elegant reactions of nickel-NHC complexes in recent years.



**Scheme 6.1** Hofmann's C-CN oxidative addition of benzonitrile with bis(NHC) complex **6.1**

A current project of interest in the Love group, spearheaded by PhD candidate Eric G. Bowes, is the development of a series of P,N-type ligands. While these ligands were designed for platinum-

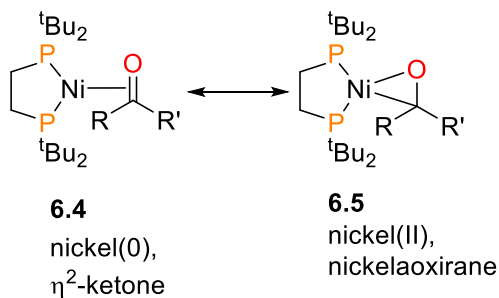
catalyzed C-H activation, we believe that their asymmetry, hemilability and tunability would offer interesting reactivity complementary to that of the simple dtbpe ligand (Scheme 6.2).



**Scheme 6.2** A 2-nickela(II)oxetane supported by a P,N-type ancillary ligand

More specifically, the projects described in this Thesis are far from exhausted. For example, mechanistic studies into the isomerization of **2.14** to **2.20**, further catalytic hydroboration experiments of **3.15** using more reactive boranes like HBcat, and kinetic experiments on the formation of **4.21** to determine the order in nickel would all shed new light into these systems.

Finally, an ongoing collaborative project with the Kennepohl group at UBC aims to explore the electronic structure of many of the formally nickel(0)  $\pi$ -complexes described in this Thesis. In particular, our groups are interested in using core spectroscopic methods such as XAS to determine where these complexes lie along the Dewar-Chatt-Duncanson spectrum (i.e., whether they are more accurately described as  $\eta^2$ -complexes such as **6.4** or nickelacyclopropanes such as **6.5**, Scheme 6.3), what factors play a role in the extent of this back-bonding, how these data align with some of the current methods that are commonly used to assign metal oxidation states (i.e. NMR coupling constants), and most importantly, whether this insight will lead to new modes of reactivity for these complexes.



**Scheme 6.3** Resonance structures of a (dtbpe)nickel ketone complex

## References

- [1] Johansson Seechurn, C. C.; Kitching, M. O.; Colacot, T. J.; Snieckus, V. *Angew. Chem. Int. Ed.* **2012**, *51*, 5062-85.
- [2] Hartwig, J. F. *Acc. Chem. Res.* **1998**, *31*, 852-860.
- [3] Hartwig, J. F. *Inorg. Chem.* **2007**, *46*, 1936-1947.
- [4] Hanley, P. S.; Hartwig, J. F. *Angew. Chem. Int. Ed.* **2013**, *52*, 8510-8525.
- [5] Hartwig, J. F. *Nature* **2008**, *455*, 314-22.
- [6] Ritleng, V.; Henrion, M.; Chetcuti, M. J. *ACS Catal.* **2016**, 890-906.
- [7] Renaud, J.-L.; Gaillard, S. *Top. Organomet. Chem.* **2015**, *50*, 83-144.
- [8] Corma, A.; Leyva-Perez, A.; Sabater, M. J. *Chem. Rev.* **2011**, *111*, 1657-712.
- [9] Kolb, H. C.; VanNieuwenhze, M. S.; Sharpless, K. B. *Chem. Rev.* **1994**, *94*, 2483-2547.
- [10] Joergensen, K. A.; Schioett, B. *Chem. Rev.* **1990**, *90*, 1483-1506.
- [11] Dauth, A.; Love, J. A. *Chem. Rev.* **2011**, *111*, 2010-2047.
- [12] Wilke, G. *Angew. Chem. Int. Ed. Engl.* **1988**, *27*, 185-206.
- [13] Biilmann, E. *Ber. Dtsch. Chem. Ges.* **1900**, *33*, 1641-1655.
- [14] De Pasquale, R. J. *J. Chem. Soc., Chem. Commun.* **1973**, 157.

- [15] Park, W. R. R.; Wright, G. F. *J. Org. Chem.* **1954**, *19*, 1325-1330.
- [16] Sharpless, K. B.; Teranishi, A. Y.; Backvall, J. E. *J. Am. Chem. Soc.* **1977**, *99*, 3120-3128.
- [17] Göbel, T.; Sharpless, K. B. *Angew. Chem. Int. Ed. Engl.* **1993**, *32*, 1329-1331.
- [18] Nelson, D. W.; Gypser, A.; Ho, P. T.; Kolb, H. C.; Kondo, T.; Kwong, H.-L.; McGrath, D. V.; Rubin, A. E.; Norrby, P.-O.; Gable, K. P.; Sharpless, K. B. *J. Am. Chem. Soc.* **1997**, *119*, 1840-1858.
- [19] Corey, E. J.; Noe, M. C. *J. Am. Chem. Soc.* **1996**, *118*, 11038-11053.
- [20] DelMonte, A. J.; Haller, J.; Houk, K. N.; Sharpless, K. B.; Singleton, D. A.; Strassner, T.; Thomas, A. A. *J. Am. Chem. Soc.* **1997**, *119*, 9907-9908.
- [21] Milstein, D. *J. Am. Chem. Soc.* **1982**, *104*, 5227-5228.
- [22] Zlota, A. A.; Frolow, F.; Milstein, D. *J. Am. Chem. Soc.* **1990**, *112*, 6411-6413.
- [23] Calhorda, M. J.; Galvao, A. M.; Unaleroglu, C.; Zlota, A. A.; Frolow, F.; Milstein, D. M. *Organometallics* **1993**, *12*, 3316-3325.
- [24] Ho, S. C.; Hentges, S.; Grubbs, R. H. *Organometallics* **1988**, *7*, 780-782.
- [25] Hartwig, J. F.; Bergman, R. G.; Andersen, R. A. *J. Am. Chem. Soc.* **1990**, *112*, 3234-3236.
- [26] Hartwig, J. F.; Bergman, R. G.; Andersen, R. A. *Organometallics* **1991**, *10*, 3344-3362.
- [27] Hartwig, J. F.; Bergman, R. G.; Andersen, R. A. *Organometallics* **1991**, *10*, 3326-3344.
- [28] Klein, D. P.; Hayes, J. C.; Bergman, R. G. *J. Am. Chem. Soc.* **1988**, *110*, 3704-3706.

- [29] Bazan, G. C.; Schrock, R. R.; O'Regan, M. B. *Organometallics* **1991**, *10*, 1062-1067.
- [30] Sundermeyer, J.; Weber, K.; Pritzkow, H. *Angew. Chem. Int. Ed. Engl.* **1993**, *32*, 731-733.
- [31] de Bruin, B.; Boerakker, M. J.; Donners, J. J. J. M.; Christiaans, B. E. C.; Schlebos, P. P. J.; de Gelder, R.; Smits, J. M. M.; Spek, A. L.; Gal, A. W. *Angew. Chem. Int. Ed. Engl.* **1997**, *36*, 2064-2067.
- [32] de Bruin, B.; Boerakker, M. J.; Verhagen, J. A. W.; de Gelder, R.; Smits, J. M. M.; Gal, A. W. *Chem. Eur. J.* **2000**, *6*, 298-312.
- [33] Krom, M.; Coumans, R. G. E.; Smits, J. M. M.; Gal, A. W. *Angew. Chem. Int. Ed.* **2001**, *40*, 2106-2108.
- [34] Krom, M.; Coumans, R. G. E.; Smits, J. M. M.; Gal, A. W. *Angew. Chem. Int. Ed.* **2002**, *41*, 576-579.
- [35] Dauth, A.; Love, J. A. *Angew. Chem. Int. Ed.* **2010**, *49*, 9219-24.
- [36] Tejel, C.; Ciriano, M. A.; Sola, E.; del Rio, M. P.; Rios-Moreno, G.; Lahoz, F. J.; Oro, L. A. *Angew. Chem. Int. Ed.* **2005**, *44*, 3267-71.
- [37] del Rio, M. P.; Ciriano, M. A.; Tejel, C. *Angew. Chem. Int. Ed.* **2008**, *47*, 2502-5.
- [38] Blum, O.; Milstein, D. *J. Am. Chem. Soc.* **1995**, *117*, 4582-4594.
- [39] Day, V. W.; Klemperer, W. G.; Lockledge, S. P.; Main, D. J. *J. Am. Chem. Soc.* **1990**, *112*, 2031-2033.
- [40] Flood, T. C.; Iimura, M.; Perotti, J. M.; Rheingold, A. L.; E. Concolino, T. *Chem. Commun.* **2000**, 1681-1682.

- [41] Ghatak, T.; Sarkar, M.; Dinda, S.; Dutta, I.; Rahaman, S. M.; Bera, J. K. *J. Am. Chem. Soc.* **2015**, *137*, 6168-71.
- [42] Mindiola, D. J.; Hillhouse, G. L. *J. Am. Chem. Soc.* **2002**, *124*, 9976-9977.
- [43] Nielsen, D. K.; Doyle, A. G. *Angew. Chem. Int. Ed.* **2011**, *50*, 6056-9.
- [44] Molinaro, C.; Jamison, T. F. *J. Am. Chem. Soc.* **2003**, *125*, 8076-7.
- [45] Beaver, M. G.; Jamison, T. F. *Org. Lett.* **2011**, *13*, 4140-4143.
- [46] Aye, K.-T.; Ferguson, G.; Lough, A. J.; Puddephatt, R. J. *Angew. Chem. Int. Ed. Engl.* **1989**, *28*, 767-768.
- [47] Aye, K. T.; Gelmini, L.; Payne, N. C.; Vittal, J. J.; Puddephatt, R. J. *J. Am. Chem. Soc.* **1990**, *112*, 2464-2465.
- [48] Khusnutdinova, J. R.; Newman, L. L.; Zavalij, P. Y.; Lam, Y.-F.; Vedernikov, A. N. *J. Am. Chem. Soc.* **2008**, *130*, 2174-2174.
- [49] Cinellu, M. A.; Minghetti, G.; Cocco, F.; Stoccoro, S.; Zucca, A.; Manassero, M. *Angew. Chem. Int. Ed.* **2005**, *44*, 6892-5.
- [50] Szuromi, E.; Shan, H.; Sharp, P. R. *J. Am. Chem. Soc.* **2003**, *125*, 10522-10523.
- [51] Weliange, N. M.; Sharp, P. R. *Organometallics* **2012**, *31*, 6823-6833.
- [52] Szuromi, E.; Wu, J.; Sharp, P. R. *J. Am. Chem. Soc.* **2006**, *128*, 12088-12089.
- [53] Wu, J.; Sharp, P. R. *Organometallics* **2008**, *27*, 1234-1241.
- [54] Weliange, N. M.; Szuromi, E.; Sharp, P. R. *J. Am. Chem. Soc.* **2009**, *131*, 8736-8737.
- [55] Campora, J.; Gutierrez, E.; Monge, A.; Palma, P.; Poveda, M. L.; Ruiz, C.; Carmona, E. *Organometallics* **1994**, *13*, 1728-1745.
- [56] Vicic, D. A.; Jones, W. D. *J. Am. Chem. Soc.* **1999**, *121*, 4070-4071.

- [57] Han, R.; Hillhouse, G. L. *J. Am. Chem. Soc.* **1998**, *120*, 7657-7658.
- [58] Morton, M. S.; Lachicotte, R. J.; Vicic, D. A.; Jones, W. D. *Organometallics* **1999**, *18*, 227-234.
- [59] Sivaramakrishna, A.; Makhubela, B. C. E.; Moss, J. R.; Smith, G. S. *J. Organomet. Chem.* **2010**, *695*, 1627-1633.
- [60] Koo, K.; Hillhouse, G. L. *Organometallics* **1995**, *14*, 4421-4423.
- [61] Koo, K.; Hillhouse, G. L. *Organometallics* **1996**, *15*, 2669-2671.
- [62] Matsunaga, P. T.; Hess, C. R.; Hillhouse, G. L. *J. Am. Chem. Soc.* **1994**, *116*, 3665-3666.
- [63] Lin, B. L.; Clough, C. R.; Hillhouse, G. L. *J. Am. Chem. Soc.* **2002**, *124*, 2890-2891.
- [64] Huang, C.-Y.; Doyle, A. G. *J. Am. Chem. Soc.* **2012**, *134*, 9541-9544.
- [65] Jensen, K. L.; Standley, E. A.; Jamison, T. F. *J. Am. Chem. Soc.* **2014**, *136*, 11145-52.
- [66] Zhang, S.; Wei, J.; Zhan, M.; Luo, Q.; Wang, C.; Zhang, W. X.; Xi, Z. *J. Am. Chem. Soc.* **2012**, *134*, 11964-7.
- [67] Matsunaga, P. T.; Hillhouse, G. L. *J. Am. Chem. Soc.* **1993**, *115*, 2075-2077.
- [68] Matsunaga, P. T.; Mavropoulos, J. C.; Hillhouse, G. L. *Polyhedron* **1995**, *14*, 175-185.
- [69] Yamamoto, T.; Ishizu, J.; Kohara, T.; Komiya, S.; Yamamoto, A. *J. Am. Chem. Soc.* **1980**, *102*, 3758-3764.
- [70] Kim, Y.-J.; Osakada, K.; Sugita, K.; Yamamoto, T.; Yamamoto, A. *Organometallics* **1988**, *7*, 2182-2188.

- [71] Koo, K.; Hillhouse, G. L.; Rheingold, A. L. *Organometallics* **1995**, *14*, 456-460.
- [72] Carmona, E.; Gutierrez-Puebla, E.; Marin, J. M.; Monge, A.; Paneque, M.; Poveda, M. L.; Ruiz, C. *J. Am. Chem. Soc.* **1989**, *111*, 2883-2891.
- [73] Han, R.; Hillhouse, G. L. *J. Am. Chem. Soc.* **1997**, *119*, 8135-8136.
- [74] Koo, K.; Hillhouse, G. L. *Organometallics* **1998**, *17*, 2924-2925.
- [75] Mindiola, D. J.; Hillhouse, G. L. *J. Am. Chem. Soc.* **2001**, *123*, 4623-4624.
- [76] Mindiola, D. J.; Hillhouse, G. L. *Chem. Commun.* **2002**, 1840-1841.
- [77] Waterman, R.; Hillhouse, G. L. *J. Am. Chem. Soc.* **2003**, *125*, 13350-13351.
- [78] Mindiola, D. J.; Waterman, R.; Iluc, V. M.; Cundari, T. R.; Hillhouse, G. L. *Inorg. Chem.* **2014**, *53*, 13227-38.
- [79] Harrold, N. D.; Waterman, R.; Hillhouse, G. L.; Cundari, T. R. *J. Am. Chem. Soc.* **2009**, *131*, 12872-12873.
- [80] Laskowski, C. A.; Miller, A. J. M.; Hillhouse, G. L.; Cundari, T. R. *J. Am. Chem. Soc.* **2011**, *133*, 771-773.
- [81] Laskowski, C. A.; Hillhouse, G. L. *Organometallics* **2009**, *28*, 6114-6120.
- [82] Harrold, N. D.; Hillhouse, G. L. *Chem. Sci.* **2013**, *4*, 4011.
- [83] Mankad, N. P.; Antholine, W. E.; Szilagyi, R. K.; Peters, J. C. *J. Am. Chem. Soc.* **2009**, *131*, 3878-3880.
- [84] Jazdzewski, B. A.; Holland, P. L.; Pink, M.; Young, V. G.; Spencer, D. J. E.; Tolman, W. B. *Inorg. Chem.* **2001**, *40*, 6097-6107.
- [85] Harkins, S. B.; Mankad, N. P.; Miller, A. J. M.; Szilagyi, R. K.; Peters, J. C. *J. Am. Chem. Soc.* **2008**, *130*, 3478-3485.
- [86] Ge, Y.-W.; Ye, Y.; Sharp, P. R. *J. Am. Chem. Soc.* **1994**, *116*, 8384-8385.

- [87] Bai, G.; Stephan, D. W. *Angew. Chem. Int. Ed.* **2007**, *46*, 1856-9.
- [88] Dick, A. R.; Remy, M. S.; Kampf, J. W.; Sanford, M. S. *Organometallics* **2007**, *26*, 1365-1370.
- [89] Osakada, K.; Maeda, M.; Nakamura, Y.; Yamamoto, T.; Yamamoto, A. *J. Chem. Soc. Chem. Commun.* **1986**, 442-443.
- [90] Munjanja, L.; Brennessel, W. W.; Jones, W. D. *Organometallics* **2015**, *34*, 4574.
- [91] van der Boom, M. E.; Liou, S.-Y.; Ben-David, Y.; Vigalok, A.; Milstein, D. *Angew. Chem. Int. Ed. Engl.* **1997**, *36*, 625-626.
- [92] Van der Boom, M. E.; Liou, S.-Y.; Ben-David, Y.; Shimon, L. J.; Milstein, D. *J. Am. Chem. Soc.* **1998**, *120*, 6531-6541.
- [93] Weissman, H.; Shimon, L. J. W.; Milstein, D. *Organometallics* **2004**, *23*, 3931-3940.
- [94] van der Boom, M. E.; Liou, S.-Y.; Shimon, L. J. W.; Ben-David, Y.; Milstein, D. *Inorg. Chim. Acta* **2004**, *357*, 4015-4023.
- [95] Williams, B. S.; Holland, A. W.; Goldberg, K. I. *J. Am. Chem. Soc.* **1999**, *121*, 252-253.
- [96] Williams, B. S.; Goldberg, K. I. *J. Am. Chem. Soc.* **2001**, *123*, 2576-2587.
- [97] Smythe, N. A.; Grice, K. A.; Williams, B. S.; Goldberg, K. I. *Organometallics* **2009**, *28*, 277-288.
- [98] Luinstra, G. A.; Labinger, J. A.; Bercaw, J. E. *J. Am. Chem. Soc.* **1993**, *115*, 3004-3005.
- [99] Dick, A. R.; Kampf, J. W.; Sanford, M. S. *J. Am. Chem. Soc.* **2005**, *127*, 12790-12791.

- [100] Gary, J. B.; Sanford, M. S. *Organometallics* **2011**, *30*, 6143-6149.
- [101] Racowski, J. M.; Dick, A. R.; Sanford, M. S. *J. Am. Chem. Soc.* **2009**, *131*, 10974-10983.
- [102] Fu, Y.; Li, Z.; Liang, S.; Guo, Q.-X.; Liu, L. *Organometallics* **2008**, *27*, 3736-3742.
- [103] Canty, A. J.; Denney, M. C.; Skelton, B. W.; White, A. H. *Organometallics* **2004**, *23*, 1122-1131.
- [104] Canty, A. J.; Denney, M. C.; van Koten, G.; Skelton, B. W.; White, A. H. *Organometallics* **2004**, *23*, 5432-5439.
- [105] Camasso, N. M.; Perez-Temprano, M. H.; Sanford, M. S. *J. Am. Chem. Soc.* **2014**, *136*, 12771-5.
- [106] Powers, D. C.; Ritter, T. *Nat. Chem.* **2009**, *1*, 302-309.
- [107] Powers, D. C.; Geibel, M. A. L.; Klein, J. E. M. N.; Ritter, T. *J. Am. Chem. Soc.* **2009**, *131*, 17050-17051.
- [108] Powers, D. C.; Xiao, D. Y.; Geibel, M. A. L.; Ritter, T. *J. Am. Chem. Soc.* **2010**, *132*, 14530-14536.
- [109] Powers, D. C.; Ritter, T. *Acc. Chem. Res.* **2011**, *45*, 840-850.
- [110] Ochiai, M.; Lin, Y.-S.; Yamada, J.; Misawa, H.; Arai, S.; Matsumoto, K. *J. Am. Chem. Soc.* **2004**.
- [111] Zhao, X.; Dong, V. M. *Angew. Chem. Int. Ed.* **2011**, *50*, 932-4.
- [112] Muto, K.; Yamaguchi, J.; Lei, A.; Itami, K. *J. Am. Chem. Soc.* **2013**, *135*, 16384-7.

- [113] Lejkowski, M. L.; Lindner, R.; Kageyama, T.; Bodizs, G. E.; Plessow, P. N.; Muller, I. B.; Schafer, A.; Rominger, F.; Hofmann, P.; Futter, C.; Schunk, S. A.; Limbach, M. *Chem. Eur. J.* **2012**, *18*, 14017-25.
- [114] Manbeck, K. A.; Kundu, S.; Walsh, A. P.; Brennessel, W. W.; Jones, W. D. *Organometallics* **2012**, *31*, 5018-5024.
- [115] Kundu, S.; Brennessel, W. W.; Jones, W. D. *Organometallics* **2011**, *30*, 5147-5154.
- [116] Kundu, S.; Snyder, B. E. R.; Walsh, A. P.; Brennessel, W. W.; Jones, W. D. *Polyhedron* **2013**, *58*, 99-105.
- [117] Lee, E.; Yandulov, D. V. *J. Organomet. Chem.* **2011**, *696*, 4095-4103.
- [118] Schaub, T.; Backes, M.; Plietzsch, O.; Radius, U. *Dalton Trans.* **2009**, 7071-7079.
- [119] Ney, J. E.; Wolfe, J. P. *J. Am. Chem. Soc.* **2006**, *128*, 15415-15422.
- [120] Schaub, T.; Backes, M.; Radius, U. *Chem. Commun.* **2007**, 2037-2039.
- [121] Zhou, W.; Schultz, J. W.; Rath, N. P.; Mirica, L. M. *J. Am. Chem. Soc.* **2015**, *137*, 7604-7607.
- [122] Camasso, N. M.; Sanford, M. S. *Science* **2015**, *347*, 1218-1220.
- [123] Zhao, P.; Incarvito, C. D.; Hartwig, J. F. *J. Am. Chem. Soc.* **2006**, *128*, 9642-9643.
- [124] Yamamoto, Y.; Sugawara, K.; Han, X.-H. *J. Chem. Soc., Dalton Trans.* **2002**, 195-211.
- [125] de Bruin, B.; Boerakker, M. J.; de Gelder, R.; Smits, J. M. M.; Gal, A. W. *Angew. Chem. Int. Ed.* **1999**, *38*, 219-222.
- [126] Alcock, N. W.; Bryars, K. H.; Pringle, P. G. *J. Organomet. Chem.* **1990**, *386*, 399-410.

- [127] de Bruin, B.; Budzelaar, P. H.; Gal, A. W. *Angew. Chem. Int. Ed.* **2004**, *43*, 4142-57.
- [128] de Bruin, B.; Brands, J. A.; Donners, J. J. J. M.; Donners, M. P. J.; de Gelder, R.; Smits, J. M. M.; Gal, A. W.; Spek, A. L. *Chem. Eur. J.* **1999**, *5*, 2921-2936.
- [129] de Bruin, B.; Verhagen, J. A. W.; Schouten, C. H. J.; Gal, A. W.; Feichtinger, D.; Plattner, D. A. *Chem. Eur. J.* **2001**, *7*, 416-422.
- [130] Yamamoto, Y.; Han, X.-H.; Ma, J.-F. *Angew. Chem. Int. Ed.* **2000**, *39*, 1965-1968.
- [131] Wu, J.; Sharp, P. R. *Organometallics* **2008**, *27*, 4810-4816.
- [132] Ghosh, K.; Pattanayak, S.; Chakravorty, A. *Organometallics* **1998**, *17*, 1956-1960.
- [133] Ghosh, K.; Chattopadhyay, S.; Pattanayak, S.; Chakravorty, A. *Organometallics* **2001**, *20*, 1419-1423.
- [134] Ferstl, W.; Sakodinskaya, I. K.; Beydoun-Sutter, N.; Le Borgne, G.; Pfeffer, M.; Ryabov, A. D. *Organometallics* **1997**, *16*, 411-418.
- [135] Drover, M. W.; Beh, D. W.; Kennepohl, P.; Love, J. A. *Chem. Eur. J.* **2014**, *20*, 13345-55.
- [136] Krug, C.; Hartwig, J. F. *J. Am. Chem. Soc.* **2002**, *124*, 1674-1679.
- [137] Krug, C.; Hartwig, J. F. *Organometallics* **2004**, *23*, 4594-4607.
- [138] Tejel, C.; Ciriano, M. A.; Passarelli, V. *Chem. Eur. J.* **2011**, *17*, 91-5.
- [139] Fatah, A.; El Ayoubi, R.; Gornitzka, H.; Ranaivonjatovo, H.; Escudié, J. *Eur. J. Inorg. Chem.* **2008**, *2008*, 2007-2013.
- [140] Luca, O. R.; Crabtree, R. H. *Chem. Soc. Rev.* **2013**, *42*, 1440-59.
- [141] Kaim, W.; Schwederski, B. *Coord. Chem. Rev.* **2010**, *254*, 1580-1588.
- [142] Wang, M.; Weyhermuller, T.; Wieghardt, K. *Chem. Eur. J.* **2014**, *20*, 9037-44.

- [143] Scarborough, C. C.; Sproules, S.; Weyhermuller, T.; DeBeer, S.; Wieghardt, K. *Inorg. Chem.* **2011**, *50*, 12446-62.
- [144] Darmon, J. M.; Stieber, S. C.; Sylvester, K. T.; Fernandez, I.; Lobkovsky, E.; Semproni, S. P.; Bill, E.; Wieghardt, K.; DeBeer, S.; Chirik, P. J. *J. Am. Chem. Soc.* **2012**, *134*, 17125-37.
- [145] Broere, D. L.; de Bruin, B.; Reek, J. N.; Lutz, M.; Dechert, S.; van der Vlugt, J. I. *J. Am. Chem. Soc.* **2014**, *136*, 11574-7.
- [146] Chirik, P. J.; Wieghardt, K. *Science* **2010**, *327*, 794-5.
- [147] Jazdzewski, B. A.; Tolman, W. B. *Coord. Chem. Rev.* **2000**, *200-202*, 633-685.
- [148] Blackmore, K. J.; Ziller, J. W.; Heyduk, A. F. *Inorg. Chem.* **2005**, *44*, 5559-61.
- [149] Haneline, M. R.; Heyduk, A. F. *J. Am. Chem. Soc.* **2006**, *128*, 8410-1.
- [150] Dauth, A.; Rigling, C.; Tsoung, J.; Love, J. A. *Chem. Eur. J.* **2013**, *19*, 17180-17191.
- [151] Garcia, J. J.; Brunkan, N. M.; Jones, W. D. *J. Am. Chem. Soc.* **2002**, *124*, 9547-9555s.
- [152] Feller, M.; Diskin-Posner, Y.; Shimon, L. J. W.; Ben-Ari, E.; Milstein, D. *Organometallics* **2012**, *31*, 4083-4101.
- [153] Zenkina, O. V.; Keske, E. C.; Kochhar, G. S.; Wang, R.; Crudden, C. M. *Dalton Trans.* **2013**, *42*, 2282-93.
- [154] Rubio, M.; Suárez, A. s.; del Río, D.; Galindo, A. n.; Álvarez, E.; Pizzano, A. *Organometallics* **2009**, *28*, 547-560.
- [155] Delgado-Jaime, M. U.; Conrad, J. C.; Fogg, D. E.; Kennepohl, P. *Inorg. Chim. Acta* **2006**, *359*, 3042-3047.

- [156] Scarborough, C. C.; Lancaster, K. M.; DeBeer, S.; Weyhermuller, T.; Sproules, S.; Wieghardt, K. *Inorg. Chem.* **2012**, *51*, 3718-32.
- [157] Sproules, S.; Wieghardt, K. *Coord. Chem. Rev.* **2011**, *255*, 837-860.
- [158] Nelson, R. C.; Miller, J. T. *Catal. Sci. Technol.* **2012**, *2*, 461-470.
- [159] Westre, T. E.; Kennepohl, P.; DeWitt, J. G.; Hedman, B.; Hodgson, K. O.; Solomon, E. I. *J. Am. Chem. Soc.* **1997**, *119*, 6297-6314.
- [160] Praetorius, J. M.; Allen, D. P.; Wang, R.; Webb, J. D.; Grein, F.; Kennepohl, P.; Crudden, C. M. *J. Am. Chem. Soc.* **2008**, *130*, 3724-5.
- [161] Cipot-Wechsler, J.; Covelli, D.; Praetorius, J. M.; Hearn, N.; Zenkina, O. V.; Keske, E. C.; Wang, R.; Kennepohl, P.; Crudden, C. M. *Organometallics* **2012**, *31*, 7306-7315.
- [162] Desnoyer, A. N.; Behyan, S.; Patrick, B. O.; Dauth, A.; Love, J. A.; Kennepohl, P. *Inorg. Chem.* **2016**, *55*, 13-15.
- [163] Budzelaar, Peter H. M.; Blok, Arno N. J. *Eur. J. Inorg. Chem.* **2004**, *2004*, 2385-2391.
- [164] Lyaskovskyy, V.; de Bruin, B. *ACS Catal.* **2012**, *2*, 270-279.
- [165] Britovsek, G. J.; England, J.; White, A. J. *Inorg. Chem.* **2005**, *44*, 8125-34.
- [166] Yakelis, N. A.; Bergman, R. G. *Organometallics* **2005**, *24*, 3579-3581.
- [167] Pan, C.; Luo, F.; Wang, W.; Ye, Z.; Cheng, J. *Tetrahedron Lett.* **2009**, *50*, 5044-5046.
- [168] Webb, S. M. *Phys. Scr.* **2005**, *T115*, 1011-1014.
- [169] van Wüllen, C. *J. Chem. Phys.* **1998**, *109*, 392-399.
- [170] Lenthe, E. v.; Baerends, E. J.; Snijders, J. G. *J. Chem. Phys.* **1993**, *99*, 4597-4610.

- [171] Neese, F.; Wennmohs, F.; Hansen, A.; Becker, U. *Chem. Phys.* **2009**, *356*, 98-109.
- [172] Yang, Z.-Y. *J. Am. Chem. Soc.* **1996**, *118*, 8140-8141.
- [173] Jacobsen, E. N. *Acc. Chem. Res.* **2000**, *33*, 421-431.
- [174] Pfenninger, A. *Synthesis* **1986**, *1986*, 89-116.
- [175] Linker, T. *Angew. Chem. Int. Ed. Engl.* **1997**, *36*, 2060-2062.
- [176] Zhang, W.; Loebach, J. L.; Wilson, S. R.; Jacobsen, E. N. *J. Am. Chem. Soc.* **1990**, *112*, 2801-2803.
- [177] Larrow, J. F.; Schaus, S. E.; Jacobsen, E. N. *J. Am. Chem. Soc.* **1996**, *118*, 7420-7421.
- [178] Tokunaga, M.; Larrow, J. F.; Kakiuchi, F.; Jacobsen, E. N. *Science* **1997**, *277*, 936-938.
- [179] Pineschi, M. *Eur. J. Org. Chem.* **2006**, *2006*, 4979-4988.
- [180] Nugent, W. A.; RajanBabu, T. V. *J. Am. Chem. Soc.* **1988**, *110*, 8561-8562.
- [181] RajanBabu, T. V.; Nugent, W. A. *J. Am. Chem. Soc.* **1989**, *111*, 4525-4527.
- [182] RajanBabu, T. V.; Nugent, W. A.; Beattie, M. S. *J. Am. Chem. Soc.* **1990**, *112*, 6408-6409.
- [183] Gansäuer, A.; Pierobon, M.; Bluhm, H. *Angew. Chem. Int. Ed.* **1998**, *37*, 101-103.
- [184] Gansauer, A.; Shi, L.; Otte, M. *J. Am. Chem. Soc.* **2010**, *132*, 11858-9.
- [185] Gansauer, A.; Hildebrandt, S.; Michelmann, A.; Dahmen, T.; von Laufenberg, D.; Kube, C.; Fianu, G. D.; Flowers, R. A., 2nd *Angew. Chem. Int. Ed.* **2015**, *54*, 7003-6.
- [186] Prina Cerai, G.; Morandi, B. *Chem. Commun.* **2016**, *52*, 9769-72.
- [187] Zhao, Y.; Weix, D. J. *J. Am. Chem. Soc.* **2014**, *136*, 48-51.

- [188] Nakano, K.; Nozaki, K. *Top. Organomet. Chem.* **2006**, *18*, 223-238.
- [189] Lee, J. T.; Thomas, P. J.; Alper, H. *J. Org. Chem.* **2001**, *66*, 5424-5426.
- [190] Getzler, Y. D. Y. L.; Mahadevan, V.; Lobkovsky, E. B.; Coates, G. W. *J. Am. Chem. Soc.* **2002**, *124*, 1174-1175.
- [191] North, M.; Pasquale, R.; Young, C. *Green Chem.* **2010**, *12*, 1514.
- [192] Halle, L. F.; Armentrout, P. B.; Beauchamp, J. L. *Organometallics* **1983**, *2*, 1829-1833.
- [193] Yang, Z. Y. *J. Org. Chem.* **2004**, *69*, 2394-403.
- [194] Schlodder, R.; Ibers, J. A.; Lenarda, M.; Graziani, M. *J. Am. Chem. Soc.* **1974**, *96*, 6893-6900.
- [195] Lenarda, M.; Ros, R.; Traverso, O.; Pitts, W. D.; Baddley, W. H.; Graziani, M. *Inorg. Chem.* **1977**, *16*, 3178-3182.
- [196] Matsunaga, P. T.; Hillhouse, G. L. *Angew. Chem. Int. Ed. Engl.* **1994**, *33*, 1748-1749.
- [197] King, A. E.; Stieber, S. C. E.; Henson, N. J.; Kozimor, S. A.; Scott, B. L.; Smythe, N. C.; Sutton, A. D.; Gordon, J. C. *Eur. J. Inorg. Chem.* **2016**, *2016*, 1635-1640.
- [198] Tamaki, T.; Nagata, M.; Ohashi, M.; Ogoshi, S. *Chem. Eur. J.* **2009**, *15*, 10083-91.
- [199] Dorta, R.; Stevens, E. D.; Hoff, C. D.; Nolan, S. P. *J. Am. Chem. Soc.* **2003**, *125*, 10490-1.
- [200] Dorta, R.; Stevens, E. D.; Scott, N. M.; Costabile, C.; Cavallo, L.; Hoff, C. D.; Nolan, S. P. *J. Am. Chem. Soc.* **2005**, *127*, 2485-95.

- [201] Scott, N. M.; Clavier, H.; Mahjoor, P.; Stevens, E. D.; Nolan, S. P. *Organometallics* **2008**, *27*, 3181-3186.
- [202] Ogoshi, S.; Nagata, M.; Kurosawa, H. *J. Am. Chem. Soc.* **2006**, *128*, 5350-5351.
- [203] Amaike, K.; Muto, K.; Yamaguchi, J.; Itami, K. *J. Am. Chem. Soc.* **2012**, *134*, 13573-6.
- [204] Jin, D.; Williard, P. G.; Hazari, N.; Bernskoetter, W. H. *Chem. Eur. J.* **2014**, *20*, 3205-11.
- [205] Schultz, M.; Eisenträger, F.; Regius, C.; Rominger, F.; Hanno-Igels, P.; Jakob, P.; Gruber, I.; Hofmann, P. *Organometallics* **2012**, *31*, 207-224.
- [206] Hao, J.; Vabre, B.; Mougang-Soume, B.; Zargarian, D. *Chem. Eur. J.* **2014**, *20*, 12544-52.
- [207] Fischer, R.; Langer, J.; Malassa, A.; Walther, D.; Gorls, H.; Vaughan, G. *Chem. Commun.* **2006**, 2510-2.
- [208] Harrison, D. J.; Daniels, A. L.; Korobkov, I.; Baker, R. T. *Organometallics* **2015**, *34*, 5683-5686.
- [209] Doi, R.; Kikushima, K.; Ohashi, M.; Ogoshi, S. *J. Am. Chem. Soc.* **2015**, *137*, 3276-82.
- [210] Campora, J.; Matas, I.; Palma, P.; Graiff, C.; Tiripicchio, A. *Organometallics* **2005**, *24*, 2827-2830.
- [211] Maya, C. M.; Campora, J.; Carmona, E.; Matas, I.; Palma, P.; Gutierrez-Puebla, E.; Monge, A. *Chem. Eur. J.* **2007**, *13*, 3675-87.
- [212] Iglesias, A. L.; Muñoz-Hernández, M.; García, J. J. *J. Organomet. Chem.* **2007**, *692*, 3498-3507.

- [213] González-Sebastián, L.; Flores-Alamo, M.; García, J. J. *Organometallics* **2012**, *31*, 8200-8207.
- [214] Maleckis, A.; Sanford, M. S. *Organometallics* **2014**, *33*, 3831-3839.
- [215] Porschke, K.-R.; Pluta, C.; Proft, B.; Lutz, F.; Kruger, C. *Z. Naturforsch.* **1993**, *48B*, 608-626.
- [216] Bach, I.; Porschke, K.-R.; Goddard, R.; Kopiske, C.; Kruger, C.; Rufinska, A.; Seevogel, K. *Organometallics* **1996**, *15*, 4959-4966.
- [217] Bach, I.; Goddard, R.; Kopiske, C.; Seevogel, K.; Porschke, K.-R. *Organometallics* **1999**, *18*, 10-20.
- [218] Melenkivitz, R.; Mindiola, D. J.; Hillhouse, G. L. *J. Am. Chem. Soc.* **2002**, *124*, 3846-3847.
- [219] Ganushevich, Y. S.; Miluykov, V. A.; Polyancev, F. M.; Latypov, S. K.; Lönnecke, P.; Hey-Hawkins, E.; Yakhvarov, D. G.; Sinyashin, O. G. *Organometallics* **2013**, *32*, 3914-3919.
- [220] Latypov, S. K.; Polyancev, F. M.; Ganushevich, Y. S.; Miluykov, V. A.; Sinyashin, O. G. *Dalton Trans.* **2016**, *45*, 2053-9.
- [221] Blank, B.; Glatz, G.; Kempe, R. *Chem. Asian J.* **2009**, *4*, 321-7.
- [222] Ball, G. E.; Cullen, W. R.; Fryzuk, M. D.; James, B. R.; Rettig, S. J. *Organometallics* **1991**, *10*, 3767-3769.
- [223] Lopez, J. A.; Mereiter, K.; Paneque, M.; Poveda, M. L.; Serrano, O.; Trofimenko, S.; Carmona, E. *Chem. Commun.* **2006**, 3921-3.
- [224] Ghisolfi, A.; Condello, F.; Fliedel, C.; Rosa, V.; Braunstein, P. *Organometallics* **2015**, *34*, 2255-2260.

- [225] Lee, J.-H.; Jeon, H.-T.; Kim, Y.-J.; Lee, K.-E.; Ok Jang, Y.; Lee, S. W. *Eur. J. Inorg. Chem.* **2011**, *2011*, 1750-1761.
- [226] Campora, J.; Palma, P.; del Rio, D.; Lopez, J. A.; Valerga, P. *Chem. Commun.* **2004**, 1490-1.
- [227] Abo-Amer, A.; McCready, M. S.; Zhang, F.; Puddephatt, R. J. *Can. J. Chem.* **2012**, *90*, 46-54.
- [228] Ogoshi, S.; Tonomori, K.-I.; Oka, M.-A.; Kurosawa, H. *J. Am. Chem. Soc.* **2006**, *128*, 7077-7086.
- [229] Kitiachvili, K.; Mindiola, D. J.; Hillhouse, G. L. *J. Am. Chem. Soc.* **2004**, *126*, 10554-10555.
- [230] Cámpora, J.; Gutiérrez-Puebla, E.; López, J. A.; Monge, A.; Palma, P.; del Río, D.; Carmona, E. *Angew. Chem. Int. Ed.* **2001**, *40*, 3641.
- [231] Cámpora, J.; López, J. A.; Palma, P.; Valerga, P.; Spillner, E.; Carmona, E. *Angew. Chem. Int. Ed.* **1999**, *38*, 147-151.
- [232] Komber, H.; Senkovskyy, V.; Tkachov, R.; Johnson, K.; Kiriya, A.; Huck, W. T. S.; Sommer, M. *Macromolecules* **2011**, *44*, 9164-9172.
- [233] Desnoyer, A. N.; Bowes, E. G.; Patrick, B. O.; Love, J. A. *J. Am. Chem. Soc.* **2015**, *137*, 12748-51.
- [234] Desnoyer, A. N.; Friese, F. W.; Chiu, W.; Drover, M. W.; Patrick, B. O.; Love, J. A. *Chem. Eur. J.* **2016**, *22*, 4070-4077.
- [235] Mindiola, D. J.; Waterman, R.; Jenkins, D. M.; Hillhouse, G. L. *Inorg. Chim. Acta* **2003**, *345*, 299-308.

- [236] Cope, A. C.; Trumbull, P. A.; Trumbull, E. R. *J. Am. Chem. Soc.* **1958**, *80*, 2844-2849.
- [237] Prandi, J.; Namy, J. L.; Menoret, G.; Kagan, H. B. *J. Organomet. Chem.* **1985**, *285*, 449-460.
- [238] Archelas, A.; Furstoss, R. *J. Org. Chem.* **1999**, *64*, 6112-6114.
- [239] Niwayama, S.; Noguchi, H.; Ohno, M.; Kobayashi, S. *Tetrahedron Lett.* **1993**, *34*, 665-668.
- [240] Robinson, M. W. C.; Pillinger, K. S.; Mabbett, I.; Timms, D. A.; Graham, A. E. *Tetrahedron* **2010**, *66*, 8377-8382.
- [241] Lamb, J. R.; Jung, Y.; Coates, G. W. *Org. Chem. Front.* **2015**, *2*, 346-349.
- [242] Jurgens, E.; Wucher, B.; Rominger, F.; Tornroos, K. W.; Kunz, D. *Chem. Commun.* **2015**, *51*, 1897-900.
- [243] Kulasegaram, S.; Kulawiec, R. J. *J. Org. Chem.* **1994**, *59*, 7195-7196.
- [244] Kulasegaram, S.; Kulawiec, R. J. *J. Org. Chem.* **1997**, *62*, 6547-6561.
- [245] Kulasegaram, S.; Kulawiec, R. J. *Tetrahedron* **1998**, *54*, 1361-1374.
- [246] Standley, E. A.; Tasker, S. Z.; Jensen, K. L.; Jamison, T. F. *Acc. Chem. Res.* **2015**, *48*, 1503-14.
- [247] Anderson, J. S.; Iluc, V. M.; Hillhouse, G. L. *Inorg. Chem.* **2010**, *49*, 10203-7.
- [248] Drover, M. W.; Schafer, L. L.; Love, J. A. *Angew. Chem. Int. Ed.* **2016**.
- [249] Kabalka, G. W.; Yu, S.; Li, N.-S. *Tet Lett* **1997**, *38*, 5455-5458.
- [250] Koren-Selfridge, L.; Londino, H. N.; Vellucci, J. K.; Simmons, B. J.; Casey, C. P.; Clark, T. B. *Organometallics* **2009**, *28*, 2085-2090.
- [251] Gridnev, I. D.; Miyaura, N.; Suzuki, A. *Organometallics* **1993**, *12*, 589-592.

- [252] Kaithal, A.; Chatterjee, B.; Gunanathan, C. *Org. Lett.* **2015**, *17*, 4790-3.
- [253] MacMillan, S. N.; Hill Harman, W.; Peters, J. C. *Chem. Sci.* **2014**, *5*, 590-597.
- [254] Arrowsmith, M.; Hadlington, T. J.; Hill, M. S.; Kociok-Kohn, G. *Chem. Commun.* **2012**, *48*, 4567-9.
- [255] Carter, C. A. G.; Vogels, C. M.; Harrison, D. J.; Gagnon, M. K. J.; Norman, D. W.; Langler, R. F.; Baker, R. T.; Westcott, S. A. *Organometallics* **2001**, *20*, 2130-2132.
- [256] Iluc, V. M.; Hillhouse, G. L. *Tetrahedron* **2006**, *62*, 7577-7582.
- [257] Aubé, J. *Chem. Soc. Rev.* **1997**, *26*, 269-277.
- [258] Adam, W.; Saha-Möller, C. R.; Ganeshpure, P. A. *Chem. Rev.* **2001**, *101*, 3499-3548.
- [259] Pellarin, K. R.; Puddephatt, R. J. *Organometallics* **2013**, *32*, 3604-3610.
- [260] Huang, C. Y.; Doyle, A. G. *Chem. Rev.* **2014**, *114*, 8153-98.
- [261] Allen, C. P.; Benkovics, T.; Turek, A. K.; Yoon, T. P. *J. Am. Chem. Soc.* **2009**, *131*, 12560-1.
- [262] Michaelis, D. J.; Shaffer, C. J.; Yoon, T. P. *J. Am. Chem. Soc.* **2007**, *129*, 1866-7.
- [263] Michaelis, D. J.; Ischay, M. A.; Yoon, T. P. *J. Am. Chem. Soc.* **2008**, *130*, 6610-5.
- [264] Williamson, K. S.; Yoon, T. P. *J. Am. Chem. Soc.* **2012**, *134*, 12370-3.
- [265] Davis, F. A.; Lamendola, J.; Nadir, U.; Kluger, E. W.; Sedergran, T. C.; Panunto, T. W.; Billmers, R.; Jenkins, R.; Turchi, I. J. *J. Am. Chem. Soc.* **1980**, *102*, 2000-2005.
- [266] Waterman, R.; Hillhouse, G. L. *J. Am. Chem. Soc.* **2008**, *130*, 12628-12629.
- [267] Braslau, R.; O'Bryan, G.; Nilsen, A.; Henise, J.; Thongpaisanwong, T.; Murphy, E.; Mueller, L.; Ruehl, J. *Synthesis* **2005**, 1496-1506.

- [268] Hazari, N.; Mountford, P. *Acc. Chem. Res.* **2005**, *38*, 839-49.
- [269] Groom, L. R.; Russell, A. F.; Schwarz, A. D.; Mountford, P. *Organometallics* **2014**, *33*, 1002-1019.
- [270] Peng, X.; Zhu, Y.; Ramirez, T. A.; Zhao, B.; Shi, Y. *Org. Lett.* **2011**, *13*, 5244-7.
- [271] Poulten, R. C.; Lopez, I.; Llobet, A.; Mahon, M. F.; Whittlesey, M. K. *Inorg. Chem.* **2014**, *53*, 7160-9.
- [272] Li, Y.; Jiang, L.; Wang, L.; Gao, H.; Zhu, F.; Wu, Q. *Appl. Organomet. Chem.* **2006**, *20*, 181-186.
- [273] Yao, S.; Bill, E.; Milsmann, C.; Wieghardt, K.; Driess, M. *Angew. Chem. Int. Ed.* **2008**, *47*, 7110-3.
- [274] Engelmann, X.; Yao, S.; Farquhar, E. R.; Szilvasi, T.; Kuhlmann, U.; Hildebrandt, P.; Driess, M.; Ray, K. *Angew. Chem. Int. Ed.* **2017**, *56*, 297-301.
- [275] Dible, B. R.; Sigman, M. S. *J. Am. Chem. Soc.* **2003**, *125*, 872-3.
- [276] Dible, B. R.; Sigman, M. S.; Arif, A. M. *Inorg. Chem.* **2005**, *44*, 3774-6.
- [277] Manditmutsira, B. S.; Yamarik, J. L.; Brunold, T. C.; Gu, W.; Cramer, S. P.; Riordan, C. G. *J. Am. Chem. Soc.* **2001**, *123*, 9194-9195.
- [278] Fujita, K.; Schenker, R.; Gu, W.; Brunold, T. C.; Cramer, S. P.; Riordan, C. G. *Inorg. Chem.* **2004**, *43*, 3324-6.
- [279] Mazimba, O.; Majinda, R. R.; Masesane, I. B. *Tetrahedron Lett.* **2009**, *50*, 5927-5929.
- [280] Corey, E. J.; Chaykovsky, M. *J. Am. Chem. Soc.* **1965**, *87*, 1353-1364.
- [281] Fluxá, V. S.; Jenny, T. A.; Bochet, C. G. *Tetrahedron Lett.* **2005**, *46*, 3793-3795.
- [282] Nagaki, A.; Takizawa, E.; Yoshida, J. *Chem. Eur. J.* **2010**, *16*, 14149-58.

- [283] Garcia Ruano, J. L.; Aleman, J.; Fajardo, C.; Parra, A. *Org. Lett.* **2005**, *7*, 5493-6.
- [284] Ogoshi, S.; Oka, M. A.; Kurosawa, H. *J. Am. Chem. Soc.* **2004**, *126*, 11802-3.
- [285] Ogoshi, S.; Hoshimoto, Y.; Ohashi, M. *Chem. Commun.* **2010**, *46*, 3354-6.
- [286] Hoshimoto, Y.; Yabuki, H.; Kumar, R.; Suzuki, H.; Ohashi, M.; Ogoshi, S. *J. Am. Chem. Soc.* **2014**, *136*, 16752-5.
- [287] Fioroni, G.; Fringuelli, F.; Pizzo, F.; Vaccaro, L. *Green Chem.* **2003**, *5*, 425-428.
- [288] Garcia, J. J.; Jones, W. D. *Organometallics* **2000**, *19*, 5544-5545.
- [289] Turkyilmaz, F.; Kehr, G.; Li, J.; Daniliuc, C. G.; Tesch, M.; Studer, A.; Erker, G. *Angew. Chem. Int. Ed.* **2016**, *55*, 1470-1473.
- [290] Varlamov, V. T.; Denisov, E. T.; Chatgialoglu, C. *J. Org. Chem.* **2001**, *66*, 6317-6322.
- [291] Cowley, R. E.; Eckert, N. A.; Vaddadi, S.; Figg, T. M.; Cundari, T. R.; Holland, P. L. *J. Am. Chem. Soc.* **2011**, *133*, 9796-811.
- [292] Plessow, P. N.; Weigel, L.; Lindner, R.; Schäfer, A.; Rominger, F.; Limbach, M.; Hofmann, P. *Organometallics* **2013**, *32*, 3327-3338.
- [293] Atesin, T. A.; Li, T.; Lachaize, S.; Brennessel, W. W.; Garcia, J. J.; Jones, W. D. *J. Am. Chem. Soc.* **2007**, *129*, 7562-9.
- [294] Liu, L.; Montgomery, J. *J. Am. Chem. Soc.* **2006**, *128*, 5348-9.
- [295] Ho, C. Y.; Ohmiya, H.; Jamison, T. F. *Angew. Chem. Int. Ed.* **2008**, *47*, 1893-5.
- [296] Gable, K. P.; Phan, T. N. *J. Am. Chem. Soc.* **1994**, *116*, 833-839.
- [297] MacLeod, K. C.; Patrick, B. O.; Smith, K. M. *Organometallics* **2012**, *31*, 6681-6689.
- [298] Higgs, A. T.; Zinn, P. J.; Sanford, M. S. *Organometallics* **2010**, *29*, 5446-5449.

- [299] Schultz, M.; Plessow, P. N.; Rominger, F.; Weigel, L. *Acta Crystallogr. C* **2013**, *69*, 1437-47.
- [300] Bour, J. R.; Camasso, N. M.; Sanford, M. S. *J. Am. Chem. Soc.* **2015**, *137*, 8034-7.
- [301] Schultz, J. W.; Fuchigami, K.; Zheng, B.; Rath, N. P.; Mirica, L. M. *J. Am. Chem. Soc.* **2016**.
- [302] Ohashi, M.; Takeda, I.; Ikawa, M.; Ogoshi, S. *J. Am. Chem. Soc.* **2011**, *133*, 18018-21.
- [303] Gonzalez-Sebastian, L.; Flores-Alamo, M.; Garcia, J. J. *Dalton Trans.* **2011**, *40*, 9116-22.
- [304] Frisch, M. J.; Trucks, G. W.; Schlegel, H. B.; Scuseria, G. E.; Robb, M. A.; Cheeseman, J. R.; Scalmani, G.; Barone, V.; Mennucci, B.; Petersson, G. A.; Nakatsuji, H.; Caricato, M.; Li, X.; Hratchian, H. P.; Izmaylov, A. F.; Bloino, J.; Zheng, G.; Sonnenberg, J. L.; Hada, M.; Ehara, M.; Toyota, K.; Fukuda, R.; Hasegawa, J.; Ishida, M.; Nakajima, T.; Honda, Y.; Kitao, O.; Nakai, H.; Vreven, T.; Montgomery Jr., J. A.; Peralta, J. E.; Ogliaro, F.; Bearpark, M. J.; Heyd, J.; Brothers, E. N.; Kudin, K. N.; Staroverov, V. N.; Kobayashi, R.; Normand, J.; Raghavachari, K.; Rendell, A. P.; Burant, J. C.; Iyengar, S. S.; Tomasi, J.; Cossi, M.; Rega, N.; Millam, N. J.; Klene, M.; Knox, J. E.; Cross, J. B.; Bakken, V.; Adamo, C.; Jaramillo, J.; Gomperts, R.; Stratmann, R. E.; Yazyev, O.; Austin, A. J.; Cammi, R.; Pomelli, C.; Ochterski, J. W.; Martin, R. L.; Morokuma, K.; Zakrzewski, V. G.; Voth, G. A.; Salvador, P.; Dannenberg, J. J.; Dapprich, S.;

- Daniels, A. D.; Farkas, Ö.; Foresman, J. B.; Ortiz, J. V.; Cioslowski, J.; Fox, D. J. *Gaussian 09*, Gaussian, Inc.: Wallingford, CT, USA, 2009.
- [305] Becke, A. D. *Physical Review A* **1988**, *38*, 3098-3100.
- [306] Perdew, J. *Physical Review B* **1986**, *33*, 8822-8824.
- [307] Ishizu, J.; Yamamoto, T.; Yamamoto, A. *Chem. Lett.* **1976**, *5*, 1091-1094.
- [308] Yamamoto, T.; Ishizu, J.; Kohara, T.; Komiya, S.; Yamamoto, A. *J. Am. Chem. Soc.* **1980**, *102*, 3758-3764.
- [309] Zapf, A. *Angew. Chem. Int. Ed.* **2003**, *42*, 5394-9.
- [310] Muto, K.; Yamaguchi, J.; Musaev, D. G.; Itami, K. *Nat. Commun.* **2015**, *6*, 7508.
- [311] Mesganaw, T.; Garg, N. K. *Org. Process Res. Dev.* **2013**, *17*, 29-39.
- [312] Rosen, B. M.; Quasdorf, K. W.; Wilson, D. A.; Zhang, N.; Resmerita, A. M.; Garg, N. K.; Percec, V. *Chem. Rev.* **2011**, *111*, 1346-416.
- [313] Quasdorf, K. W.; Tian, X.; Garg, N. K. *J. Am. Chem. Soc.* **2008**, *130*, 14422-14423.
- [314] Guan, B.-T.; Wang, Y.; Li, B.-L.; Yu, D.-G.; Shi, Z.-J. *J. Am. Chem. Soc.* **2008**, *130*, 14468-14470.
- [315] Su, B.; Cao, Z. C.; Shi, Z. J. *Acc. Chem. Res.* **2015**, *48*, 886-96.
- [316] LaBerge, N. A.; Love, J. A. *Eur. J. Org. Chem.* **2015**, *2015*, 5546-5553.
- [317] Ariyananda, P. W. G.; Kieber-Emmons, M. T.; Yap, G. P. A.; Riordan, C. G. *Dalton Trans.* **2009**, 4359-4369.
- [318] Kallane, S. I.; Braun, T.; Braun, B.; Mebs, S. *Dalton Trans.* **2014**, *43*, 6786-801.
- [319] Kallane, S. I.; Braun, T.; Teltewskoi, M.; Braun, B.; Herrmann, R.; Laubenstein, R. *Chem. Commun.* **2015**, *51*, 14613-6.
- [320] Ahrens, T.; Kohlmann, J.; Ahrens, M.; Braun, T. *Chem. Rev.* **2015**, *115*, 931-72.

- [321] Sun, A. D.; Love, J. A. *Dalton Trans.* **2010**, 39, 10362-10374.
- [322] Countryman, R.; Penfold, B. R. *J. Chem. Soc., Chem. Commun.* **1971**, 1598.
- [323] Nakazawa, H.; Nosaka, H.; Kushi, Y.; Yoneda, H. *Organometallics* **1990**, 9, 1958-1963.
- [324] Matas, I.; Cámpora, J.; Palma, P.; Álvarez, E. *Organometallics* **2009**, 28, 6515-6523.
- [325] Flores-Gaspar, A.; Pinedo-González, P.; Crestani, M. G.; Muñoz-Hernández, M.; Morales-Morales, D.; Warsop, B. A.; Jones, W. D.; García, J. J. *J. Mol. Catal. A: Chem.* **2009**, 309, 1-11.
- [326] Cornella, J.; Gomez-Bengoia, E.; Martin, R. *J. Am. Chem. Soc.* **2013**, 135, 1997-2009.
- [327] Sylvester, K. T.; Wu, K.; Doyle, A. G. *J. Am. Chem. Soc.* **2012**, 134, 16967-70.
- [328] Martin, R.; Buchwald, S. L. *Acc. Chem. Res.* **2008**, 41, 1461-1473.
- [329] Pignolet, L. H.; Horrocks, W. *J. Am. Chem. Soc.* **1968**, 90, 922-926.
- [330] Dougherty, W. G.; Rangan, K.; O'Hagan, M. J.; Yap, G. P. A.; Riordan, C. G. *J. Am. Chem. Soc.* **2008**, 130, 13510-13511.
- [331] Shaver, A.; Morris, S.; Desjardins, A. *Inorg. Chim. Acta* **1989**, 161, 11-12.
- [332] Yamashina, Y.; Kataoka, Y.; Ura, Y. *Eur. J. Inorg. Chem.* **2014**, 2014, 4073-4078.
- [333] Fitzpatrick, J.; Kalyvas, H.; Shearer, J.; Kim, E. *Chem. Commun.* **2013**, 49, 5550-2.
- [334] Buchwald, S. L.; Nielsen, R. B.; Dewan, J. C. *J. Am. Chem. Soc.* **1987**, 109, 1591-1593.
- [335] Yu, D. G.; Li, B. J.; Shi, Z. J. *Acc. Chem. Res.* **2010**, 43, 1486-95.

- [336] Han, F. S. *Chem. Soc. Rev.* **2013**, *42*, 5270-98.
- [337] Yoshikai, N.; Matsuda, H.; Nakamura, E. *J. Am. Chem. Soc.* **2008**, *130*, 15258-9.
- [338] Hong, X.; Liang, Y.; Houk, K. N. *J. Am. Chem. Soc.* **2014**, *136*, 2017-25.
- [339] Bennett, M. A.; Hockless, D. C. R.; Wenger, E. *Organometallics* **1995**, *14*, 2091-2101.
- [340] Kim, Y.-J.; Sato, R.; Maruyama, T.; Osakada, K.; Yamamoto, T. *J. Chem. Soc., Dalton Trans.* **1994**, 943-948.
- [341] Xu, H.; Muto, K.; Yamaguchi, J.; Zhao, C.; Itami, K.; Musaev, D. G. *J. Am. Chem. Soc.* **2014**, *136*, 14834-44.
- [342] Meng, L.; Kamada, Y.; Muto, K.; Yamaguchi, J.; Itami, K. *Angew. Chem. Int. Ed.* **2013**, *52*, 10048-51.
- [343] Koch, E.; Takise, R.; Studer, A.; Yamaguchi, J.; Itami, K. *Chem. Commun.* **2015**, *51*, 855-7.
- [344] Cornella, J.; Jackson, E. P.; Martin, R. *Angew. Chem. Int. Ed.* **2015**, *54*, 4075-8.
- [345] Tobisu, M.; Shimasaki, T.; Chatani, N. *Angew. Chem. Int. Ed.* **2008**, *47*, 4866-9.
- [346] Alvarez-Bercedo, P.; Martin, R. *J. Am. Chem. Soc.* **2010**, *132*, 17352-17353.
- [347] Cornella, J.; Zarate, C.; Martin, R. *Chem. Soc. Rev.* **2014**, *43*, 8081-97.
- [348] Lancaster, K. M.; Roemelt, M.; Ettenhuber, P.; Hu, Y.; Ribbe, M. W.; Neese, F.; Bergmann, U.; DeBeer, S. *Science* **2011**, *334*, 974-977.
- [349] Wiig, J. A.; Hu, Y.; Lee, C. C.; Ribbe, M. W. *Science* **2012**, *337*, 1672-5.
- [350] Wiig, J. A.; Hu, Y.; Ribbe, M. W. *Nat. Commun.* **2015**, *6*, 8034.
- [351] Ramaswamy, S. *Science* **2011**, *334*, 914-5.
- [352] Hong, S. H.; Day, M. W.; Grubbs, R. H. *J. Am. Chem. Soc.* **2004**, *126*, 7414-7415.

- [353] Ballmann, J.; Yeo, A.; MacKay, B. A.; van Rijt, S.; Patrick, B. O.; Fryzuk, M. D. *Chem. Commun.* **2010**, *46*, 8794-6.
- [354] Man, W. L.; Xie, J.; Pan, Y.; Lam, W. W.; Kwong, H. K.; Ip, K. W.; Yiu, S. M.; Lau, K. C.; Lau, T. C. *J. Am. Chem. Soc.* **2013**, *135*, 5533-6.
- [355] Fox, A. R.; Arnold, P. L.; Cummins, C. C. *J. Am. Chem. Soc.* **2010**, *132*, 3250-3251.
- [356] Teets, T. S.; Nocera, D. G. *Inorg. Chem.* **2012**, *51*, 7192-201.
- [357] Caskey, S. R.; Stewart, M. H.; Kivela, J. E.; Sootsman, J. R.; Johnson, M. J. A.; Kampf, J. W. *J. Am. Chem. Soc.* **2005**, *127*, 16750-16751.
- [358] Hejl, A.; Trnka, T. M.; Day, M. W.; Grubbs, R. H. *Chem. Commun.* **2002**, 2524-2525.
- [359] Schenck, H. A.; Lenkowski, P. W.; Choudhury-Mukherjee, I.; Ko, S. H.; Stables, J. P.; Patel, M. K.; Brown, M. L. *Bioorg. Med. Chem.* **2004**, *12*, 979-93.
- [360] Billard, T.; Roques, N.; Langlois, B. R. *J. Org. Chem.* **1999**, *64*, 3813-3820.
- [361] Lee, C. K.; Yu, J. S.; Lee, H.-J. *J. Heterocycl. Chem.* **2002**, *39*, 1207-1217.
- [362] Vujjini, S. K.; Datla, V. R. K. R.; Badarla, K. R.; Vetukuri, V. N. K. V. P. R.; Bandichhor, R.; Kagga, M.; Cherukupally, P. *Tetrahedron Lett.* **2014**, *55*, 3885-3887.
- [363] Chen, H. W.; Papparizos, C.; Fackler, J. P. *Inorg. Chim. Acta* **1985**, *96*, 137-149.
- [364] Liang, L. C.; Chien, P. S.; Lee, P. Y.; Lin, J. M.; Huang, Y. L. *Dalton Trans.* **2008**, 3320-7.
- [365] Scholl, M.; Ding, S.; Lee, C. W.; Grubbs, R. H. *Org. Lett.* **1999**, *1*, 953-956.
- [366] Vougioukalakis, G. C.; Grubbs, R. H. *Chem. Rev.* **2010**, *110*, 1746-87.

- [367] Marion, N.; Nolan, S. P. *Acc. Chem. Res.* **2008**, *41*, 1440-9.
- [368] Diez-Gonzalez, S.; Marion, N.; Nolan, S. P. *Chem. Rev.* **2009**, *109*, 3612-76.
- [369] Kantchev, E. A.; O'Brien, C. J.; Organ, M. G. *Angew. Chem. Int. Ed.* **2007**, *46*, 2768-813.
- [370] Valente, C.; Calimsiz, S.; Hoi, K. H.; Mallik, D.; Sayah, M.; Organ, M. G. *Angew. Chem. Int. Ed.* **2012**, *51*, 3314-32.
- [371] Brendel, M.; Braun, C.; Rominger, F.; Hofmann, P. *Angew. Chem. Int. Ed.* **2014**, *53*, 8741-5.
- [372] Laskowski, C. A.; Bungum, D. J.; Baldwin, S. M.; Del Ciello, S. A.; Iluc, V. M.; Hillhouse, G. L. *J. Am. Chem. Soc.* **2013**, *135*, 18272-5.
- [373] Olechnowicz, F.; Hillhouse, G. L.; Jordan, R. F. *Inorg. Chem.* **2015**, *54*, 2705-12.
- [374] Harrold, N. D.; Corcos, A. R.; Hillhouse, G. L. *J. Organomet. Chem.* **2016**, *813*, 46-54.
- [375] Laskowski, C. A.; Hillhouse, G. L. *Chem. Sci.* **2011**, *2*, 321-325.
- [376] Kumar, R.; Tokura, H.; Nishimura, A.; Mori, T.; Hoshimoto, Y.; Ohashi, M.; Ogoshi, S. *Org. Lett.* **2015**, *17*, 6018-21.
- [377] Hoshimoto, Y.; Hayashi, Y.; Ohashi, M.; Ogoshi, S. *Chem. Asian J.* **2017**, *12*, 278-282.

## Appendix A: Crystallographic Data

**2.14[BAr<sup>F</sup><sub>4</sub>]:** included in the lattice is one half-molecule of water, disordered in two orientations as well as about an inversion center. As a result of this disorder the water hydrogen atoms could not be located and were thus not included in the refinement model. The missing hydrogen atoms were, however, included in the final empirical formula. Additionally, four of the six CF<sub>3</sub> groups are disordered, with rotation of the fluorine atoms about the C-C bond. In each case the disorder was modeled in two orientations in most cases this was simply the three fluorine atoms rotating about the C-C bond however in the case of the CF<sub>3</sub> group containing C43, the carbon atom is also disordered.

**2.27[BAr<sup>F</sup><sub>4</sub>]:** the material crystallizes with one half-molecule of disordered hexane in the asymmetric unit. Each disordered half-molecule is related to the second *via* inversion symmetry. In addition to the disordered hexane, significant regions containing residual electron density were located, however no reasonable model for this electron density could be found. As a result the PLATON/SQUEEZE program was used to generate a data set free of any solvent in that region.

**3.34:** The material crystallizes as a two-component 'split crystal' with components one and two related by a 4.0° rotation about the (0.517 1.00 0.021) real axis. Data were integrated for both components, including both overlapped and non-overlapped reflections. In total 143802 reflections were integrated (59924 from component one only, 59370 from component two only, 24508 overlapped). The structure was solved by direct methods using non-overlapped data from the major twin component. The material was crystallized from pentanes, with solvent molecules present and disordered over multiple sites in the asymmetric unit. Attempts to model the disorder were unsuccessful, and thus the PLATON/SQUEEZE program was used to generate a 'solvent-

free' data set, de-twinning data set. 135 electrons were removed from the unit cell, or the equivalent of roughly 3 pentane molecules. Subsequent refinements were carried out using an HKLF 5 format data set containing complete data from component one and overlaps from component 2.

**4.21:** One *t*-butyl group is disordered in two orientations, about the P2 – C21 bond. All non-hydrogen atoms were refined anisotropically. H2 and H3 were located in difference maps and refined isotropically. All other hydrogen atoms were placed in calculated positions.

**4.23:** The material crystallizes with one molecule of solvent H<sub>2</sub>O in the asymmetric unit. All non-hydrogen atoms were refined anisotropically. All O-H hydrogen atoms were located in difference maps and refined isotropically. All other hydrogen atoms were placed in calculated positions.

**4.35:** The material crystallizes with two crystallographically independent molecules in the asymmetric unit. One of the molecules is also disordered with respect to the orientation of all the atoms except for one P(*t*-Bu)<sub>2</sub> group. All non-hydrogen atoms were refined anisotropically. All hydrogen atoms were placed in calculated positions.

**4.37:** The material crystallizes with solvent benzene in the lattice. The benzene molecule resides with one half-molecule residing on a two-fold rotation axis.

**5.20:** The material crystallizes with considerable disorder. In most cases the disorder was modeled over two sites, in others three fragments were modeled and the sum of the occupancies was restrained to sum to 1.00. In some cases the SADI and EADP constraints were employed to maintain reasonable geometries and anisotropic displacement parameters.

**5.21:** One of the independent molecules in the unit cell containing Ni(2) consists of a disordered diphosphine (dtbpe) ligand fragment. In particular, disorder in the ethylene bridge was oriented in

two orientations C(51)-C(52) [58/42]. Likewise, three *t*Bu groups were also modeled in two orientations C(35): [59/41], C(43): [52/48] and finally, C(47): [62/38]. RIGU body restraints were employed on all atoms. This disorder and moderately high R1 (11.05%) value are attributed to poor crystal quality (despite numerous attempts at growing superior quality crystals).

**5.25:** This material was non-merohedral twinned and the two partially overlapping diffraction patterns were indexed separately. Refinements were carried out using an HKLF5 format data set. It is noteworthy that two level A alerts corresponding to Ni1A and Ni2A are present:

PLAT307\_ALERT\_2\_A Isolated Metal Atom (Unusual !)

These isolated metal atoms were q-peaks that were assigned as partially occupied Ni sites (with occupancies of <10% using EADP constraints). Q-peaks for the remainder of the Ni-containing molecules were not observed, due to the degree of disorder being relatively small.

**5.37:** The trifluoroacetate  $-\text{CF}_3$  groups were modeled over two positions C(2): [77/23] and C(4): [71/29]. One  $-\text{CF}_3$  group still gives an A-level checkcif alert due to large ADP max/min ratios. RIGU body restraints were employed on all atoms.

**Table A1** Crystallographic data for **2.14[BAr<sup>F</sup><sub>4</sub>]** and **2.27[BAr<sup>F</sup><sub>4</sub>]**.

Compound	<b>2.14[BAr<sup>F</sup><sub>4</sub>]</b>	<b>2.27[BAr<sup>F</sup><sub>4</sub>]</b>
Empirical formula	C <sub>60</sub> H <sub>45</sub> BF <sub>24</sub> N <sub>4</sub> O <sub>5,5</sub> Rh	C <sub>56</sub> H <sub>43</sub> BF <sub>24</sub> N <sub>4</sub> O <sub>2</sub> Rh
Formula weight	1479.72	1373.66
Temperature/K	90(2)	100(2)
Crystal system	triclinic	triclinic
Space group	P-1	P-1
a/Å	9.5642(13)	9.7614(11)
b/Å	18.249(2)	17.681(2)
c/Å	19.551(3)	18.517(2)
α/°	116.345(3)	65.050(6)
β/°	96.706(4)	85.142(6)
γ/°	91.811(4)	75.089(6)
V/Å <sup>3</sup>	3023.8(7)	2799.0(6)
Z	2	2
ρ/ g/cm <sup>-3</sup>	1.625	1.630
μ/ mm <sup>-1</sup>	0.411	0.432
F(000)	1486.0	1378.0
Crystal size/ mm <sup>3</sup>	0.570 × 0.270 × 0.110	0.23 × 0.16 × 0.09
Radiation	MoKα (λ = 0.71073)	MoKα (λ = 0.71073)
2θ range for data collection/°	4.7 to 56.908	2.426 to 56.788
Index ranges	-12 ≤ h ≤ 12, -24 ≤ k ≤ 24, -26 ≤ l ≤ 26	-12 ≤ h ≤ 12, -24 ≤ k ≤ 24, -26 ≤ l ≤ 26
Independent reflections	15109 [R <sub>int</sub> = 0.0539, R <sub>sigma</sub> = 0.0489]	13918 [R <sub>int</sub> = ?, R <sub>sigma</sub> = 0.0610]
Data/restraints/parameters	15109/1746/986	13918/1426/861
Goodness-of-fit on F <sup>2</sup>	1.033	1.106
R [I ≥ 2θ (I)] (R <sub>1</sub> , wR <sub>2</sub> )	R <sub>1</sub> = 0.0474, wR <sub>2</sub> = 0.1183	R <sub>1</sub> = 0.0708, wR <sub>2</sub> = 0.1414
R (all data) (R <sub>1</sub> , wR <sub>2</sub> )	R <sub>1</sub> = 0.0593, wR <sub>2</sub> = 0.1242	R <sub>1</sub> = 0.1052, wR <sub>2</sub> = 0.1513
Largest diff. peak/hole / (e Å <sup>-3</sup> )	1.34/-1.52	2.19/-1.44

$$R_1 = \frac{\sum ||F_o| - |F_c||}{\sum |F_o|}; wR_2 = \left[ \frac{\sum (w(F_o^2 - F_c^2)^2)}{\sum w(F_o^2)^2} \right]^{1/2}$$

**Table A2** Crystallographic data for **3.22**, **3.23** and **3.24**

Compound	<b>3.22</b>	<b>3.23</b>	<b>3.24</b>
Empirical formula	C <sub>19</sub> H <sub>42</sub> Cl <sub>2</sub> NiP <sub>2</sub>	C <sub>26</sub> H <sub>48</sub> NiOP <sub>2</sub>	C <sub>26</sub> H <sub>48</sub> NiOP <sub>2</sub>
Formula weight	462.07	497.29	497.29
Temperature/K	90(2)	90(2)	100(2)
Crystal system	triclinic	Monoclinic	Triclinic
Space group	<i>P1</i>	<i>P2<sub>1</sub>/c</i>	<i>P-1</i>
a/Å	8.9572(5)	10.362(2)	11.052(2)
b/Å	11.0247(6)	18.079(4)	16.462(4)
c/Å	12.861(7)	15.092(3)	16.470(4)
α/°	87.662(4)	90	101.828(6)
β/°	89.449(4)	103.086(3)	96.795(7)
γ/°	67.075(4)	90	107.865(7)
V/Å <sup>3</sup>	1168.7(6)	2753.9(10)	2738.1(10)
Z	2	4	4
ρ/ g/cm <sup>-3</sup>	1.313	1.199	1.206
μ/ mm <sup>-1</sup>	4.575	0.835	0.840
F(000)	496.0	1080.0	1080.0
Crystal size/ mm <sup>3</sup>	0.19 × 0.05 × 0.02	0.36 × 0.24 × 0.08	0.3 × 0.23 × 0.06
Radiation	CuKα (λ = 1.54178)	MoKα (λ = 0.71073)	MoKα (λ = 0.71073)
2θ range for data collection/°	6.878 to 114.11	3.57 to 60.436	4.172 to 60.17
Index ranges	-9 ≤ h ≤ 9, -11 ≤ k ≤ 11, -13 ≤ l ≤ 13	-14 ≤ h ≤ 14, -25 ≤ k ≤ 25, -21 ≤ l ≤ 21	-15 ≤ h ≤ 15, -20 ≤ k ≤ 23, -23 ≤ l ≤ 21
Independent reflections	5789 [R <sub>int</sub> = 0.0605, R <sub>sigma</sub> = 0.0760]	8106 [R <sub>int</sub> = 0.0523, R <sub>sigma</sub> = 0.0489]	15294 [R <sub>int</sub> = 0.0435, R <sub>sigma</sub> = 0.0520]
Data/restraints/parameters	5789/417/457	8106/258/287	15294/0/567
Goodness-of-fit on F <sup>2</sup>	1.057	1.068	1.009
R [I>=2θ (I)] (R1, wR2)	R <sub>1</sub> = 0.0552, wR <sub>2</sub> = 0.1364	R <sub>1</sub> = 0.0514, wR <sub>2</sub> = 0.1133	R <sub>1</sub> = 0.0368, wR <sub>2</sub> = 0.0772
R (all data) (R1, wR2)	R <sub>1</sub> = 0.0648, wR <sub>2</sub> = 0.1432	R <sub>1</sub> = 0.0733, wR <sub>2</sub> = 0.1237	R <sub>1</sub> = 0.0649, wR <sub>2</sub> = 0.0878
Largest diff. peak/hole / (e Å <sup>-3</sup> )	0.72/-0.39	1.62/-0.59	0.66/-0.43

$$R1 = \frac{\sum ||F_o| - |F_c||}{\sum |F_o|}; wR2 = \left[ \frac{\sum (w(F_o^2 - F_c^2)^2)}{\sum w(F_o^2)^2} \right]^{1/2}$$

**Table A3** Crystallographic data for **3.26**, **3.29** and **3.30**

Compound	<b>3.26</b>	<b>3.29</b>	<b>3.30</b>
Empirical formula	C <sub>37</sub> H <sub>64</sub> NiOP <sub>2</sub>	C <sub>27</sub> H <sub>50</sub> NiOP <sub>2</sub>	C <sub>46</sub> H <sub>64</sub> NiO <sub>2</sub> P <sub>2</sub>
Formula weight	645.53	511.32	769.62
Temperature/K	90(2)	90(2)	90(2)
Crystal system	Monoclinic	Triclinic	Triclinic
Space group	<i>P</i> 2 <sub>1</sub> / <i>n</i>	<i>P</i> -1	<i>P</i> -1
<i>a</i> /Å	11.1033(8)	8.1301(5)	12.5155(6)
<i>b</i> /Å	19.8882(15)	11.2513(7)	13.4517(6)
<i>c</i> /Å	16.7137(13)	16.1662(11)	14.9812(7)
$\alpha$ /°	90	78.3890(10)	71.1380(10)
$\beta$ /°	98.369(2)	76.4770(10)	67.3550(10)
$\gamma$ /°	90	79.5650(10)	67.1180(10)
<i>V</i> /Å <sup>3</sup>	3651.5(5)	1394.35(15)	2099.38(17)
<i>Z</i>	4	2	2
$\rho$ / g/cm <sup>-3</sup>	1.174	1.218	1.217
$\mu$ / mm <sup>-1</sup>	0.645	0.827	0.574
<i>F</i> (000)	1408.0	556.0	828.0
Crystal size/ mm <sup>3</sup>	0.32 × 0.22 × 0.12	0.25 × 0.18 × 0.12	0.44 × 0.23 × 0.18
Radiation	MoK $\alpha$ ( $\lambda$ = 0.71073)	MoK $\alpha$ ( $\lambda$ = 0.71073)	MoK $\alpha$ ( $\lambda$ = 0.71073)
2 $\theta$ range for data collection/°	3.204 to 58.336	2.628 to 58.28	3.008 to 58.398
Index ranges	-15 ≤ <i>h</i> ≤ 14, -27 ≤ <i>k</i> ≤ 24, -22 ≤ <i>l</i> ≤ 22	-11 ≤ <i>h</i> ≤ 11, -15 ≤ <i>k</i> ≤ 15, -22 ≤ <i>l</i> ≤ 22	-17 ≤ <i>h</i> ≤ 17, -18 ≤ <i>k</i> ≤ 9, - 20 ≤ <i>l</i> ≤ 20
Independent reflections	9848 [R <sub>int</sub> = 0.0335, R <sub>sigma</sub> = 0.0293]	7514 [R <sub>int</sub> = 0.0185, R <sub>sigma</sub> = 0.0174]	11020 [R <sub>int</sub> = 0.0224, R <sub>sigma</sub> = 0.0353]
Data/restraints/parameters	9848/0/384	7514/0/293	11020/0/476
Goodness-of-fit on <i>F</i> <sup>2</sup>	1.047	1.041	1.024
R [ <i>I</i> ≥ 2 $\theta$ ( <i>I</i> )] (R <sub>1</sub> , wR <sub>2</sub> )	R <sub>1</sub> = 0.0288, wR <sub>2</sub> = 0.0656	R <sub>1</sub> = 0.0233, wR <sub>2</sub> = 0.0557	R <sub>1</sub> = 0.0354, wR <sub>2</sub> = 0.0826
R (all data) (R <sub>1</sub> , wR <sub>2</sub> )	R <sub>1</sub> = 0.0373, wR <sub>2</sub> = 0.0692	R <sub>1</sub> = 0.0270, wR <sub>2</sub> = 0.0585	R <sub>1</sub> = 0.0471, wR <sub>2</sub> = 0.0894
Largest diff. peak/hole / (e Å <sup>-3</sup> )	0.41/-0.23	0.47/-0.29	0.76/-0.33

$$R_1 = \frac{\sum ||F_o| - |F_c||}{\sum |F_o|}; wR_2 = \left[ \frac{\sum (w(F_o^2 - F_c^2)^2)}{\sum w(F_o^2)^2} \right]^{1/2}$$

**Table A4** Crystallographic data for **3.34**, **3.37** and **3.53**

Compound	<b>3.34</b>	<b>3.37</b>	<b>3.53</b>
Empirical formula	C <sub>34</sub> H <sub>56</sub> NiOP <sub>2</sub>	C <sub>34</sub> H <sub>56</sub> NiO <sub>2</sub> P <sub>2</sub>	C <sub>32</sub> H <sub>53</sub> NNiO <sub>2</sub> P <sub>2</sub> S
Formula weight	601.43	617.43	636.46
Temperature/K	90(2)	90(2)	90(2)
Crystal system	Triclinic	Monoclinic	monoclinic
Space group	<i>P</i> -1	<i>P</i> 2 <sub>1</sub> / <i>n</i>	Cc
<i>a</i> /Å	12.4215(9)	9.2927(3)	15.205(2)
<i>b</i> /Å	14.5174(11)	19.0278(7)	16.403(3)
<i>c</i> /Å	23.7123(17)	19.4186(7)	13.947(2)
$\alpha$ /°	98.580(2)	90	90
$\beta$ /°	94.124(2)	96.536(2)	102.508(5)
$\gamma$ /°	114.652(2)	90	90
<i>V</i> /Å <sup>3</sup>	3799.7(5)	3411.3(2)	3396.0(9)
<i>Z</i>	4	4	4
$\rho$ /g/cm <sup>-3</sup>	1.051	1.202	1.245
$\mu$ /mm <sup>-1</sup>	0.616	0.690	0.755
<i>F</i> (000)	1304.0	1336.0	1368.0
Crystal size/mm <sup>3</sup>	0.10 × 0.12 × 0.24	0.48 × 0.33 × 0.2	0.27 × 0.18 × 0.12
Radiation	MoK $\alpha$ ( $\lambda$ = 0.71073)	MoK $\alpha$ ( $\lambda$ = 0.71073)	MoK $\alpha$ ( $\lambda$ = 0.71073)
2 $\theta$ range for data collection/°	3.148 to 61.108	3.006 to 58.332	3.7 to 60.156
Index ranges	-17 ≤ <i>h</i> ≤ 17, -20 ≤ <i>k</i> ≤ 20, 0 ≤ <i>l</i> ≤ 33	-12 ≤ <i>h</i> ≤ 11, -21 ≤ <i>k</i> ≤ 26, -25 ≤ <i>l</i> ≤ 26	-21 ≤ <i>h</i> ≤ 19, -23 ≤ <i>k</i> ≤ 22, -19 ≤ <i>l</i> ≤ 19
Independent reflections	23295 [R <sub>int</sub> = 0.042, R <sub>sigma</sub> = 0.0307]	7382 [R <sub>int</sub> = 0.0307, R <sub>sigma</sub> = 0.0503]	7937 [R <sub>int</sub> = 0.0472, R <sub>sigma</sub> = 0.0597]
Data/restraints/parameters	23295/672/712	7382/0/366	7937/2/365
Goodness-of-fit on <i>F</i> <sup>2</sup>	1.05	1.009	1.000
R [ <i>I</i> ≥ 2 $\theta$ ( <i>I</i> )] (R <sub>1</sub> , wR <sub>2</sub> )	R <sub>1</sub> = 0.038, wR <sub>2</sub> = 0.099	R <sub>1</sub> = 0.0372, wR <sub>2</sub> = 0.0796	R <sub>1</sub> = 0.0361, wR <sub>2</sub> = 0.0756
R (all data) (R <sub>1</sub> , wR <sub>2</sub> )	R <sub>1</sub> = 0.049, wR <sub>2</sub> = 0.104	R <sub>1</sub> = 0.0564, wR <sub>2</sub> = 0.0870	R <sub>1</sub> = 0.0449, wR <sub>2</sub> = 0.0790
Largest diff. peak/hole / (e Å <sup>-3</sup> )	0.64/-0.37	0.48/-0.27	0.87/-0.38

$$R_1 = \Sigma ||F_o| - |F_c|| / \Sigma |F_o|; wR_2 = [\Sigma(w(F_o^2 - F_c^2)^2) / \Sigma w(F_o^2)^2]^{1/2}$$

**Table A5** Crystallographic data for **3.54**, **3.57** and **3.62**

Compound	<b>3.54</b>	<b>3.57</b>	<b>3.62</b>
Empirical formula	C <sub>25</sub> H <sub>46</sub> NiOP <sub>2</sub>	C <sub>25</sub> H <sub>48</sub> NNiO <sub>2</sub> P <sub>2</sub> S	C <sub>35</sub> H <sub>61</sub> NNiOP <sub>2</sub>
Formula weight	483.27	547.37	632.52
Temperature/K	90(2)	90(2)	90(2)
Crystal system	monoclinic	monoclinic	monoclinic
Space group	<i>P2<sub>1</sub>/c</i>	<i>P2<sub>1</sub>/n</i>	<i>P2<sub>1</sub>/n</i>
<i>a</i> /Å	15.728(3)	9.3856(15)	11.3153(15)
<i>b</i> /Å	20.763(4)	21.845(3)	17.650(2)
<i>c</i> /Å	16.376(3)	14.090(2)	17.536(2)
$\alpha$ /°	90	90	90
$\beta$ /°	96.899(4)	98.119(4)	103.453(3)
$\gamma$ /°	90	90	90
<i>V</i> /Å <sup>3</sup>	5309.3(18)	2859.9(8)	3406.0(8)
<i>Z</i>	8	4	4
$\rho$ / g/cm <sup>-3</sup>	1.209	1.2712	1.2334
$\mu$ / mm <sup>-1</sup>	0.865	0.884	0.691
<i>F</i> (000)	2096.0	1183.1	1378.6
Crystal size/ mm <sup>3</sup>	0.25 × 0.18 × 0.09	0.19 × 0.13 × 0.1	0.24 × 0.16 × 0.11
Radiation	MoK $\alpha$ ( $\lambda$ = 0.71073)	Mo K $\alpha$ ( $\lambda$ = 0.71073)	Mo K $\alpha$ ( $\lambda$ = 0.71073)
2 $\theta$ range for data collection/°	2.608 to 60.334	3.46 to 58.22	3.32 to 58.42
Index ranges	-22 ≤ <i>h</i> ≤ 22, -28 ≤ <i>k</i> ≤ 29, -23 ≤ <i>l</i> ≤ 23	-6 ≤ <i>h</i> ≤ 12, -29 ≤ <i>k</i> ≤ 29, - 19 ≤ <i>l</i> ≤ 19	-15 ≤ <i>h</i> ≤ 15, -23 ≤ <i>k</i> ≤ 24, -14 ≤ <i>l</i> ≤ 24
Independent reflections	15653 [ <i>R</i> <sub>int</sub> = 0.0489, <i>R</i> <sub>sigma</sub> = 0.0363]	7688 [ <i>R</i> <sub>int</sub> = 0.0356, <i>R</i> <sub>sigma</sub> = 0.0316]	9175 [ <i>R</i> <sub>int</sub> = 0.0415, <i>R</i> <sub>sigma</sub> = 0.0374]
Data/restraints/parameters	15653/0/555	7688/0/305	9175/0/376
Goodness-of-fit on <i>F</i> <sup>2</sup>	1.012	0.804	1.025
<i>R</i> [ <i>I</i> ≥ 2 $\theta$ ( <i>I</i> )] ( <i>R</i> <sub>1</sub> , <i>wR</i> <sub>2</sub> )	<i>R</i> <sub>1</sub> = 0.0330, <i>wR</i> <sub>2</sub> = 0.0799	<i>R</i> <sub>1</sub> = 0.0262, <i>wR</i> <sub>2</sub> = 0.0925	<i>R</i> <sub>1</sub> = 0.0359, <i>wR</i> <sub>2</sub> = 0.0859
<i>R</i> (all data) ( <i>R</i> <sub>1</sub> , <i>wR</i> <sub>2</sub> )	<i>R</i> <sub>1</sub> = 0.0464, <i>wR</i> <sub>2</sub> = 0.0863	<i>R</i> <sub>1</sub> = 0.0318, <i>wR</i> <sub>2</sub> = 0.1002	<i>R</i> <sub>1</sub> = 0.0488, <i>wR</i> <sub>2</sub> = 0.0927
Largest diff. peak/hole / (e Å <sup>-3</sup> )	1.94/-0.71	0.48/-0.41	1.39/-0.36

$$R1 = \Sigma ||F_o| - |F_c|| / \Sigma |F_o|; wR2 = [\Sigma(w(F_o^2 - F_c^2)^2) / \Sigma w(F_o^2)]^{1/2}$$

**Table A6** Crystallographic data for **4.21**, **4.23** and **4.28**

Compound	<b>4.21</b>	<b>4.23</b>	<b>4.28</b>
Empirical formula	C <sub>24</sub> H <sub>48</sub> NiO <sub>2</sub> P <sub>2</sub>	C <sub>24</sub> H <sub>52</sub> NiO <sub>2</sub> P <sub>2</sub>	C <sub>25</sub> H <sub>50</sub> NiO <sub>2</sub> P <sub>2</sub>
Formula weight	489.27	493.30	503.30
Temperature/K	90(2)	100(2)	90(2)
Crystal system	monoclinic	monoclinic	monoclinic
Space group	P2 <sub>1</sub> /n	P2 <sub>1</sub> /c	P2 <sub>1</sub> /c
a/Å	10.4190(7)	11.1398(8)	16.124(3)
b/Å	21.2112(14)	16.7554(12)	8.7411(16)
c/Å	11.8560(9)	15.4593(11)	19.627(4)
α/°	90	90	90
β/°	95.930(2)	110.118(2)	103.322(4)
γ/°	90	90	90
V/Å <sup>3</sup>	2606.1(3)	2709.4(3)	2691.7(8)
Z	4	4	4
ρ/ g/cm <sup>-3</sup>	1.247	1.209	1.242
μ/ mm <sup>-1</sup>	0.884	0.851	0.858
F(000)	1064.0	1080.0	1096.0
Crystal size/ mm <sup>3</sup>	0.18 × 0.17 × 0.06	0.36 × 0.13 × 0.08	0.07 × 0.20 × 0.28
Radiation	MoKα (λ = 0.71073)	MoKα (λ = 0.71073)	MoKα (λ = 0.71073)
2θ range for data collection/°	3.84 to 60.132	3.712 to 60.234	4.266 to 60.11
Index ranges	-14 ≤ h ≤ 14, -29 ≤ k ≤ 29, -16 ≤ l ≤ 16	-15 ≤ h ≤ 15, -23 ≤ k ≤ 19, -21 ≤ l ≤ 19	-20 ≤ h ≤ 22, -12 ≤ k ≤ 12, -27 ≤ l ≤ 27
Independent reflections	7634 [R <sub>int</sub> = 0.0404, R <sub>sigma</sub> = 0.0351]	7936 [R <sub>int</sub> = 0.0464, R <sub>sigma</sub> = 0.0441]	7888 [R <sub>int</sub> = 0.0441, R <sub>sigma</sub> = 0.0425]
Data/restraints/parameters	7634/324/313	7936/0/282	7888/0/284
Goodness-of-fit on F <sup>2</sup>	1.022	1.019	1.015
R [I>=2θ (I)] (R1, wR2)	R <sub>1</sub> = 0.0332, wR <sub>2</sub> = 0.0768	R <sub>1</sub> = 0.0313, wR <sub>2</sub> = 0.0687	R <sub>1</sub> = 0.0332, wR <sub>2</sub> = 0.0703
R (all data) (R1, wR2)	R <sub>1</sub> = 0.0482, wR <sub>2</sub> = 0.0831	R <sub>1</sub> = 0.0470, wR <sub>2</sub> = 0.0746	R <sub>1</sub> = 0.0522, wR <sub>2</sub> = 0.0768
Largest diff. peak/hole / (e Å <sup>-3</sup> )	0.55/-0.34	0.44/-0.32	0.81/-0.32

$$R1 = \sum ||F_o| - |F_c|| / \sum |F_o|; wR2 = [\sum (w(F_o^2 - F_c^2)^2) / \sum w(F_o^2)^2]^{1/2}$$

**Table A7** Crystallographic data for **4.35**, **4.38** and **4.44/4.45**

Compound	<b>4.35</b>	<b>4.37</b>	<b>4.44/4.45</b>
Empirical formula	C <sub>24</sub> H <sub>48</sub> NiOP <sub>2</sub>	C <sub>28</sub> H <sub>49</sub> NiO <sub>3</sub> P <sub>2</sub>	C <sub>74</sub> H <sub>144</sub> Ni <sub>3</sub> O <sub>6</sub> P <sub>6</sub>
Formula weight	473.27	557.34	1491.83
Temperature/K	100(2)	90(2)	90(2)
Crystal system	monoclinic	orthorhombic	triclinic
Space group	P2 <sub>1</sub> /n	Pbcn	P-1
a/Å	16.0749(15)	15.5113(17)	11.2511(5)
b/Å	20.0552(17)	21.773(2)	18.2996(8)
c/Å	16.1820(13)	17.3548(19)	21.9366(11)
α/°	90	90	90.897(3)
β/°	102.859(3)	90	104.140(2)
γ/°	90	90	101.716(2)
V/Å <sup>3</sup>	5086.0(8)	5861.1(11)	4278.3(3)
Z	8	8	2
ρ/g/cm <sup>-3</sup>	1.236	1.263	1.158
μ/mm <sup>-1</sup>	0.901	0.797	2.157
F(000)	2064.0	2392.0	1620.0
Crystal size/mm <sup>3</sup>	0.5 × 0.5 × 0.43	0.20 × 0.11 × 0.02	0.12 × 0.08 × 0.05
Radiation	MoKα (λ = 0.71073)	MoKα (λ = 0.71073)	CuKα (λ = 1.54178)
2θ range for data collection/°	3.23 to 57.096	3.224 to 45.064	4.164 to 115.938
Index ranges	-21 ≤ h ≤ 20, -26 ≤ k ≤ 26, -21 ≤ l ≤ 21	-12 ≤ h ≤ 16, -23 ≤ k ≤ 23, -18 ≤ l ≤ 17	-12 ≤ h ≤ 11, -20 ≤ k ≤ 20, -24 ≤ l ≤ 24
Independent reflections	12890 [R <sub>int</sub> = 0.0321, R <sub>sigma</sub> = 0.0367]	3853 [R <sub>int</sub> = 0.1026, R <sub>sigma</sub> = 0.0688]	11463 [R <sub>int</sub> = 0.0617, R <sub>sigma</sub> = 0.1003]
Data/restraints/parameters	12890/684/689	3853/307/320	11463/810/838
Goodness-of-fit on F <sup>2</sup>	1.061	1.115	1.050
R [I>=2θ (I)] (R1, wR2)	R <sub>1</sub> = 0.0450, wR <sub>2</sub> = 0.0908	R <sub>1</sub> = 0.0827, wR <sub>2</sub> = 0.1937	R <sub>1</sub> = 0.0897, wR <sub>2</sub> = 0.2588
R (all data) (R1, wR2)	R <sub>1</sub> = 0.0683, wR <sub>2</sub> = 0.1017	R <sub>1</sub> = 0.1292, wR <sub>2</sub> = 0.2166	R <sub>1</sub> = 0.1189, wR <sub>2</sub> = 0.2853
Largest diff. peak/hole / (e Å <sup>-3</sup> )	0.86/-0.81	1.14/-0.49	1.04/-0.65

$$R1 = \Sigma ||F_o| - |F_c|| / \Sigma |F_o|; wR2 = [\Sigma(w(F_o^2 - F_c^2)^2) / \Sigma w(F_o^2)]^{1/2}$$

**Table A8** Crystallographic data for **4.46**.

Compound	<b>4.46</b>
Empirical formula	C <sub>31</sub> H <sub>53</sub> NiO <sub>4</sub> P <sub>2</sub>
Formula weight	610.38
Temperature/K	90(2)
Crystal system	monoclinic
Space group	P2 <sub>1</sub> /n
a/Å	16.768(2)
b/Å	21.219(3)
c/Å	18.794(3)
α/°	90
β/°	106.254(8)
γ/°	90
V/Å <sup>3</sup>	6419.8(15)
Z	8
ρ/g/cm <sup>-3</sup>	1.263
μ/mm <sup>-1</sup>	2.063
F(000)	2632.0
Crystal size/mm <sup>3</sup>	0.23 × 0.05 × 0.04
Radiation	CuKα (λ = 1.54178)
2θ range for data collection/°	6.43 to 114.3
Index ranges	-6 ≤ h ≤ 18, -23 ≤ k ≤ 22, - 20 ≤ l ≤ 20
Independent reflections	8541 [R <sub>int</sub> = 0.0714, R <sub>sigma</sub> = 0.0776]
Data/restraints/parameters	8541/678/704
Goodness-of-fit on F <sup>2</sup>	1.015
R [I >= 2θ (I)] (R1, wR2)	R <sub>1</sub> = 0.0483, wR <sub>2</sub> = 0.1023
R (all data) (R1, wR2)	R <sub>1</sub> = 0.0871, wR <sub>2</sub> = 0.1192
Largest diff. peak/hole / (e Å <sup>-3</sup> )	0.71/-0.31

$$R1 = \frac{\sum ||F_o| - |F_c||}{\sum |F_o|}; wR2 = \left[ \frac{\sum (w(F_o^2 - F_c^2)^2)}{\sum w(F_o^2)^2} \right]^{1/2}$$

**Table A9** Crystallographic data for **5.17**, **5.20** and **5.21**.

Compound	<b>5.17</b>	<b>5.20</b>	<b>5.21</b>
Empirical formula	C <sub>27</sub> H <sub>47</sub> F <sub>3</sub> NiOP <sub>2</sub>	C <sub>22.02</sub> H <sub>45.04</sub> F <sub>3</sub> NiOP <sub>2</sub> S	C <sub>26</sub> H <sub>45</sub> F <sub>3</sub> NiOP <sub>2</sub> S
Formula weight	565.29	535.59	583.33
Temperature/K	90(2)	90(2)	90(2)
Crystal system	Monoclinic	Tetragonal	Orthorhombic
Space group	<i>P</i> 2 <sub>1</sub> / <i>n</i>	<i>P</i> 4 <sub>2</sub> / <i>n</i>	<i>Pbca</i>
<i>a</i> /Å	19.063(4)	22.854(6)	18.882(2)
<i>b</i> /Å	16.461(3)	22.854(6)	15.801(2)
<i>c</i> /Å	20.536(4)	10.245(3)	39.081(5)
$\alpha$ /°	90	90	90
$\beta$ /°	114.500(4)	90	90
$\gamma$ /°	90	90	90
<i>V</i> /Å <sup>3</sup>	5864(2)	5351(3)	11660(2)
<i>Z</i>	8	8	16
$\rho$ / g/cm <sup>-3</sup>	1.281	1.330	1.329
$\mu$ / mm <sup>-1</sup>	0.807	0.955	0.883
<i>F</i> (000)	2416.0	2289.0	4960.0
Crystal size/ mm <sup>3</sup>	0.28 × 0.13 × 0.10	0.25 × 0.05 × 0.04	0.36 × 0.29 × 0.12
Radiation	MoK $\alpha$ ( $\lambda$ = 0.71073)	MoK $\alpha$ ( $\lambda$ = 0.71073)	MoK $\alpha$ ( $\lambda$ = 0.71073)
2 $\theta$ range for data collection/°	3.298 to 60.196	3.564 to 55.644	3 to 50.858
Index ranges	-26 ≤ <i>h</i> ≤ 26, -23 ≤ <i>k</i> ≤ 23, -28 ≤ <i>l</i> ≤ 26	-30 ≤ <i>h</i> ≤ 29, -30 ≤ <i>k</i> ≤ 29, -13 ≤ <i>l</i> ≤ 13	-22 ≤ <i>h</i> ≤ 22, -18 ≤ <i>k</i> ≤ 19, -47 ≤ <i>l</i> ≤ 47
Independent reflections	17187 [R <sub>int</sub> = 0.0468, R <sub>sigma</sub> = 0.0417]	6354 [R <sub>int</sub> = 0.0608, R <sub>sigma</sub> = 0.0248]	10702 [R <sub>int</sub> = 0.0936, R <sub>sigma</sub> = 0.0346]
Data/restraints/parameters	17187/0/639	6354/552/525	10702/708/739
Goodness-of-fit on <i>F</i> <sup>2</sup>	1.008	1.031	1.129
R [ <i>I</i> ≥ 2 $\theta$ ( <i>I</i> )] (R <sub>1</sub> , wR <sub>2</sub> )	R <sub>1</sub> = 0.0341, wR <sub>2</sub> = 0.0817	R <sub>1</sub> = 0.0328, wR <sub>2</sub> = 0.0754	R <sub>1</sub> = 0.1105, wR <sub>2</sub> = 0.2740
R (all data) (R <sub>1</sub> , wR <sub>2</sub> )	R <sub>1</sub> = 0.0525, wR <sub>2</sub> = 0.0912	R <sub>1</sub> = 0.0512, wR <sub>2</sub> = 0.0858	R <sub>1</sub> = 0.1269, wR <sub>2</sub> = 0.2865
Largest diff. peak/hole / (e Å <sup>-3</sup> )	0.91/-0.36	0.47/-0.39	2.62/-1.19

$$R1 = \frac{\sum ||F_o| - |F_c||}{\sum |F_o|}; wR2 = \left[ \frac{\sum (w(F_o^2 - F_c^2)^2)}{\sum w(F_o^2)} \right]^{1/2}$$

**Table A10** Crystallographic data for **5.24**, **5.25** and **5.27**.

Compound	<b>5.24</b>	<b>5.25</b>	<b>5.27</b>
Empirical formula	C <sub>21</sub> H <sub>48</sub> NiP <sub>2</sub> S	C <sub>25</sub> H <sub>48</sub> P <sub>2</sub> SNi	C <sub>22</sub> H <sub>50</sub> NiP <sub>2</sub> S <sub>2</sub>
Formula weight	453.30	501.34	499.39
Temperature/K	90(2)	90(2)	90(2)
Crystal system	Monoclinic	Triclinic	Monoclinic
Space group	<i>P2<sub>1</sub>/n</i>	<i>P-1</i>	<i>P2<sub>1</sub>/n</i>
<i>a</i> /Å	8.8670(16)	11.3578(9)	8.5261(6)
<i>b</i> /Å	19.924(4)	15.7134(13)	15.5496(11)
<i>c</i> /Å	13.866(3)	16.3475(13)	20.1936(13)
$\alpha$ /°	90	68.824(2)	90
$\beta$ /°	97.386(3)	80.825(2)	96.1010(10)
$\gamma$ /°	90	84.268(2)	90
<i>V</i> /Å <sup>3</sup>	2429.4(8)	2682.9(4)	2662.1(3)
<i>Z</i>	4	4	4
$\rho$ / g/cm <sup>-3</sup>	1.239	1.241	1.246
$\mu$ / mm <sup>-1</sup>	1.020	0.930	1.012
<i>F</i> (000)	992.0	1088.0	1088.0
Crystal size/ mm <sup>3</sup>	0.52 × 0.28 × 0.24	0.23 × 0.15 × 0.08	0.32 × 0.24 × 0.24
Radiation	MoK $\alpha$ ( $\lambda$ = 0.71073)	MoK $\alpha$ ( $\lambda$ = 0.71073)	MoK $\alpha$ ( $\lambda$ = 0.71073)
2 $\theta$ range for data collection/°	3.598 to 58.54	2.696 to 58.266	3.312 to 54.986
Index ranges	-12 ≤ <i>h</i> ≤ 12, -26 ≤ <i>k</i> ≤ 27, -18 ≤ <i>l</i> ≤ 18	-15 ≤ <i>h</i> ≤ 15, -19 ≤ <i>k</i> ≤ 21, 0 ≤ <i>l</i> ≤ 22	-11 ≤ <i>h</i> ≤ 11, -20 ≤ <i>k</i> ≤ 20, -26 ≤ <i>l</i> ≤ 26
Independent reflections	6548 [ <i>R</i> <sub>int</sub> = 0.0411, <i>R</i> <sub>sigma</sub> = 0.0402]	14252 [ <i>R</i> <sub>sigma</sub> = 0.0518]	6084 [ <i>R</i> <sub>int</sub> = 0.0192, <i>R</i> <sub>sigma</sub> = 0.0157]
Data/restraints/parameters	6548/0/240	14252/0/558	6084/0/258
Goodness-of-fit on <i>F</i> <sup>2</sup>	1.195	1.085	1.069
<i>R</i> [ <i>I</i> ≥ 2 $\theta$ ( <i>I</i> )] ( <i>R</i> <sub>1</sub> , <i>wR</i> <sub>2</sub> )	<i>R</i> <sub>1</sub> = 0.0508, <i>wR</i> <sub>2</sub> = 0.1495	<i>R</i> <sub>1</sub> = 0.0562, <i>wR</i> <sub>2</sub> = 0.1309	<i>R</i> <sub>1</sub> = 0.0196, <i>wR</i> <sub>2</sub> = 0.0471
<i>R</i> (all data) ( <i>R</i> <sub>1</sub> , <i>wR</i> <sub>2</sub> )	<i>R</i> <sub>1</sub> = 0.0668, <i>wR</i> <sub>2</sub> = 0.1618	<i>R</i> <sub>1</sub> = 0.0757, <i>wR</i> <sub>2</sub> = 0.1397	<i>R</i> <sub>1</sub> = 0.0232, <i>wR</i> <sub>2</sub> = 0.0510
Largest diff. peak/hole / (e Å <sup>-3</sup> )	2.39/-0.84	1.45/-1.01	0.39/-0.18

$$R1 = \sum ||F_o| - |F_c|| / \sum |F_o|; wR2 = [\sum(w(F_o^2 - F_c^2)^2) / \sum w(F_o^2)]^{1/2}$$

**Table A11** Crystallographic data for **5.30**, **5.35** and **5.37**.

Compound	<b>5.30</b>	<b>5.35</b>	<b>5.37</b>
Empirical formula	C <sub>22</sub> H <sub>45</sub> F <sub>3</sub> NiO <sub>2</sub> P <sub>2</sub>	C <sub>26</sub> H <sub>48</sub> NiO <sub>2</sub> P <sub>2</sub>	C <sub>22</sub> H <sub>40</sub> F <sub>6</sub> NiO <sub>4</sub> P <sub>2</sub>
Formula weight	519.23	513.29	603.19
Temperature/K	90(2)	90(2)	90(2)
Crystal system	Monoclinic	Monoclinic	Monoclinic
Space group	<i>P2<sub>1</sub>/n</i>	<i>C2/c</i>	<i>P2<sub>1</sub>/n</i>
<i>a</i> /Å	16.4020(11)	23.532(3)	8.6157(9)
<i>b</i> /Å	19.6669(13)	23.545(3)	16.2943(17)
<i>c</i> /Å	16.8982(11)	40.359(5)	20.128(2)
$\alpha$ /°	90	90	90
$\beta$ /°	104.942(2)	98.465(4)	92.248(2)
$\gamma$ /°	90	90	90
<i>V</i> /Å <sup>3</sup>	5266.6(6)	22117(4)	2823.6(5)
<i>Z</i>	8	32	4
$\rho$ / g/cm <sup>-3</sup>	1.310	1.233	1.419
$\mu$ / mm <sup>-1</sup>	0.895	0.837	0.865
<i>F</i> (000)	2224.0	8896.0	1264.0
Crystal size/ mm <sup>3</sup>	0.4 × 0.27 × 0.21	0.24 × 0.15 × 0.11	0.31 × 0.26 × 0.14
Radiation	MoK $\alpha$ ( $\lambda$ = 0.71073)	MoK $\alpha$ ( $\lambda$ = 0.71073)	MoK $\alpha$ ( $\lambda$ = 0.71073)
2 $\theta$ range for data collection/°	3.086 to 58.426	2.04 to 52.878	3.216 to 61.076
Index ranges	-22 ≤ <i>h</i> ≤ 22, -17 ≤ <i>k</i> ≤ 26, -23 ≤ <i>l</i> ≤ 23	-29 ≤ <i>h</i> ≤ 17, -29 ≤ <i>k</i> ≤ 29, -50 ≤ <i>l</i> ≤ 50	-12 ≤ <i>h</i> ≤ 12, -23 ≤ <i>k</i> ≤ 23, -28 ≤ <i>l</i> ≤ 28
Independent reflections	14236 [ <i>R</i> <sub>int</sub> = 0.0308, <i>R</i> <sub>sigma</sub> = 0.0285]	22758 [ <i>R</i> <sub>int</sub> = 0.1479, <i>R</i> <sub>sigma</sub> = 0.0827]	8623 [ <i>R</i> <sub>int</sub> = 0.0208, <i>R</i> <sub>sigma</sub> = 0.0171]
Data/restraints/parameters	14236/0/567	22758/0/1169	8623/369/384
Goodness-of-fit on <i>F</i> <sup>2</sup>	1.071	1.193	1.049
<i>R</i> [ <i>I</i> ≥ 2 $\theta$ ( <i>I</i> )] ( <i>R</i> <sub>1</sub> , <i>wR</i> <sub>2</sub> )	<i>R</i> <sub>1</sub> = 0.0484, <i>wR</i> <sub>2</sub> = 0.1196	<i>R</i> <sub>1</sub> = 0.0826, <i>wR</i> <sub>2</sub> = 0.1680	<i>R</i> <sub>1</sub> = 0.0267, <i>wR</i> <sub>2</sub> = 0.0652
<i>R</i> (all data) ( <i>R</i> <sub>1</sub> , <i>wR</i> <sub>2</sub> )	<i>R</i> <sub>1</sub> = 0.0629, <i>wR</i> <sub>2</sub> = 0.1279	<i>R</i> <sub>1</sub> = 0.1209, <i>wR</i> <sub>2</sub> = 0.1839	<i>R</i> <sub>1</sub> = 0.0303, <i>wR</i> <sub>2</sub> = 0.0671
Largest diff. peak/hole / (e Å <sup>-3</sup> )	2.28/-0.66	1.37/-0.72	0.81/-0.37

$$R1 = \sum ||F_o| - |F_c|| / \sum |F_o|; wR2 = [\sum(w(F_o^2 - F_c^2)^2) / \sum w(F_o^2)]^{1/2}$$

**Table A12** Crystallographic data for **5.38**.

Compound	<b>5.38</b>
Empirical formula	C <sub>26</sub> H <sub>54</sub> NiO <sub>8</sub> P <sub>2</sub>
Formula weight	615.34
Temperature/K	90(2)
Crystal system	Monoclinic
Space group	<i>P2<sub>1</sub>/c</i>
<i>a</i> /Å	18.352(3)
<i>b</i> /Å	10.1685(19)
<i>c</i> /Å	17.216(3)
$\alpha$ /°	90
$\beta$ /°	92.095(4)
$\gamma$ /°	90
<i>V</i> /Å <sup>3</sup>	3210.5(10)
<i>Z</i>	4
$\rho$ / g/cm <sup>-3</sup>	1.273
$\mu$ / mm <sup>-1</sup>	0.745
<i>F</i> (000)	1328.0
Crystal size/ mm <sup>3</sup>	0.35 × 0.25 × 0.12
Radiation	MoK $\alpha$ ( $\lambda$ = 0.71073)
2 $\theta$ range for data collection/°	2.22 to 58.45
Index ranges	-25 ≤ <i>h</i> ≤ 25, -13 ≤ <i>k</i> ≤ 13, -23 ≤ <i>l</i> ≤ 23
Independent reflections	8617 [ <i>R</i> <sub>int</sub> = 0.0328, <i>R</i> <sub>sigma</sub> = 0.0304]
Data/restraints/parameters	8617/0/352
Goodness-of-fit on <i>F</i> <sup>2</sup>	1.084
<i>R</i> [ <i>I</i> ≥ 2 $\theta$ ( <i>I</i> )] ( <i>R</i> <sub>1</sub> , <i>wR</i> <sub>2</sub> )	<i>R</i> <sub>1</sub> = 0.0474, <i>wR</i> <sub>2</sub> = 0.1184
<i>R</i> (all data) ( <i>R</i> <sub>1</sub> , <i>wR</i> <sub>2</sub> )	<i>R</i> <sub>1</sub> = 0.0640, <i>wR</i> <sub>2</sub> = 0.1281
Largest diff. peak/hole / (e Å <sup>-3</sup> )	1.58/-1.21

$$R1 = \frac{\sum ||F_o| - |F_c||}{\sum |F_o|}; wR2 = \frac{[\sum(w(F_o^2 - F_c^2)^2)]^{1/2}}{\sum w(F_o^2)^{1/2}}$$

## Appendix B: NMR Spectra

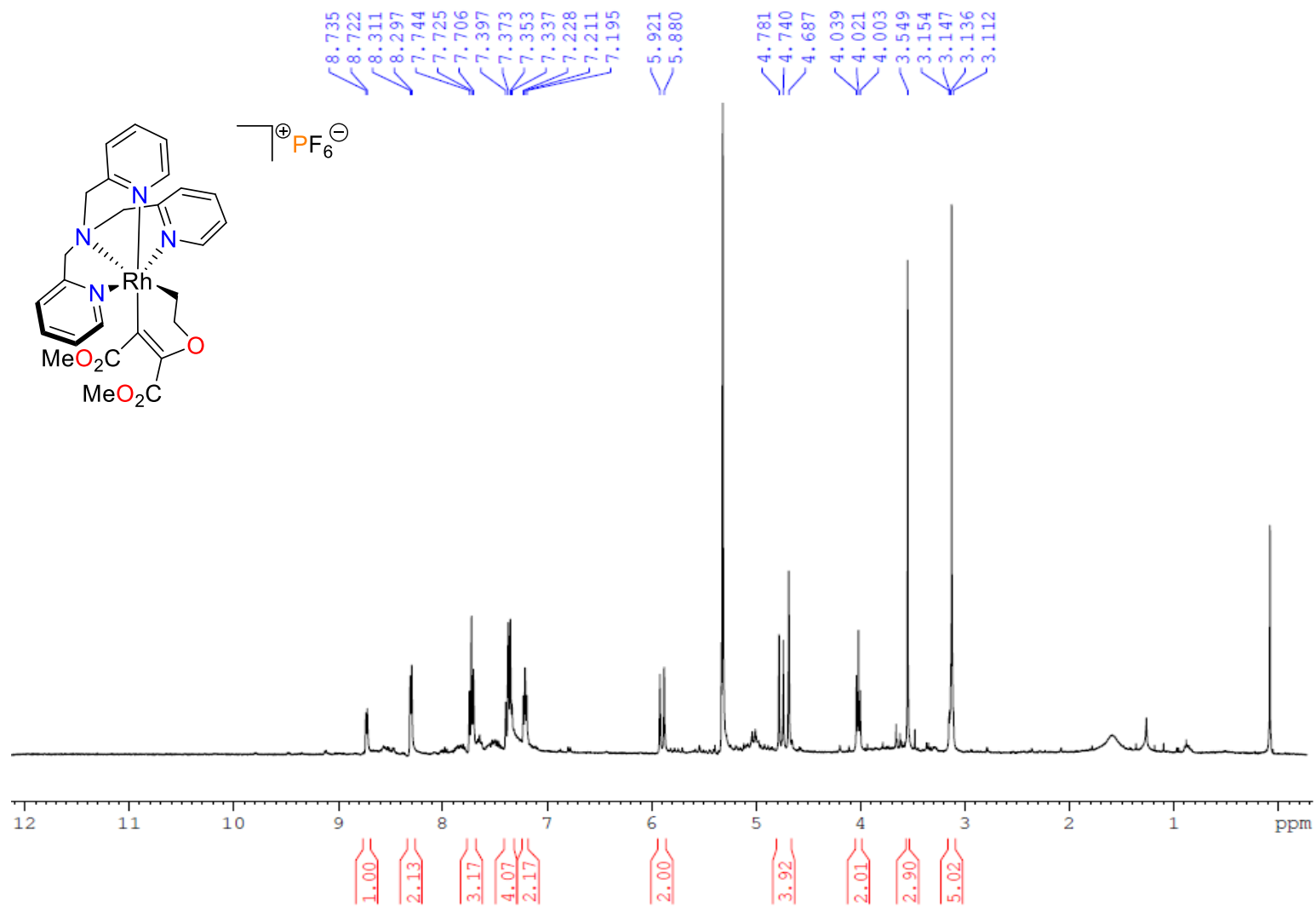


**Figure B2.1.**  $^1\text{H}$  NMR spectrum (400 MHz,  $\text{CD}_2\text{Cl}_2$ , 25 °C) of **2.13**.

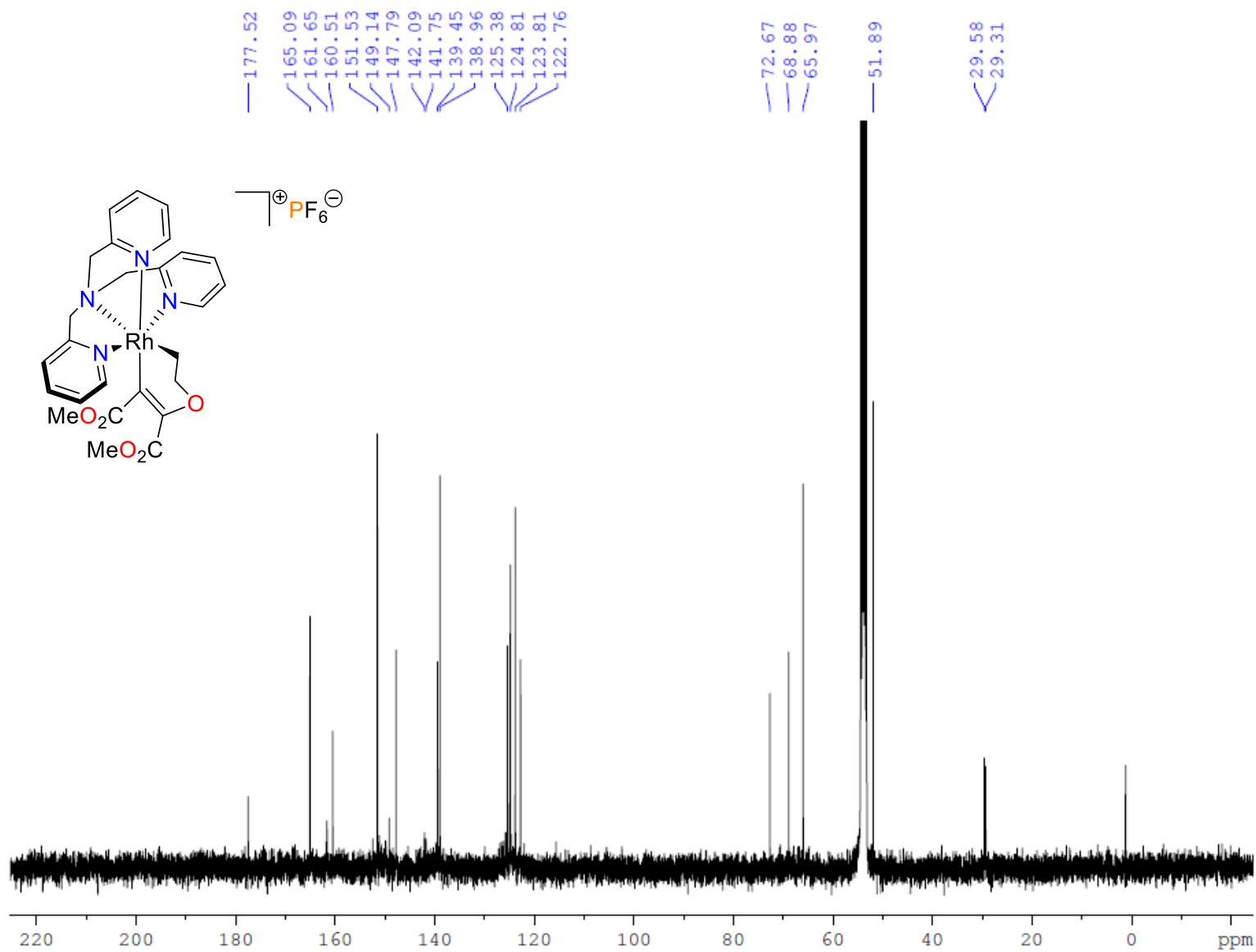


**Figure B2.2.**  $^{13}\text{C}\{^1\text{H}\}$  NMR spectrum (100 MHz,  $\text{CD}_2\text{Cl}_2$ , 25 °C) of **2.13**.

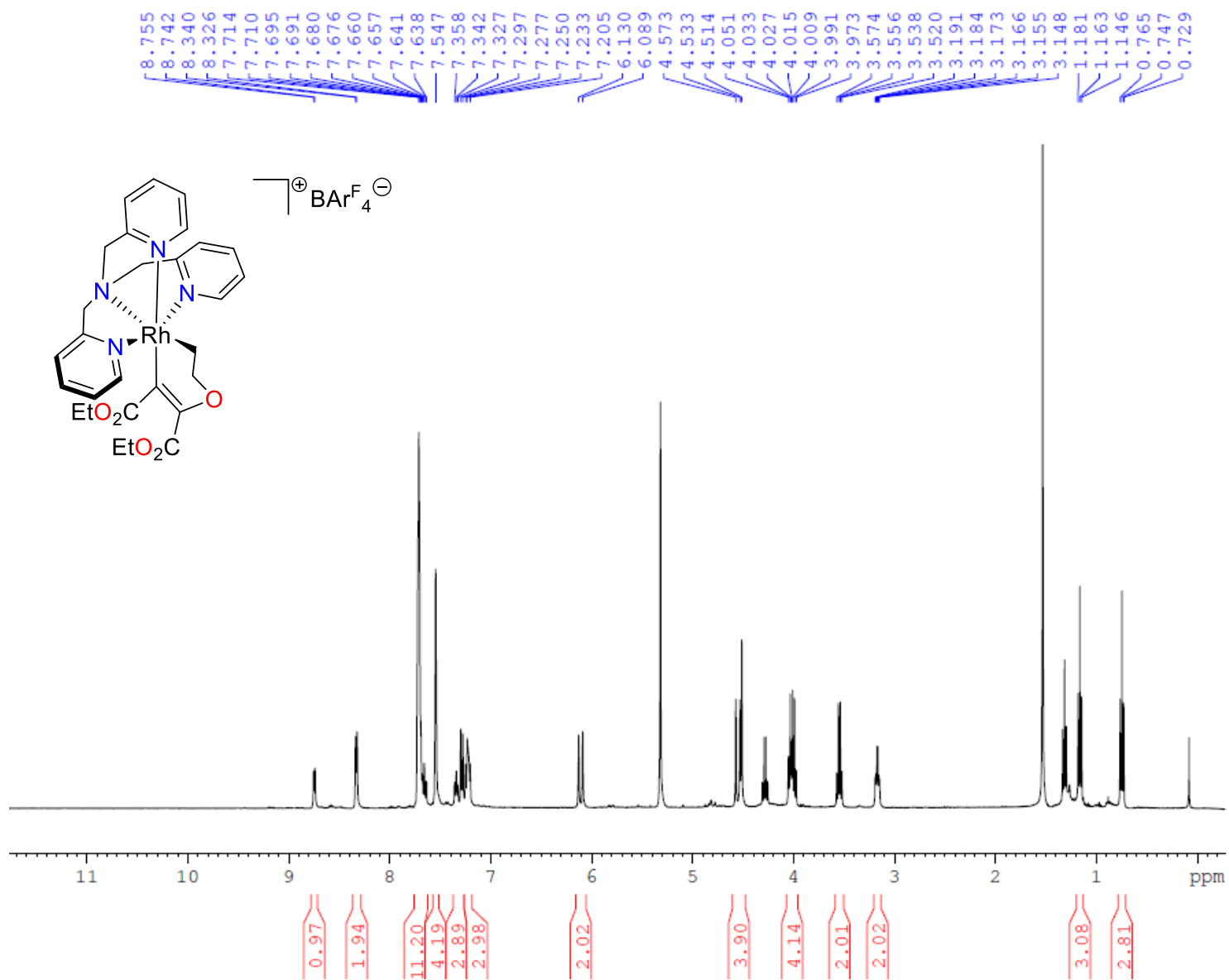


**Figure B2.3.** <sup>1</sup>H NMR spectrum (400 MHz, CD<sub>2</sub>Cl<sub>2</sub>, 25 °C) of 2.14[BarF<sub>4</sub>].

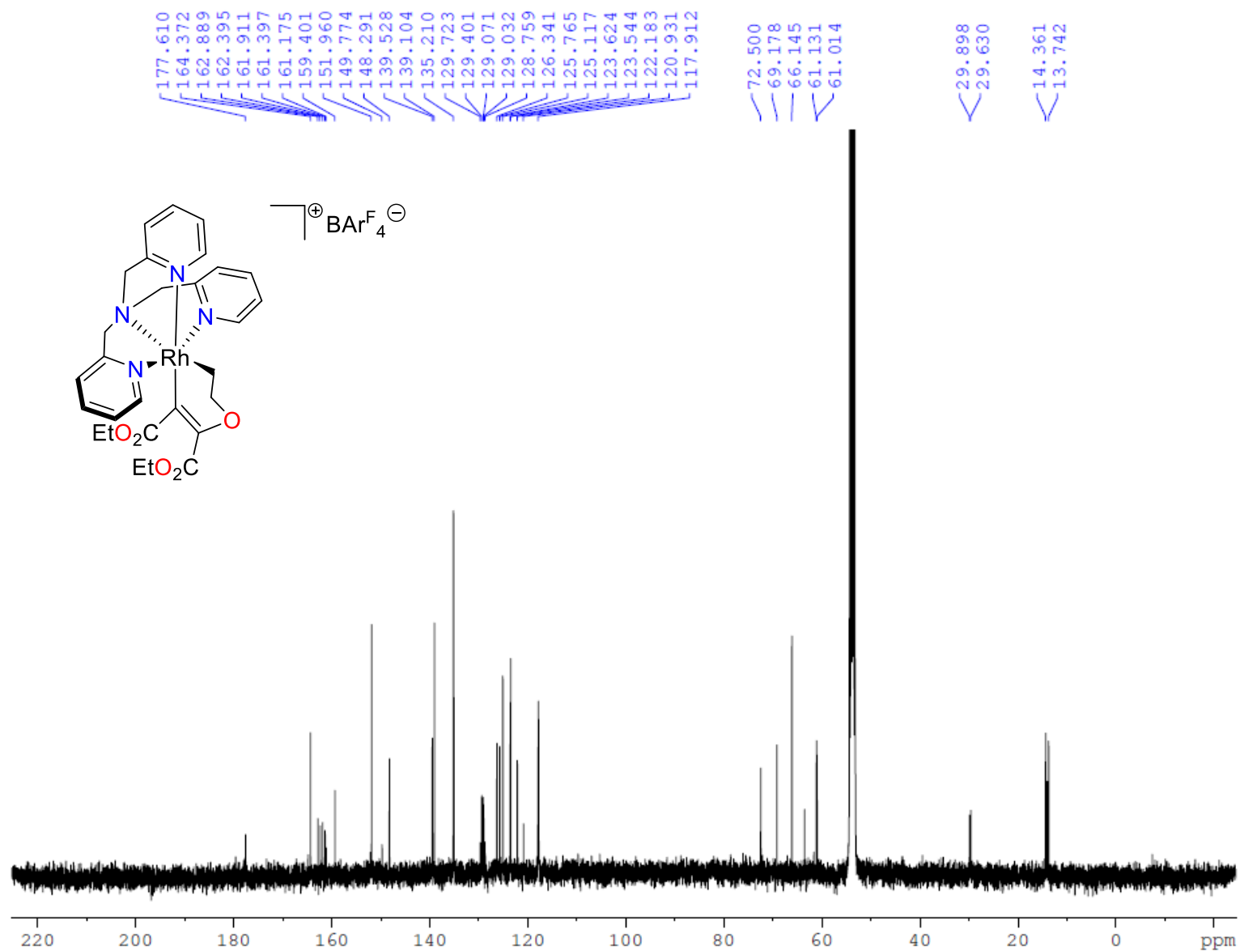


**Figure B2.4.**  $^{13}\text{C}\{^1\text{H}\}$  NMR spectrum (100 MHz,  $\text{CD}_2\text{Cl}_2$ ,  $25^\circ\text{C}$ ) of **2.14** $[\text{BArF}_4]$ .

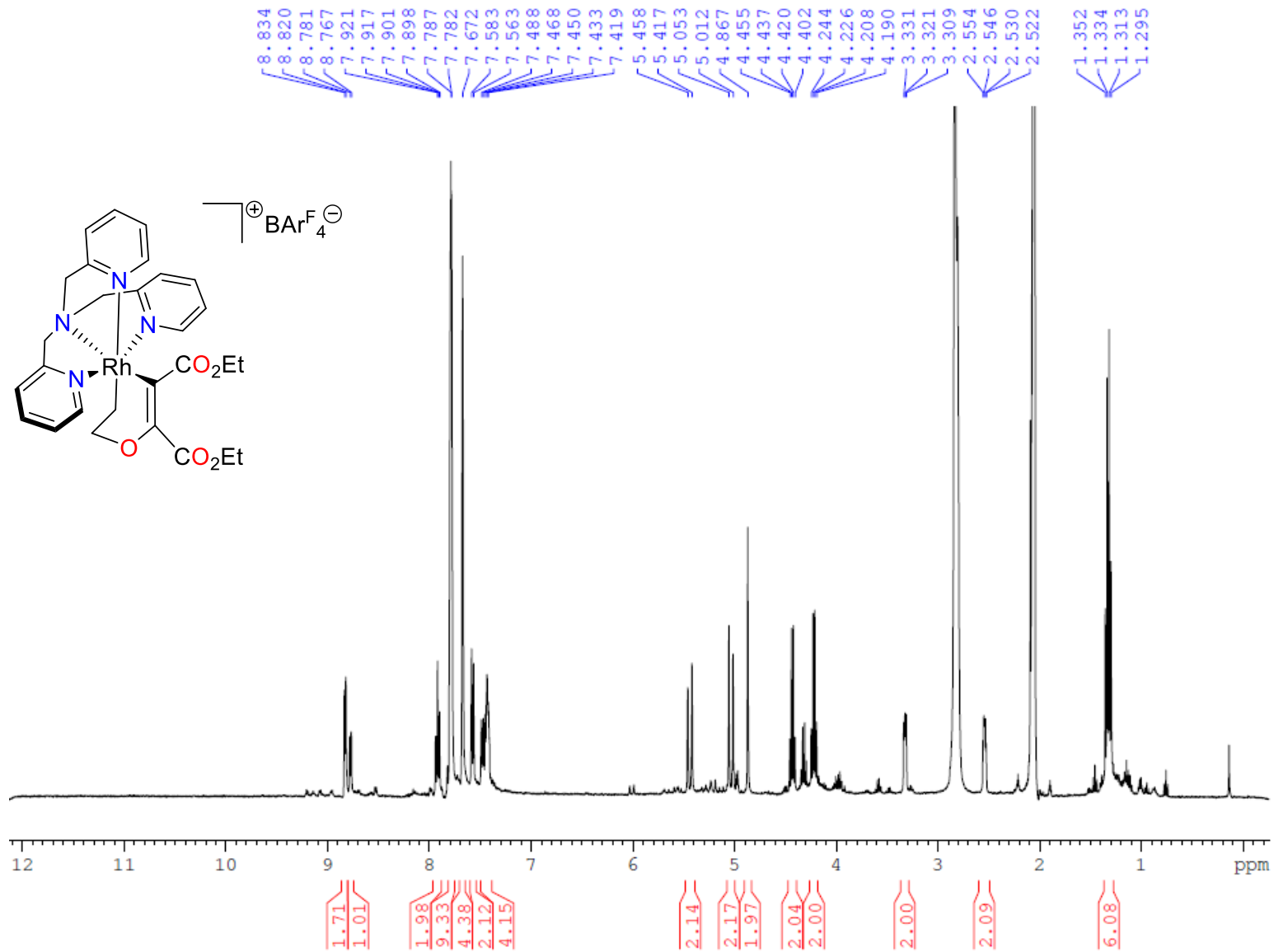


**Figure B2.5.**  $^1\text{H}$  NMR spectrum (400 MHz, acetone- $d_6$ , 25 °C) of **2.20** $[\text{BArF}_4]$ .

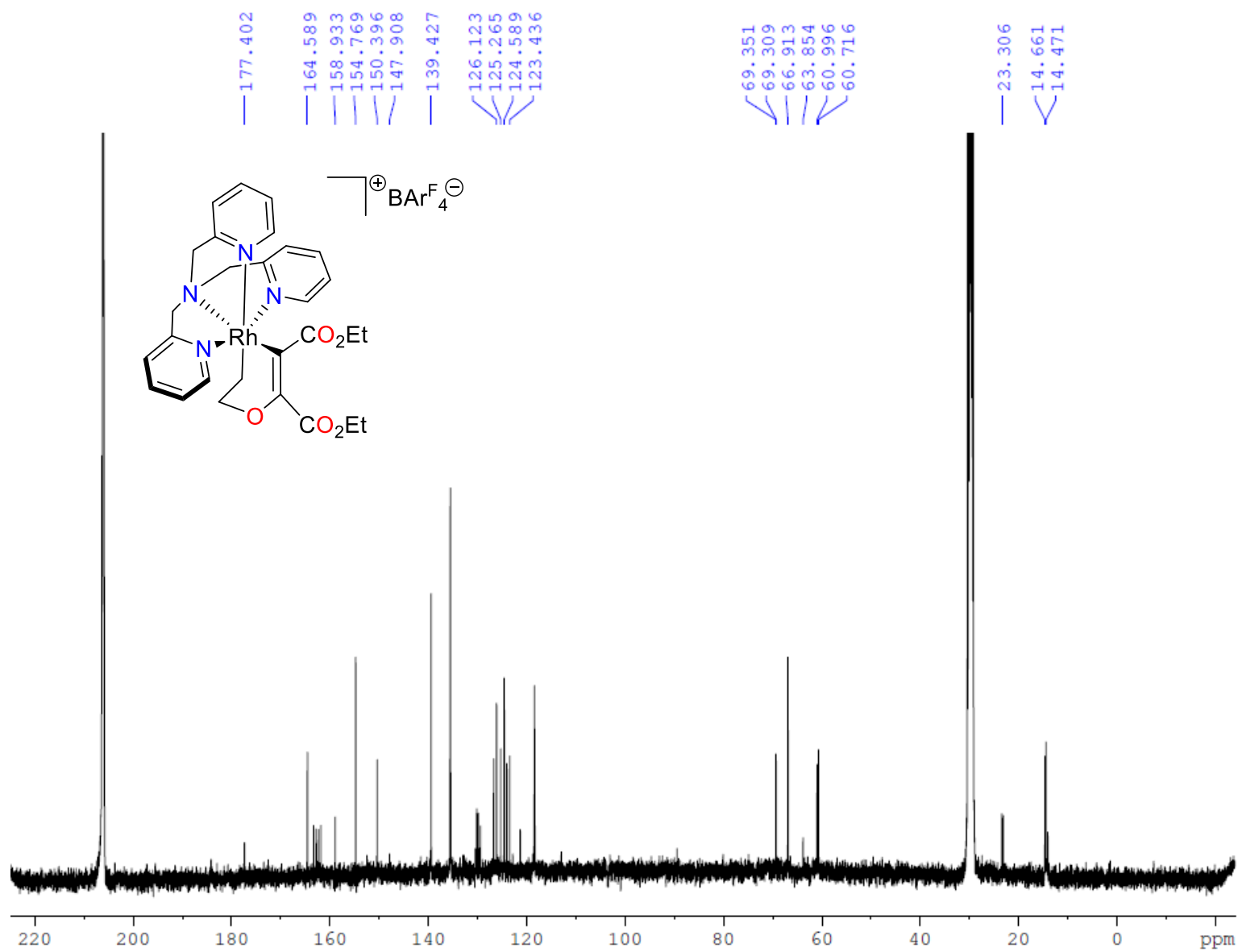


**Figure B2.6.**  $^{13}\text{C}\{^1\text{H}\}$  NMR spectrum (100 MHz, acetone- $d_6$ , 25 °C) of **2.20** $[\text{BArF}_4]$ .

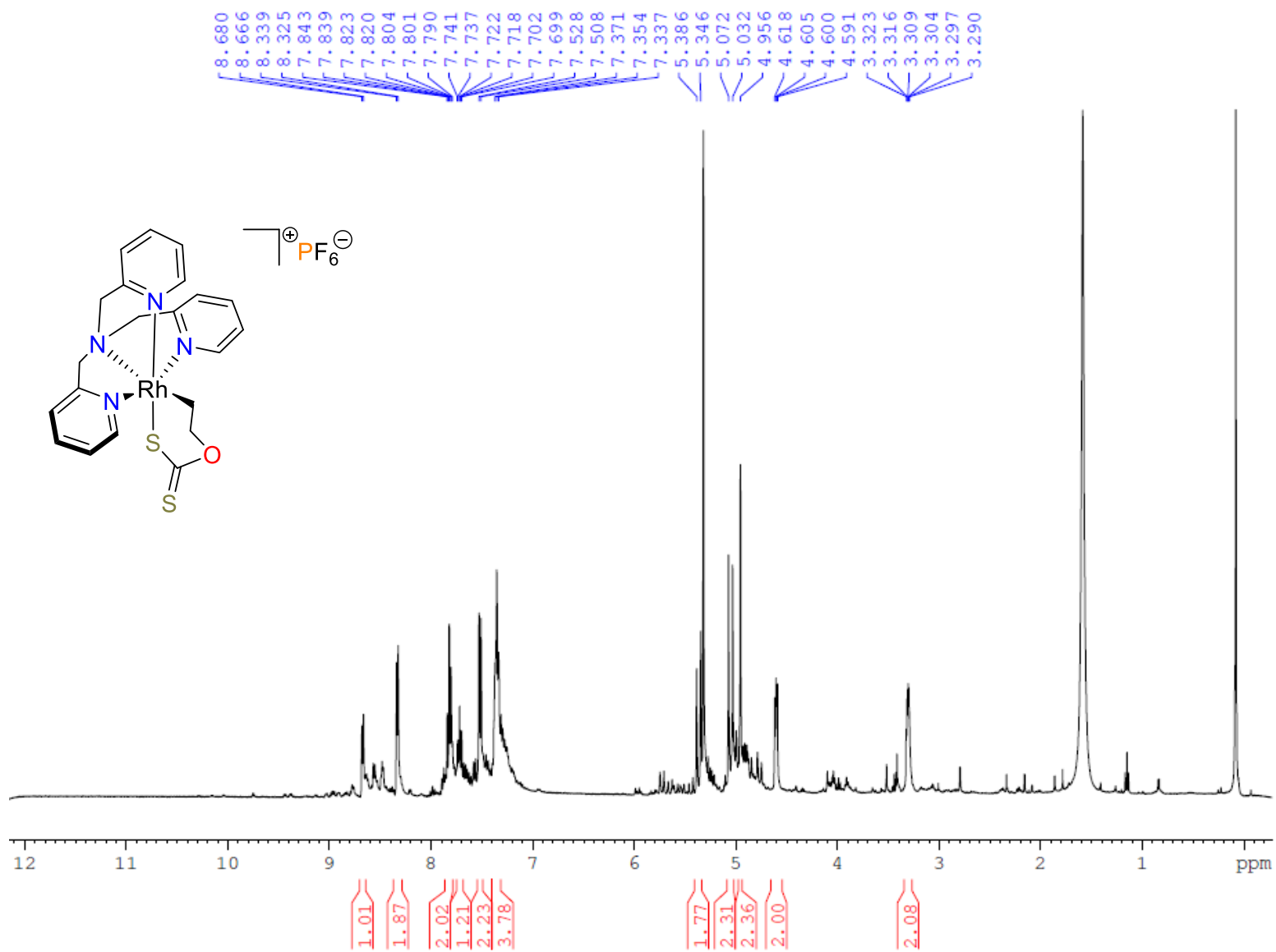


**Figure B2.7.**  $^1\text{H}$  NMR spectrum (400 MHz,  $\text{CD}_2\text{Cl}_2$ , 25 °C) of **2.22**.

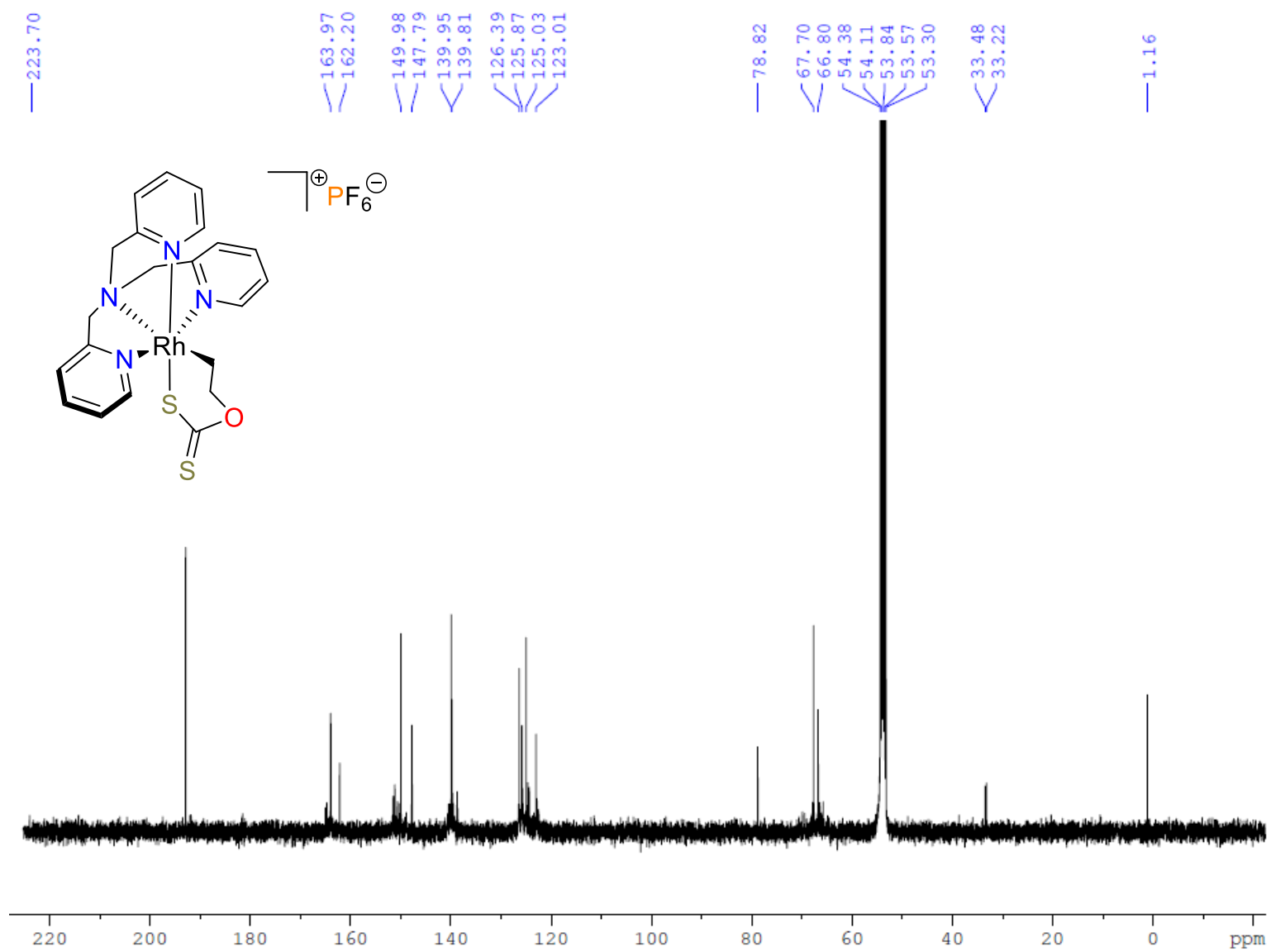


**Figure B2.8.**  $^{13}\text{C}\{^1\text{H}\}$  NMR spectrum (100 MHz,  $\text{CD}_2\text{Cl}_2$ , 25 °C) of **2.22**.

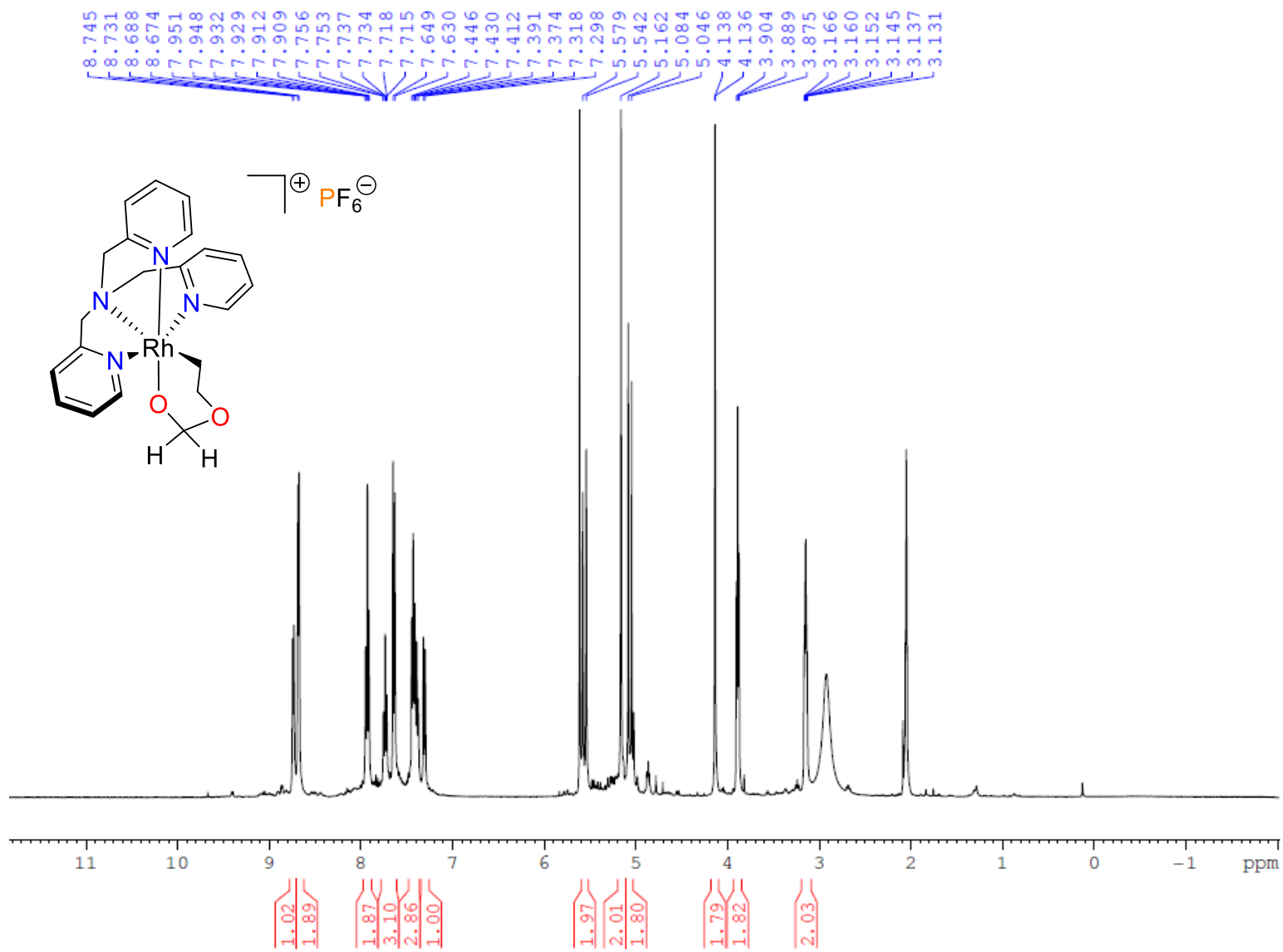


**Figure B2.9.**  $^1\text{H}$  NMR spectrum (400 MHz, acetone- $d_6$ , 25 °C) of **2.27**.

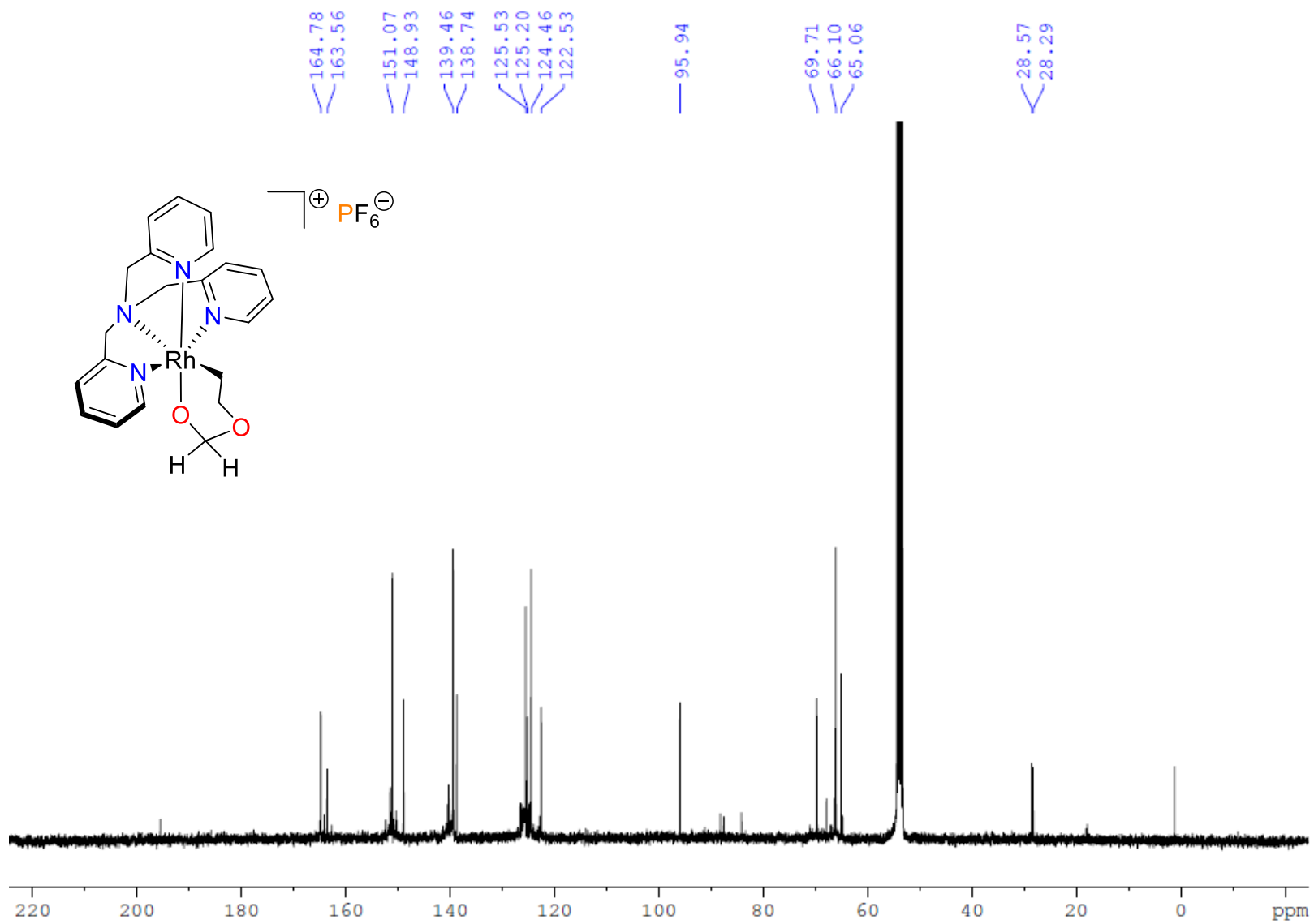


**Figure B2.10.**  $^{13}\text{C}\{^1\text{H}\}$  NMR spectrum (100 MHz,  $\text{CD}_2\text{Cl}_2$ , 25 °C) of **2.27**.

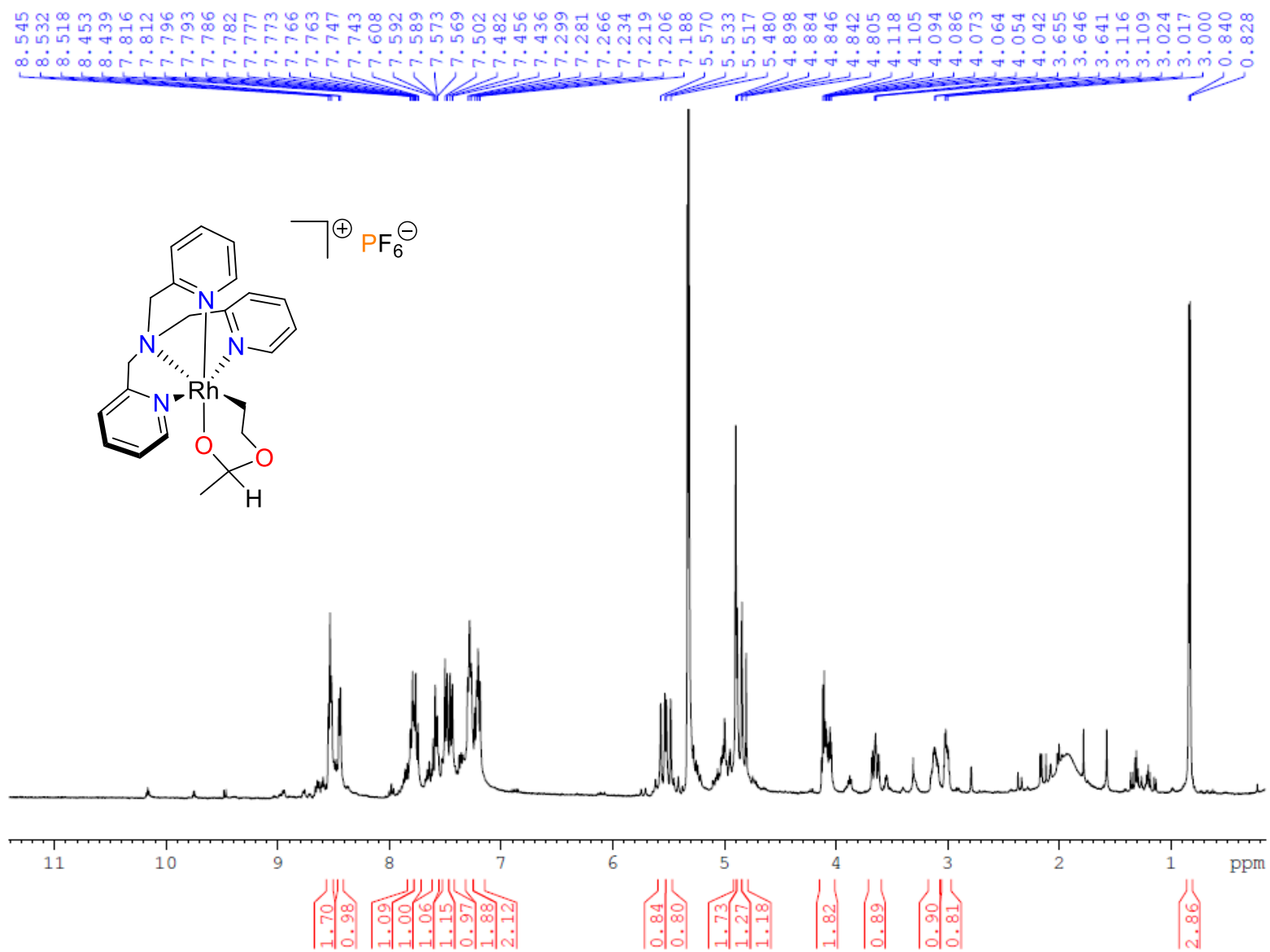


**Figure B2.11.**  $^1\text{H}$  NMR spectrum (400 MHz,  $\text{CD}_2\text{Cl}_2$ , 25 °C) of **2.28**.

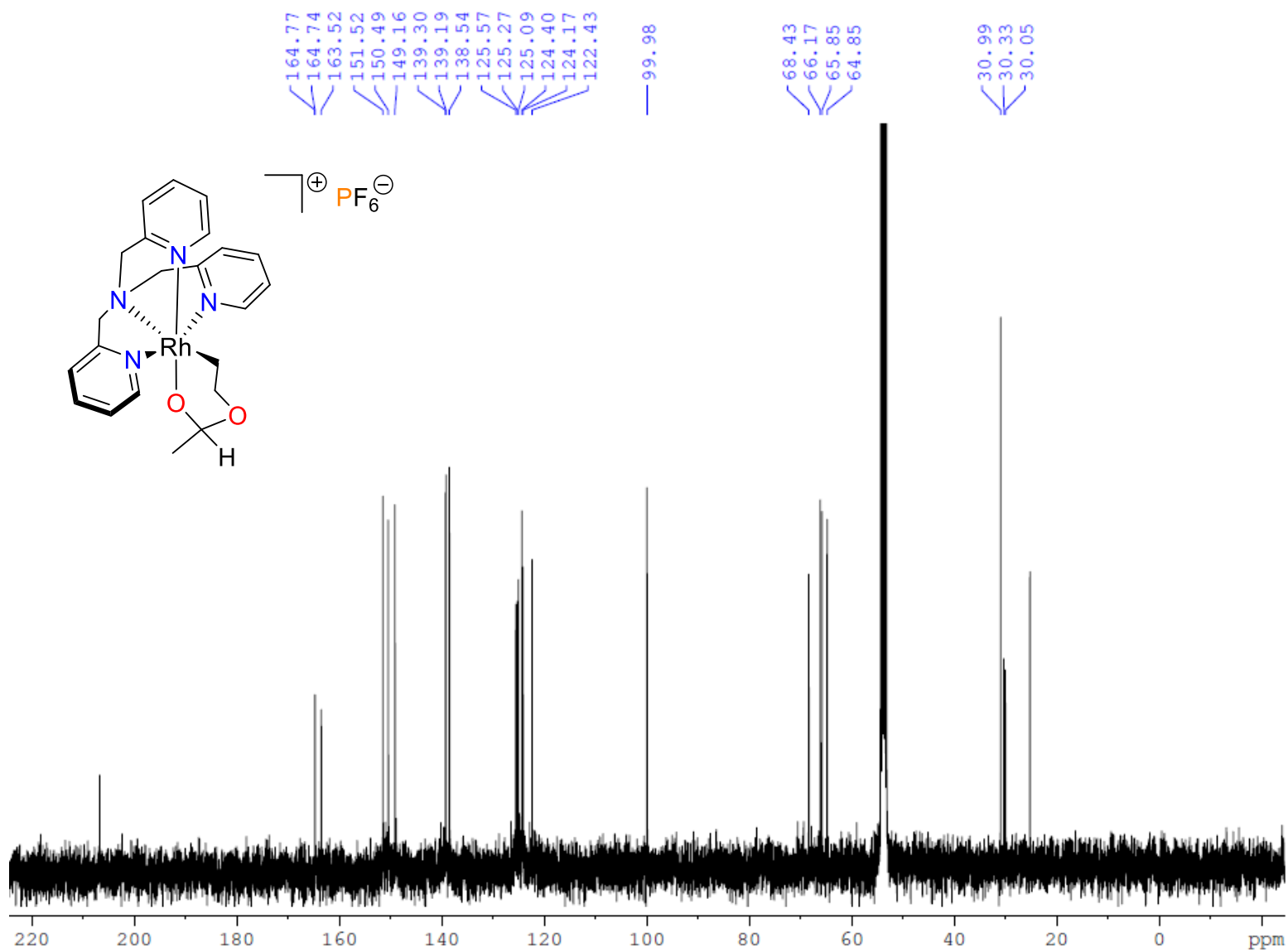


**Figure B2.12.**  $^{13}\text{C}\{^1\text{H}\}$  NMR spectrum (100 MHz,  $\text{CD}_2\text{Cl}_2$ , 25 °C) of **2.28**.

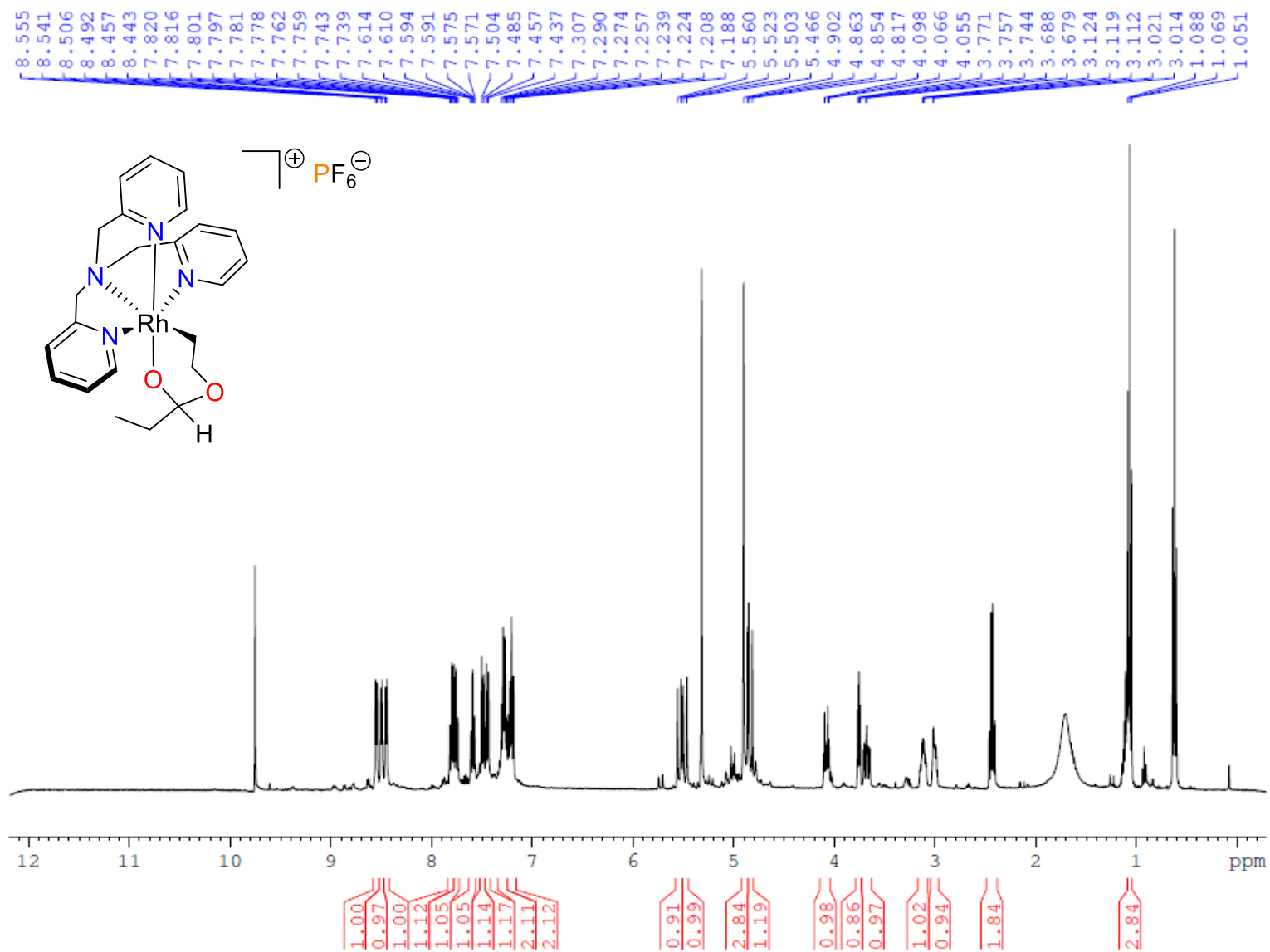


**Figure B2.13.**  $^1\text{H}$  NMR spectrum (400 MHz,  $\text{CD}_2\text{Cl}_2$ , 25 °C) of **2.29**.

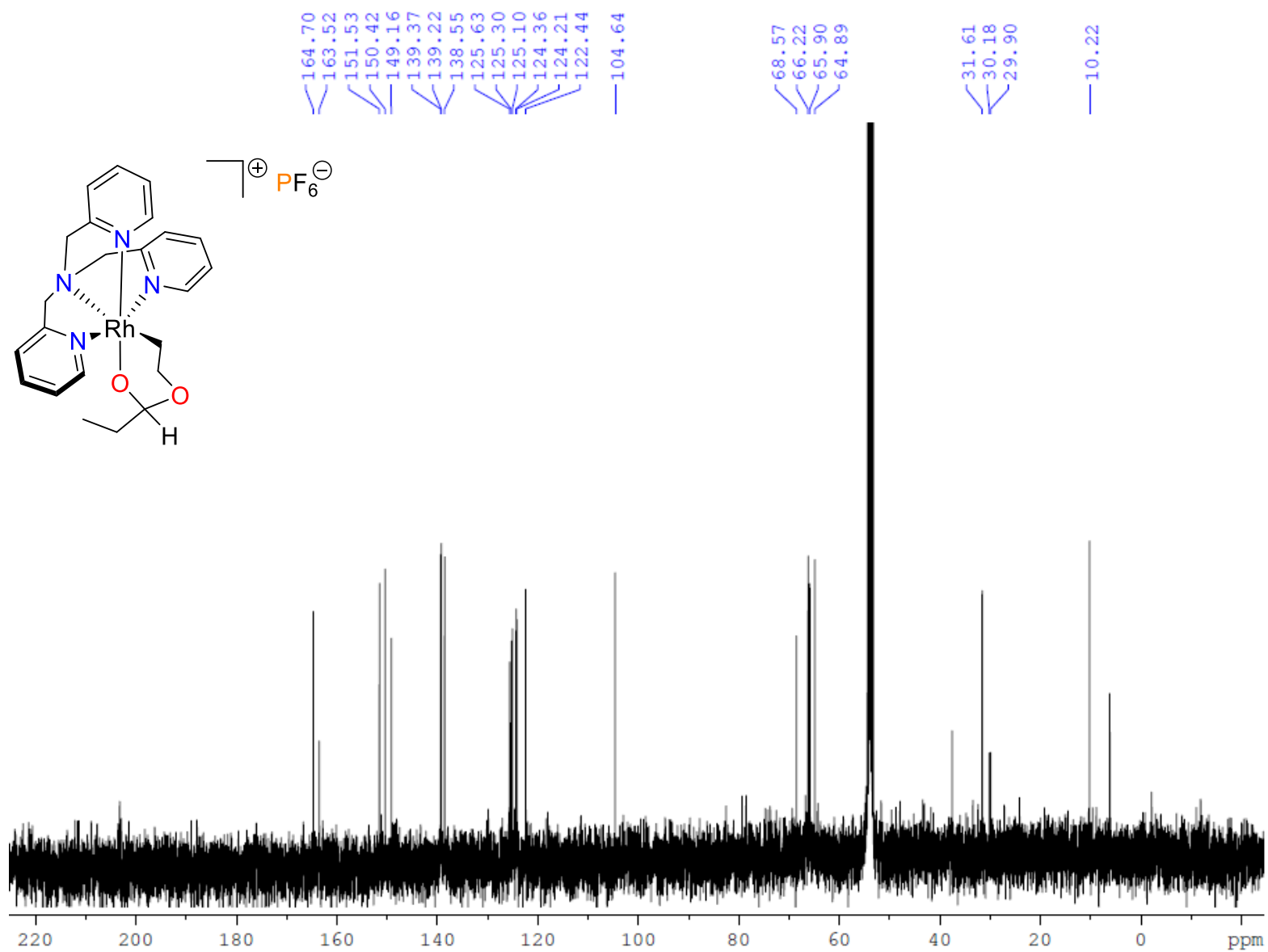


**Figure B2.14.**  $^{13}\text{C}\{^1\text{H}\}$  NMR spectrum (100 MHz,  $\text{CD}_2\text{Cl}_2$ , 25 °C) of **2.29**.

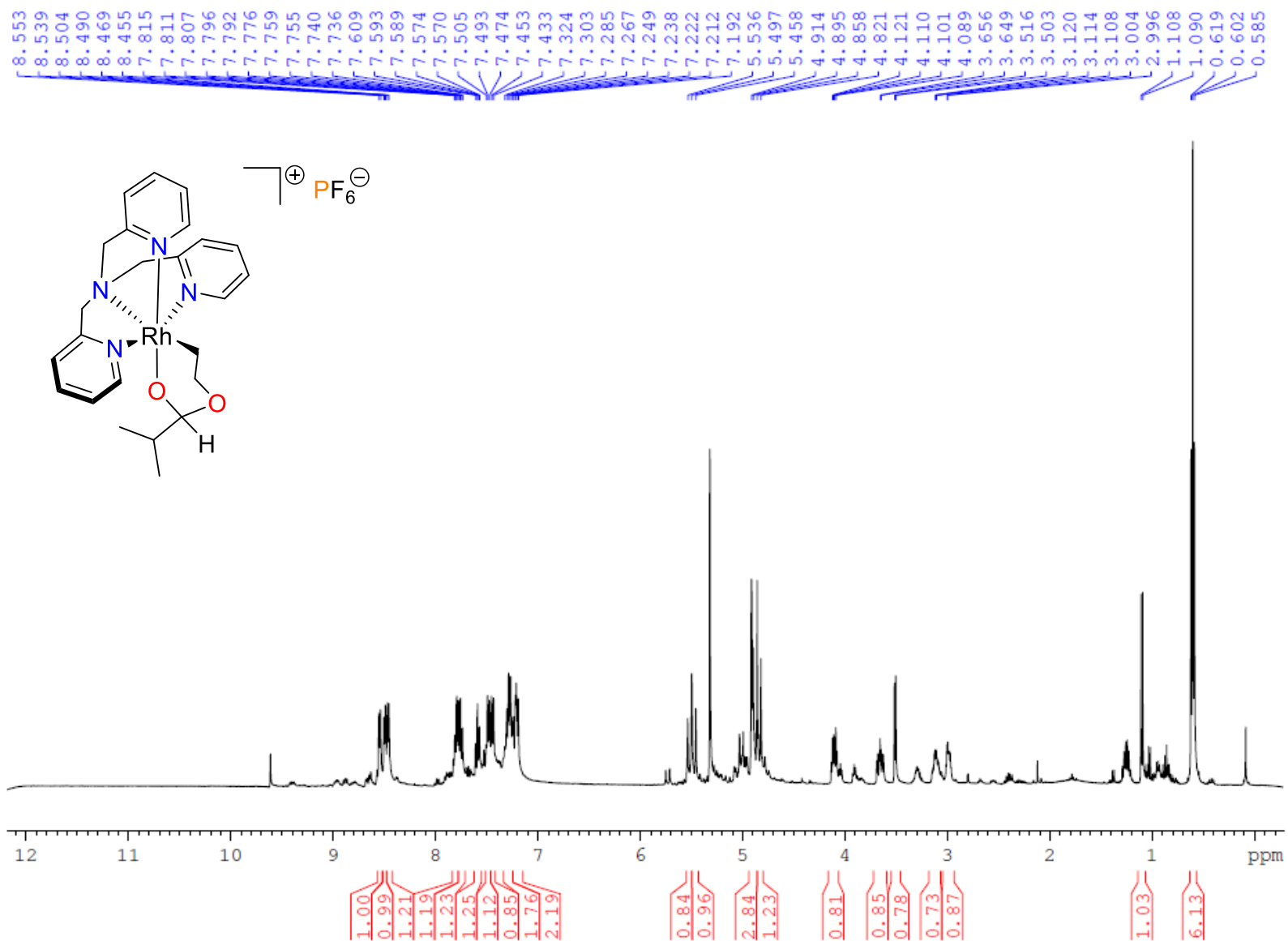


**Figure B2.15.**  $^1\text{H}$  NMR spectrum (400 MHz,  $\text{CD}_2\text{Cl}_2$ , 25 °C) of **2.30**.

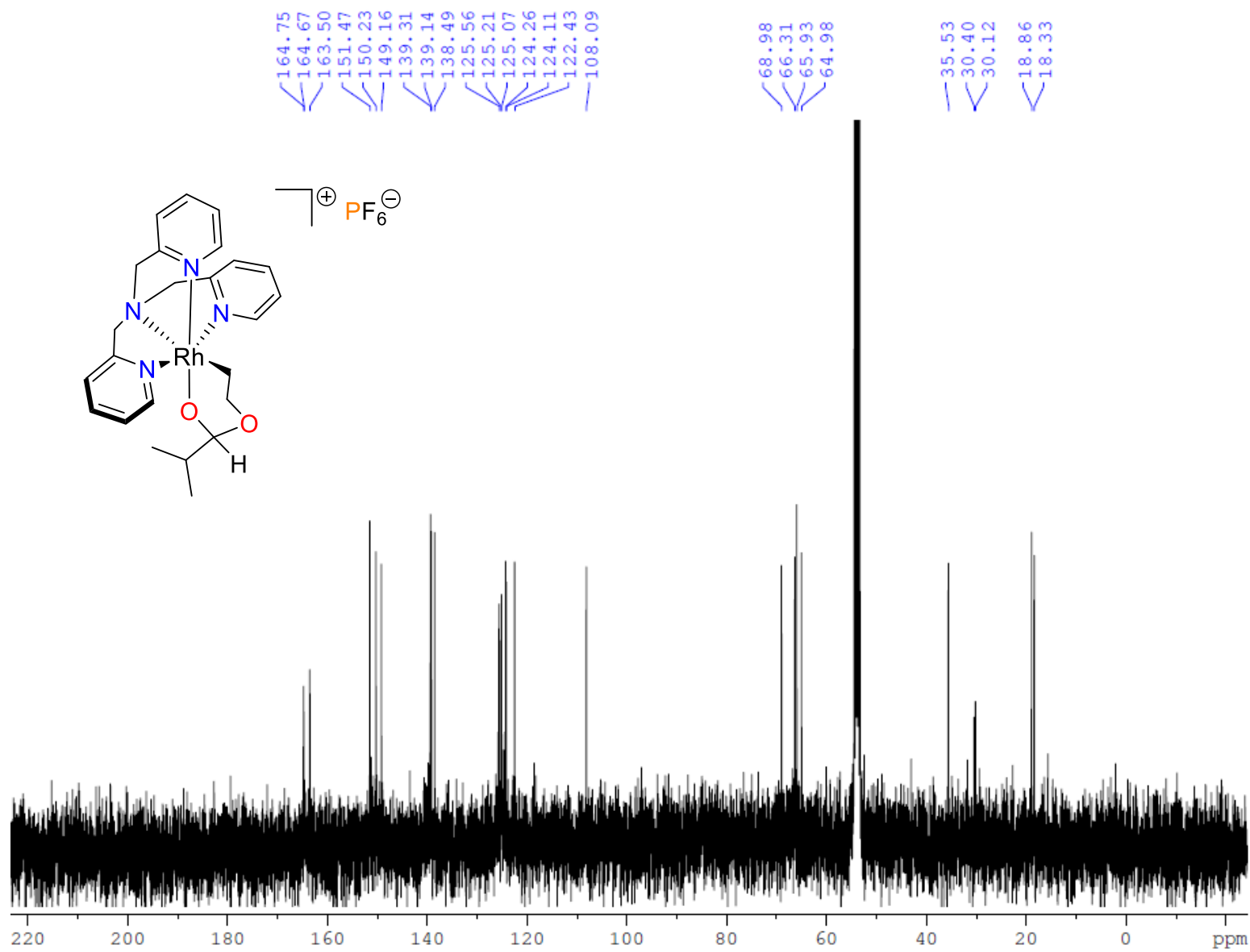


**Figure B2.16.**  $^{13}\text{C}\{^1\text{H}\}$  NMR spectrum (100 MHz,  $\text{CD}_2\text{Cl}_2$ , 25 °C) of **2.30**.

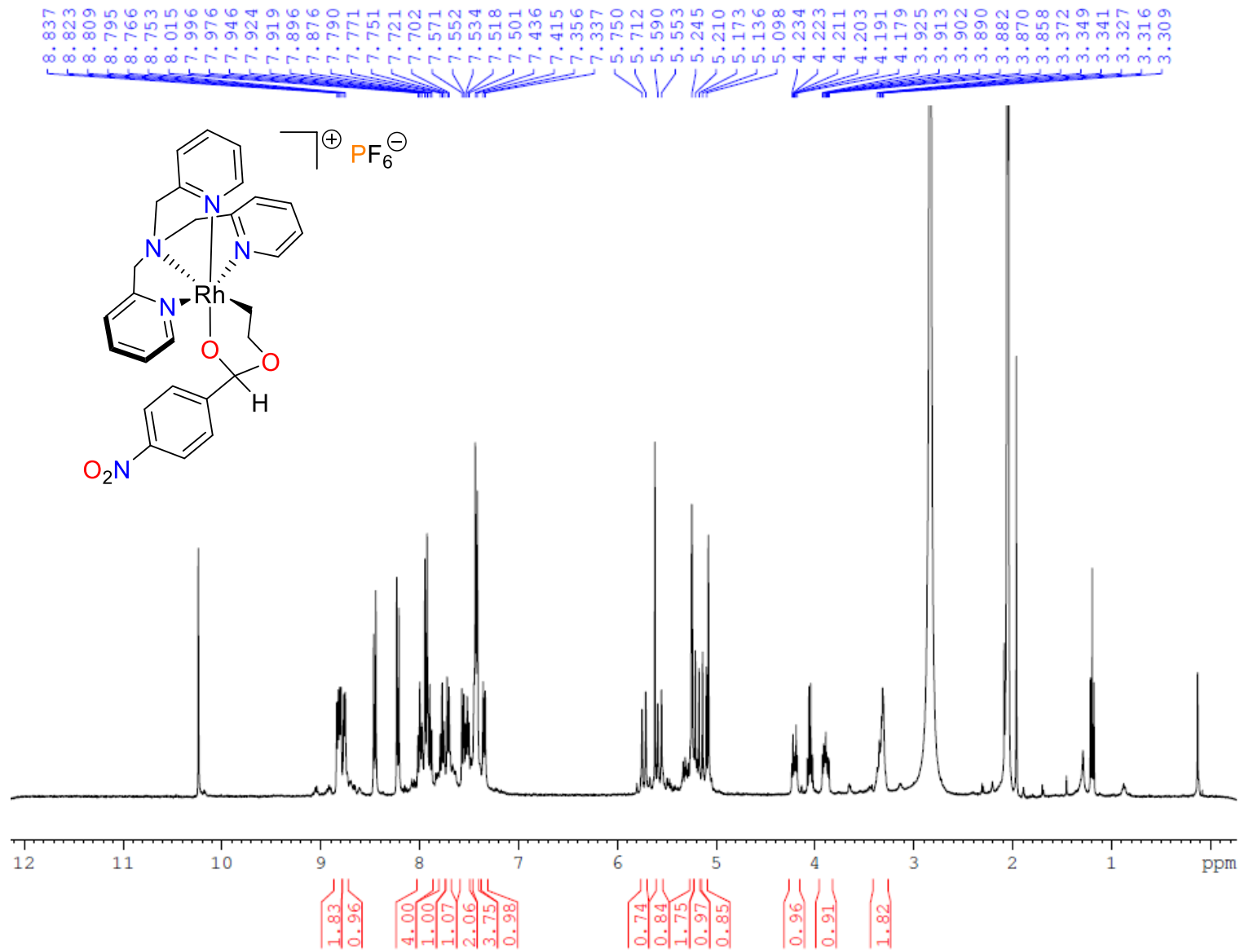


**Figure B2.17.**  $^1\text{H}$  NMR spectrum (400 MHz,  $\text{CD}_2\text{Cl}_2$ , 25 °C) of **2.31**.

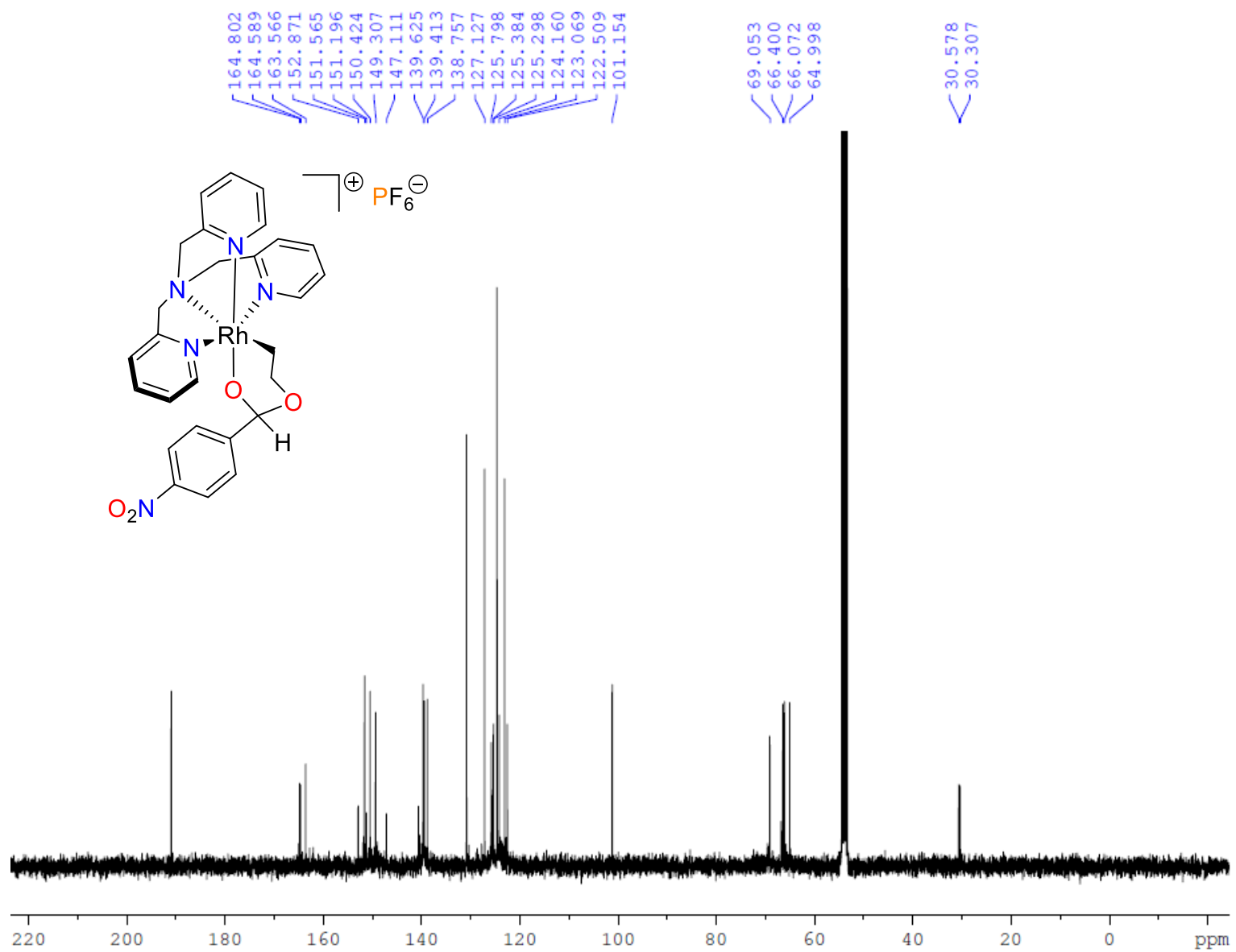


**Figure B2.18.**  $^{13}\text{C}\{^1\text{H}\}$  NMR spectrum (100 MHz,  $\text{CD}_2\text{Cl}_2$ , 25 °C) of 2.31.

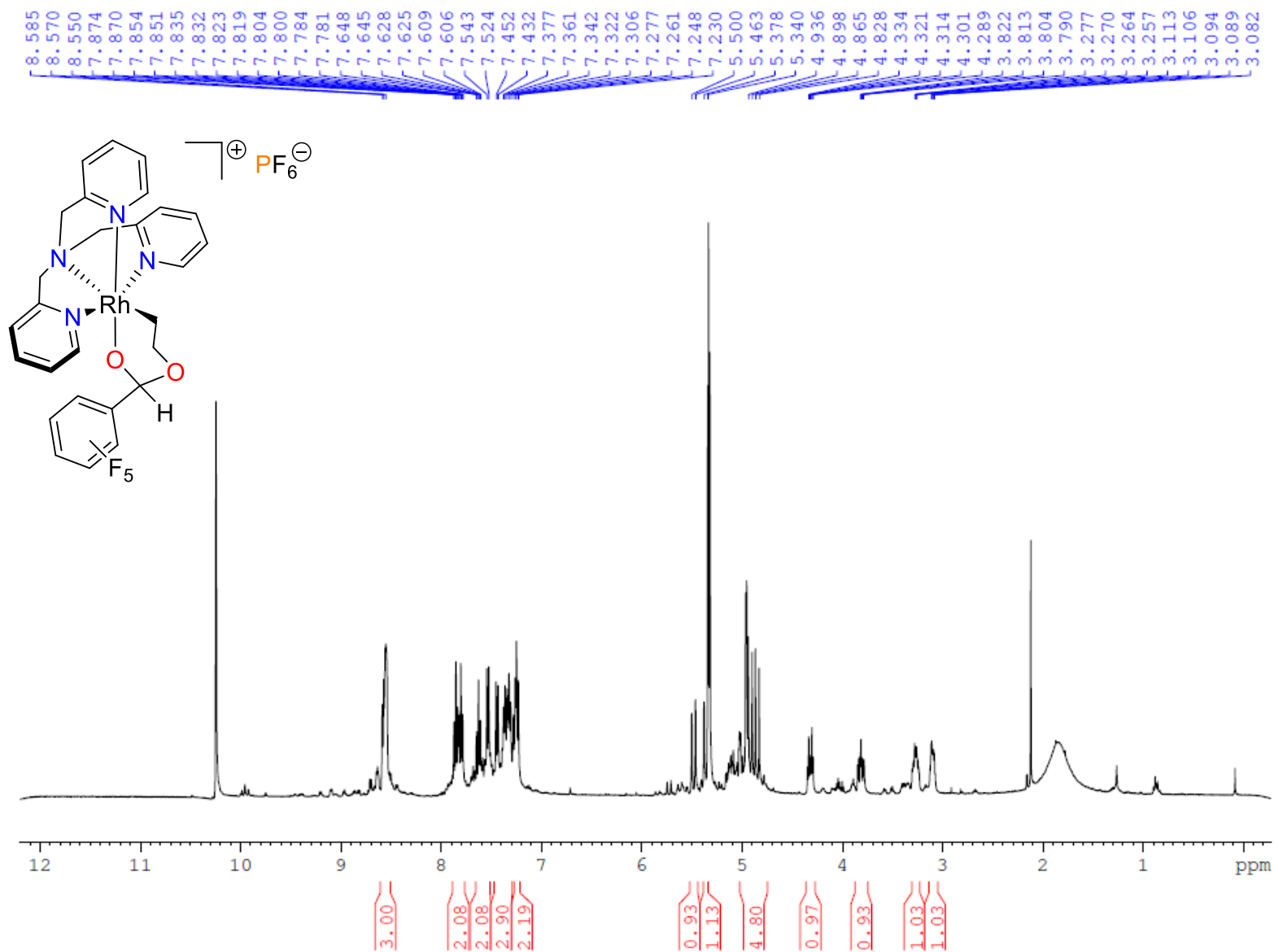


**Figure B2.19.**  $^1\text{H}$  NMR spectrum (400 MHz,  $\text{CD}_2\text{Cl}_2$ , 25 °C) of **2.22**.

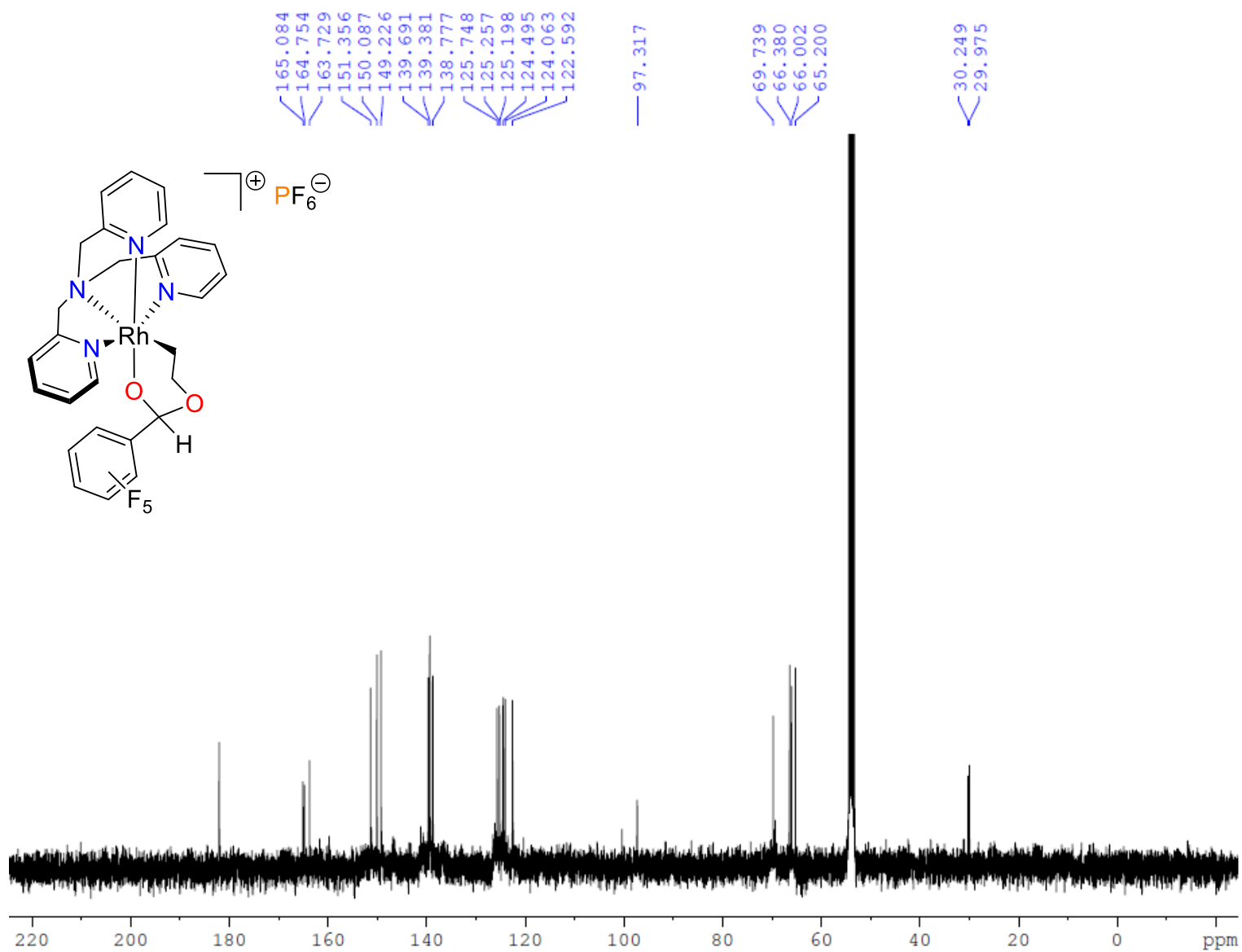


**Figure B2.20.** <sup>13</sup>C{<sup>1</sup>H} NMR spectrum (100 MHz, CD<sub>2</sub>Cl<sub>2</sub>, 25 °C) of **2.22**.

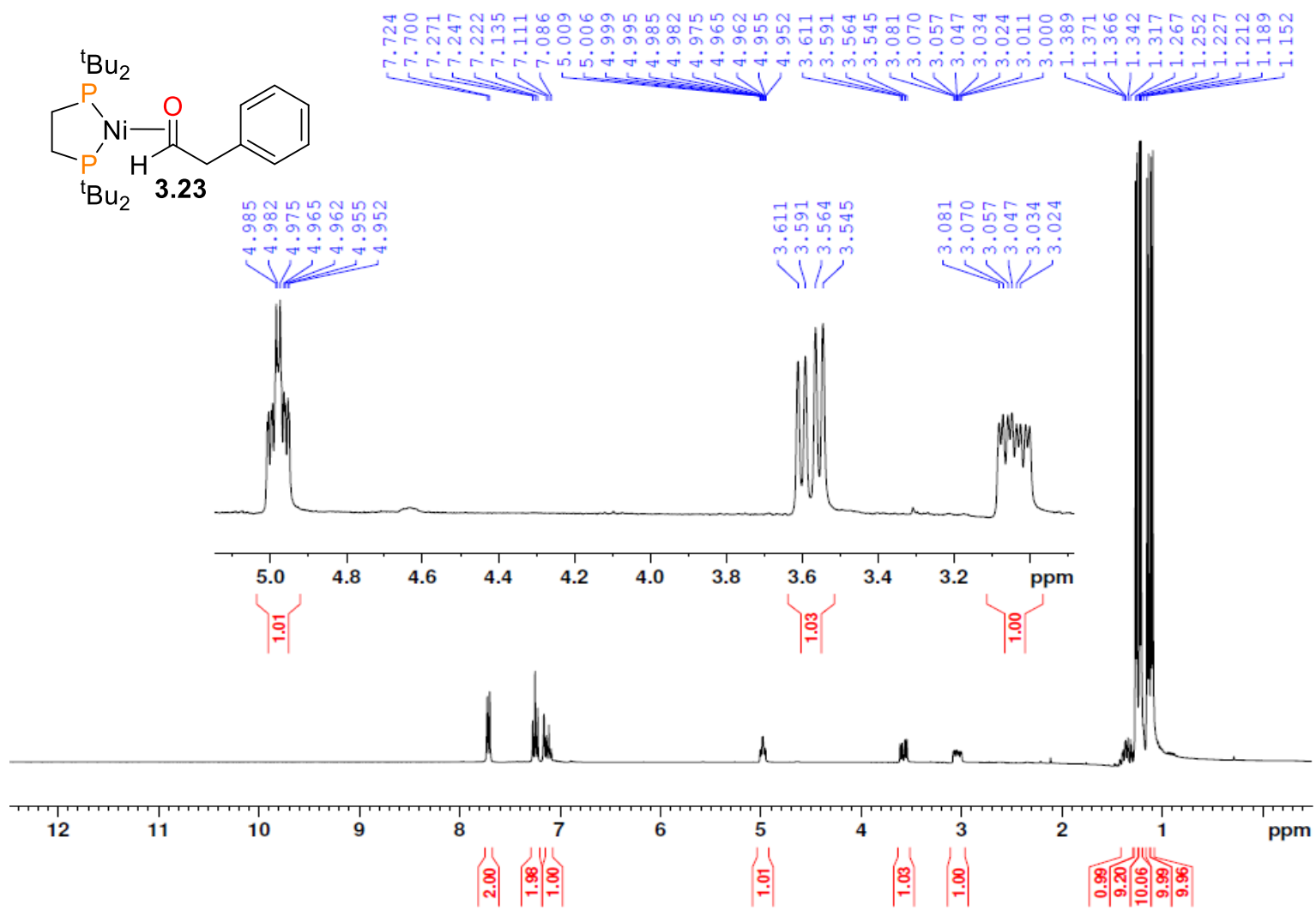


**Figure B3.1.** <sup>1</sup>H NMR spectrum (300 MHz, C<sub>6</sub>D<sub>6</sub>, 25 °C) of **3.23**. Inset shows the resonances assigned to **H1** and **H2**.

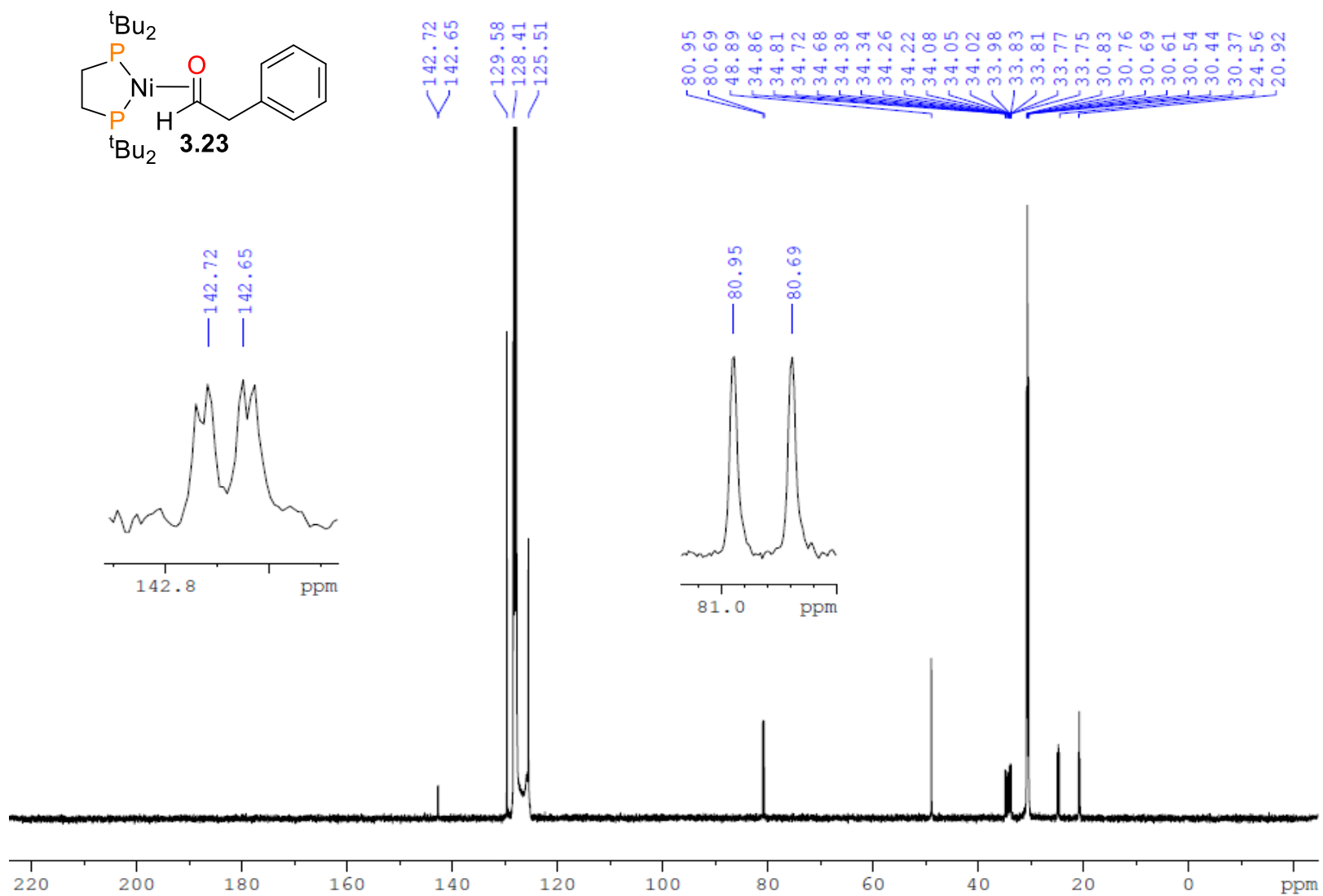


**Figure B3.2.**  $^{13}\text{C}\{^1\text{H}\}$  NMR spectrum (100 MHz,  $\text{C}_6\text{D}_6$ , 25 °C) of **3.23**.

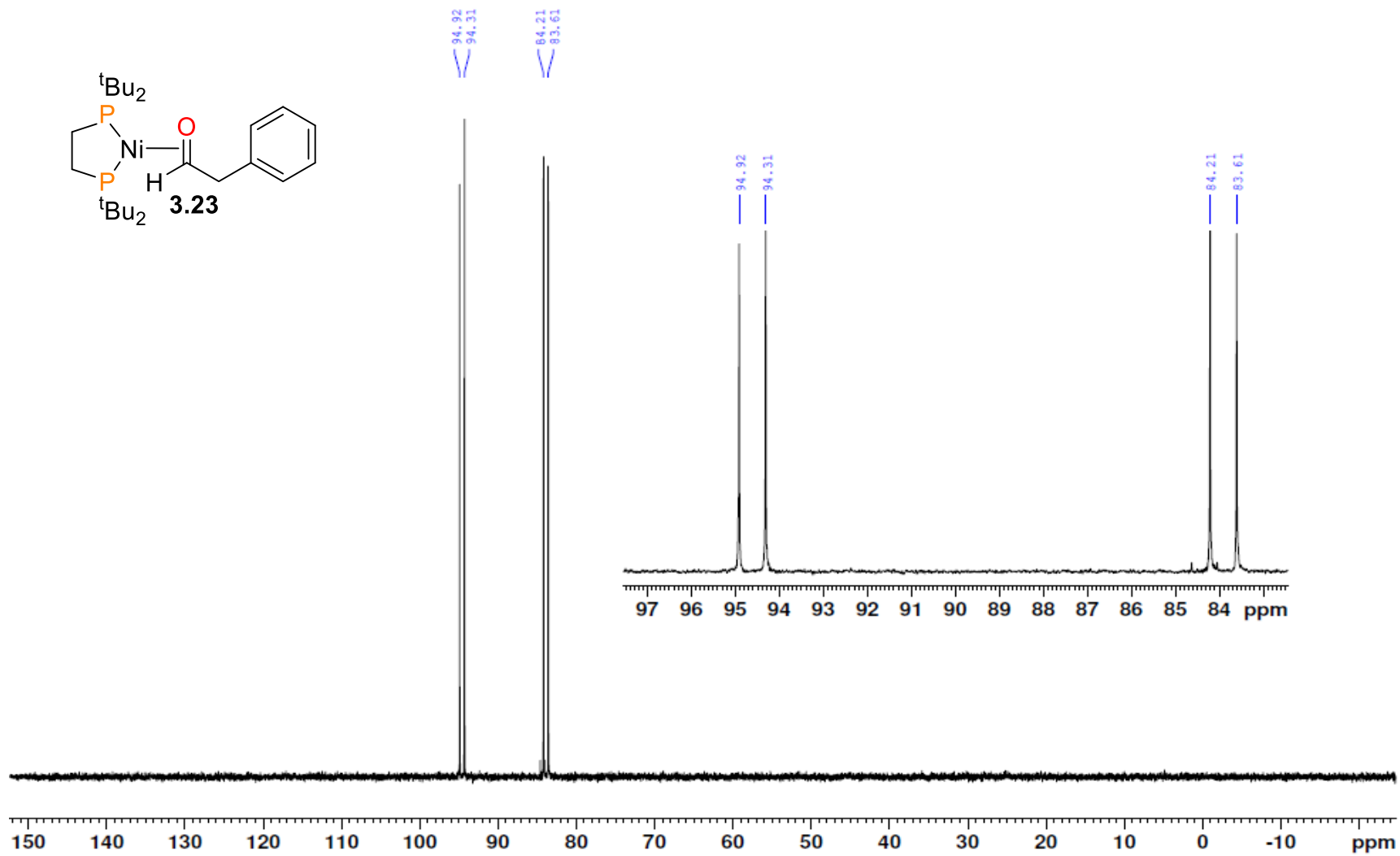


**Figure B3.3.**  $^{31}\text{P}\{^1\text{H}\}$  NMR spectrum (162 MHz,  $\text{C}_6\text{D}_6$ , 25 °C) of **3.23**.

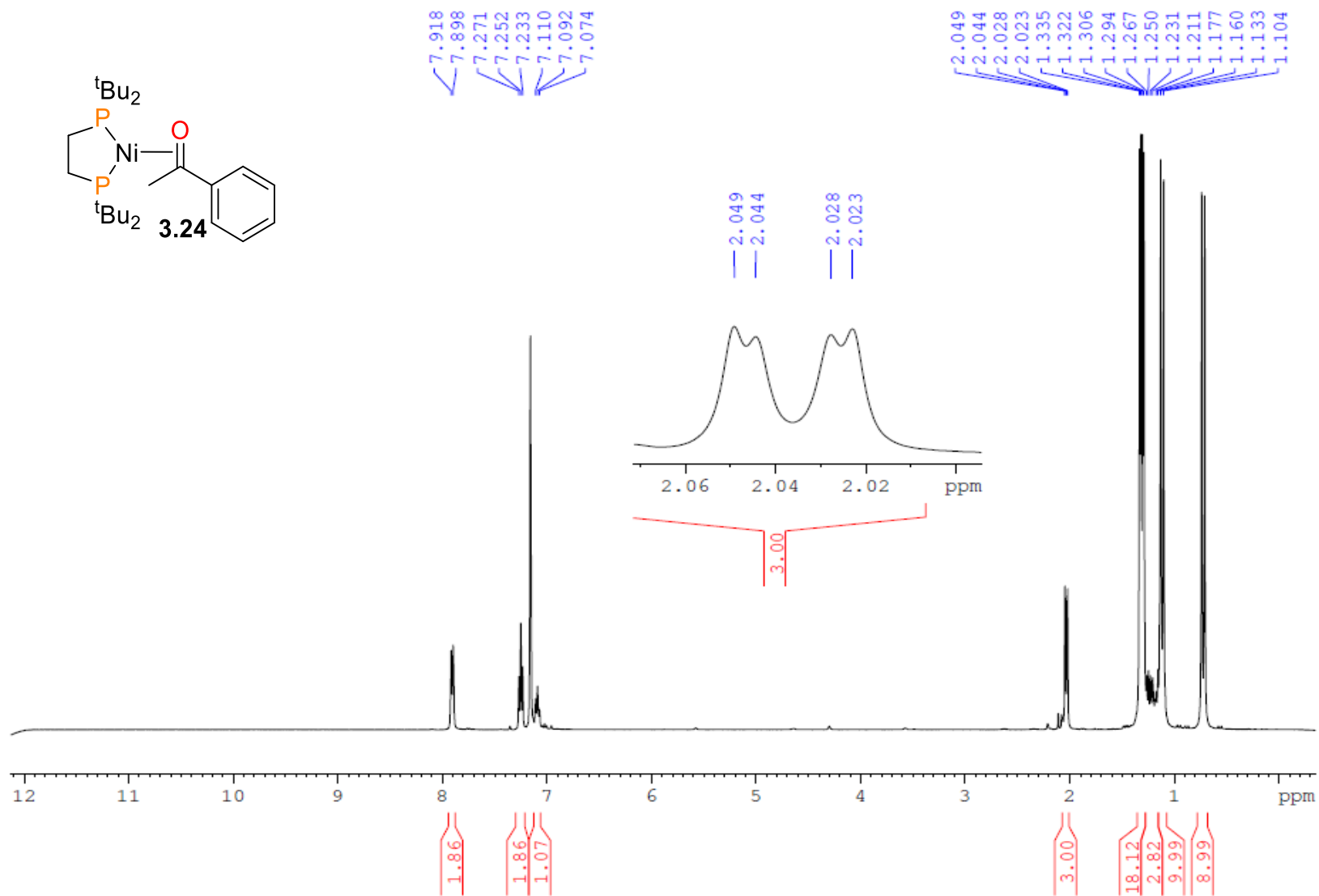


**Figure B3.4.**  $^1\text{H}$  NMR spectrum (400 MHz,  $\text{C}_6\text{D}_6$ , 25  $^\circ\text{C}$ ) of **3.24**.

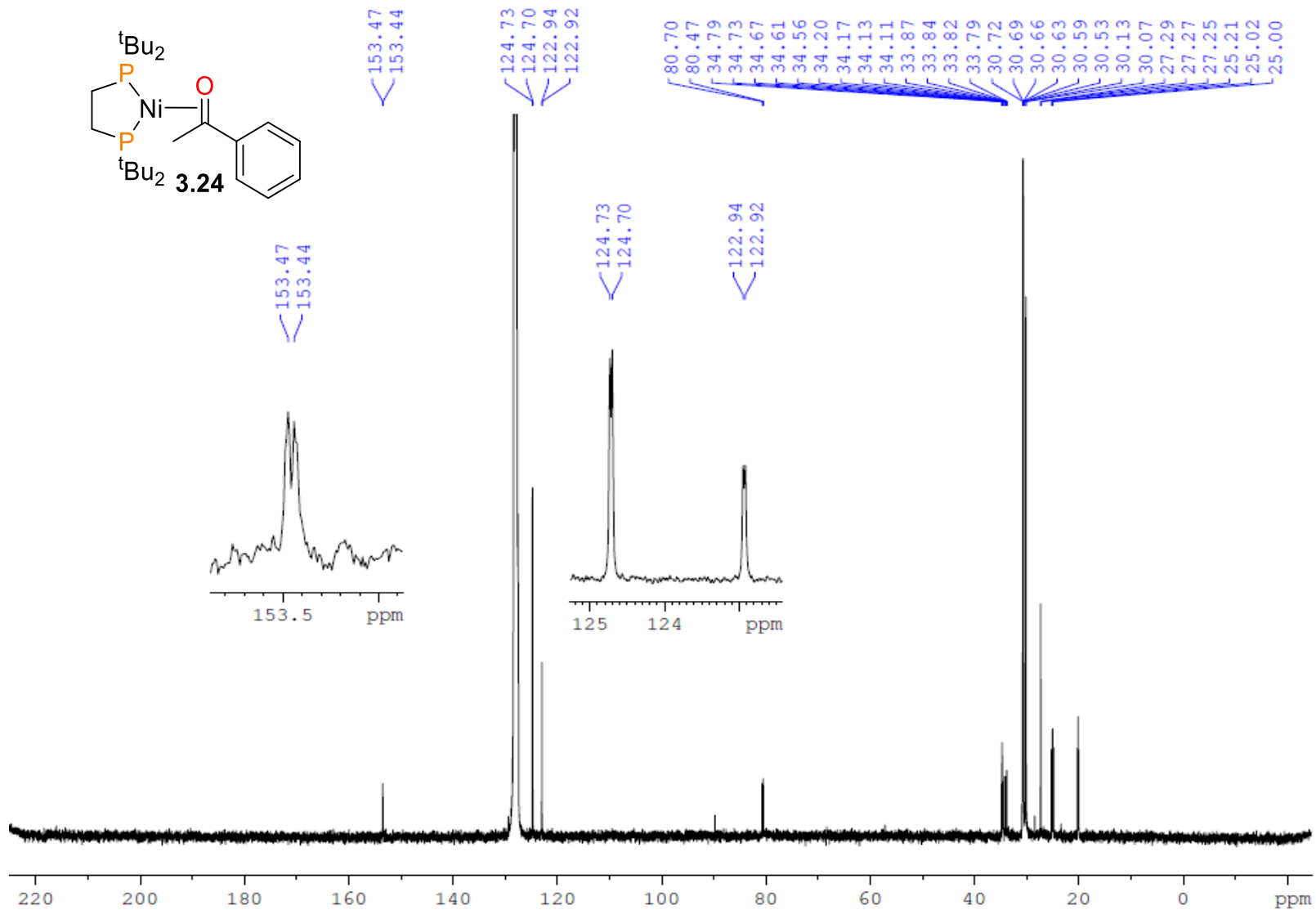


**Figure B3.5.**  $^{13}\text{C}\{^1\text{H}\}$  NMR spectrum (100 MHz,  $\text{C}_6\text{D}_6$ , 25 °C) of **3.24**.

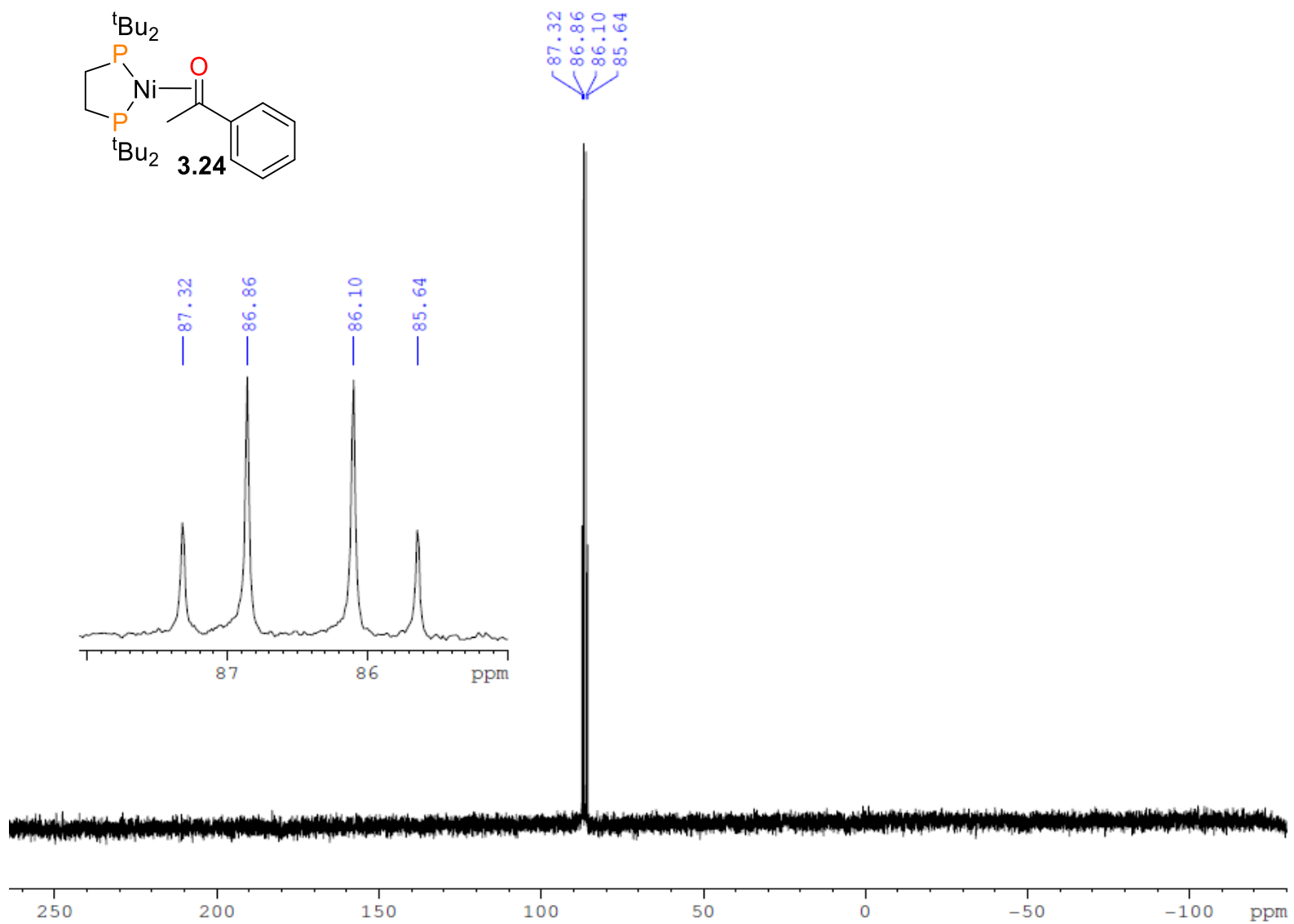


**Figure B3.6.**  $^{31}\text{P}\{^1\text{H}\}$  NMR spectrum (162 MHz,  $\text{C}_6\text{D}_6$ , 25 °C) of **3.24**.

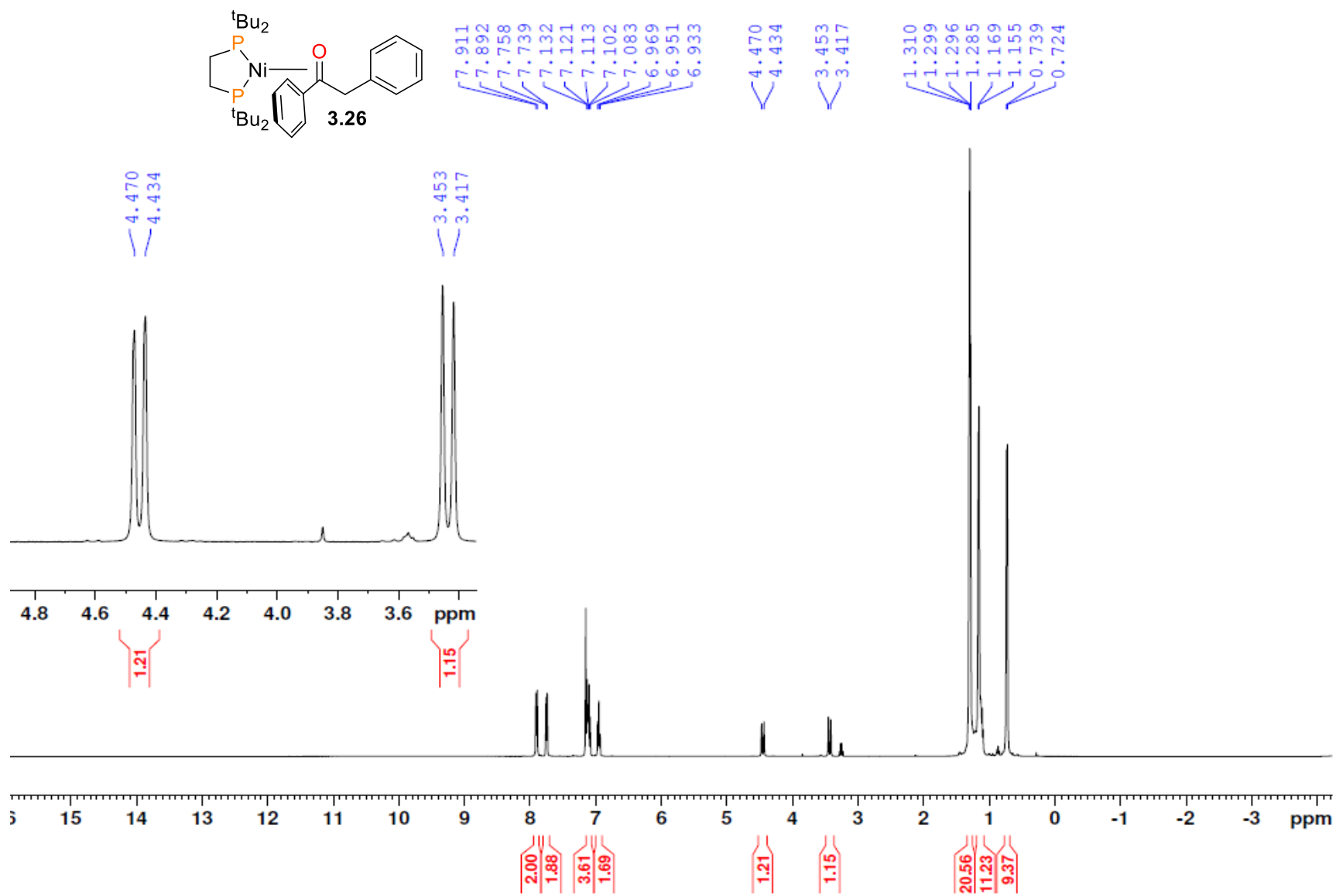


**Figure B3.7.**  $^1\text{H}\{^{31}\text{P}\}$  NMR spectrum (400 MHz,  $\text{C}_6\text{D}_6$ , 25 °C) of **3.26**.

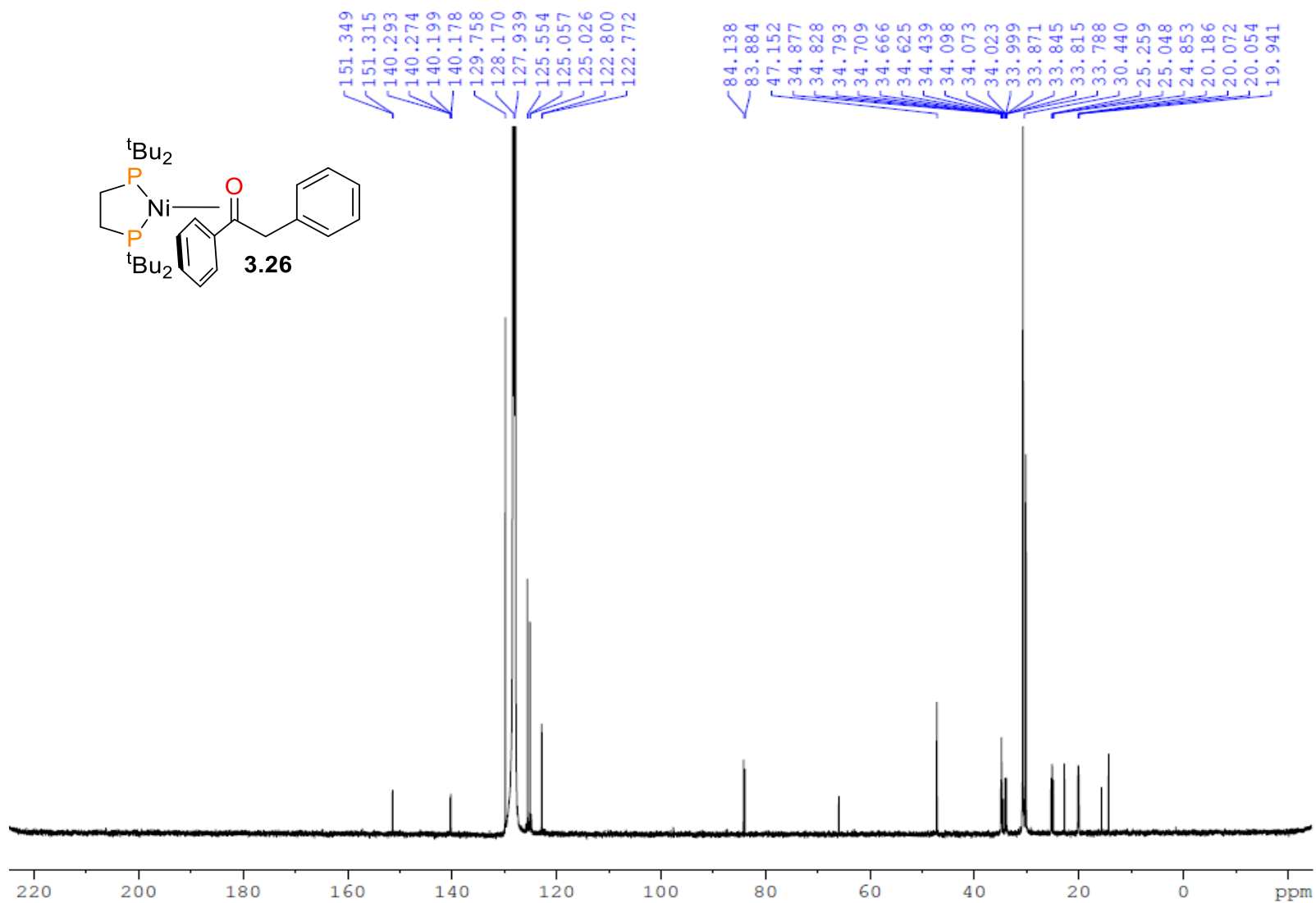


**Figure B3.8.**  $^{13}\text{C}\{^1\text{H}\}$  NMR spectrum (100 MHz,  $\text{C}_6\text{D}_6$ , 25 °C) of **3.26**. Inset shows the resonance assigned for C1.

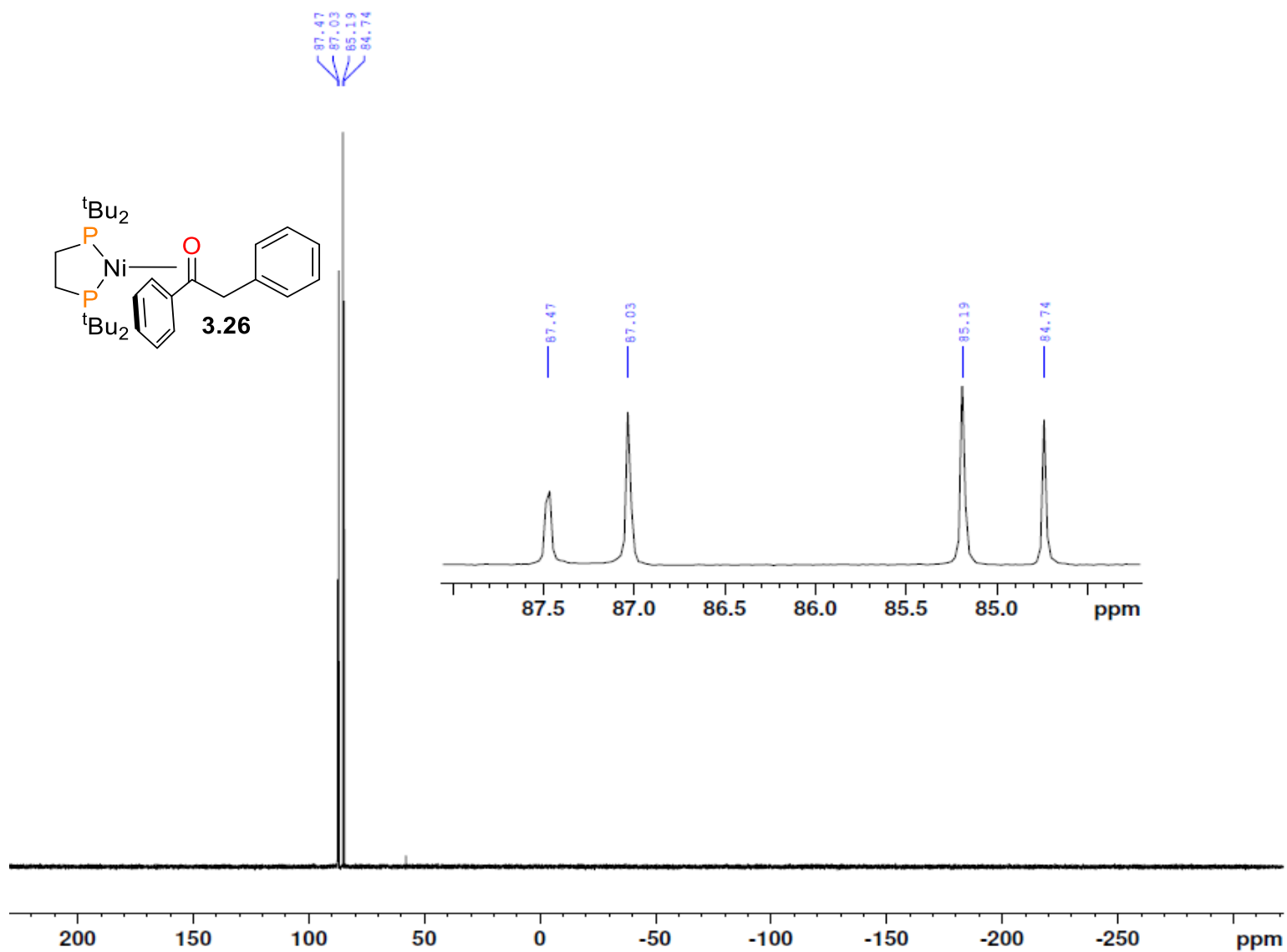


**Figure B3.9.**  $^{31}\text{P}\{^1\text{H}\}$  NMR spectrum (162 MHz,  $\text{C}_6\text{D}_6$ , 25 °C) of **3.26**.

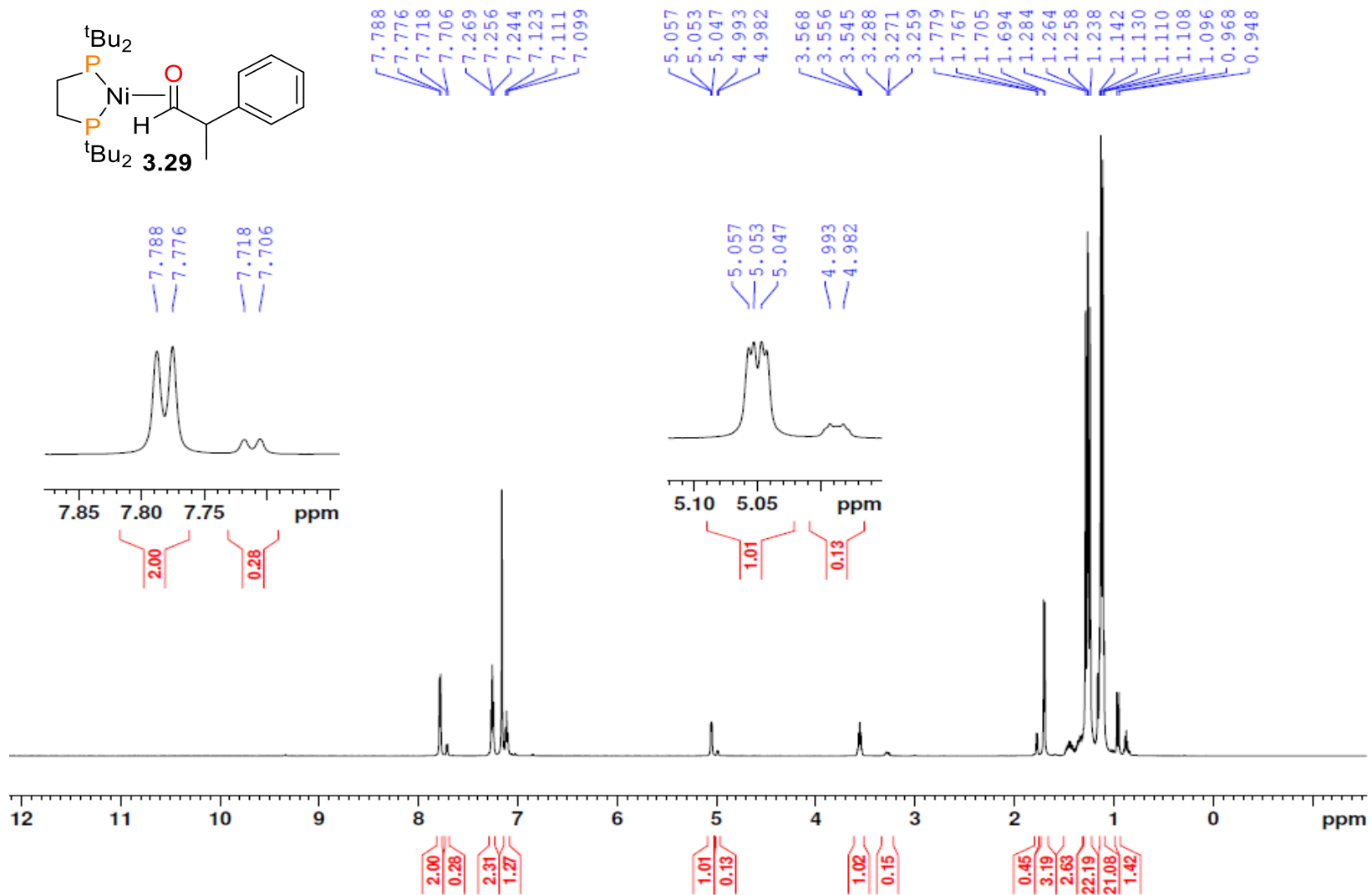


**Figure B3.10.**  $^1\text{H}$  NMR spectrum (600 MHz,  $\text{C}_6\text{D}_6$ , 25  $^\circ\text{C}$ ) of **3.29**. Left inset shows the resonances assigned to **H5** of both diastereomers, right inset shows resonances assigned to **H1** of both diastereomers.

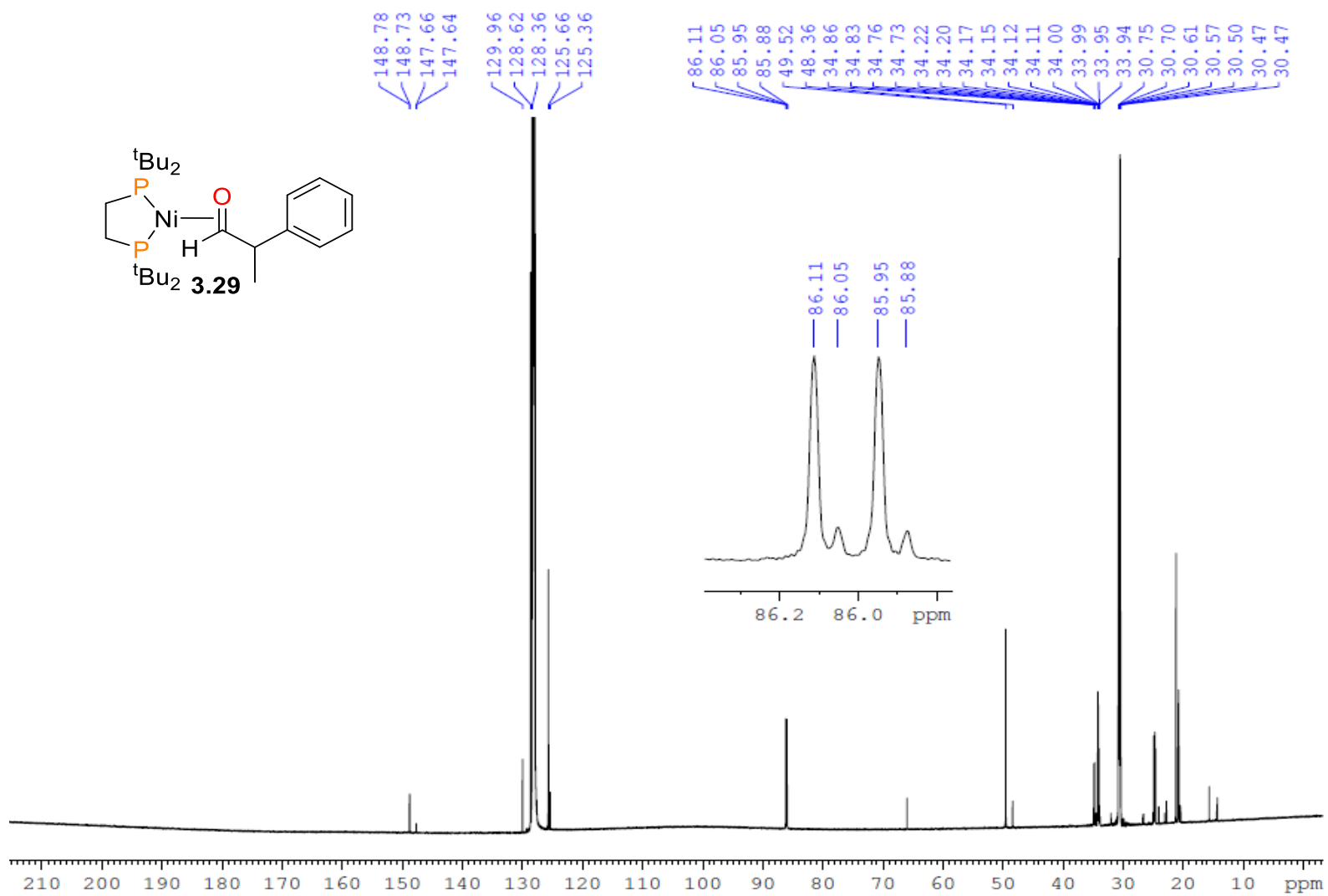


**Figure B3.11.**  $^{13}\text{C}\{^1\text{H}\}$  NMR spectrum (125 MHz,  $\text{C}_6\text{D}_6$ , 25 °C) of **3.29**. Inset shows the resonance assigned to C1 of both diastereomers.

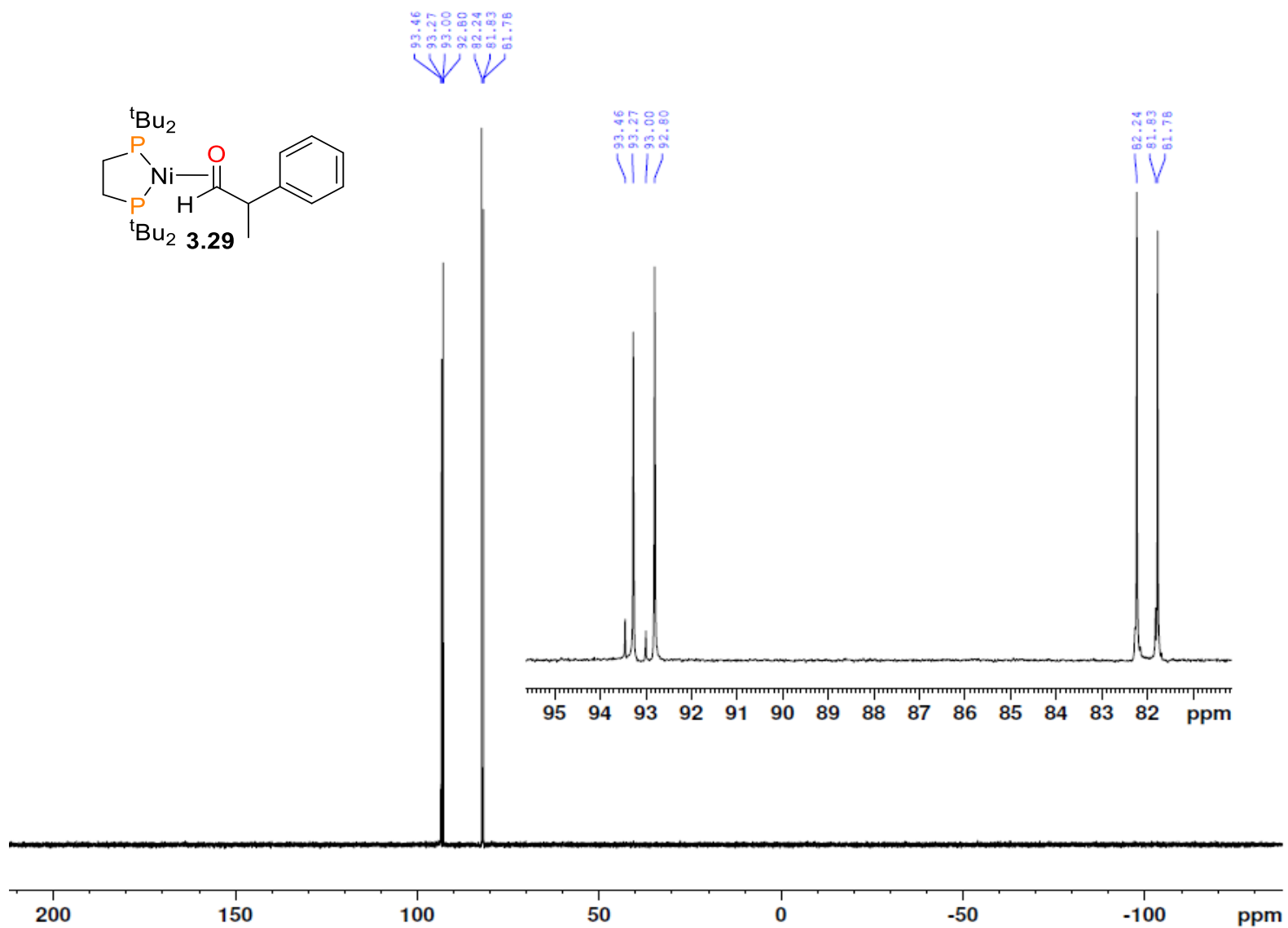


**Figure B3.12.**  $^{31}\text{P}\{^1\text{H}\}$  NMR spectrum (162 MHz,  $\text{C}_6\text{D}_6$ , 25 °C) of **3.29**.

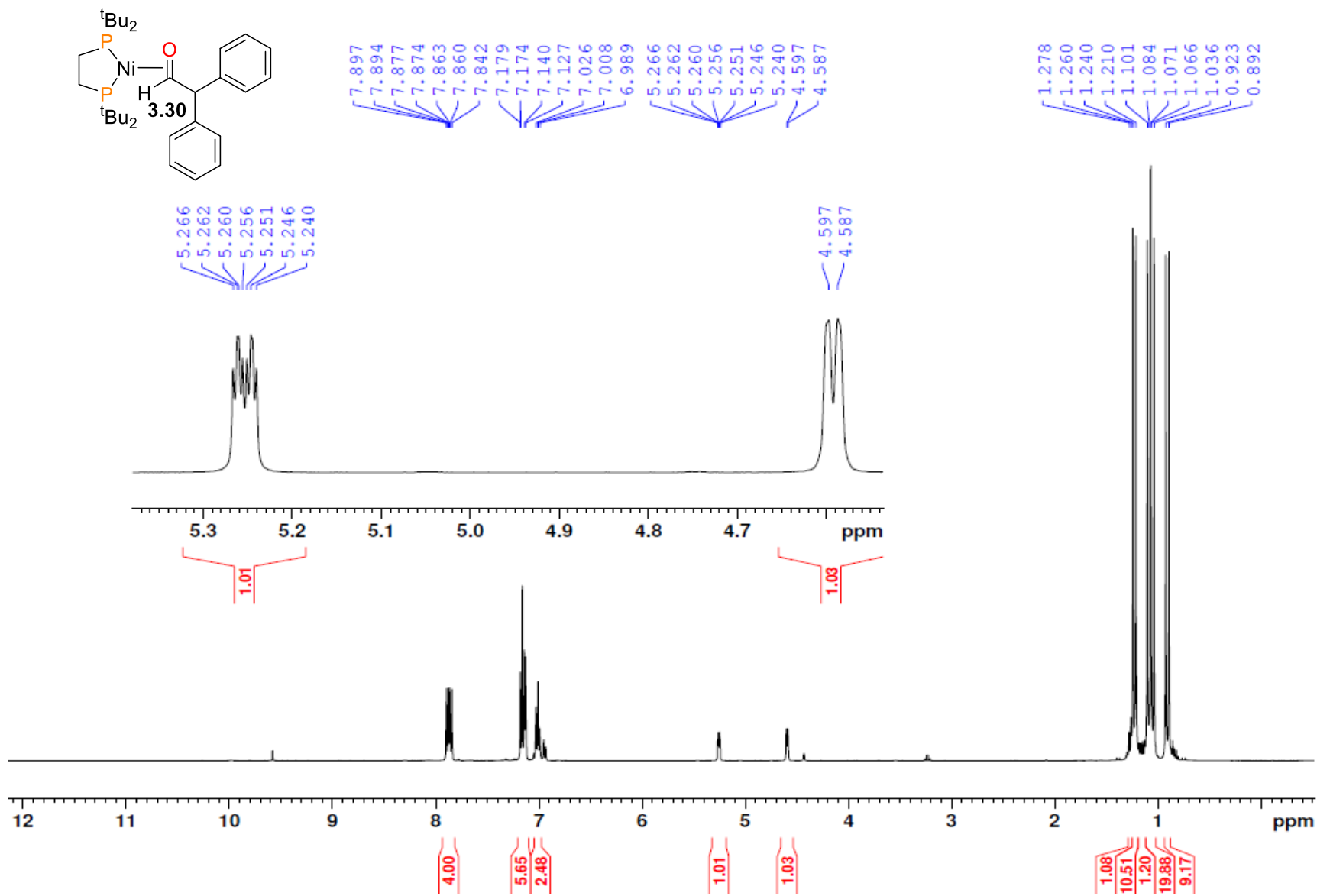


**Figure B3.13.** <sup>1</sup>H NMR spectrum (400 MHz, C<sub>6</sub>D<sub>6</sub>, 25 °C) of **3.30**. Inset shows the resonances assigned for C1 and C2.

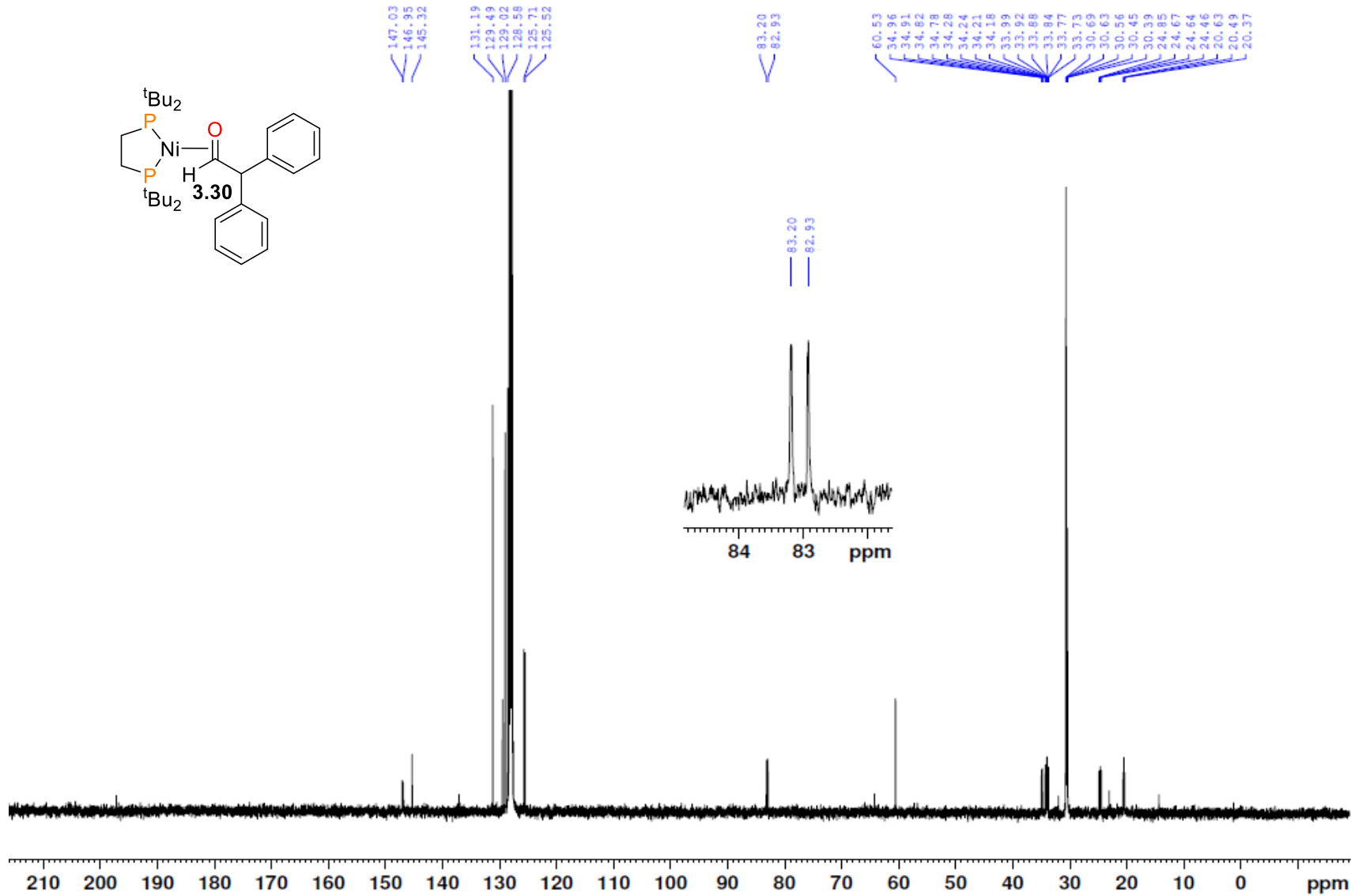


**Figure B3.14.**  $^{13}\text{C}\{^1\text{H}\}$  NMR spectrum (100 MHz,  $\text{C}_6\text{D}_6$ , 25 °C) of **3.30**. Inset shows the resonance assigned for C1.

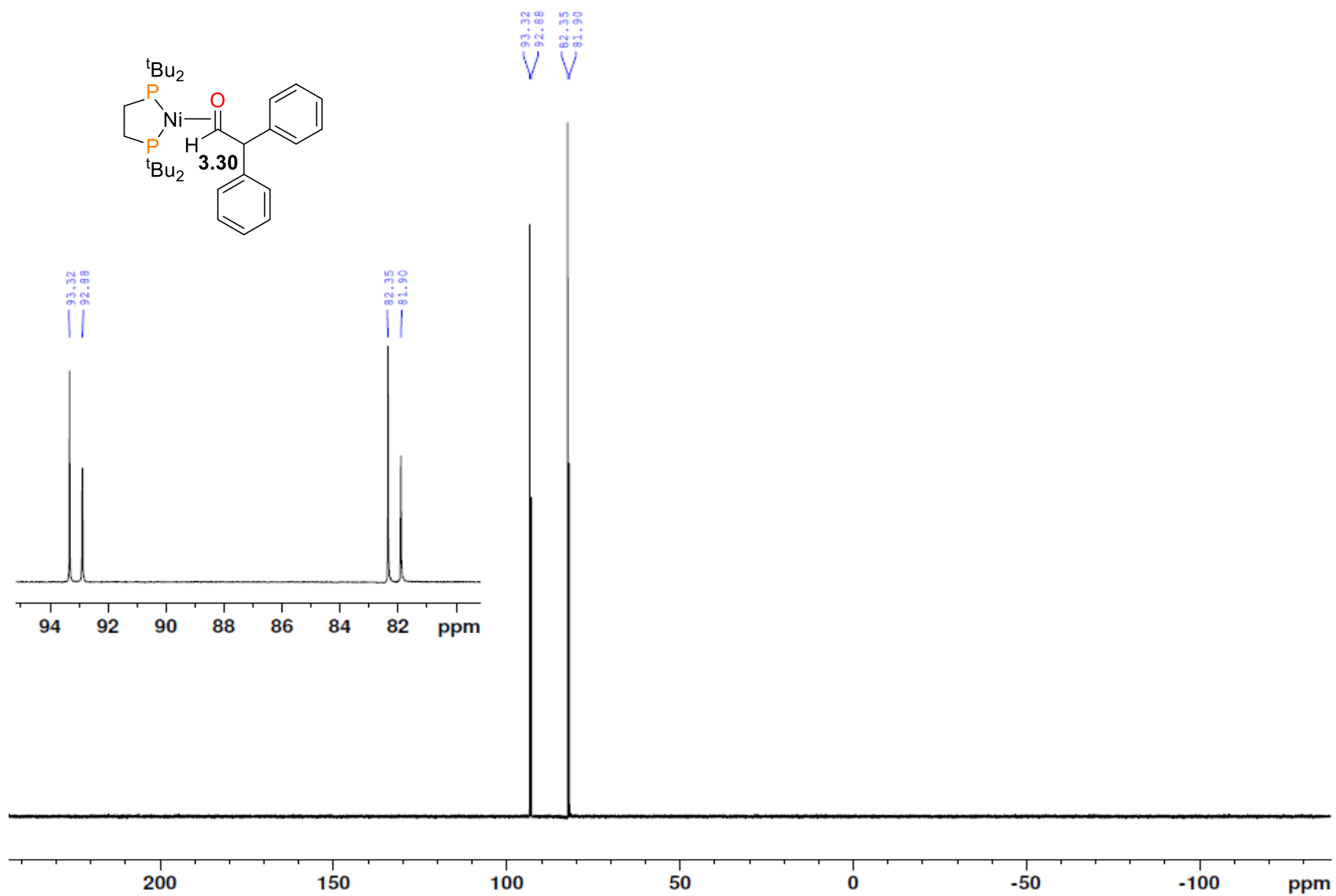


**Figure B3.15.**  $^{31}\text{P}\{^1\text{H}\}$  NMR spectrum (162 MHz,  $\text{C}_6\text{D}_6$ , 25 °C) of **3.30**.

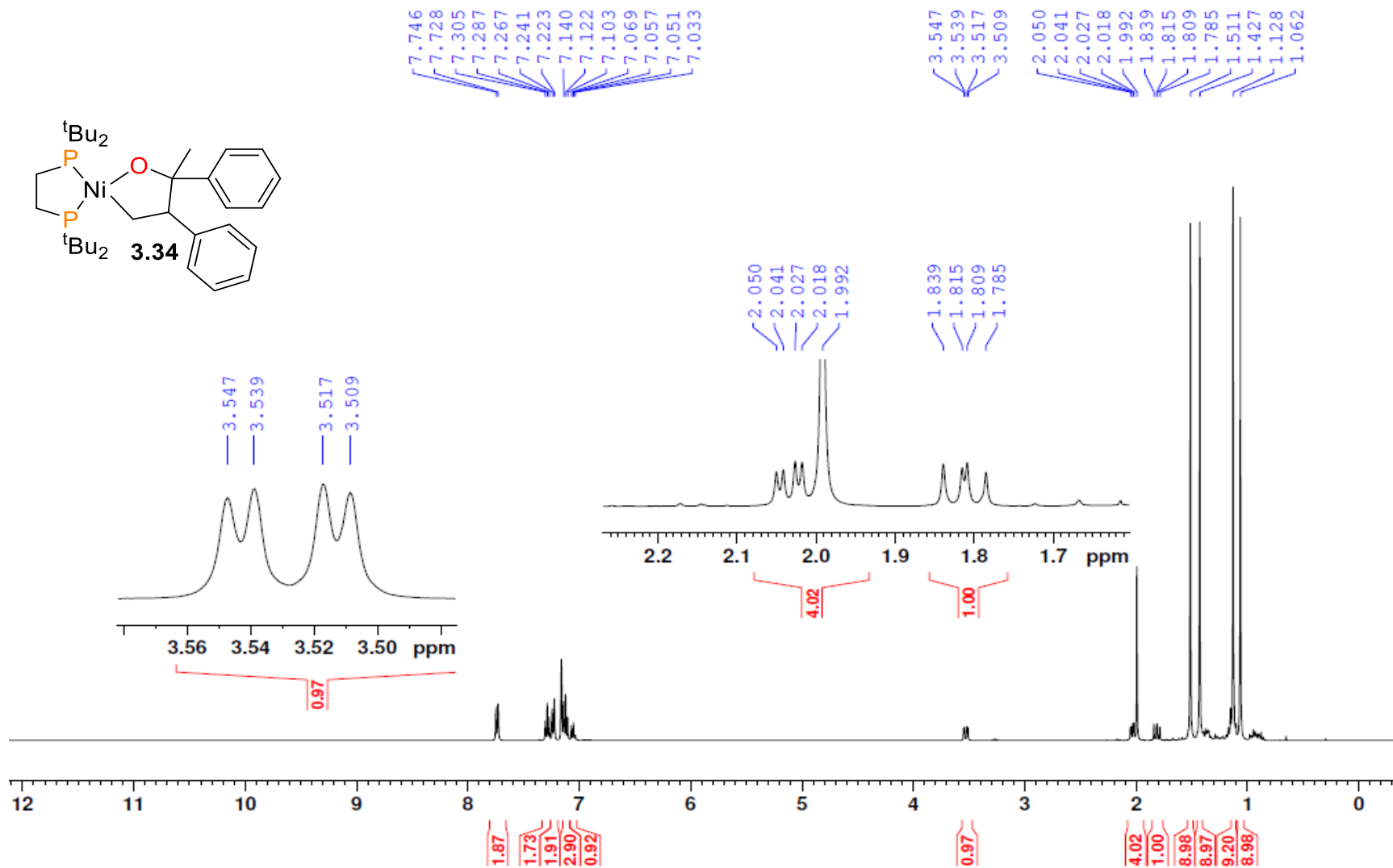


**Figure B3.16.**  $^1\text{H}\{^{31}\text{P}\}$  NMR spectrum (400 MHz,  $\text{C}_6\text{D}_6$ , 25 °C) of **3.34**. The left inset shows the resonance assigned to **H2**, while the right shows the resonances of **H3** and **H4**.

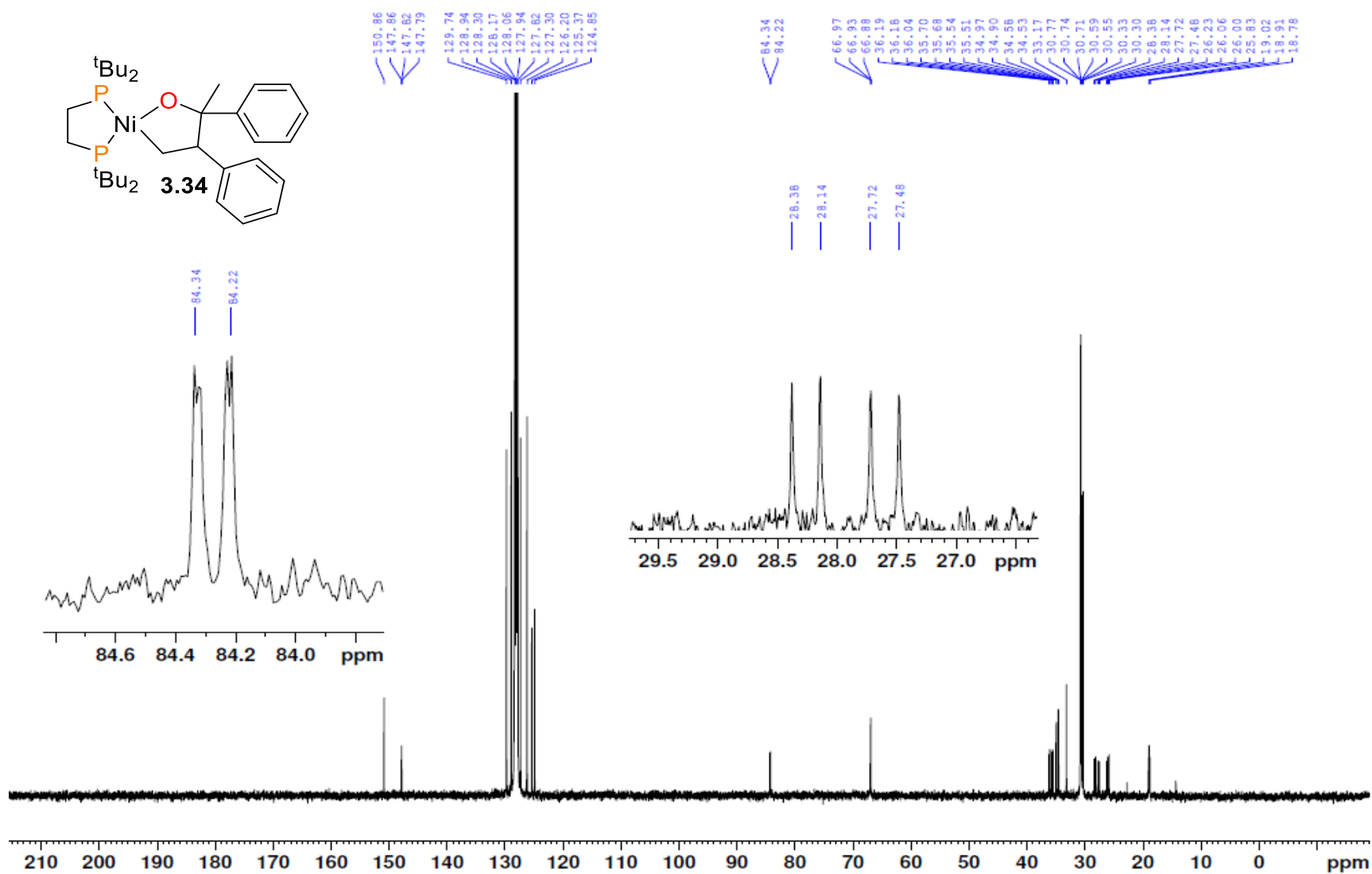


**Figure B3.17.**  $^{13}\text{C}\{^1\text{H}\}$  NMR spectrum (100 MHz,  $\text{C}_6\text{D}_6$ , 25 °C) of **3.34**. The left inset shows the resonance assigned for C1, while the right shows the resonance for C3.

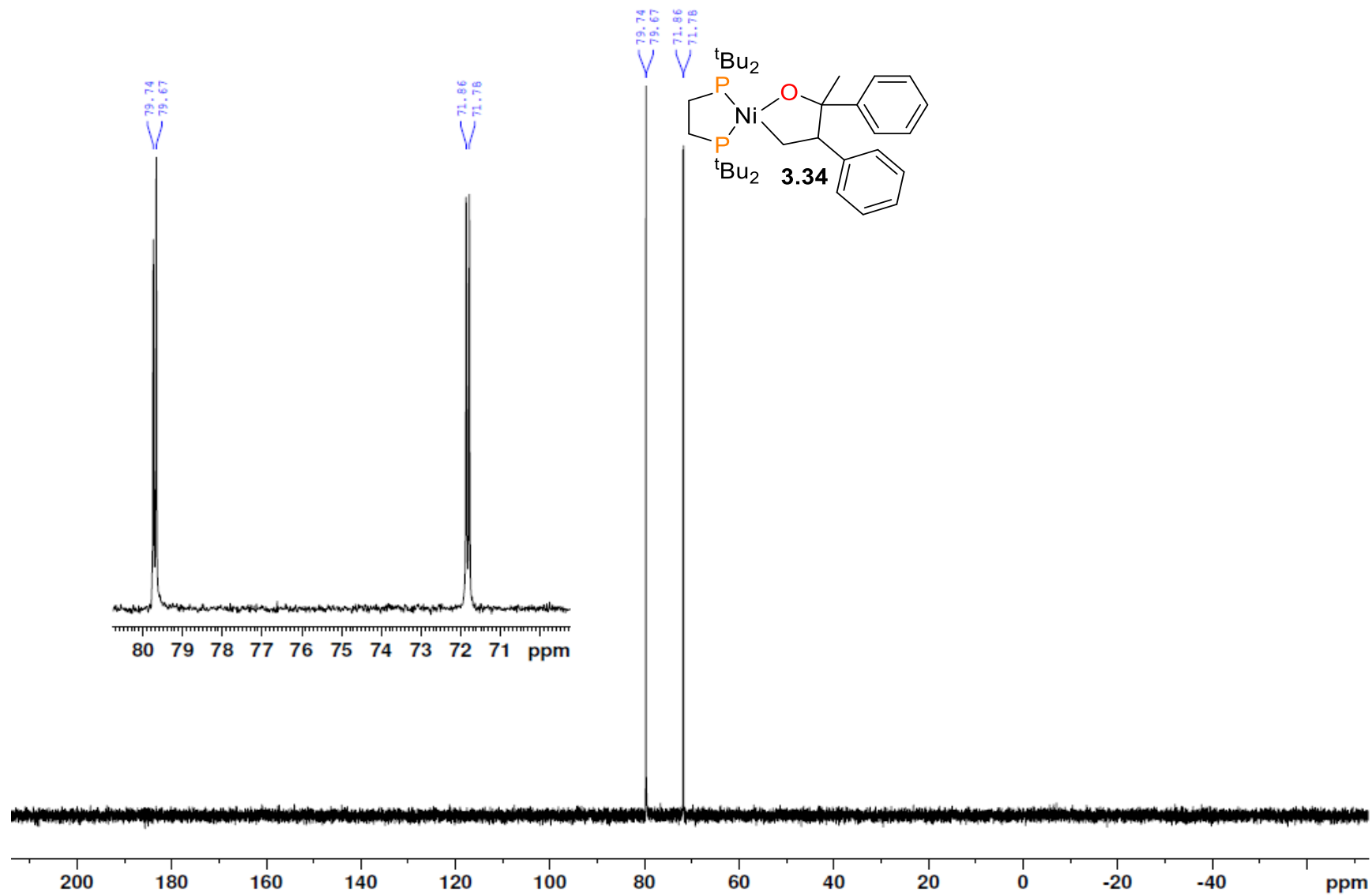


**Figure B3.18.**  $^{31}\text{P}\{^1\text{H}\}$  NMR spectrum (162 MHz,  $\text{C}_6\text{D}_6$ , 25 °C) of **3.34**.

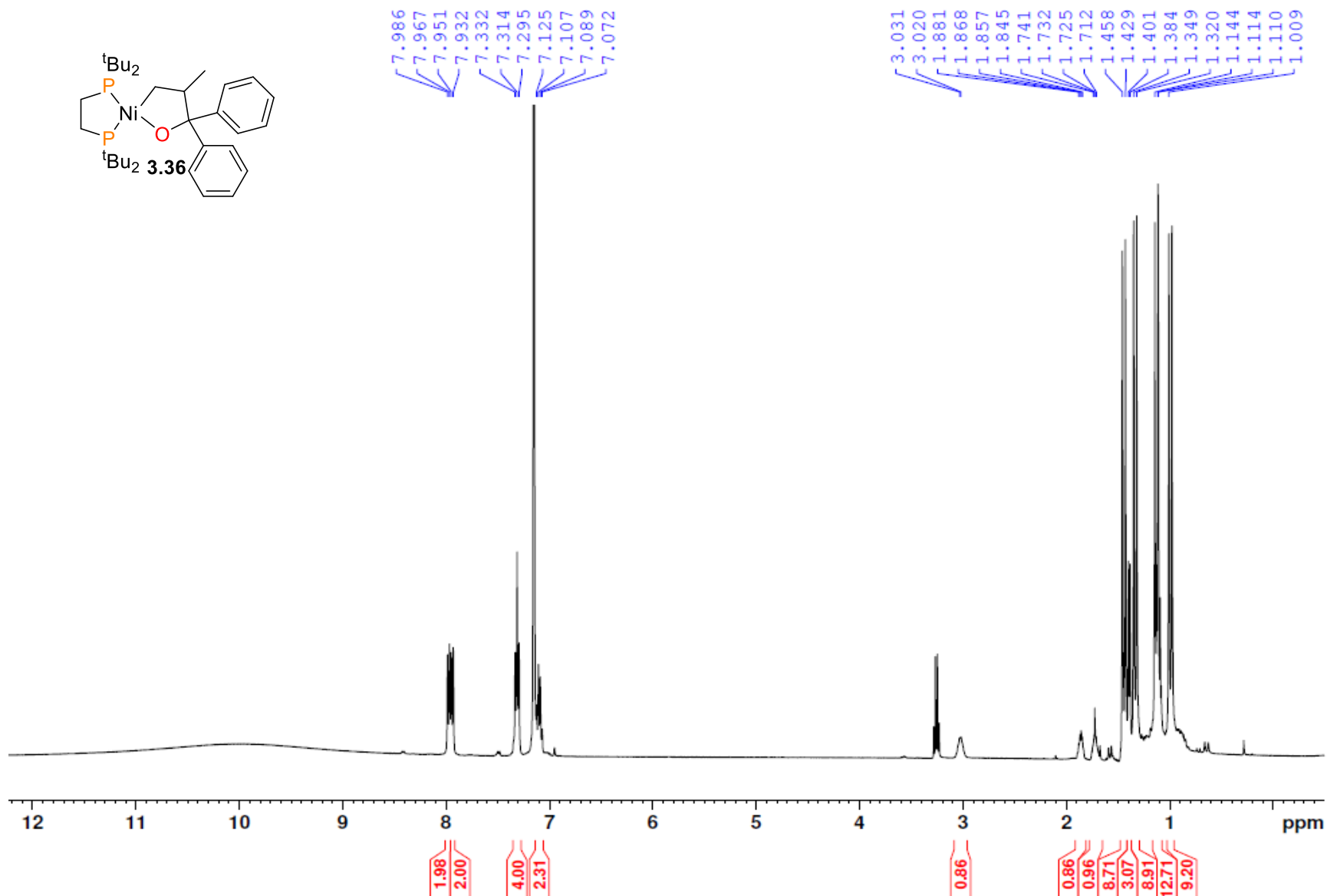


**Figure B3.19.**  $^1\text{H}$  NMR spectrum (400 MHz,  $\text{C}_6\text{D}_6$ , 25 °C) of **3.36**.

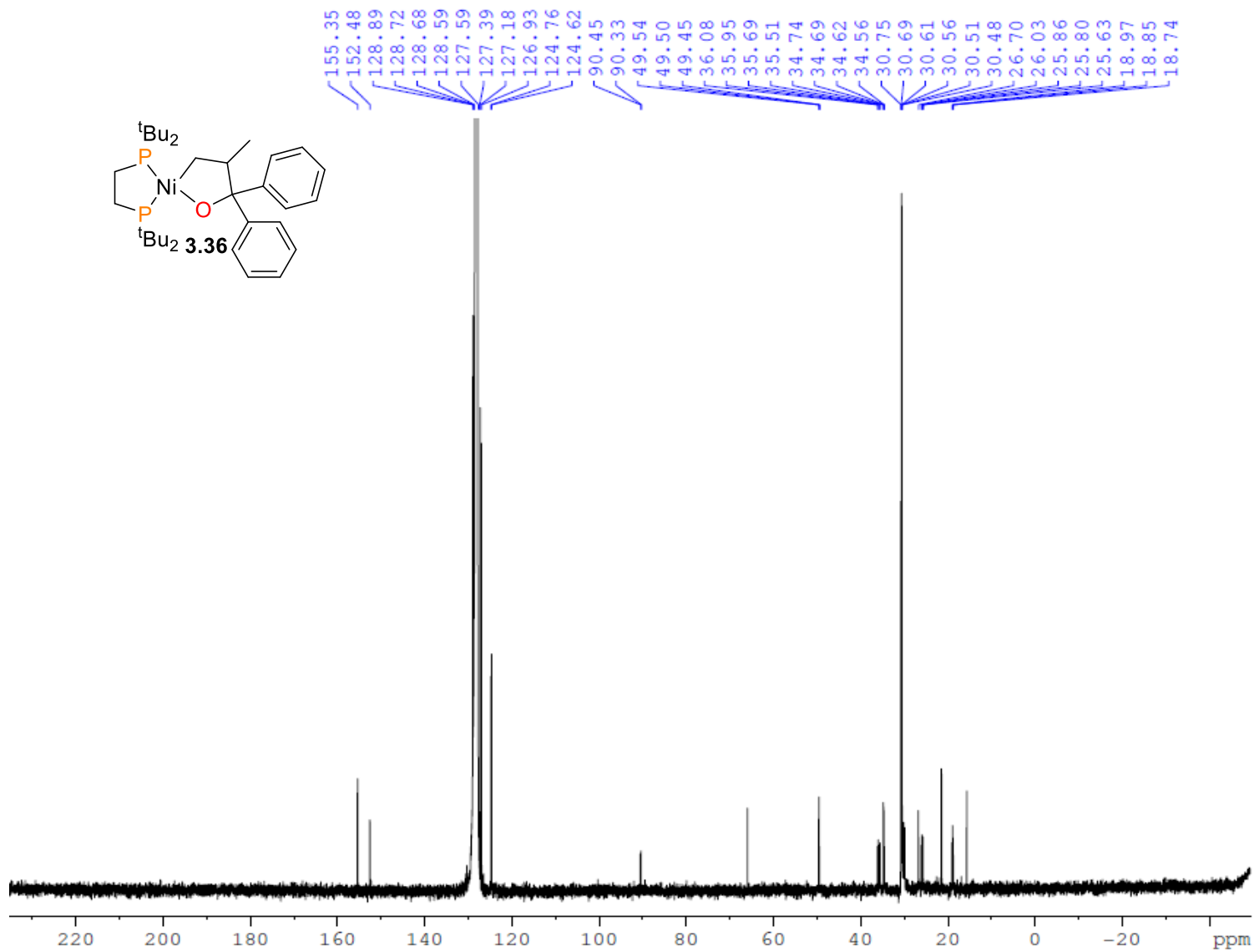


**Figure B3.20.**  $^{13}\text{C}\{^1\text{H}\}$  NMR spectrum (100 MHz,  $\text{C}_6\text{D}_6$ , 25 °C) of **3.36**.

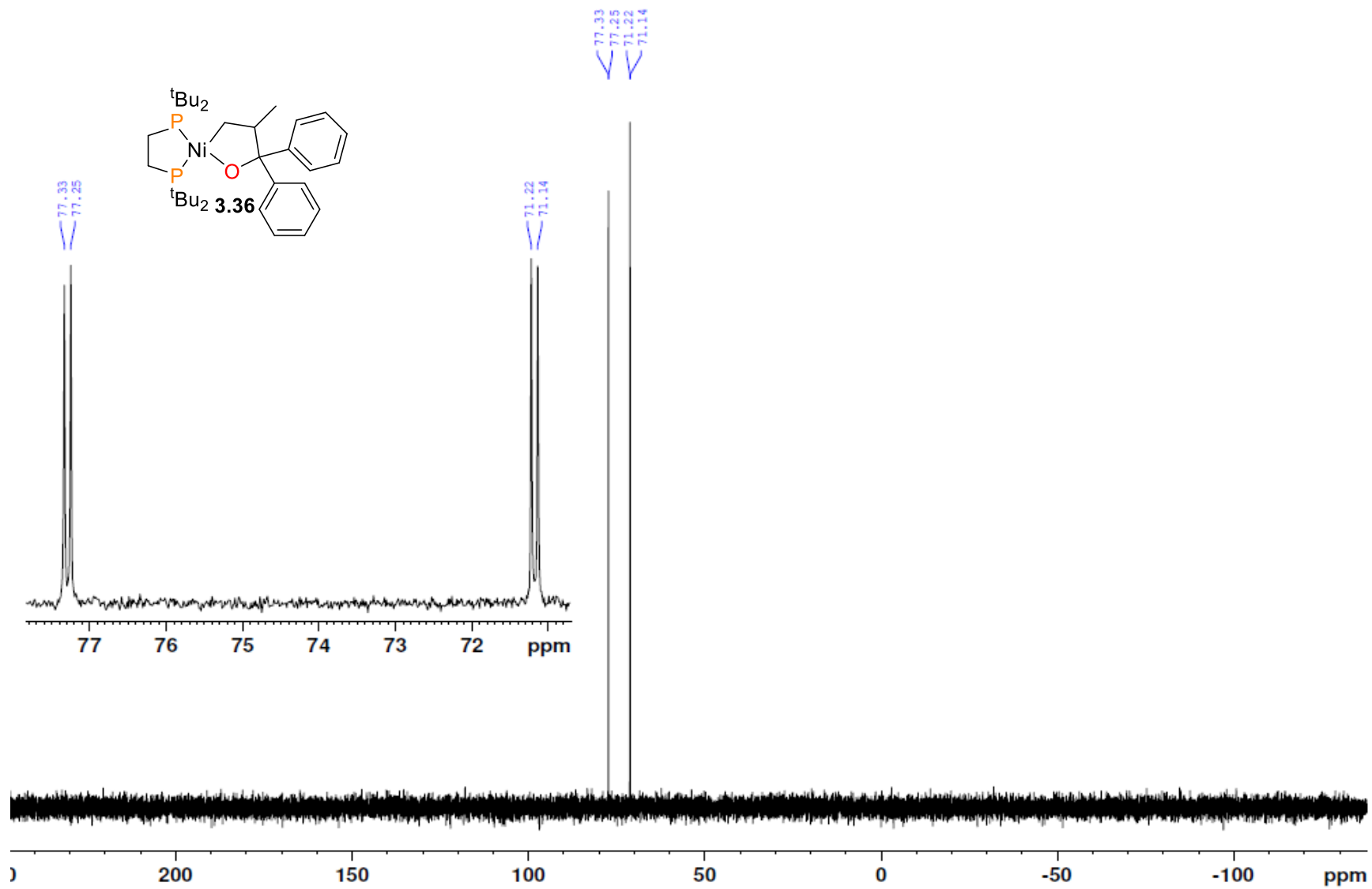


**Figure B3.21.**  $^{31}\text{P}\{^1\text{H}\}$  NMR spectrum ( $162\text{ MHz}$ ,  $\text{C}_6\text{D}_6$ ,  $25^\circ\text{C}$ ) of **3.36**.

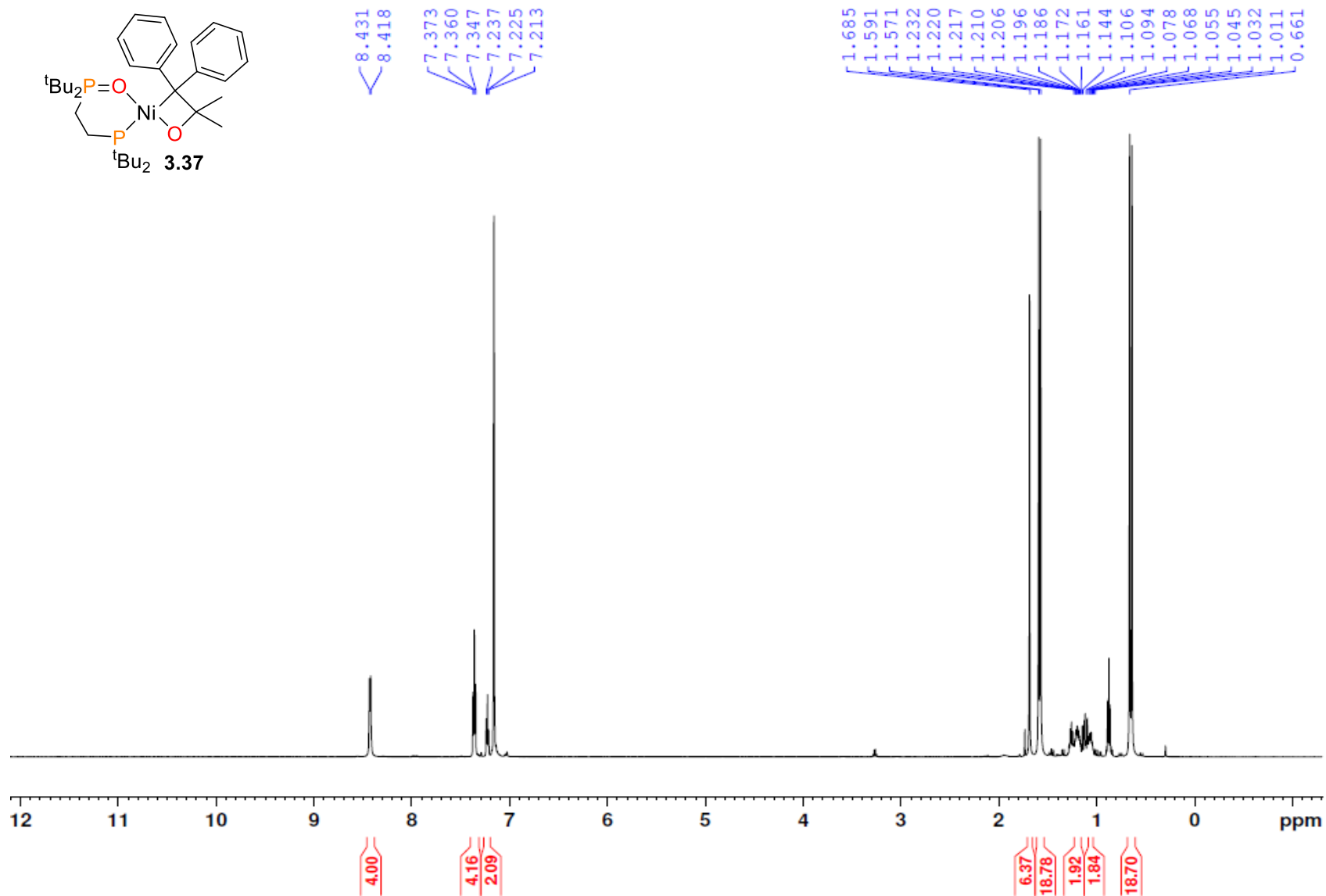


**Figure B3.22.**  $^1\text{H}$  NMR spectrum (400 MHz,  $\text{C}_6\text{D}_6$ , 25  $^\circ\text{C}$ ) of **3.37**.

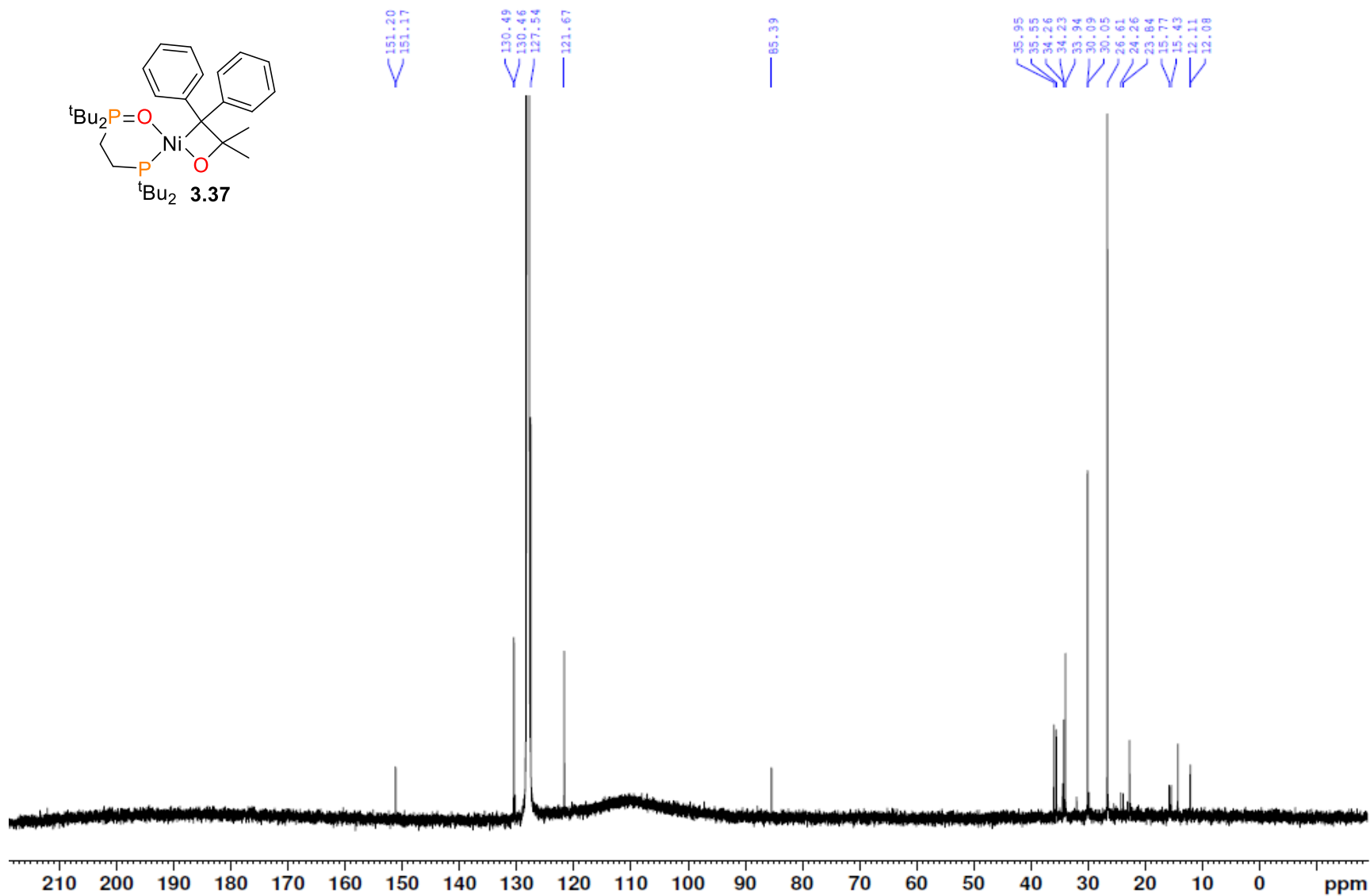


**Figure B3.23.**  $^{13}\text{C}\{^1\text{H}\}$  NMR spectrum (100 MHz,  $\text{C}_6\text{D}_6$ , 25 °C) of **3.37**.

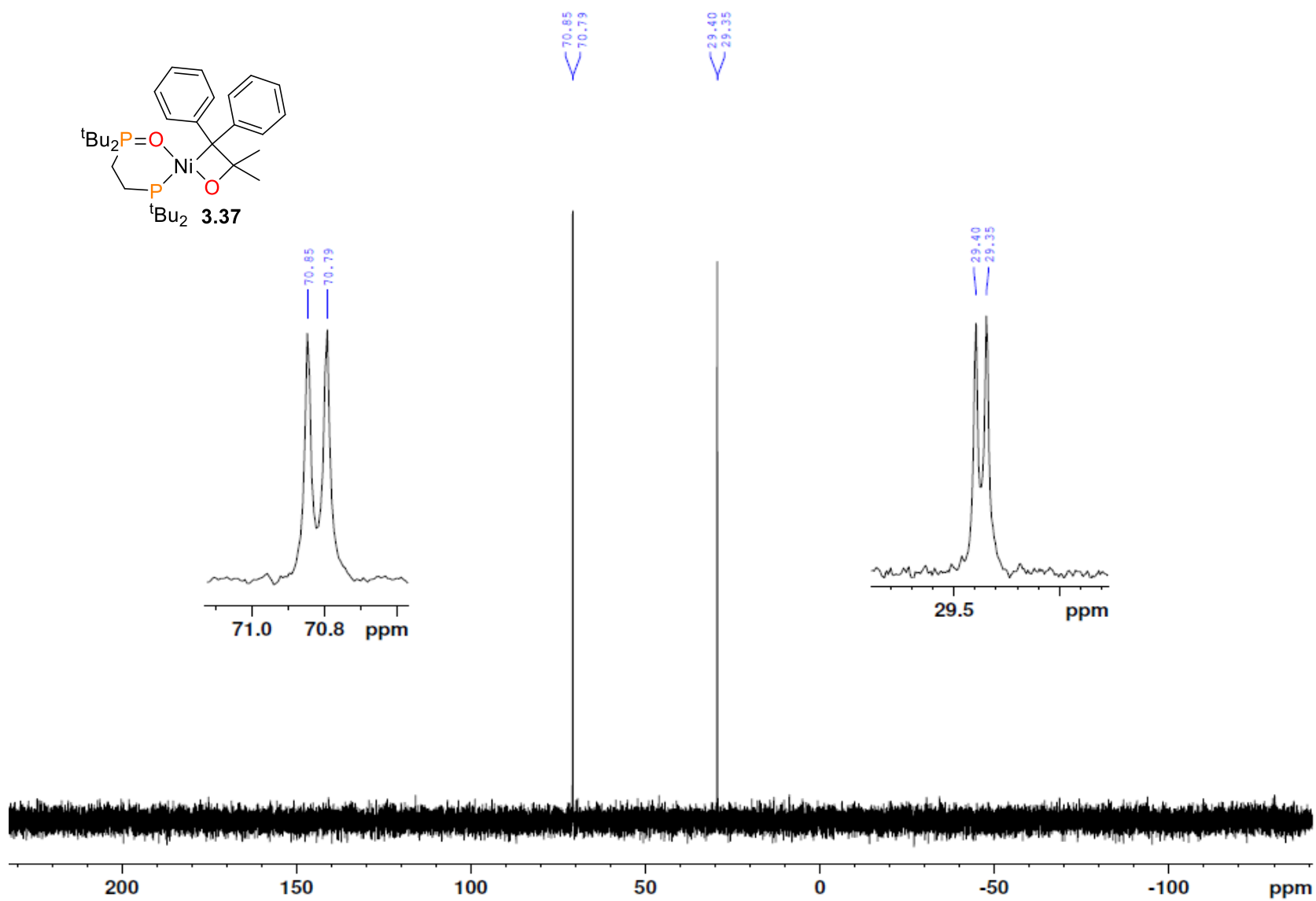


**Figure B3.24.**  $^{31}\text{P}\{^1\text{H}\}$  NMR spectrum (162 MHz,  $\text{C}_6\text{D}_6$ , 25 °C) of **3.37**.

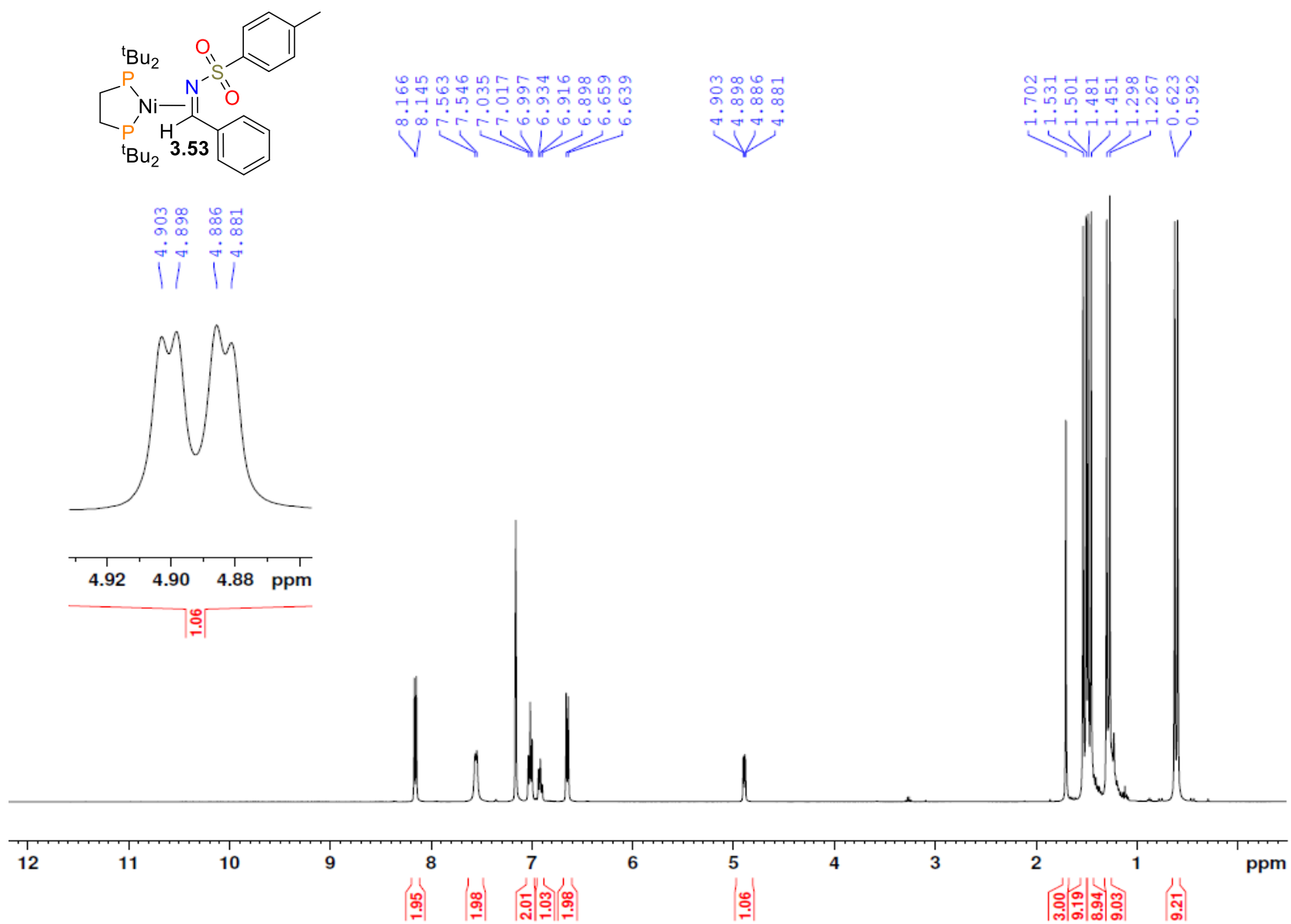


**Figure B3.25.**  $^1\text{H}$  NMR spectrum (400 MHz,  $\text{C}_6\text{D}_6$ , 25 °C) of **3.53**. Inset shows **H1** resonance.



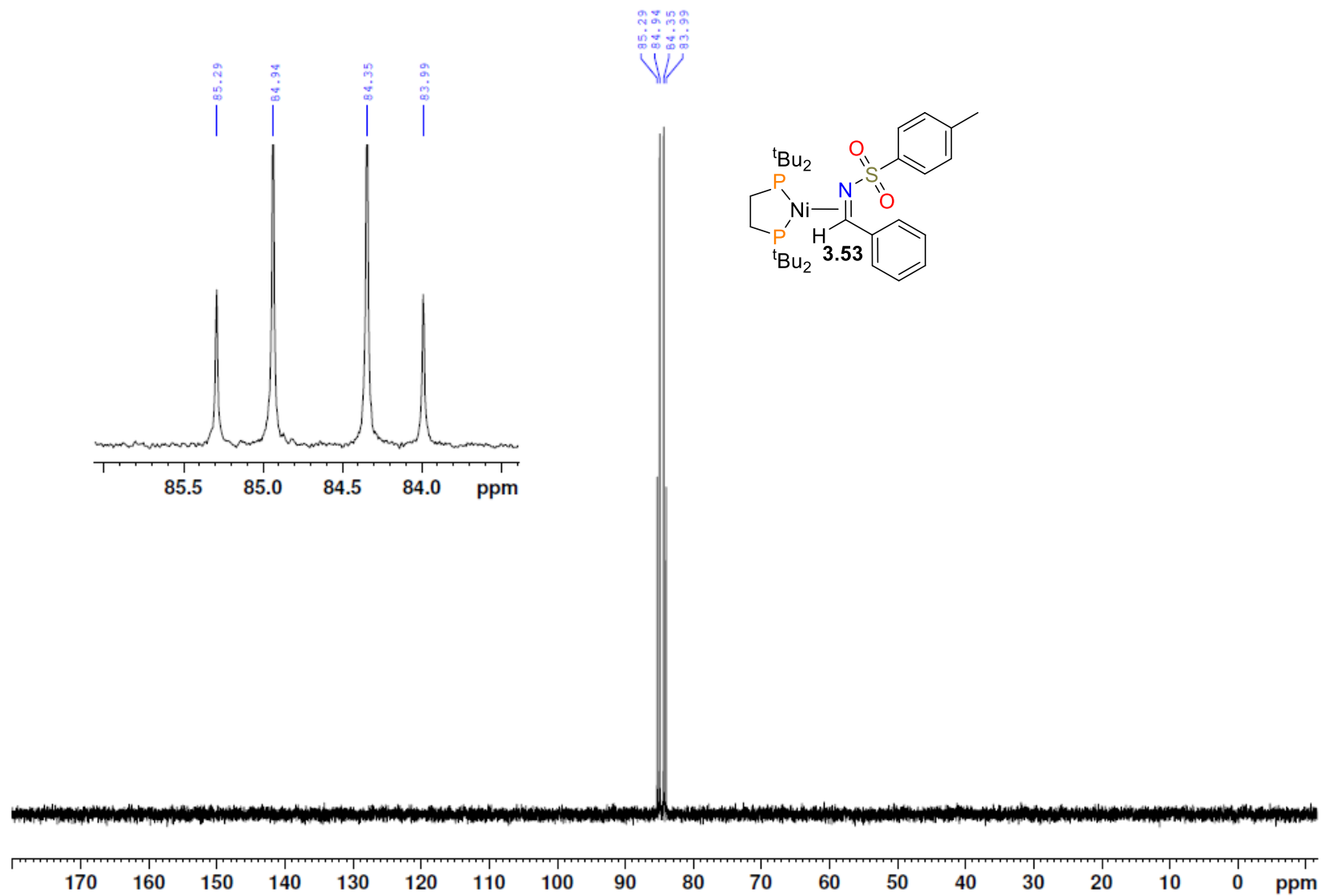


**Figure B3.27.**  $^{31}\text{P}\{^1\text{H}\}$  NMR spectrum (120 MHz,  $\text{C}_6\text{D}_6$ , 25 °C) of **3.53**.

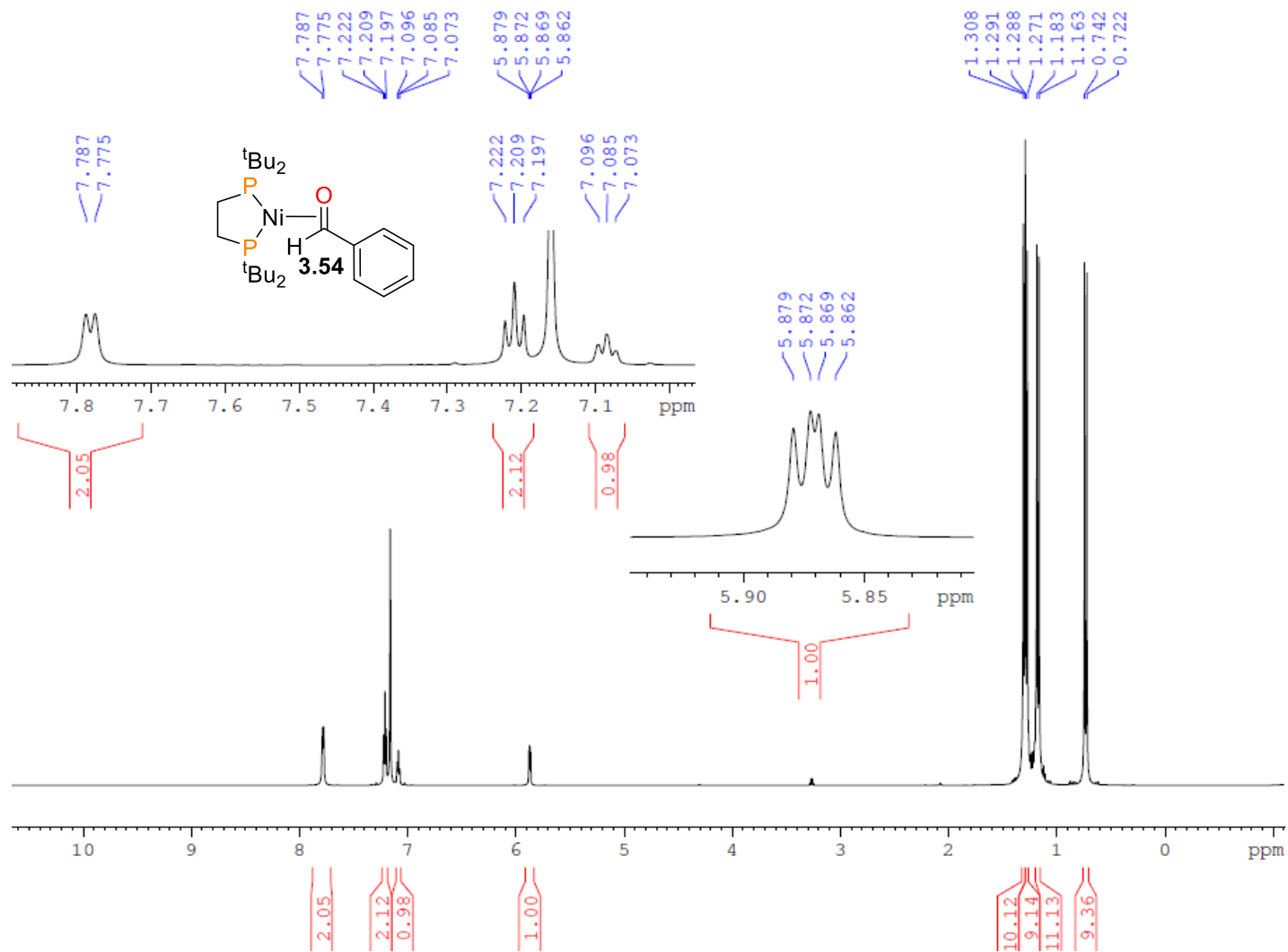


**Figure B3.28.**  $^1\text{H}$  NMR spectrum (600 MHz,  $\text{C}_6\text{D}_6$ , 25  $^\circ\text{C}$ ) of **3.54**. Left inset shows the aromatic resonances, while the right shows the **H1** resonance.

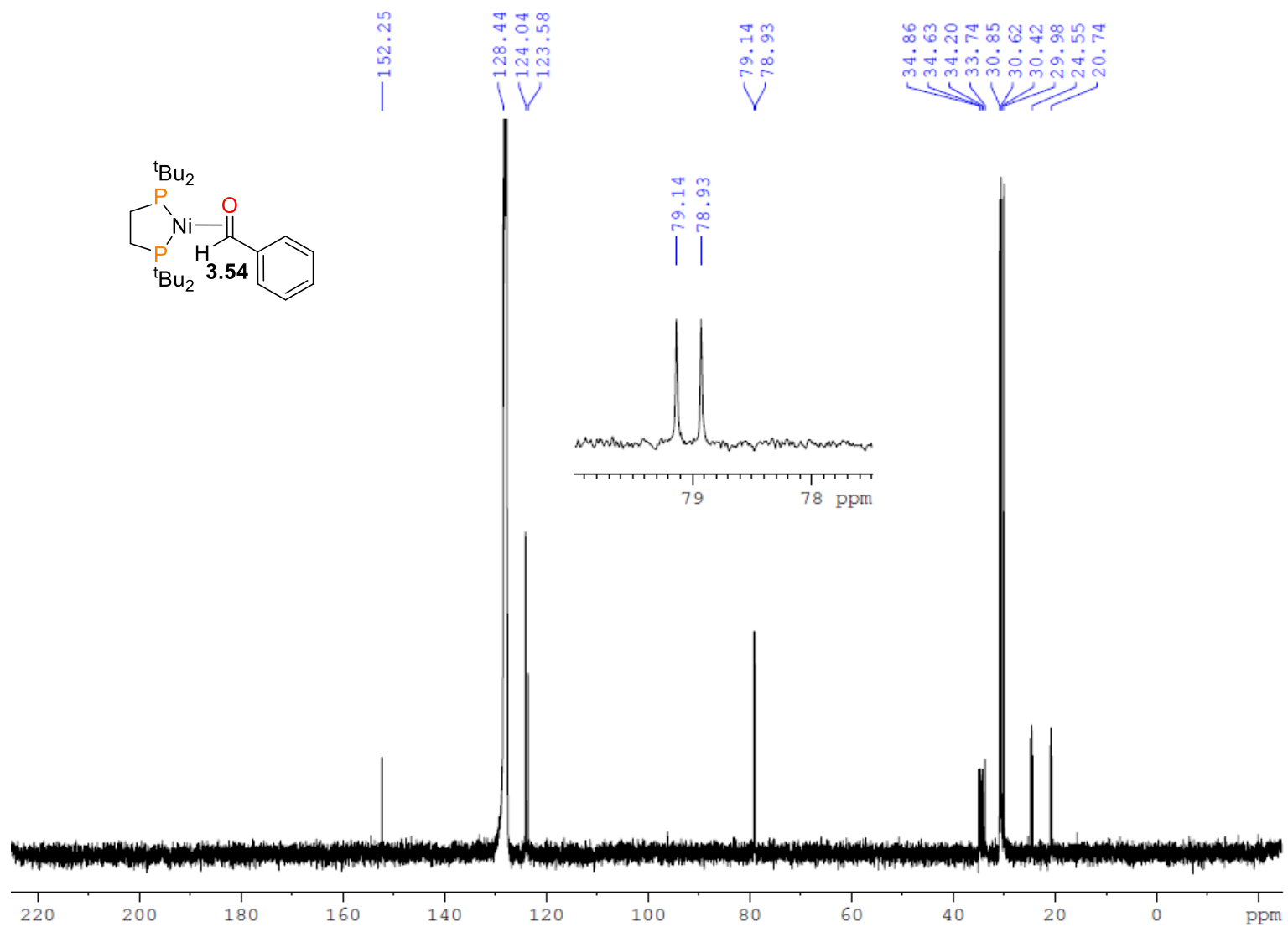


**Figure B3.29.**  $^{13}\text{C}\{^1\text{H}\}$  NMR spectrum (100 MHz,  $\text{C}_6\text{D}_6$ , 25 °C) of **3.54**. Inset shows the C1 resonance.

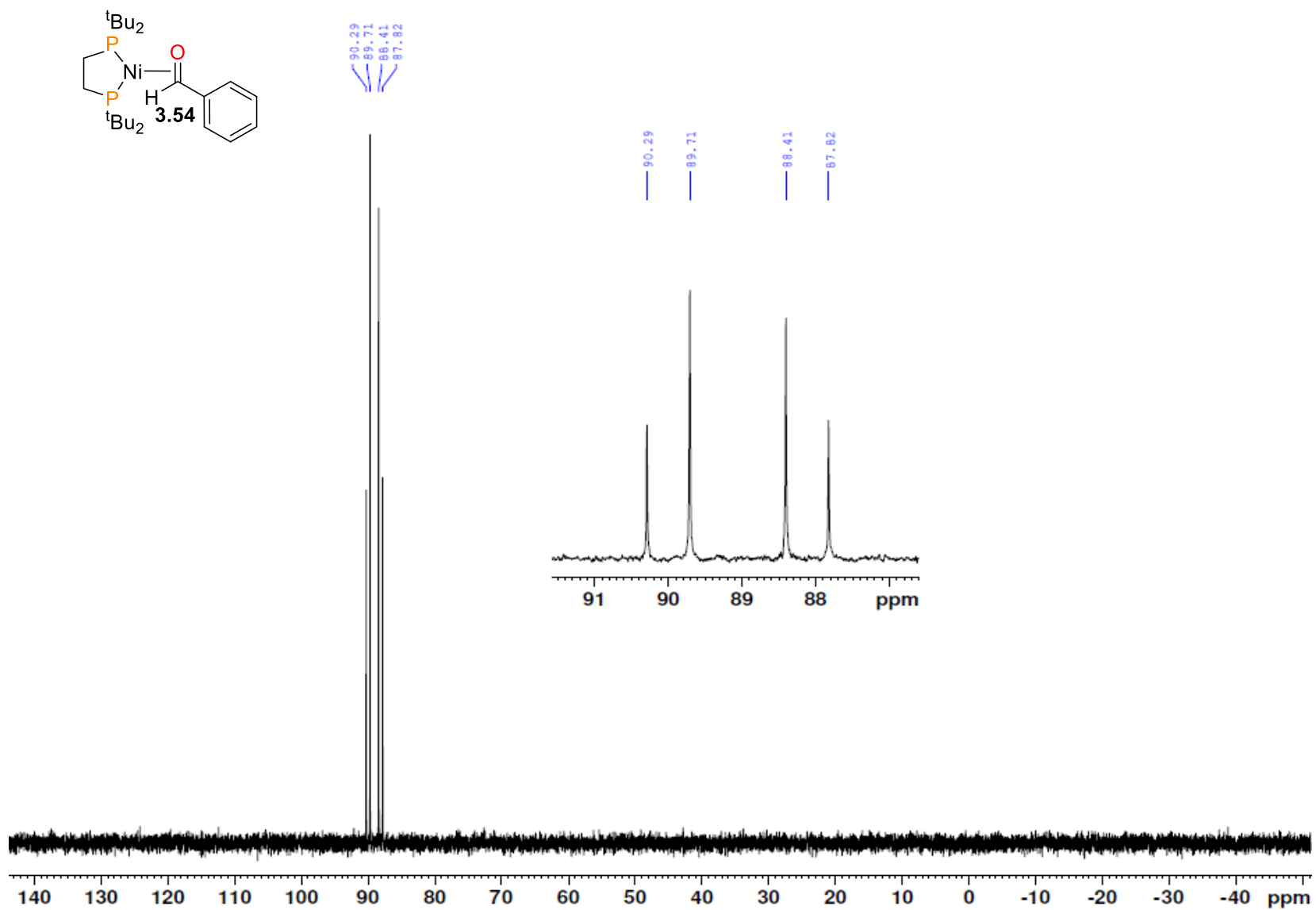


**Figure B3.30.**  $^{31}\text{P}\{^1\text{H}\}$  NMR spectrum (162 MHz,  $\text{C}_6\text{D}_6$ , 25 °C) of **3.54**.

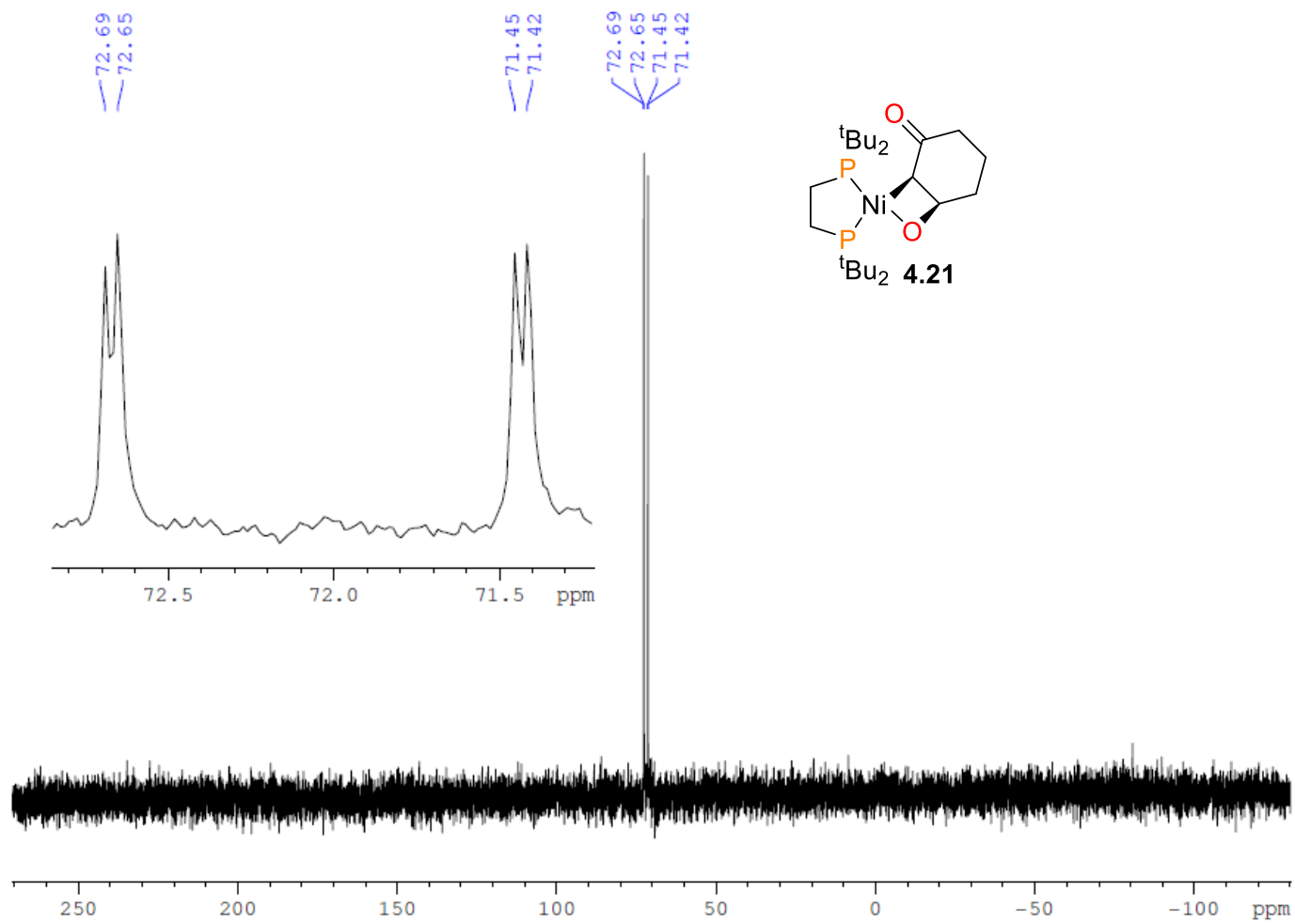


**Figure B4.1.**  $^{31}\text{P}\{^1\text{H}\}$  NMR spectrum (162 MHz, 25 °C,  $\text{C}_6\text{D}_6$ ) of **4.21**.

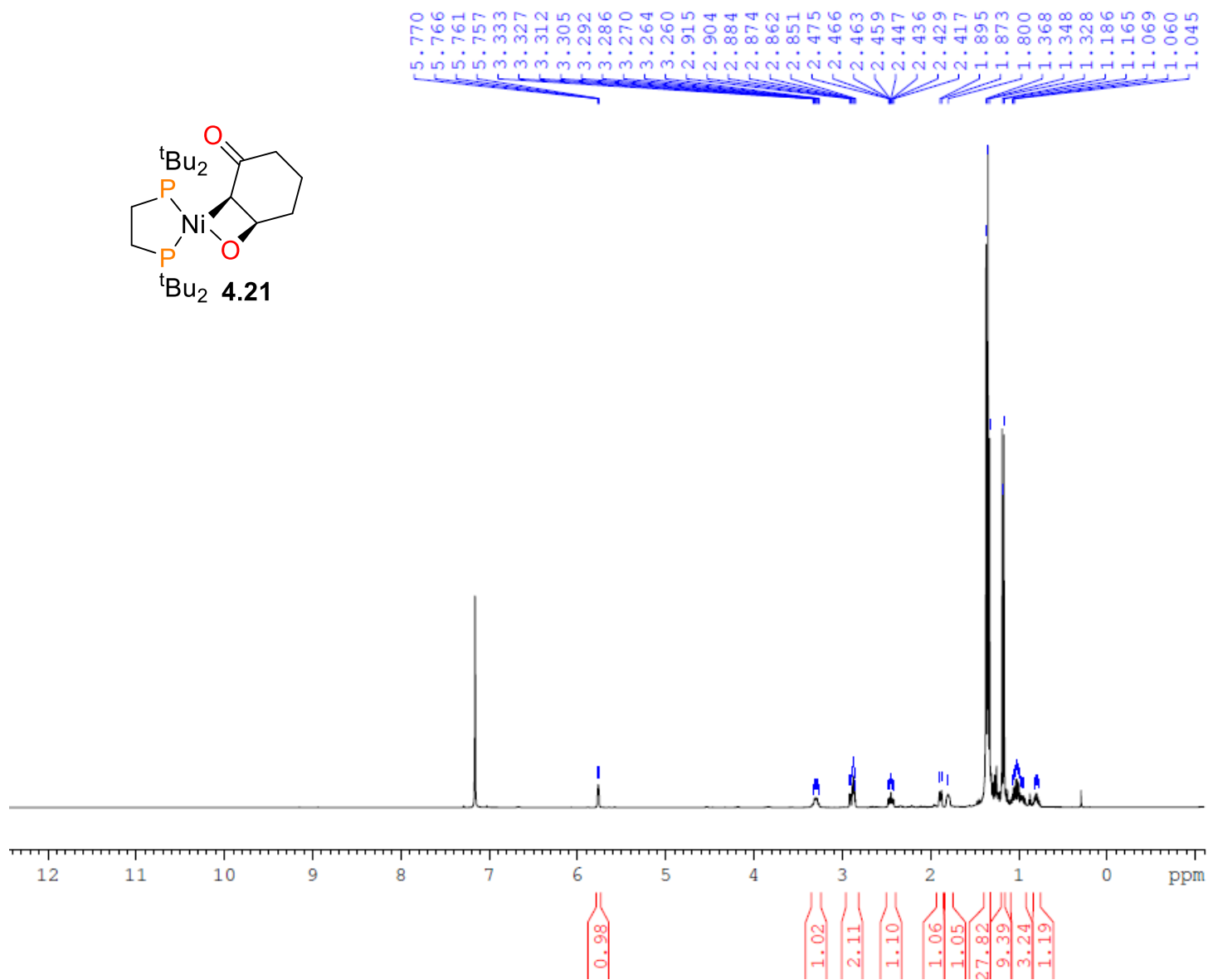


**Figure B4.2.**  $^1\text{H}$  NMR spectrum (600 MHz, 25 °C,  $\text{C}_6\text{D}_6$ ) of **4.21**.

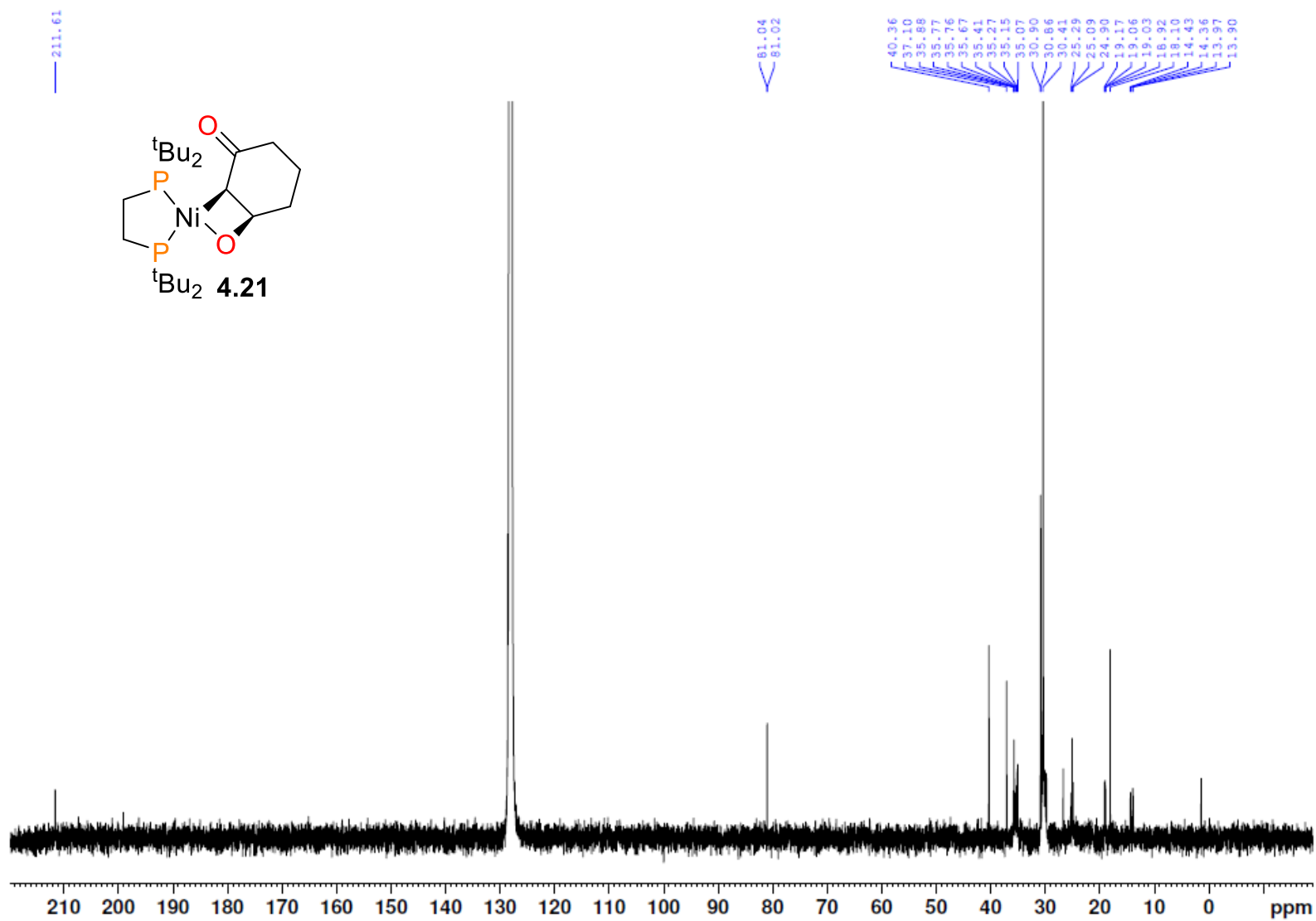


**Figure B4.3.**  $^{13}\text{C}$  NMR spectrum (150 MHz, 25 °C,  $\text{C}_6\text{D}_6$ ) of **4.21**.

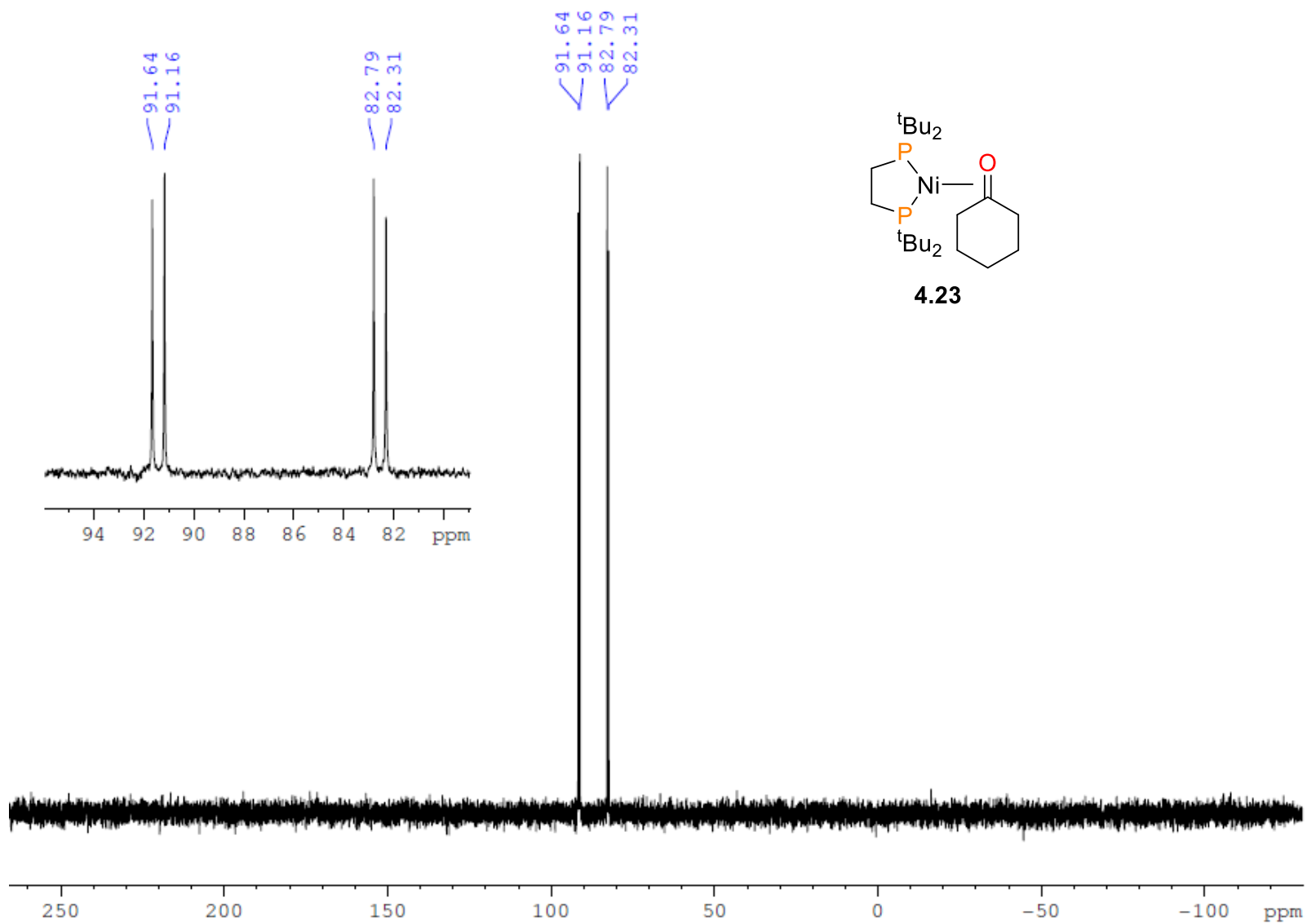


**Figure B4.4.**  $^{31}\text{P}$  NMR spectrum (162 MHz, 25 °C,  $\text{C}_6\text{D}_6$ ) of **4.23**.

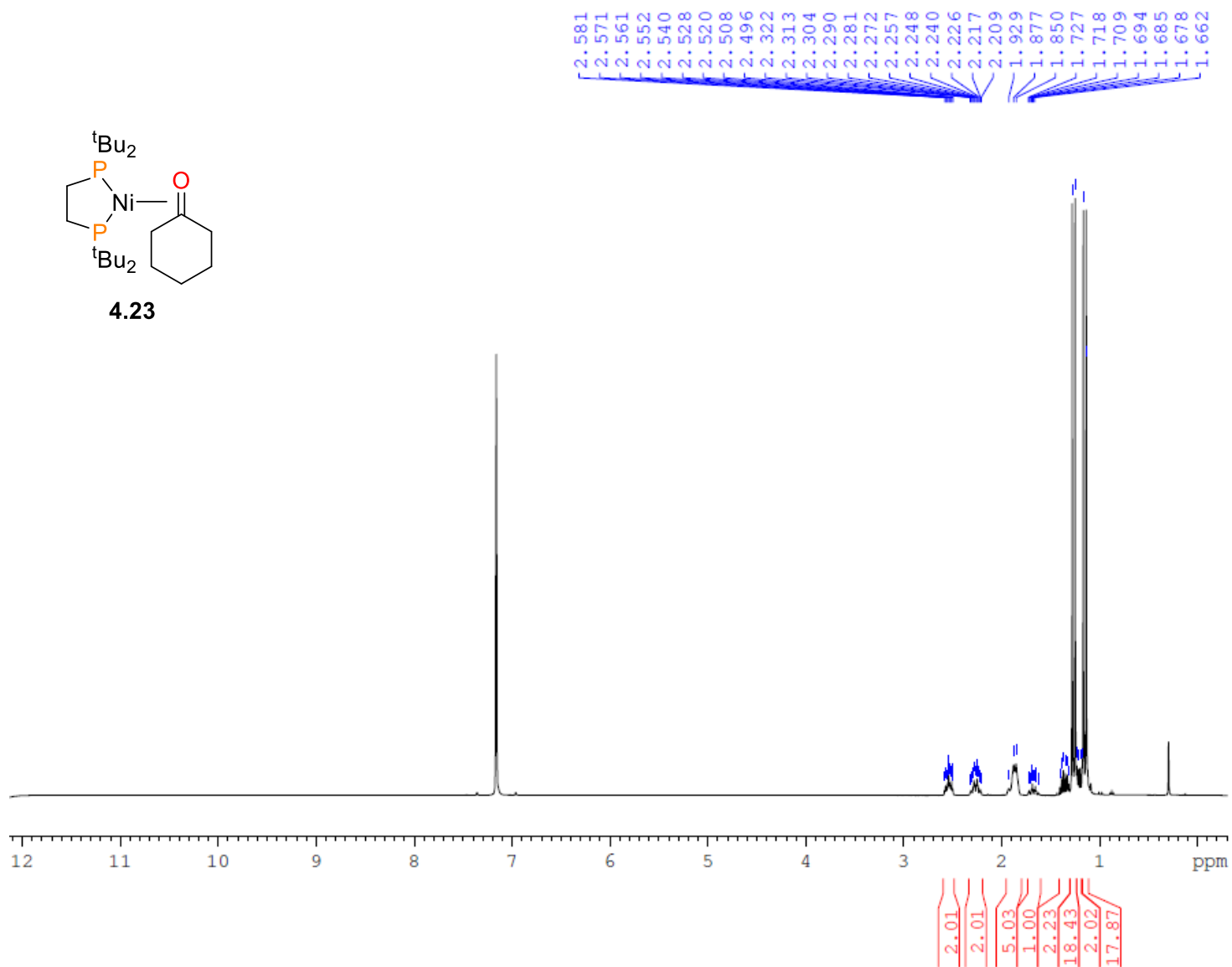


**Figure B4.5.** <sup>1</sup>H NMR spectrum (400 MHz, 25 °C, C<sub>6</sub>D<sub>6</sub>) of **4.23**.

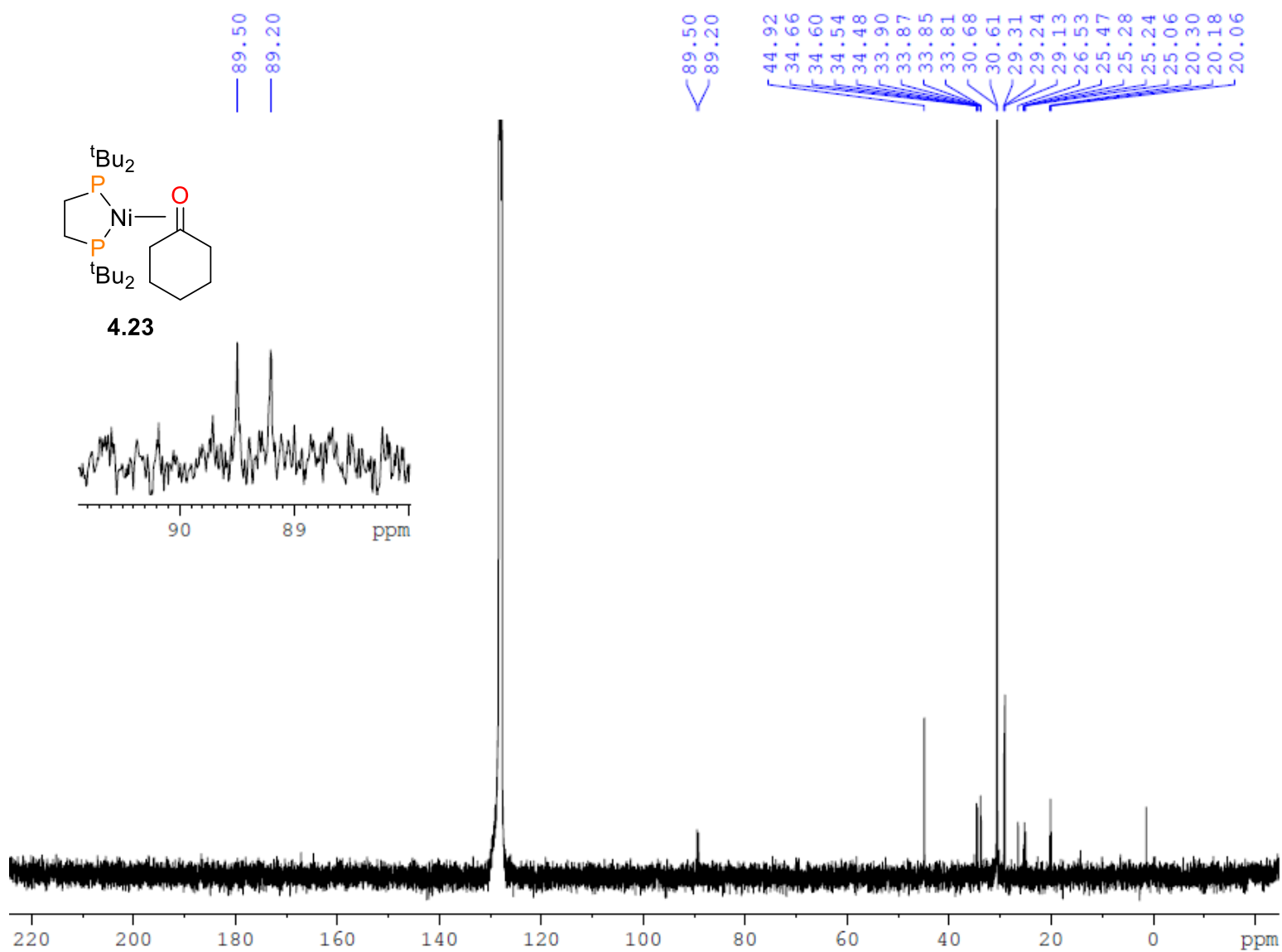


**Figure B4.6.** <sup>13</sup>C NMR spectrum (100 MHz, 25 °C, C<sub>6</sub>D<sub>6</sub>) of **4.23**. Inset shows resonance assigned for **C1**.

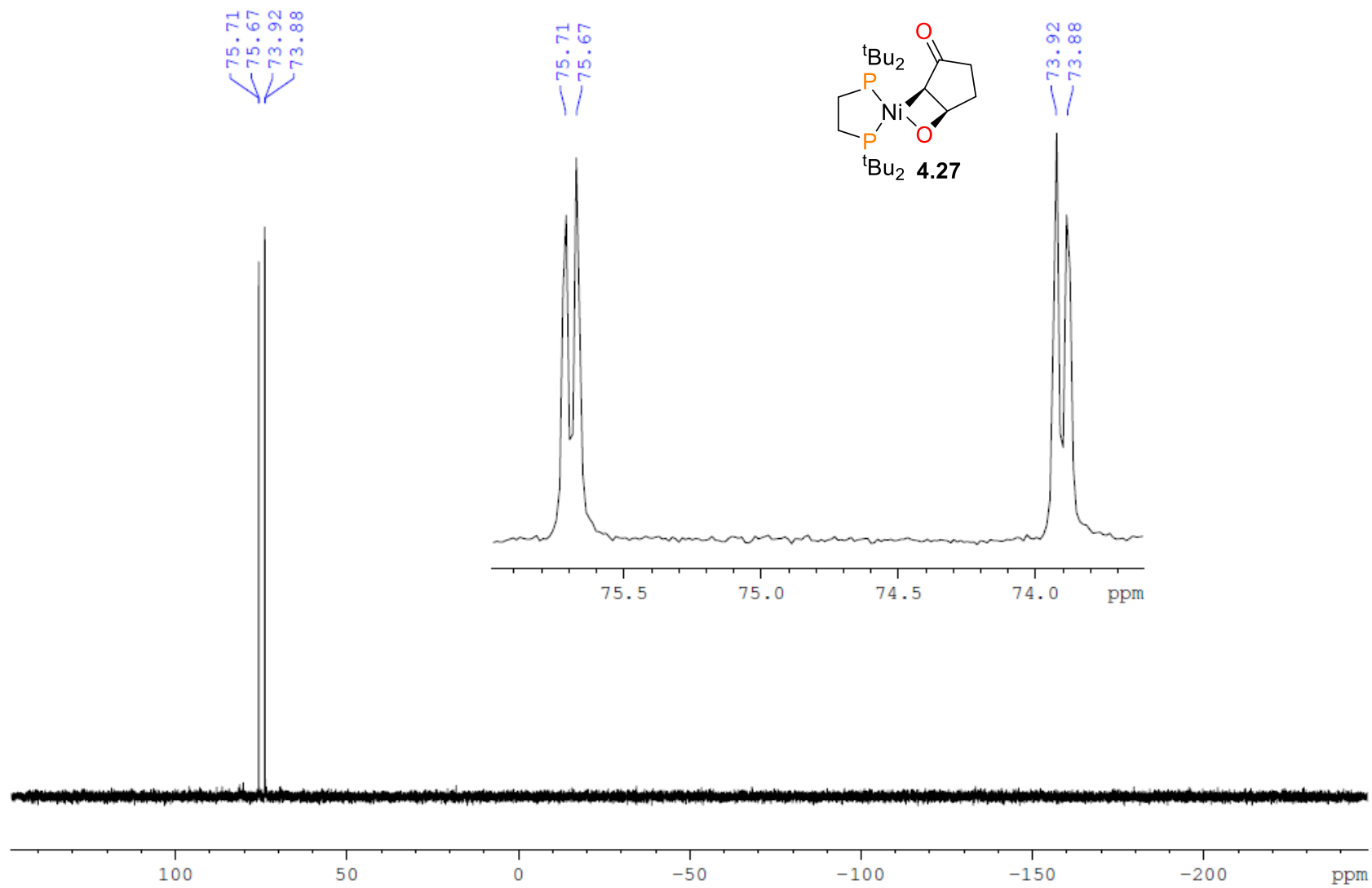


**Figure B4.7.**  $^{31}\text{P}$  NMR spectrum (162 MHz, 25 °C,  $\text{C}_6\text{D}_6$ ) of **4.27**.

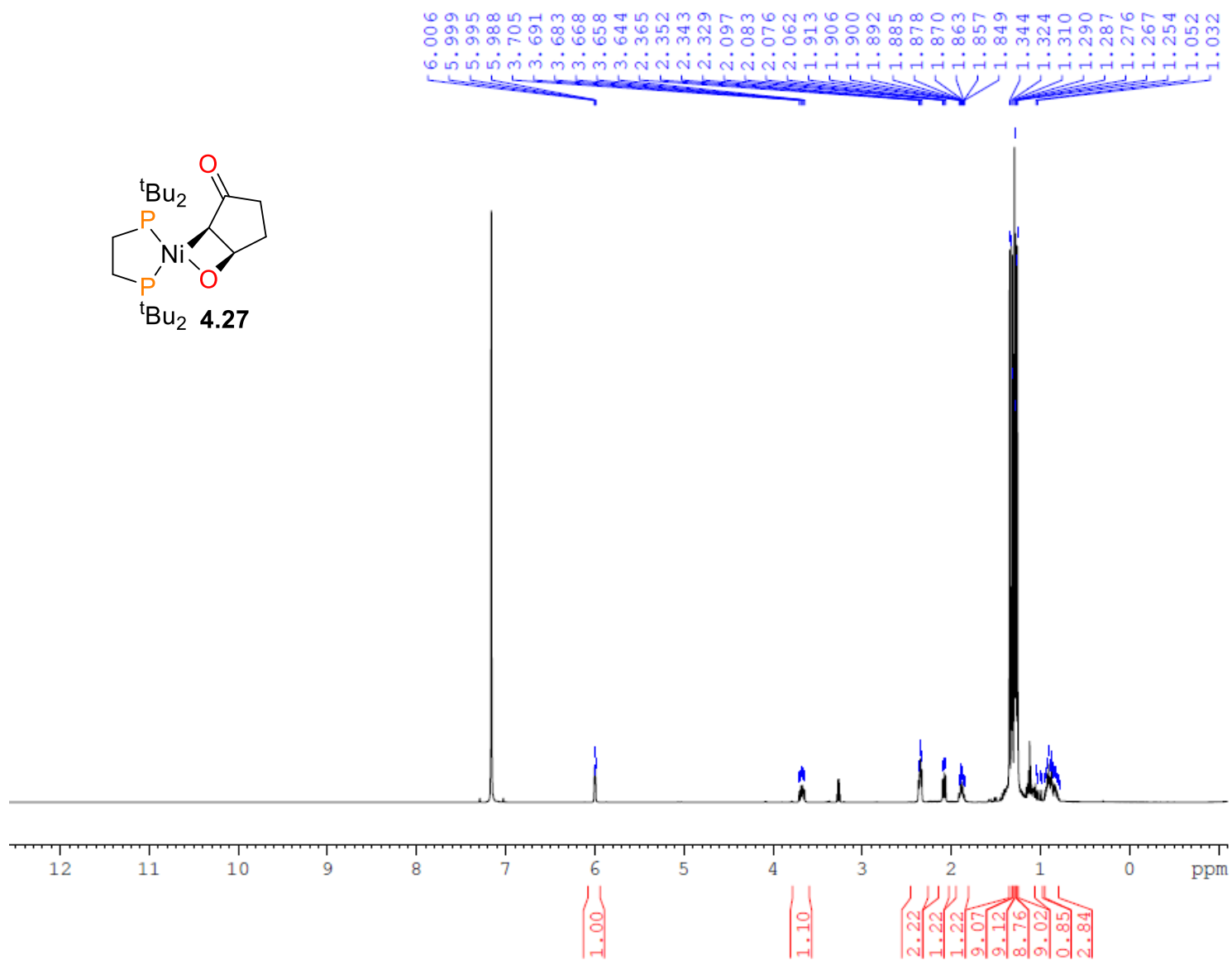


**Figure B4.8.**  $^1\text{H}$  NMR spectrum (600 MHz, 25 °C,  $\text{C}_6\text{D}_6$ ) of **4.27**.

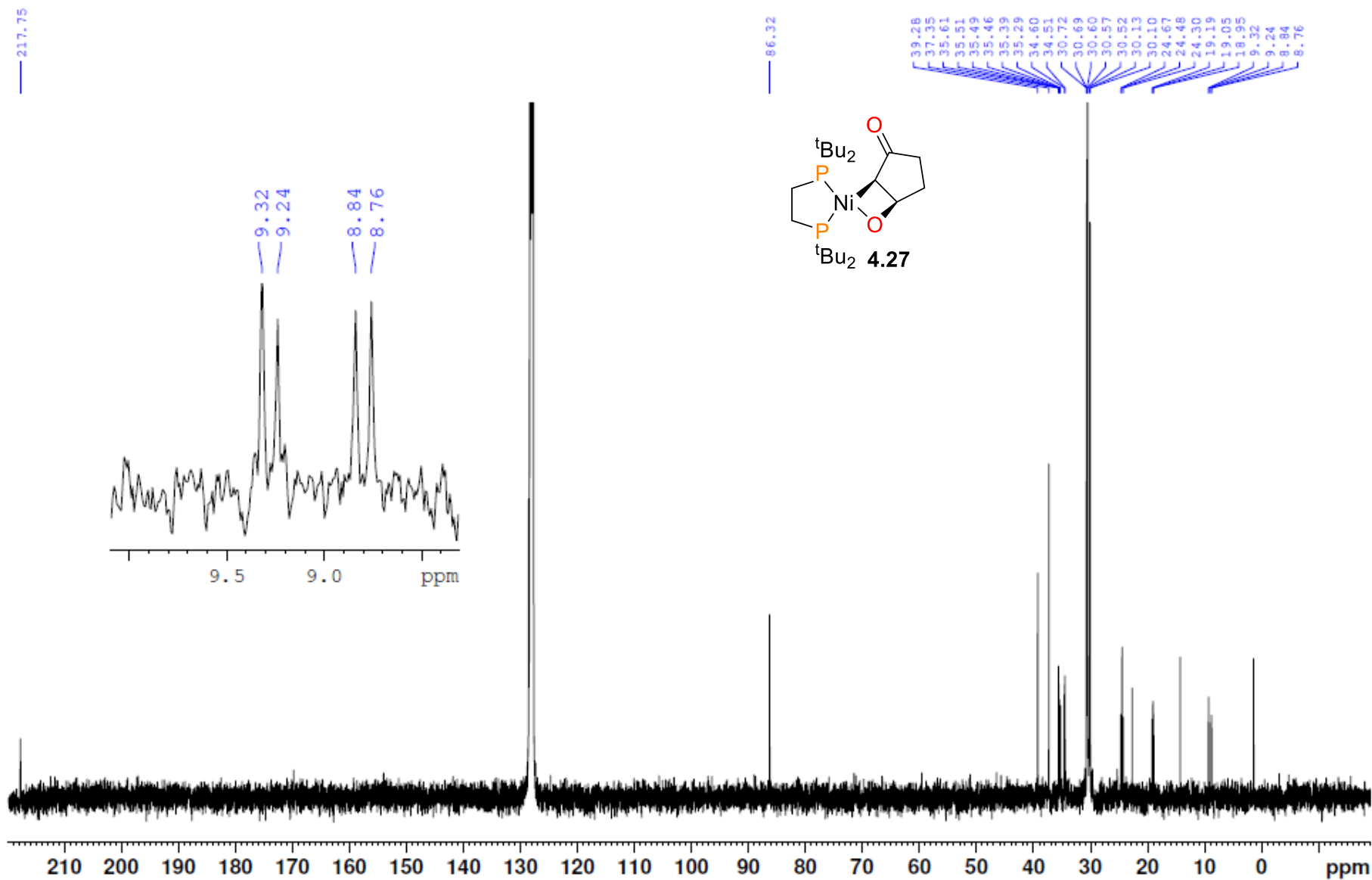


**Figure B4.9.**  $^{13}\text{C}$  NMR spectrum (100 MHz, 25 °C,  $\text{C}_6\text{D}_6$ ) of **4.27**. Inset shows resonance assigned for **C3**.

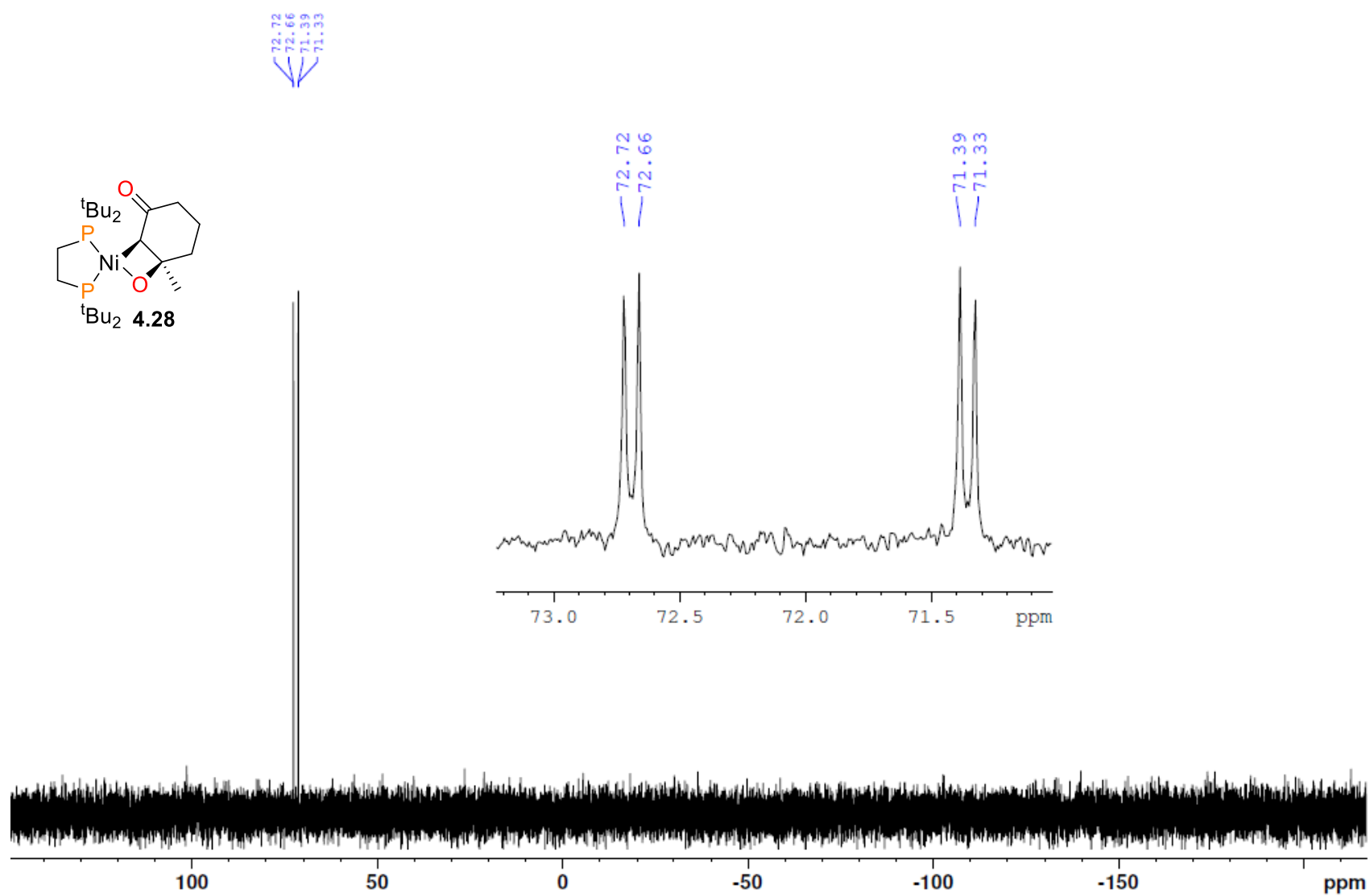


**Figure B4.10.**  $^{31}\text{P}$  NMR spectrum (162 MHz, 25 °C,  $\text{C}_6\text{D}_6$ ) of **4.28**.

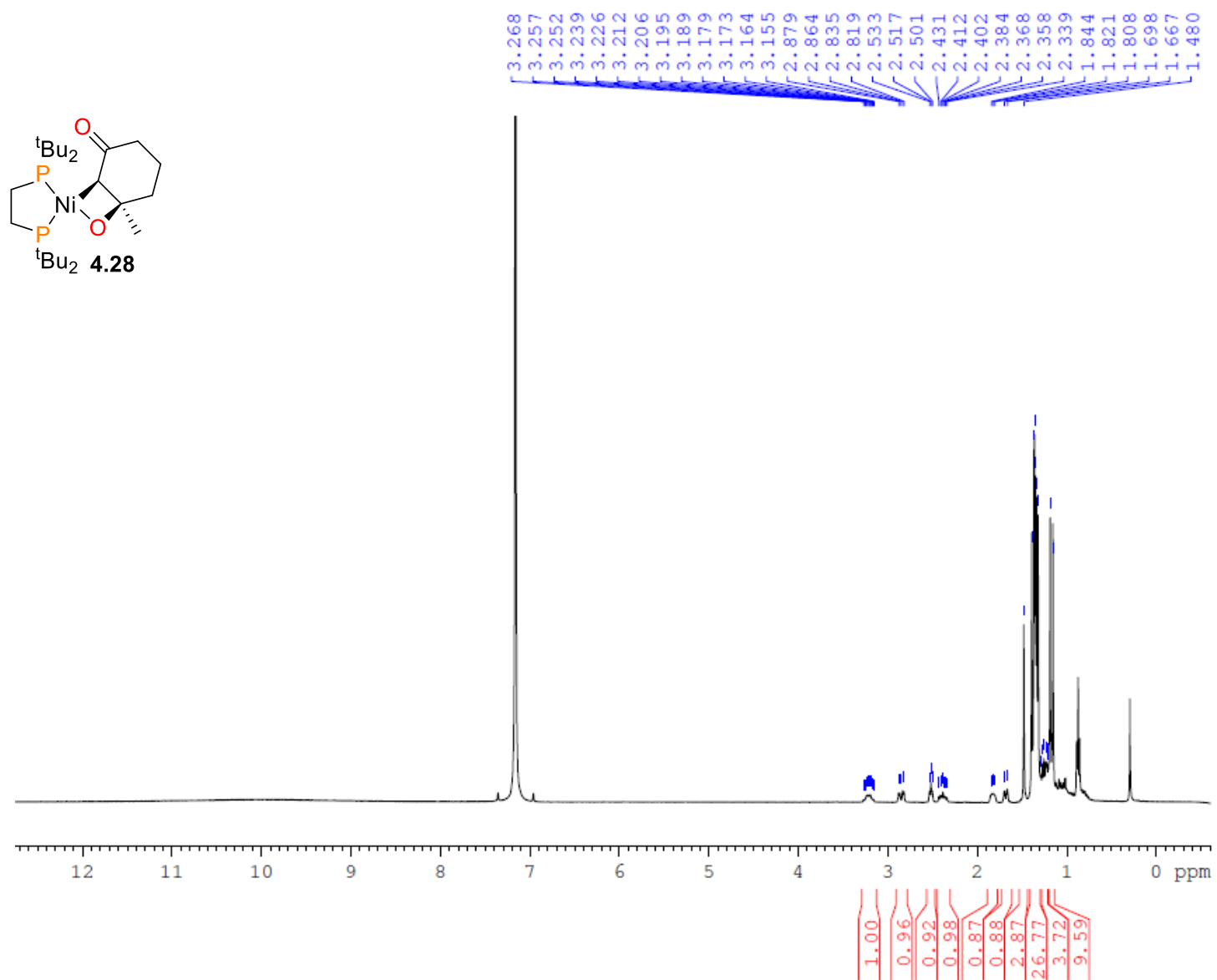


**Figure B4.11.**  $^1\text{H}$  NMR spectrum (400 MHz, 25 °C,  $\text{C}_6\text{D}_6$ ) of **4.28**.

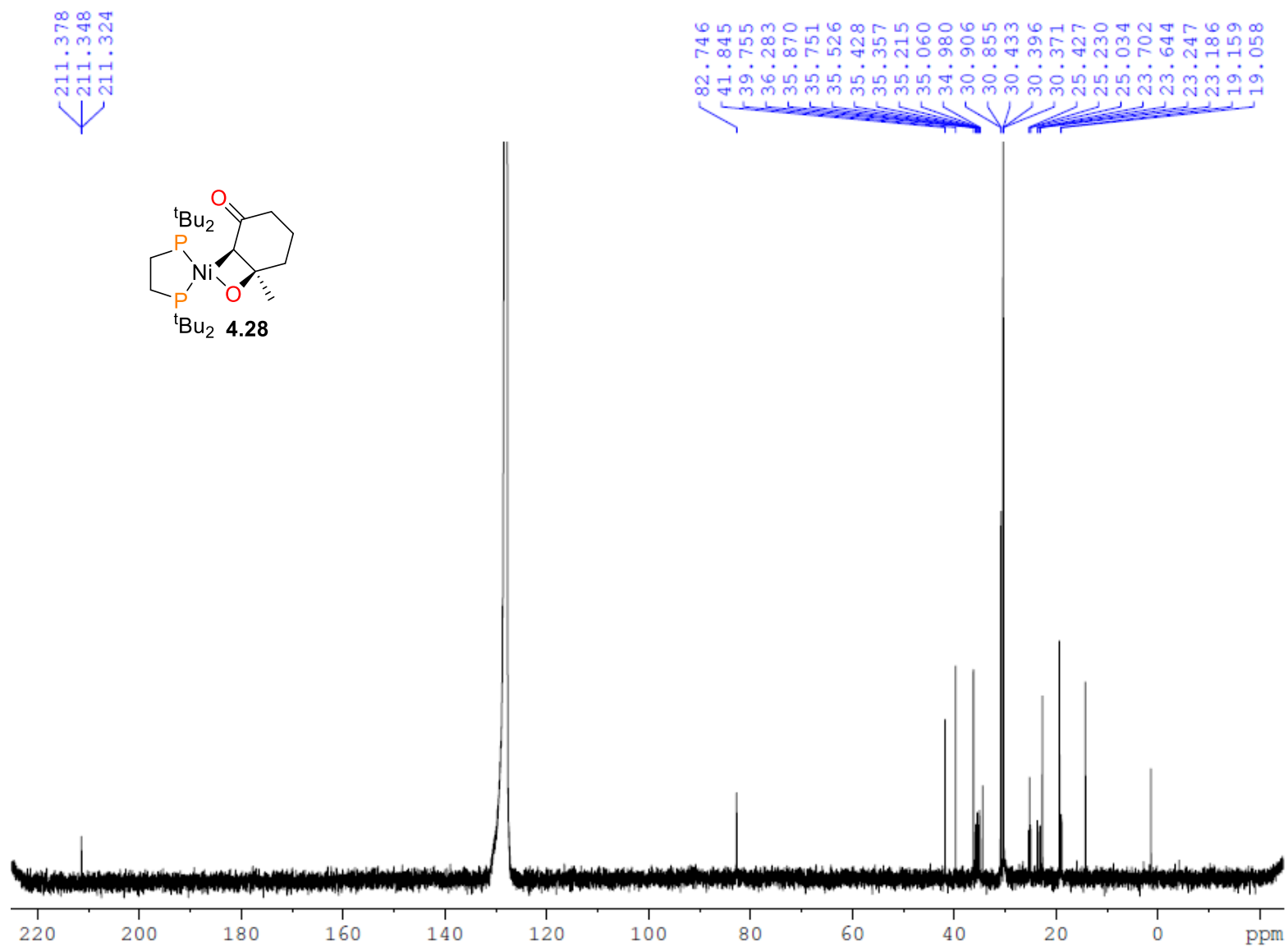


**Figure B4.12.** <sup>13</sup>C NMR spectrum (100 MHz, 25 °C, C<sub>6</sub>D<sub>6</sub>) of **4.28**.

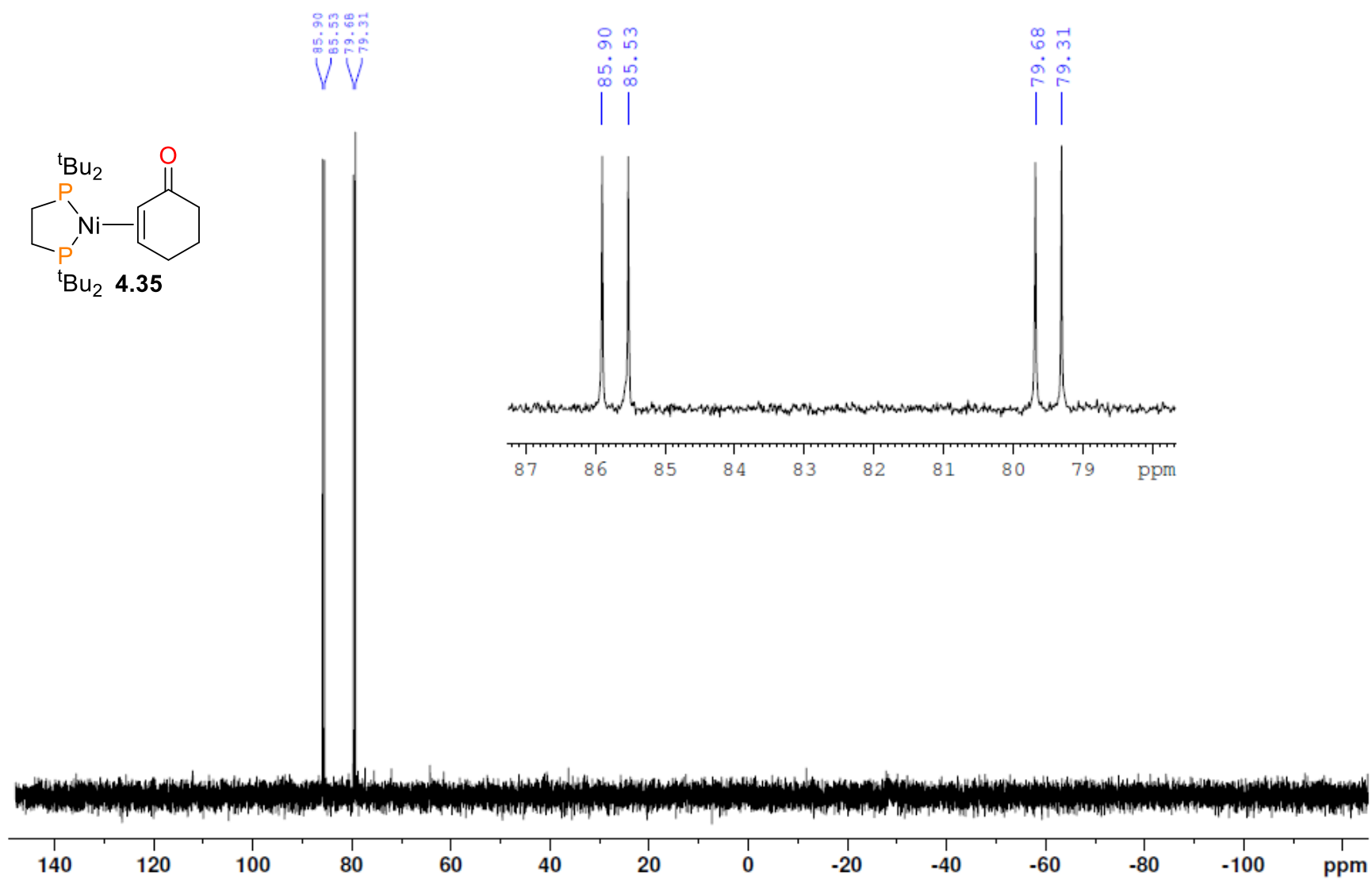


**Figure B4.13.**  $^{31}\text{P}$  NMR spectrum (162 MHz, 25 °C,  $\text{C}_6\text{D}_6$ ) of **4.35**.

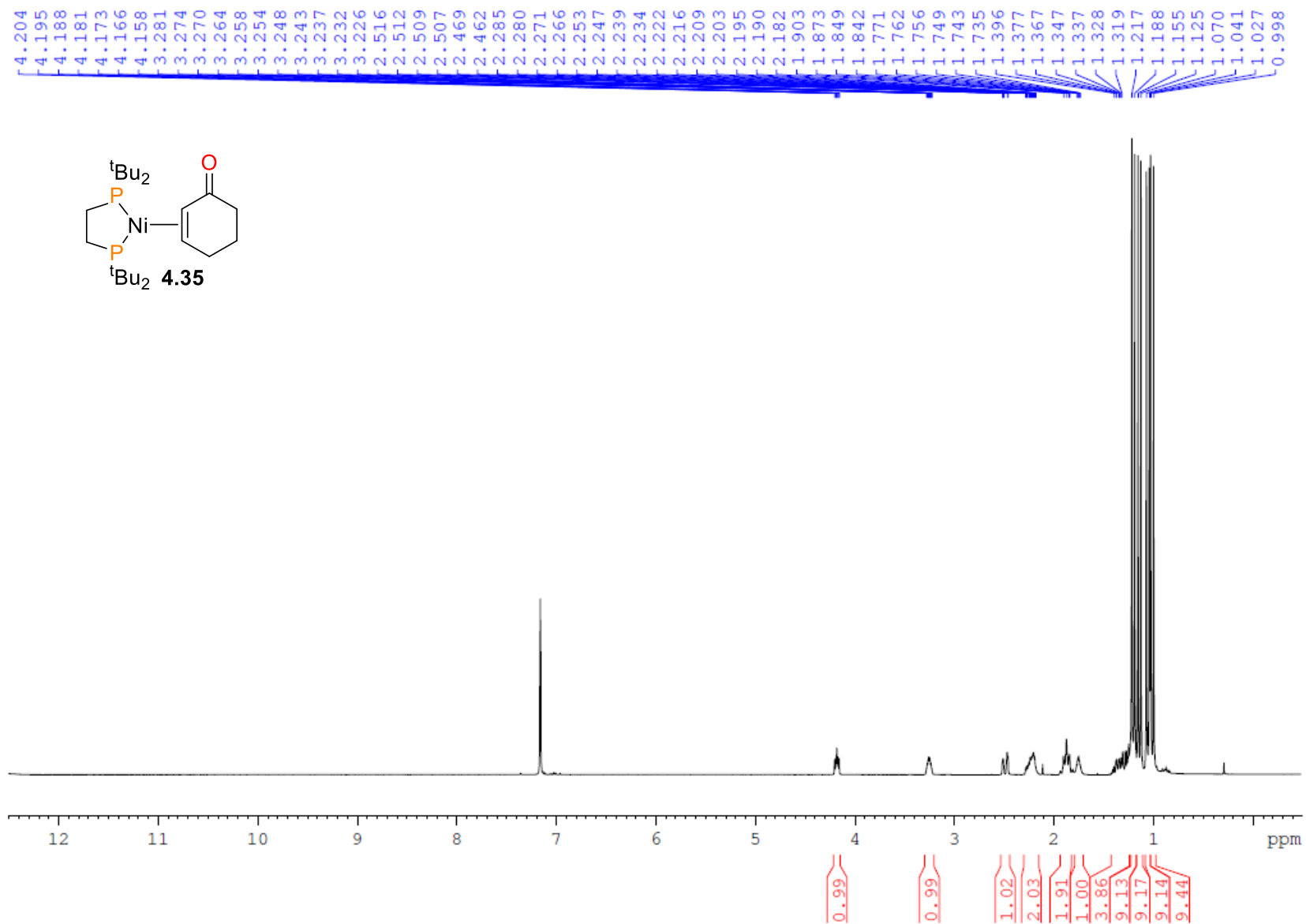


**Figure B4.14.** <sup>1</sup>H NMR spectrum (400 MHz, 25 °C, C<sub>6</sub>D<sub>6</sub>) of **4.35**.

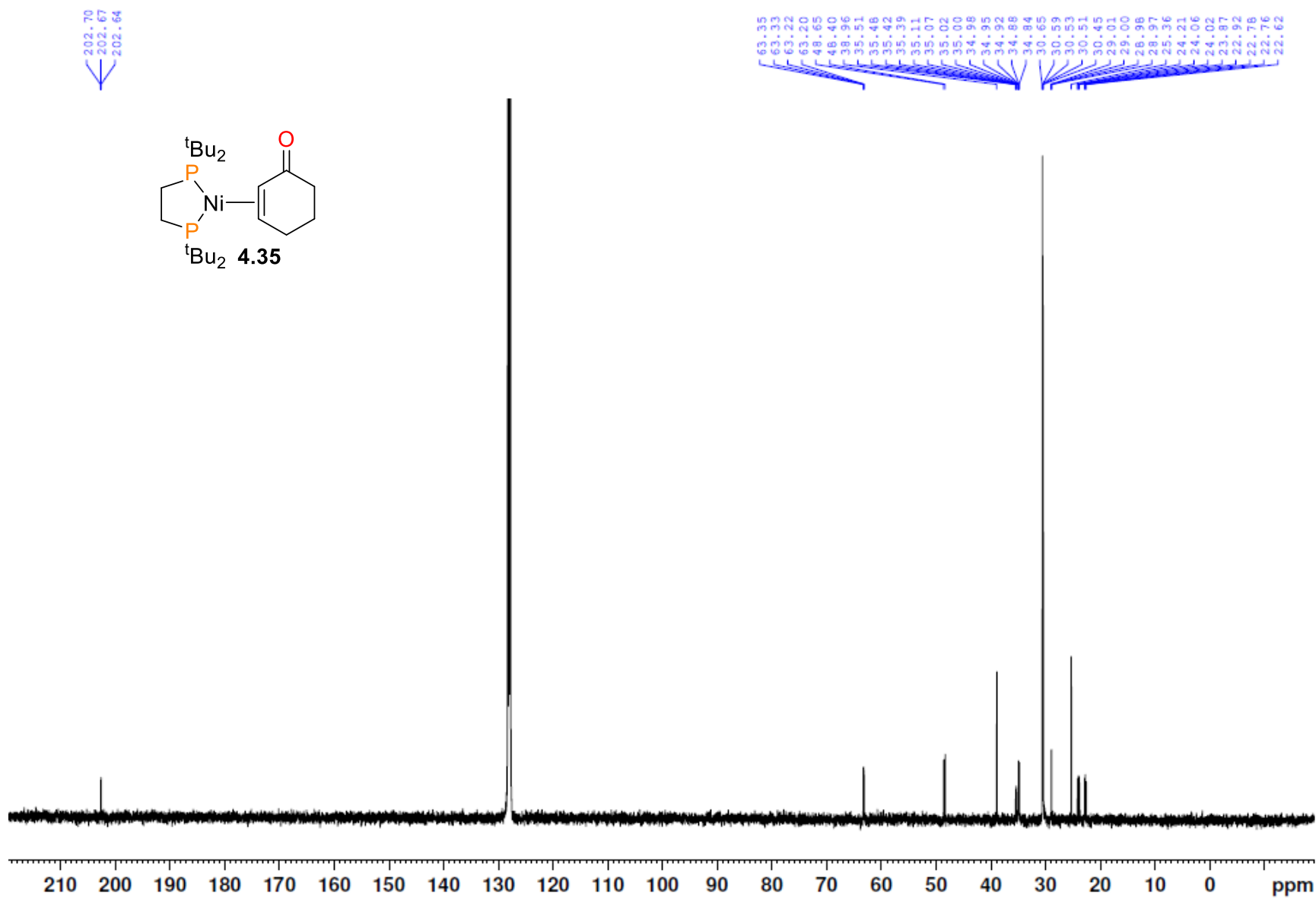


**Figure B4.15.**  $^{13}\text{C}$  NMR spectrum (100 MHz, 25 °C,  $\text{C}_6\text{D}_6$ ) of **4.35**.

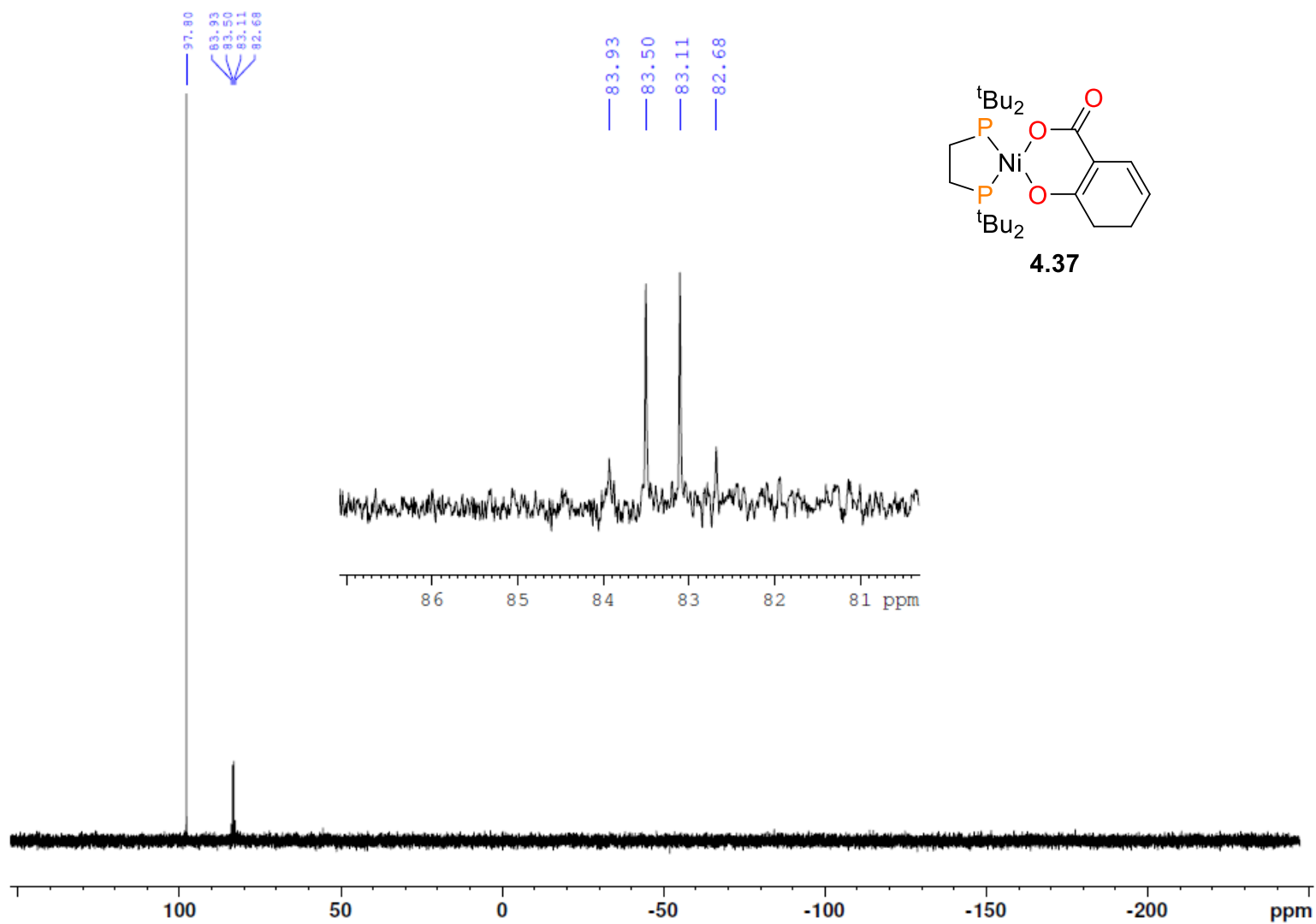


**Figure B4.16.**  $^{31}\text{P}$  NMR spectrum (121 MHz, 25 °C,  $\text{CD}_2\text{Cl}_2$ ) of a mixture of **4.37** and **4.38**. The large resonance at 97.8 ppm is due to **4.37**. Inset shows the resonances for **4.37**.

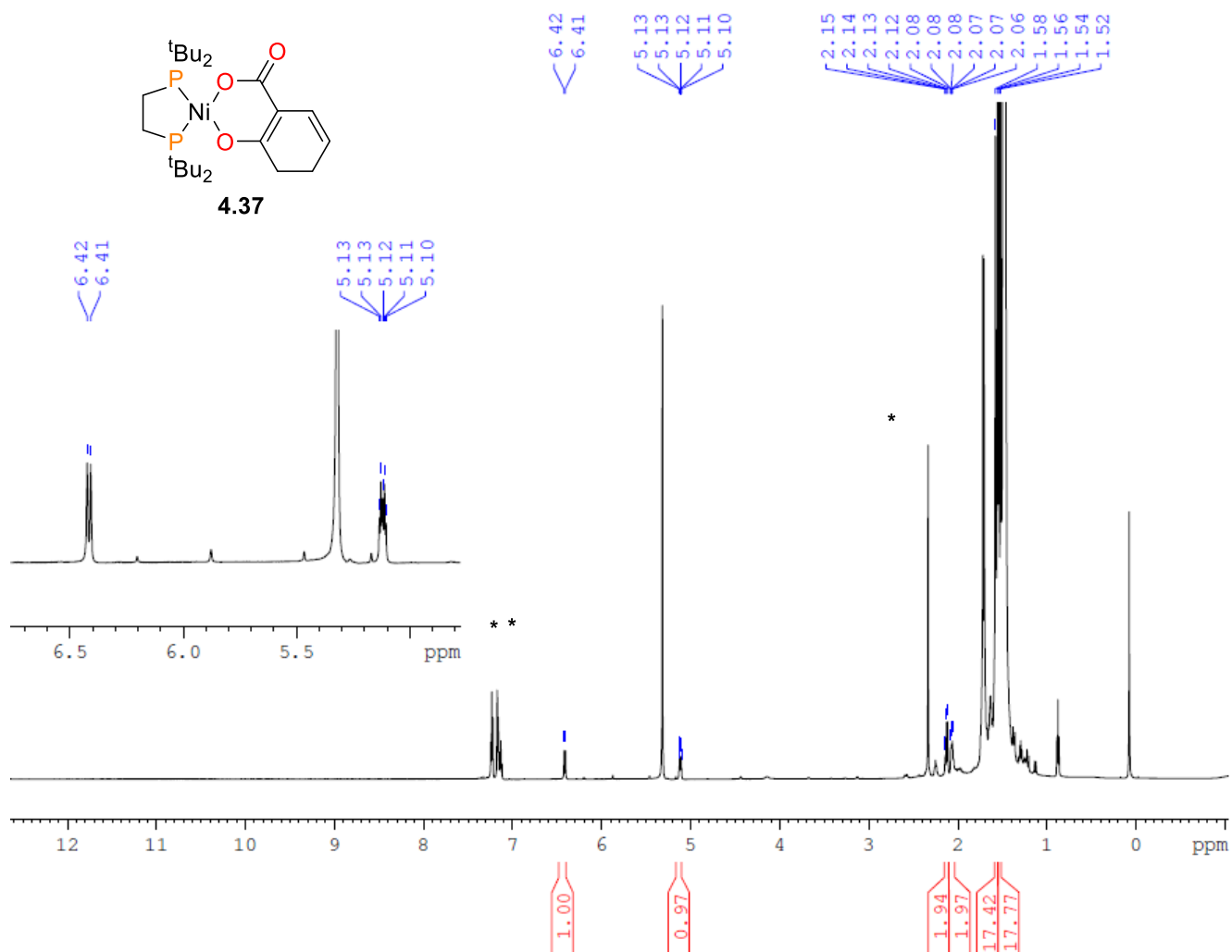


**Figure B4.17.**  $^1\text{H}$  NMR spectrum (600 MHz, 25 °C,  $\text{CD}_2\text{Cl}_2$ ) of a mixture of **4.36** and **4.37**. Resonances marked with \* are from one equivalent of co-crystallized toluene. The large resonances between 1 and 2 ppm are due to **4.36**. Inset shows the resonances of **H1** and **H6** of **4.37** in the olefinic region.

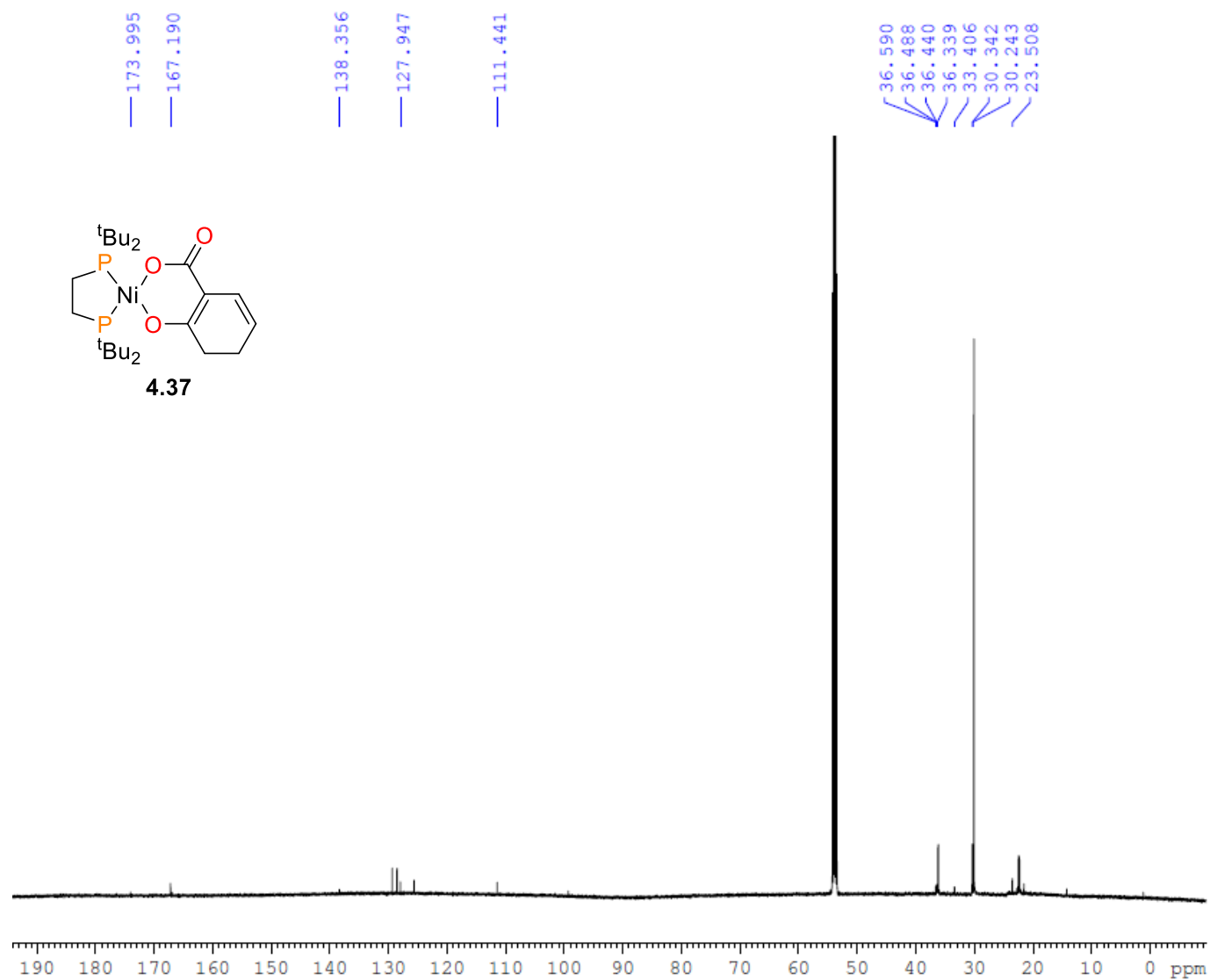


**Figure B4.18.**  $^{13}\text{C}$  NMR spectrum (150 MHz, 25 °C,  $\text{CD}_2\text{Cl}_2$ ) of a mixture of **4.36** and **4.37**. The spectrum also contains one equivalent of co-crystallized toluene.

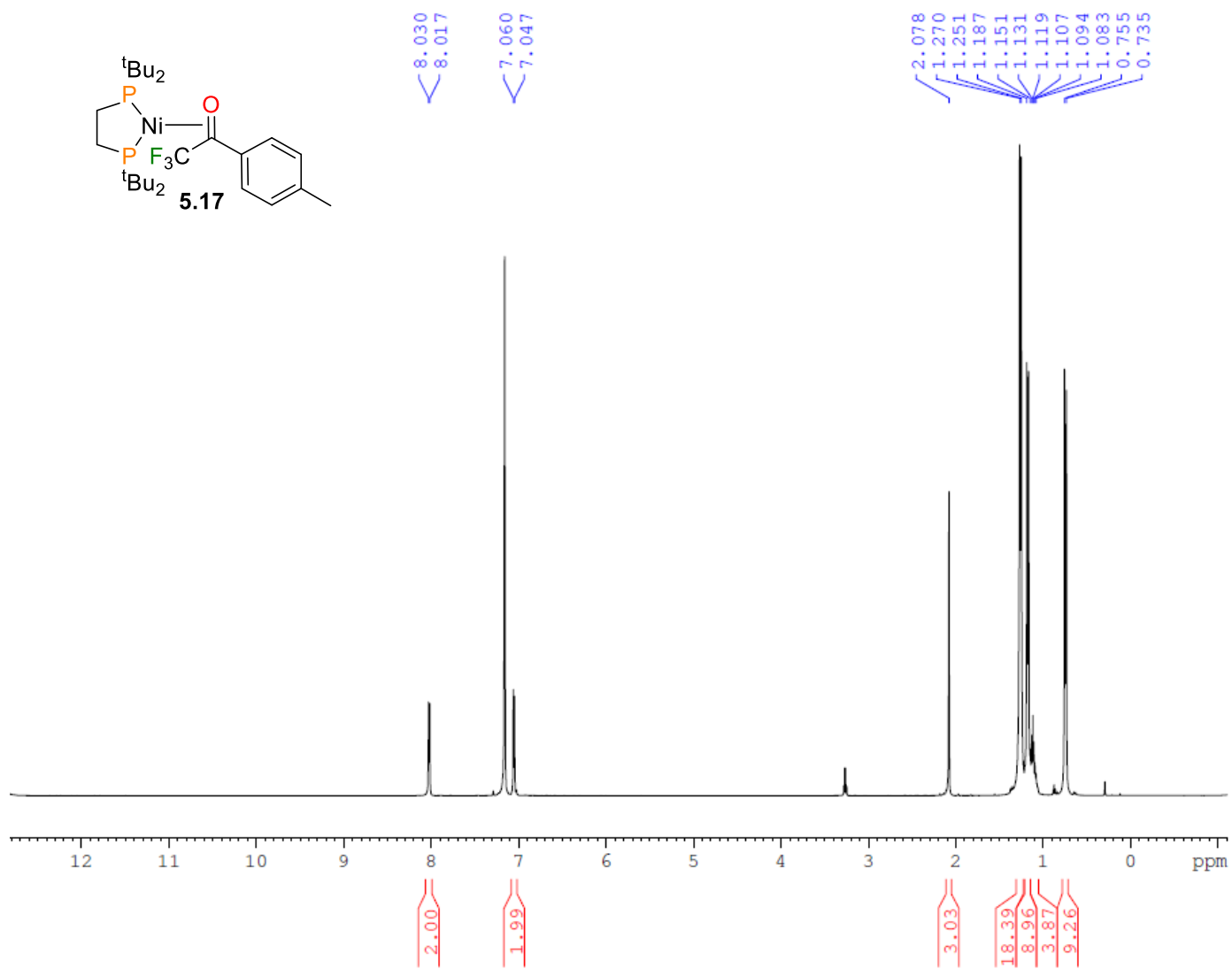


**Figure B5.1.** <sup>1</sup>H NMR spectrum (400 MHz, 25 °C, C<sub>6</sub>D<sub>6</sub>) of **5.17**.

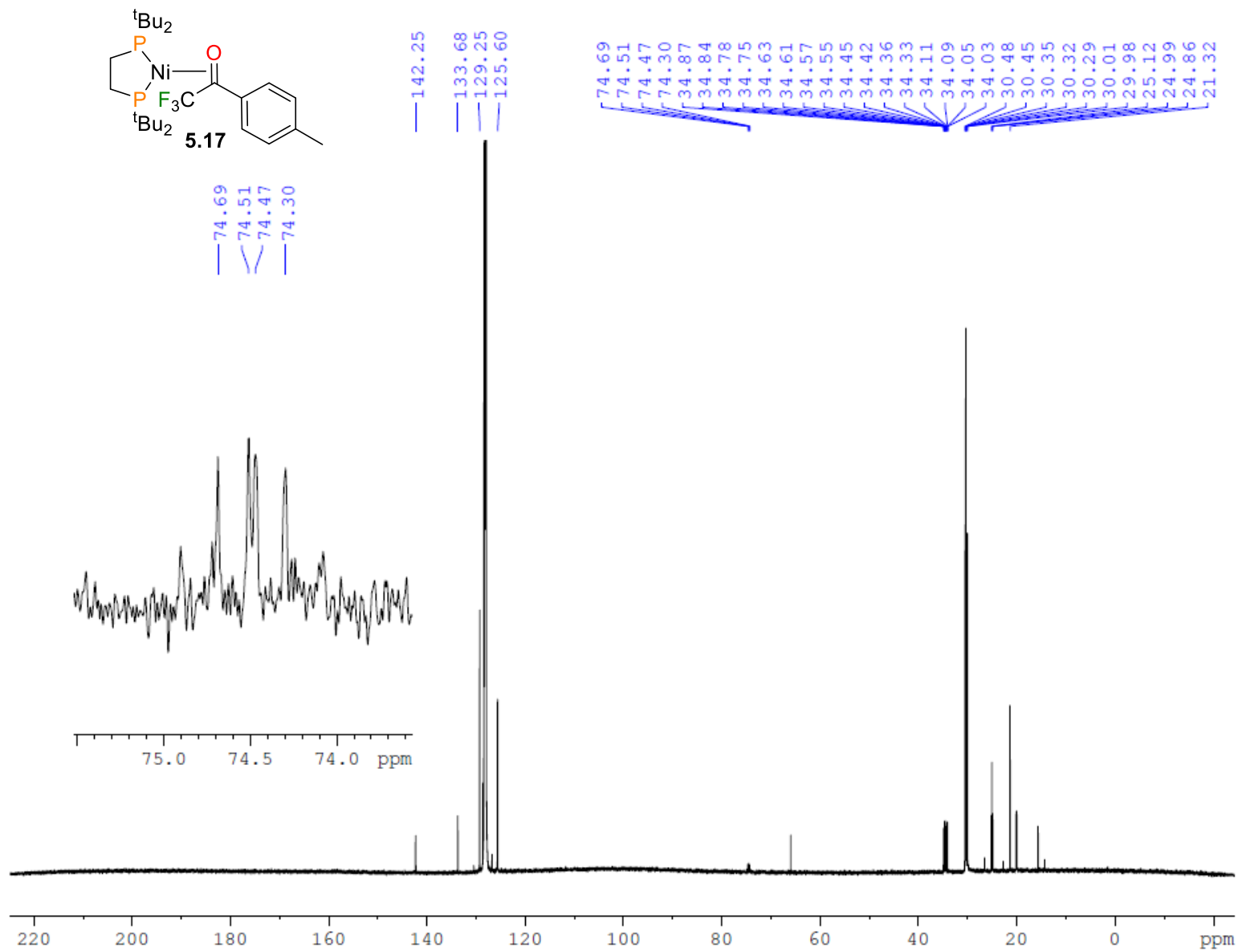


**Figure B5.2.** <sup>13</sup>C{<sup>1</sup>H} NMR spectrum (100 MHz, 25 °C, C<sub>6</sub>D<sub>6</sub>) of **5.17**. The inset shows the resonance assigned for C2.

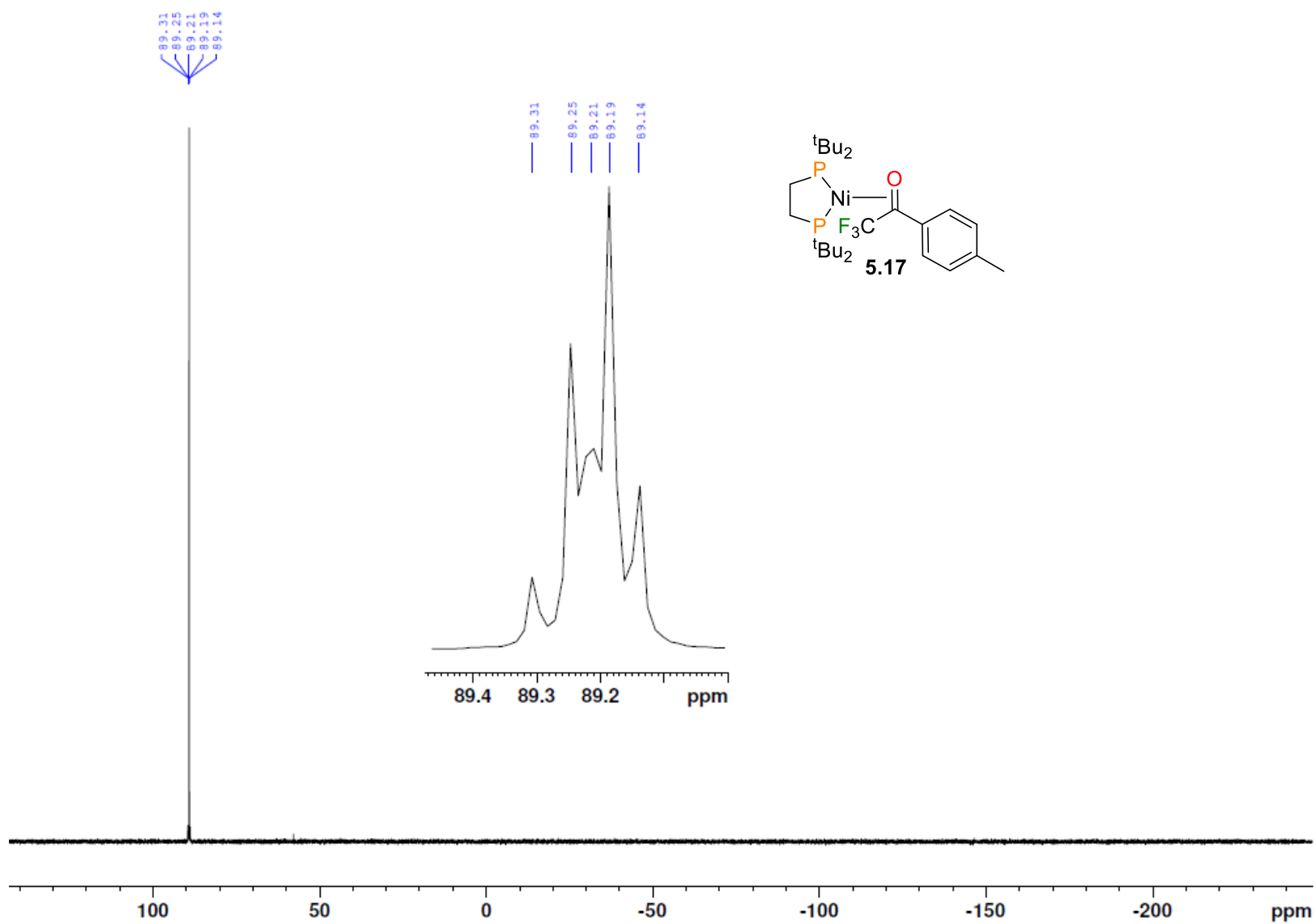


**Figure B5.3.**  $^{31}\text{P}\{^1\text{H}\}$  NMR spectrum (162 MHz, 25 °C,  $\text{C}_6\text{D}_6$ ) of **5.17**.

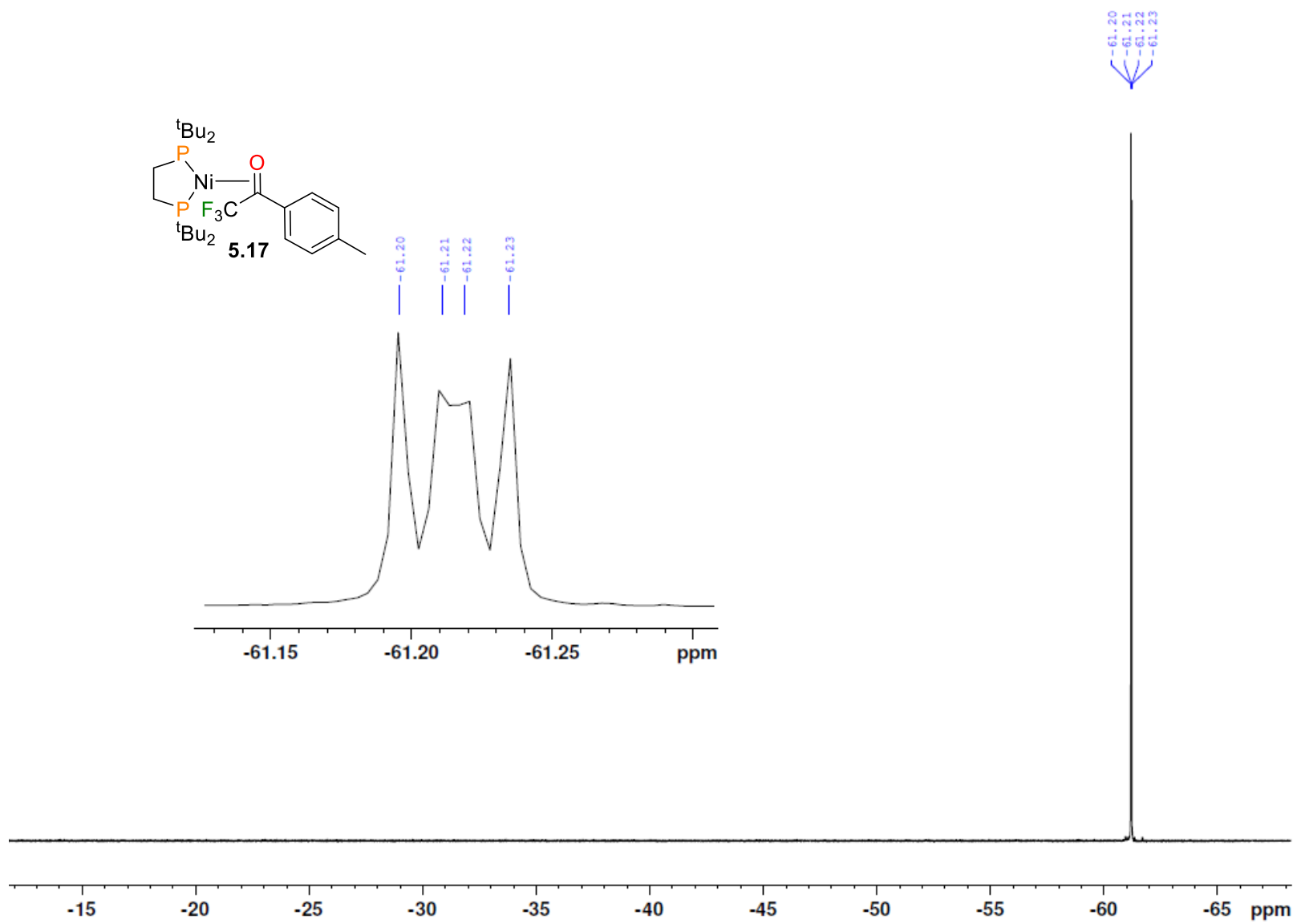


**Figure B5.4.**  $^{19}\text{F}\{^1\text{H}\}$  NMR spectrum (380 MHz, 25 °C,  $\text{C}_6\text{D}_6$ ) of **5.17**.

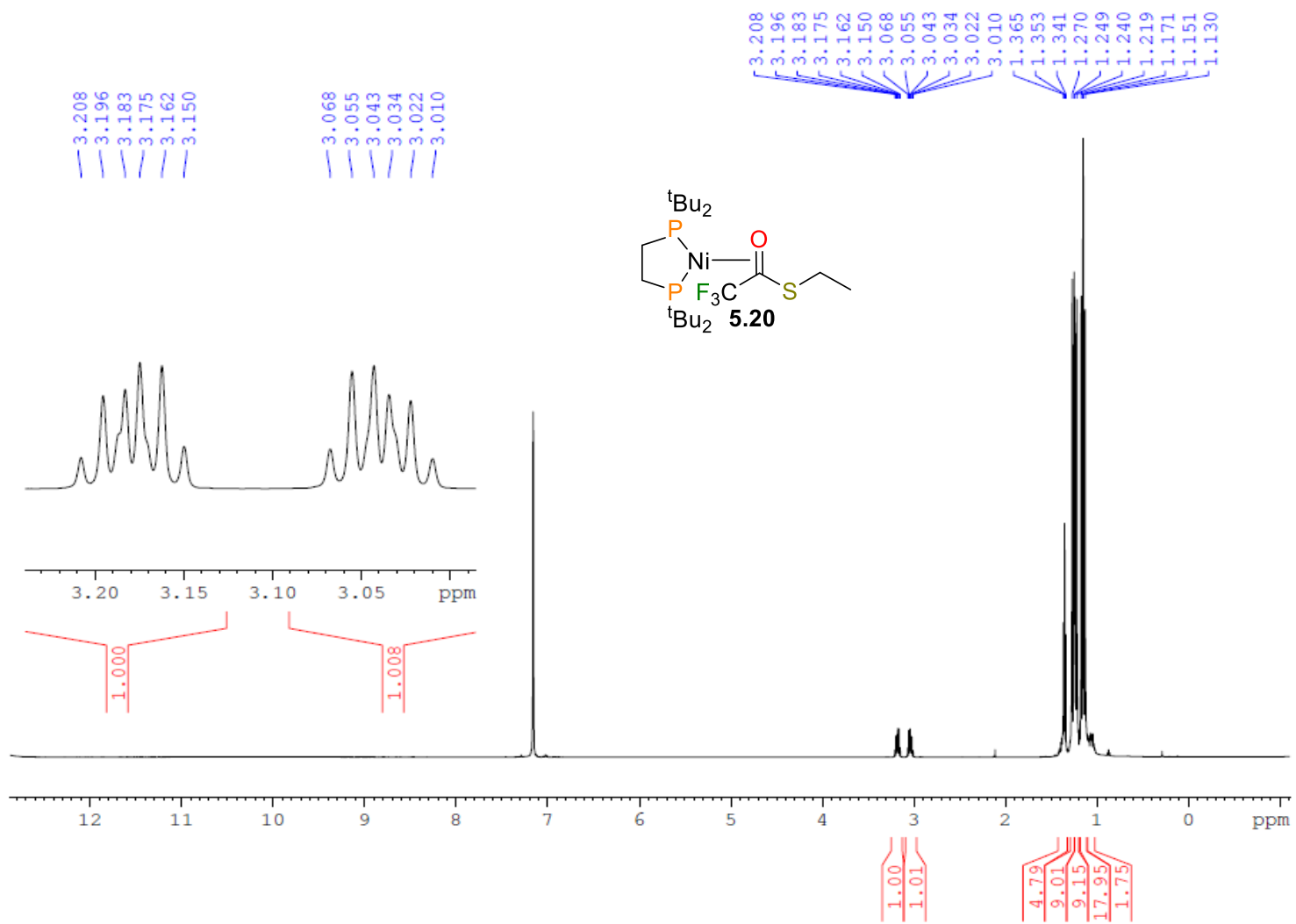


**Figure B5.5.** <sup>1</sup>H NMR spectrum (600 MHz, 25 °C, C<sub>6</sub>D<sub>6</sub>) of **5.20**. The inset shows the resonances assigned to the diastereotopic H<sub>3</sub> protons.

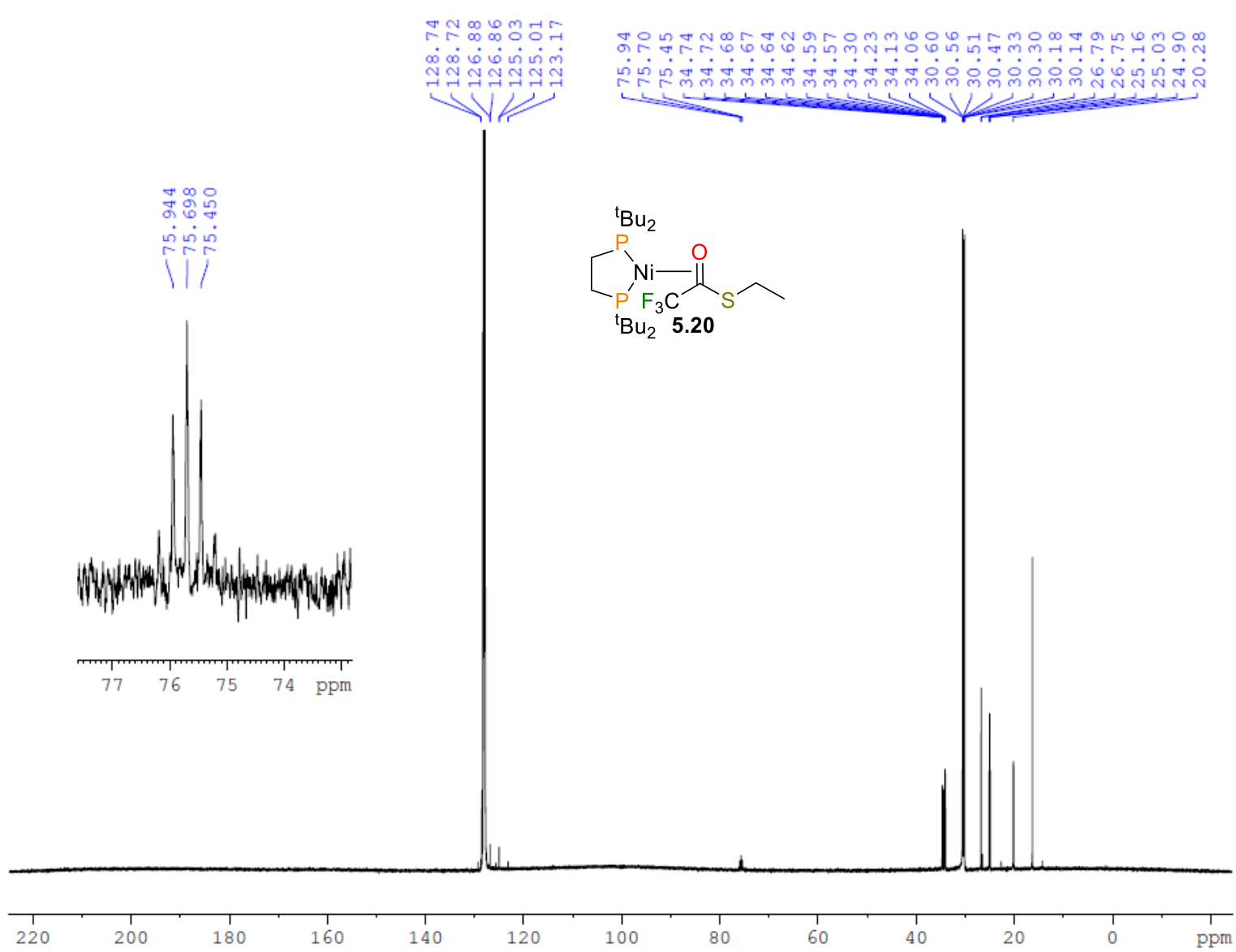


**Figure B5.6.**  $^{13}\text{C}\{^1\text{H}\}$  NMR spectrum (150 MHz, 25 °C,  $\text{C}_6\text{D}_6$ ) of **5.20**. The inset shows the resonance assigned to C2.

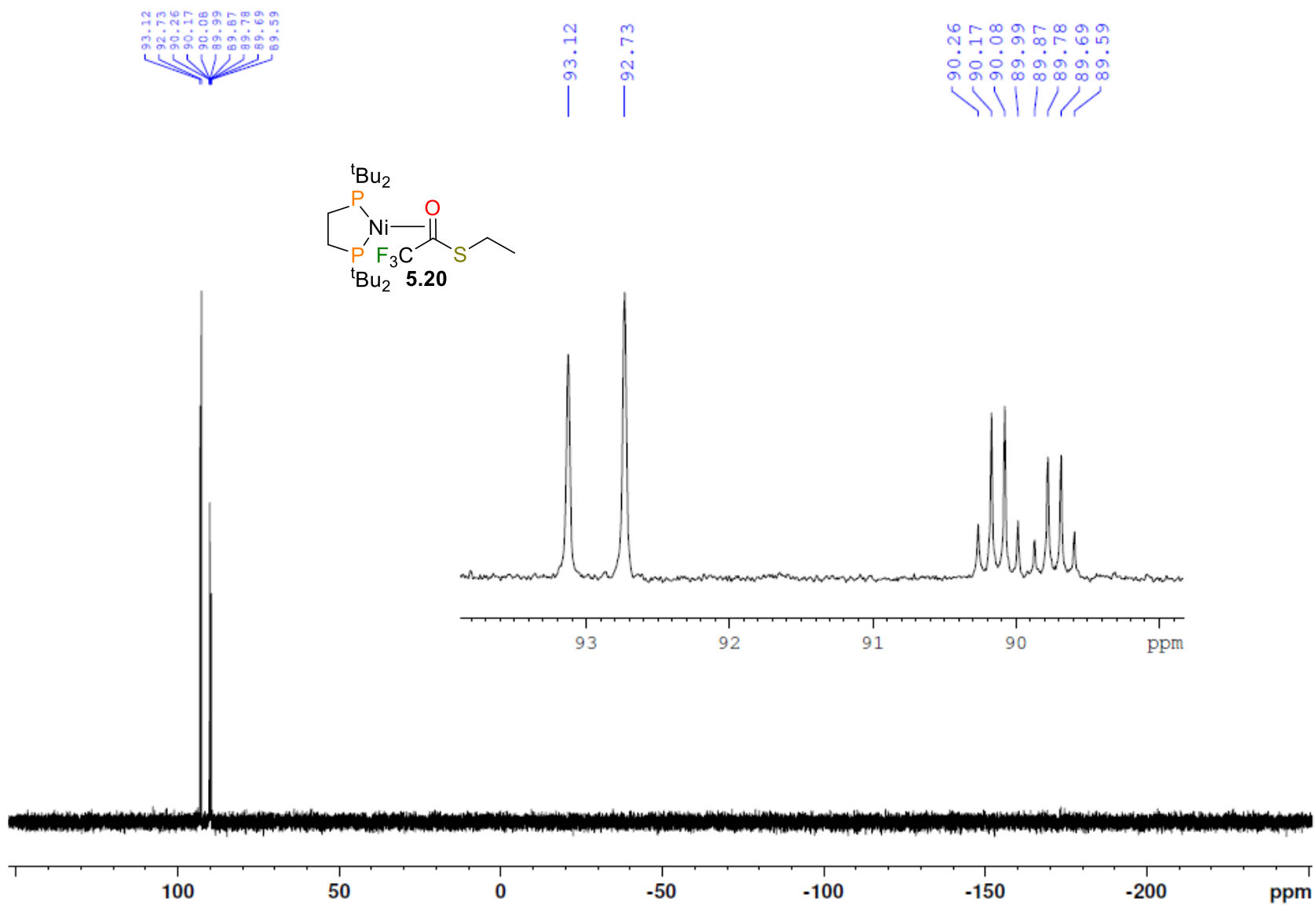


**Figure B5.7.**  $^{31}\text{P}\{^1\text{H}\}$  NMR spectrum (162 MHz, 25 °C,  $\text{C}_6\text{D}_6$ ) of **5.20**.

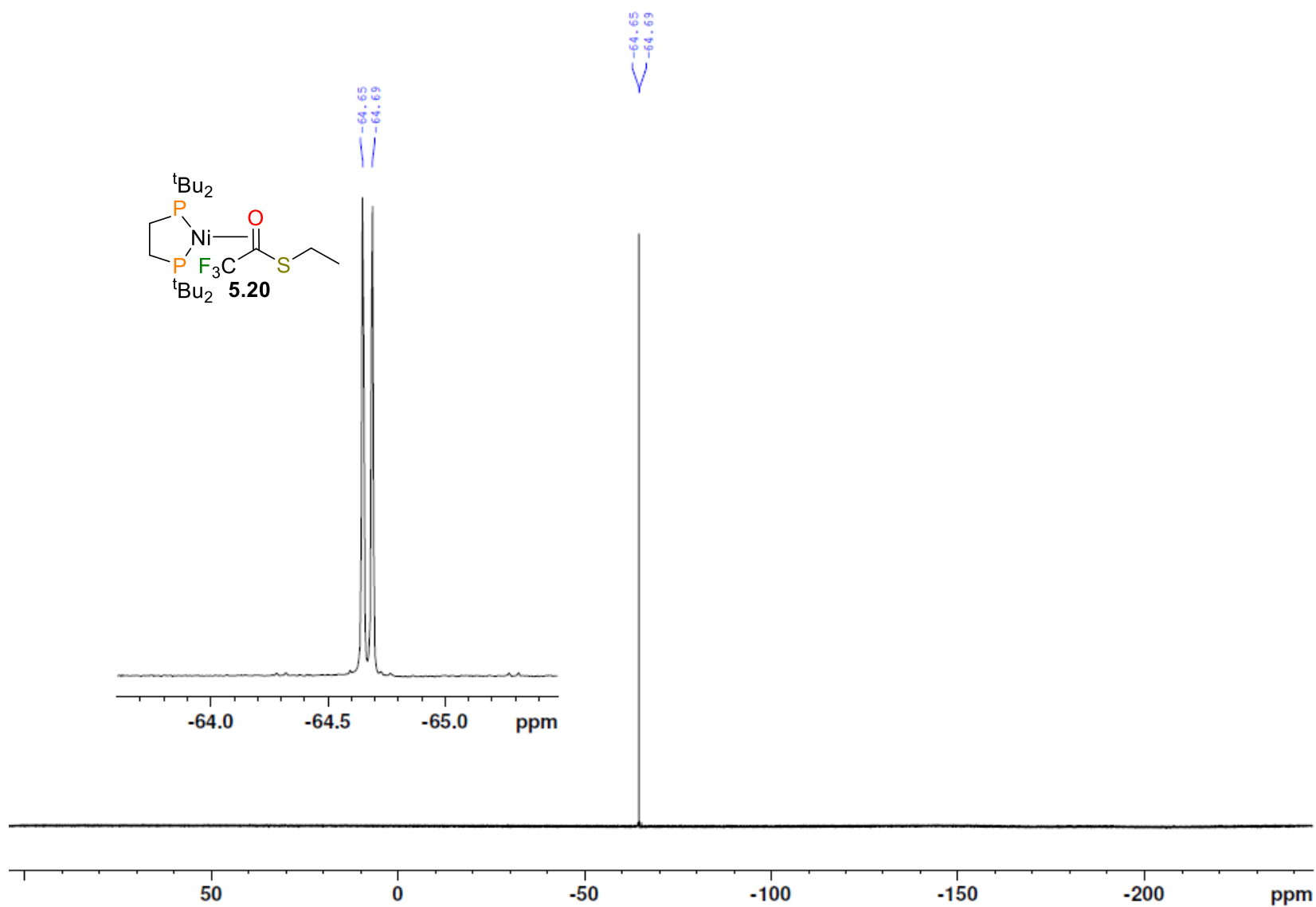


**Figure B5.8.**  $^{19}\text{F}\{^1\text{H}\}$  NMR spectrum (280 MHz, 25 °C,  $\text{C}_6\text{D}_6$ ) of **5.20**.

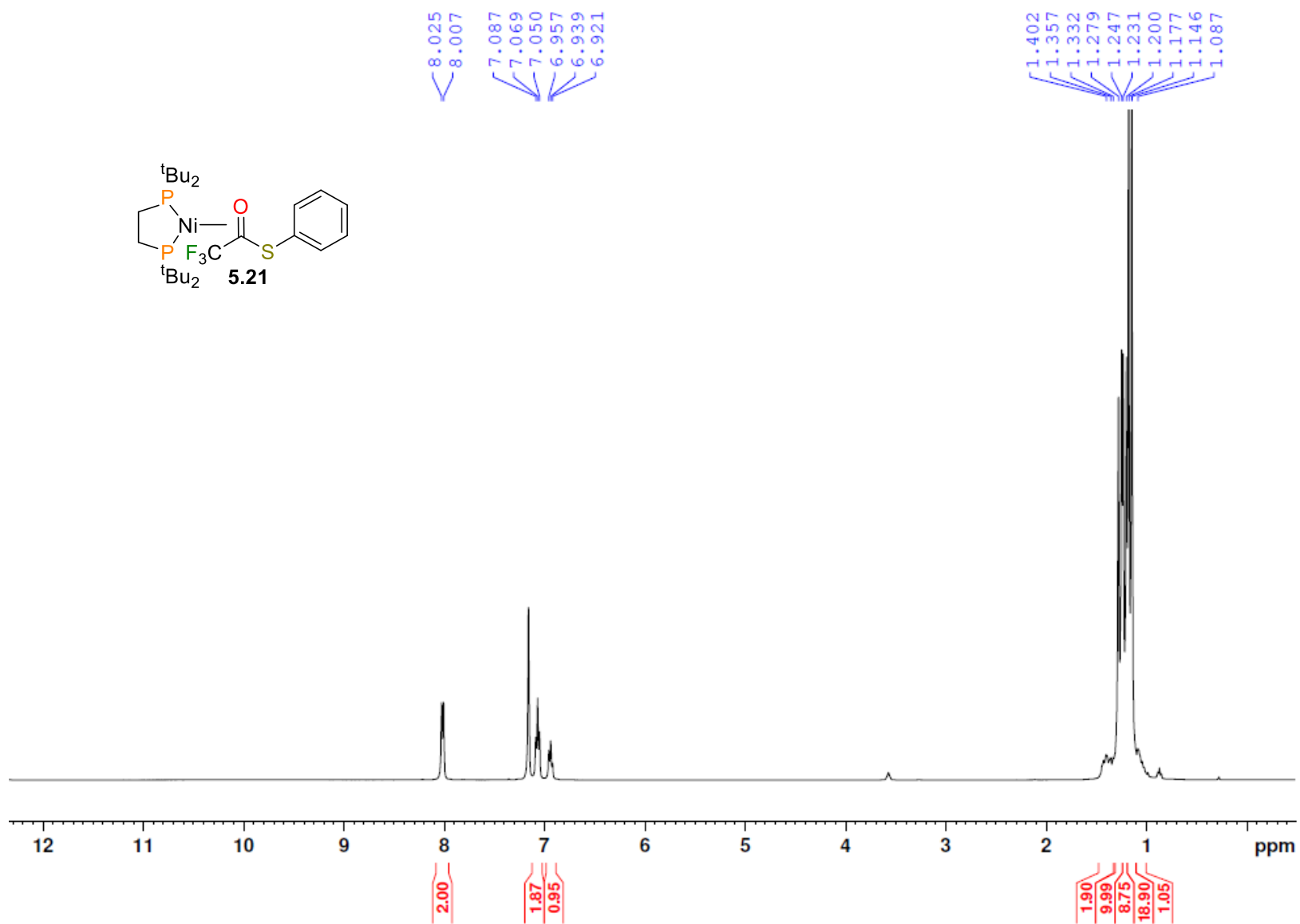


**Figure B5.9.**  $^1\text{H}$  NMR spectrum (400 MHz, 25 °C,  $\text{C}_6\text{D}_6$ ) of **5.21**.

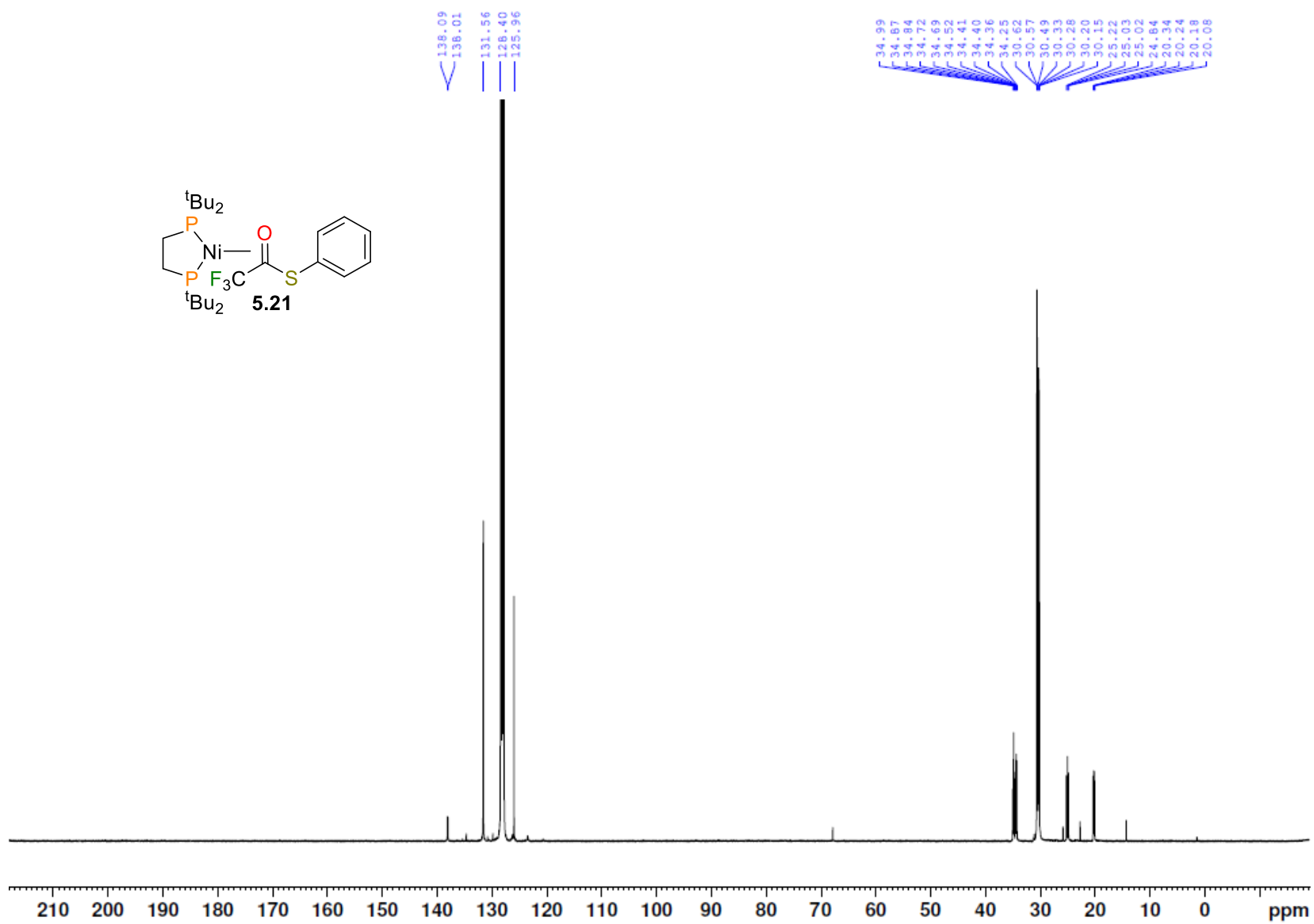


**Figure B5.10.** <sup>13</sup>C{<sup>1</sup>H} NMR spectrum (100 MHz, 25 °C, C<sub>6</sub>D<sub>6</sub>) of **5.21**.

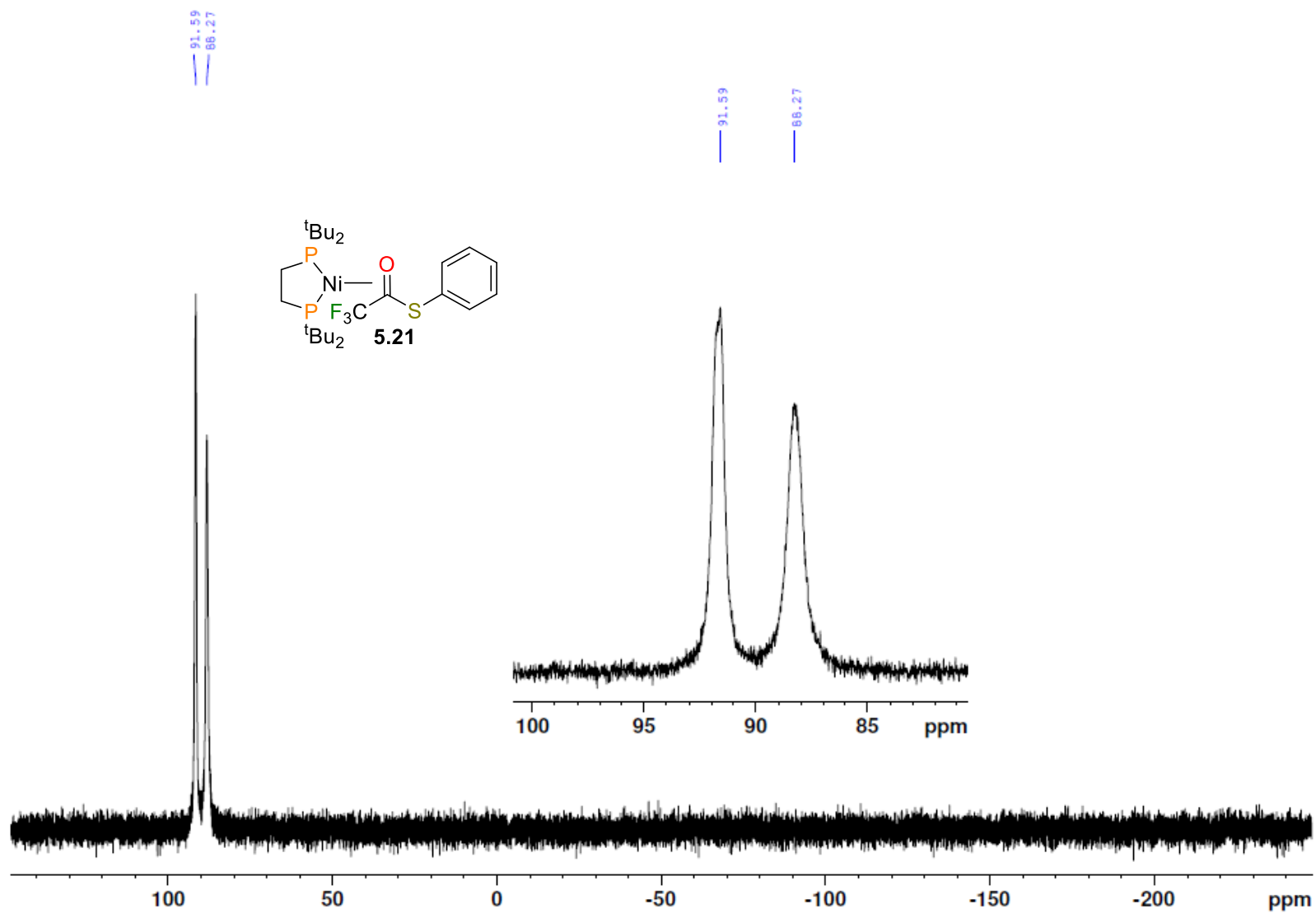


**Figure B5.11.**  $^{31}\text{P}\{^1\text{H}\}$  NMR spectrum (162 MHz, 25 °C,  $\text{C}_6\text{D}_6$ ) of **5.21**.

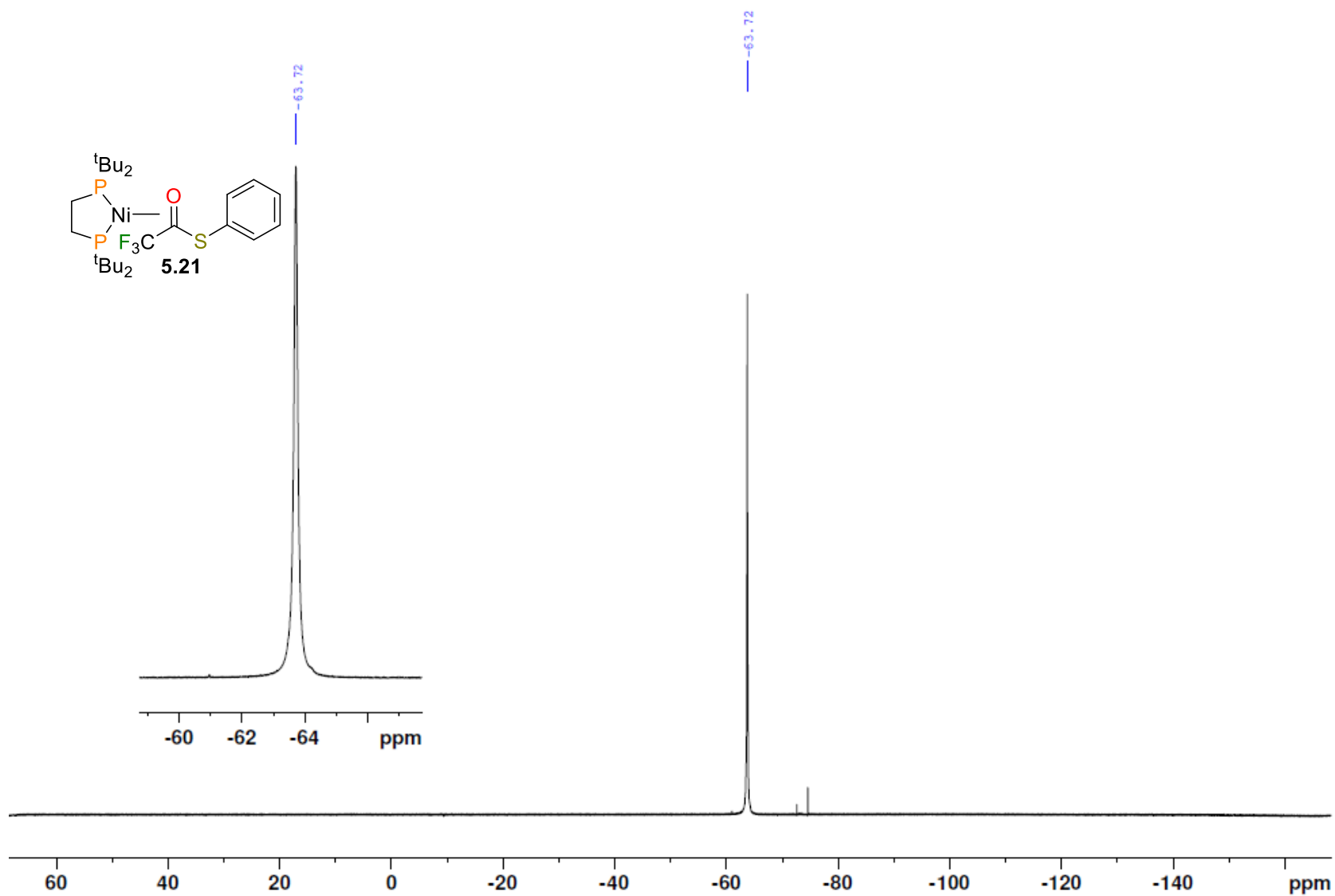


**Figure B5.12.**  $^{19}\text{F}\{^1\text{H}\}$  NMR spectrum (380 MHz, 25 °C,  $\text{C}_6\text{D}_6$ ) of **5.21**.



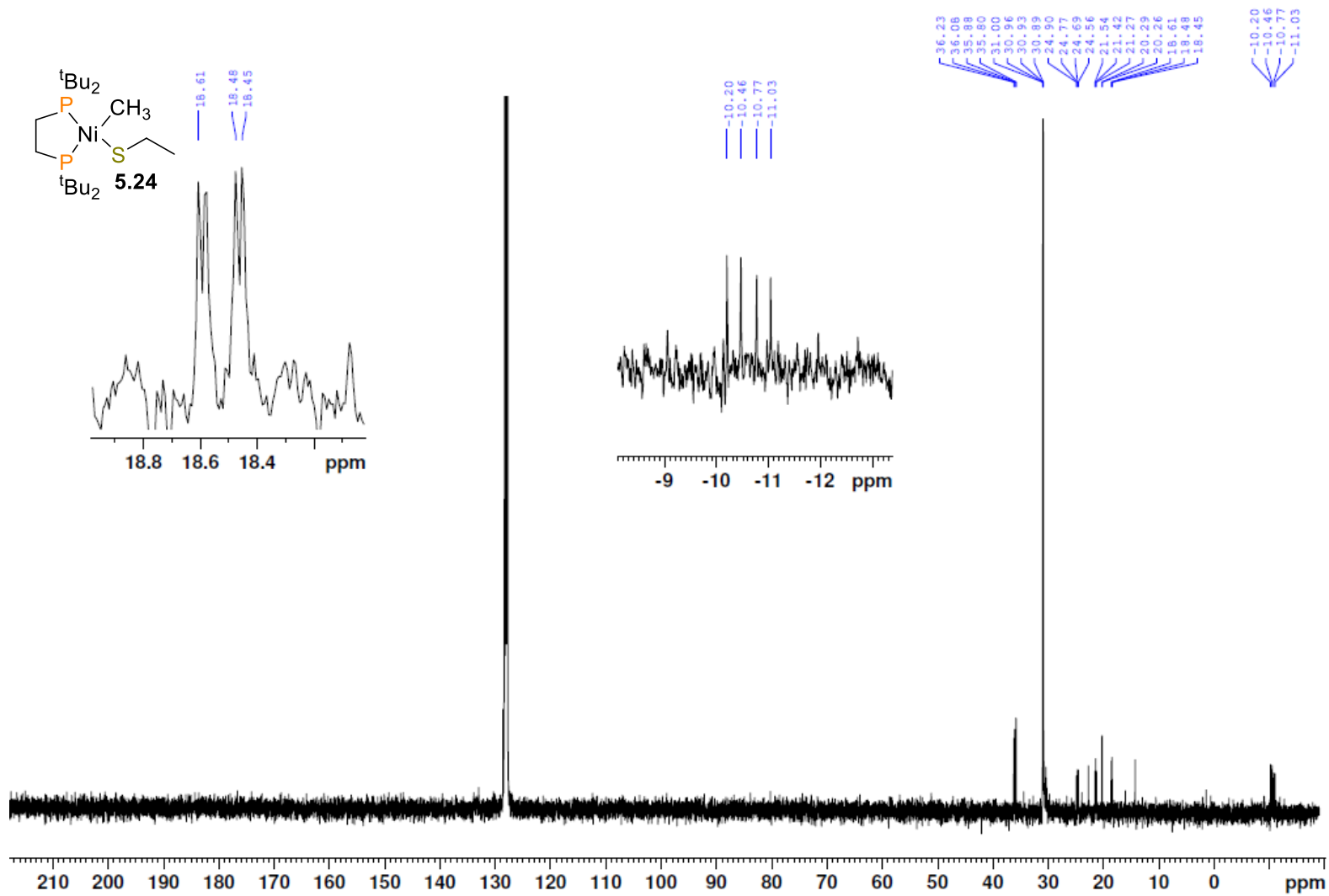


**Figure B5.14.**  $^{13}\text{C}\{^1\text{H}\}$  NMR spectrum (100 MHz, 25 °C,  $\text{C}_6\text{D}_6$ ) of **5.24**. The inset shows the resonances assigned to **C2** (left) and **C1** (right).



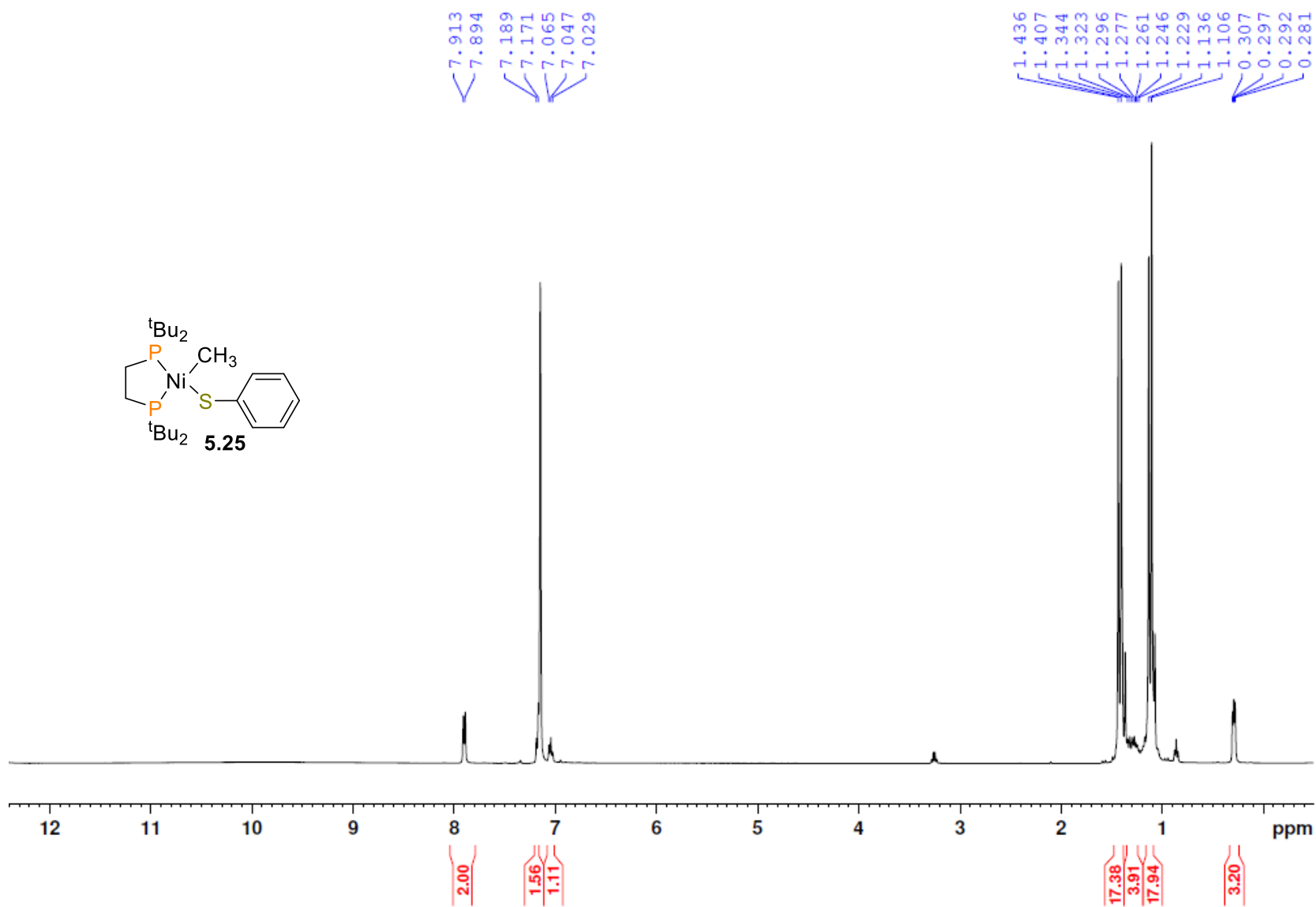


**Figure B5.16.** <sup>1</sup>H NMR spectrum (400 MHz, 25 °C, C<sub>6</sub>D<sub>6</sub>) of **5.25**.

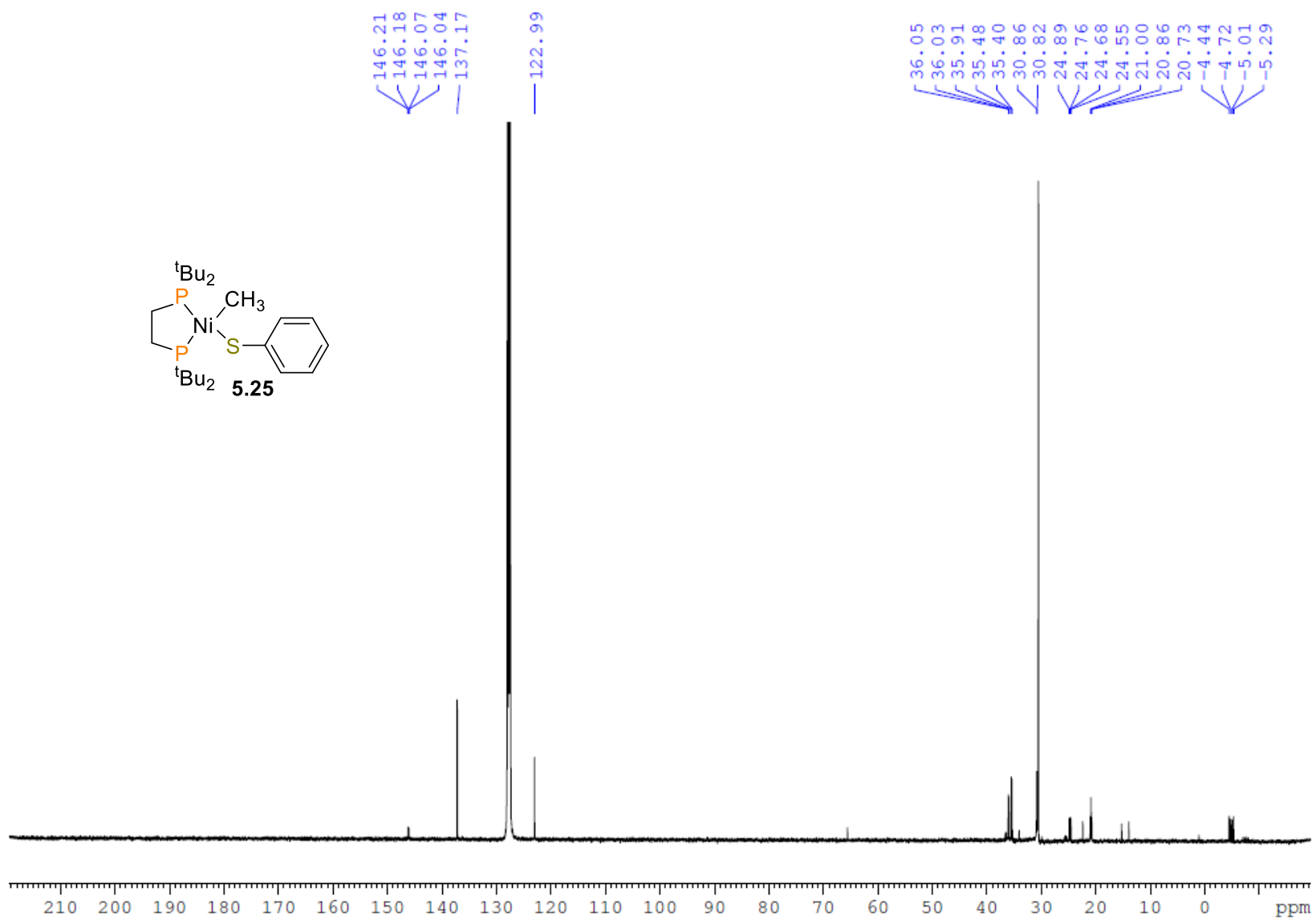


**Figure B5.17.**  $^{13}\text{C}\{^1\text{H}\}$  NMR spectrum (100 MHz, 25 °C,  $\text{C}_6\text{D}_6$ ) of **5.25**.

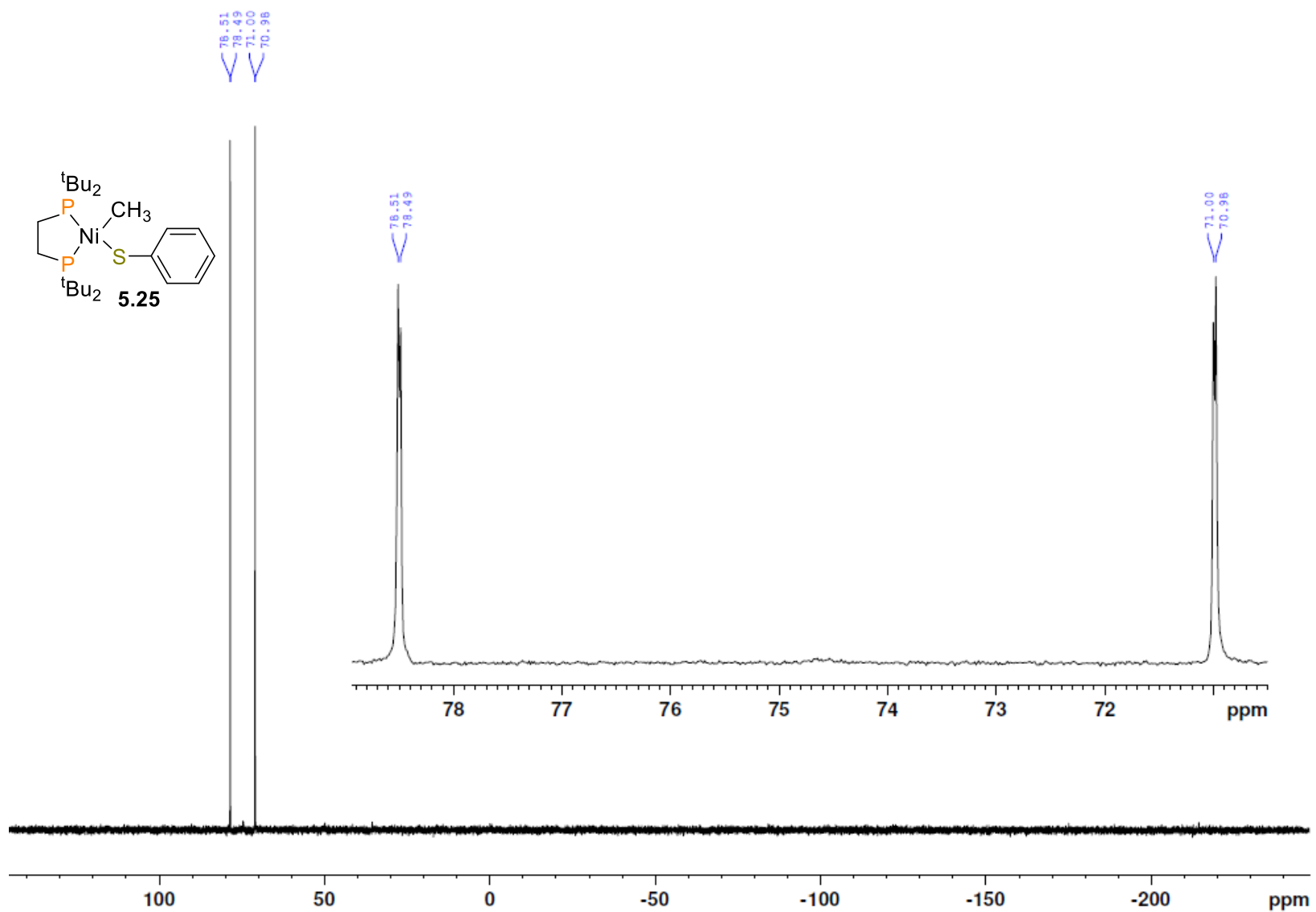


**Figure B5.18.**  $^{31}\text{P}\{^1\text{H}\}$  NMR spectrum (162 MHz, 25 °C,  $\text{C}_6\text{D}_6$ ) of **5.25**.

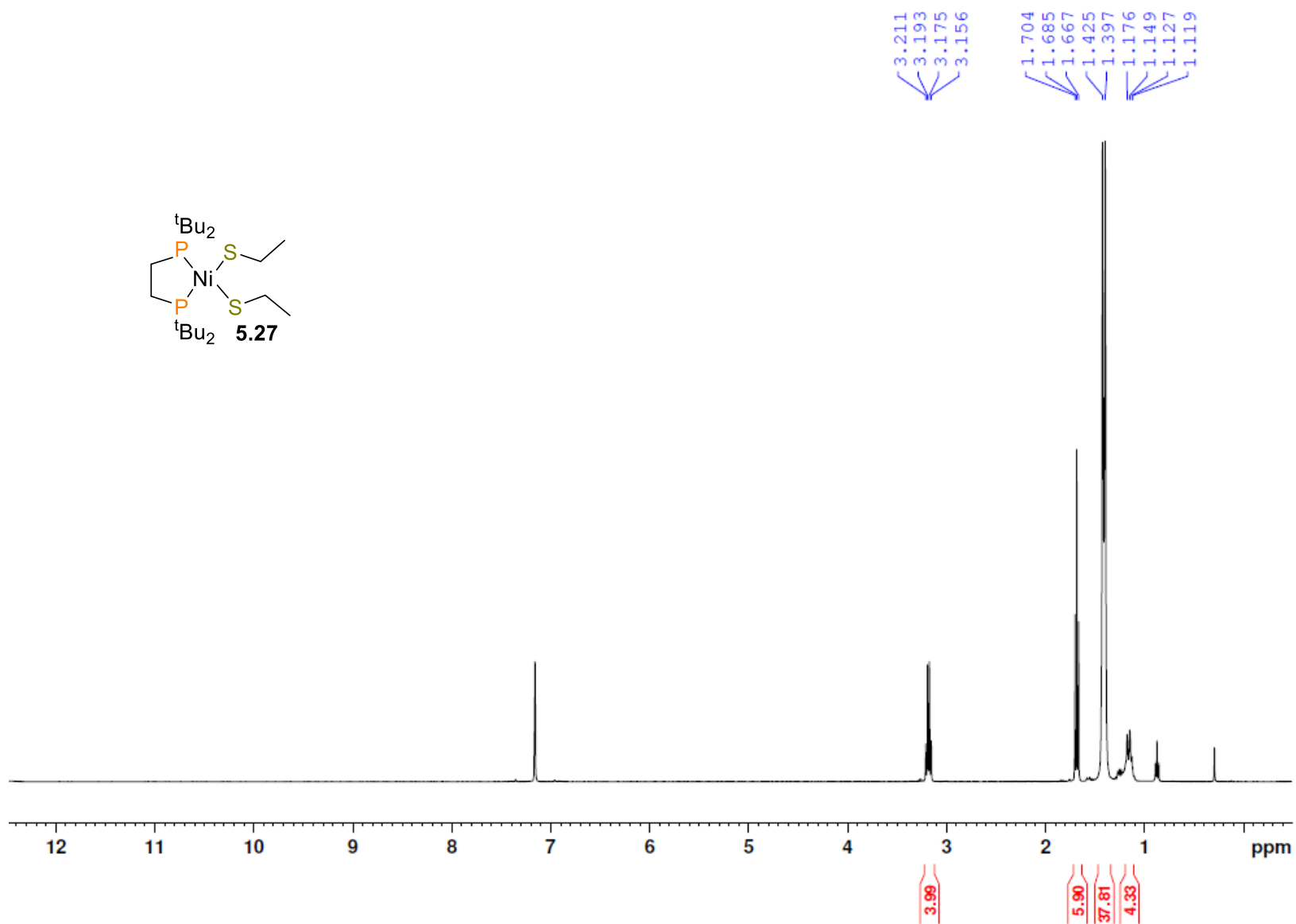


**Figure B5.19.**  $^1\text{H}$  NMR spectrum (400 MHz, 25 °C,  $\text{C}_6\text{D}_6$ ) of **5.27**.

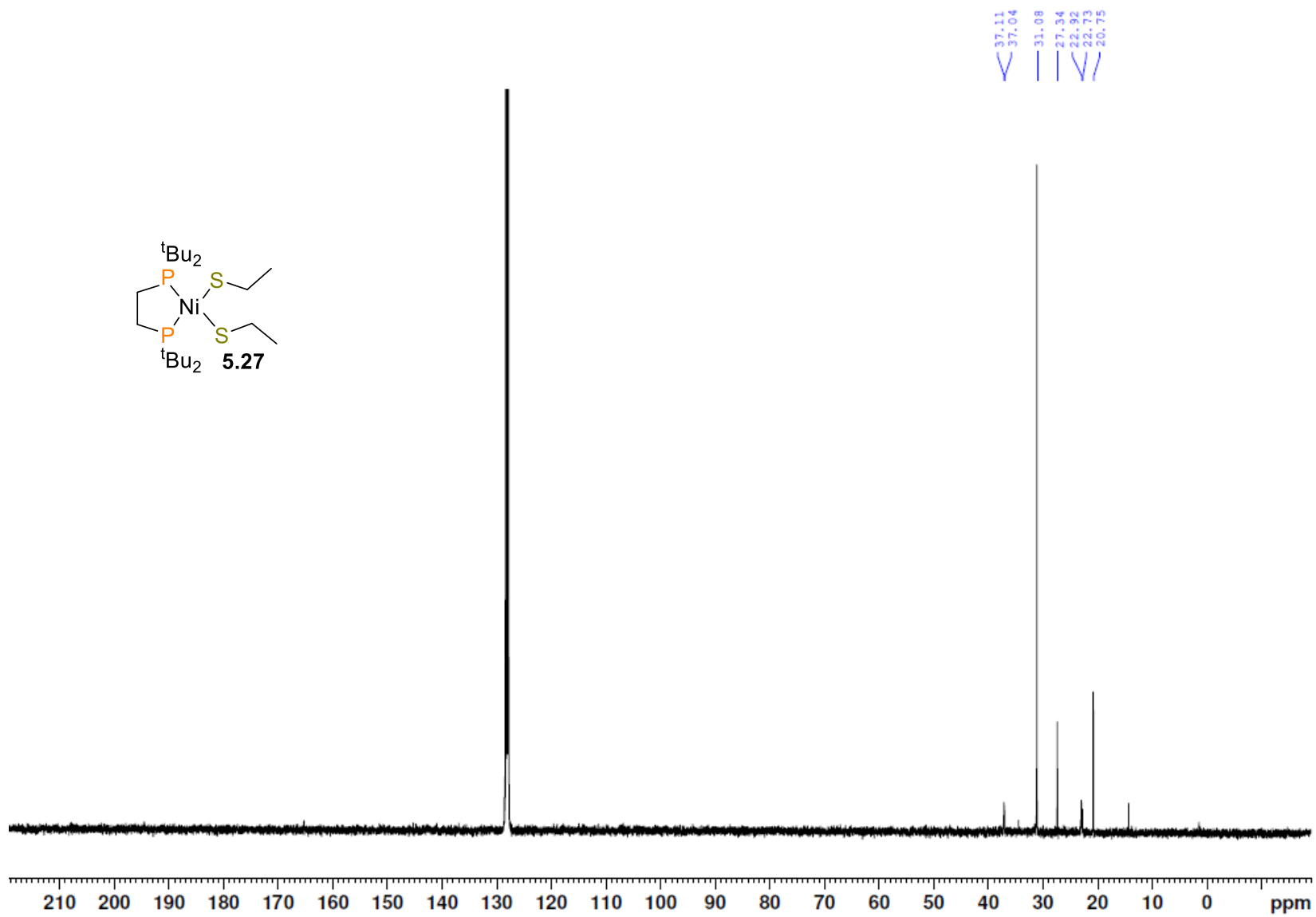


**Figure B5.20.**  $^{13}\text{C}\{^1\text{H}\}$  NMR spectrum (100 MHz, 25 °C,  $\text{C}_6\text{D}_6$ ) of **5.27**.

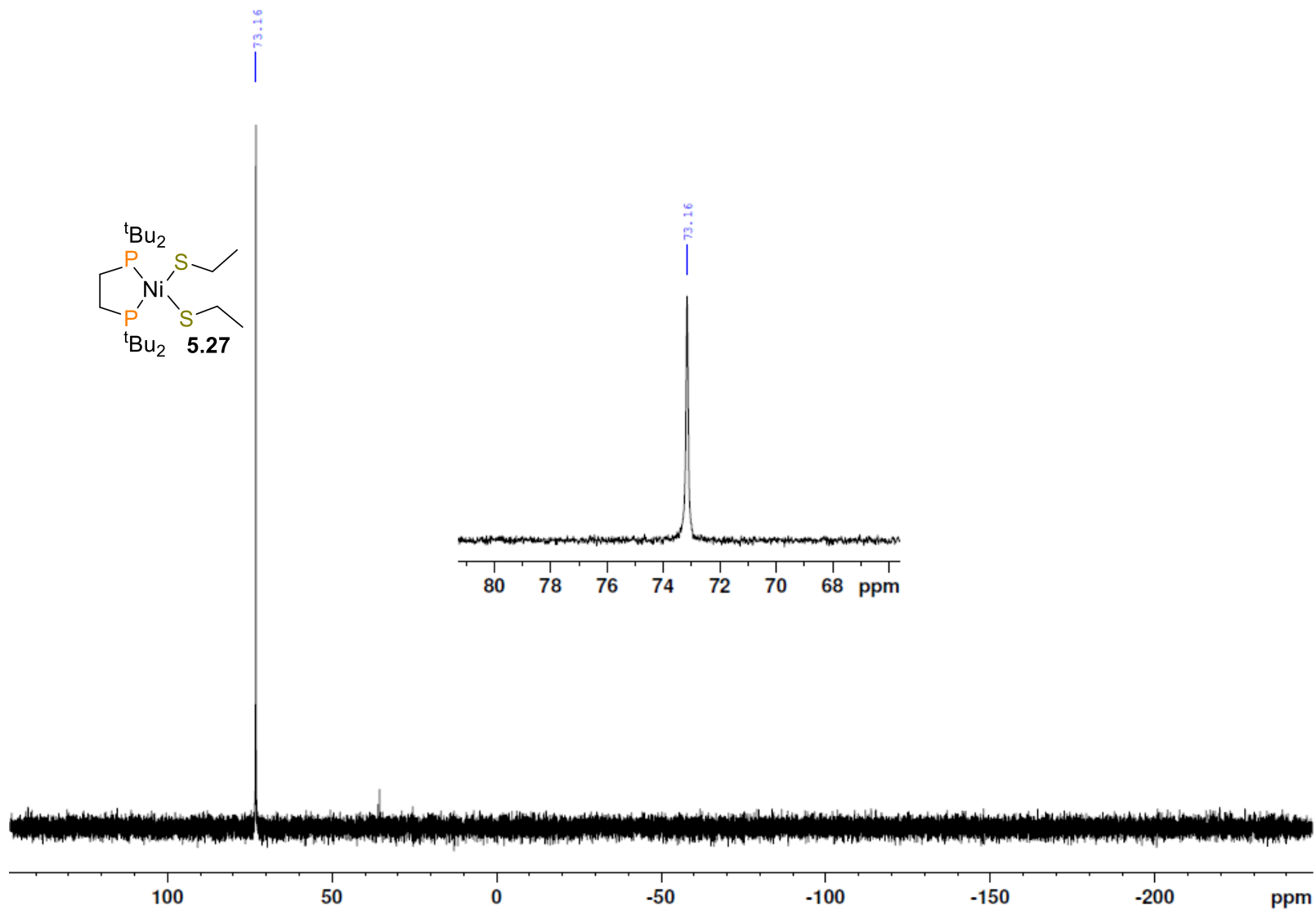


**Figure B5.21.**  $^{31}\text{P}\{^1\text{H}\}$  NMR spectrum (162 MHz, 25 °C,  $\text{C}_6\text{D}_6$ ) of **5.27**.

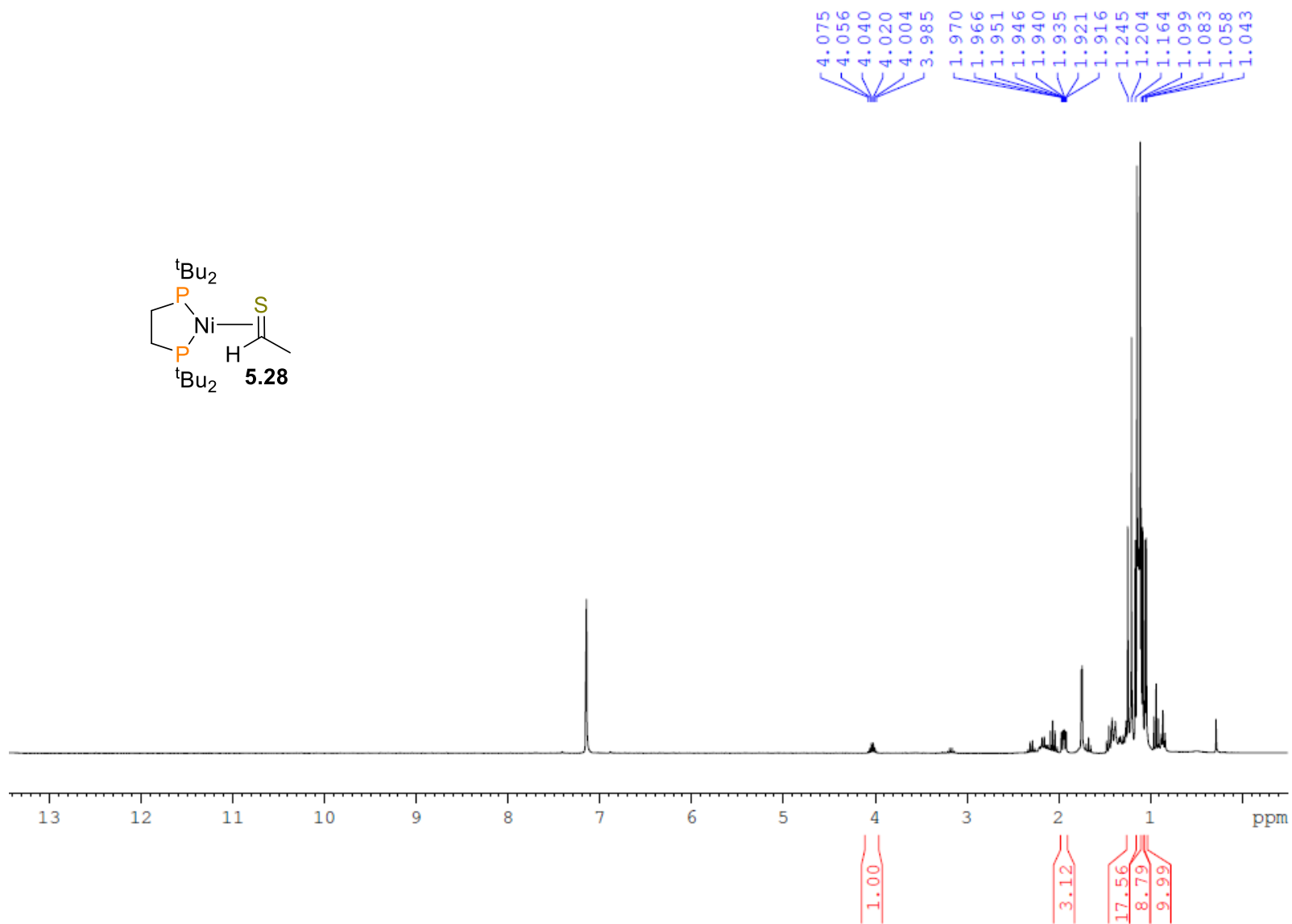


**Figure B5.22.** <sup>1</sup>H NMR spectrum (300 MHz, 25 °C, C<sub>6</sub>D<sub>6</sub>) of **5.28**.

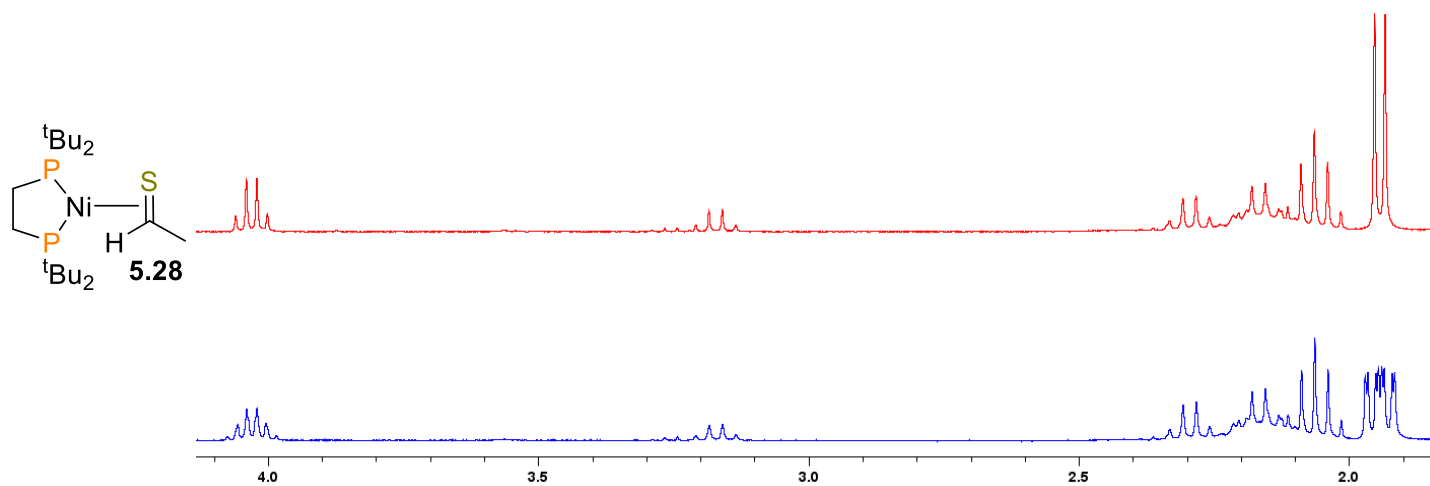


**Figure B5.23.** Selective  $^1\text{H}$  NMR spectrum (300 MHz, 25 °C,  $\text{C}_6\text{D}_6$ ) of **5.28** with  $^{31}\text{P}$  coupling (blue, bottom) and  $^{31}\text{P}$  decoupling (red, top).

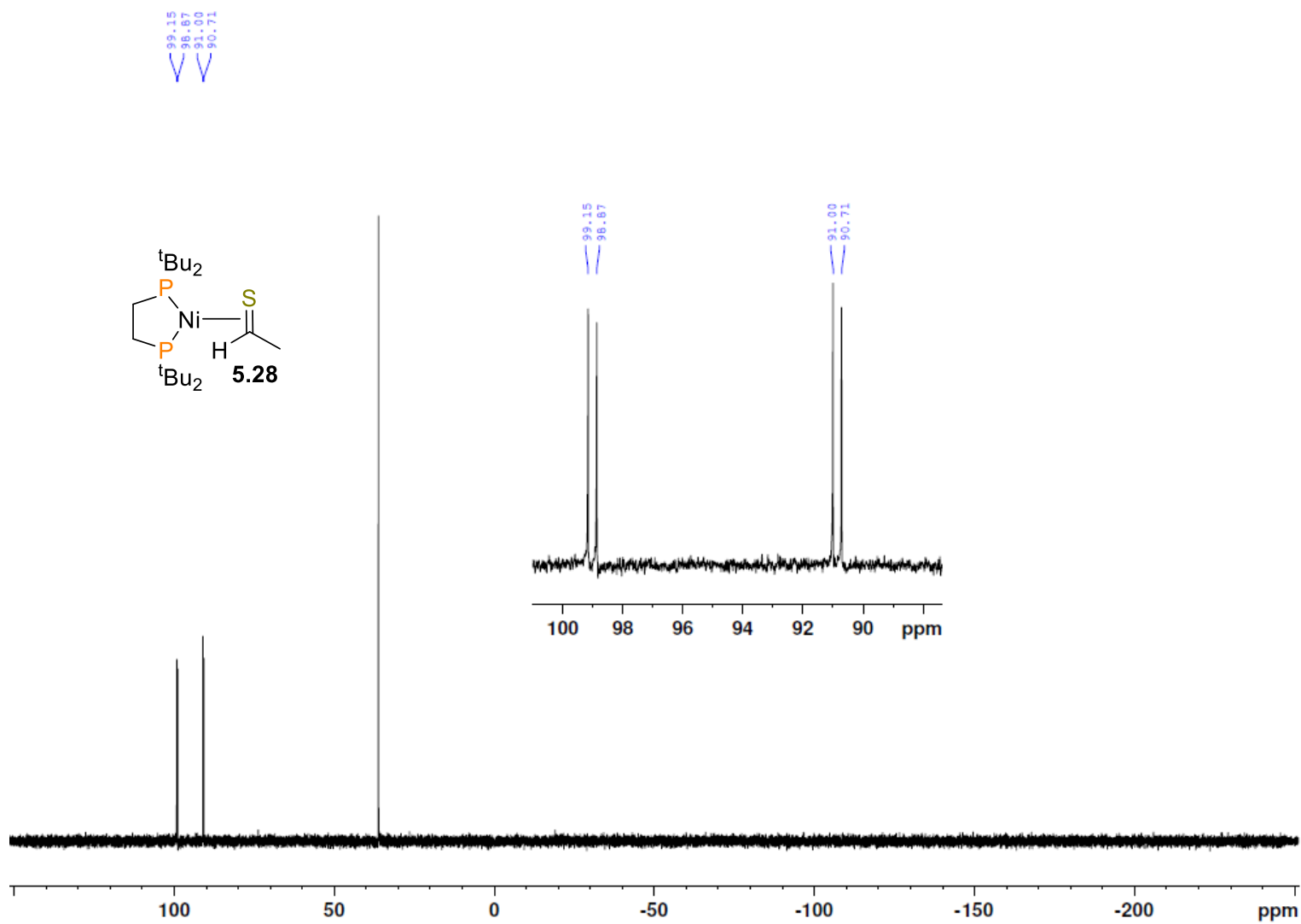


**Figure B5.24.**  $^{31}\text{P}\{^1\text{H}\}$  NMR spectrum (120 MHz, 25 °C,  $\text{C}_6\text{D}_6$ ) of **5.28**. The large singlet at 36 ppm is free dtbpe, formed during the thermolysis of **5.27** to generate **5.28**.

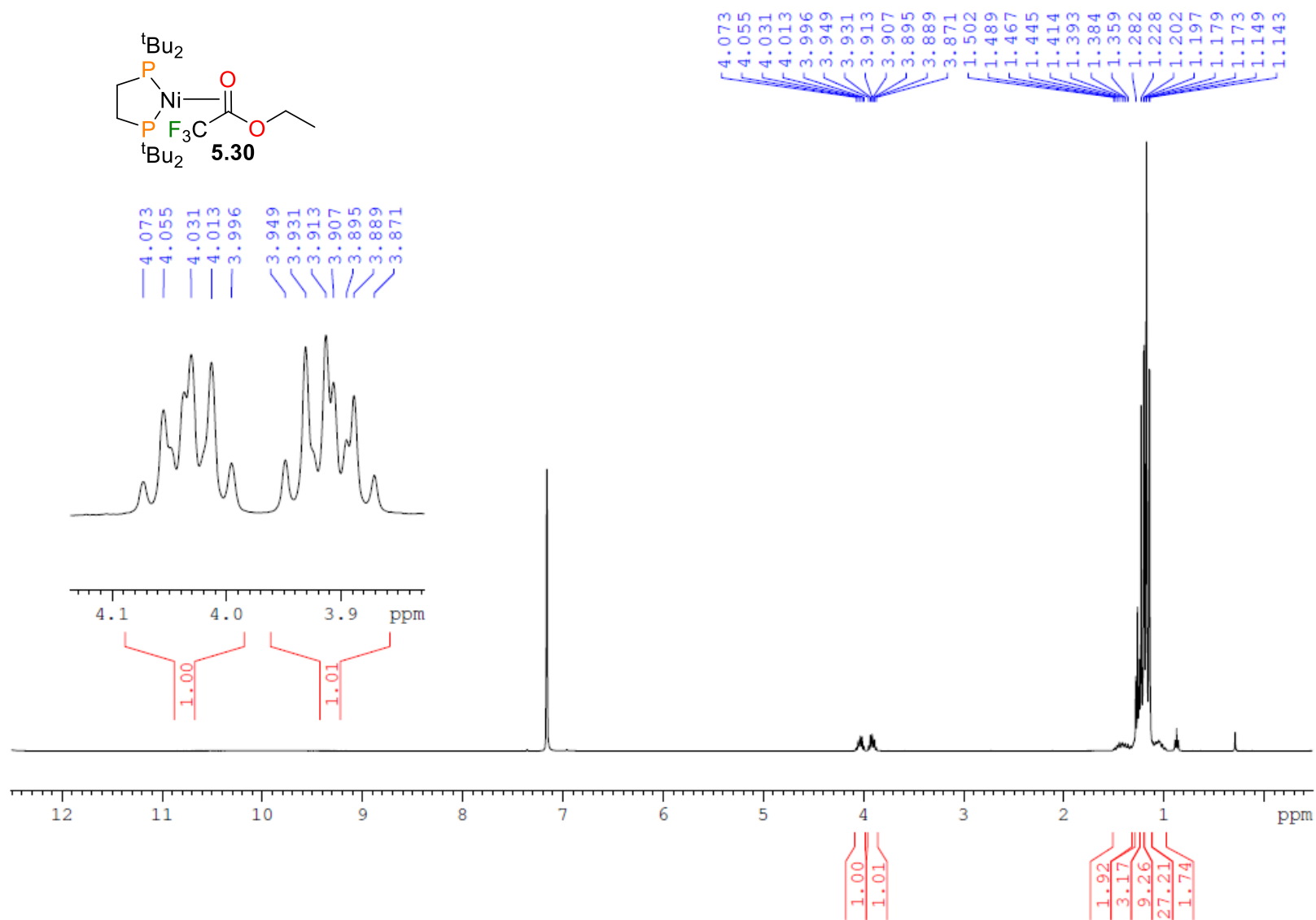


**Figure B5.25.**  $^1\text{H}$  NMR spectrum (400 MHz, 25 °C,  $\text{C}_6\text{D}_6$ ) of **5.30**. The inset shows the resonances assigned to **H3**.

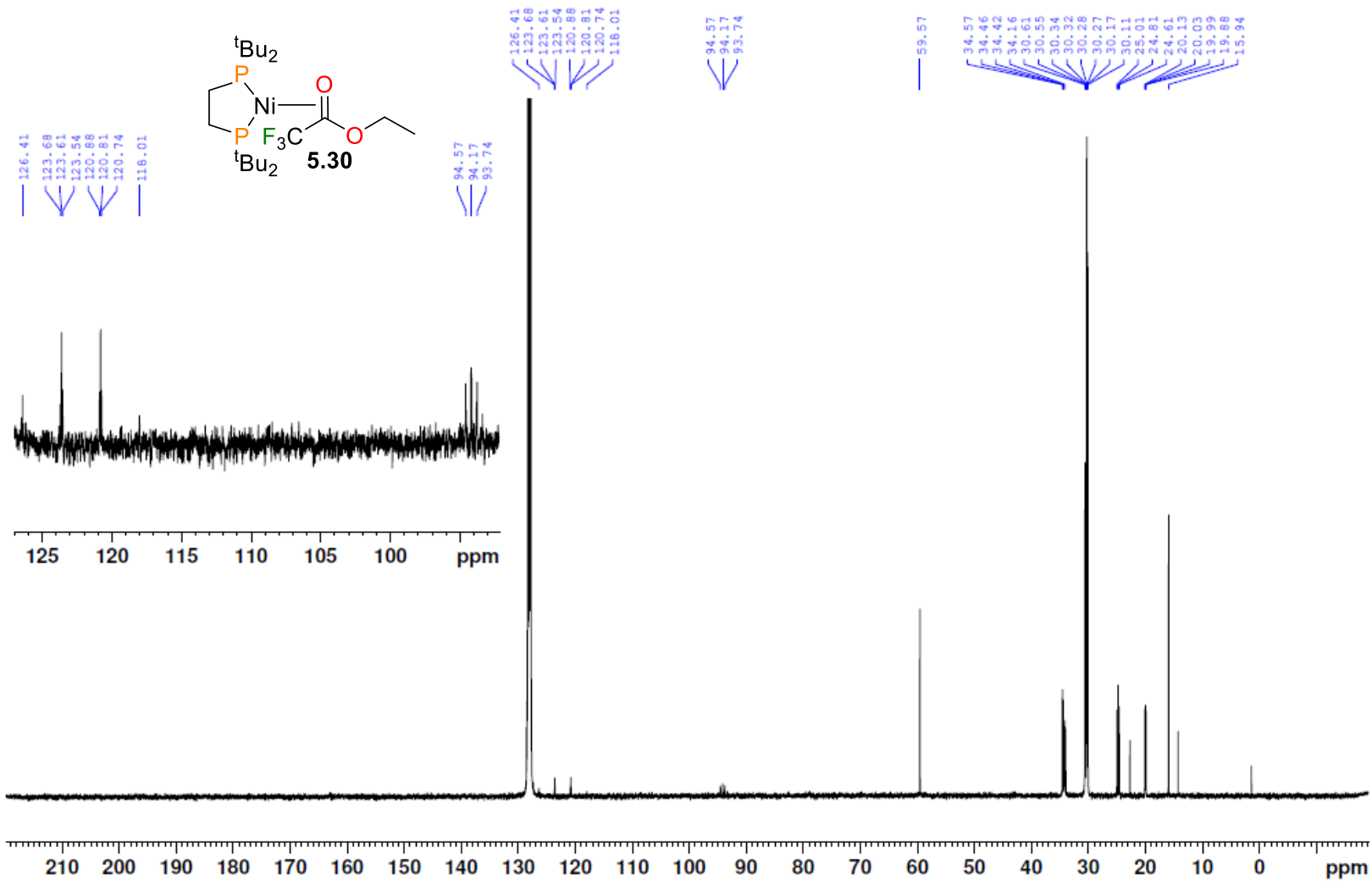


**Figure B5.26.**  $^{13}\text{C}\{^1\text{H}\}$  NMR spectrum (100 MHz, 25 °C,  $\text{C}_6\text{D}_6$ ) of **5.30**. The inset shows the resonance assigned to **C1** (left) and **C2** (right).

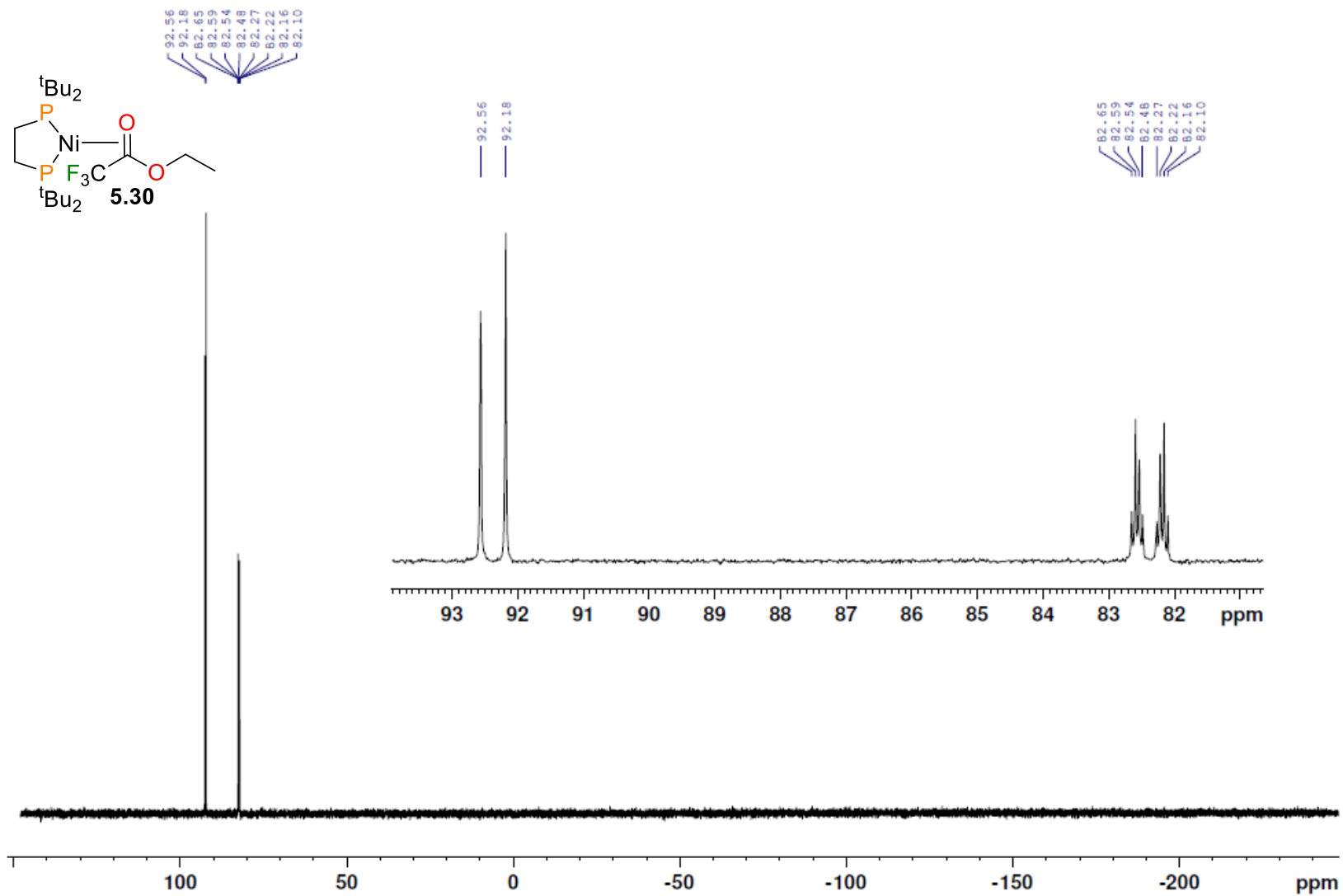


**Figure B5.27.**  $^{31}\text{P}\{^1\text{H}\}$  NMR spectrum (162 MHz, 25 °C,  $\text{C}_6\text{D}_6$ ) of **5.30**.

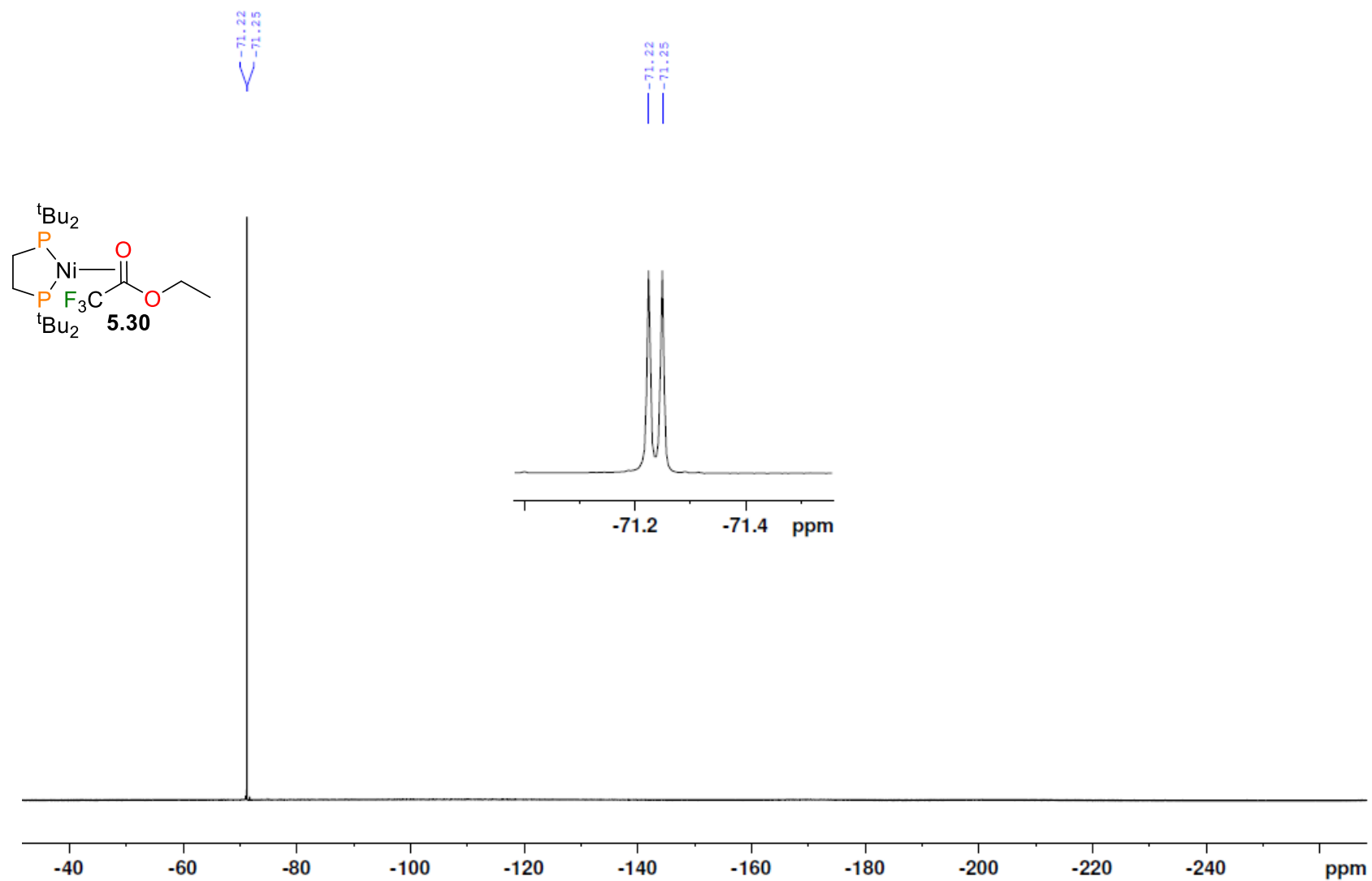


**Figure B5.28.**  $^{19}\text{F}\{^1\text{H}\}$  NMR spectrum (380 MHz, 25 °C,  $\text{C}_6\text{D}_6$ ) of **5.30**.

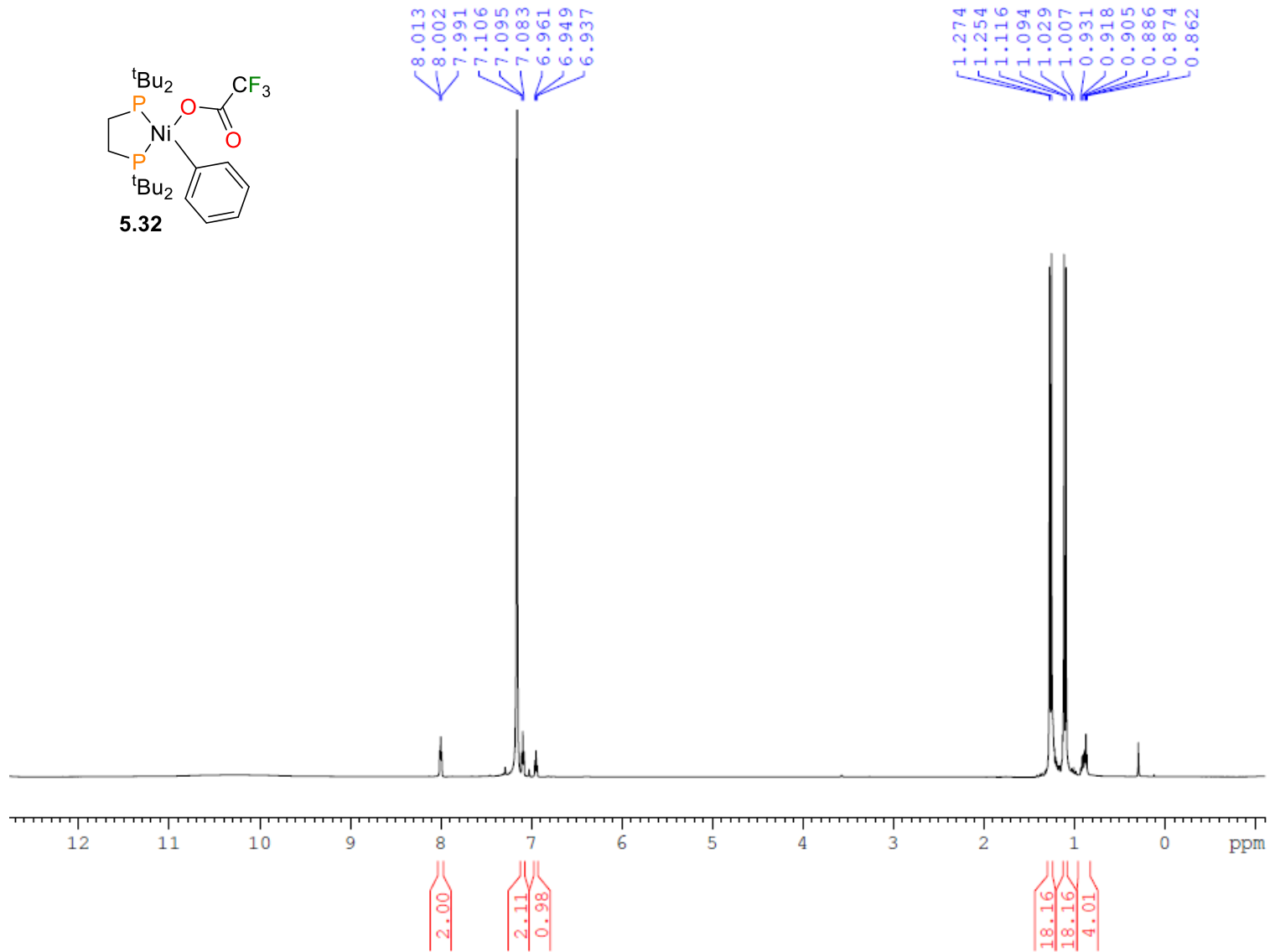


**Figure B5.29.** <sup>1</sup>H NMR spectrum (400 MHz, 25 °C, C<sub>6</sub>D<sub>6</sub>) of **5.32**.

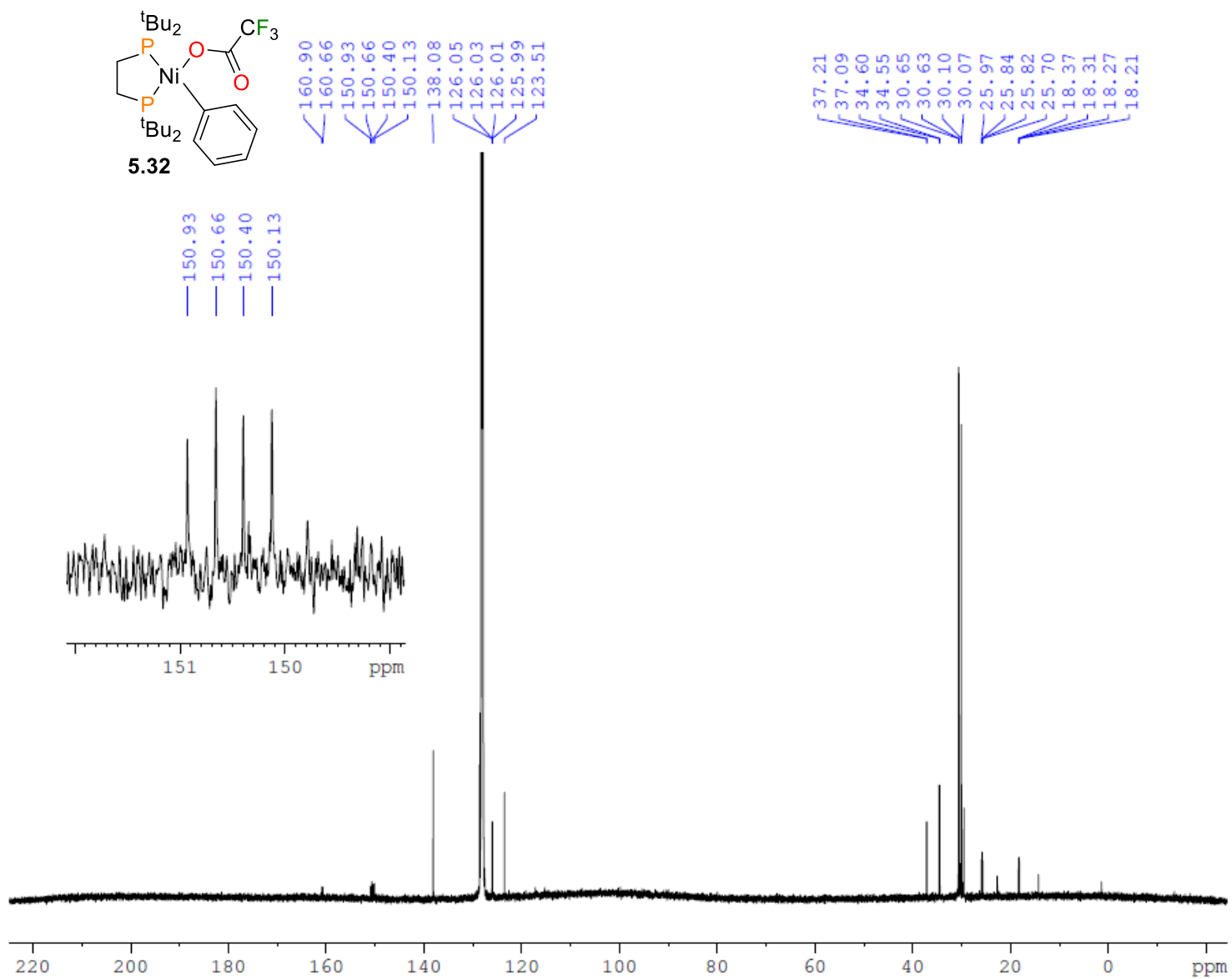


**Figure B5.30.**  $^{13}\text{C}\{^1\text{H}\}$  NMR spectrum (100 MHz, 25 °C,  $\text{C}_6\text{D}_6$ ) of **5.32**. The inset shows the resonance assigned to C3.

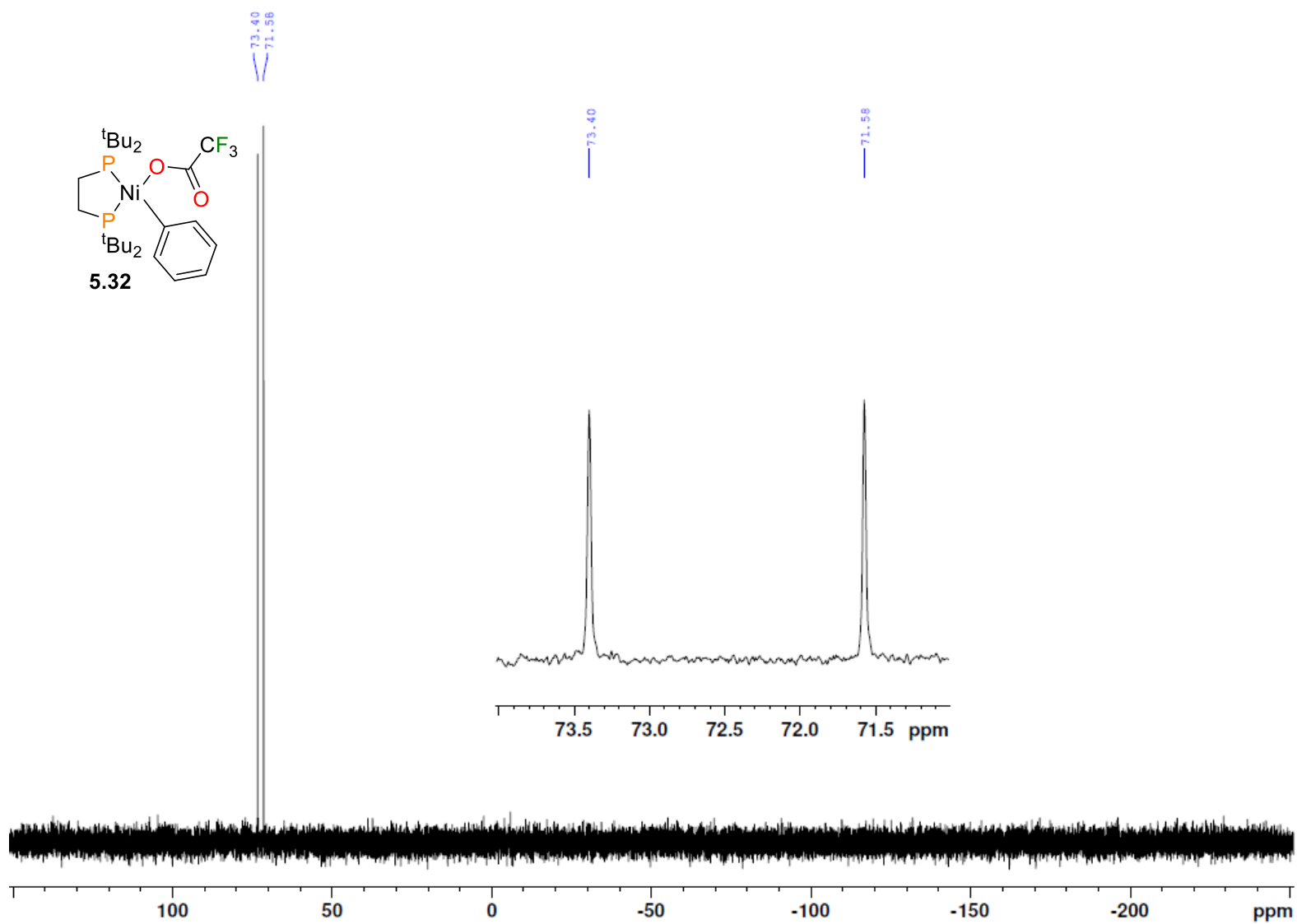
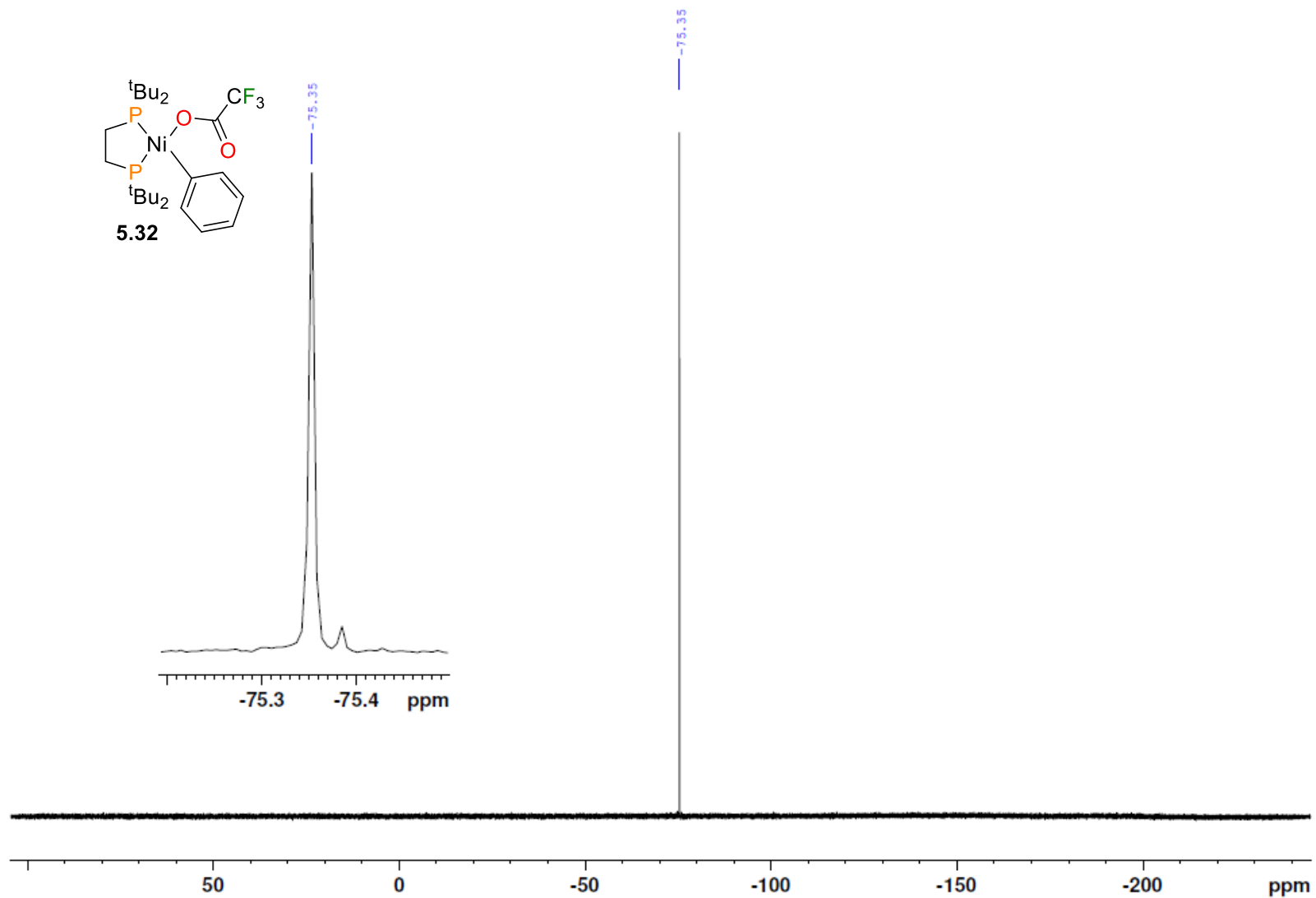
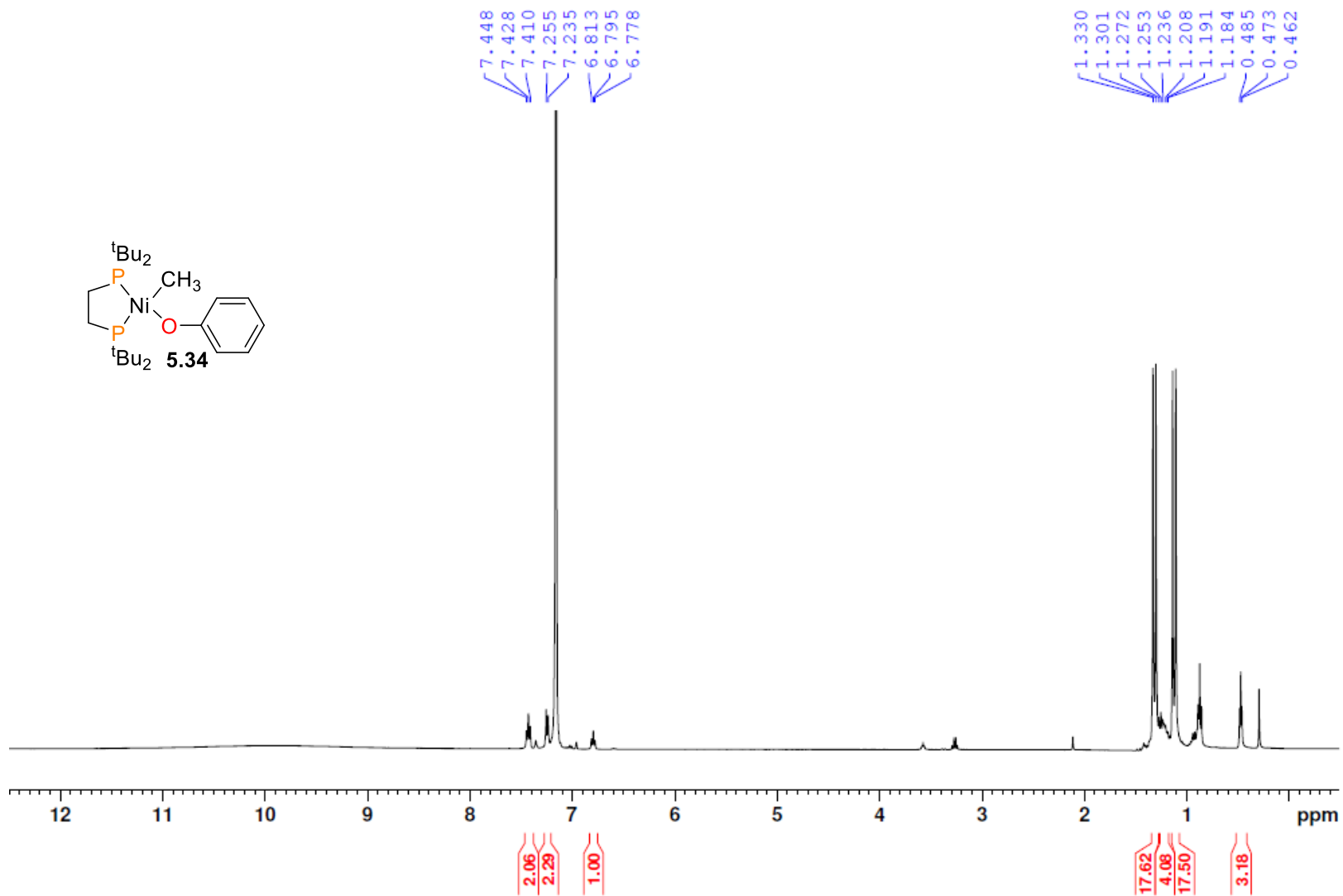


Figure B5.31.  $^{31}\text{P}\{^1\text{H}\}$  NMR spectrum (162 MHz, 25 °C,  $\text{C}_6\text{D}_6$ ) of **5.32**.



**Figure B5.32.**  $^{19}\text{F}\{^1\text{H}\}$  NMR spectrum (380 MHz, 25 °C,  $\text{C}_6\text{D}_6$ ) of **5.32**.



**Figure B5.33.** <sup>1</sup>H NMR spectrum (400 MHz, 25 °C, C<sub>6</sub>D<sub>6</sub>) of 5.34.

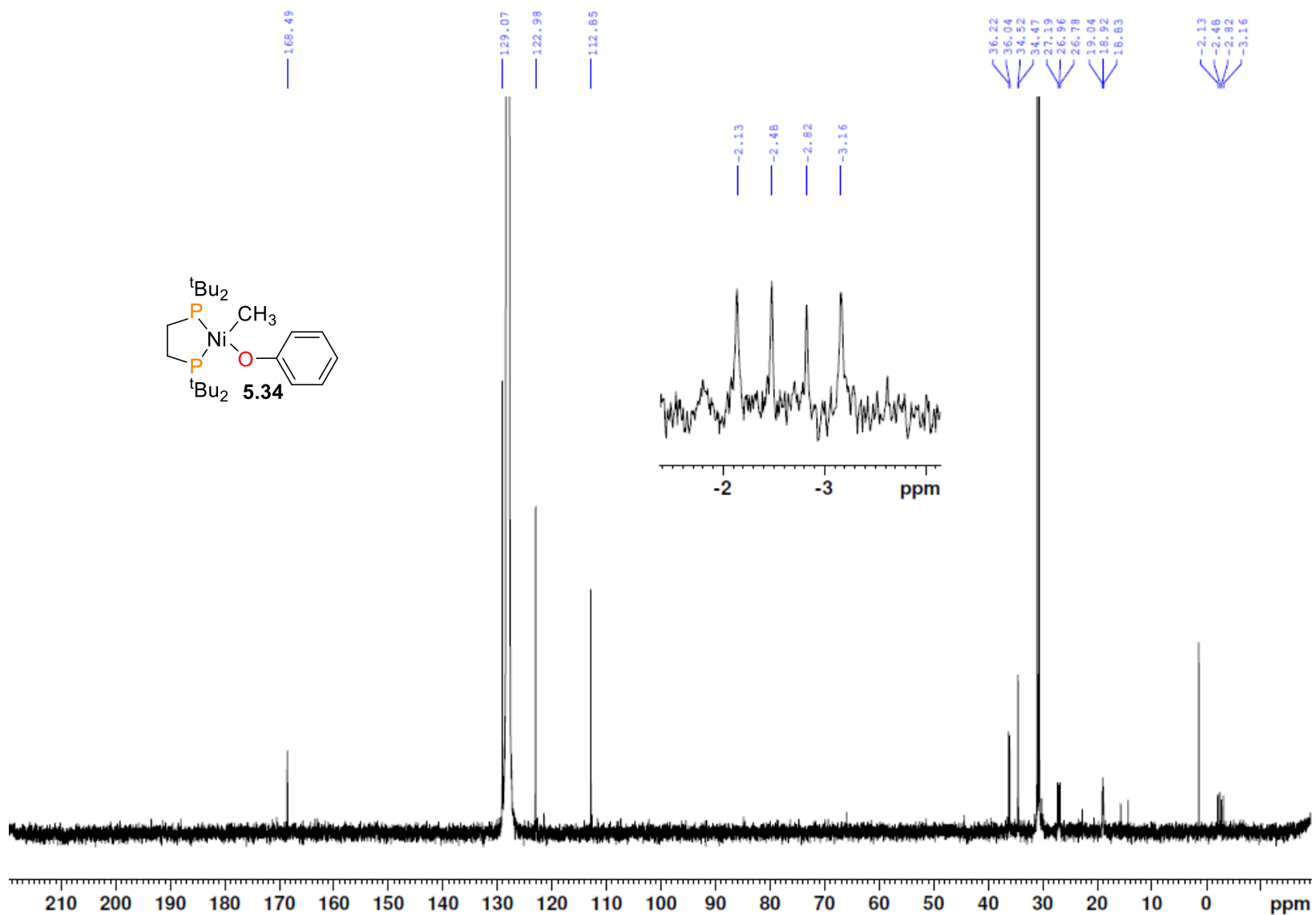


**Figure B5.34.**  $^{13}\text{C}\{^1\text{H}\}$  NMR spectrum (100 MHz, 25 °C,  $\text{C}_6\text{D}_6$ ) of **5.34**. The inset shows the resonance assigned to C1.

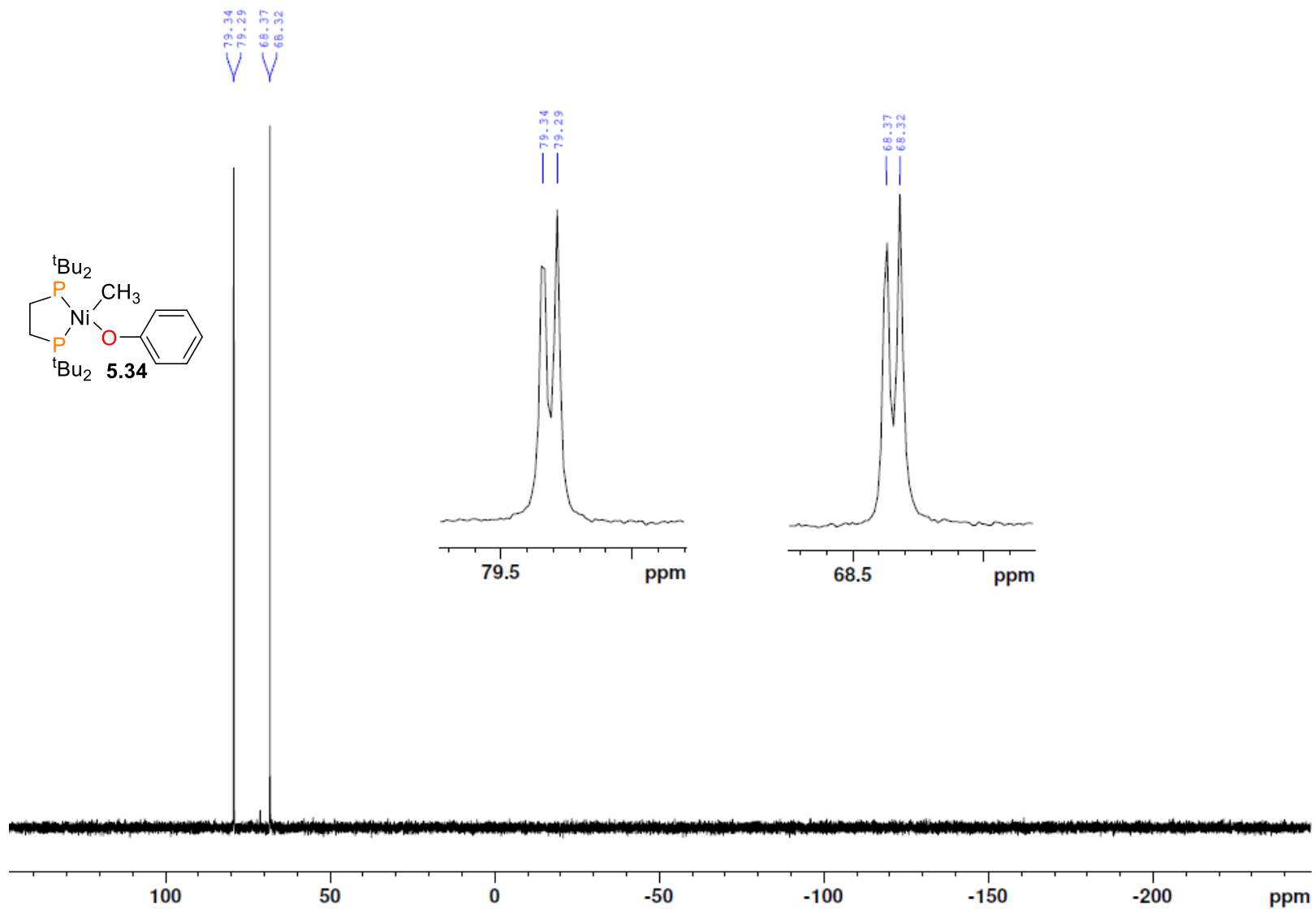


**Figure B5.35.**  $^{31}\text{P}\{^1\text{H}\}$  NMR spectrum (162 MHz, 25 °C,  $\text{C}_6\text{D}_6$ ) of **5.34**.

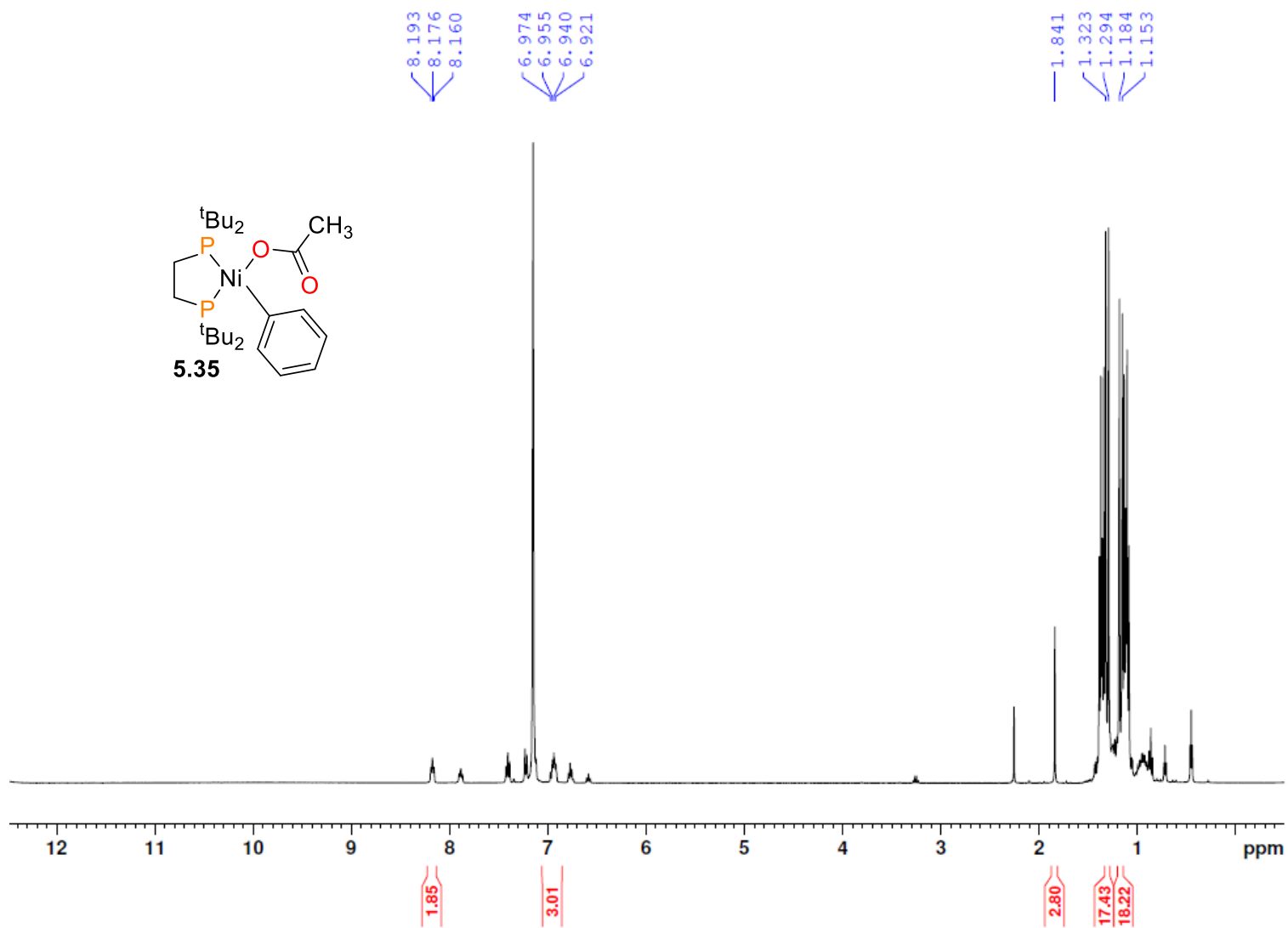


**Figure B5.36.** <sup>1</sup>H NMR spectrum (400 MHz, 25 °C, C<sub>6</sub>D<sub>6</sub>) of a mixture found to contain complex **5.34**, complex **5.35** and other unidentified products. The labelled resonances are those assigned to **5.35**.

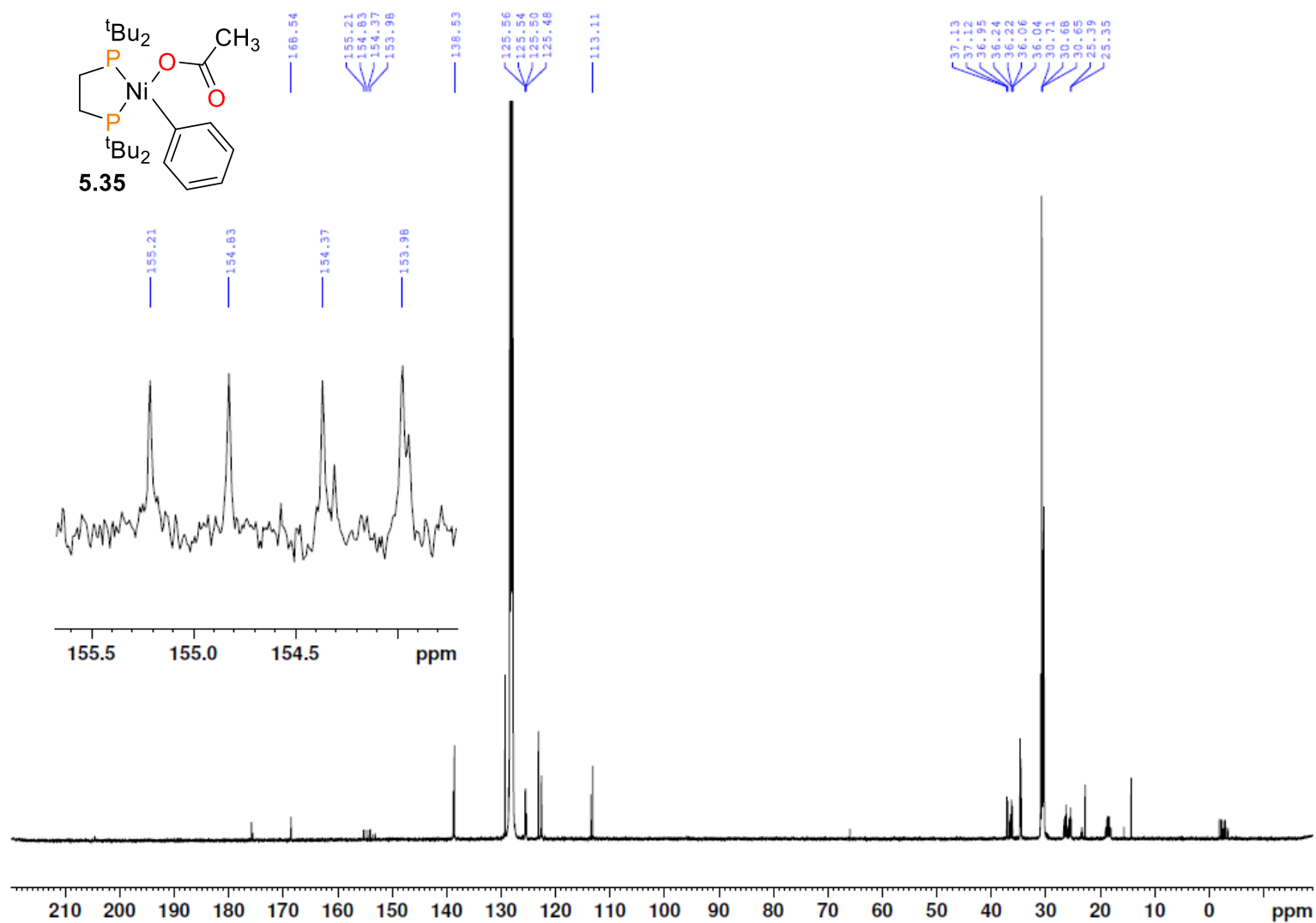


**Figure B5.37.** <sup>13</sup>C{<sup>1</sup>H} NMR spectrum (100 MHz, 25 °C, C<sub>6</sub>D<sub>6</sub>) of a mixture found to contain complex **5.34**, complex **5.35** and other unidentified products. The labelled resonances are those assigned to **5.35**. The inset shows the resonance assigned to **C3**.

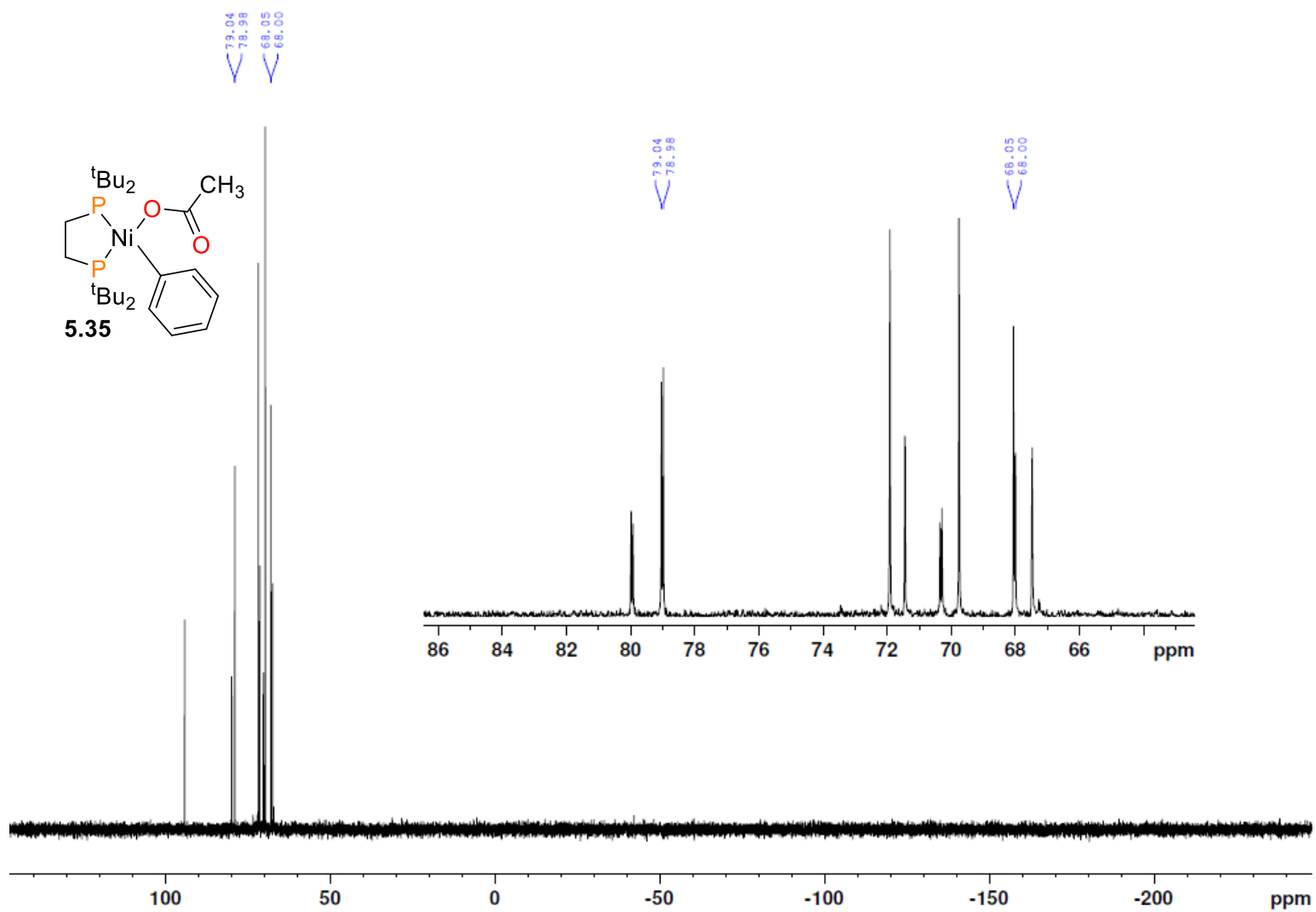


**Figure B5.38.**  $^{31}\text{P}\{^1\text{H}\}$  NMR spectrum (162 MHz, 25 °C,  $\text{C}_6\text{D}_6$ ) of a mixture found to contain complex **5.34**, complex **5.35** and other unidentified products. The labelled resonances are those assigned to **5.35**.

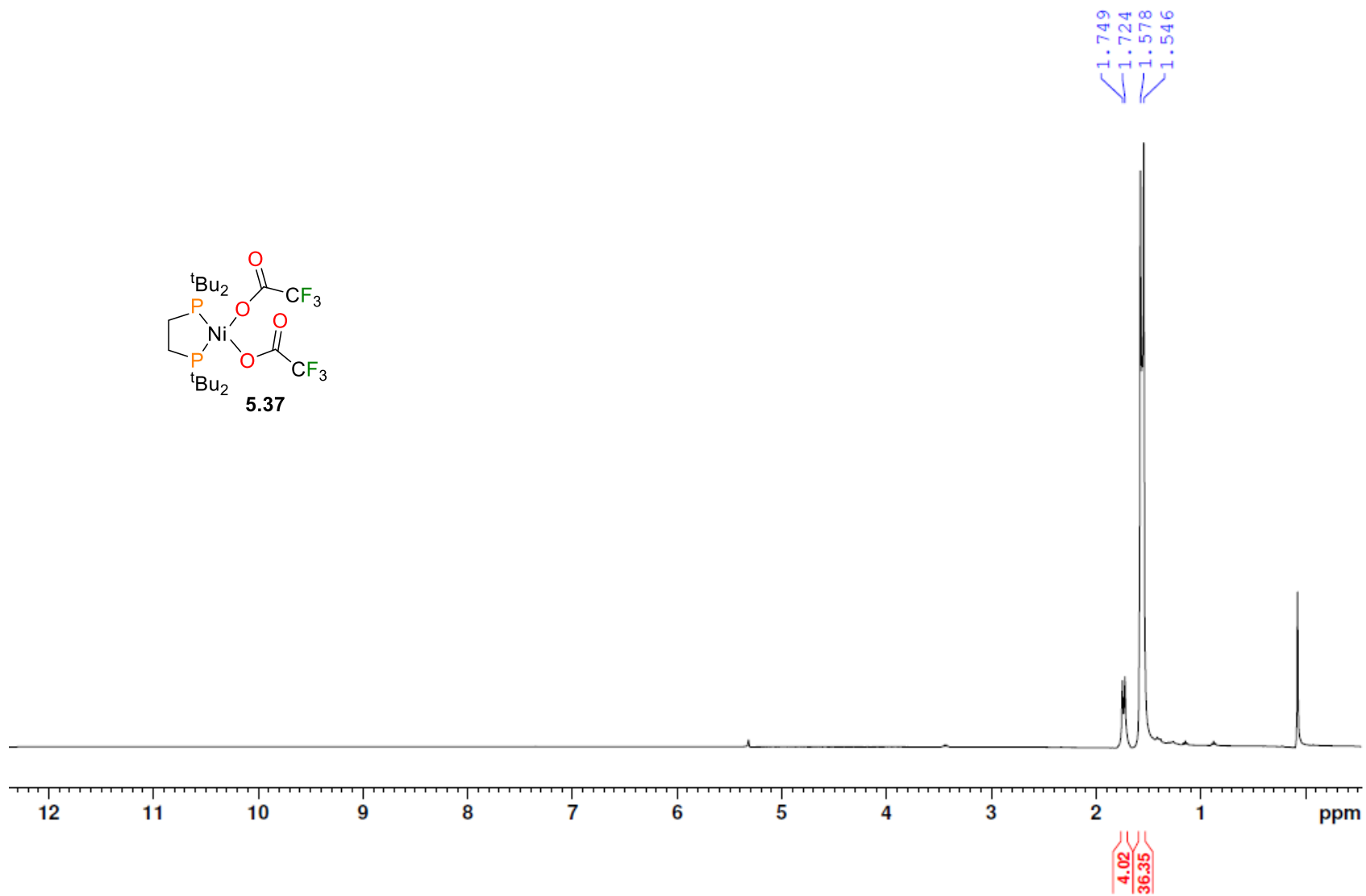


**Figure B5.39.**  $^1\text{H}$  NMR spectrum (400 MHz, 25 °C,  $\text{CD}_2\text{Cl}_2$ ) of **5.37**.

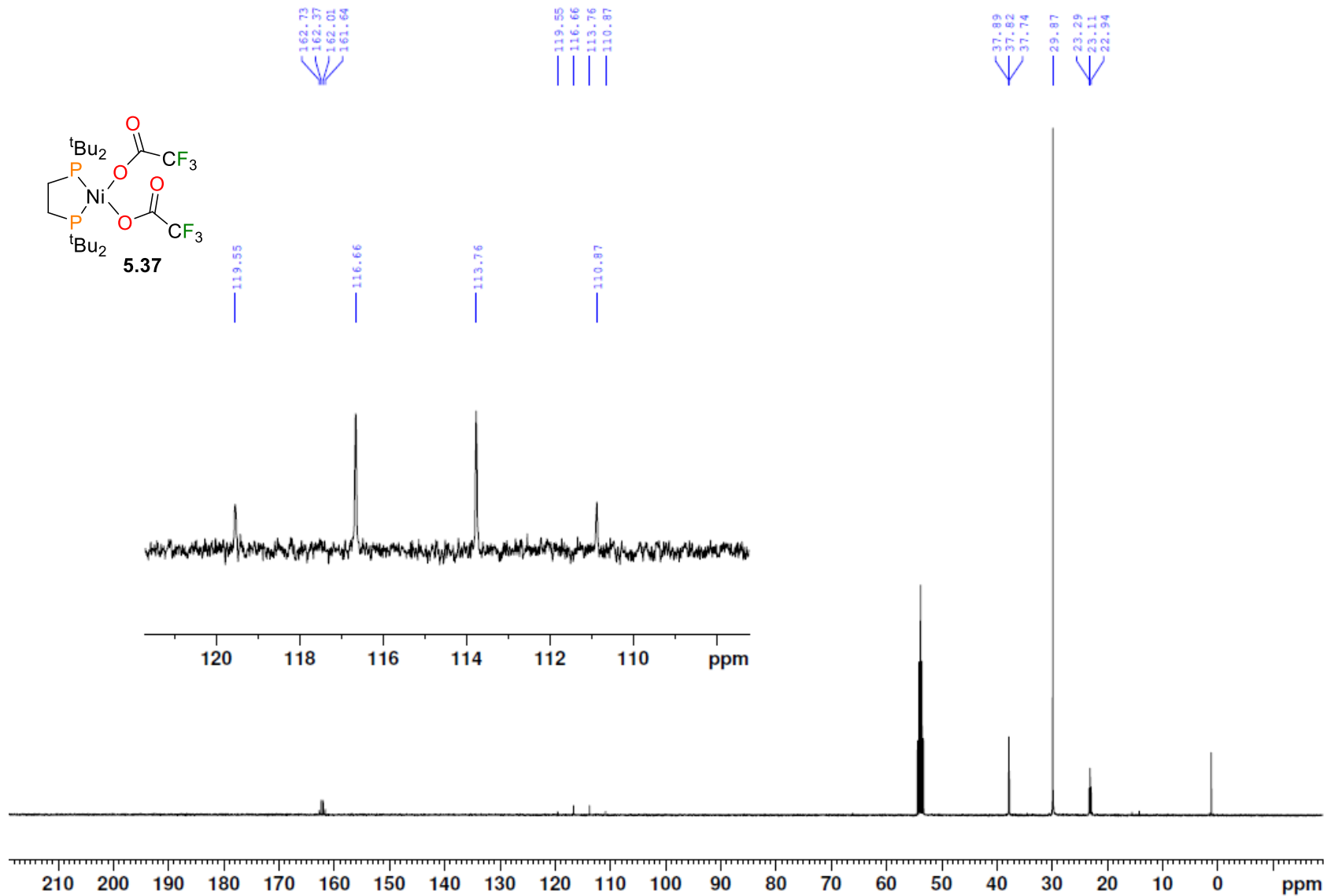


**Figure B5.40.**  $^{13}\text{C}\{^1\text{H}\}$  NMR spectrum (100 MHz, 25 °C,  $\text{CD}_2\text{Cl}_2$ ) of **5.37**. Inset shows the resonance assigned to C1.

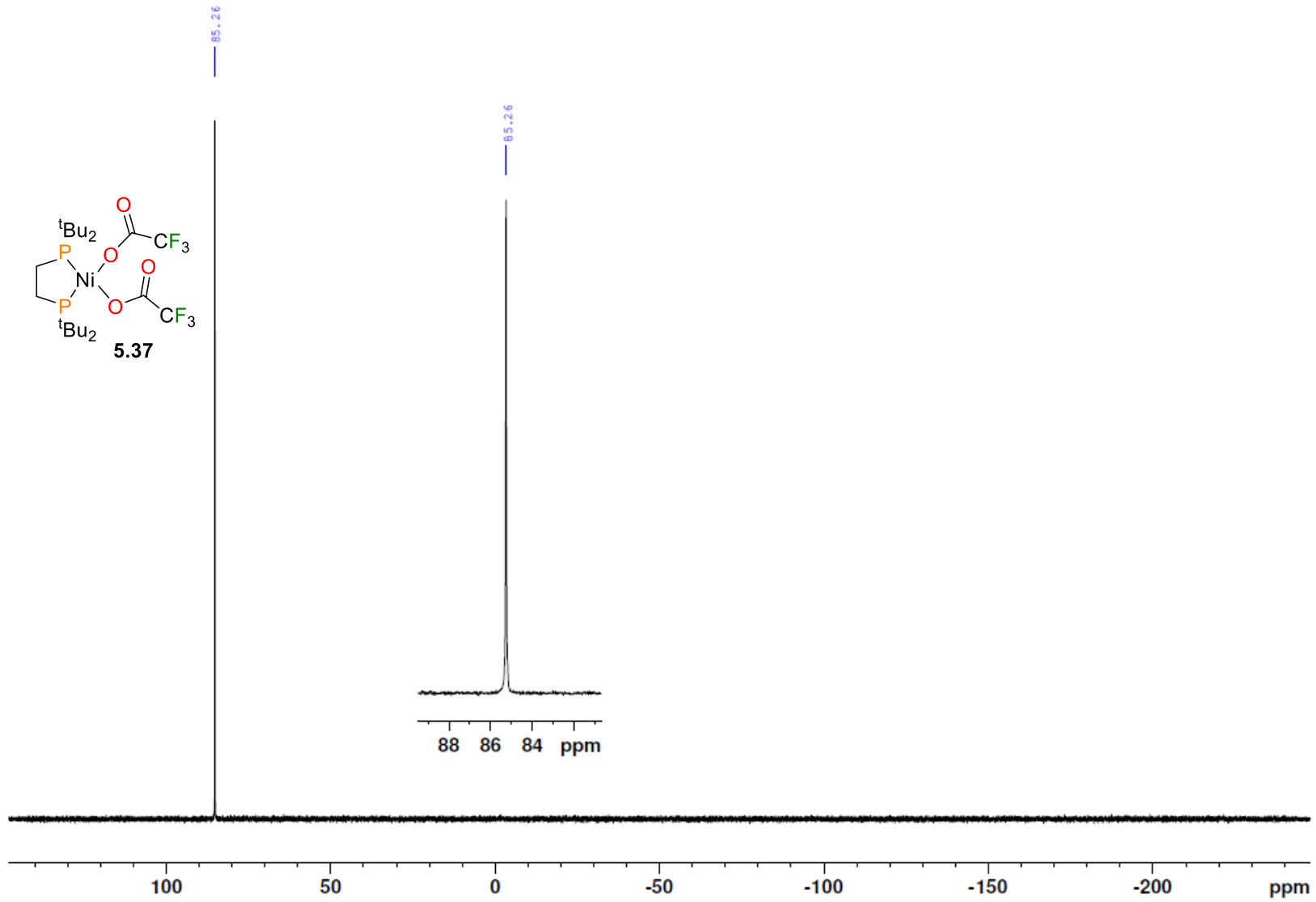


**Figure B5.41.**  $^{31}\text{P}\{^1\text{H}\}$  NMR spectrum (162 MHz, 25 °C,  $\text{CD}_2\text{Cl}_2$ ) of **5.37**.

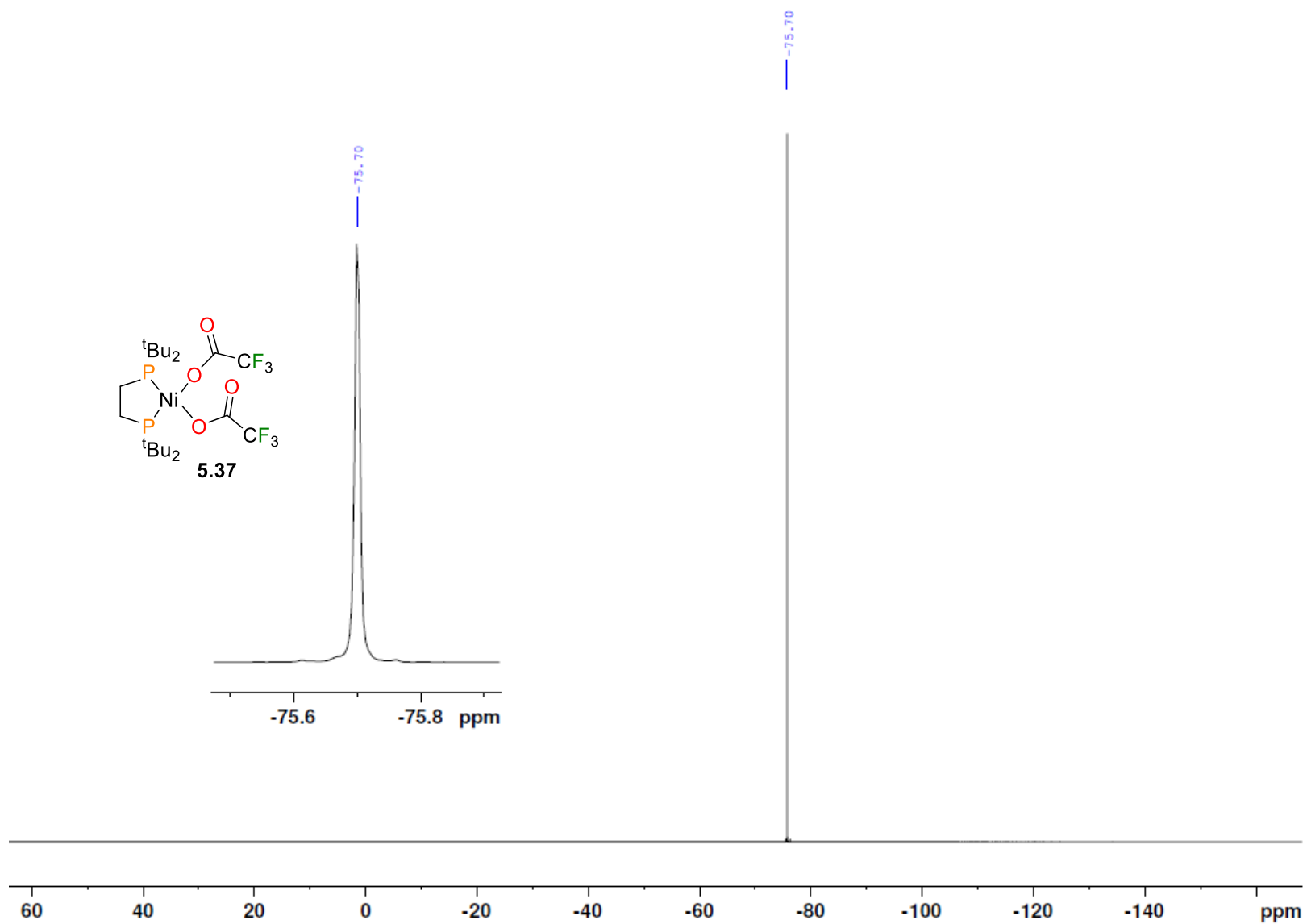


**Figure B5.42.**  $^{19}\text{F}\{^1\text{H}\}$  NMR spectrum (380 MHz, 25 °C,  $\text{CD}_2\text{Cl}_2$ ) of **5.37**.

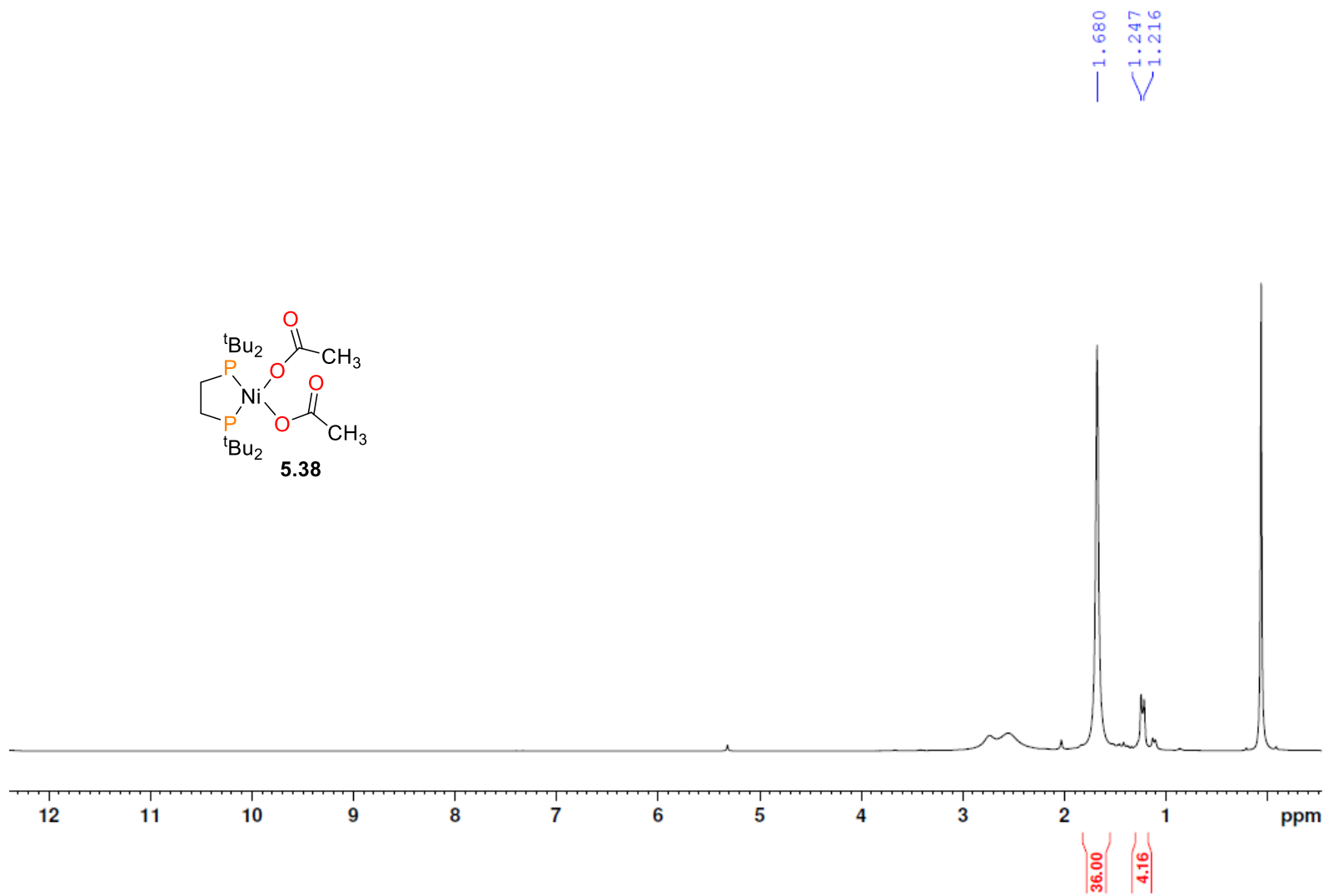


**Figure B5.43.**  $^1\text{H}$  NMR spectrum (400 MHz, 25 °C,  $\text{CD}_2\text{Cl}_2$ ) of **5.38**.

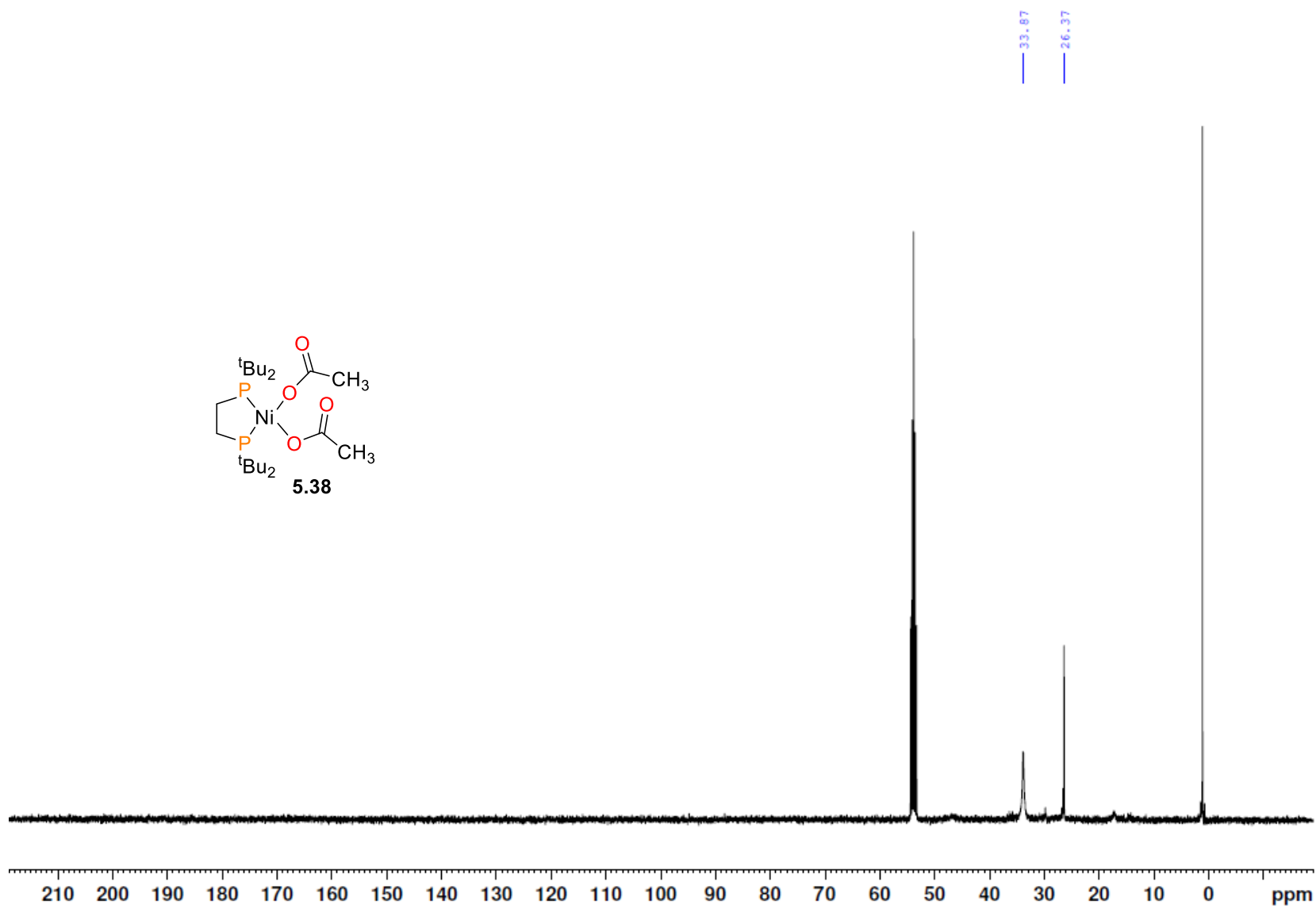


**Figure B5.44.**  $^{13}\text{C}\{^1\text{H}\}$  NMR spectrum (100 MHz, 25 °C,  $\text{CD}_2\text{Cl}_2$ ) of **5.38**.

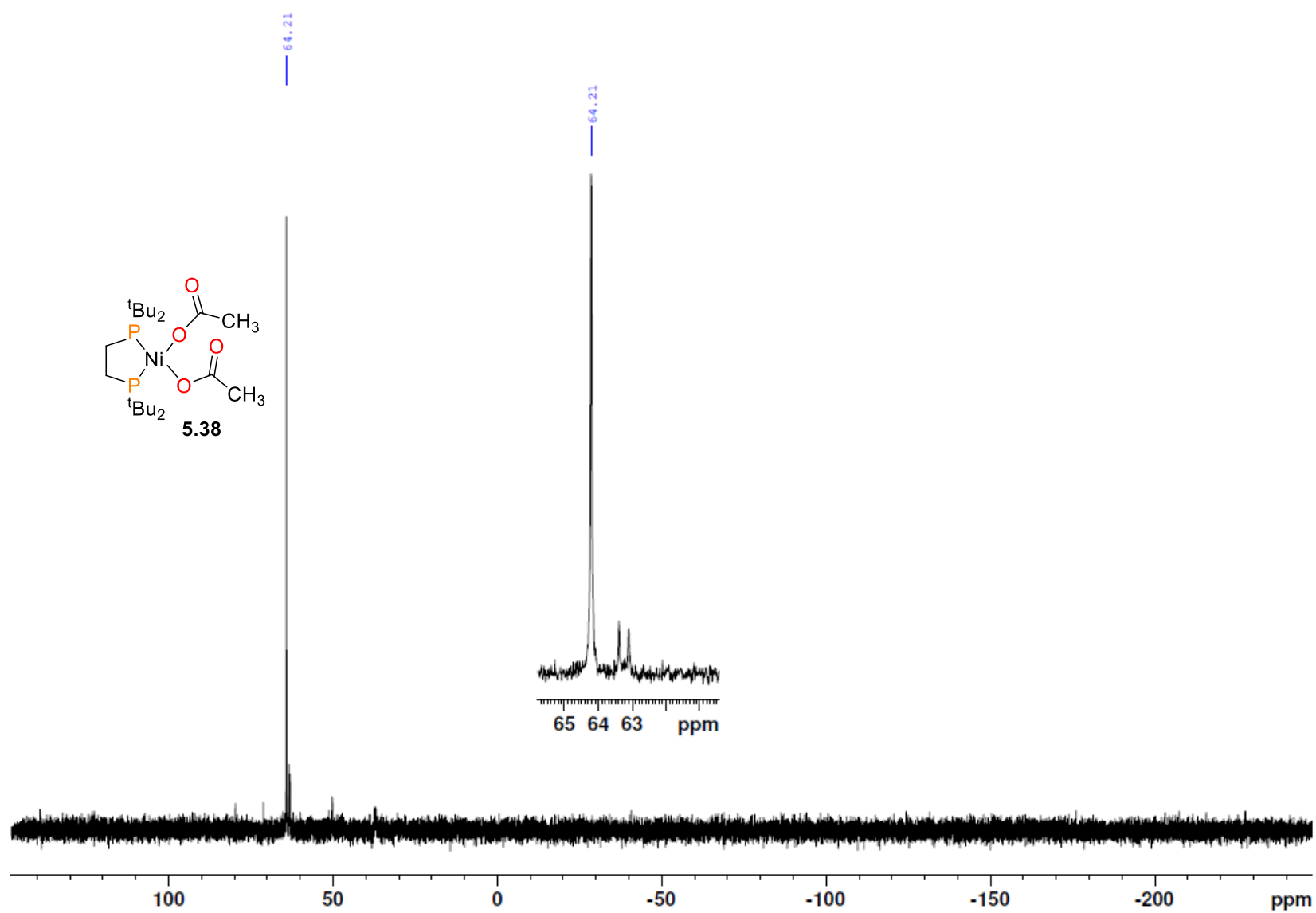


**Figure B5.45.**  $^{31}\text{P}\{^1\text{H}\}$  NMR spectrum (162 MHz, 25 °C,  $\text{CD}_2\text{Cl}_2$ ) of **5.38**.